Models That Go Ouch

by

Daina Simone Ross

October 2020

Supervised by

Professor Mark Taylor

&

Associate Professor Kenneth Pope

Submitted to the College of Science and Engineering in partial fulfilment of the requirements for the degree Bachelor of Engineering (Robotics)(Honours)/Master of Engineering (Electronics) at Flinders University – Adelaide Australia

Declaration

I certify that this work does not incorporate without acknowledgment any material previously submitted for a degree or diploma in any university; and that to the best of my knowledge and belief it does not contain any material previously published or written by another person except where due reference is made in the text.

Daina Simone Ross

1/11/2020

ACKNOWLEDGEMENTS

I would like to express my sincere gratitude to my supervisors, Professor Mark Taylor and Associate Professor Kenneth Pope, for their ongoing guidance and support throughout the duration of this project.

I will also be forever thankful to my family and friends for their unwavering encouragement, reassurance and patience along the way.

Abstract

Knee prostheses, particularly those used in knee arthroplasties, are commonly designed using mechanical modelling methods. Despite the benefits of these methods, there are persistent issues regarding chronic post-operative pain following implantation of prosthetic devices. As one of the significant indicators for revision surgery, it is important that the occurrence of chronic post-operative pain is mitigated. The integration of mechanical and neural modelling methods is yet to be explored extensively but may offer a solution to the issue. With integrated modelling methods, potential pain or discomfort may be predicted during the design phase, allowing for modifications to alleviate predicted complications prior to the device being physically created and implanted.

As a first step towards developing a complete integrated mechanical/neural model for the knee, this project focused on adapting the Hodgkin-Huxley neural model for a single Ruffini ending. However, there is a significant lack of understanding regarding fundamental behaviours of the Ruffini and limited experimental data available. As a result, there are numerous discrepancies in the literature, in particular regarding what and how the Ruffini senses. Currently, Khalsa et al. (1996) provides the most complete set of experimental data that describes Ruffini behaviour and so this data was used as a guide for adaptation of the neural model (Khalsa, Hoffman et al. 1996).

The Khalsa et al. (1996) experiment was replicated using computer modelling methods. This was expected to assist in determining what the Ruffini senses and the physical properties involved in how it senses. The specimen used in the original experiment was replicated using FEBio, while the Ruffini neural response was replicated using a Matlab adaptation of the Hodgkin-Huxley model. Successful integration of the mechanical and neural models was achieved, and the models were tested extensively using three material types and eighteen neural model input stimuli.

None of the material/input stimuli combinations produced results that adequately described the original results, and the ‘correct’ input stimulus for the neural model is still unclear. Given that none of the models tested were able to adequately replicate the original results, two possible conclusions can be drawn: either there are physical features or characteristics missing from the mechanical or neural model that play part in the Ruffini behaviour, or there may have been complications in the original results that make them difficult to replicate (e.g. responses are from multiple Ruffini endings, or interference from other neurons). Overall, the goals of the project were not achieved and as such there is still an abundance of future work to be completed, including further adaptations to the mechanical and neural model and physically re-performing the original experiment.

Contents

List of Figures

List of Tables

1 Introduction

A knee arthroplasty is a surgical operation during which the patient's knee joint is reconstructed or replaced, either partially or totally, with artificial parts. The surgery may either be an initial knee replacement (primary surgery) or re-operation on a previous knee replacement (revision surgery), and has the aim of providing the patient with relief from pain and correcting physical deformities or misalignments within the joint (Wylde, Dieppe et al. 2007; Coolican 2015; Foran and Fischer 2015; Orthopedics SA 2019). Knee arthroplasty is currently accepted as the international standard treatment for both degenerative and rheumatologic knee diseases, including osteoarthritis and rheumatoid arthritis, but is also sometimes selected as a path of treatment for sporting knee injuries when other forms of treatment have failed to provide any benefit or relief to the patient (Kurtz, Ong et al. 2011; Orthopedics SA 2019).

The total number of knee arthroplasties performed annually in Australia is rapidly increasing, to the point where knee replacement surgery is becoming almost as common as a heart attack or stroke (Australian Orthopedic Association 2018; Kim, Pearson-Chauhan et al. 2018; Australian Orthopedic Association 2019). In 2018 in Australia, there were 65,266 primary and revision knee replacement surgeries performed – a 2.2% increase in knee arthroplasty surgeries compared with the previous year (Australian Orthopedic Association 2018; Australian Orthopedic Association 2019). This increase in number of annual knee arthroplasties has been observed internationally too; in the United States, there were approximately 700,000 knee arthroplasties performed in 2010, however this number has been predicted to grow to 3.48 million by 2030 based on projection of observed trends (Kim, Pearson-Chauhan et al. 2018).

Alongside the increasing number of knee arthroplasties being performed annually, both nationally and internationally, there is an increasing incidence of post-operative patient dissatisfaction (Skou, Graven-Nielsen et al. 2013; Kim, Pearson-Chauhan et al. 2018; Orthopedics SA 2019). Various scoring systems have been developed as an attempt to quantify patient satisfaction to determine the success of the surgery and causes for dissatisfaction (Wylde, Dieppe et al. 2007; Coolican 2015). From these scoring systems, chronic and persistent post-operative pain and knee instability have been identified as significant sources of patient dissatisfaction following knee arthroplasty (Coolican 2015; Kim, Pearson-Chauhan et al. 2018; Orthopedics SA 2019). Pain and instability following knee arthroplasty can stem from a range of identifiable causes including infection, part loosening, incorrect part sizing, part misalignment, and soft tissue impingement. However, there are a proportion of patients who present with symptoms of post-operative pain and instability but

show no obvious indication of the cause (Wylde, Dieppe et al. 2007; Coolican 2015; Kim, Pearson-Chauhan et al. 2018; Orthopedics SA 2019).

A systematic review of total hip and knee replacement surgery outcomes indicated that approximately 20% of all primary total knee replacement patients reported experiencing chronic post-operative pain (Beswick, Wylde et al. 2012). As one of the most significant sources of patient dissatisfaction, it is unsatisfactory for such a large proportion of knee arthroplasty patients to be experiencing chronic post-operative pain (Coolican 2015). Additionally, the Hip, Knee and Shoulder Arthroplasty 2018 Annual Report indicated that 19% of revision arthroplasties performed in 2018 were undertaken in an attempt to rectify chronic pain caused by, or which had not been alleviated by, previously performed primary arthroplasties (Australian Orthopedic Association 2018).The rising number of knee arthroplasties performed each year, combined with an increasing proportion of patients experiencing dissatisfaction following surgery, can be expected to result in an increase in the number of revision surgeries being performed. The likelihood of requiring multiple revision surgeries has been identified as 4-5 times greater than the risk of requiring an initial revision surgery (Skou, Graven-Nielsen et al. 2013; Australian Orthopedic Association 2019). Therefore, it is clearly undesirable for the rate of initial revision surgeries to increase.

Recently, the use of mechanical modelling methods in knee prosthesis design (including those used for knee arthroplasties) has become increasingly common (Bendjaballah, Shirazi-Adl et al. 1997; Halloran, Petrella et al. 2005; Trad, Barkaoui et al. 2018). Utilising mechanical modelling allows for the prediction of contact stresses and pressures that may occur within and around the prosthetic device and joint following implantation. As a result, there is an opportunity to revise the design and mitigate potential complications that may have occurred due to these stresses and pressures (Halloran, Petrella et al. 2005). In theory, modifying the prosthesis to reduce the occurrence and /or magnitude of the predicted forces should improve both the longevity and comfort of the prosthesis once implanted and as such, reduce the need for revision surgeries. However, even with mechanical modelling in current practice, the continually increasing incidence of chronic pain and discomfort experienced following knee arthroplasties indicates that this mechanical modelling method alone is not enough to predict the discomfort that may be elicited by any particular prosthesis once it has been implanted.

The combination of neural modelling with mechanical modelling may offer a potential solution to this problem. Neural modelling, which models the neural response of the body to various input

stimuli, could be adapted specifically for the receptors within the knee in order to determine how the stresses and contact pressures within a particular prosthesis design might be physically received by the patient following knee arthroplasty. Combining the two modelling methods is a concept which has not yet been explored in-depth, particularly with specific application to the knee. If successful, it could offer invaluable improvements in the medical field - it would re-imagine the way prostheses are designed, providing the potential to improve patient satisfaction levels through early prediction and mitigation of pain points during the design process. As a result, the occurrence of chronic post-operative pain would be expected to reduce, which would in turn reduce the number of revision surgeries that are required.

2 Literature Review

In order to successfully integrate neural and mechanical models specific to the knee, a fundamental understanding of human knee structure and how pain or discomfort is sensed within the knee is required. An in-depth analysis of existing literature in these areas was undertaken, along with an analysis of existing neural and mechanical model combinations.

2.1 Anatomy and Physiology of the Human Knee

2.1.1 Overview of the Knee Joint

The human knee is a complex hinge joint that is formed by the femur, tibia and patella and is supported by various surrounding ligaments, tendons, muscles and cartilage (Souza and Doan 2010; Gaillard, Shabani et al. 2015; Orthopedics SA 2019). The arrangement of the joint's supporting elements and bones constrain the knee to a range of motion across three planes, allowing for six degrees of freedom comprised of three rotational and three translational motions (Komdeur, Pollo et al. 2002; Gaillard, Shabani et al. 2015; Jawad and Michael 2017). The greatest range of motion in the knee joint is flexion/extension (rotation) in the sagittal plane (Komdeur, Pollo et al. 2002). The remaining motions the knee is capable of, but with a more limited range, include internal/external rotation, varus/valgus rotation, anterior/posterior gliding, medial/lateral shifting, and compression/distraction (translation proximally/distally) (Figure 1) (Komdeur, Pollo et al. 2002; Gaillard, Shabani et al. 2015; Jawad and Michael 2017).

Figure 1. The six degrees of freedom of motion of the knee (Komdeur, Pollo et al. 2002).

Both the intra-articular and extra-articular structures of the knee joint contribute to joint reinforcement and stability during movement in the prescribed degrees of freedom, ensuring that the joint's range of motion is smooth and controlled (Gaillard, Shabani et al. 2015; Wodowski, Swigler et al. 2016; Orthopedics SA 2019). Extensive research regarding the knee joint and associated structures has led to an understanding that the ligaments of the knee are primarily responsible for joint stabilization, while the muscles, cartilage, and other structures surrounding the knee provide secondary support (Katonis, Papoutsidakis et al. 2008; Gaillard, Shabani et al. 2015; Jawad and Michael 2017). Figure 2 illustrates the anatomy of the knee joint, detailing some of the structures which play an important role in knee stabilization.

This image has been removed due to copyright restrictions. Available online from [http://www.avalonorthopaedic.com.au/managing-complex-knee-injuries/]

Figure 2. Illustration of the human knee showing primary structures pertinent to stability and movement (Avalon Orthopedic 2019)

The contribution of ligaments to knee stability and reinforcement of the joint is understood to be due to their extensive nerve supply which allows for proprioception (Gaillard, Shabani et al. 2015). The ligaments documented to have involvement in the primary support and stabilization of the knee joint include the patellar ligament, the medial and lateral collateral ligaments, and the anterior and posterior cruciate ligaments (Komdeur, Pollo et al. 2002; Jawad and Michael 2017). These ligaments all assist in preventing excessive displacements and rotations, therefore protecting the joint from unstable, uncontrolled movements that could result in injury to the joint structures (Jawad and Michael 2017). In particular, the anterior cruciate ligament (ACL) and the posterior cruciate ligament (PCL) have been identified as key ligaments that contribute to joint stabilization and reinforcement, with the ACL recognised to contribute to approximately 85% of the knee joint stabilization functionality (Komdeur, Pollo et al. 2002; Souza and Doan 2010; Jawad and Michael 2017).

There are multiple muscle groups that contribute to secondary support and active stabilization of the knee joint as well as being responsible for initiation of joint motion (Katonis, Papoutsidakis et al. 2008). The two main muscle groups contributing to this are the quadriceps and the hamstrings, while other smaller muscles involved include the gastrocnemius, plantaris and popliteus muscles (Souza and Doan 2010; Jawad and Michael 2017).

The knee joint contains three fat pads - the quadriceps fat pad, the prefemoral fat pad, and the infrapatellar fat pad, all of which are located anteriorly within the knee (Souza and Doan 2010). While not all of the functions of the fat pads are known, there is speculation that they may contribute to stability and biomechanical support of the joint due to being rich in vascularization and innervation, similar to the other supporting structures of the knee (Souza and Doan 2010; Gaillard, Shabani et al. 2015).

Another structure of the knee joint that is considered to assist in reinforcing knee stability is the joint capsule (Müller 1982). The joint capsule is strong, dense, collagen-rich connective tissue that attaches to the knee joint bones, sealing the joint space (Ralphs and Benjamin 1994; Souza and Doan 2010). The inner surface of the capsule is lined by a synovial membrane, and both the capsule

tissue itself and the synovial tissue are highly innervated (Ralphs and Benjamin 1994). The innervation of these tissues indicates that the joint capsule, alongside the other supporting structures, provides some stability and proprioception to the joint (Müller 1982; Ralphs and Benjamin 1994).

2.2 Neurons and the Nervous System

2.2.1 Sensory Receptors

Sensory receptors convey information regarding the internal body and the surrounding environment by converting stimuli into neural impulses (known as action potentials), which are then interpreted by the central nervous system (Widmaier, Raff et al. 2014; Wodowski, Swigler et al. 2016). These action potentials are only produced by the receptor if the strength of the given stimuli is above a given threshold, and the threshold varies between receptor types (Halata, Wagner et al. 1999). The various types of sensory receptors are classified according to the types of stimuli that activate them, or by their location within the body (Jawad and Michael 2017). In general, the types of sensory receptors include mechanoreceptors, chemoreceptors, thermoreceptors, photoreceptors, and nociceptors (Widmaier, Raff et al. 2014).

Literature indicates that the types of receptors identified specifically within the internal knee are mechanoreceptors and nociceptors (Gillquist 1996; Katonis, Papoutsidakis et al. 2008; Wodowski, Swigler et al. 2016; Jawad and Michael 2017). Mechanoreceptors respond to mechanical stimuli such as pressure, stretch or vibration (Widmaier, Raff et al. 2014). One class of mechanoreceptor that is found within the knee is the proprioceptor, which provides the body with an awareness of its relative position in space (Johnson 2003; Wodowski, Swigler et al. 2016). Nociceptors are a type of receptor that detect noxious stimuli thereby allowing the body to interpret harmful stimuli as pain thereby preventing further tissue damage or injury (Widmaier, Raff et al. 2014). Nociceptors may respond to a range of stimuli including thermal, mechanical or chemical (Widmaier, Raff et al. 2014).

While many aspects of human physiology are agreed upon, there is still some degree of controversy in regards to the types and locations of mechanoreceptors within the human knee (Wodowski, Swigler et al. 2016). This is due to limited research directly involving the human knee and its sensory receptors, although there have been multiple studies related to receptors located in other parts of the human body (such as the skin). On the other hand, there have been a number of studies performed relating to receptors in animals (Freeman and Wyke 1967; Burgess and Clark 1969; Halata, Wagner et al. 1999; Grigg 2001).

A major study by Freeman and Wyke (1967) identified four types of receptors within the cat knee – Ruffini endings, Pacinian corpuscles, Golgi-tendon organs, and free nerve endings (Freeman and Wyke 1967). This has been a widely accepted study that has been used by other researchers to draw conclusions regarding the human knee. There are a number of weaknesses in applying this

study directly to the human knee, including the lack of evidence that the cat and human knee are directly comparable. In addition, the study was conducted using cats' knees with a small sample size of 31 individual cats and a total of 41 knees. However compared to other related studies performed on cats this was the most significant sample (Freeman and Wyke 1967; Burgess and Clark 1969; Grigg 2001).

There have also been studies completed on knee joints of other animal species including rats, rabbits and sheep. One particular study involving sheep identified three of the four types of receptors classified by Freeman and Wyke (1967) within the sheep knee, including Ruffini endings, Pacinian corpuscles and free nerve endings (Halata, Wagner et al. 1999). The study also confirmed the rich supply of sensory nerves within the sheep ACL. The strengths of this study include the sheep knee joint being easily accessible for sample dissection, as well as the human and sheep knee joint and ligaments sharing anatomical similarities. However, there are always limitations in drawing conclusions regarding the human knee receptors from a non-human study.

There have been two studies involving mechanoreceptors in human knees that have produced different findings to Freeman and Wyke (1967) (Schutte, Dabezies et al. 1987; Katonis, Papoutsidakis et al. 2008). Specifically, both studies found fewer receptors overall, and the study by Katonis et al. (2008) identified only three of the four receptor types classified by Freeman and Wyke (1967). The weaknesses in these two studies include their reliance on cadaver samples, amputation samples and samples obtained as a result of surgery. Samples obtained under these circumstances may not be representative of healthy human knees as there may have been diseased or damaged tissues amongst the samples or potential deterioration of sensory receptors. The use of human samples has allowed these studies to add some value to the body of knowledge regarding receptors in the human knee, however they have also created uncertainty by producing conflicting results compared to the Freeman and Wyke (1967) classifications.

More recently, a human study was conducted which attempted to map the distributions of all mechanoreceptors within the ligaments and tendons surrounding the knee, as well as distinguish the types and densities of receptors (Çabuk and Kuşku Çabuk 2016). The study indicated the presence of three of the four receptor types identified by Freeman and Wyke (1967), however in contrast to other studies, the receptors identified were Golgi tendon organs, Ruffini endings and free nerve endings. A strength of this study is the use of a contemporary histological technique, while the weaknesses of the study are the small sample size of 8 cadavers and the possibility of deteriorated cadaver tissues.

Research regarding the densities of receptor types within the knee is variable between studies, mainly due to the varied sampling methodologies which included cadavers and damaged knee tissue, as well as varied species (Schultz, Miller et al. 1984; Schutte, Dabezies et al. 1987; Katonis, Papoutsidakis et al. 2008; Çabuk and Kuşku Çabuk 2016). Therefore, precise numbers of receptors within various structure of the human knee have not been accurately established.

Despite there being some uncertainty as a result of conflicting studies, the Freeman and Wyke (1967) classification remains the predominant and most widely accepted study regarding receptors within the knee. Therefore, the receptors that will be further investigated will be those classified by Freeman and Wyke (1967). These receptor types, their structures and their functionality are summarised in Table 1. It should be noted that naming conventions of the receptor types differ between studies, however the names that will be used in the present paper are those listed in Table 1.

Table 1. Summary of the four receptor types identified by Freeman and Wyke (1967), including morphology and physiological function

Type	Common Name	Location (in the knee)	Structure and Size	Parent Axon	Perceived Stimulus	Activation Threshold	Adaptation
I	Ruffini ending	Joint capsule, ligaments.	Variable depending on species. Generally elongated with tapering ends, encapsulated. 20μm-150μm in diameter, up to 600μm in length.	Myelinated, 5μm-10μm in diameter.	Stretch, tissue displacement.	Low	Slow
II	Pacinian corpuscle	Fat pads, joint capsule, ligaments, menisci.	Elongated, oval-shaped, encapsulated, multi-laminated. Up to 4mm length.	Myelinated, 8-15μm in diameter.	Compression, pressure, vibration.	Low	Fast
III	Golgi tendon organ	Tendons, ligaments, joint capsule, menisci.	Elongated with tapering ends, encapsulated. Up to 600μm in length, 100μm in width.	Myelinated, 14μm - 16μm in diameter.	Stretch (extreme, end limit).	High	Slow
IV	Free nerve ending	All articular tissues except bone.	Unencapsulated, branching or tightly meshed. 0.5μm-1.5μm in diameter.	Unmyelinated, 1-2μm in diameter OR Myelinated, 2-4μm in diameter.	Noxious mechanical stimuli.	High	Slow

2.2.2 Ruffini Endings

Type I receptors, or Ruffini endings, are generally described as globular encapsulated corpuscles, appearing elongated with narrowing ends (Freeman and Wyke 1967; Zimny and Wink 1991; Fleming and Luo 2013). However, the findings regarding structure of the Ruffini are variable between studies. For example, Halata et al. (1985) described finding five types of Ruffini endings, all with varying shape and size, whereas Freeman and Wyke (1967) only described two variations of Ruffini ending (Freeman and Wyke 1967; Halata, Rettig et al. 1985). Regardless of structural differences reported in the literature, multiple researchers agree that Ruffini endings are embedded in the surrounding tissue. Two studies indicated that this is achieved by the intertwining of unmyelinated nerve fibres within the receptor capsule with the collagen fibres of the embedding tissue (Zimny and Wink 1991; Magee, Zachazewski et al. 2007). Figure 3 is an interpretive illustration by Das et al. (2017), adapted from Hall's (2015) representation of the Ruffini ending, which depicts this intertwining of nerve fibres with the collagen fibres within the receptor capsule (Hall 2015; Das, Soni et al. 2017).

This image has been removed due to copyright restrictions. Available online from [https://www.oatext.com/pdf/MDDE-2-116.pdf]

Figure 3. Interpretive illustration of a singular of Ruffini ending (Das, Soni et al. 2017).

Figure 4Figure 5 shows a gold chloride stain of a Ruffini ending within the glenoid capsule from the shoulder of a human cadaver, while Figure 5 shows a gold chloride stain of the Ruffini ending within the ACL of a rabbit (Aydog, Korkusuz et al. 2006; Witherspoon, Smirnova et al. 2014). Despite anatomical differences and potentially differing neuronal structures between the two species, the intertwining of the Ruffini ending fibres with the surrounding tissue is evident in both images.

This image has been removed due to copyright restrictions. Available online from [https://onlinelibrary.wiley.com/doi/full/10.1111/joa.12215]

Figure 4. Gold chloride stain of a Ruffini ending within the glenoid capsule of a cadaver (Witherspoon, Smirnova et al. 2014).

This image has been removed due to copyright restrictions. Available online from [https://link.springer.com/article/10.1007%2Fs00167-005-0673-2]

Figure 5. Gold chloride stain of Ruffini ending in the rabbit ACL (Aydog, Korkusuz et al. 2006)

The size of Ruffini endings has also been documented to vary, particularly between species, ranging from 20μm to 150μm in diameter, and up to 600μm in length (Freeman and Wyke 1967; Zimny and Wink 1991; Halata, Wagner et al. 1999). The parent axon of the Ruffini ending is a myelinated nerve fibre, generally 5μm-10μm in diameter (Freeman and Wyke 1967; Magee, Zachazewski et al. 2007). Ruffini endings are usually found in clusters of three to six, and are dispersed three-dimensionally within the tissue they are located in (Freeman and Wyke 1967). All capsules within the cluster are innervated by individual myelinated terminal axon branches approximately 2μm-5μm in diameter which originate from the same parent axon (Freeman and Wyke 1967; Magee, Zachazewski et al. 2007). It has been documented that a parent axon of a Ruffini ending will only innervate other Ruffini endings and not other receptor types (Freeman and Wyke 1967).

The locations of the Ruffini endings has been reported differently across studies. One study indicated that they are not present on either cruciate ligament and are less frequently found in the medial and lateral collateral ligaments (Freeman and Wyke 1967), while another study suggested that they are found in more significant numbers in the PCL and ACL than in the lateral collateral ligament (Çabuk and Kuşku Çabuk 2016). The former study also indicated that the Ruffini is most prevalent in the joint capsule, while the latter suggested prevalence in the popliteal tendon. These differing results may be due to the subjects used in each of the studies, with the former study using samples from cats while the latter study involved human cadavers. In that regard, the latter study is more applicable to the anatomy of the human knee, and therefore provides a more accurate representation of the receptor locations. There is general consensus that Ruffini endings tend to be located within deeper tissues of the knee joint, and are not present in the fat pads and synovial membrane (Freeman and Wyke 1967; Zimny and Wink 1991; Halata, Wagner et al. 1999).

Ruffini endings are primarily responsive to mechanical stimuli in the form of tissue deformation caused by stretch or displacement (Zimny and Wink 1991; Magee, Zachazewski et al. 2007; Fleming and Luo 2013). This responsiveness to the mechanical stimuli occurs for a range of joint positions, and as such the Ruffini ending is classified as a type of proprioceptor (Freeman and Wyke 1967; Magee, Zachazewski et al. 2007). A number of studies identified that the embedded nature of Ruffini endings allowed the sensing of deformation in the surrounding tissues, via transmission of tension through collagen fibres to the nerve terminal (Zimny and Wink 1991; Halata, Wagner et al. 1999; Magee, Zachazewski et al. 2007; Fleming and Luo 2013). The orientation of both the collagen fibres and the Ruffini structure are suggested to determine the directional sensitivity for tissue stretch, although the orientation of the Ruffini ending respective

to the collagen and other tissue fibres is unclear (Grigg and Hoffman 1982; Magee, Zachazewski et al. 2007). A study by Khalsa et al. (1996) indicated that Ruffini endings have a preferred direction of stretch sensitivity (Khalsa, Hoffman et al. 1996). Magee et al. (2007) suggested that this stretch sensitivity was along the long axis of the Ruffini capsule, however it is still unclear which orientation the Ruffini ending would be respective to the tissue fibres (Magee, Zachazewski et al. 2007). On the contrary, Palmer et al. (2012), proposed that the Ruffini does not have a preferred direction of stretch sensitivity itself, and that direction of stretch sensitivity depends instead on the material properties of the surrounding tissue in which the Ruffini is embedded (Palmer, Taylor et al. 2012).

In a study relating to Ruffini endings within the skin, it was suggested that the receptors were also sensitive to velocity (Fleming and Luo 2013). Other studies involving Ruffini endings in knees have not indicated a similar finding in relation to velocity sensitivity, which raises the possibility of the Ruffini endings having different properties depending on their location within the body.

Ruffini endings have been identified to have a low stimulus threshold before producing an action potential response (Halata, Wagner et al. 1999; Kahanov and Kato 2007). The exact threshold value is not clear however, as a number of experimental studies report variations in the threshold values recorded (ranging between 5kPa and 80kPa) (Eklund and Skoglund 1960; Grigg and Hoffman 1982; Khalsa, Hoffman et al. 1996). This variability in values could be reflective of differences in methodology between the experiments, but it may also be due to variations in the structure of the Ruffini endings or possibly differences between the tissues from which they were obtained. These mechanoreceptors are slowly adapting, meaning that the receptor response is sustained for the duration of the stimulus, provided the stimulus strength remains above the activation threshold (Johnson 2003; Kahanov and Kato 2007; Magee, Zachazewski et al. 2007).

2.2.3 Pacinian Corpuscle

Type II receptors, or Pacinian corpuscles, are elongated, oval-shaped, encapsulated end organs which can reach up to 4mm in length in humans (Kahanov and Kato 2007; Fleming and Luo 2013). Pacinian corpuscles in humans are significantly longer than those found in other species such as cats, where the length has been found to only reach up to 280μm (Freeman and Wyke 1967; Magee, Zachazewski et al. 2007). Each corpuscle has a thick multi-laminated connective tissue capsule, which results in an onion-like cross sectional appearance (Freeman and Wyke 1967; Fleming and Luo 2013). In the knee joint, Pacinian corpuscles are usually distributed in clusters of two to four corpuscles (Freeman and Wyke 1967). Each corpuscle within a cluster is innervated

by a thin myelinated axon (4-5μm in diameter), branching from a single myelinated parent axon (8-15μm in diameter) (Freeman and Wyke 1967). Figure 6 depicts an interpretation by Das et al. (2017) of the Pacinian corpuscle from within the human body, while Figure 7 shows a gold chloride stain image of a cluster of Pacinian corpuscles taken from a rabbit ACL (Aydog, Korkusuz et al. 2006). Comparing the interpretive image with the histological stain, it is clear that the shape of the Pacinian corpuscle is consistent, despite the anatomical differences between human and rabbit.

This image has been removed due to copyright restrictions. Available online from [https://www.oatext.com/pdf/MDDE-2-116.pdf]

Figure 6. Das et al. (2017) interpretation of the Pacinian corpuscle from the human body (Das, Soni et al. 2017).

This image has been removed due to copyright restrictions. Available online from [https://link.springer.com/article/10.1007%2Fs00167-005-0673-2]

Figure 7. Gold chloride stain of Pacinian corpuscle cluster in the rabbit ACL (Aydog, Korkusuz et al. 2006)

The locations of Pacinian corpuscles vary significantly between species (Fleming and Luo 2013). In humans and other primates they are mostly located within fat pads of hands and feet, but are also found in joints, muscles, tendons and also some internal organs (Halata, Wagner et al. 1999; Fleming and Luo 2013). Freeman and Wyke (1967) studied cat knees and found that Pacinian corpuscles were entirely absent from all ligaments, menisci and synovial tissue (Freeman and Wyke 1967). This contrasts with a number of other studies. A broad review of human and animal studies by Katonis et al. (2008) found large numbers of Pacinian corpuscles present within the ACL and PCL (Katonis, Papoutsidakis et al. 2008). Halata et al. (1999) recorded the presence of these corpuscles within the ACL of sheep (Halata, Wagner et al. 1999). Magee et al. (2007) documented the presence of Pacinian corpuscles within the human knee joint capsule, ligaments and menisci (Magee, Zachazewski et al. 2007). This difference in documented locations supports the premise that there is significant interspecies variability. Despite there being variations in studies involving the different species, there are also similarities. In particular, Pacinian corpuscles within the knee are mostly found medially and laterally to the joint and are predominantly located within the fibrous and fatty structures within the joint capsule (Freeman and Wyke 1967; Magee, Zachazewski et al. 2007).

Pacinian corpuscles are sensitive to mechanical stimuli in the form of compression, and as such are classified as a type of proprioceptor. In particular, they are responsive to joint compression and increases in joint hydrostatic pressure (Magee, Zachazewski et al. 2007). Pacinian corpuscles are also considered to be sensitive to vibrations internal and external to the body (Magee, Zachazewski et al. 2007; Fleming and Luo 2013; Jawad and Michael 2017). Various researchers agree that Pacinian corpuscles are not sensitive to stretch (Magee, Zachazewski et al. 2007; Fleming and Luo 2013; Jawad and Michael 2017).

These receptors function as low-threshold, and rapidly adapting proprioceptors (Halata, Wagner et al. 1999; Kahanov and Kato 2007). Two studies agree that the Pacinian corpuscle's ability to sense and rapidly adapt to a stimulus is due to the layered structure of the capsule (Johnson 2003; Fleming and Luo 2013). Johnson (2003) further suggested that the layers of the corpuscle move past each other and dissipate the pressure from the capsule into surrounding tissue (Johnson 2003). The change in neural membrane pressure during the onset and release of a stimulus is suggested to activate the receptor response, to which the receptor adapts and then returns to an inactive state (Johnson 2003). Johnson (2003) also indicated that, within the skin, Pacinian corpuscles are most sensitive to stimuli ranging between 200Hz - 300Hz. However, the literature is unclear whether this threshold can be extrapolated for Pacinian corpuscles located within the knee.

2.2.4 Golgi Tendon Organ

Type III receptors, or Golgi tendon organs (GTO), have been identified by researchers as 'spray-like' endings enclosed within a fine elongated tissue capsule with narrowing ends (Zimny and Wink 1991; Magee, Zachazewski et al. 2007). GTOs within the knee joint have been described as appearing similar to Ruffini endings but tend to be larger and have a thicker innervating parent axon (Zimny and Wink 1991; Magee, Zachazewski et al. 2007). The parent axon is myelinated, and can range from 14μm-16μm in diameter (Zimny and Wink 1991). These receptors have been documented to reach up to 600μm in length and 100μm in width (Zimny and Wink 1991). Figure 8 is an illustration of the Golgi tendon organ by Das et al. (2017), which appears to be very similar to the Ruffini ending depicted in Figure 3, as was expected based on the consensus within the literature that the two receptor types have very similar structures. Figure 9 shows a gold chloride stain of a Golgi tendon organ within the lateral collateral ligament of a cadaver elbow, where the distinctive elongated shape of the GTO described in the literature can clearly be observed (Kholinne, Lee et al. 2018).

This image has been removed due to copyright restrictions. Available online from [https://www.oatext.com/pdf/MDDE-2-116.pdf]

Figure 8. Illustration by Das et al. (2017) of the Golgi tendon organ from the human knee (Das, Soni et al. 2017).

This image has been removed due to copyright restrictions. Available online from [https://www.sciencedirect.com/science/article/pii/S2214687317303527?via%3Dihub]

Figure 9. Gold chloride stain of a Golgi tendon organ in the lateral collateral ligament of a human elbow (Kholinne, Lee et al. 2018).

There have been conflicting studies regarding the presence of GTO's within the knee, with three studies failing to identify the presence of these receptors (Schutte, Dabezies et al. 1987; Halata, Wagner et al. 1999; Katonis, Papoutsidakis et al. 2008). However, four studies did identify GTO's within the knee (Freeman and Wyke 1967; Zimny and Wink 1991; Magee, Zachazewski et al. 2007; Çabuk and Kuşku Çabuk 2016). In those studies that did identify the presence of GTO's, they were only located within the tendons, ligaments, joint capsule, and menisci of the knee (Zimny and Wink 1991; Magee, Zachazewski et al. 2007; Çabuk and Kuşku Çabuk 2016). They have been reported to be most abundant within the PCL and the popliteal tendon, but have also been identified in smaller numbers within the patellar tendon and the semitendinosus tendon (Çabuk and Kuşku Çabuk 2016).

GTOs have been identified as a type of proprioceptor due to their sensitivity to stretch (Zimny and Wink 1991; Magee, Zachazewski et al. 2007). Three studies have found GTOs to be inactive while the knee joint is stationary and indicated that they only become active towards the extreme limits of joint movement (Zimny and Wink 1991; Kahanov and Kato 2007; Magee, Zachazewski et al. 2007). It is considered that because of this limit detection, GTO's have high activation thresholds (Zimny and Wink 1991; Magee, Zachazewski et al. 2007). They have also been identified as slowly adapting receptors, producing action potentials for the entire duration of a stimulus above the given threshold (Kahanov and Kato 2007; Magee, Zachazewski et al. 2007).

2.2.5 Free Nerve Endings

Type IV receptors, or free nerve endings, can be further classified as Type IV(a) or IV(b). Type IV(b) endings will not be covered in this discussion as they have only been found within articular blood vessels, and are therefore not specifically related to the function of the knee joint (Freeman and Wyke 1967). Hence, the only free nerve endings referred to from this point forward will be Type IV(a).

Unlike the other three types of receptors described, free nerve endings are non-corpuscular, presenting either as tightly meshed unmyelinated nerve fibres (0.5μm-1.5μm in diameter) or branching unmyelinated axon terminals (<1μm in diameter) (Freeman and Wyke 1967; Zimny and Wink 1991; Halata, Wagner et al. 1999; Jawad and Michael 2017). Both formations of free nerve endings branch from parent axons that can either be unmyelinated C fibres (1-2μm in diameter) or thinly myelinated Aδ fibres (2-4μm in diameter) (Halata, Rettig et al. 1985; Zimny and Wink 1991; Johnson 2003). Two studies have indicated the identical morphological structure of free nerve endings across species and in varying locations (Heppelmann, Messlinger et al. 1995; Halata, Wagner et al. 1999). Therefore, it is plausible to extrapolate information pertaining to free nerve endings within non-human species to the human knee. Figure 10 is an illustration by Poláček (1966) depicting a branching free nerve ending (Poláček 1966). Figure 11 shows an immunohistochemical stain of a network of free nerve endings from a cadaver wrist (Rein, Semisch et al. 2015). It is clear from the similarities between the illustration and the immunohistochemical stain that there are minimal discrepancies regarding the structure of free nerve endings regardless of species or location, most likely due to being commonly identified and having been studied more widely than the other receptor types.

This image has been removed due to copyright restrictions. Available online from [https://musculoskeletalkey.com/neurophysiology-of-the-joints-and-muscles/]

Figure 10. Illustration by Poláček (1966), depicting the branching terminals of a free nerve ending (Poláček 1966).

This image has been removed due to copyright restrictions. Available online from [https://pubmed.ncbi.nlm.nih.gov/26024577]

Figure 11. An immunohistochemical stain of the free nerve endings from the wrist of a cadaver (Rein, Semisch et al. 2015).

In all species studied, free nerve endings are the most commonly identified receptor type within the knee (Halata, Wagner et al. 1999; Çabuk and Kuşku Çabuk 2016). In the human knee specifically, they have also been documented as the most widely distributed receptor type and are located within most of the articular tissues (Freeman and Wyke 1967; Halata, Rettig et al. 1985; Zimny and Wink 1991; Magee, Zachazewski et al. 2007). Tightly meshed free nerve endings are mostly found within the fibrous and fat tissues of the joint, including the joint capsule and fat pads, but have been reported as absent from ligaments, menisci and synovial tissues (Freeman and Wyke 1967). In contrast, terminal free nerve endings are most abundant in both the intra- and extra-

articular ligaments but are also found in joint capsule tendons and deeper within the joint capsule, although , in much smaller numbers, (Freeman and Wyke 1967). This latter form of free nerve ending has not been documented within the menisci or synovial tissues (Freeman and Wyke 1967). Numerous studies identified free nerve endings within ligaments of the knee, and it is assumed that these were the latter form of free nerve ending (Schutte, Dabezies et al. 1987; Johansson, Sjölander et al. 1991; Zimny and Wink 1991; Halata, Wagner et al. 1999; Çabuk and Kuşku Çabuk 2016). Both Çabuk and Kuşku Çabuk (2016) and Halata et al. (1999) reported that free nerve endings were primarily located within the cruciate ligaments compared with other structures of the knee joint (Halata, Wagner et al. 1999; Çabuk and Kuşku Çabuk 2016).

Free nerve endings are nociceptors that respond to noxious stimuli, transmitting information regarding pain or inflammation at the receptor site to the central nervous system (Zimny and Wink 1991; Lobenhoffer, Biedert et al. 1996; Halata, Wagner et al. 1999). Although documented to respond to other types of noxious stimuli, free nerve endings within the articular structures of the knee tend to primarily respond to harmful mechanical stimuli (Halata, Wagner et al. 1999; Magee, Zachazewski et al. 2007). This includes functioning alongside proprioceptors where they may elicit a pain response at extreme limits of movement that may result in tissue damage, although the main role of the nociceptor depends on its location (Çabuk and Kuşku Çabuk 2016). Johnson (2003) suggested that the type of pain experienced depends on the fibre the receptor response originates from (Johnson 2003). It is suggested that receptors innervated by the unmyelinated C fibres to generate a burning sensation, while those innervated by Aδ fibres generate a pricking or tickling sensation (Johnson 2003).

Free nerve endings have been documented to have a high threshold, so a neural response tends to be triggered only for potentially damaging stimuli rather than during general movement (Halata, Wagner et al. 1999; Kahanov and Kato 2007; Magee, Zachazewski et al. 2007). In contrast to this, a study investigating changes to nociceptor response under experimental arthritic conditions indicated increases to sensitivity of free nerve endings in inflamed or swollen joints, therefore triggering neural responses at a lower threshold (Schaible and Schmidt 1985; Magee, Zachazewski et al. 2007). Free nerve endings are also documented to be slow-adapting receptors, which is suggested to be due to the nature of the stimuli activating the receptor (Johnson 2003). The process of slow adaptation to the stimulus allows the central nervous system to maintain alertness to potential tissue damage for the duration of the noxious stimulus, thereby increasing protection for the body (Johnson 2003; Widmaier, Raff et al. 2014).

2.3 Computational Modelling of Knees and Neurons

2.3.1 Finite Element Method

The Finite Element Method (FEM) is a numerical approach that is widely used in modelling the behavior of physical objects or systems. FEM modelling has direct application to the calculations associated with the design and simulation of prostheses, including those used in knee arthroplasties (Bendjaballah, Shirazi-Adl et al. 1997; Halloran, Petrella et al. 2005; Trad, Barkaoui et al. 2018).

Findings from Halloran et al. (2005) have indicated that a complete understanding of joint contact mechanics, kinetics, and kinematics is crucial to designing successful knee replacement prostheses (Halloran, Petrella et al. 2005). Various structures and biomechanical behaviours of the human knee can be simulated using FEM models to aid in this understanding (Villa, Migliavacca et al. 2004; Halloran, Petrella et al. 2005; Muller 2014). FEM modelling of the knee joint also allows prediction of mechanical properties that may be created by knee replacement prostheses, including stresses, deformations, and contact pressures (Villa, Migliavacca et al. 2004; Halloran, Petrella et al. 2005; Peña, Calvo et al. 2006). In turn, through stress analysis, it is possible to predict the success of knee arthroplasties and potentially prevent premature failure of knee protheses (Villa, Migliavacca et al. 2004; Halloran, Petrella et al. 2005).

The application of FEM modelling to prosthetic design allows for changes to be made to geometrical elements and material components of prostheses prior to the production of prototypes (Villa, Migliavacca et al. 2004; Muller 2014). In addition to delivering a more effective prosthesis design, this method also results in time and cost savings (Muller 2014). Furthermore, the flexibility of a computational model provides the opportunity for model modification to account for differences in anatomy of individual patients (Muller 2014; Trad, Barkaoui et al. 2018).

Whilst FEM modelling has considerable strengths in its application to the knee, it also presents limitations. More specifically, the performance of the model is dependent on how accurately the model is constructed, particularly in regard to the structure, dimensions and material (Panagiotopoulou 2009). This limitation is especially relevant when considering FEM modelling of the human knee due to its extremely complex structure, and as such, accurate modelling has proven to be difficult (Bendjaballah, Shirazi-Adl et al. 1997; Haut Donahue, Hull et al. 2002; Halloran, Petrella et al. 2005; Trad, Barkaoui et al. 2018). Additionally, the FEM calculations are only approximate due to the analysis being performed on a model rather than the real object, hence the importance of creating as accurate a model as possible (Panagiotopoulou 2009).

Regardless of the limitations presented, the strengths and benefits in using FEM modelling, particularly for applications such as knee prosthesis design, far outweigh the weaknesses (Muller 2014).

2.3.2 The Hodgkin-Huxley Model

The Hodgkin-Huxley model provides a mathematical description of current flow through ion-selective channels across neural membranes (Hodgkin and Huxley 1952; Nelson and Rinzel 1998). Current flow through these channels (above a given threshold) results in the generation of action potentials, and as such this model has provided the basis for understanding of neural responses (Appali, van Rienen et al. 2012). Hodgkin and Huxley (1952) based their studies on the axon of a giant squid, which allowed them to develop a mathematical model comprised of differential equations to describe the ion channels and ionic current (Hodgkin and Huxley 1952; Nelson and Rinzel 1998).

Other models describing neural response have been developed since publication of the Hodgkin-Huxley model in 1952, yet the Hodgkin-Huxley model is currently still the most established and widely accepted model in medicine and biological sciences (Nelson and Rinzel 1998). However, there are some limitations to the model.

Firstly, the model is based upon research involving the giant squid axon, which raises questions in regard to applicability to human neurons. In particular, the giant squid axon is much thicker (up to 1mm in diameter) than human axons (typically 1μm in diameter) (Nelson and Rinzel 1998). Thicker axons have faster conduction velocity, which results in the capacity for greater frequency of action potentials (Sadegh-Zadeh 2017). The model could be improved if adjustments are made to account for these differences in firing frequency across species. Also, the squid axon is unmyelinated whereas human axons can be myelinated or unmyelinated. Myelination is understood to increase the speed of action potentials, however it is unclear whether myelination may also influence action potential generation (Snaidero and Simons 2014; McDougall, Vargas Riad et al. 2018). Furthermore, the squid axon has evolved to produce rapid neural response specifically for the purpose of generating propulsive motion (Santamaria and Bower 2009). Many other species require a greater range of responses, and as such have more complex axon function than found in the squid which means the extrapolation of these results may be compromised (Nelson and Rinzel 1998; Santamaria and Bower 2009).

The model is a point neuron model which means it considers only how individual neurons respond to input voltage and does not take into account the combined effect of multiple neurons (Xu, Wen et al. 2008; Johnson and Chartier 2017). It also does not address the complexity of neurons, including size and shape (Xu, Wen et al. 2008). Also, although the model effectively describes aspects of the neural response, it is only based on the electrical aspects of the neuron (Appali, van Rienen et al. 2012). The model cannot describe other aspects of the action potential that are of non-electrical nature, including heat release and morphological changes in the axon itself (Appali, van Rienen et al. 2012).

Despite limitations of the model, experimentation has demonstrated it to be effective in capturing most significant elements of the action potential (Appali, van Rienen et al. 2012). The mathematical nature of the model means that it can be adapted through minor adjustments to variables. For example, Xu et al. (2008) was able to adapt the model to take into account myelinated axons and muscle fibres in their study pertaining to the neural response of nociceptors in human skin (Xu, Wen et al. 2008). Similarly, Bell and Holmes (1992) were able to adapt the model to represent the neural response specifically from Pacinian corpuscles (Bell and Holmes 1992). The adaptations made to the model in these studies indicate that many of the model's limitations regarding application to human neural response can be mitigated through minor adaptations, and for this reason the model continues to have relevance regardless of its age (Santamaria and Bower 2009; Krouchev, Rattay et al. 2015).

2.3.3 Integrative Work

Researchers have considered combining various neural response models to produce an overall model that will more accurately replicate and describe neural responses within humans. For example, Appali et al. (2012) discussed the benefits of potentially combining the Hodgkin-Huxley model with the Soliton theory model to better describe both electrical and non-electrical aspects of action potentials (Appali, van Rienen et al. 2012).

Interestingly, there has been limited research involving the combination of a mechanical model with a neural model, such as the FEM model and the Hodgkin-Huxley model described in the previous subsections. Two studies created a biological FEM model of a fingertip, and combined the FEM model analysis results with mechanoreceptor threshold values obtained from experimental data (Dandekar, Raju et al. 2003; Wu, Krajnak et al. 2006). By combining this data, both studies were able to predict the responses of various mechanoreceptors in the fingertip under a range of conditions. Another study by Quindlen-Hotek and Barocas (2018) created an FEM

model of Pacinian corpuscles embedded within skin, and combined this with a model to replicate the action potentials produced by the receptors (Quindlen-Hotek and Barocas 2018). The study allowed for investigation into the mechanical properties of Pacinian corpuscles by simulating the receptor response when vibration was applied to the FEM model.

The few studies mentioned are all related to model combinations with application for skin, and there is evidently a significant lack of research in this area with specific application for the knee. Given the importance of FEM modelling in the successful design of prosthetics for knee arthroplasties, there is appropriate reason for investigation into the development of a more informative model. This could be achieved through combination of an FEM model of the human knee with an adapted Hodgkin-Huxley model for simulation of proprioception and nociception by the knee's receptors. This model combination could provide designers of knee prostheses with greater insight into how the body may respond to the prosthesis following a knee arthroplasty, potentially predicting pain or instability that the patient may experience. This may assist to reduce the increasing level of post-operative patient dissatisfaction, and in turn reduce the number of revision surgeries performed.

Although FEM modelling is already successfully used in prosthesis design, there is clearly a gap in relation to integrating FEM with Hodgkin-Huxley neural models, and even more specifically when applied to the knee. The Hodgkin-Huxley model has already proven to be adaptable, and as such, modification for specific application to the receptors within the human knee is likely to be achievable. However, there is an obvious lack of clarity in existing research regarding which receptors are actually present, their morphology, and their physiological responses – an understanding that is critical for accurate adaptation of the Hodgkin-Huxley model. Additionally, the Hodgkin-Huxley model has been developed to describe a single neural response only, so there may be challenges in accounting for combined responses from multiple receptors of varying types. Despite this, there is a range of experimental data across species and anatomical locations that could potentially be extrapolated for development of the model. Although this extrapolated data may not be ideal, it is the most complete data available at this time and could still provide a basis for replicating a receptor response that is somewhat comparable to that found in the human knee.

3 Methodology

The first step towards developing a combined FEM and Hodgkin-Huxley model for the knee is to adapt individual neural models for each of the four types of mechanoreceptors within the knee. The individual neural models will then need to be combined to form a single neural model representative of all the mechanoreceptors in the knee, and that single neural model can then be integrated with an FEM model. Given the sizeable scale of the proposed work, this project is focused on the development of the Hodgkin-Huxley neural model for one receptor type only. The Ruffini ending was selected for the first neural model adaptation because, of the four identified receptors, the current literature indicates it has the most experimental data available relating to neural responses.

Despite having experimental results on which to base adaptions to the Ruffini neural model on, accurately adapting the model is not a simple task. There is still a significant lack of understanding in the field regarding the fundamental properties of the Ruffini ending, including their size and structure, how they sense their surrounding environment, and to what they are sensitive. This makes it extremely difficult to correctly adapt the model, as there is little understanding regarding the Ruffini's sensitivities and what will actually trigger a neural response – a key component required to develop the neural model.

Currently, Khasla et al. (1996) provides the most complete set of experimental data available for Ruffini ending neural responses. The experiment performed by Khalsa et al. has been replicated in this project in an attempt to gain a better understanding of how the properties of the Ruffini and surrounding tissue might affect the neural response, and what adaptations may be required for the neural model. The experiment replication was implemented via computer modelling, using Matlab and FEBio. An overview of the original Khalsa et al. experiment is provided in Chapter 3.1, followed by the methodology for the experiment replication in Chapter 3.2 – Chapter 3.4.

3.1 Khalsa et al. (1996) Experiment: An Overview

The original experiment by Khalsa et al. (1996) documented Ruffini behaviour by stretching the joint capsules from the left knees of cats and recording the neural responses of Ruffini endings located within the capsules (Khalsa, Hoffman et al. 1996). This section provides an overview of the method and results reported by Khalsa et al.

The joint capsules were prepared with spherical surface markers for tracking displacement caused by the stretching, and the locations of the Ruffini endings were identified within a radius of 0.5mm. An example of a prepared specimen is given in Figure 12.

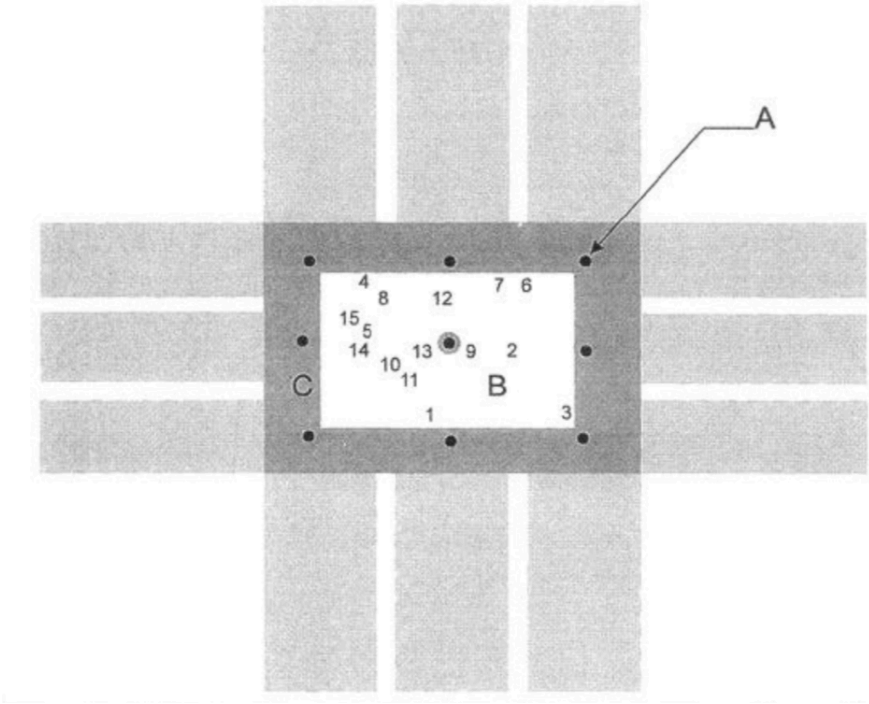

Figure 12. Example of a prepared specimen, with relative locations of the Ruffini endings (numbered) and surface markers in the experiment performed by Khalsa et al. (1996) (Khalsa, Hoffman et al. 1996). This image has been reproduced with permission from The American Physiological Society.

The joint capsules were then placed into a stretching apparatus and stretched in six different loading regimes. The loading regimes identified were uniform, biaxial, uniaxial x, uniaxial y, positive shear and negative shear loading (Figure 13).

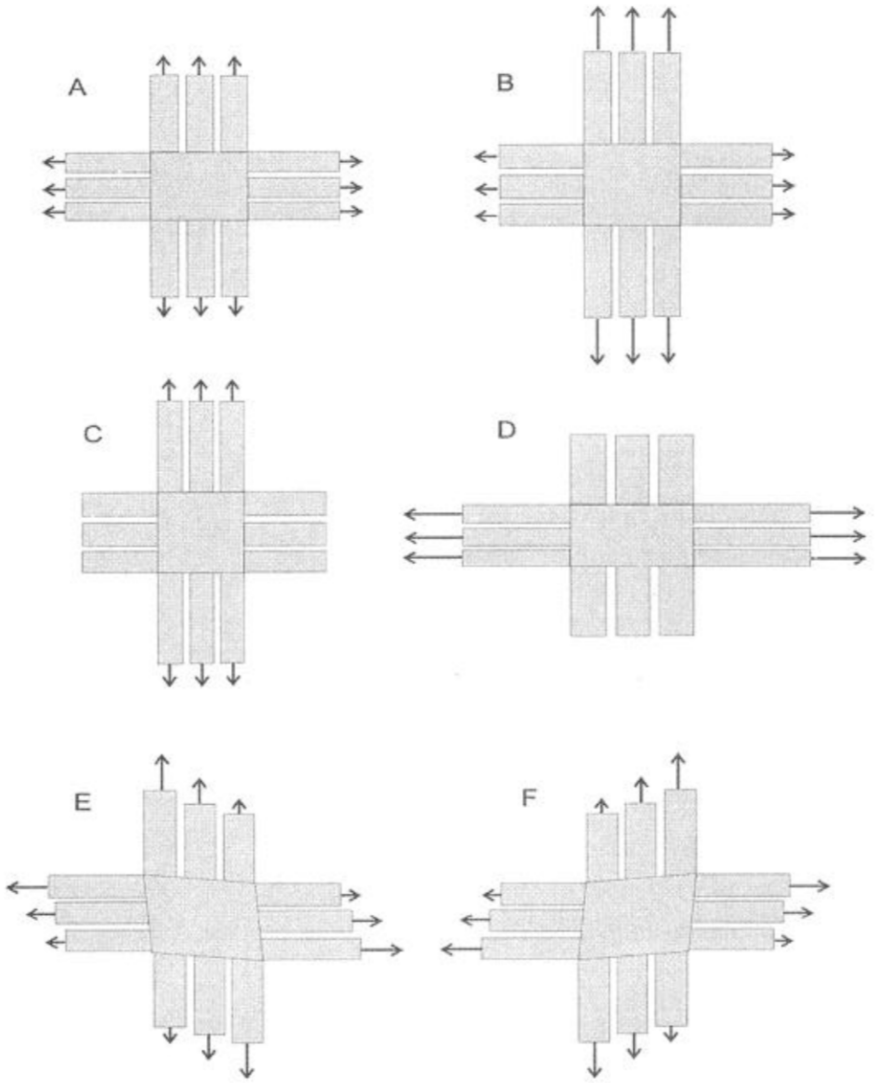

Figure 13. Experimental loading regimes used to stretch the joint capsule in the experiment performed by Khalsa et. al: A. Uniform, B. Biaxial (Y), C. Uniaxial Y, D. Uniaxial X, E. Negative Shear, F. Positive Shear. (Khalsa, Hoffman et al. 1996). This image has been reproduced with permission from The American Physiological Society.

Neural responses from the Ruffini endings were measured and the corresponding in-plane stresses and strains were calculated. The apparent in-plane strain was calculated using optical tracking of the surface markers before and after 4 seconds of deformation in the selected loading regime, while the apparent in-plane stress was calculated from the loads measured along the specimen edges. The local stress around the Ruffini ending was estimated using interpolation.

The results for one neuron were presented by Khalsa et al. in the plot shown in Figure 14, with the neural response (NR) (i.e. firing frequency) plotted against six different stress variables for each of the loading regimes. These results were for neuron 13 which according to Khalsa et al. was a 'typical' neuron (i.e. 'Y-biased'), that was located in the centre of the specimen. The neural response results were not explicitly reported, or the raw results documented in the original paper – only summaries and results plots were provided.

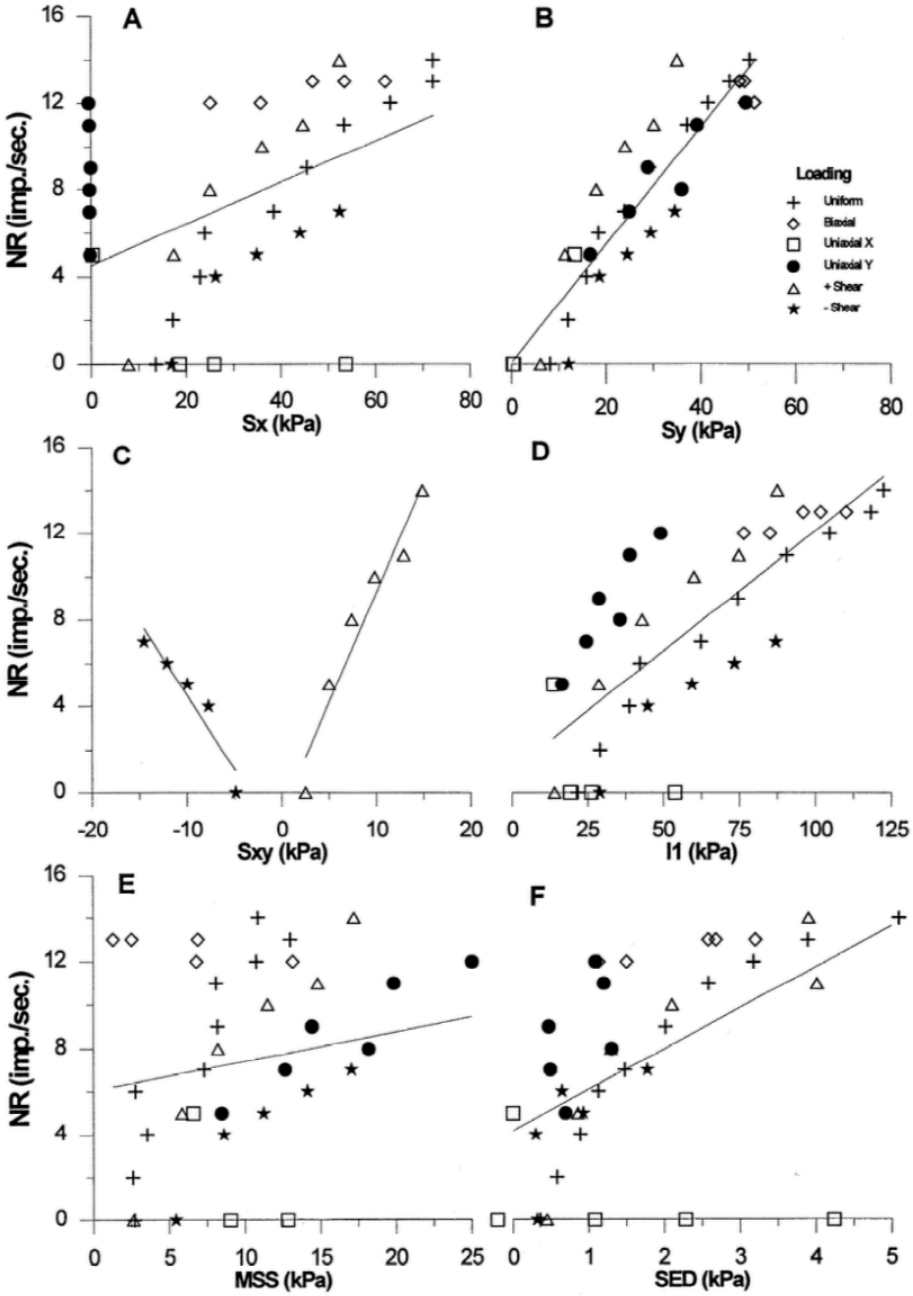

Figure 14. Relationships between neural response and various stress variables for one neuron (Neuron 13), as presented in the Khalsa et al. (1996) study. A: X stress. B: Y stress. C: shear stress. D: 1st invariant of the stress tensor (I1). E: Maximum shear stress (MSS). F: strain energy density (SED) (Khalsa, Hoffman et al. 1996). This image has been reproduced with permission from The American Physiological Society.

3.2 FEBio Modelling

The specimen used in the Khalsa et al. experiment was replicated using the FEBio software suite. FEBio was also used to apply the loads for each loading regime to the specimen.

3.2.1 Modelling the Specimen

The FEBio replica of the joint capsule specimen was created as a 7.5mm x 5mm x 0.5mm rectangular model consisting of 150 elements (Figure 15). The size of the specimen used in the Khalsa et al. experiment was not explicitly stated but was determined under the assumption that the example specimen diagram provided was to scale (Figure 12). Based on the 0.5mm radius spherical markers that were indicated in Figure 12, the capsule size was measured and scaled accordingly. The resulting size of the specimen was found to be similar to the cat knee specimen sizes documented by Hoffman et al. (1985) (Hoffman, Grigg et al. 1985).

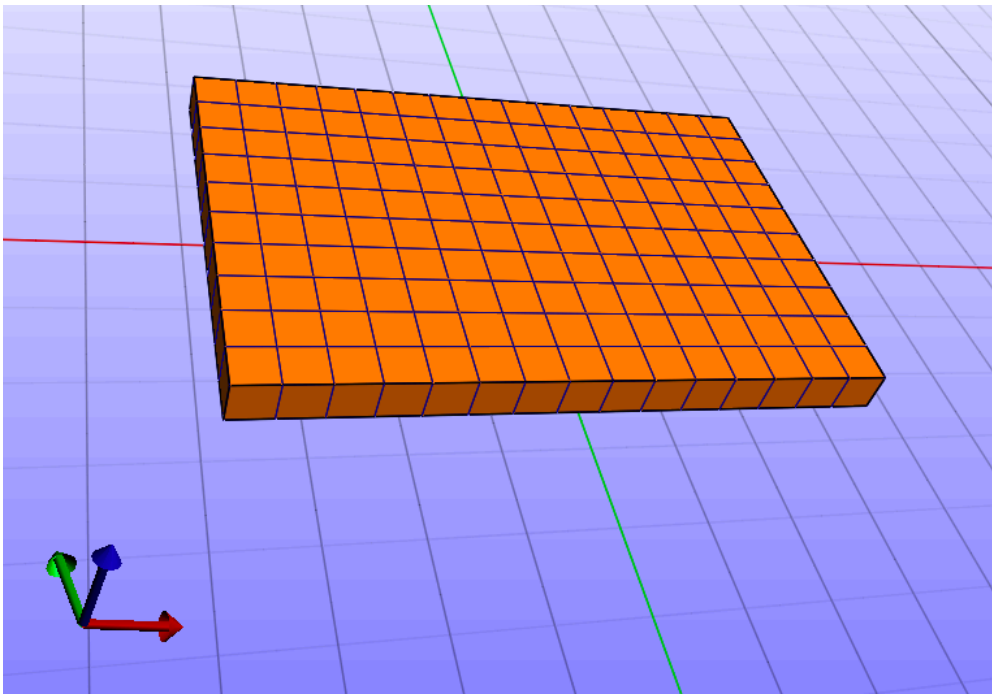

Figure 15. FEBio model replica of the Khalsa et al. (1996) joint capsule specimen.

The loading tabs shown in the example specimen in Figure 12 were not modelled. The tabs were required in the physical experiment to eliminate stress concentrations caused by the attachment points between the stretching apparatus and the specimen. This, however, was not an issue in the computer model and so modelling the tabs was unnecessary.

Given that the results reported by Khalsa were for a neuron located in the centre of the specimen, the FEBio element located in the corresponding central position on the model was identified as element 75. Element 75 was used as the location for stress and strain observation in the model, replicating the location for the apparent local stresses and strains reported by Khalsa et al. for neuron 13.

3.2.2 Model Material

In literature, biological soft tissues are generally recognised as non-linear materials that exhibit inelastic and anisotropic properties and nearly incompressible behaviours (Fung 1993; Humphrey 2003). Collagen fibres in particular are known to demonstrate transversely orthotropic material properties (Fung 1993). These characteristics were considered when replicating the joint capsule specimen used in the original Khalsa et al. experiment, particularly given the collagen-rich nature of the joint capsule. As such, three different materials were tested for the FEBio model in an attempt to find the most suitable model to provide the best replication of the original experiment results. In doing so, it was hoped that some understanding would be gained regarding how material properties of the surrounding tissue may play part in the neural response produced by the Ruffini ending.

The three FEBio materials selected for testing were isotropic elastic, orthotropic elastic, and coupled transversely isotropic Mooney Rivlin. All of the material property values required for FEBio implementation of these materials were selected based on values found in the literature (Fung 1993; Humphrey 2003). While the three materials were modelled as closely as possible to encompass the identified characteristics of soft tissue, not all of the chosen materials would generally be considered appropriate for soft tissue modelling. Regardless, it allowed the opportunity to explore the effect of material properties on the Ruffini neural response and hence the responses when using different material models could be compared.

The isotropic material was not expected to produce an accurate replication of the original experiment results due to the elastic and isotropic properties of the material as well as its application for modelling compressible materials. These properties do not correspond to the characteristics that would be expected for the joint capsule based on literature findings. However, the material was selected for initial testing due to the simplicity of modelling the material in FEBio, requiring fewer properties to be defined to implement the material in the model. The minimal effort and time cost involved meant that the material was worth testing on the chance that the results would be reasonable regardless of the material properties not aligning to what is generally understood about biological soft tissues.

The orthotropic elastic material was the second material selected, as it provided the opportunity to incorporate anisotropic properties into the model. Unlike other anisotropic FEBio materials, this material was relatively simple to implement in FEBio (again due to few material properties requiring definition). However, like the isotropic material, this material also exhibits elastic and

compressible material behaviours. As such, it was not expected to provide completely accurate results, but it was expected to provide an improvement compared to the isotropic elastic results.

The third material selected was the coupled transversely isotropic Mooney Rivlin material. This material, like the orthotropic material, was selected for the anisotropic properties it would add to the model. However, this material also allowed for fibre reinforcement of one fibre family along a single direction (e.g. collagen fibres aligned along a single direction, as may be found in joint capsule tissue) and implemented hyper-elastic material behaviour. This was a more complex material to implement compared to the isotropic and orthotropic materials, however of the three materials selected this material reflected the most similarities to biological tissue described in literature. As such, it was expected to provide the most accurate results of the three materials.

3.2.3 Loading Regimes and Applied Loads

The FEBio model from Figure 15 was duplicated six times - one model for each of the six loading regimes used by Khalsa et al. (pictured in Figure 13).

Boundary conditions were applied to each bottom row node along the left and front faces of the model, as indicated by the arrows in Figure 16. The nodes along the left face, indicated with red arrows, were fixed in the X direction. The nodes along the front face, indicated with yellow arrows, were fixed in the Y direction. The node in the bottom left corner, indicated by the green arrow, was also fixed in the Z direction. These boundary conditions were applied to fix the model in space while still allowing for deformation in the X, Y and Z directions without producing a necking effect.

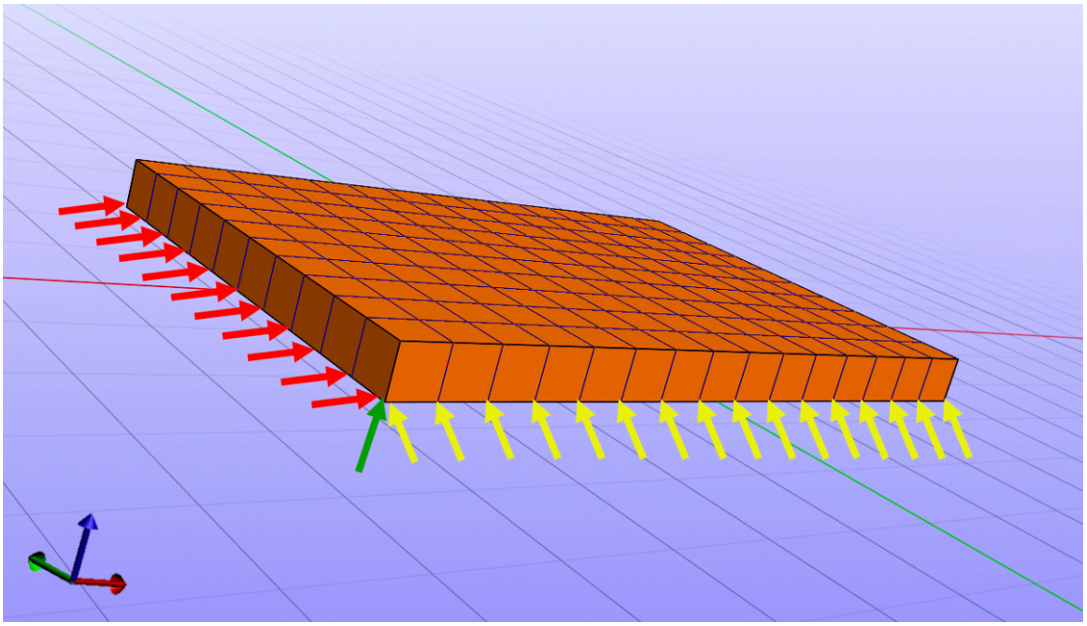

Figure 16. Location of fixed position boundary conditions on the FEBio model as indicated by the coloured arrows. Red: nodes fixed in the X direction. Yellow: nodes fixed in the Y direction. Green: node fixed in the z direction.

Each model was set up with the load magnitudes corresponding to the given loading regime. The loads were applied to the opposite sides of the model to the boundary conditions (i.e. to the right and back faces). These were specified as nodal loads, to ensure that each load was applied uniformly along the model face.

The magnitudes of the loads applied to the specimen in the original experiment were back-calculated using Figure 14. Given that stress can be defined as the force per unit area, the calculation was made based on the surface area of the selected model face and the maximum stress recorded in that direction (i.e. maximum X stress or Y stress) for each loading regime.

The maximum stresses were estimated from the Khalsa et al. results figure. Later in the project, the Khalsa et al. results figure was digitized so the actual values of each marker on the figure were identified, but at the time of load calculation this digitization had not been performed. Time constraints did not permit running all the experiments again with the adjusted applied loads after digitization of the data. Recalculating the applied loads based on the actual maximum stresses could be performed in future project work, however it is unlikely to make a significant difference in the results as the estimated maximum stresses were similar to the actual maximum stresses (Table 2).

Table 2. Estimated maximum stress versus actual maximum stress from Khalsa et al. results in Figure 14.

Loading Regime	Estimated Max X Stress (KPa)	Actual Max X Stress (KPa)	Estimated Max Y Stress (KPa)	Actual Max Y Stress (KPa)
Uniform	72	72.2848	50	50.2788
Biaxial	62	62.1748	51	51.2067
Uniaxial X	53	53.7854	15	13.3107
Uniaxial Y	0	-0.0314	50	49.4352
Shear Positive	52	52.5252	35	34.9769
Shear Negative	52	52.5392	34	34.3858

Based on the dimensions of the model, the surface areas of the right (X) and back (Y) faces were 2.5mm^2 and 3.75mm^2 respectively. Due to applying a nodal load rather than a surface load, the total load calculated had to be divided by the number of nodes on that face (i.e. 22 for the X face, 32 for the Y face). The total load applied to the X and Y faces for each loading regime, as well as the nodal load applied (i.e. the point load applied to each node) are provided in Table 3.

Table 3. Total and nodal loads to be applied to the x and y faces of the model

Loading Regime	Total Load X (N)	Nodal Load X (N)	Total Load Y (N)	Nodal Load Y (N)
Uniform	0.18	0.00818	0.27	0.00844
Biaxial	0.155	0.00705	0.191	0.00598
Uniaxial X	0.133	0.00602	0.0563	0.00176
Uniaxial Y	0.000	0.000	0.188	0.00586
Shear Positive	0.13	0.00591	0.131	0.00410
Shear Negative	0.13	0.00591	0.128	0.00398

3.3 Hodgkin-Huxley Model

The Hodgkin-Huxley neural model used in this project was based on a Matlab adaptation for the original Hodgkin-Huxley mathematical model, developed by Jahn (2013). As such, the original Matlab code modelled the neural response of the axon of a giant squid. The code was subsequently modified for thermal nociceptors within the human skin by Azin Janani at Flinders University to replicate the findings and results presented by Xu et al. (Xu, Wen et al. 2008; Jahn 2013). This involved adjusting the code such that the neural response (firing rate) of the model was suitable for a human neuron rather than a giant squid neuron.

As summarised in Table 1, the literature findings indicate that the Ruffini ending and free nerve endings have similar action potential responses. Despite having different firing activation thresholds to produce a neural response, both neurons are slow-adapting meaning that they have

continuous firing while a stimulus above the given threshold is applied. Due to this similarity, the Hodgkin-Huxley model adapted by Janani (originally by Jahn (2013)) was not significantly modified for this project – only minor adjustments were made. The first adaptation involved modifying the model to accept stress (or another mechanical variable) as the model input, rather than temperature. The second modification was made to the model's induced current equation, to change the neuron firing activation threshold. No adaptations were made to the output of the model, which was presented as an action potential spike train.

3.3.1 Input Stimuli

The Hodgkin-Huxley model was adapted to accept a mechanical input rather than a thermal input. Given the numerous discrepancies within the literature regarding the fundamental properties of the Ruffini ending, it was unclear what mechanical stimuli the Ruffini might be sensitive to. Therefore, eighteen different mechanical stimuli were tested as the neural model inputs and the responses of the Ruffini (produced by the Hodgkin-Huxley model) to each stimulus were recorded. The eighteen stimuli are listed in Table 4.

The Matlab code was modified such that the input stimulus could be scaled, or even combined with another type of stimulus. However, for this project all inputs were tested individually only and with a scale of 1, except in the case of no firing produced by the model. In those cases, the scale of the input was increased by a factor of 10 until firing was produced. This was to compensate for any potential errors in modifications made to scaling of the firing activation threshold.

Table 4. List of tested input stimuli to the Hodgkin-Huxley neural model.

Input Number	Mechanical Stimulus
1	X Stress (Sx)
2	Y Stress (Sy)
3	Shear Stress (Sxy)
4	1st Invariant Stress Tensor (I1)
5	Maximum Shear Stress (MSS)
6	Strain Energy Density (SED)
7	Hydrostatic Pressure (HS)
8	1st Principal Stress (S1)
9	2nd Principal Stress (S2)
10	3rd Principal Stress (S3)
11	Deviatoric Stress 1 (Dev1)
12	Deviatoric Stress 2 (Dev2)
13	Deviatoric Stress 3 (Dev3)

14	Shear A
15	Shear B
16	Shear C
17	X Strain (Ex)
18	Y Strain (Ey)

3.3.2 Induced Current Equation

The induced current equation (I_ST equation), represents the total stimulation induced current comprised of the current produced by the neuron's heat, chemical and mechanical gated ion channels (Xu, Wen et al. 2008). When above a given threshold, this induced current results in the activation of neural firing. Modifications were made to the induced current equation to alter the activation threshold for neural firing of the Ruffini ending.

The I_ST equation in the Hodgkin-Huxley model for the thermal nociceptor model was exponential, however when adapting the equation for the Ruffini ending the equation was modified to be linear for simplicity. Khalsa et al. reported the maximum and minimum stress and strain values that resulted in firing during the original experiment. The maximum and minimum I_ST current values required for firing activation in the thermal nociceptor model were also identified. This was achieved through trial and error, by testing various thermal inputs to the model and identifying when a neural response was produced and the corresponding I_ST value. To modify the firing activation threshold to be suitable for the Ruffini, the reported maximum and minimum mechanical values were linearly mapped to the maximum and minimum I_ST current values identified. Therefore, a mechanical input to the model within the maximum/minimum mechanical range would result in neural firing, while outside of this range no firing would be produced. This was achieved with Equation 1, where the mechanical input is the input to the neural model, mech_min and mech_max are the minimum and maximum mechanical values for firing activation, and IST_min and IST_max are the maximum and minimum I_ST current values for firing activation. I_shift was introduced in the original Xu et al. (2008) code to prevent firing below the specified threshold value, and so this was still included in the modified equation.

Equation 1: $$I_{ST} = \left(\frac{(\text{mechanical input} - mech\_min)*(IST\_max - IST\_min)}{(mech\_max - mech\_min)} + IST\_min\right) + I\_shift$$

The mech_min and mech_max values used in the I_ST equation had to be modified depending on the mechanical input being used. When the mechanical input was a stress value, these mech_min and mech_max values were based on the maximum and minimum stress values causing firing in

the original experiment. Alternatively, when strain was used as a mechanical input to the model, the mech_min and mech_max values were based on the maximum and minimum strain values reported to cause neural firing.

3.4 Matlab Code Development

3.4.1 Automating the Experiment

Matlab code was developed by Associate Professor Kenneth Pope to automate the computer modelled experiment, providing efficiency and the flexibility to easily adapt and run the entire experiment via Matlab as many times as required. A script was developed to automatically create the six FEBio experiments (i.e. each loading regime) via Matlab, while another script automatically ran the experiments and facilitated seamless integration of the FEBio models with the Hodgkin-Huxley neural model. Mechanical variable values (e.g. X stress) resulting from the FEBio experiments were read directly from the FEBio results file into the Hodgkin-Huxley Matlab model as the neural model input stimulus. The neural response (NR) (i.e. firing frequency) was then derived from the action potential spike train output by the Hodgkin-Huxley model. The neural responses for each loading regime were then plotted against six mechanical variables to be presented in the same format as the results figure provided by Khalsa et al. (Figure 14). Presenting the results in this format allowed for direct visual comparisons between the replicated and original results. Using this method, upon inspection of each results subplot it was simple to visually identify whether distinct characteristics of the original results had been reproduced (e.g. if the Sx plot had uniaxial Y loading points firing with zero Sx stress).

Minor adjustments were made to these Matlab scripts to fine-tune the tests that were run and ensure the output of the results was occurring as expected. This included adjusting the scripts so that the Matlab-developed FEBio model matched the model created using the FEBio graphical user interface (e.g. defining size and shape of the model, specifying the applied loads, selecting material and material properties). Modifications were made to allow additional mechanical variable options for selection as the input stimulus to the neural model. Also, there were adjustments made to provide alternative visualisation of the neural response results in addition to plotting them in the same format as the original results. This allowed for improved and quantifiable analysis of the results.

3.4.2 Digitizing Khalsa et al. (1996) Results

The results figure presented by Khasla et al. (Figure 14) was digitized to allow the results from the computer modelled experiment replication to be quantified against the original experiment results.

This digitization was performed using the Grabit graphical user interface on Matlab. The Khalsa et al. results figure was obtained from a digital copy of the original paper. Using Grabit, the points for each individual loading regime per subplot were manually selected from the results figure and each set of points was saved as an array Matlab. The average firing rates of each loading regime across the six subplots was calculated from the selected points to reduce the variability in the accuracy of the values due to the manual selection of the points. Then, adapting the code developed by Kenneth Pope for presenting the results in the same format as the original results figure, the digitized results were plotted in the original format (Figure 17). Producing this digital copy of the results was important as it provided quantifiable values for the neural responses recorded by Khalsa et al. which had not actually been explicitly reported in the paper. However, the accuracy of the digitized original results is limited by the image resolution and precision of the manual selection using the cursor on the Grabit interface.

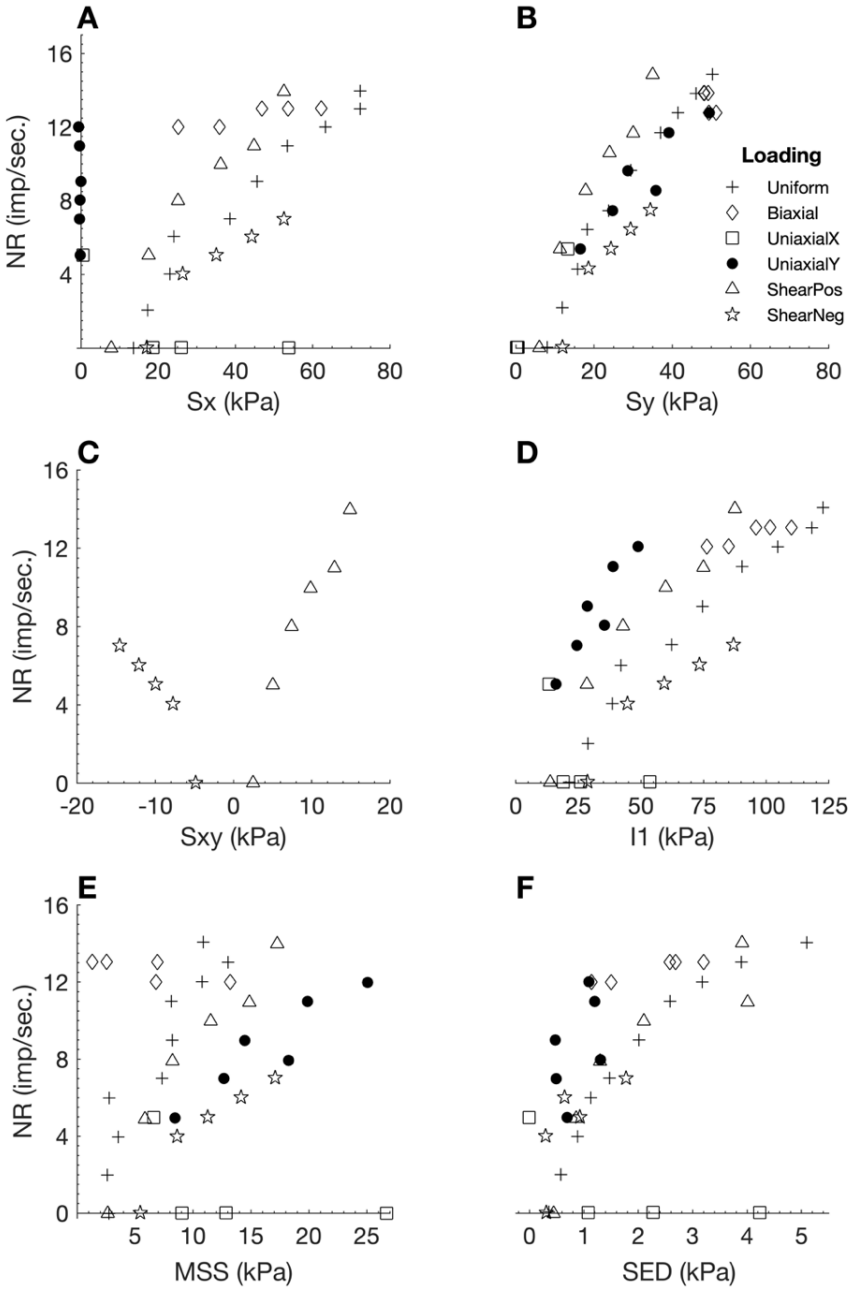

Figure 17. Digitization of the results figure provided in the electronic paper by Khalsa et al. (1996)

3.4.3 Linear regression plots

While the results of the replicated experiment were plotted in the same form as the original experiment results (Figure 17), visual comparisons between the replicated and original plots is not adequate to determine how well the model replicates the results. Instead, it is important that there is a quantifiable method of determining the success of the results replication.

With the flexibility of the digitized original experiment results, the linear regression of the replicated results versus the original experiment results was able to be calculated. The R^2 fit, Root Mean Square Error (RMSE), and the slope values were calculated for each individual loading

regime and also the overall experiment (i.e. all loading regimes combined), for each material/input stimulus combination that was tested. This provided quantification for determining exactly how well the replicated results fit the original dataset. The regression plot of the results (original versus replicated, for all loading regimes) was produced via Matlab in order to visually emphasise the likeness and differences between the replicated values and the original values.

If the replicated experiment results were a perfect replica of the original results, the plotted points would be completely linear (Figure 18). The regression calculations would present with an R^2 value of 1, an RMSE of 0, and a slope of 1. Given that the likelihood of perfectly replicating the results is slim, for the replicated results to be considered as an adequate relative fit to the original data the R^2 value should be at least 0.7 (however an R^2 fit closer to 1 is more desirable). If adequate relative fit is achieved but the slope is not 1 (or close to 1), then it is likely that simple tuning adjustments may be required to the neural model to alter the magnitude of the results. Adequate absolute fit of the data is indicated with an RMSE value close to 0, however tuning the magnitude to improve the slope will improve the absolute fit of the data so it is more important to initially consider the relative fit.

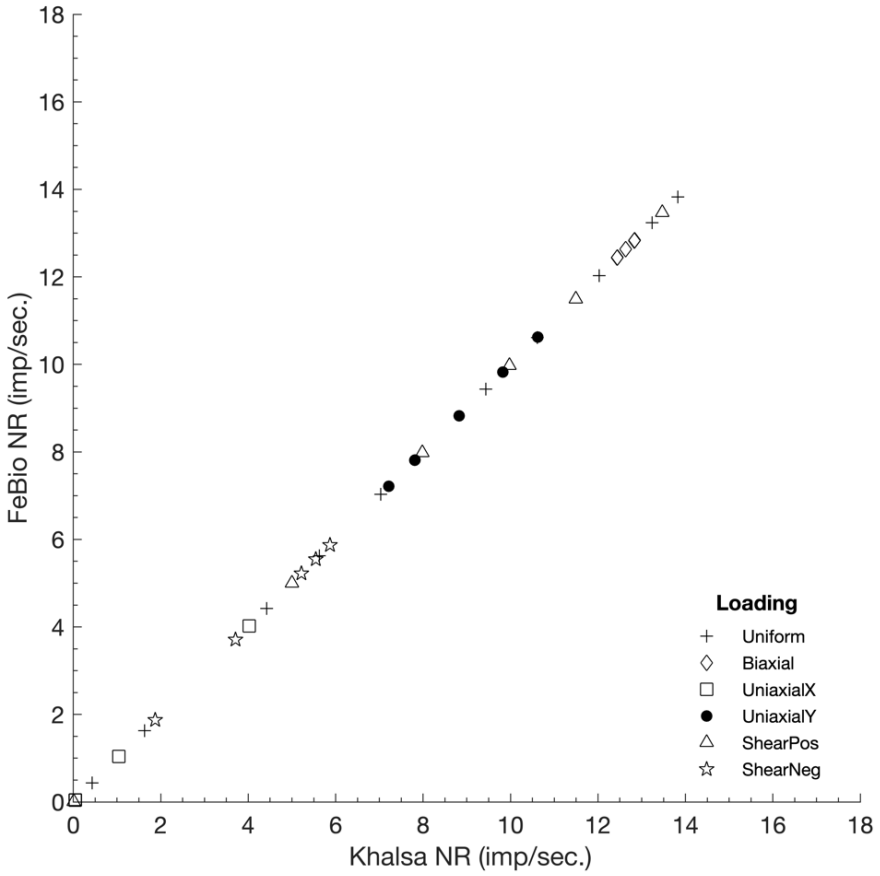

Figure 18. Linear regression plot of the original Khalsa et al. (1996) results versus perfectly replicated FEBio results.

4 Results

This project considered three material types (isotropic elastic, orthotropic elastic, and coupled transversely isotropic Mooney Rivlin) and eighteen input stimuli. Each material/input stimulus combination was tested, and the results were presented in three ways. Firstly, the results were plotted in the same form as the Khalsa et al. results to allow for basic comparison of the replicated figure to the original experiment results figure. Secondly, a regression plot of the original versus replicated neural responses was provided as a direct visual comparison of the differences between the original and the replicated results. Thirdly, the linear regression statistical measures of the original versus replicated neural responses were calculated for each individual loading regime, and for the total plot (i.e. all loading regimes combined).

4.1 Isotropic Elastic Material

The first test was performed using the isotropic elastic material. To implement this material in FEBio, three material properties were required to be defined: density, Young's modulus, and Poisson's ratio. The values selected for each material property were based on findings in literature regarding biological tissue properties. These are provided in Table 5.

Table 5. Isotropic elastic material properties required by FEBio and values selected.

Isotropic Material Property	**Value Selected**
Density	1
Young's Modulus	1
Poisson's Ratio	0.49

The model was tested with all eighteen input stimuli listed in Chapter 3.3.1 Input Stimuli. A summary of the linear regression statistical measures for the total plot (i.e. considering all loading regimes), for each input stimulus are given in Table 6.

Table 6. Linear regression statistical measures for the isotropic elastic material model, considering total plot (all loading regimes).

** Numerical quirk in the result caused by zero firing produced in the replicated results*

Input Stimulus	**R^2**	**RMSE**	**Slope**
X Stress (Sx)	0.1578	4.4106	0.4218
Y Stress (Sy)	0.2866	3.9820	0.5576
XY Stress (Sxy)	0.0789	1.0887	0.0704
1st Invariant Stress Tensor (I1)	0.2525	5.7699	0.7407
Maximum Shear Stress (MSS)	0.2486	2.2465	0.2854
Strain Energy Density (SED)	0.1746	1.2602	0.1280
Hydrostatic Pressure (HS)	0.2273	2.8302	0.3390
1st Principal Stress (S1)	0.2389	3.9735	0.4918
2nd Principal Stress (S2)	0.2065	4.3202	0.4869
3rd Principal Stress (S3)	0.1840	2.8193	0.2957
Deviatoric Stress 1 (Dev1)	0.1684	1.7656	0.1755
Deviatoric Stress 2 (Dev2)	0.1630	1.5032	0.1465
Deviatoric Stress 3 (Dev3) *	NaN	0.0000	0.0000
Shear A	0.0002	0.8685	-0.0024
Shear B	0.1906	2.2367	0.2397
Shear C	0.2486	2.2465	0.2854
X Strain (Ex)	0.0819	3.6571	0.2412
Y Strain (Ey)	0.3047	3.1996	0.4679
Average	**0.1890**	**2.6766**	**0.2984**

Observing the R^2 values in Table 6, none of the input stimuli tested with the isotropic material model produced an adequate relative fit for the total plot. The 'best' results (based on the relative fit) were produced when using Y strain as the neural model input. However, the replicated results were still not an adequate fit for the original results, as indicated by the R^2 value of 0.3047. The regression plot (Figure 19) particularly emphasises the differences between the original and the replicated neural response results.

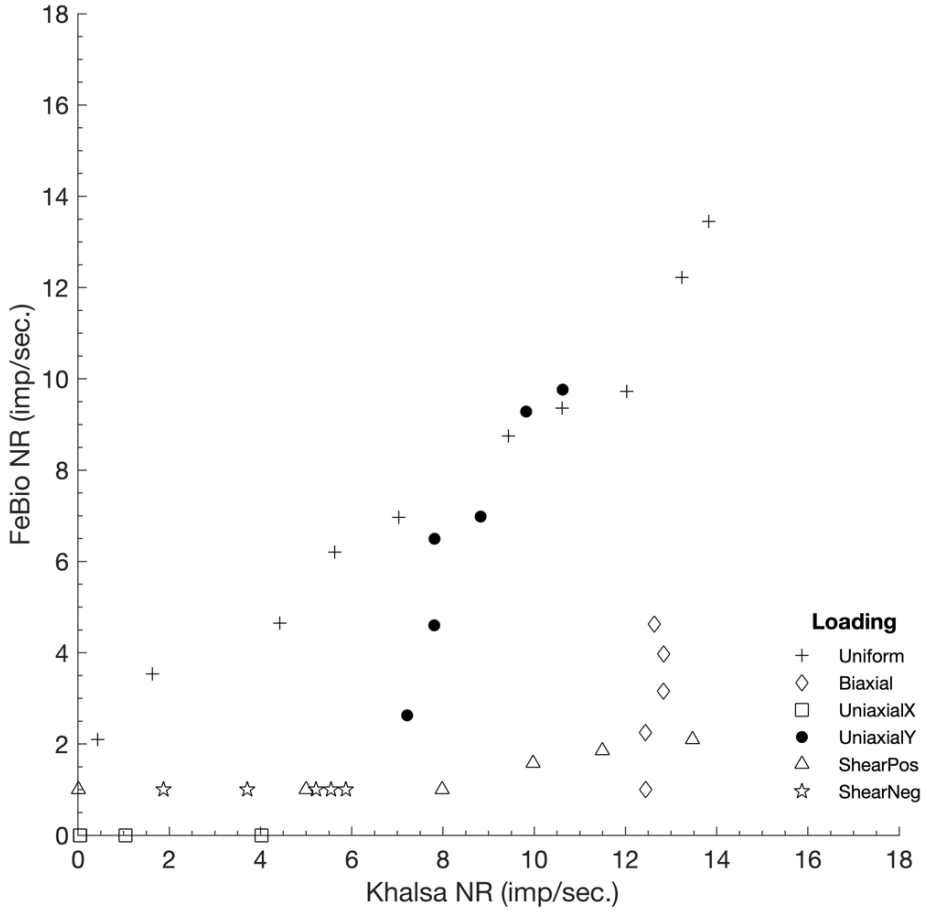

Figure 19. Regression plot of neural response (NR) from the isotropic elastic material model tested using Y strain as the input to the neural model.

The Y strain results were examined in closer detail. It can be seen in Figure 19 that the plotted uniform, uniaxial Y and shear positive loading points display some linearity with a reasonable slope, as would be desired in a perfect replication of results. When considering the linear regression measures for each individual loading regime (Table 7), the results indicate that the uniform, uniaxial Y and shear positive loading did indeed provide adequate relative fits for the original data, as the R^2 values were above 0.7. While the biaxial loading result showed some linearity in Figure 19, the relative fit ($R^2 = 0.4550$) was not high enough to be considered adequate and as such the results would not be further improved with fine-tuning of the response magnitudes. No firing was produced by the uniaxial X loading resulting in a numerical quirk causing the R^2 value being calculated as 'Not a Number' (NaN). Given that the original results did produce firing for the uniaxial X loading, it is clear that the uniaxial X results were not an adequate replication of the original results. Interestingly, the shear negative loading produced a constant firing rate which resulted in Matlab calculating the R^2 as 1. Generally, an R^2 value of 1 indicates a perfect relative fit to the original results, however it is clear from Figure 19 and the other regression

measures in Table 7 that in this case the results do not currently describe the original data. This was caused by another numerical quirk.

Table 7. Linear Regression statistical measurements for each individual loading regime when using Y Strain as the neural model input stimulus from the isotropic elastic material model.

** Numerical quirk in the result caused by zero firing produced by the loading regime.*

*** Numerical quirk in the result caused by the all the replicated firing values for the loading regime being the same – not actually a perfect fit.*

Loading Regime	**R^2**	**RMSE**	**Slope**
Uniform	0.9694	0.6840	0.7634
Biaxial	0.4550	1.2192	4.9027
Uniaxial X *	NaN	0.0000	0.0000
Uniaxial Y	0.8798	1.0562	1.9313
Shear Positive	0.7225	0.2891	0.0856
Shear Negative **	1.000	0.0000	0.0000

Overall, while some individual loading regime results produced an adequate R^2 fit, there were other individual loading regimes which did not. Hence, the total plot could not be considered as a sufficient fit when using the Y strain input to the isotropic model. This was a similar pattern also observed in the results from the other tested input stimuli. This demonstrates that the combination of all loading regimes together must be considered to understand how the results overall match the original results, not just considering the fit of exclusive aspects of the results.

The Khalsa replicated results plots and the linear regression statistical measures for each individual loading regime for the remaining input stimuli are provided in **Error! Reference source not found.**.

4.2 Orthotropic Elastic Material

The second test was performed using the orthotropic elastic material. Unlike the isotropic elastic material which had the same material properties in all directions, the orthotropic elastic material allowed the defining of different properties for different planes or axes of symmetry.

A study by Hoffman et al. (1985) identified that there are three regions of stiffness in the joint capsule (Hoffman, Grigg et al. 1985). As indicated in Figure 20, the first and third layers of the joint capsule differ in stiffness by a ratio of approximately 1:5. Based on this finding, it was determined that a stiffness study would be performed on the orthotropic elastic material to determine whether the stiffness in the surrounding tissue would affect the replicated Ruffini

response. The stiffness (Young's modulus) of the joint capsule was increased to the maximum value allowed in FEBio for a single direction, while keeping the stiffness in the other two directions constant. The maximum allowed stiffness in FEBio was dependent on the values selected for the other material properties.

Figure 20. Varying regions of stiffness within the joint capsule (Hoffman, Grigg et al. 1985). Image by Palmer (Palmer 2013).

To implement the orthotropic elastic material in FEBio, ten material properties had to be defined: density, shear modulus (X, Y and Z directions), Young's modulus (X, Y and Z directions), and Poisson's ratio (X, Y and Z directions). Two sources indicated that material properties (particularly Poisson's ratio) were dependent with respect to the direction of fibre alignment (Fung 1993; Little and Khalsa 2005). The values for material properties were selected based on these two sources. Six combinations of material properties and stiffness directions (Table 8) were tested for the stiffness study. These tests were intended to help determine how the surrounding material properties affected the ability to adequately replicate the original Khalsa et al. results, and as a result indicate whether surrounding material properties play a part in how or what the Ruffini senses.

Table 8. The six test combinations for the orthotropic elastic material model

Test	**Test Description**
1	Increasing X stiffness with same Poisson's ratios for all directions (Poisson's value 1)
2	Increasing X stiffness with same Poisson's ratios for all directions (Poisson's value 2)
3	Increasing X stiffness with differing Poisson's ratios for each direction
4	Increasing Y stiffness with same Poisson's ratios for all directions (Poisson's value 1)
5	Increasing Y stiffness with same Poisson's ratios for all directions (Poisson's value 2)
6	Increasing Y stiffness with differing Poisson's ratios for each direction

The material properties selected for each test are provided in Appendix B. Also included in Appendix B are the Khalsa replicated results plots and the linear regression measures for each individual loading regime for all tested stimuli, the linear regression measures of the total plots for each test.

When compared with the average relative fit of the isotropic test, the average relative fit of the results was improved for all orthotropic tests except Test 4. However, similar to the results of the isotropic elastic material test, all input stimuli for all six orthotropic elastic tests produced R^2 values below 0.7. As such, none of the tests provided an adequate replication of the original results.

Of the six tests performed, Test 3 provided the best average improvement of relative total plot fits. The highest relative total plot fit for Test 3 was produced when using Y strain as the neural model input (Table 9), however only resulted in an R^2 value of 0.3508.

Table 9. Linear regression measures for total plot results (i.e. considering all loading regimes combined), for each input stimulus tested with the orthotropic elastic model 3.

** Numerical quirk in the result caused by zero firing produced in the replicated results*

Input Stimuli	**R^2**	**RMSE**	**Slope**
X Stress (Sx)	0.1725	4.4296	0.4467
Y Stress (Sy)	0.2808	4.1426	0.5718
Shear Stress (Sxy)	0.0736	1.7552	0.1093
1st Invariant Stress Tensor (I1)	0.2664	5.8166	0.7743
Maximum Shear Stress (MSS)	0.2962	2.4903	0.3568
Strain Energy Density (SED)	0.1747	1.2616	0.1282
Hydrostatic Pressure (HS)	0.2327	3.0274	0.3683
1st Principal Stress (S1)	0.2747	4.5111	0.6132
2nd Principal Stress (S2)	0.2540	3.0820	0.3972
3rd Principal Stress (S3)	0.1746	8.8833	0.9024
Deviatoric Stress 1 (Dev1)	0.2917	2.4793	0.3515
Deviatoric Stress 2 (Dev2)	0.1905	0.7638	0.0819
Deviatoric Stress 3 (Dev3) *	NaN	0.0000	0.0000
Shear A	0.2252	1.4374	0.1712
Shear B	0.2609	1.5256	0.2002
Shear C	0.2962	2.4903	0.3568
X Strain (Ex)	0.1340	0.8856	0.0769
Y Strain (Ey)	0.3508	4.4411	0.7212
Average	**0.2323**	**2.9679**	**0.3682**

When inspecting the regression plot (Figure 21) and individual loading regime regression measures (Table 10) for Test 3 with the Y strain input, there are similarities to the isotropic elastic Y strain results. The linearity of the uniform, uniaxial Y and shear positive loading points can still clearly be seen in Figure 21, however there are also improvements to the linearity of the plotted shear negative loading points which were not present in the isotropic results. The regression measures confirm the adequate fit of these loading regime results to the original experiment results,

with all producing relative fits above 0.7. However, as with the isotropic results, the biaxial and uniaxial X loading regimes still do not fit the original data well ($R^2 < 0.7$, with uniaxial X loading still not producing any firing). As such the relative fit for the total plot is not adequate.

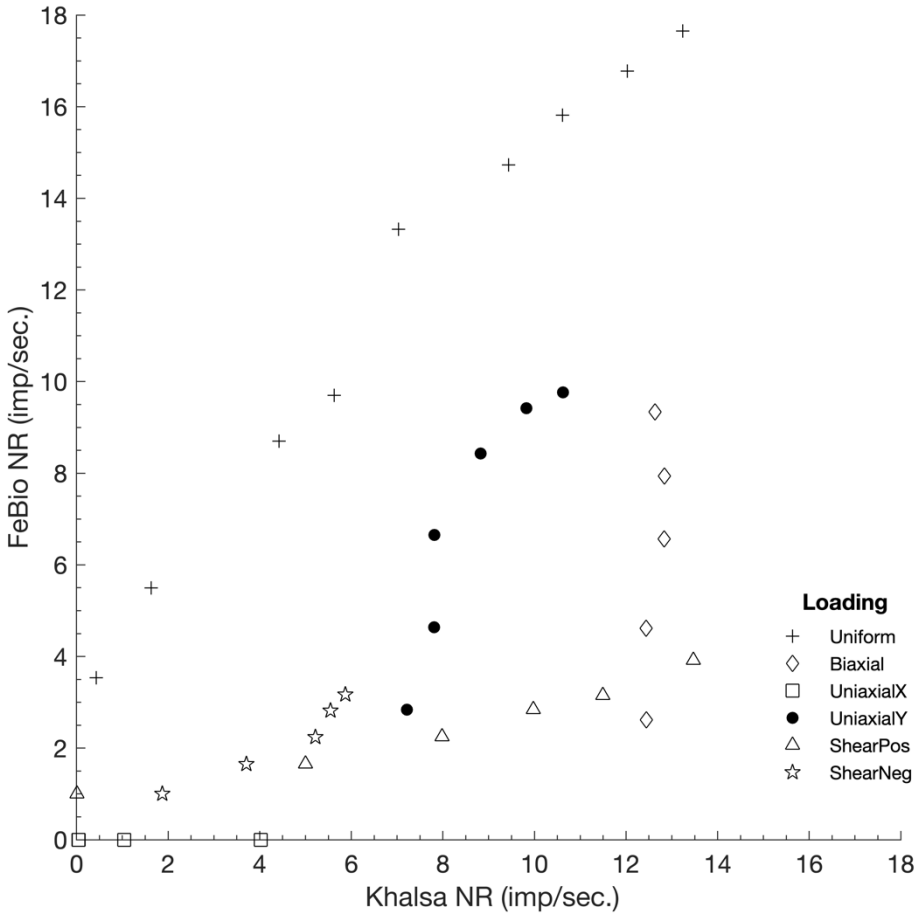

Figure 21. Regression plot of neural response (NR) from the orthotropic elastic material model 3 tested using Y strain as the input to the neural model.

Table 10. Linear regression measures for individual loading regime results from the orthotropic elastic model 3, with Ey as neural model input.

** Numerical quirk in the result caused by zero firing produced by the loading regime.*

Loading Regime	**R^2**	**RMSE**	**Slope**
Uniform	0.9795	0.7995	1.0948
Biaxial	0.4601	2.2587	9.1762
Uniaxial X *	NaN	0.0000	0.0000
Uniaxial Y	0.8357	1.2581	1.9170
Shear Positive	0.9609	0.2336	0.2124
Shear Negative	0.9259	0.2749	0.5070

While Test 3 produced the best average relative fit improvement of the six tests, the highest total plot R^2 value was actually produced in Test 1. This highest R^2 value was again produced when

using Y strain as the neural model input, but still only resulted in an R^2 value of 0.3536. This was only a 0.79% improvement compared with the highest Test 3 result, and neither result was a significant improvement compared to the best isotropic test result.

Interestingly, each orthotropic model tested with the stiffness increased in X direction resulted in the Y strain input producing the largest R^2 value, however when stiffness was increased in the Y direction, the input stimulus that resulted in the largest R^2 value was unpredictable.

Overall, the direction in which the stiffness was increased did not significantly affect the relative fit of the results, apart from altering which input stimulus produced the best R^2 value. Changing the value for the Poisson's ratio did not make any significant differences to the relative fit of the results either. Regardless of the direction of increased stiffness or Poisson's ratio values, all R^2 values produced across all tests were still considered to be unacceptable, and so none of the results provided an adequate replication of the original results.

4.3 Coupled Transversely Isotropic Mooney Rivlin Material

The final model tested was created with the coupled transversely isotropic Mooney Rivlin material. Similar to the orthotropic elastic material, this material allowed for anisotropy in different planes/axes of symmetry which was desired due to the generally anisotropic nature of biological soft tissues (Fung 1993; Humphrey 2003). More specifically, this material allowed for fibre reinforcement along a specified direction to be introduced into the model. To keep the model simple, only one type of fibre family was implemented, although there is potential for adding multiple fibre families with varying directions if future work is pursued.

Collagen fibres were selected for reinforcement in the model due to the joint capsule being heavily comprised of collagen (Ralphs and Benjamin 1994; Souza and Doan 2010). Two models were tested - both the X and Y directions of reinforcement, as the direction of fibres in the original experiment specimen was unclear. The FEBio values required to implement this model were originally based on values for a ligament but were adjusted so the model would exhibit more collagen-like stretch behaviour rather than ligament behaviour (Fung 1993; Freutel, Schmidt et al. 2014; Chakraborty, Mondal et al. 2016). This was achieved by comparing the XY displacement for the previous isotropic and orthotropic models (which had been implemented using collagen-based values identified from literature) with the XY displacement of the ligament-based Mooney Rivlin model (Figure 22). The Mooney Rivlin parameter 1 was then scaled by the factor of

difference between the displacements, until the model showed approximately the same maximum displacement as in the previous collagen-based tests.

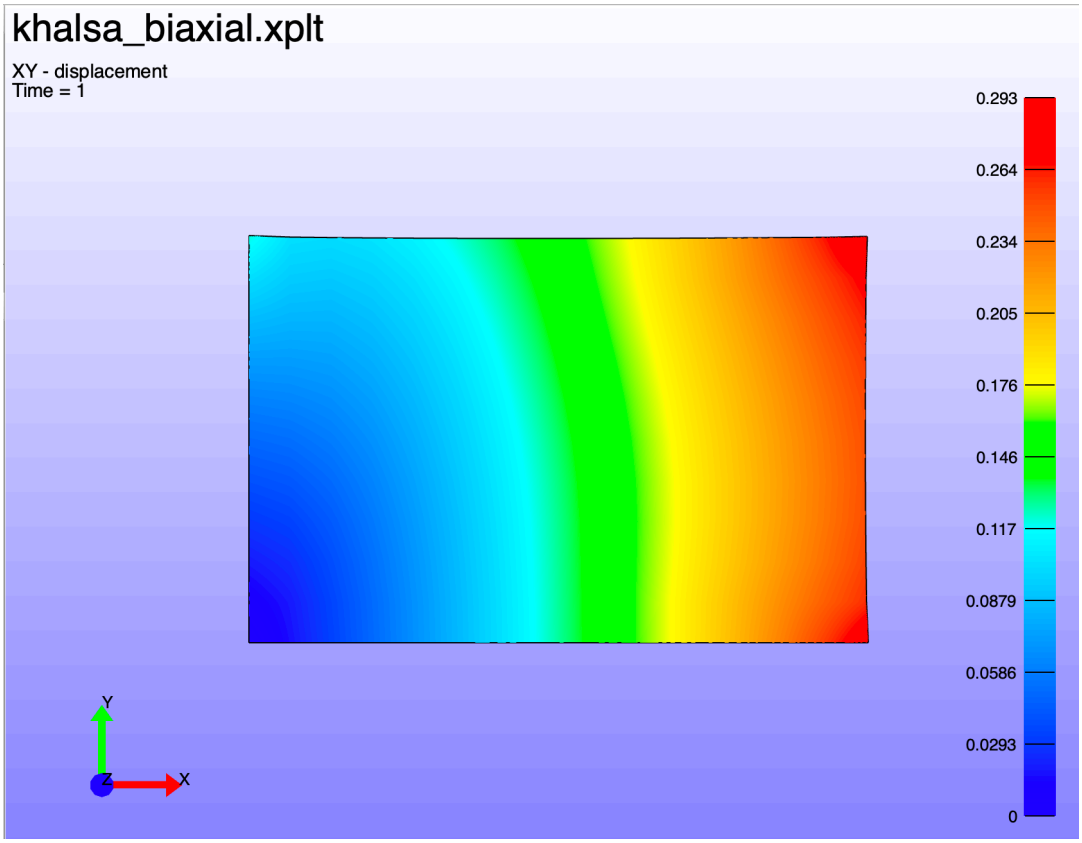

Figure 22. Scale of XY displacement (right) for Mooney Rivlin biaxial model after material property adjustment, so maximum displacement approximately matches the maximum displacement of previous isotropic and orthotropic tests.

The selected values were the same for both the X and Y fibre reinforcement tests except for specification of fibre reinforcement direction (Table 11).

Table 11. Coupled transversely isotropic Mooney Rivlin material properties required by FEBio and values selected for X fibre reinforcement test.

Mooney Rivlin Material Property	**Value Selected**
Density	1
Mooney Rivlin Parameter 1 (C1)	0.195
Mooney Rivlin Parameter 2 (C2)	0
Exponential Multiplier (C3)	0.0139
Fibre Scale Factor (C4)	116.22
Fibre Modulus - Linear Region (C5)	535.039
Bulk-like Modulus (K)	73.2
Max. Fibre Straightening Stretch (Lambda)	1
Fibre Direction	X

As found with the orthotropic tests, there were no significant differences between the regression measures produced by the two tested models, the only difference being which stimuli produced better results. The X fibre reinforced model on average produced slightly better results compared with the Y fibre reinforced model. Neither model, however, produced an average regression fit that was an improvement to the average isotropic or orthotropic model results. Regardless, the results were not significantly different from those produced by other models. As was found with every other model tested so far, no input stimuli on either X or Y reinforced model produced an adequate relative fit ($R^2 > 0.7$) to the original results. Once again, the 'best' result was produced for this material model when using the X fibre reinforced model with Y strain as the neural model input (Table 12), however this was still only 0.3011.

Table 12. Linear regression measures for total plot results produced by the coupled transversely isotropic Mooney Rivlin material model with collagen fibre reinforcement in the X direction.

** Numerical quirk in the result caused by zero firing produced in the replicated results*

Input Stimuli	**R^2**	**RMSE**	**Slope**
X Stress (Sx)	0.1183	2.5618	0.2073
Y Stress (Sy)	0.2944	2.2902	0.3267
Shear Stress (Sxy)	0.0400	2.1489	0.0969
1st Invariant Stress Tensor (I1)	0.2092	4.5110	0.5125
Maximum Shear Stress (MSS)	0.1879	1.3923	0.1479
Strain Energy Density (SED)	0.0597	0.1640	0.0091
Hydrostatic Pressure (HS)	0.2639	1.0904	0.1442
1st Principal Stress (S1)	0.1778	2.4682	0.2536
2nd Principal Stress (S2)	0.1823	2.6334	0.2747
3rd Principal Stress (S3)	0.0627	1.3656	0.0780
Deviatoric Stress 1 (Dev1)	0.0711	1.1909	0.0728
Deviatoric Stress 2 (Dev2)	0.1605	0.5013	0.0484
Deviatoric Stress 3 (Dev3) *	NaN	0.0000	0.0000
Shear A	0.0014	0.7319	0.0060
Shear B	0.1867	1.2719	0.1346
Shear C	0.1892	1.3662	0.1458
X Strain (Ex)	0.0169	0.2820	0.0082
Y Strain (Ey)	0.3011	2.4755	0.3589
Average	**0.1484**	**1.5803**	**0.3589**

Again, when analysing the result more closely, it can be seen that the uniform and uniaxial Y loading regime points are plotted linearly on the regression plot (Figure 23). The regression measures for the individual loading regimes (Table 13) indicate that those two loading regimes produced an adequate relative fit to the original results, although require some adjustment of firing

magnitude. As was seen for the isotropic material results, the biaxial, uniaxial X and shear loadings do not provide an adequate fit for the corresponding loading regime in the original results and therefore the overall relative total plot fit is unacceptable.

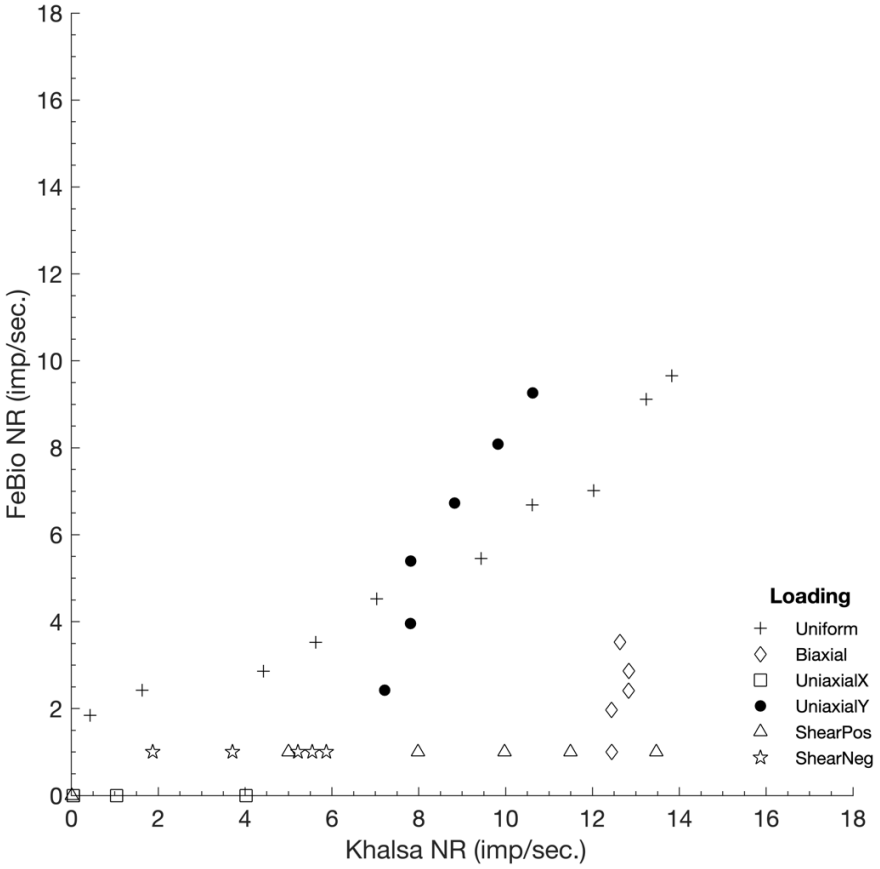

Figure 23. Regression plot of neural response (NR) from the Mooney Rivlin material model 1 (X fibre reinforced) tested using Y strain as the input to the neural model.

Table 13. Linear regression measures for individual loading regime results from the Mooney Rivlin model 1, with Ey as neural model input.

** Numerical quirk in the result caused by zero firing produced by the loading regime.*

*** Numerical quirk in the result caused by the all the replicated firing values for the loading regime being the same – not actually a perfect fit.*

Loading Regime	**R^2**	**RMSE**	**Slope**
Uniform	0.9397	0.7175	0.5618
Biaxial	0.3609	0.8799	2.9096
Uniaxial X *	NaN	0.0000	0.0000
Uniaxial Y	0.9315	0.7500	1.8691
Shear Positive	0.6424	0.2730	0.0671
Shear Negative **	1.0000	0.0000	0.0000

5 Discussion

Three material models (a total of nine sub-models) and eighteen different input stimuli were tested exhaustively, and the linear regression measures for the replicated results versus the original experiment results were calculated for every material/input stimulus combination tested. The average relative fit of the total plot results for each material model (i.e. all loading regimes) was determined in order to compare the general performance of each material. The total plot relative fits for each material/input stimulus combination have also been individually considered to account for the potential of only one input stimulus being the 'correct' input to the model and providing accurate replication of results.

Of the three tested materials, it was initially expected that the models created with the Mooney Rivlin material would provide the most accurate results due to the material having similar properties, according to literature, to those reported for biological soft tissue (i.e. anisotropy, fibre direction reinforcement, hyper-elastic non-linear behaviour). Correspondingly, the isotropic material models were expected to provide the least accurate results due to differences between the material properties and properties reported in literature for soft tissue.

Unexpectedly, the Mooney Rivlin material generally produced poorer relative fits of the total plots than both the orthotropic elastic and isotropic elastic materials. All of the orthotropic material models (except for Test 4) on average performed better than the other two materials, with orthotropic Test 3 overall providing the best average relative fit results. However, the average relative fit of both the isotropic elastic and Mooney Rivlin material results were not significantly lower than those produced by the orthotropic material tests.

Of all the model combinations tested, the best replication of the original results was produced by orthotropic elastic Test 1 using Y strain as the neural model input, although the relative fit produced by this material/input stimulus combination was only 0.3536. Although this was the best result achieved across all tests performed, it did not provide a significant improvement compared to individual results from the other tests. In some cases, the weaker performing material models, on average, combined with certain input stimuli actually produced results that provided a marginally better relative fit than that produced with other material/input stimuli combinations. For example, the X fibre reinforced Mooney Rivlin model using Y strain as the neural model input stimulus produced better results than all orthotropic tests that used Y stress as the input stimulus.

It was observed that for models where the stiffness or fibre directions were reinforced along the X direction, the results were generally better than those where the stiffness and fibre directions were reinforced along the Y direction. Also, it was found that the best results for inputs with X direction reinforcement were achieved using Y strain as the input to the neural model, and the results achieved with these combinations provided the best relative fits across all models.

Comparatively, the input stimulus that produced the best results in tests with Y direction reinforcement was unpredictable – there were no obvious patterns regarding which input stimuli produced the best results. Interestingly, Khalsa et al. had reported observing directional bias in the response of the cells, with the original results used in this project based on a 'Y-biased' neuron. It is unclear how a cell could have bias in an arbitrary direction without some method of orientation (e.g. cell orientation with respect to surrounding fibre direction). However, the minor differences observed in the results from the X and Y direction reinforcement models could be an indication of the directional bias that was observed by Khalsa et al. This could potentially support the theory proposed by Palmer et al. (2012) that the directional bias observed by Khalsa et al. was not due to the cells themselves sensing arbitrary orientation, but rather due to the properties of the surrounding material (Palmer, Taylor et al. 2012). The results, however, were not conclusive in actually proving or disproving this theory.

Overall, the regression measures for the total plot of every test performed demonstrated relative fits which were well below an acceptable value ($R^2 < 0.7$) to be considered an adequate replication of the original data. As such, these results demonstrated that none of the material/input combinations were able to adequately describe the original experiment results recorded by Khalsa et al.

Despite the relative fit of the total plots for all tests being much lower than expected, breaking down each test and considering the fit of each individual loading regime indicated more positive results. While the relative fit of the total plot was not acceptable, in many cases individual loading regimes did provide acceptable fits when compared with the corresponding loading regime from the original results. Unfortunately, in these cases the relative fit of the total plots were lowered due to other loading regimes not providing adequate fits. This further detailed analysis of individual loading regimes was useful for identifying which loading regimes were not performing correctly and analysing the effect of changes to the model. If testing is continued using this modelling method, this analysis of individual loading regimes could potentially be used to tune the model to improve fit of specific loading regimes and track any improvements. While this break-down of

individual loading regime performance is useful, it is still important overall to base any conclusions on the total plot performance. By considering the overall performance, assessments can be made as to whether the model is adequate in describing the complete set of original results, rather than just part of the result.

There could be a number of explanations for the extremely poor model performances. Firstly, it may indicate that the materials or material parameters selected were not truly representative of the material properties that would be observed in real life tissue. If the behaviour of the Ruffini was indeed reliant on the surrounding material properties and if certain characteristics of the surrounding material influenced how or what the Ruffini senses, then it is crucial that the surrounding material is modelled correctly. If this were the case, then modelling the joint capsule with materials that are not entirely representative of or accurate to a real-life joint capsule would clearly cause difficulties in attempting to accurately replicate the Ruffini responses.

Alternatively, the minor differences between the general performance of each material model could potentially be an indication that the surrounding material properties do not affect the behaviour or response of the Ruffini ending. If this is the case, then it raises numerous questions regarding what might be physically missing from the mechanical model that will allow the Khalsa et al. results to be replicated, and where this may lead future work.

Following from this, it is also possible that there are other physical characteristics of the Ruffini or surrounding material that have not yet been accounted for which may influence the Ruffini behaviour. This could potentially include the size, shape, orientation or material composition of the Ruffini, the number of Ruffini endings present, or the position of the cell in the surrounding material. These are all areas which could be investigated in future work if further adaptations to the model were to be explored.

It may be possible that the correct input stimulus to the neural model is not one of the eighteen mechanical stimuli tested in this project. Although there was a pattern observed in which using Y strain as the input stimulus to X direction reinforced models produced the best results of all the tests, the relative fits were not high enough that the material/input combination could be considered to adequately describe the Khalsa et al. results. Therefore, no conclusions can be drawn in regard to whether Y strain is the correct input for the model and the mechanical stimulus that the Ruffini senses. The poor relative fit of the replicated results could otherwise indicate that the correct input stimulus has perhaps not yet been identified or tested, and this may be why none of the stimuli

tested produced adequate replications of the original results. If this were the case, there may be difficulties in identifying what the Ruffini senses particularly given the discrepancies surrounding this in literature. It is unclear whether the Ruffini may be sensing a mechanical value that can be measured or one which is not measurable or possibly even perceivable to humans. There is also a possibility that the Ruffini could be sensing a combination of mechanical stimuli rather than just a single stimulus. Alternatively, if the surrounding material properties do impact how and what the Ruffini senses, then perhaps one of the inputs already tested is in fact correct but has not yet been combined with the correct material.

Apart from input stimulus, there may also be other adaptations that are required for the neural model. This could include adjustments to the induced current equation, or even potentially modifications to the physiological workings of the model. It is difficult to identify where the neural model may require adjustments as there is little information in literature regarding physiological level similarities between the Ruffini ending and nociceptors, as well as human neurons compared to giant squid neurons.

The explanations and conclusions that can be drawn regarding the results are limited. This is mostly significantly caused by the current lack of clear understanding in literature regarding Ruffini endings and their behaviours. Without this fundamental understanding there is little way of knowing what determines the Ruffini behaviour and responses, and as such it is extremely difficult to determine why the results do not adequately replicate the original results. Also, there is a significant lack of experimental data available that can be used to corroborate the model results, and therefore it becomes difficult to determine whether the model is correct and acting as it should.

Nevertheless, there are limitations within the project itself which may potentially explain the difficulties faced in replicating the original Khalsa et al. results. One significant limitation to the project is the possibility that the original Khalsa et al. results are not a reliable representation of Ruffini behaviour. This could be due to methods in performing the experiment, as well as unanticipated experimental complications which make the results difficult to replicate. Based on the reported methodology in the original Khalsa et al. paper, there are a number of factors in the original experiment which could have resulted in unaccounted-for complications.

Firstly, there were limitations in the method used by Khalsa et al. for localisation and isolation of the Ruffini endings. The receptive fields of Ruffini endings in the capsule were located using a

combination of the following three techniques: indentation with a blunt probe, in-plane stretching using fine forceps, and local electrical stimulation of the capsule surface using bipolar electrodes (Khalsa, Hoffman et al. 1996). However, this combination of techniques still only allowed for localisation within a radius of 0.5mm. Given that the size of the Ruffini endings are measured on a micro-scale, this 0.5mm localisation radius may not have been adequate to isolate single receptors, particularly as literature indicates that multiple Ruffini endings may branch from a single parent axon (Freeman and Wyke 1967; Magee, Zachazewski et al. 2007). This potentially means that the original results are not indicative of a single Ruffini receptor as expected, but instead multiple Ruffini receptors. However the literature also states that the parent axon of a Ruffini will only innervate other Ruffini endings (and no other receptor types), and as such, it is expected that there would not be other receptor types within the isolated receptive field (Freeman and Wyke 1967). However, it is difficult to conclude whether the methods of measuring the receptor response would be robust enough to completely isolate the Ruffini ending/s, or whether there may still be some interference from nearby receptors (with potentially overlapping receptive fields).

Another limitation of the original experiment is that it was performed 25 years ago, and as such methods for measuring the stresses, strains and neural responses have advanced since that time. In particular, in the original experiment the displacements of the surface markers on the specimen were optically tracked with a CCD camera mounted on the operating microscope over the stretching apparatus. Digital images of the control and deformed state were acquired using a frame grabber. The capsule strains were then measured optically by measuring displacements of surface markers glued onto the capsule, using a 0.25mm calibrated ruler under an operating microscope (Khalsa, Hoffman et al. 1996). This method for measuring the apparent strain experienced by the specimen is limited by the precision of the displacement measurements. Also, this technique allowed only for the apparent strain to be measured, and apparent stress to be estimated based on the loads applied to the specimen. However, the local stresses and strains may not be the same as the apparent stress and strains measured by Khalsa et al, and as such the results are limited because the local stresses and strains could not be measured.

Additionally, the extent of the results documented by Khalsa et al. is limited – only summaries of results and results plots have been provided. There was only one set of relevant data available (i.e. results for one neuron) and consequently the models developed in this project have been based on those results only. The results from this project may be more substantial if there were multiple data sets available, allowing the neural model to be corroborated across multiple neuron data sets

rather than just based on data from a single neuron. This would provide better credibility to the developed neural/mechanical model. Also, given that the raw data had not been archived, the original results had to be digitized from the figure provided in the original Khalsa et al. paper in order to be used. The digitization process, using Grabit on Matlab, results in some degree of error in the data, as the accuracy of the selected points is dependent on the image resolution and the accuracy of the manual selection of the data points on the image using a mouse cursor.

Given these numerous limitations to the original experiment and the fact that the entirety of this project has been based upon the original Khalsa et al. results, the reliability of both the mechanical and neural model and the results produced may be compromised.

Overall, the original Khalsa et al. results were not able to be adequately replicated and the outcomes of this project have not provided any clarification to the discrepancies in literature regarding fundamental Ruffini behaviours (i.e. what it senses and how). As a result, further questions have been raised and multiple avenues for future work have been exposed. Regardless of the results, successful integration between FEBio mechanical models and the Matlab adaptation of the Hodgkin-Huxley neural model was achieved. This demonstrates the possibility of combining neural and mechanical models and provides the first step towards development of a completely integrated model.

6 Conclusions

Literature relating to the combination of mechanical and neural modelling methods is sparse. While there have been some attempts at combining mechanical modelling methods with other model types, mechanical and neural modelling methods are yet to be successfully combined. The concept of combining FEM modelling with Hodgkin-Huxley neural modelling is new territory, but if successful could produce significant benefits in the medical field. When applied to applications such as prosthesis design (specifically prostheses for knee arthroplasties), this modelling combination could allow for prediction of patient pain and discomfort based on the predicted stresses and strains produced by a given prosthesis. The ability to try and test prostheses without first physically implanting them would be expected to decrease levels of patient dissatisfaction caused by chronic post-operative pain and instability, in turn leading to a reduction in the number of revision arthroplasties required.

Unfortunately, the mechanoreceptors within the human knee are still quite poorly understood, as indicated by the many discrepancies within the literature in relation to the fundamental properties of the receptors, including their size, structure, locations, material composition, and sensitivities. Consequently, creating a complete neural model of the knee to combine with an FEM model is no small feat, and given the time constraints of this project and the nature of the task at hand, it was not viable to complete the entire neural model within this project. Instead, the focus of this project was to adapt the Hodgkin-Huxley model for the Ruffini ending only, while also attempting to clarify and explain the documented Ruffini behaviours through replication of the Khalsa et al. (1996) experiment using FEBio modelling and the adapted Hodgkin-Huxley Ruffini model.

A simple rectangular model representing the joint capsule specimen used by Khalsa et al. was created with FEBio. The model was tested in the same six loading regimes that were used by Khalsa et al. (uniform, biaxial, uniaxial X and Y, positive and negative shear), with three different material types (isotropic elastic, orthotropic elastic, and coupled transversely isotropic Mooney Rivlin). This was done in an attempt to identify the effect of material properties on the behaviour of the Ruffini ending, so as to accurately reproduce the Khalsa et al. results. Successful integration between the FEBio mechanical model and the Matlab adaptation of the Hodgkin-Huxley neural model was achieved, along with exhaustive testing of three material types and eighteen input stimuli. Regardless of the material type, material properties specified for the specimen model, or the input stimulus, the results did not adequately reflect the results that were observed in the Khalsa et al. experiment.

Based on these results, it is understood that everything that has been tested and investigated up until this point still does not produce or describe the Ruffini ending behaviours that were observed by Khalsa et al. Therefore, this leads to one of two conclusions; either there is something missing from the model - whether it be the FEBio specimen model, the Ruffini ending neural model, or both - or alternatively there were abnormalities in the results recorded by Khalsa et al., perhaps due to issues with methodology. Regardless, based on these conclusions, it is clear that there are many questions still unanswered regarding Ruffini behaviour and the properties which may influence the Ruffini's response, and as such there is an abundance of future work to be undertaken.

7 Future Work

Considering the time and resources required versus the likelihood of producing expected or useful results, the best option forward would be to physically re-perform Khalsa et al. experiment, or an improved version of the experiment. While this might require more time and resources than just adjusting the computational model, it is the only way to determine if the Khalsa et al. results actually accurately describe the behaviour of the Ruffini ending, as well as to study and document other physical characteristics of the mechanoreceptor. Repeating the Khalsa et al. experiment would provide a good basis for ensuring the Ruffini neural model adaptation is based on accurately recorded Ruffini responses.

Another option for future work is to continue to make changes and adaptations to the FEBio model and Hodgkin-Huxley neural model, in an attempt to determine the properties which result in the Ruffini behaviours observed by Khalsa et al. Although repeating the Khalsa et al. experiment is ideal, adapting the current FEBio and neural model could still be a useful avenue for understanding the Ruffini ending behaviour as it is not particularly time or resource intensive. However, there always remains the risk that the Khalsa et al. results are not reliable due to complications in the original experiment that make the results difficult to reproduce. If this is the case, the FEBio and neural model developed based on the original Khalsa et al. results may not be accurate.

7.1 Repeating Khalsa et. al Experiment

As mentioned, it is recommended that the first avenue for future work is to physically re-perform the Khalsa et al. experiment due to the limitations encountered in both the original experiment and this project. While the repeated experiment may not be exactly the same as the original experiment, it provides the opportunity to obtain a new set of results for the Ruffini ending behaviours using improved methodology. This would allow for a full set of raw results to be properly archived for future use, adding to the currently limited store of experimental data in the literature regarding Ruffini behaviours. It would also assist to dispel any uncertainty regarding the accuracy and reliability of the original Khalsa et al. results. There are three particular areas identified where improvements could be made in the repeated experiment.

Firstly, the original experiment used joint capsules from the knees of adult cats. In re-performing the experiment, the joint capsules may not necessarily be from the knees of cats but instead from another animal. Due to the differences documented in literature regarding Ruffini endings in different species, it would be expected that using the Ruffini endings from another species may

produce different results to the original experiment. However, a species which has more anatomical and physiological similarities to humans could be selected instead, which would likely produce results that are more similar to the results that would be obtained from a human. This would be ideal, as the overall aim is to adapt a neural model for the human knee – if the experimental results used to tune the model are similar to human results, the neural model will be more accurate.

Secondly, techniques for neural mapping and identification have progressed beyond what was used 25 years ago. Repeating the experiment provides the opportunity to improve on areas of the original experiment methodology. In particular, the new experiment could improve upon the method for the measurement of the stress and strain in the specimen. The original experiment calculated only the apparent strain through measurement of surface marker displacement (to 0.25mm accuracy), while the average apparent stress of the joint capsule was estimated based on the loads applied from the stretching apparatus. However, the local stress and strain experienced around the Ruffini ending may not be the same as the apparent stress and strain that was calculated by Khalsa et al. The experiment could be substantially improved by using modern techniques, such as Digital Image Correlation, to measure the local strain around the Ruffini ending with high resolution. This method has already been used with success in a similar application by Palmer et al. (2017) with viscerofugal neurons within gut tissue, as well as in other biological applications (Dickinson, Taylor et al. 2012; Wentzell, Sterling Nesbitt et al. 2013; Hokka, Mirow et al. 2015; Palmer, Hibberd et al. 2017).

Finally, another point of uncertainty in the original results of the Khalsa et al. experiment was whether the results were recorded from a single Ruffini ending or from multiple endings. As the literature review indicated, Ruffini endings tend to be found in clusters of three to six with a single parent axon. Khalsa et al. noted that the location of the Ruffini endings were found within a radius of 0.5mm using a combination of three techniques, however the identified 'single receptive fields' may have included multiple receptors with the same parent axon. Therefore, it is important that in the repeated experiment it is made clear whether the results are recorded from a single Ruffini cell or from a cluster of cells (and how many within the cluster). The original experiment methodology for identifying the presence and localisation of the neurons could be improved through use of histological staining techniques, which have already been proven successful and reliable (Witherspoon, Smirnova et al. 2014; Rein, Semisch et al. 2015; Kholinne, Lee et al. 2018). If Ruffini behaviour could be recorded from individual Ruffini cells rather than a cluster, it would

become much simpler to isolate the properties of an individual cell and as a result understand how and why the response is produced.

With these three main adaptations to the re-performed experiment, and with careful recording of results, there is likely to be progress towards greater understanding of Ruffini behaviour.

7.2 FEBio and Hodgkin-Huxley Model Adaptations

There are a number of adaptations that could be made to the FEBio model and the Hodgkin-Huxley Matlab model further to what was already presented in this project. Such changes could assist in identifying which properties of the Ruffini ending and the surrounding material influence the receptor response, therefore providing a better understanding of the Ruffini ending behaviour. This could be a suitable path to explore for future work due to the relatively low resource and time costs. However as mentioned previously, if the Khalsa et al. experiment results are not accurate, then the adapted neural model may not perform as it should and understandings gained through adapting the model may not be correct.

Ideally, any changes made to the Hodgkin-Huxley model would be very minimal as the model should already be fundamentally correct, assuming that Ruffini endings and giant squid axons are fundamentally similar in their behaviours. Regardless, there may still be small adaptations required to alter the firing activation threshold for the neural model.

More significant changes are likely to be required for the FEBio model, however the order in which this work is undertaken should depend on the time required to change the model versus the perceived benefits of doing so. It should also be noted that structural changes to the FEBio model may take longer to replicate into the Matlab script for automating the running of the experiments. If the perceived benefit is small, then it may be worth using the FEBio GUI to begin with, to test if there are any significant benefits, before implementing it into the code.

7.2.1 Modelling the Cell

7.2.1.1 Single Cell Body

First and foremost, a number of changes should be made to the FEBio specimen model. The current model is a simple rectangular model, however in reality, the specimen was likely not so simple.

As such, it would be a good idea to first model a single Ruffini cell body into the specimen in order to determine the effects of the size and shape of the cell on the cell's response. This will

likely have a significant effect on the results, due to the relatively large size of the cell and its elongated shape and the stress that will concentrate around the cell body rather than being relatively uniform (as it was throughout the continuous rectangular model). This modelling should also take into account the orientation of the cell.

7.2.1.2 Cell Material Properties

Similar to the tests performed to investigate the material properties of the specimen itself, the material properties of the cell body should also be investigated. This could include investigating the effects of the cell body being fluid filled, or fibre reinforced. Given that changing the material type and material properties on FEBio is quite simple, this is a good option for future work that requires minimal time but may produce significant results. It would also help establish an understanding of the extent to which the material properties of the Ruffini ending itself affect the sensitivity of the cell to particular inputs.

7.2.1.3 Modelling Cell Cluster

If the results of modelling a simple cell and altering the material properties of that cell have still not indicated any explanation for Ruffini behaviours, the next step would be to model the Ruffini as a cluster. This could be particularly useful to test if still comparing to the original Khalsa et al. experiment results, because the Khalsa et al. experiment could not identify whether there were multiple cells within the single receptive field. If the test results improve in similarity to the Khalsa et al. results, this could potentially confirm whether or not the Khalsa et al. experiment identified and recorded responses from a single Ruffini ending or a cluster.

7.2.2 Modelling the Joint Capsule

Finally, of the changes to be made to the FEBio model, further modifications to the joint capsule could be explored. Palmer et al. (2012) indicated that the Khalsa et al. findings regarding directional sensitivities of the Ruffini may have actually been caused by the surrounding material properties. Therefore, it may be beneficial to further investigate which properties of the surrounding tissue might cause this behaviour (Palmer, Taylor et al. 2012).

There are four possible areas for investigation. Firstly, additional materials for the FEBio joint capsule model could be investigated. Only three materials were investigated in this project however there are many more materials available on FEBio - some of which may potentially provide a better simulation of soft tissue properties than the materials tested in this study.

The second area for investigation involves modelling the outer fibrous and inner synovial layers of the joint capsule rather than modelling the joint capsule as a single uniform piece of material. As fibrous and synovial materials have significantly different properties, modelling the two material layers could indeed have an effect on the results of the testing, particularly depending on where the Ruffini cell is embedded within the layers – whether it is within one material or the other, or spans across both. However, before commencing work on modelling the two layers, it would be beneficial to review the literature for any information regarding material property differences between the layers, or if there is any literature which already demonstrates whether the layers have a significant effect on the properties of the joint capsule.

The third area for investigation is modelling the three regions of stiffness of the joint capsule as identified by Hoffman et al. (1985) (Figure 20). Combining multiple stiffness layers may be significant enough to alter the way the specimen is deformed and how the stress concentrates, however the stiffness study performed on the orthotropic elastic material in this project did not indicate any major differences in Ruffini responses. Again, the results may also depend on where the Ruffini cell is embedded, and whether it spans more than one stiffness region.

Finally, further consideration could be made to modelling fibre reinforcement within the joint capsule. Multiple fibre directions were not accounted for during this project, although Khalsa et al. (1996) identified that there were varying orientations of fibre direction within the joint capsule specimen used in their experiment. Khalsa et al. (1996) also stated that the local orientation of the Ruffini endings varied depended on the fibre directions within the capsule. Modelling multiple fibre directions within the one model could be worth exploring, particularly if the cell body is also modelled, as it would provide a closer replication to the specimen used in the original experiment. This is an avenue which could provide insight into whether both/either fibre direction or cell orientation influences the Ruffini behaviour.

7.2.3 Hodgkin-Huxley Model Adaptations

The Hodgkin-Huxley model for the Ruffini ending was adapted for this project based on a Hodgkin-Huxley Matlab code adaptation for the Xu et al. (2008) modelling. The Xu et al. experiment was based on thermal nociceptors within the skin, while the adaptations made were for the Ruffini ending mechanoreceptors within the knee joint capsule. Changes were made to allow for mechanical rather than thermal input, and the I_ST equation was adapted in order to lower the firing threshold. No further adaptations were made, which leaves sections of the neural model open to explore in future work.

7.2.3.1 Inducing Current (I_ST) Equation

The I_ST equation was adapted in order to lower the firing rate of the neural model, given that the firing activation threshold of Ruffini endings is lower than free nerve endings. One I_ST equation which linearly mapped the new firing values to the original firing values was already investigated in this project. Other options for the I_ST equation should be considered, including the possibility of a non-linear equation such as the one used for the thermal nociceptor neural model, or a linear model which only uses a 'fudge factor' for scaling the input. If this avenue is explored, it would be beneficial to consider developing code to optimise any 'fudge factors' or scaling values used in the equation based on the input value or stimulus type.

7.2.3.2 Input Stimuli

Considering that there have been no conclusive results to suggest what the Ruffini ending is sensitive to and thus what the input to the Hodgkin-Huxley model should be, further work should be conducted to determine this. This could include testing other mechanical inputs apart from the eighteen that were considered in this project, as well as considering a combination of the inputs. The Matlab code has already been modified such that multiple mechanical terms can be combined, with varying scale and weighting, as the input stimulus for the Hodgkin-Huxley model. Further exploration in this area may be beneficial by aiding understanding of what the Ruffini ending actually senses and responds to.

7.2.3.3 Physiological Changes: Ionic Properties

As a final suggestion for possible changes that could be made to the models, the physiological differences between a Ruffini ending and a thermal nociceptor could be considered. More specifically, further research could investigate whether there are significant fundamental differences in terms of the ionic properties of the two receptors.

Given that the Ruffini neural model was adapted from Hodgkin-Huxley Matlab code for nociceptor response to temperature, it could be useful to determine whether the type of receptor (i.e. mechanoreceptor, thermal receptor, chemical receptor) has any correlation with the ionic properties or ion gated channels of the cell. If there were differences, then these would need to be incorporated into the Hodgkin-Huxley Ruffini model to ensure the responses are accurate.

It seems unlikely however, that these physiological changes would be significant when the Ruffini ending and nociceptor have very similar firing patterns, just with different thresholds. Also, the

literature available regarding this is likely to be quite limited given the very specific nature of the query and the lack of confirmed knowledge regarding mechanoreceptors. Therefore, this work should potentially only be pursued if all other options have been exhausted.

7.2.3.4 Alternative Hodgkin-Huxley Adaptations

Finally, it would be beneficial to also investigate other Hodgkin-Huxley adaptations which already exist in literature, especially if the adaptations are for other human receptor types. This could provide significant insight into what might be required for further adaptation of the Ruffini model or in the future, the neural models for the other mechanoreceptor types. It may also identify techniques that were successfully used during model adaptation that may also be applicable in this case.

8 Final Comments

To conclude, while there have not been any significant results to explain or describe Ruffini behaviour throughout the span of this project itself, there are many possibilities of where the project could be taken to next and how it can progress. As is commonly found in research, more questions arise as the project progresses, which is certainly the case here. This area of research is certainly innovative and there is plenty of work still to be done before significant progress is likely to be made. The end goal, however, could provide significant benefits – particularly in the medical field – and so is certainly worth exploring further.

References

Appali, R., U. van Rienen and T. Heimburg (2012). A comparison of the Hodgkin–Huxley model and the Soliton theory for the action potential in nerves. **16:** 271-279.

Australian Orthopedic Association (2018). Hip, knee and shoulder arthroplasty 2018 annual report. Adelaide, Australia, National Joint Replacement Registry.

Australian Orthopedic Association (2019). Hip, knee and shoulder arthroplasty 2019 annual report. Adelaide, Australia, National Joint Replacement Registry.

Avalon Orthopedic. (2019). "Managing complex knee injuries." Retrieved March 8, 2020, from http://www.avalonorthopaedic.com.au/managing-complex-knee-injuries/.

Aydog, S. T., P. Korkusuz, M. Doral, O. Tetik and H. Demirel (2006). "Decrease in the numbers of mechanoreceptors in rabbit ACL: The effects of ageing." Knee Surgery, Sports Traumatology, Arthroscopy: Official Journal of the ESSKA **14**: 325-329.

Bell, J. and M. Holmes (1992). "Model of the dynamics of receptor potential in a mechanoreceptor." Mathematical Biosciences **110**(2): 139-174.

Bendjaballah, M. Z., A. Shirazi-Adl and D. J. Zukor (1997). "Finite element analysis of human knee joint in varus-valgus." Clinical Biomechanics **12**(3): 139-148.

Beswick, A. D., V. Wylde, R. Gooberman-Hill, A. Blom and P. Dieppe (2012). "What proportion of patients report long-term pain after total hip or knee replacement for osteoarthritis? A systematic review of prospective studies in unselected patients." BMJ Open **2**(1): 435.

Burgess, P. R. and F. J. Clark (1969). "Characteristics of knee joint receptors in the cat." The Journal of Physiology **203**(2): 317-335.

Çabuk, H. and F. Kuşku Çabuk (2016). "Mechanoreceptors of the ligaments and tendons around the knee." Clinical Anatomy **29**(6): 789-795.

Chakraborty, S., D. Mondal and M. Motalab (2016). Constitutive modeling of the human Anterior Cruciate Ligament (ACL) under uniaxial loading using viscoelastic prony series and hyperelastic five parameter Mooney-Rivlin model. Melville, American Institute of Physics. **1754**.

Coolican, M. R. J. (2015). Aetiology of patient dissatisfaction following total knee arthroplasty. Total Knee Arthroplasty: A Comprehensive Guide. E. C. Rodríguez-Merchán and S. Oussedik. Cham, Springer International Publishing**:** 229-233.

Dandekar, K., B. I. Raju and M. A. Srinivasan (2003). "3-D finite-element models of human and monkey fingertips to investigate the mechanics of tactile sense." Journal of Biomechanical Engineering **125**(5): 682-691.

Das, S., V. Soni and J. Bellare (2017). "Evolution of root form endosseous dental implant - transformation from bone anchored to ligament anchored implants and its neurological aspects - sensory dental implants." Medical Devices and Diagnostic Engineering **2**(1).

Dickinson, A. S., A. C. Taylor and M. Browne (2012). "The influence of acetabular cup material on pelvis cortex surface strains, measured using digital image correlation." Journal of Biomechanics **45**(4): 719-723.

Eklund, G. and S. Skoglund (1960). "On the specificity of the Ruffini like joint receptors." Acta Physiologica Scandinavica **49**: 184-191.

Fleming, M. S. and W. Luo (2013). "The anatomy, function, and development of mammalian Aβ low-threshold mechanoreceptors." Frontiers in Biology **8**(4).

Foran, J. R. H. and S. J. Fischer. (2015). "Total knee replacement." Retrieved September 10, 2019, from https://orthoinfo.aaos.org/en/treatment/total-knee-replacement/.

Freeman, M. A. and B. Wyke (1967). "The innervation of the knee joint. An anatomical and histological study in the cat." Journal of Anatomy **101**(Pt 3): 505-532.

Freutel, M., H. Schmidt, L. Dürselen, A. Ignatius and F. Galbusera (2014). "Finite element modeling of soft tissues: Material models, tissue interaction and challenges." Clinical Biomechanics **29**(4): 363-372.

Fung, Y.-C. (1993). Biomechanics: Mechanical Properties of Living Tissues, New York: Springer New York.
Gaillard, R., B. Shabani, R. Ballis, P. Neyret and S. Lustig (2015). Anatomy, physiology and biomechanics of the native knee. Total Knee Arthroplasty: A Comprehensive Guide. E. C. Rodriguez-Merchan and S. Oussedik. Switzerland, Springer International.
Gillquist, J. (1996). "Knee ligaments and proprioception." Acta Orthopaedica Scandinavica **67**(6): 533-535.
Grigg, P. (2001). "Properties of sensory neurons innervating synovial joints." Cells Tissues Organs **169**(3): 218-225.
Grigg, P. and A. H. Hoffman (1982). "Properties of Ruffini afferents revealed by stress analysis of isolated sections of cat knee capsule." Journal of Neurophysiology **47**(1): 41-54.
Halata, Z., T. Rettig and W. Schulze (1985). "The ultrastructure of sensory nerve endings in the human knee joint capsule." Anatomy and Embryology **172**(3): 265-275.
Halata, Z., C. Wagner and K. I. Baumann (1999). "Sensory nerve endings in the anterior cruciate ligament (Lig. cruciatum anterius) of sheep." The Anatomical Record **254**(1): 13-21.
Hall, J. E. (2015). Guyton and Hall textbook of medical physiology, Saint Louis: Elsevier.
Halloran, J. P., A. J. Petrella and P. J. Rullkoetter (2005). "Explicit finite element modeling of total knee replacement mechanics." Journal of Biomechanics **38**(2): 323-331.
Haut Donahue, T. L., M. Hull, M. M. Rashid and C. R. Jacobs (2002). "A finite element model of the human knee joint for the study of tibio-femoral contact." Journal of Biomechanical Engineering **124**(3): 273-280.
Heppelmann, B., K. Messlinger, W. F. Neiss and R. F. Schmidt (1995). "Fine sensory innervation of the knee joint capsule by group III and group IV nerve fibers in the cat." Journal of Comparative Neurology **351**(3): 415-428.
Hodgkin, A. L. and A. F. Huxley (1952). "A quantitative description of membrane current and its application to conduction and excitation in nerve." Journal of Physiology **117**(4): 500-544.
Hoffman, A. H., P. Grigg and D. M. Flynn (1985). "A biomechanical model of the posterior knee capsule of the cat." Journal of Biomedical Engineering **107**: 140-146.
Hokka, M., N. Mirow, H. Nagel, M. Irqsusi, S. Vogt and V.-T. Kuokkala (2015). "In-vivo deformation measurements of the human heart by 3D Digital Image Correlation." Journal of Biomechanics **48**(10): 2217-2220.
Humphrey, J. D. (2003). "Continuum biomechanics of soft biological tissues." Proc. R. Soc. A-Math. Phys. Eng. Sci. **459**(2029): 3-46.
Jahn, A. (2013). "Introduction to computational modelling: Hodgkin Huxley model." Retrieved September 4, 2020, from http://andysbrainblog.blogspot.com/2013/10/introduction-to-computational-modeling.html.
Jawad, F. A. and J. G. Michael (2017). "Anatomy and physiology of knee stability." Journal of Functional Morphology and Kinesiology **2**(4): 34.
Johansson, H., P. Sjölander and P. Sojka (1991). "Receptors in the knee joint ligaments and their role in the biomechanics of the joint." Critical Reviews in Biomedical Engineering **18**(5): 341-368.
Johnson, L. R. (2003). Essential medical physiology, Elsevier Science.
Johnson, M. and S. Chartier (2017). "Spike neural models (part I): The Hodgkin-Huxley model." The Quantitative Methods for Psychology **13**: 105-119.
Kahanov, L. and M. Kato (2007). "Therapeutic effect of joint mobilization: Joint mechanoreceptors and nociceptors." Athletic Therapy Today **12**: 28-31.
Katonis, P., A. Papoutsidakis, A. Aligizakis, G. Tzanakakis, G. M. Kontakis and P. J. Papagelopoulos (2008). "Mechanoreceptors of the posterior cruciate ligament." Journal of International Medical Research **36**(3): 387-393.
Khalsa, P. S., A. H. Hoffman and P. Grigg (1996). "Mechanical states encoded by stretch-sensitive neurons in feline joint capsule." Journal of Neurophysiology **76**(1): 175-187.

Kholinne, E., H.-J. Lee, Y.-M. Lee, S.-J. Lee, M. F. Deslivia, G.-Y. Kim, S. Lim and I.-H. Jeon (2018). "Mechanoreceptor profile of the lateral collateral ligament complex in the human elbow." Asia-Pacific Journal of Sports Medicine, Arthroscopy, Rehabilitation and Technology **14**: 17-21.

Kim, D. H., K. M. Pearson-Chauhan, R. J. McCarthy and A. Buvanendran (2018). "Predictive factors for developing chronic pain after total knee arthroplasty." The Journal of arthroplasty **33**(11): 3372-3378.

Komdeur, P., F. E. Pollo and R. W. Jackson (2002). "Dynamic knee motion in anterior cruciate impairment: a report and case study." Baylor University Medical Center Proceedings **15**(3): 257-259.

Krouchev, N. I., F. Rattay, M. Sawan and A. Vinet (2015). "From squid to mammals with the HH model." PLOS One **10**(12).

Kurtz, S. M., K. L. Ong, E. Lau, M. Widmer, M. Maravic, E. Gómez-Barrena, M. d. F. de Pina, V. Manno, M. Torre, W. L. Walter, R. de Steiger, R. G. T. Geesink, M. Peltola and C. Röder (2011). "International survey of primary and revision total knee replacement." International Orthopaedics **35**(12): 1783-1789.

Little, J. S. and P. S. Khalsa (2005). "Material properties of the human lumbar facet joint capsule." Journal of Biomechanical Engineering **127**(1): 15.

Lobenhoffer, P., R. Biedert, E. Stauffer, C. Lattermann, T. G. Gerich and W. Müller (1996). "Occurrence and distribution of free nerve endings in the distal iliotibial tract system of the knee." Knee Surgery, Sports Traumatology, Arthroscopy **4**(2): 111-115.

Magee, D. J., J. E. Zachazewski and W. S. Quillen (2007). Scientific foundations and principles of practice in musculoskeletal rehabilitation-E-book, Elsevier Health Sciences.

McDougall, S., W. Vargas Riad, A. Silva-Gotay, E. R. Tavares, D. Harpalani, G.-L. Li and H. N. Richardson (2018). "Myelination of axons corresponds with faster transmission speed in the prefrontal cortex of developing male rats." eNeuro **5**(4): 203-218.

Muller, J. (2014). Computational modelling of knee implants. Computational Modelling of Biomechanics and Biotribology in the Musculoskeletal System, Elsevier**:** 417-446.

Müller, W. (1982). Anatomy. The Knee: Form, Function, and Ligament Reconstruction. W. Müller. Berlin, Heidelberg, Springer Berlin Heidelberg**:** 2-7.

Nelson, M. and J. Rinzel (1998). The Hodgkin—Huxley model. The Book of GENESIS: Exploring Realistic Neural Models with the GEneral NEural SImulation System. J. M. Bower and D. Beeman. New York, NY, Springer New York**:** 29-49.

Orthopedics SA. (2019). "Total knee replacement (TKR)." Retrieved September 23, 2019, from https://www.orthosa.com.au/treatment/total-knee-replacement/.

Palmer, G., T. J. Hibberd, T. Roose, S. J. Brookes and M. Taylor (2017). "Measurement of strains experienced by viscerofugal nerve cell bodies during mechanosensitive firing using digital image correlation."

Palmer, G., M. Taylor and T. Roose (2012). "Do Ruffini mechanoreceptors have a preferred sensing direction?" Journal of biomechanics **45**: 421.

Panagiotopoulou, O. (2009). "Finite element analysis (FEA): Applying an engineering method to functional morphology in anthropology and human biology." Annals of Human Biology **36**(5): 609-623.

Peña, E., B. Calvo, M. A. Martínez and M. Doblaré (2006). "A three-dimensional finite element analysis of the combined behavior of ligaments and menisci in the healthy human knee joint." Journal of Biomechanics **39**(9): 1686-1701.

Poláček, P. (1966). "Receptors of the joints." Acta Faculty of Medicine Brno **23**.

Quindlen-Hotek, J. and V. Barocas (2018). "A finite-element model of mechanosensation by a Pacinian corpuscle cluster in human skin." Biomechanics and Modeling in Mechanobiology **17**(4): 1053-1067.

Ralphs, J. R. and M. Benjamin (1994). "The joint capsule: structure, composition, ageing and disease." Journal of Anatomy **184**(3): 503-509.

Rein, S., M. Semisch, M. Garcia-Elias, A. Lluch, H. Zwipp and E. Hagert (2015). "Immunohistochemical mapping of sensory nerve endings in the human triangular fibrocartilage complex." Clinical orthopaedics and related research **473**(10): 3245-3253.

Sadegh-Zadeh, S.-A. (2017). "All-or-None principle and weakness of Hodgkin-Huxley mathematical model." International Journal of Mathematical and Computational Sciences **11**.

Santamaria, F. and J. M. Bower (2009). Hodgkin-Huxley models.

Schaible, H. G. and R. F. Schmidt (1985). "Effects of an experimental arthritis on the sensory properties of fine articular afferent units." Journal of Neurophysiology **54**(5): 1109-1122.

Schultz, R. A., D. C. Miller, C. S. Kerr and L. Micheli (1984). "Mechanoreceptors in human cruciate ligaments. A histological study." The Journal of Bone and Joint Surgery. American Volume **66**(7): 1072-1076.

Schutte, M. J., E. J. Dabezies, M. L. Zimny and L. T. Happel (1987). "Neural anatomy of the human anterior cruciate ligament." The Journal of Bone and Joint Surgery. American Volume **69**(2): 243-247.

Skou, S. T., T. Graven-Nielsen, S. Rasmussen, O. H. Simonsen, M. B. Laursen and L. Arendt-Nielsen (2013). "Widespread sensitization in patients with chronic pain after revision total knee arthroplasty." Pain **154**(9): 1588-1594.

Snaidero, N. and M. Simons (2014). "Myelination at a glance." Journal of Cell Science **127**(14): 2999.

Souza, R. B. and R. Doan (2010). Anatomy and physiology of the knee.

Trad, Z., A. Barkaoui, M. Chafra and J. M. R. S. Tavares (2018). Finite element models of the knee joint. FEM Analysis of the Human Knee Joint: A Review. Z. Trad, A. Barkaoui, M. Chafra and J. M. R. S. Tavares. Cham, Springer International Publishing**:** 1-34.

Villa, T., F. Migliavacca, D. Gastaldi, M. Colombo and R. Pietrabissa (2004). "Contact stresses and fatigue life in a knee prosthesis: comparison between in vitro measurements and computational simulations." Journal of Biomechanics **37**(1): 45-53.

Wentzell, S., R. Sterling Nesbitt, J. Macione and S. Kotha (2013). "Measuring strain using digital image correlation of second harmonic generation images." Journal of Biomechanics **46**(12): 2032-2038.

Widmaier, E. P., H. Raff and K. T. Strang (2014). Vander's human physiology, McGraw-Hill.

Witherspoon, J. W., I. V. Smirnova and T. E. McIff (2014). "Neuroanatomical distribution of mechanoreceptors in the human cadaveric shoulder capsule and labrum." Journal of Anatomy **225**(3): 337-345.

Wodowski, A. J., C. W. Swigler, H. Liu, K. M. Nord, P. C. Toy and W. M. Mihalko (2016). "Proprioception and knee arthroplasty." Orthopedic Clinics of North America **47**(2): 301-309.

Wu, J. Z., K. Krajnak, D. E. Welcome and R. G. Dong (2006). "Analysis of the dynamic strains in a fingertip exposed to vibrations: Correlation to the mechanical stimuli on mechanoreceptors." Journal of Biomechanics **39**(13): 2445-2456.

Wylde, V., P. Dieppe, S. Hewlett and I. Learmonth (2007). "Total knee replacement: is it really an effective procedure for all?" The Knee **14**(6): 417-423.

Xu, F., T. Wen, T. J. Lu and K. A. Seffen (2008). "Modeling of nociceptor transduction in skin thermal pain sensation." Journal of Biomechanical Engineering **130**(4): 13.

Zimny, M. L. and C. S. Wink (1991). "Neuroreceptors in the tissues of the knee joint." Journal of Electromyography and Kinesiology **1**(3): 148-157.

Appendix A: Isotropic Elastic Material Results

A.1 Test 1

A.1.1 X Stress (Sx)

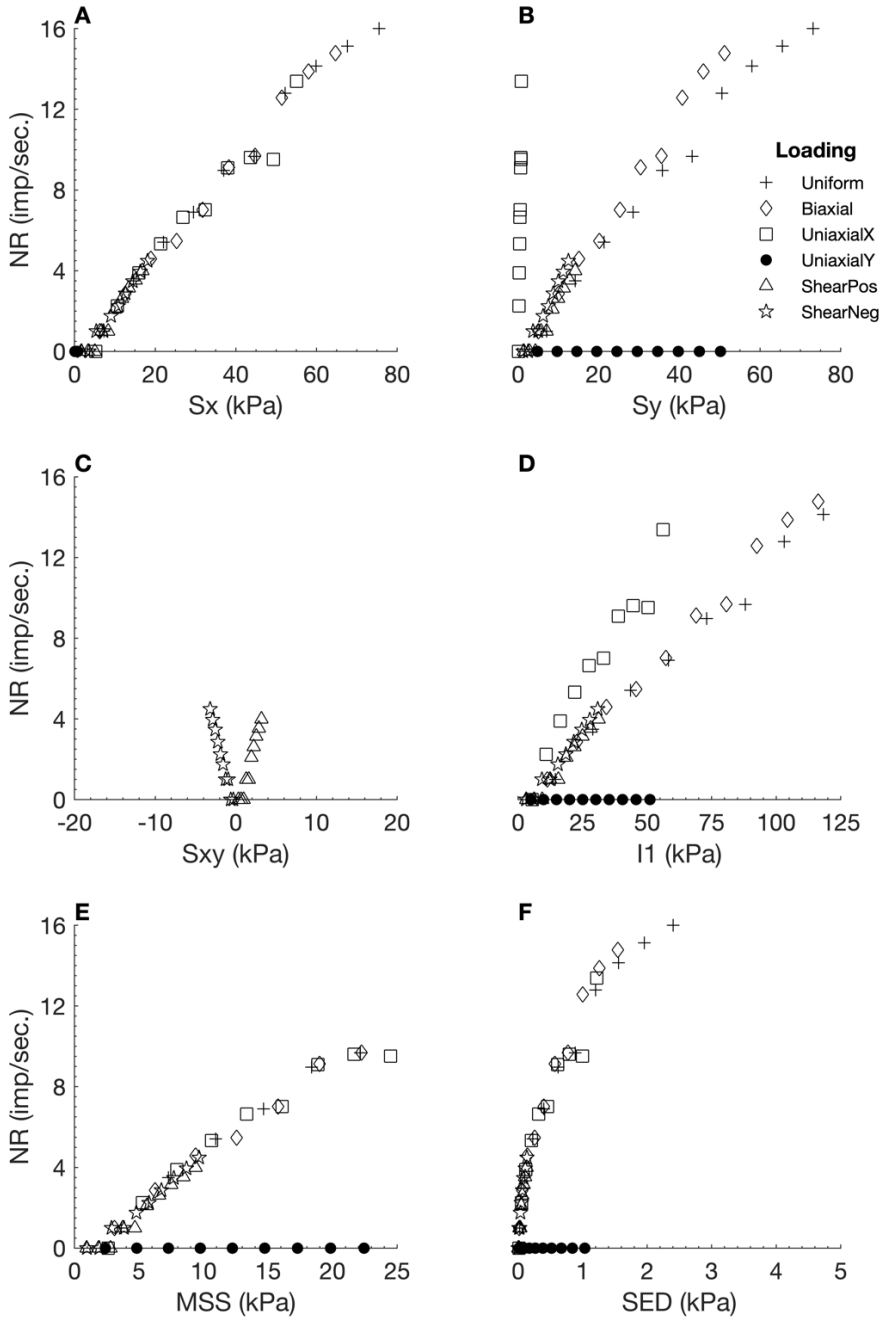

Figure A - 1. Neural responses (NR) output by the isotropic elastic FEBio model using Sx as the neural model input, plotted against six different stress variables. Sx: X stress. Sy: Y stress. Sxy: shear stress. I1: 1st invariant stress tensor. MSS: maximum shear stress. SED: strain energy density.

Table A - 1. Linear regression measures for individual loading regime results from the isotropic elastic model with Sx as neural model input.

Loading Regime	**R^2**	**RMSE**	**Slope**
Uniform	0.9857	0.6524	1.0745
Biaxial	0.4347	2.0246	7.8125
Uniaxial X	0.4794	2.0225	-0.8415
Uniaxial Y	NaN	0.0000	0.0000
Shear Positive	0.6746	0.5411	0.1429
Shear Negative	0.7736	0.4122	0.3976

A.1.2 Y Stress (Sy)

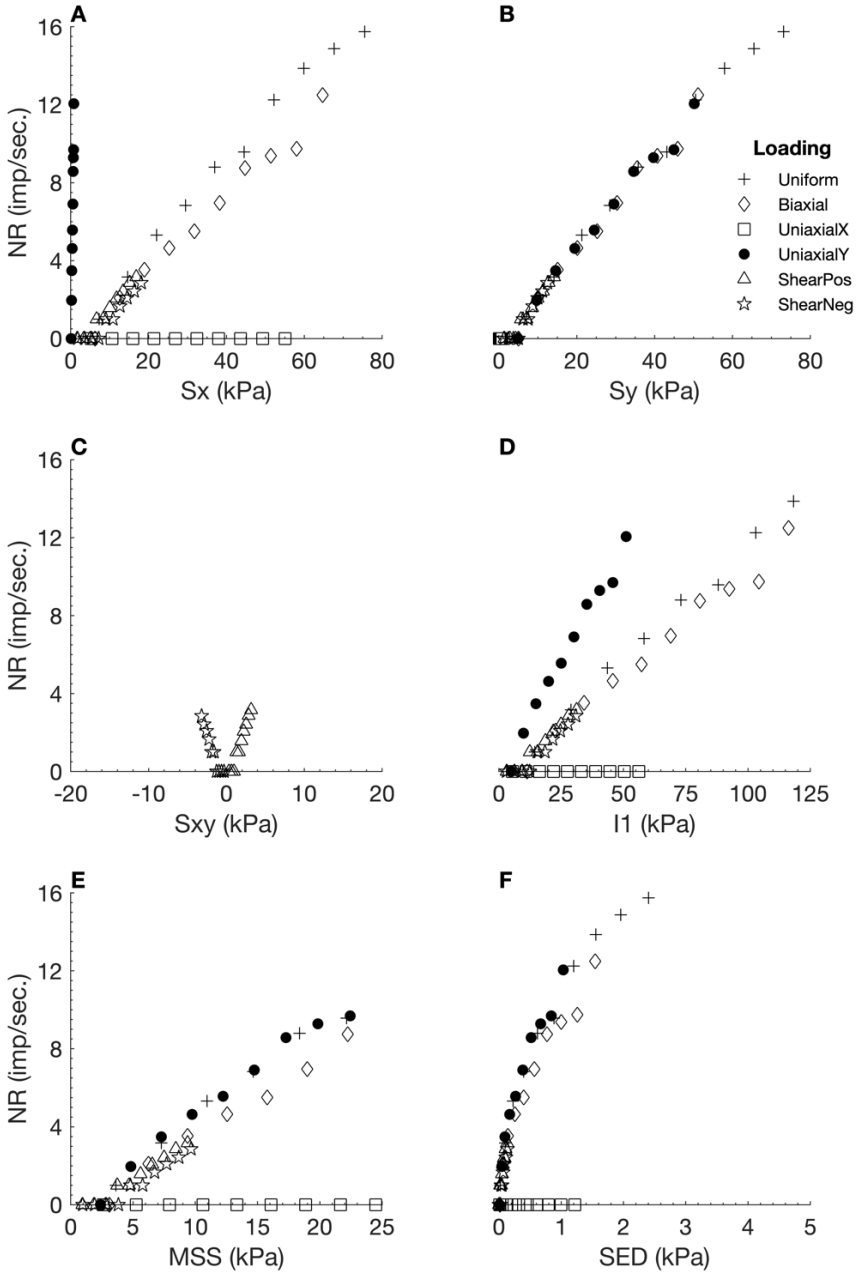

Figure A - 2. Neural responses (NR) output by the isotropic elastic FEBio model using Sy as the neural model input, plotted against six different stress variables. Sx: X stress. Sy: Y stress. Sxy: shear stress. I1: 1st invariant stress tensor. MSS: maximum shear stress. SED: strain energy density.

Table A - 2. Linear regression measures for individual loading regime results from the isotropic elastic model with Sy as neural model input.

Loading Regime	R^2	RMSE	Slope
Uniform	0.9892	0.5590	1.0595
Biaxial	0.4815	1.8109	7.6790
Uniaxial X	NaN	0.0000	0.0000
Uniaxial Y	0.8876	0.9385	1.7822
Shear Positive	0.7143	0.4102	0.1189
Shear Negative	0.2318	0.4526	0.1297

A.1.3 Shear Stress (Sxy)

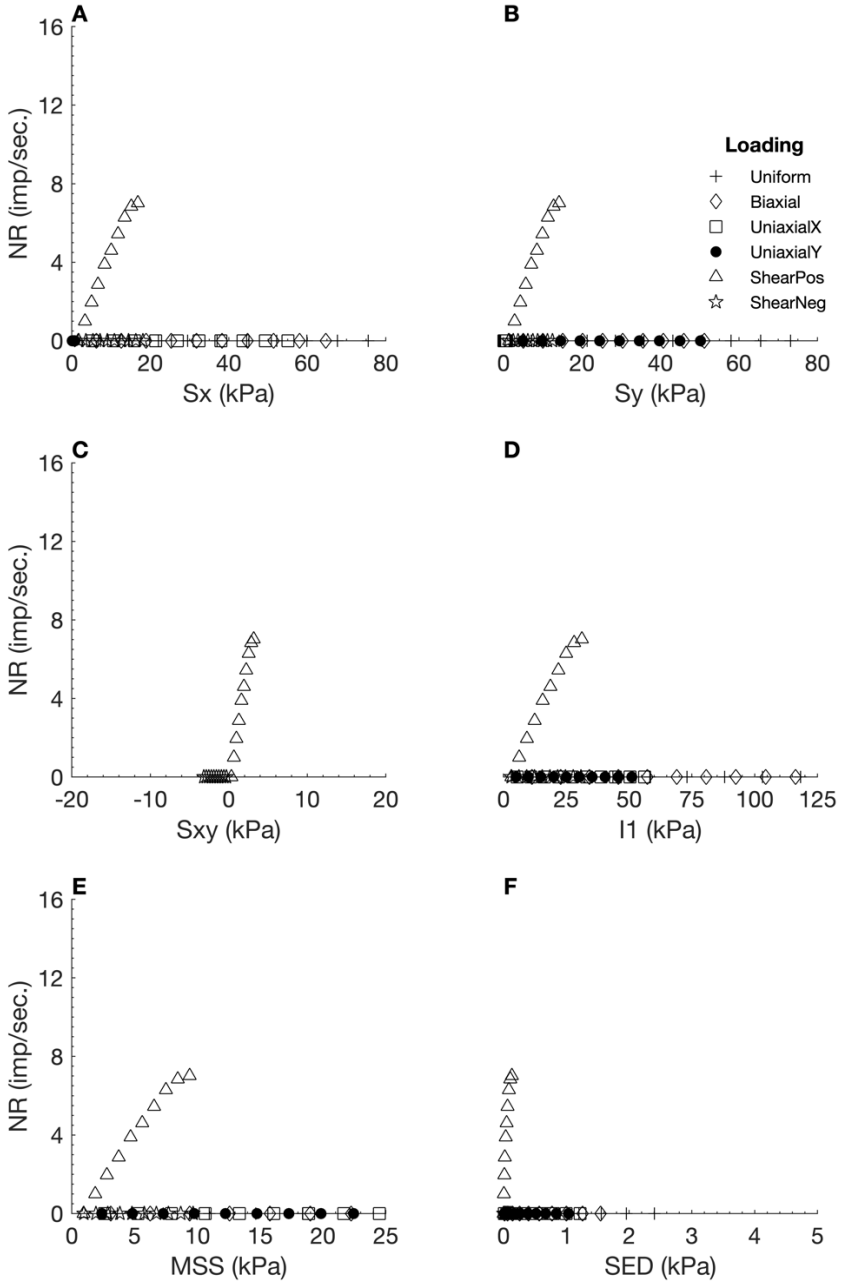

Figure A - 3. Neural responses (NR) output by the isotropic elastic FEBio model using Sxy as the neural model input, plotted against six different stress variables. Sx: X stress. Sy: Y stress. Sxy: shear stress. I1: 1st invariant stress tensor. MSS: maximum shear stress. SED: strain energy density.

Table A - 3. Linear regression measures for individual loading regime results from the isotropic elastic model with Sxy as neural model input.

Loading Regime	R^2	RMSE	Slope
Uniform	NaN	0.0000	0.0000
Biaxial	NaN	0.0000	0.0000
Uniaxial X	NaN	0.0000	0.0000
Uniaxial Y	NaN	0.0000	0.0000
Shear Positive	0.9559	0.4099	0.3499
Shear Negative	NaN	0.0000	0.0000

A.1.4 1st Invariant Stress Tensor (I1)

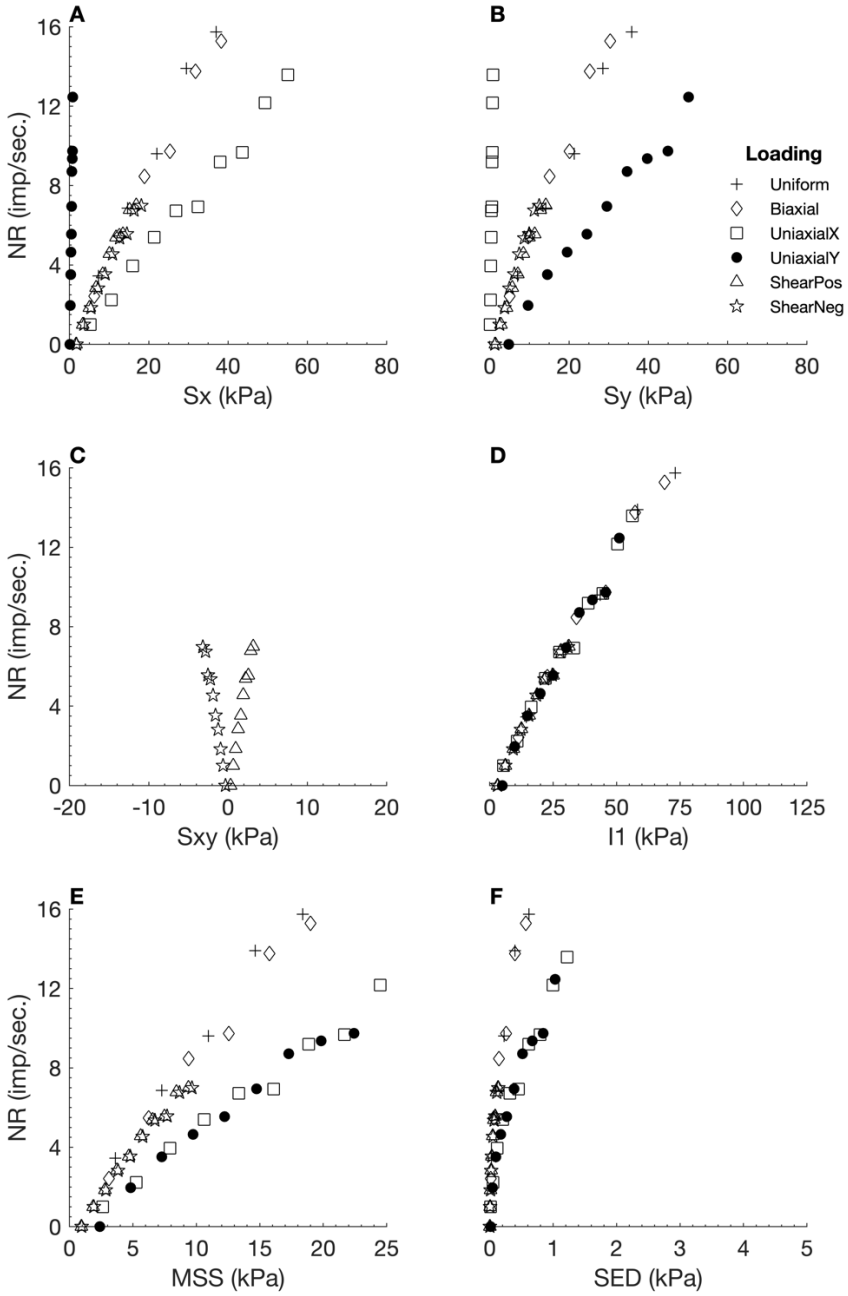

Figure A - 4. Neural responses (NR) output by the isotropic elastic FEBio model using I1 as the neural model input, plotted against six different stress variables. Sx: X stress. Sy: Y stress. Sxy: shear stress. I1: 1st invariant stress tensor. MSS: maximum shear stress. SED: strain energy density.

Table A - 4. Linear regression measures for individual loading regime results from the isotropic elastic model with I1 as neural model input.

Loading Regime	R^2	RMSE	Slope
Uniform	0.9666	1.2325	1.3144
Biaxial	0.3509	3.9951	12.9266
Uniaxial X	0.3333	1.9306	-0.5918
Uniaxial Y	0.8855	0.9505	1.7865
Shear Positive	0.9557	0.3960	0.3373
Shear Negative	0.8970	0.5217	0.8036

A.1.5 Maximum Shear Stress (MSS)

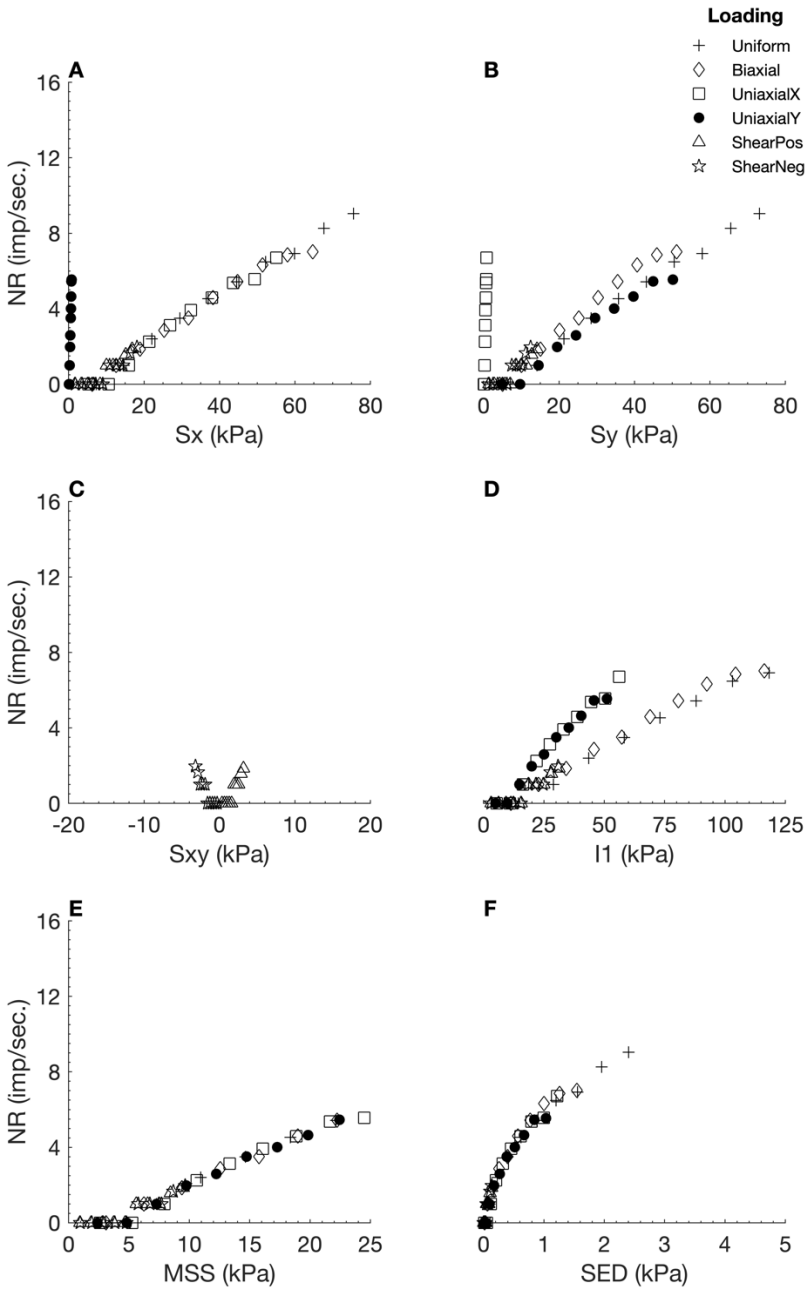

Figure A - 5. Neural responses (NR) output by the isotropic elastic FEBio model using MSS as the neural model input, plotted against six different stress variables. Sx: X stress. Sy: Y stress. Sxy: shear stress. I1: 1st invariant stress tensor. MSS: maximum shear stress. SED: strain energy density.

Table A - 5. Linear regression measures for individual loading regime results from the isotropic elastic model with MSS as neural model input.

Loading Regime	**R^2**	**RMSE**	**Slope**
Uniform	0.9906	0.3112	0.6348
Biaxial	0.4309	1.2260	4.6951
Uniaxial X	0.0886	1.2487	-0.1689
Uniaxial Y	0.9387	0.3950	1.0449
Shear Positive	0.3035	0.3809	0.0461
Shear Negative	NaN	0.0000	0.0000

A.1.6 Strain Energy Density (SED)

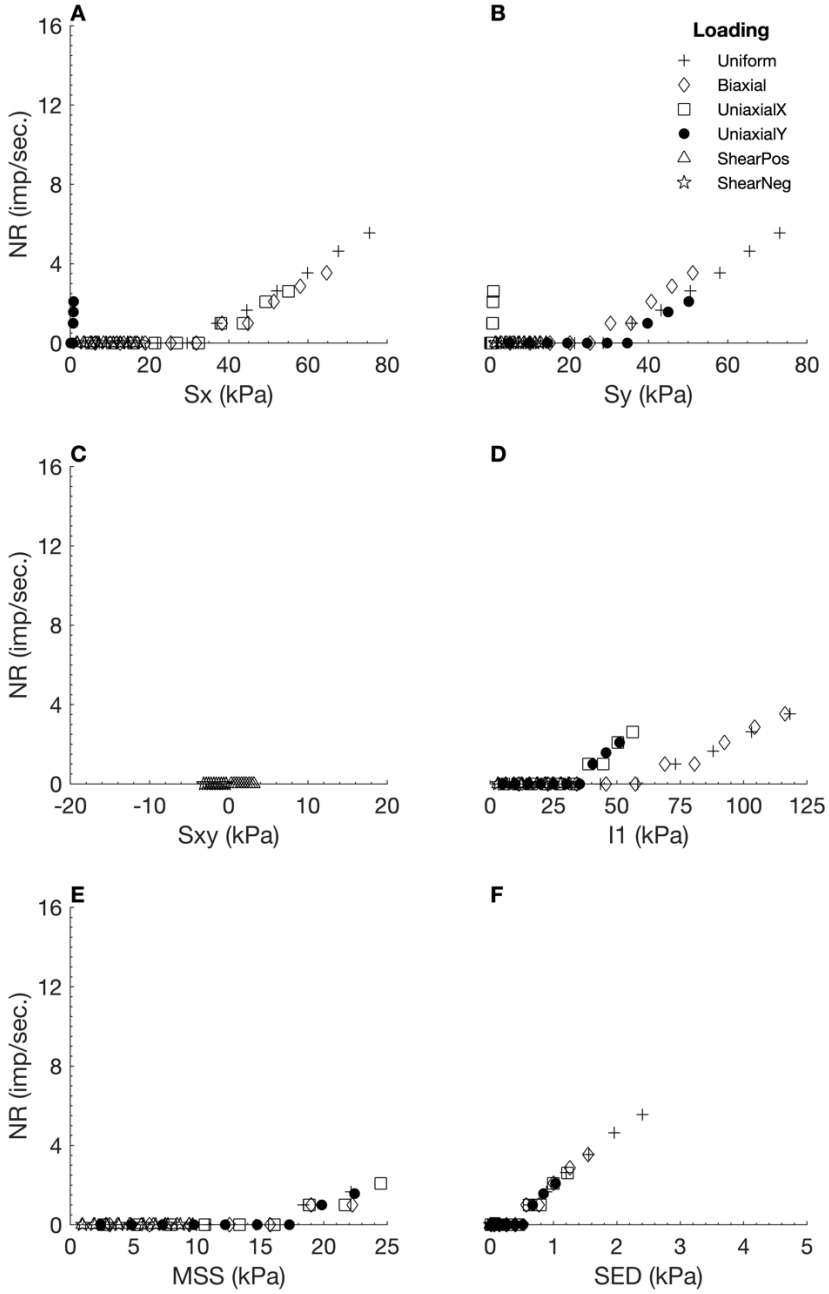

Figure A - 6. Neural responses (NR) output by the isotropic elastic FEBio model using SED as the neural model input, plotted against six different stress variables. Sx: X stress. Sy: Y stress. Sxy: shear stress. I1: 1st invariant stress tensor. MSS: maximum shear stress. SED: strain energy density.

Table A - 6. Linear regression measures for individual loading regime results from the isotropic elastic model with SED as neural model input.

Loading Regime	R^2	RMSE	Slope
Uniform	0.8488	0.8623	0.4052
Biaxial	NaN	0.0000	0.0000
Uniaxial X	NaN	0.0000	0.0000
Uniaxial Y	NaN	0.0000	0.0000
Shear Positive	NaN	0.0000	0.0000
Shear Negative	NaN	0.0000	0.0000

A.1.7 Hydrostatic Pressure (HS)

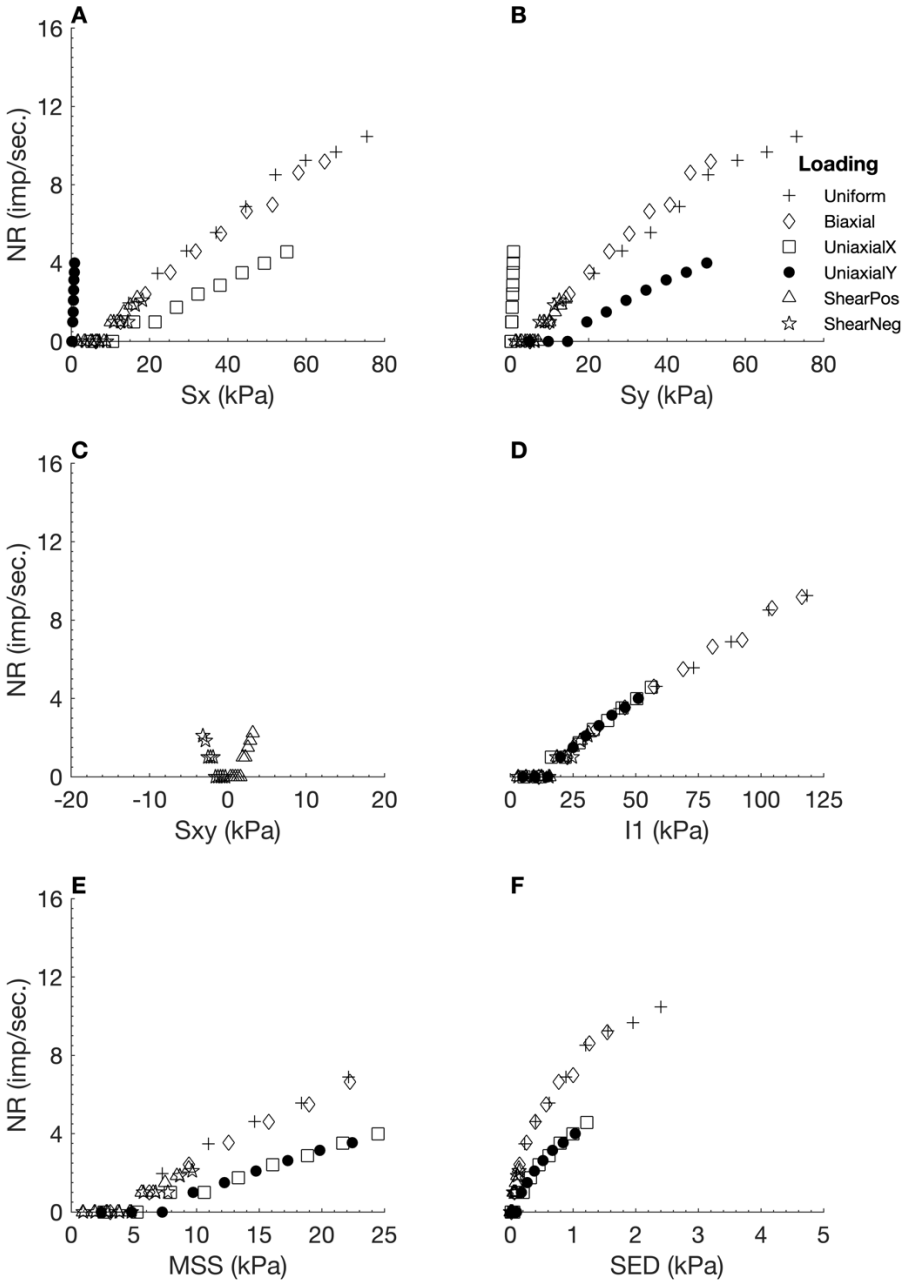

Figure A - 7. Neural responses (NR) output by the isotropic elastic FEBio model using HS as the neural model input, plotted against six different stress variables. Sx: X stress. Sy: Y stress. Sxy: shear stress. I1: 1st invariant stress tensor. MSS: maximum shear stress. SED: strain energy density.

Table A - 7. Linear regression measures for individual loading regime results from the isotropic elastic model with HS as neural model input.

Loading Regime	R^2	RMSE	Slope
Uniform	0.9904	0.3666	0.7383
Biaxial	0.4386	1.6083	6.2559
Uniaxial X	0.2082	0.6292	-0.1399
Uniaxial Y	0.9677	0.1826	0.6750
Shear Positive	0.3035	0.3809	0.0461
Shear Negative	NaN	0.0000	0.0000

A.1.8 1st Principle Stress (S1)

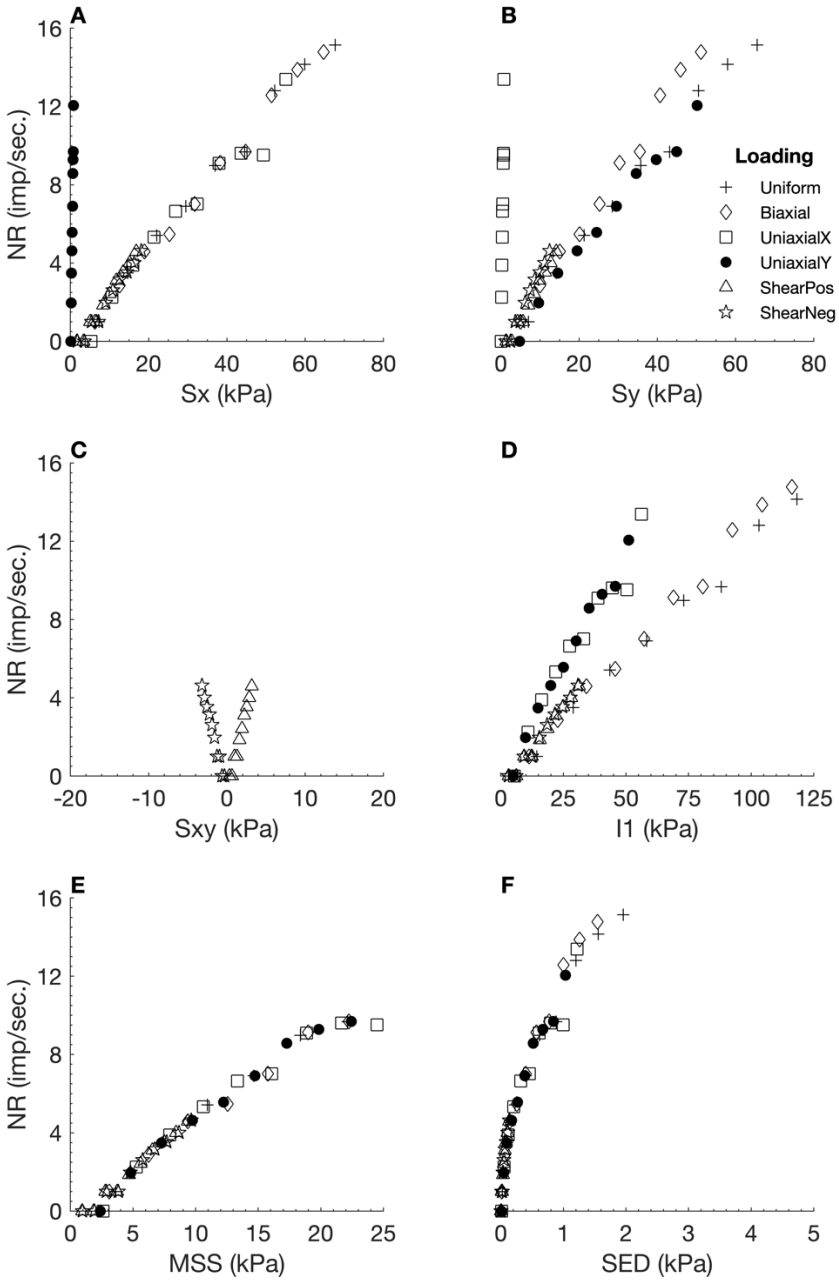

Figure A - 8. Neural responses (NR) output by the isotropic elastic FEBio model using S1 as the neural model input, plotted against six different stress variables. Sx: X stress. Sy: Y stress. Sxy: shear stress. I1: 1st invariant stress tensor. MSS: maximum shear stress. SED: strain energy density.

Table A - 8. Linear regression measures for individual loading regime results from the isotropic elastic model with S1 as neural model input.

Loading Regime	R^2	RMSE	Slope
Uniform	0.9856	0.6542	1.0752
Biaxial	0.4346	2.0244	7.8104
Uniaxial X	0.4795	2.0223	-0.8416
Uniaxial Y	0.8876	0.9386	1.7822
Shear Positive	0.8402	0.4353	0.1831
Shear Negative	0.7331	0.4926	0.4259

A.1.9 2nd Principle Stress (S2)

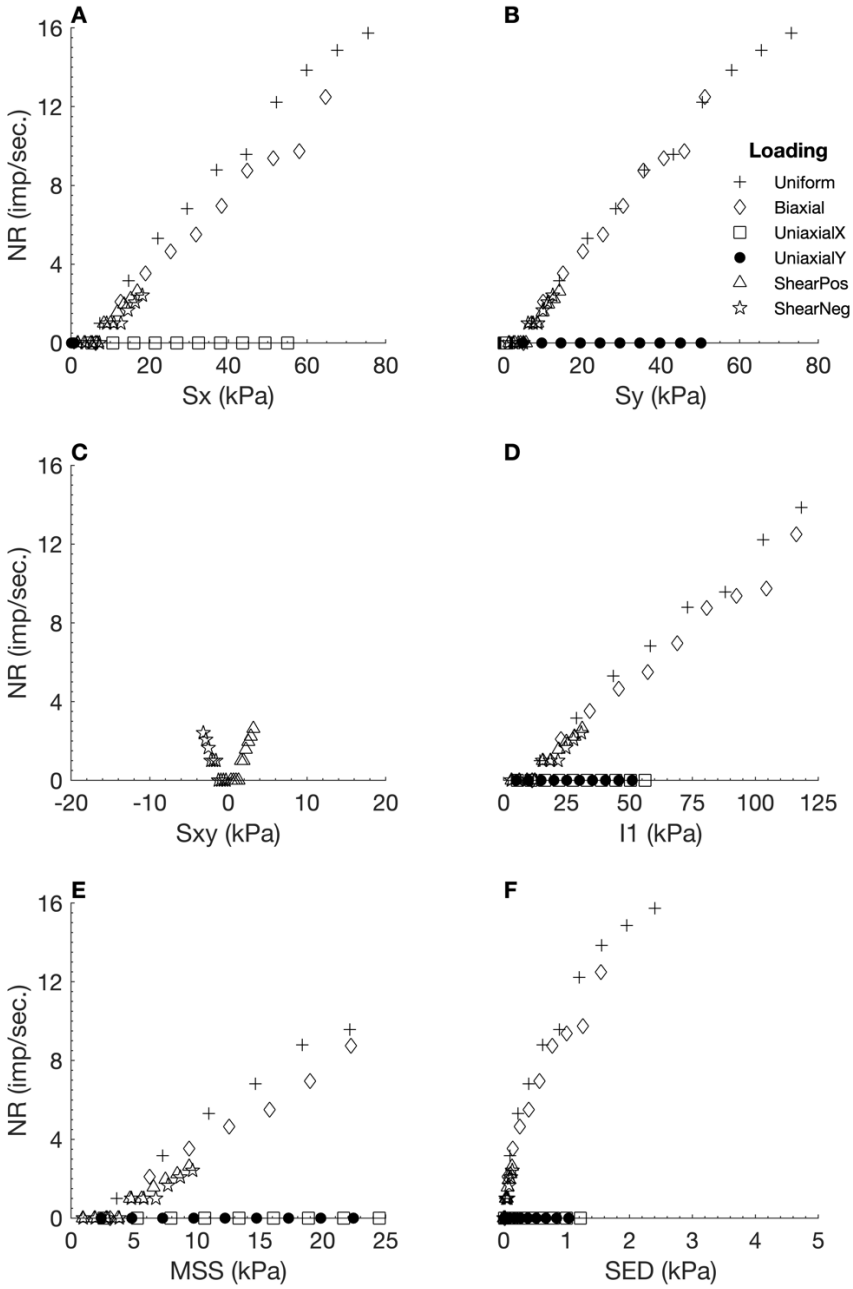

Figure A - 9. Neural responses (NR) output by the isotropic elastic FEBio model using S2 as the neural model input, plotted against six different stress variables. Sx: X stress. Sy: Y stress. Sxy: shear stress. I1: 1st invariant stress tensor. MSS: maximum shear stress. SED: strain energy density.

Table A - 9. Linear regression measures for individual loading regime results from the isotropic elastic model with S2 as neural model input.

Loading Regime	R^2	RMSE	Slope
Uniform	0.9892	0.5578	1.0586
Biaxial	0.4813	1.8115	7.6785
Uniaxial X	NaN	0.0000	0.0000
Uniaxial Y	NaN	0.0000	0.0000
Shear Positive	0.5096	0.4043	0.0756
Shear Negative	0.2318	0.4526	0.1297

A.1.10 3rd Principle Stress (S3)

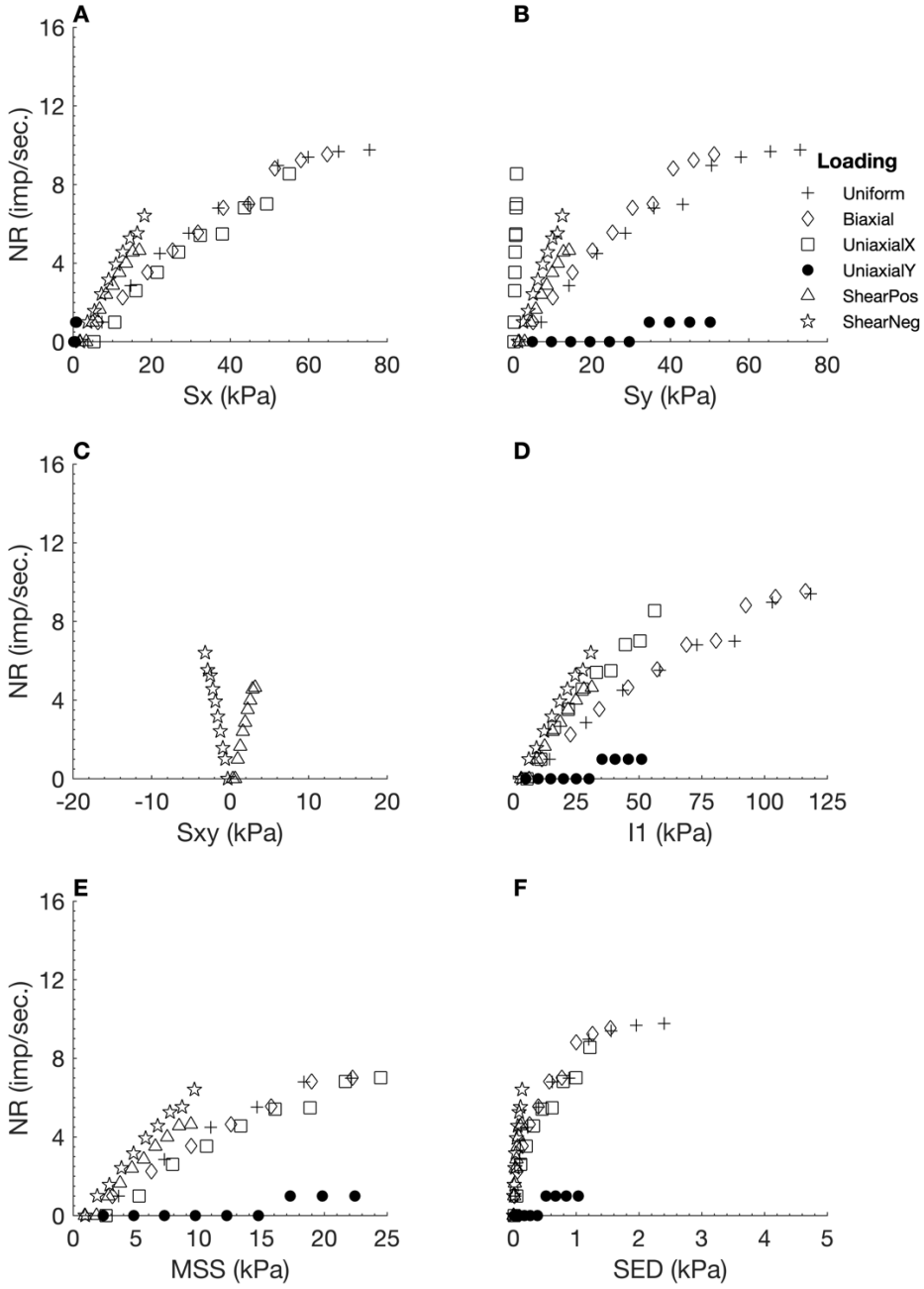

Figure A - 10. Neural responses (NR) output by the isotropic elastic FEBio model using S3 as the neural model input, plotted against six different stress variables. Sx: X stress. Sy: Y stress. Sxy: shear stress. I1: 1st invariant stress tensor. MSS: maximum shear stress. SED: strain energy density.

Table A - 10. Linear regression measures for individual loading regime results from the isotropic elastic model with S3 as neural model input.

Loading Regime	R^2	RMSE	Slope
Uniform	0.9673	0.5867	0.6324
Biaxial	0.4512	1.5618	6.2315
Uniaxial X	0.3574	1.5553	-0.5030
Uniaxial Y	NaN	0.0000	0.0000
Shear Positive	0.8701	0.4861	0.2308
Shear Negative	0.8855	0.4791	0.6953

A.1.11 Deviatoric Stress 1 (Dev1)

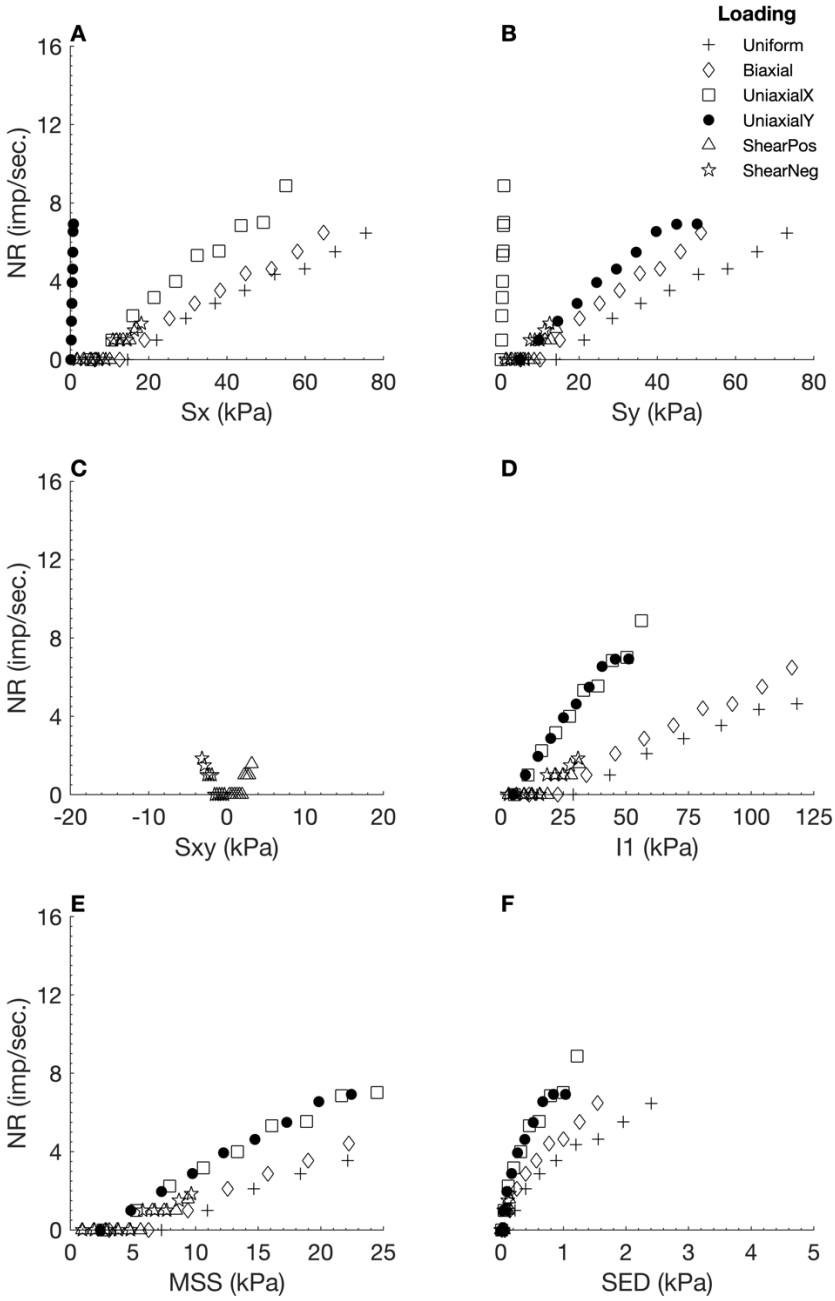

Figure A - 11. Neural responses (NR) output by the isotropic elastic FEBio model using Dev1 as the neural model input, plotted against six different stress variables. Sx: X stress. Sy: Y stress. Sxy: shear stress. I1: 1st invariant stress tensor. MSS: maximum shear stress. SED: strain energy density.

Table A - 11. Linear regression measures for individual loading regime results from the isotropic elastic model with Dev1 as neural model input.

Loading Regime	R^2	RMSE	Slope
Uniform	0.9776	0.3583	0.4698
Biaxial	0.3652	1.1738	3.9184
Uniaxial X	0.3760	1.3447	-0.4526
Uniaxial Y	0.9375	0.4915	1.2861
Shear Positive	NaN	0.0000	0.0000
Shear Negative	NaN	0.0000	0.0000

A.1.12 Deviatoric Stress 2 (Dev2)

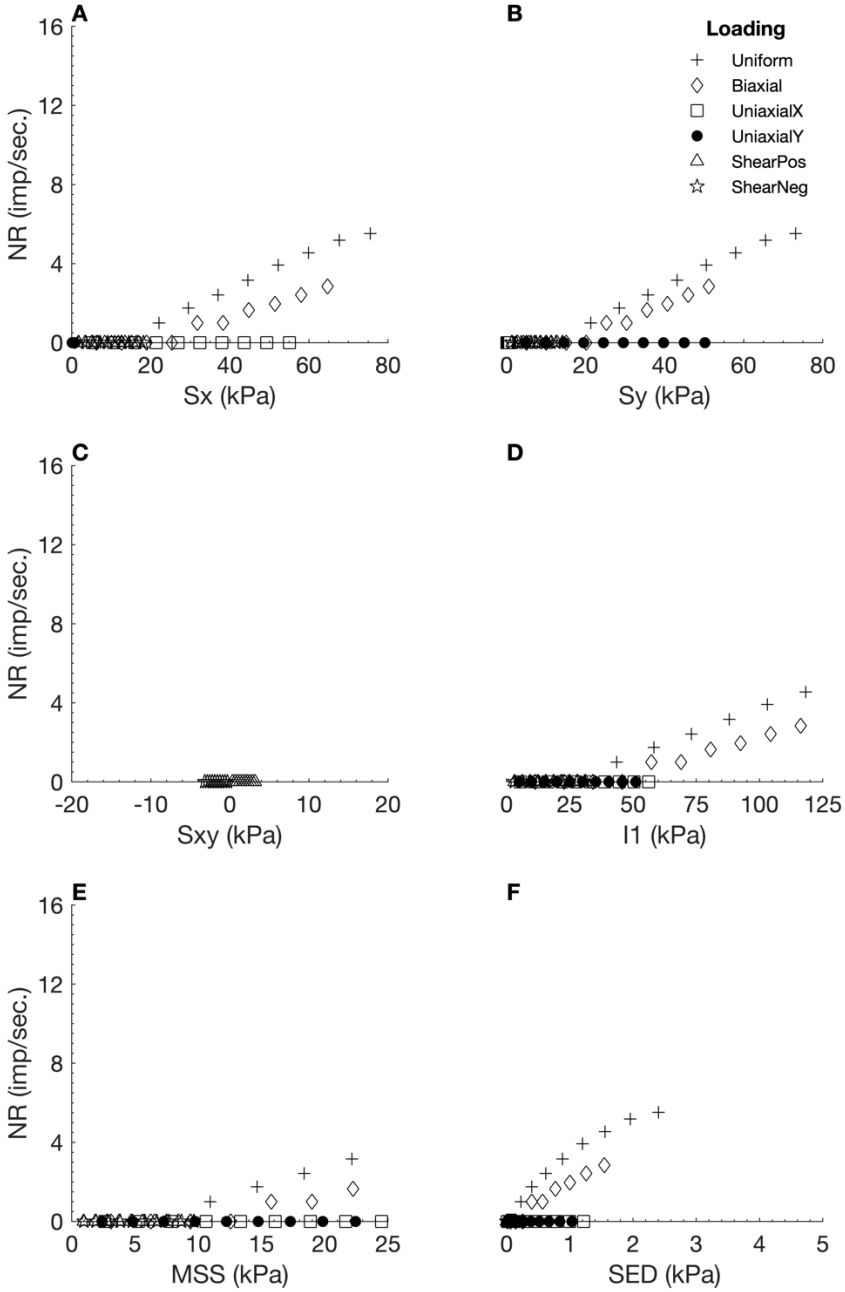

Figure A - 12. Neural responses (NR) output by the isotropic elastic FEBio model using Dev2 as the neural model input, plotted against six different stress variables. Sx: X stress. Sy: Y stress. Sxy: shear stress. I1: 1st invariant stress tensor. MSS: maximum shear stress. SED: strain energy density.

Table A - 12. Linear regression measures for individual loading regime results from the isotropic elastic model with Dev2 as neural model input.

Loading Regime	R^2	RMSE	Slope
Uniform	0.9893	0.2242	0.4281
Biaxial	0.0001	0.5164	-0.0233
Uniaxial X	NaN	0.0000	0.0000
Uniaxial Y	NaN	0.0000	0.0000
Shear Positive	NaN	0.0000	0.0000
Shear Negative	NaN	0.0000	0.0000

A.1.13 Deviatoric Stress 3 (Dev3)

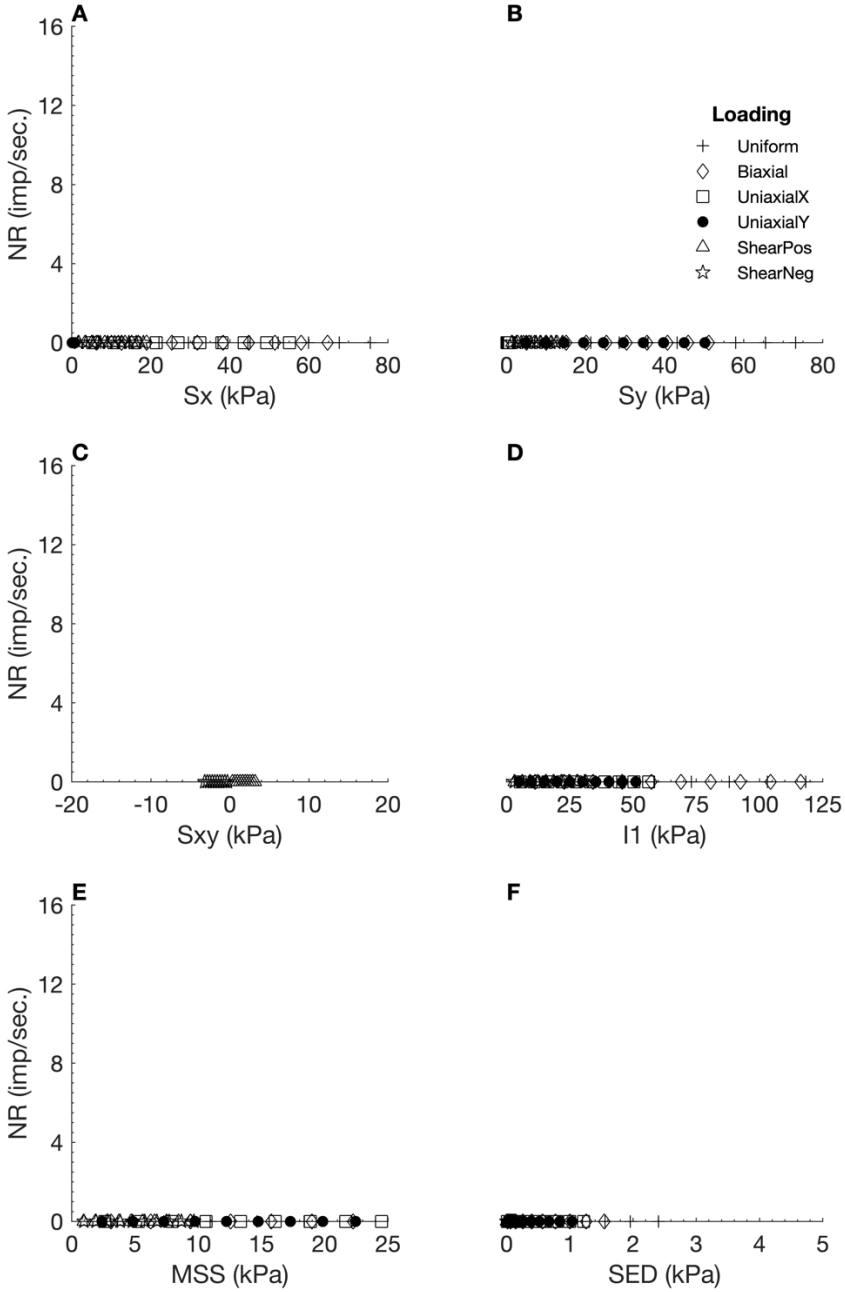

Figure A - 13. Neural responses (NR) output by the isotropic elastic FEBio model using Dev3 as the neural model input, plotted against six different stress variables. Sx: X stress. Sy: Y stress. Sxy: shear stress. I1: 1st invariant stress tensor. MSS: maximum shear stress. SED: strain energy density.

Table A - 13. Linear regression measures for individual loading regime results from the isotropic elastic model with Dev3 as neural model input.

Loading Regime	R^2	RMSE	Slope
Uniform	NaN	0.0000	0.0000
Biaxial	NaN	0.0000	0.0000
Uniaxial X	NaN	0.0000	0.0000
Uniaxial Y	NaN	0.0000	0.0000
Shear Positive	NaN	0.0000	0.0000
Shear Negative	NaN	0.0000	0.0000

A.1.14 Shear Stress A

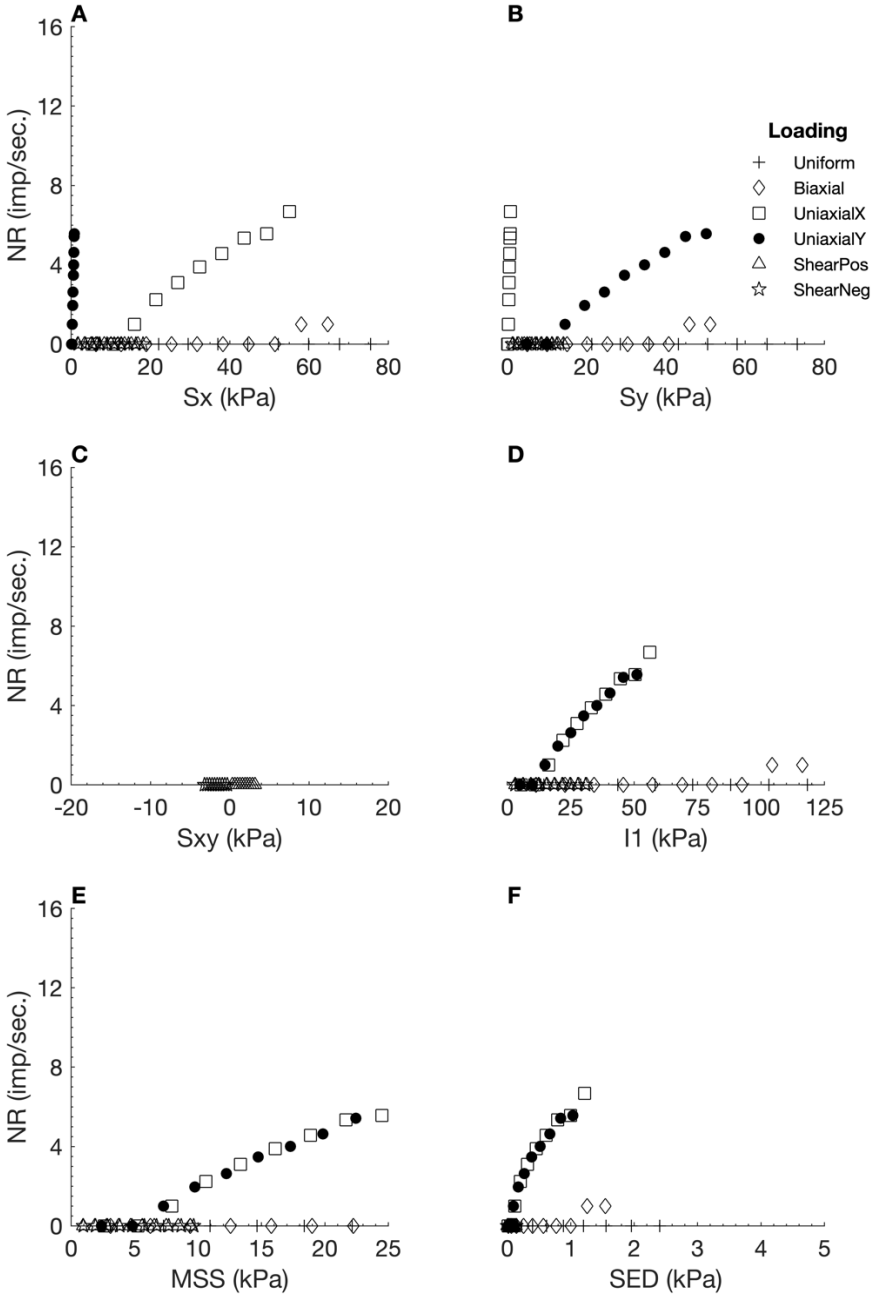

Figure A - 14. Neural responses (NR) output by the isotropic elastic FEBio model using ShearA as the neural model input, plotted against six different stress variables. Sx: X stress. Sy: Y stress. Sxy: shear stress. I1: 1st invariant stress tensor. MSS: maximum shear stress. SED: strain energy density.

Table A - 14. Linear regression measures for individual loading regime results from the isotropic elastic model with ShearA as neural model input.

Loading Regime	**R^2**	**RMSE**	**Slope**
Uniform	NaN	0.0000	0.0000
Biaxial	NaN	0.0000	0.0000
Uniaxial X	0.0889	1.2456	-0.1687
Uniaxial Y	0.9395	0.3915	1.0425
Shear Positive	NaN	0.0000	0.0000
Shear Negative	NaN	0.0000	0.0000

A.1.15 Shear Stress B

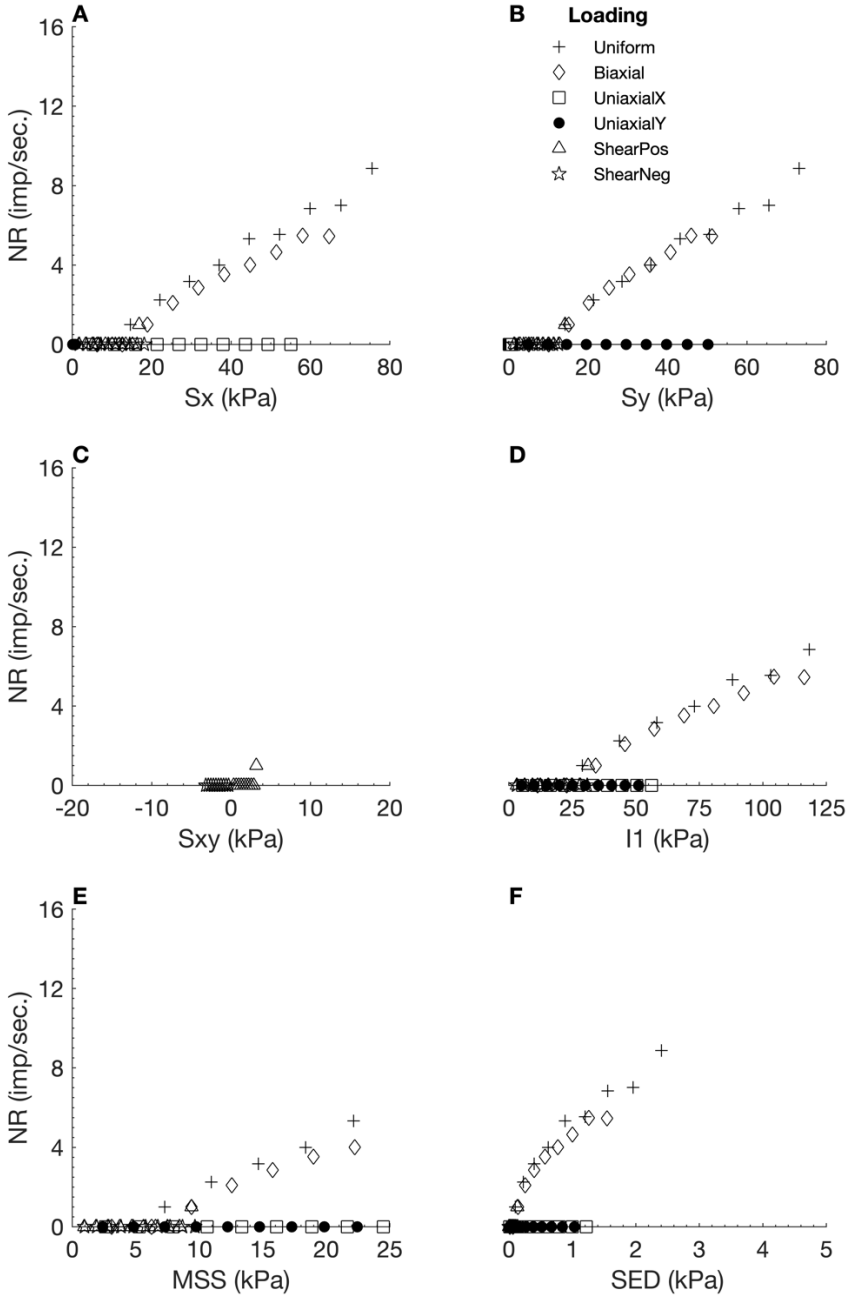

Figure A - 15. Neural responses (NR) output by the isotropic elastic FEBio model using ShearB as the neural model input, plotted against six different stress variables. Sx: X stress. Sy: Y stress. Sxy: shear stress. I1: 1st invariant stress tensor. MSS: maximum shear stress. SED: strain energy density.

Table A - 15. Linear regression measures for individual loading regime results from the isotropic elastic model with ShearB as neural model input.

Loading Regime	R^2	RMSE	Slope
Uniform	0.9785	0.4403	0.5896
Biaxial	0.3661	1.1680	3.9058
Uniaxial X	NaN	0.0000	0.0000
Uniaxial Y	NaN	0.0000	0.0000
Shear Positive	NaN	0.0000	0.0000
Shear Negative	NaN	0.0000	0.0000

A.1.16 Shear Stress C

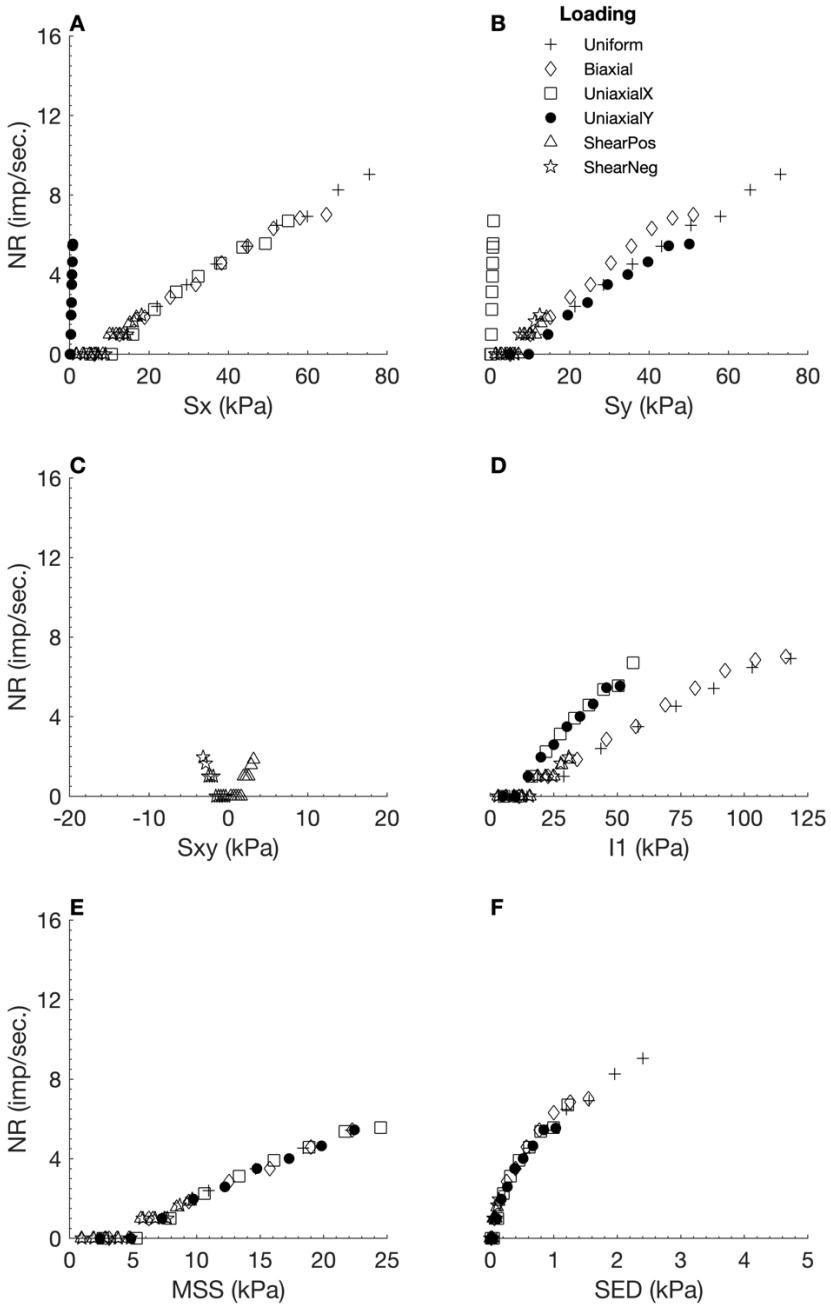

Figure A - 16. Neural responses (NR) output by the isotropic elastic FEBio model using ShearC as the neural model input, plotted against six different stress variables. Sx: X stress. Sy: Y stress. Sxy: shear stress. I1: 1st invariant stress tensor. MSS: maximum shear stress. SED: strain energy density.

Table A - 16. Linear regression measures for individual loading regime results from the isotropic elastic model with ShearC as neural model input.

Loading Regime	R^2	RMSE	Slope
Uniform	0.9906	0.3112	0.6348
Biaxial	0.4309	1.2260	4.6951
Uniaxial X	0.0886	1.2487	-0.1689
Uniaxial Y	0.9387	0.3950	1.0449
Shear Positive	0.3035	0.3809	0.0461
Shear Negative	NaN	0.0000	0.0000

A.1.17 X Strain (Ex)

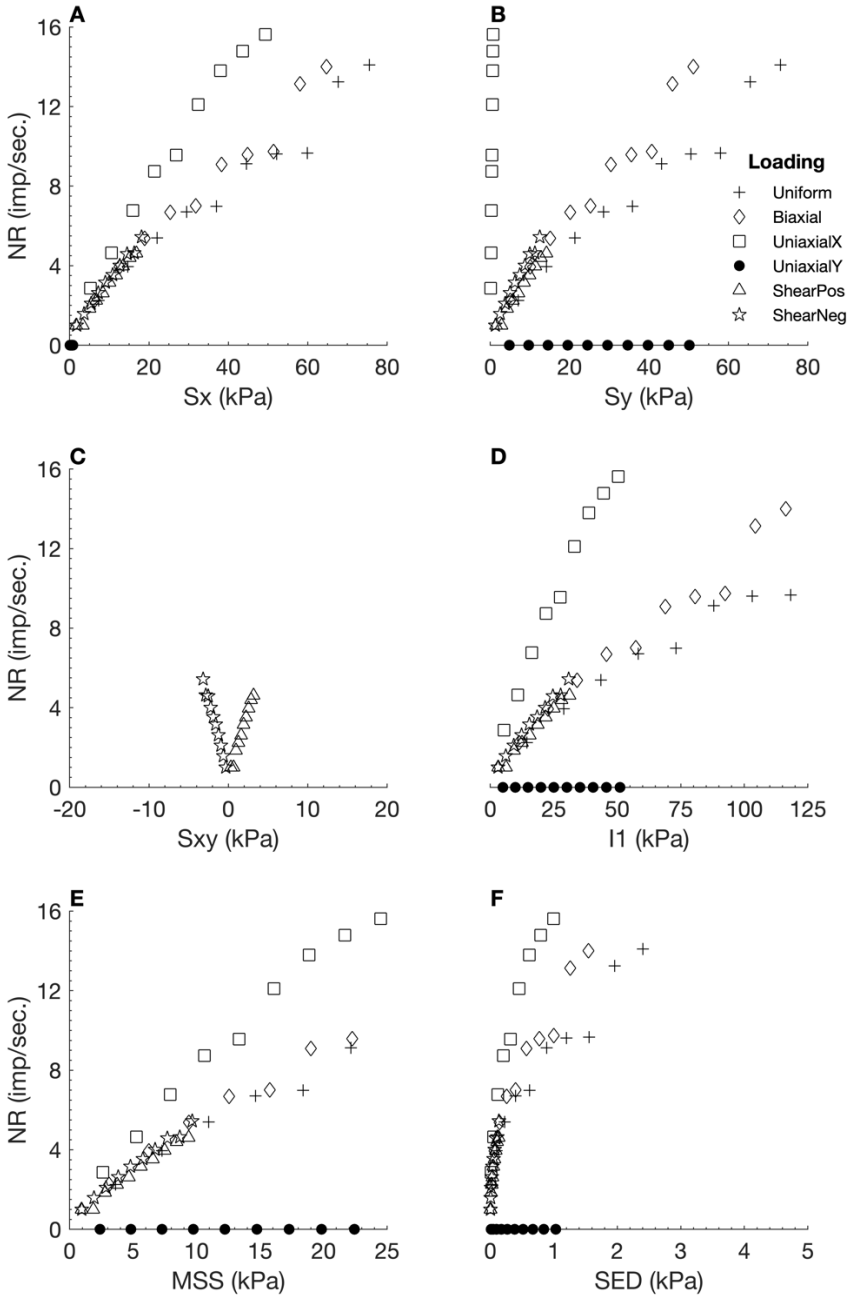

Figure A - 17. Neural responses (NR) output by the isotropic elastic FEBio model using Ex as the neural model input, plotted against six different stress variables. Sx: X stress. Sy: Y stress. Sxy: shear stress. I1: 1st invariant stress tensor. MSS: maximum shear stress. SED: strain energy density.

Table A - 17. Linear regression measures for individual loading regime results from the isotropic elastic model with Ex as neural model input.

Loading Regime	R^2	RMSE	Slope
Uniform	0.9475	0.9243	0.7786
Biaxial	0.5449	1.5433	7.4316
Uniaxial X	0.3492	2.5178	-0.7997
Uniaxial Y	NaN	0.0000	0.0000
Shear Positive	0.8828	0.3338	0.1680
Shear Negative	0.8868	0.3304	0.4825

A.1.18 Y Strain (Ey)

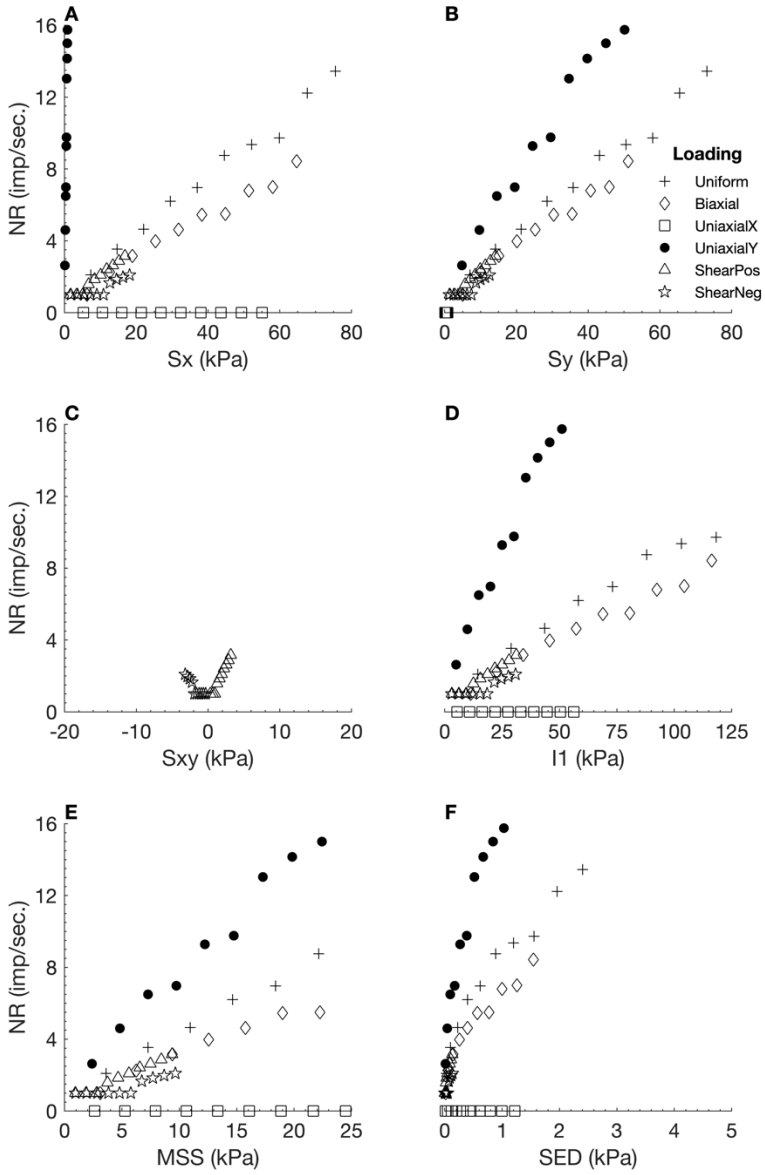

Figure A - 18. Neural responses (NR) output by the isotropic elastic FEBio model using Ey as the neural model input, plotted against six different stress variables. Sx: X stress. Sy: Y stress. Sxy: shear stress. I1: 1st invariant stress tensor. MSS: maximum shear stress. SED: strain energy density.

Appendix B: Orthotropic Elastic Material Results

B.1 Test 1

Table B - 1. Values selected for material properties during FEBio implementation of orthotropic elastic material test 1.

Orthotropic Material Property	Value Selected
Density	1
Young's Modulus (X)	2.6
Young's Modulus (Y)	1
Young's Modulus (Z)	1
Shear Modulus (XY)	0.9
Shear Modulus (YZ)	0.345
Shear Modulus (XZ)	0.345
Poisson's Ratio (XY)	0.45
Poisson's Ratio (YZ)	0.45
Poisson's Ratio (XZ)	0.45

Table B - 2. Linear regression measures for total plot results (i.e. considering all loading regimes combined), for each input stimulus tested with the orthotropic elastic model 1.

Input Stimuli	R^2	RMSE	Slope
X Stress (Sx)	0.1650	4.3936	0.4315
Y Stress (Sy)	0.2862	4.0749	0.5699
Shear Stress (Sxy)	0.0795	1.3171	0.0855
1st Invariant Stress Tensor (I1)	0.2545	5.8150	0.7506
Maximum Shear Stress (MSS)	0.2495	2.2739	0.2896
Strain Energy Density (SED)	0.1747	1.2610	0.1282
Hydrostatic Pressure (HS)	0.2305	2.9756	0.3597
1st Principal Stress (S1)	0.2533	3.9731	0.5112
2nd Principal Stress (S2)	0.2054	4.3724	0.4910
3rd Principal Stress (S3)	0.2178	6.4738	0.7546
Deviatoric Stress 1 (Dev1)	0.1894	1.7983	0.1920
Deviatoric Stress 2 (Dev2)	0.1639	1.3866	0.1356
Deviatoric Stress 3 (Dev3)	NaN	0.0000	0.0000
Shear A	0.0002	0.8184	-0.0024
Shear B	0.1908	2.2294	0.2392
Shear C	0.2495	2.2739	0.2896
X Strain (Ex)	0.0802	1.8441	0.1203
Y Strain (Ey)	0.3536	4.0991	0.6696
Average	**0.1967**	**2.8545**	**0.3342**

B.1.1 X Stress (Sx)

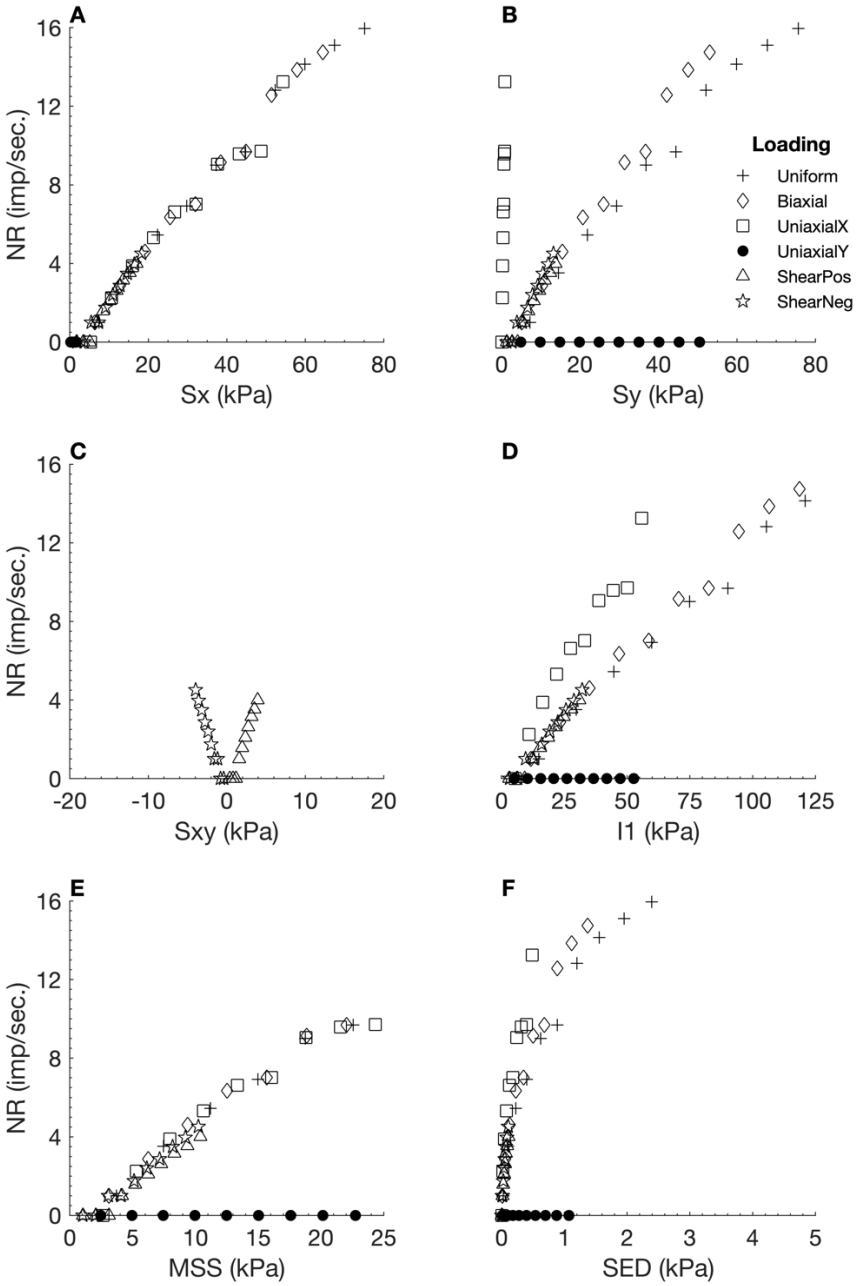

Figure B - 1. Neural responses (NR) output by the orthotropic elastic FEBio model 1 using Sx as the neural model input, plotted against six different stress variables. Sx: X stress. Sy: Y stress. Sxy: shear stress. I1: 1st invariant stress tensor. MSS: maximum shear stress. SED: strain energy density.

Table B - 3. Linear regression measures for individual loading regime results from the orthotropic elastic model 1, with Sx as neural model input.

Loading Regime	R^2	RMSE	Slope
Uniform	0.9855	0.6552	1.0716
Biaxial	0.5056	2.0135	8.9605
Uniaxial X	0.4805	2.0151	-0.8404
Uniaxial Y	NaN	0.0000	0.0000
Shear Positive	0.7165	0.5491	0.1601
Shear Negative	0.7737	0.4120	0.3975

B.1.2 Y Stress (Sy)

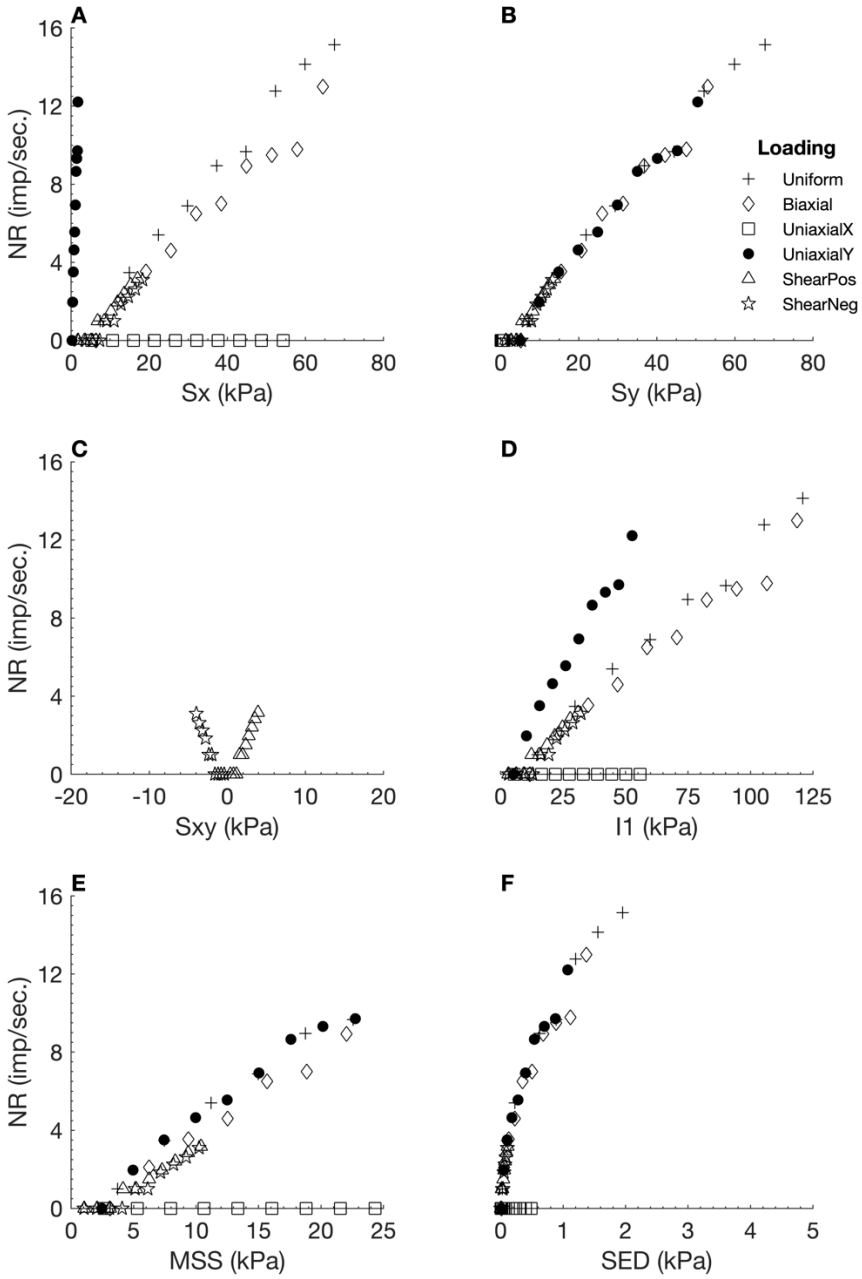

Figure B - 2. Neural responses (NR) output by the orthotropic elastic FEBio model 1 using Sy as the neural model input, plotted against six different stress variables. Sx: X stress. Sy: Y stress. Sxy: shear stress. I1: 1st invariant stress tensor. MSS: maximum shear stress. SED: strain energy density.

Table B - 4. Linear regression measures for individual loading regime results from the orthotropic elastic model 1, with Sy as neural model input.

Loading Regime	R^2	RMSE	Slope
Uniform	0.9858	0.6501	1.0759
Biaxial	0.3680	2.2632	7.5998
Uniaxial X	NaN	0.0000	0.0000
Uniaxial Y	0.8857	0.9489	1.7847
Shear Positive	0.7167	0.3956	0.1154
Shear Negative	0.2318	0.4526	0.1297

B.1.3 Shear Stress (Sxy)

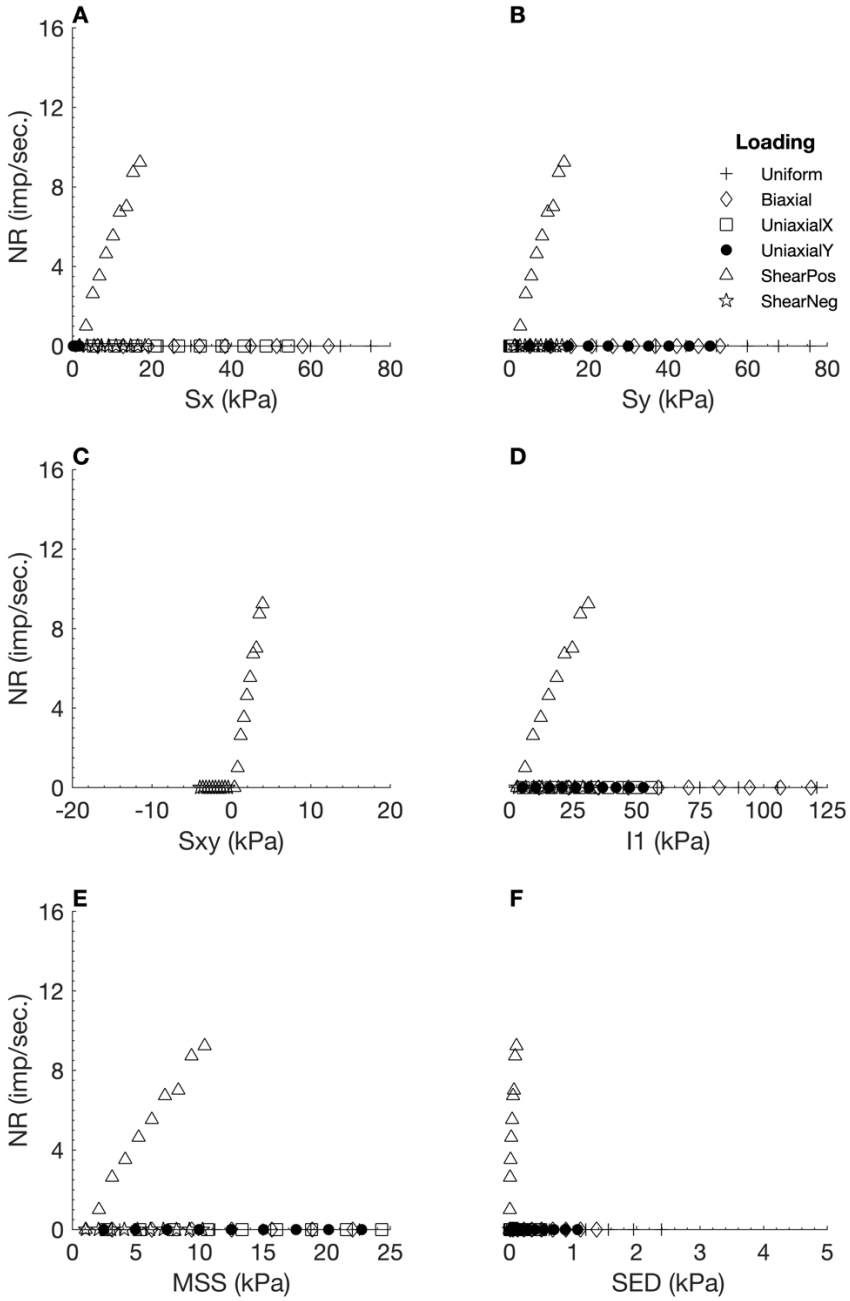

Figure B - 3. Neural responses (NR) output by the orthotropic elastic FEBio model 1 using Sxy as the neural model input, plotted against six different stress variables. Sx: X stress. Sy: Y stress. Sxy: shear stress. I1: 1st invariant stress tensor. MSS: maximum shear stress. SED: strain energy density.

Table B - 5. Linear regression measures for individual loading regime results from the orthotropic elastic model 1, with Sxy as neural model input.

Loading Regime	R^2	RMSE	Slope
Uniform	NaN	0.0000	0.0000
Biaxial	NaN	0.0000	0.0000
Uniaxial X	NaN	0.0000	0.0000
Uniaxial Y	NaN	0.0000	0.0000
Shear Positive	0.9593	0.4775	0.4254
Shear Negative	NaN	0.0000	0.0000

B.1.4 1st Invariant Stress Tensor (I1)

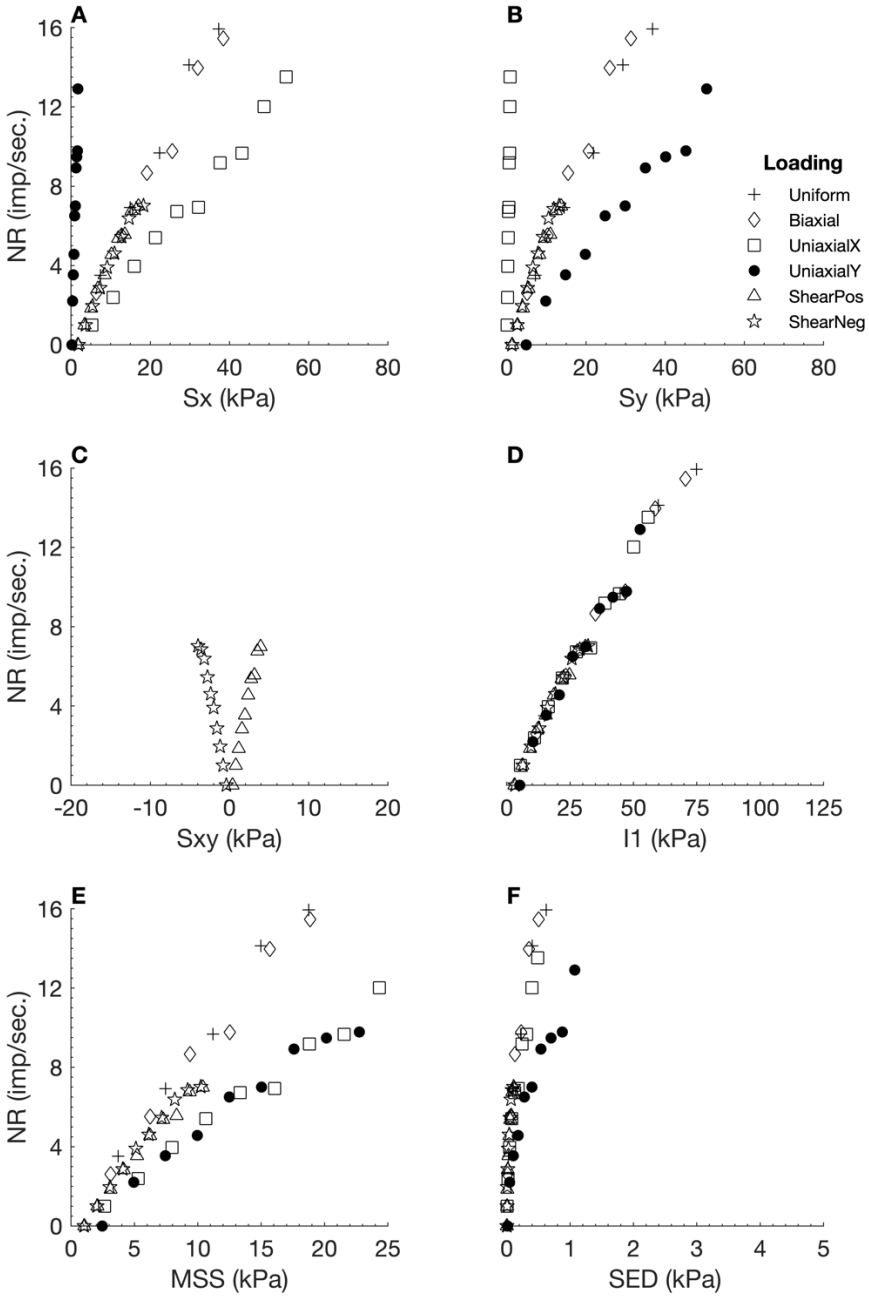

Figure B - 4. Neural responses (NR) output by the orthotropic elastic FEBio model 1 using I1 as the neural model input, plotted against six different stress variables. Sx: X stress. Sy: Y stress. Sxy: shear stress. I1: 1st invariant stress tensor. MSS: maximum shear stress. SED: strain energy density.

Table B - 6. Linear regression measures for individual loading regime results from the orthotropic elastic model 1, with I1 as neural model input.

Loading Regime	R^2	RMSE	Slope
Uniform	0.9655	1.2645	1.3277
Biaxial	0.3492	4.0153	12.9428
Uniaxial X	0.3637	1.8660	-0.6117
Uniaxial Y	0.8982	0.9449	1.8964
Shear Positive	0.9558	0.3944	0.3364
Shear Negative	0.8798	0.6130	0.8653

B.1.5 Maximum Shear Stress (MSS)

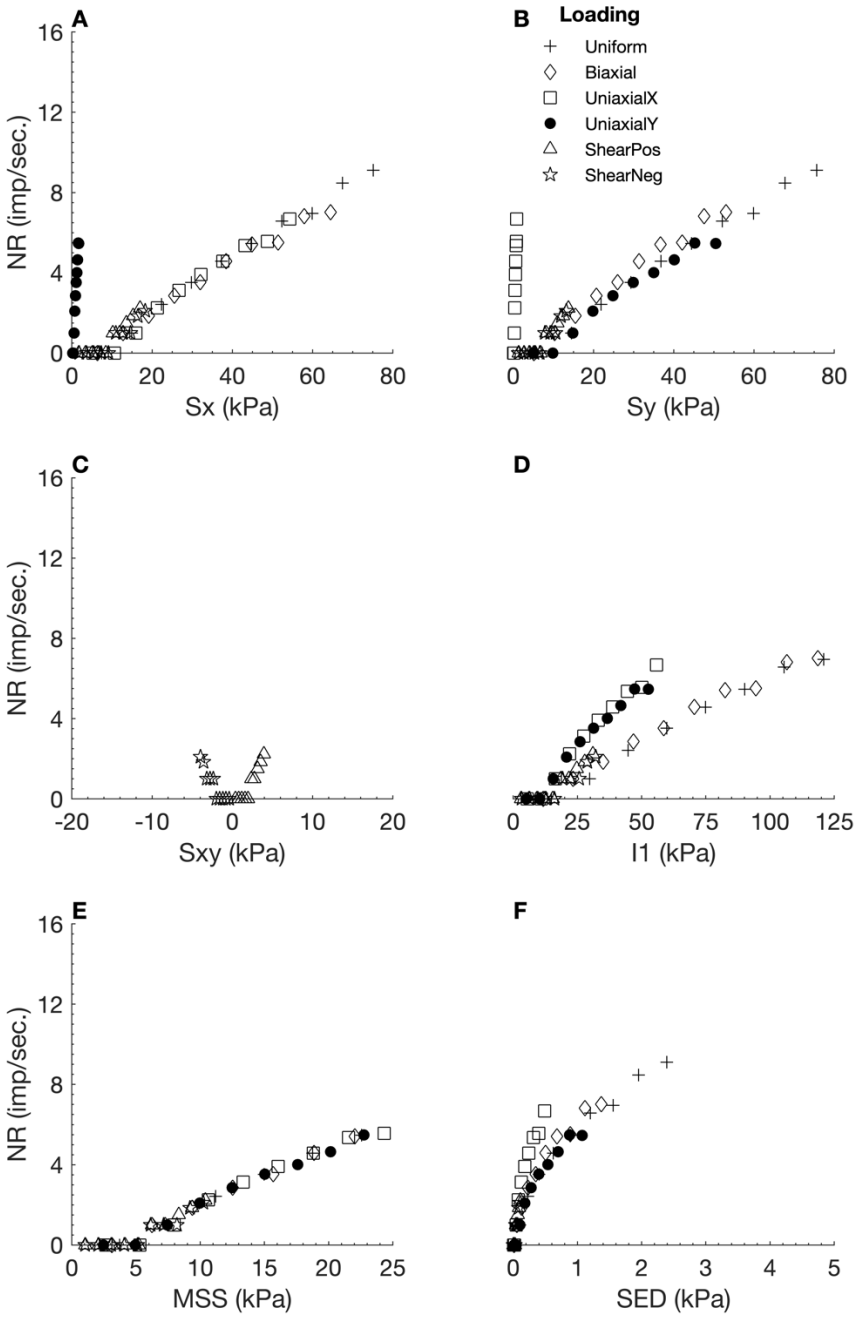

Figure B - 5. Neural responses (NR) output by the orthotropic elastic FEBio model 1 using MSS as the neural model input, plotted against six different stress variables. Sx: X stress. Sy: Y stress. Sxy: shear stress. I1: 1st invariant stress tensor. MSS: maximum shear stress. SED: strain energy density.

Table B - 7. Linear regression measures for individual loading regime results from the orthotropic elastic model 1, with MSS as neural model input.

Loading Regime	R^2	RMSE	Slope
Uniform	0.9901	0.3247	0.6436
Biaxial	0.4274	1.2339	4.6912
Uniaxial X	0.0886	1.2490	-0.1689
Uniaxial Y	0.9380	0.4128	1.0852
Shear Positive	0.3035	0.3809	0.0461
Shear Negative	NaN	0.0000	0.0000

B.1.6 Strain Energy Density (SED)

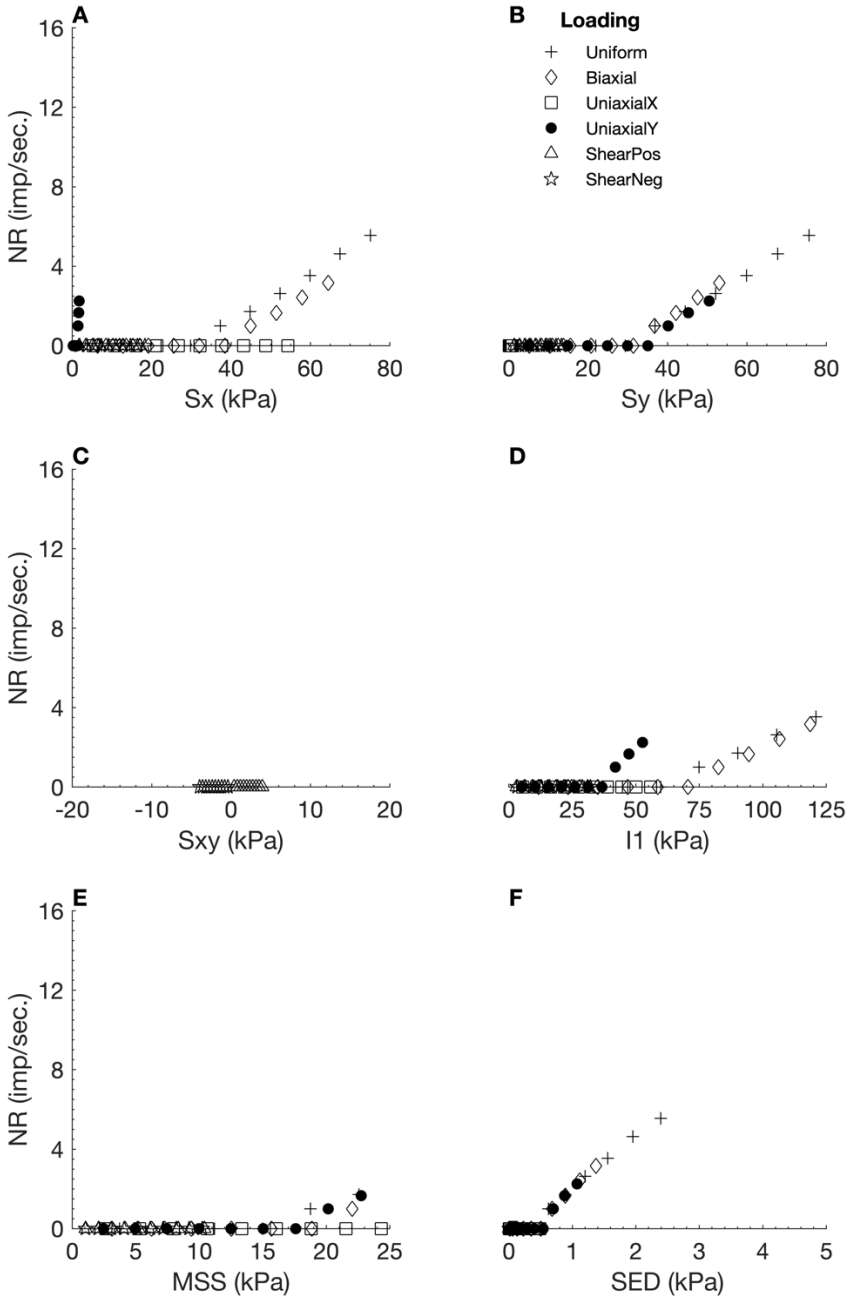

Figure B - 6. Neural responses (NR) output by the orthotropic elastic FEBio model 1 using SED as the neural model input, plotted against six different stress variables. Sx: X stress. Sy: Y stress. Sxy: shear stress. I1: 1st invariant stress tensor. MSS: maximum shear stress. SED: strain energy density.

Table B - 8. Linear regression measures for individual loading regime results from the orthotropic elastic model 1, with SED as neural model input.

Loading Regime	R^2	RMSE	Slope
Uniform	0.8516	0.8535	0.4055
Biaxial	NaN	0.0000	0.0000
Uniaxial X	NaN	0.0000	0.0000
Uniaxial Y	NaN	0.0000	0.0000
Shear Positive	NaN	0.0000	0.0000
Shear Negative	NaN	0.0000	0.0000

B.1.7 Hydrostatic Pressure (HS)

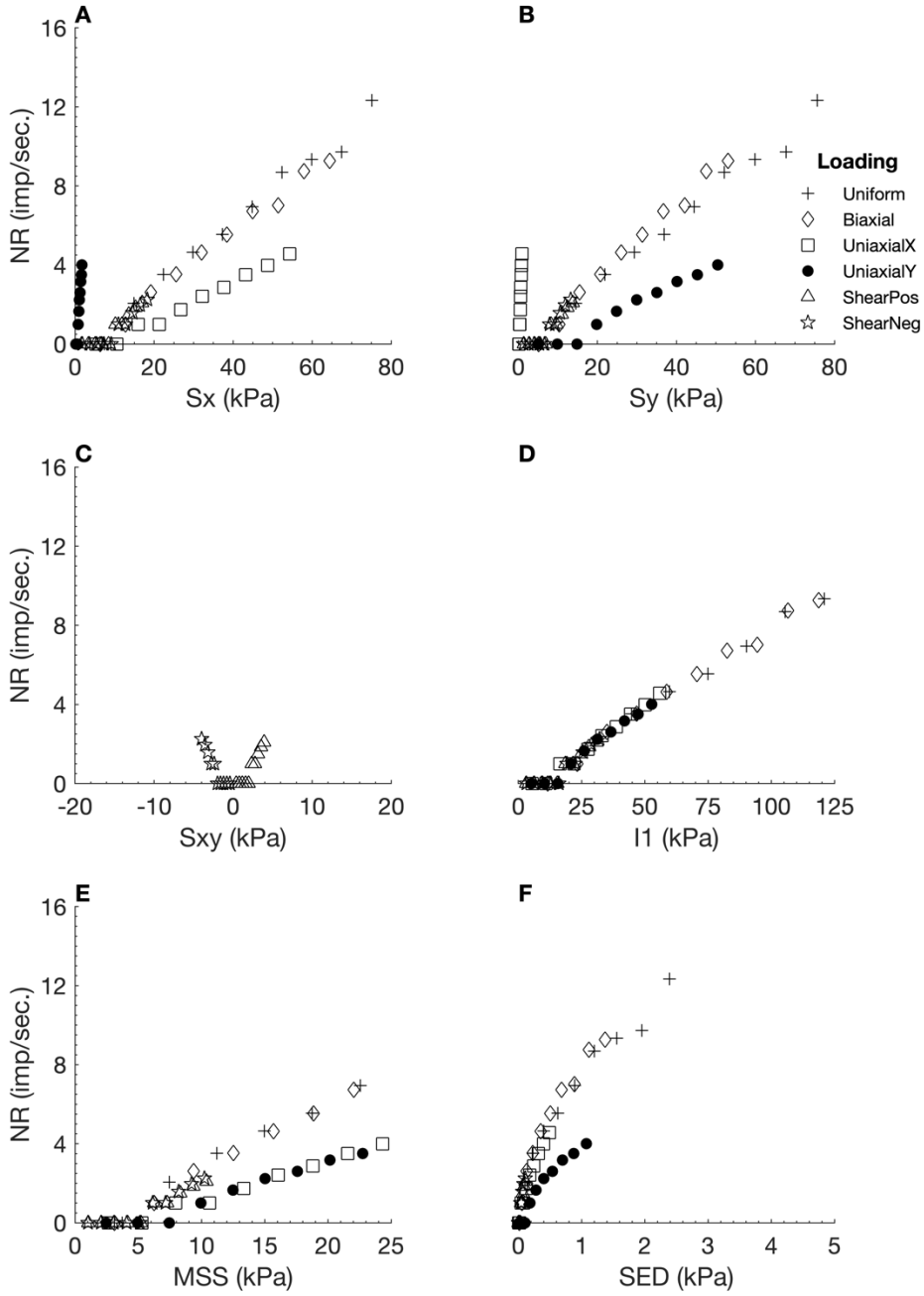

Figure B - 7. Neural responses (NR) output by the orthotropic elastic FEBio model 1 using HS as the neural model input, plotted against six different stress variables. Sx: X stress. Sy: Y stress. Sxy: shear stress. I1: 1st invariant stress tensor. MSS: maximum shear stress. SED: strain energy density.

Table B - 9. Linear regression measures for individual loading regime results from the orthotropic elastic model 1, with HS as neural model input.

Loading Regime	**R^2**	**RMSE**	**Slope**
Uniform	0.9731	0.6672	0.7953
Biaxial	0.4662	1.5794	6.4951
Uniaxial X	0.2082	0.6292	-0.1399
Uniaxial Y	0.9716	0.1839	0.7265
Shear Positive	0.3035	0.3809	0.0461
Shear Negative	NaN	0.0000	0.0000

B.1.8 1st Principle Stress (S1)

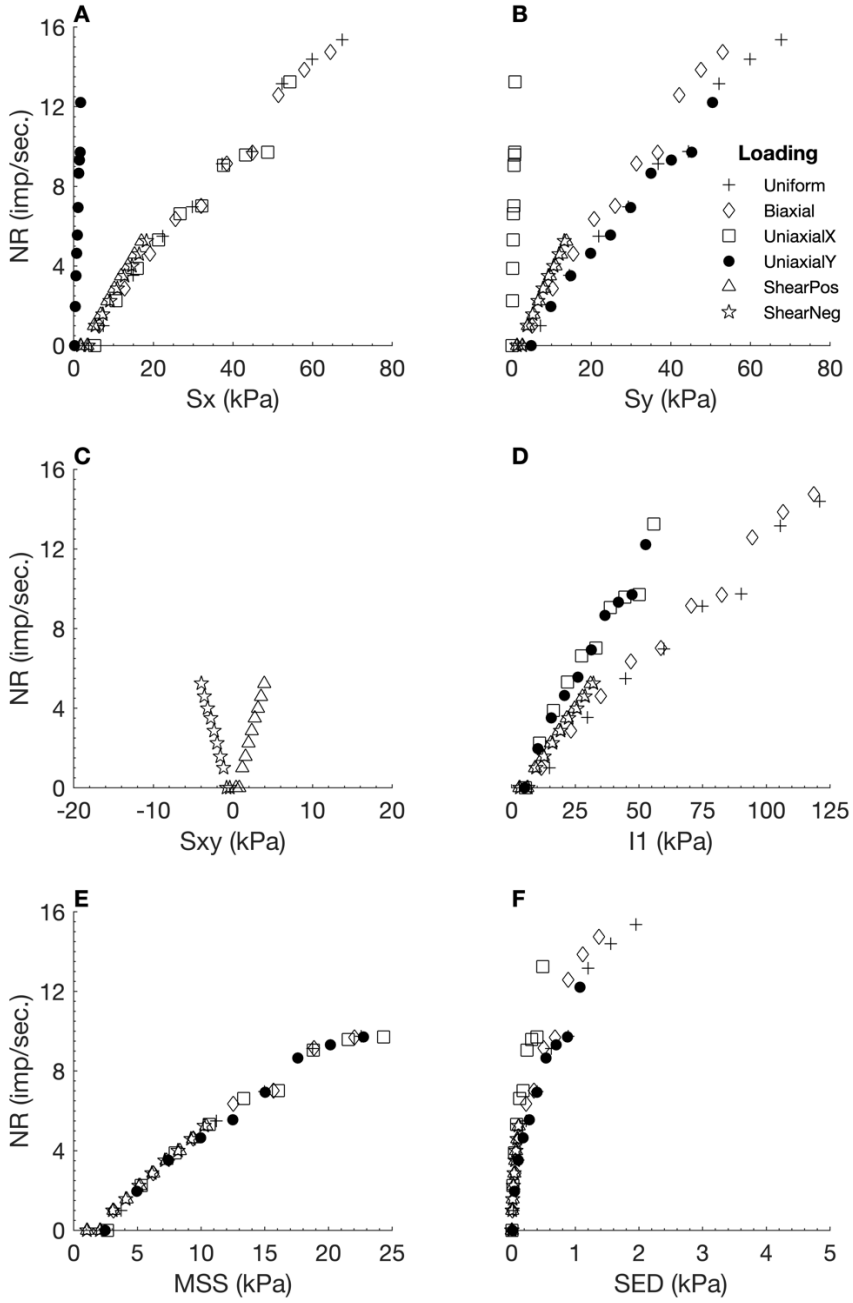

Figure B - 8. Neural responses (NR) output by the orthotropic elastic FEBio model 1 using S1 as the neural model input, plotted against six different stress variables. Sx: X stress. Sy: Y stress. Sxy: shear stress. I1: 1st invariant stress tensor. MSS: maximum shear stress. SED: strain energy density.

Table B - 10. Linear regression measures for individual loading regime results from the orthotropic elastic model 1, with S1 as neural model input.

Loading Regime	R^2	RMSE	Slope
Uniform	0.9841	0.7018	1.0941
Biaxial	0.5060	2.0135	8.9672
Uniaxial X	0.4805	2.0151	-0.8404
Uniaxial Y	0.8856	0.9490	1.7847
Shear Positive	0.8705	0.4718	0.2244
Shear Negative	0.7665	0.5484	0.5185

B.1.9 2nd Principle Stress (S2)

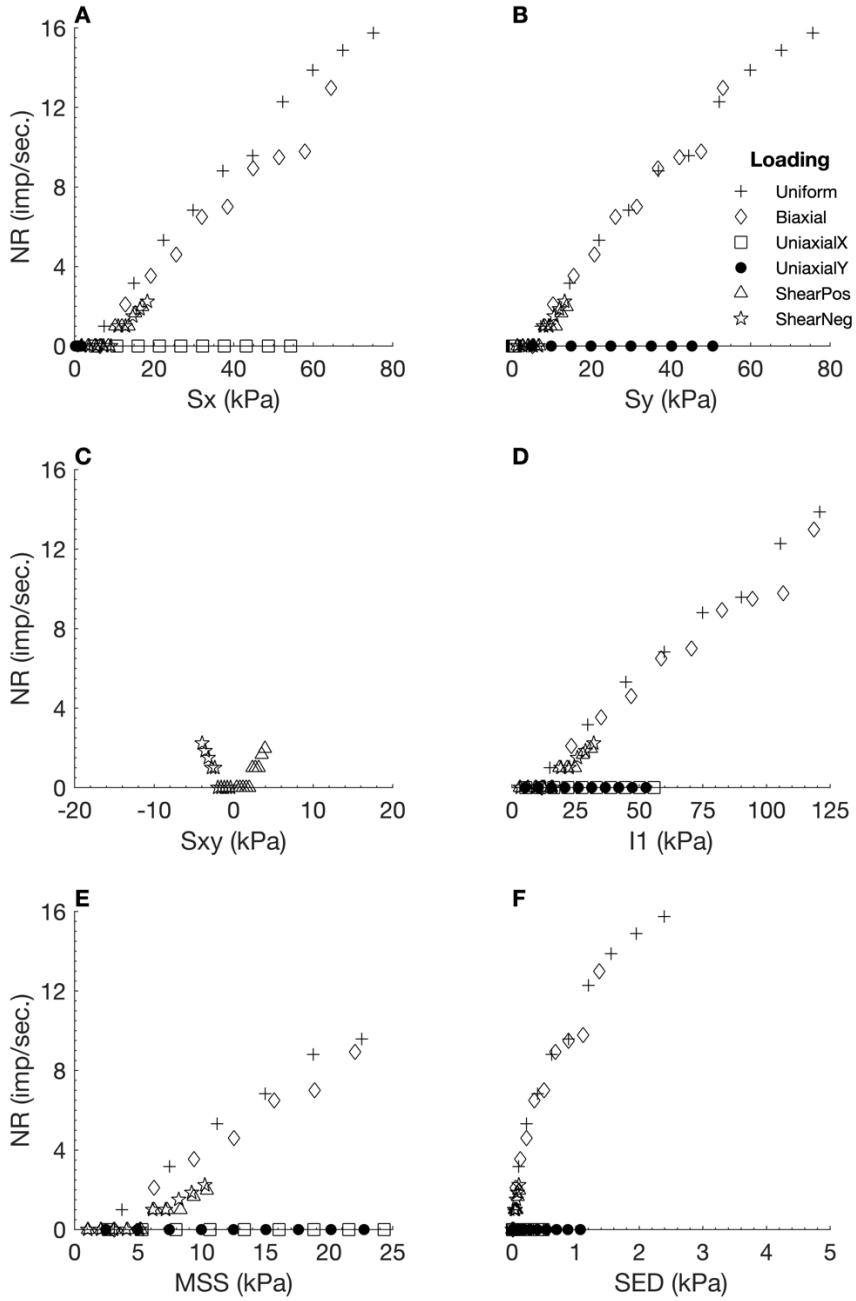

Figure B - 9. Neural responses (NR) output by the orthotropic elastic FEBio model 1 using S2 as the neural model input, plotted against six different stress variables. Sx: X stress. Sy: Y stress. Sxy: shear stress. I1: 1st invariant stress tensor. MSS: maximum shear stress. SED: strain energy density.

Table B - 11. Linear regression measures for individual loading regime results from the orthotropic elastic model 1, with S2 as neural model input.

Loading Regime	R^2	RMSE	Slope
Uniform	0.9891	0.5602	1.0602
Biaxial	0.3685	2.2619	7.6041
Uniaxial X	NaN	0.0000	0.0000
Uniaxial Y	NaN	0.0000	0.0000
Shear Positive	0.3035	0.3809	0.0461
Shear Negative	NaN	0.0000	0.0000

B.1.10 3rd Principle Stress (S3)

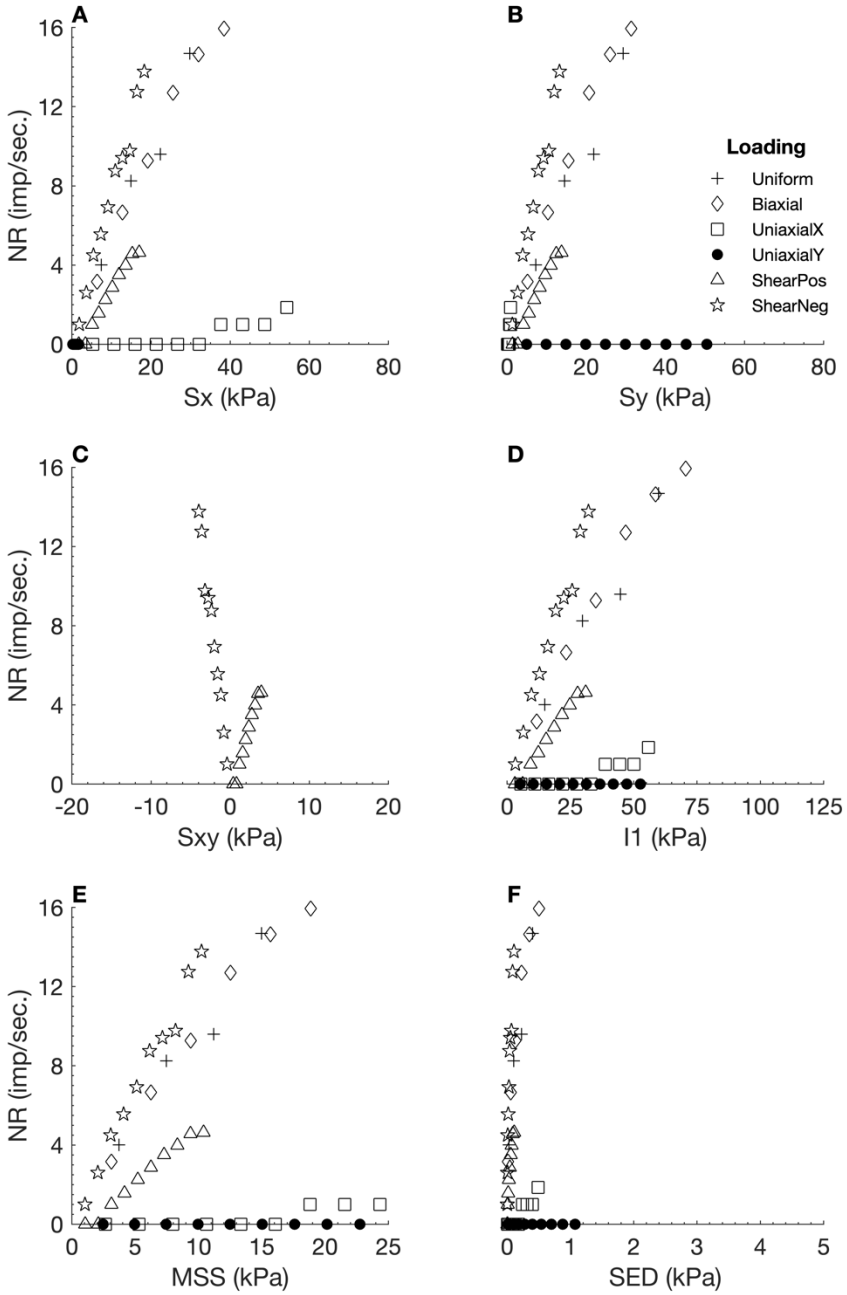

Figure B - 10. Neural responses (NR) output by the orthotropic elastic FEBio model 1 using S3 as the neural model input, plotted against six different stress variables. Sx: X stress. Sy: Y stress. Sxy: shear stress. I1: 1st invariant stress tensor. MSS: maximum shear stress. SED: strain energy density.

Table B - 12. Linear regression measures for individual loading regime results from the orthotropic elastic model 1, with S3 as neural model input.

Loading Regime	R^2	RMSE	Slope
Uniform	0.9409	1.5263	1.2082
Biaxial	0.4316	4.0069	15.3664
Uniaxial X	NaN	0.0000	0.0000
Uniaxial Y	NaN	0.0000	0.0000
Shear Positive	0.8701	0.4737	0.2249
Shear Negative	0.9269	0.7343	1.3639

B.1.11 Deviatoric Stress 1 (Dev1)

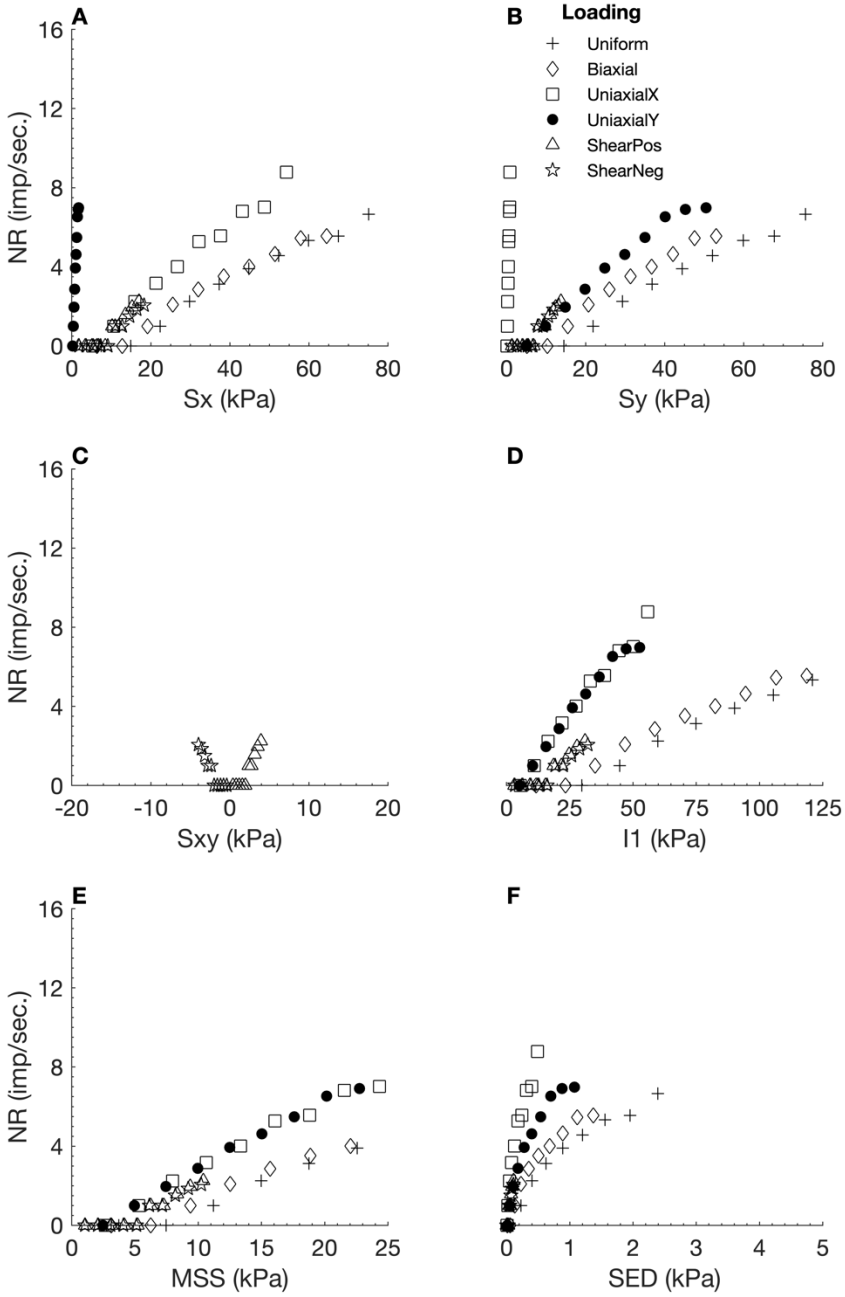

Figure B - 11. Neural responses (NR) output by the orthotropic elastic FEBio model 1 using Dev1 as the neural model input, plotted against six different stress variables. Sx: X stress. Sy: Y stress. Sxy: shear stress. I1: 1st invariant stress tensor. MSS: maximum shear stress. SED: strain energy density.

Table B - 13. Linear regression measures for individual loading regime results from the orthotropic elastic model 1, with Dev1 as neural model input.

Loading Regime	R^2	RMSE	Slope
Uniform	0.9812	0.3446	0.4942
Biaxial	0.3667	1.1658	3.9039
Uniaxial X	0.3753	1.3451	-0.4521
Uniaxial Y	0.9371	0.4928	1.2857
Shear Positive	0.3035	0.3809	0.0461
Shear Negative	NaN	0.0000	0.0000

B.1.12 Deviatoric Stress 2 (Dev2)

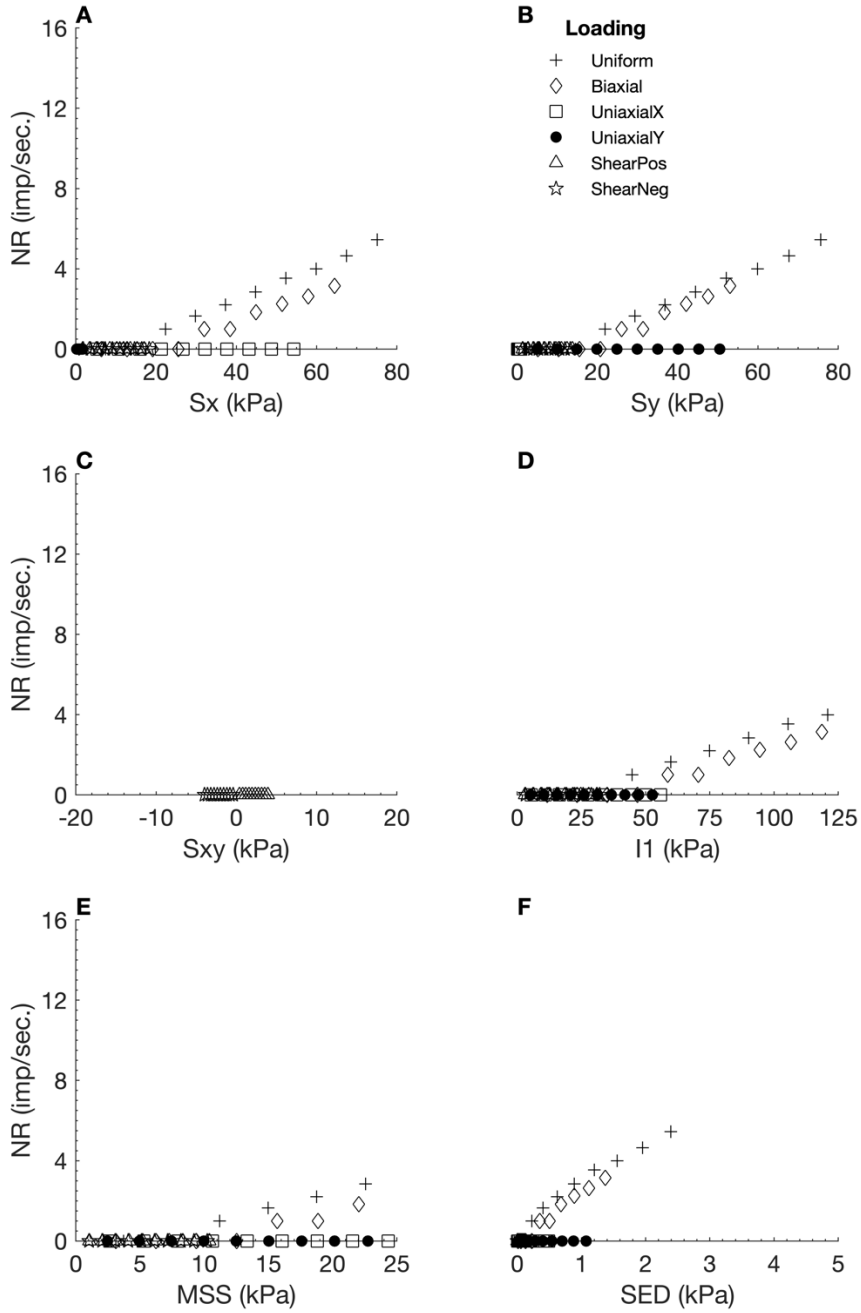

Figure B - 12. Neural responses (NR) output by the orthotropic elastic FEBio model 1 using Dev2 as the neural model input, plotted against six different stress variables. Sx: X stress. Sy: Y stress. Sxy: shear stress. I1: 1st invariant stress tensor. MSS: maximum shear stress. SED: strain energy density.

Table B - 14. Linear regression measures for individual loading regime results from the orthotropic elastic model 1, with Dev2 as neural model input.

Loading Regime	R^2	RMSE	Slope
Uniform	0.9798	0.2855	0.3946
Biaxial	0.0001	0.5164	-0.0233
Uniaxial X	NaN	0.0000	0.0000
Uniaxial Y	NaN	0.0000	0.0000
Shear Positive	NaN	0.0000	0.0000
Shear Negative	NaN	0.0000	0.0000

B.1.13 Deviatoric Stress 3 (Dev3)

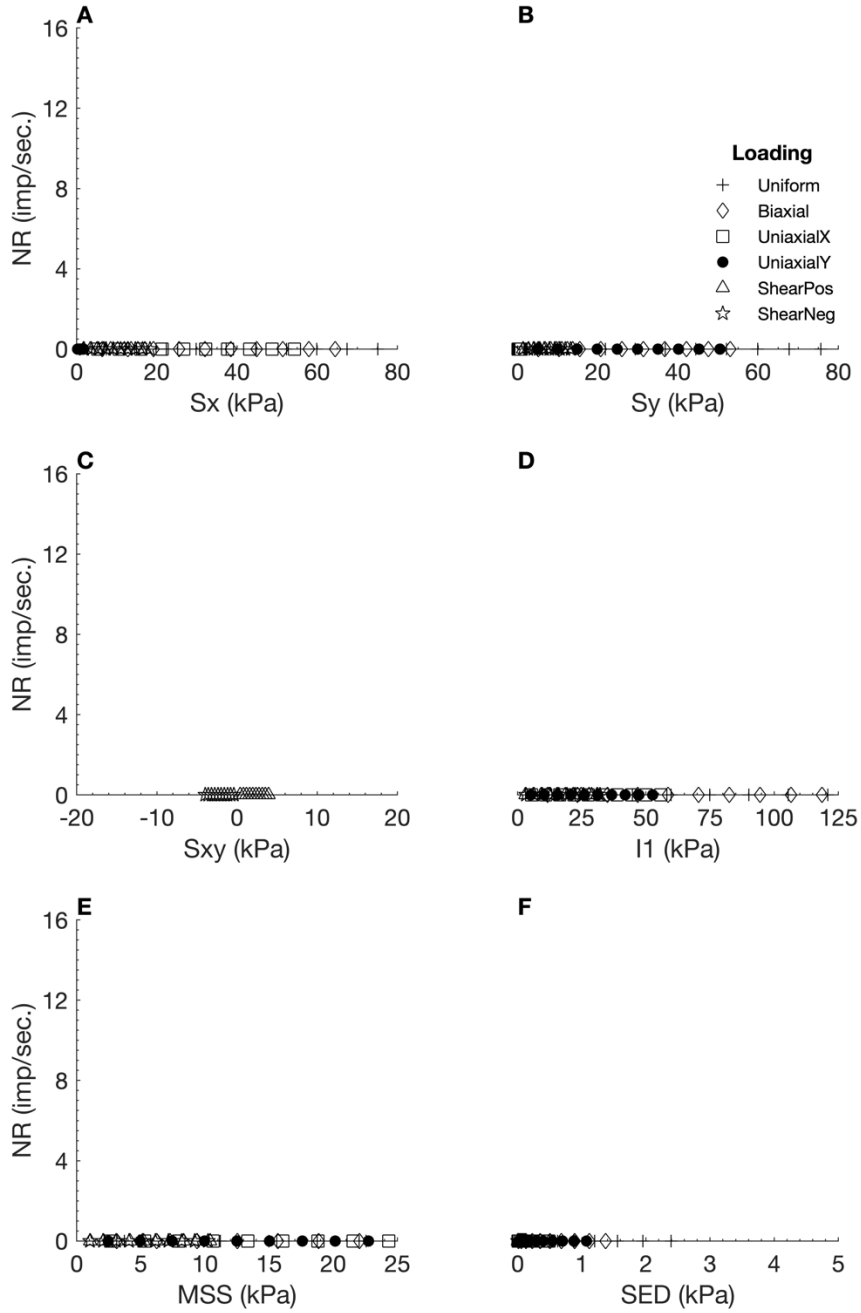

Figure B - 13. Neural responses (NR) output by the orthotropic elastic FEBio model 1 using Dev3 as the neural model input, plotted against six different stress variables. Sx: X stress. Sy: Y stress. Sxy: shear stress. I1: 1st invariant stress tensor. MSS: maximum shear stress. SED: strain energy density.

Table B - 15. Linear regression measures for individual loading regime results from the orthotropic elastic model 1, with Dev3 as neural model input.

Loading Regime	R^2	RMSE	Slope
Uniform	NaN	0.0000	0.0000
Biaxial	NaN	0.0000	0.0000
Uniaxial X	NaN	0.0000	0.0000
Uniaxial Y	NaN	0.0000	0.0000
Shear Positive	NaN	0.0000	0.0000
Shear Negative	NaN	0.0000	0.0000

B.1.14 Shear Stress A

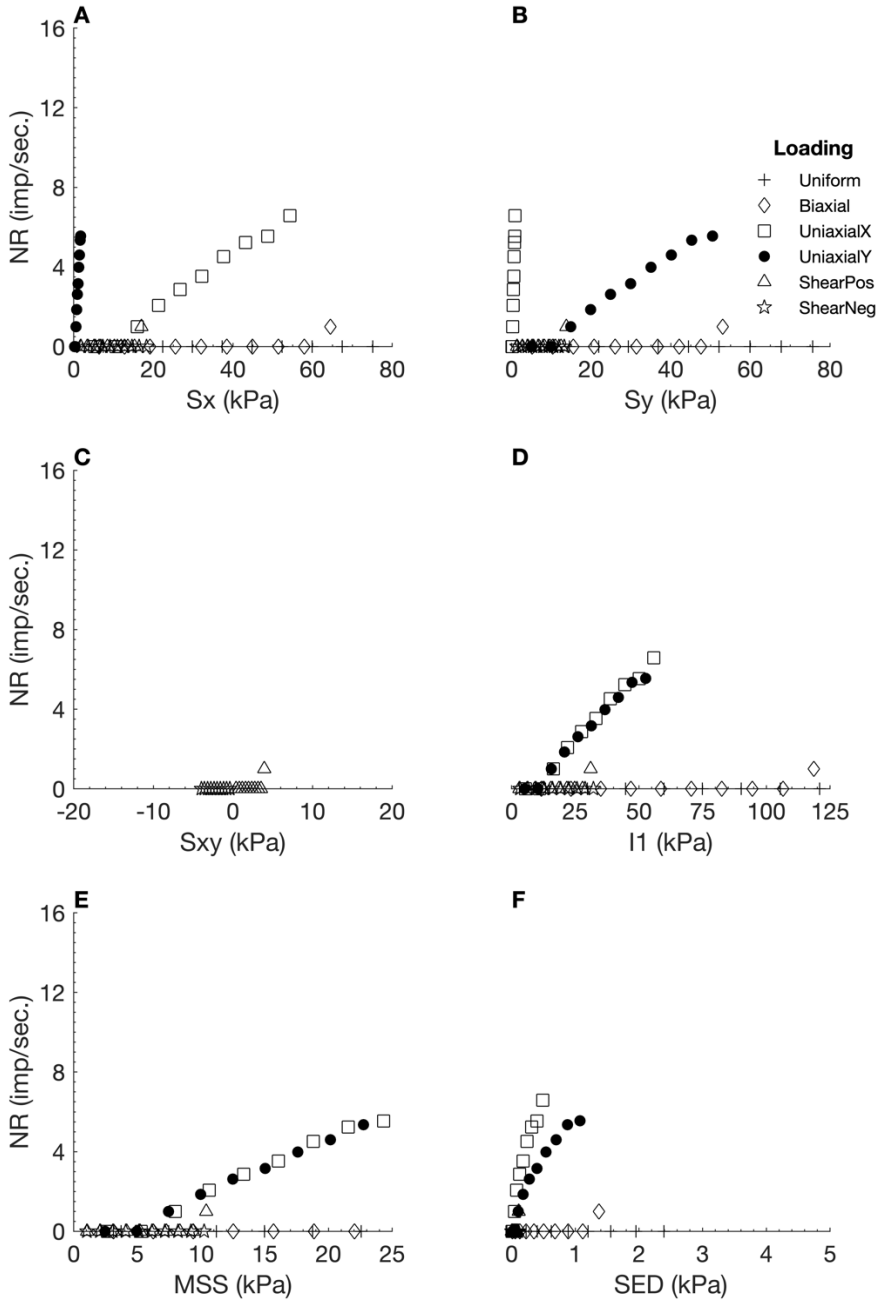

Figure B - 14. Neural responses (NR) output by the orthotropic elastic FEBio model 1 using ShearA as the neural model input, plotted against six different stress variables. Sx: X stress. Sy: Y stress. Sxy: shear stress. I1: 1st invariant stress tensor. MSS: maximum shear stress. SED: strain energy density.

Table B - 16. Linear regression measures for individual loading regime results from the orthotropic elastic model 1, with ShearA as neural model input.

Loading Regime	R^2	RMSE	Slope
Uniform	NaN	0.0000	0.0000
Biaxial	NaN	0.0000	0.0000
Uniaxial X	0.0987	1.1473	-0.1646
Uniaxial Y	0.9299	0.3943	0.9706
Shear Positive	NaN	0.0000	0.0000
Shear Negative	NaN	0.0000	0.0000

B.1.15 Shear Stress B

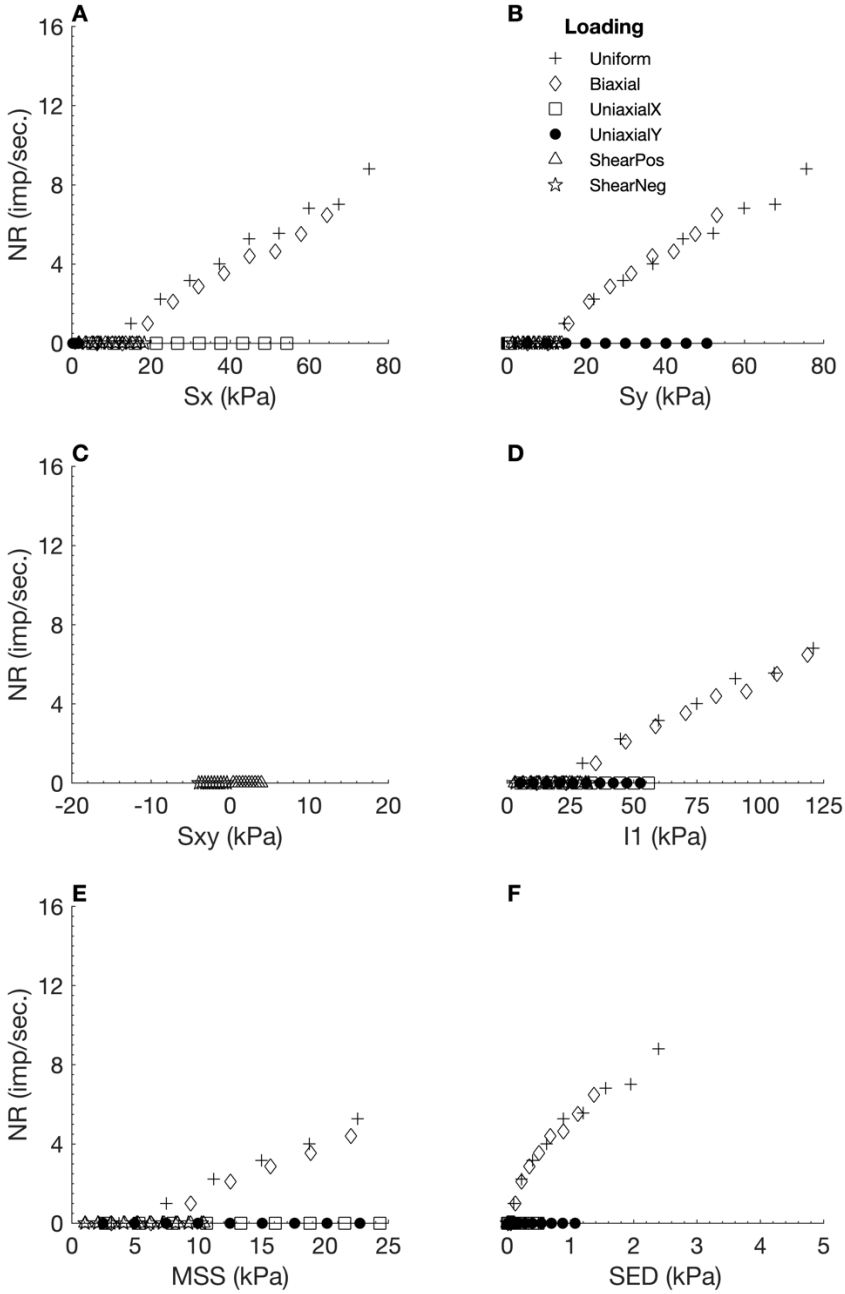

Figure B - 15. Neural responses (NR) output by the orthotropic elastic FEBio model 1 using ShearB as the neural model input, plotted against six different stress variables. Sx: X stress. Sy: Y stress. Sxy: shear stress. I1: 1st invariant stress tensor. MSS: maximum shear stress. SED: strain energy density.

Table B - 17. Linear regression measures for individual loading regime results from the orthotropic elastic model 1, with ShearB as neural model input.

Loading Regime	R^2	RMSE	Slope
Uniform	0.9801	0.4217	0.5873
Biaxial	0.3652	1.1740	3.9187
Uniaxial X	NaN	0.0000	0.0000
Uniaxial Y	NaN	0.0000	0.0000
Shear Positive	NaN	0.0000	0.0000
Shear Negative	NaN	0.0000	0.0000

B.1.16 Shear Stress C

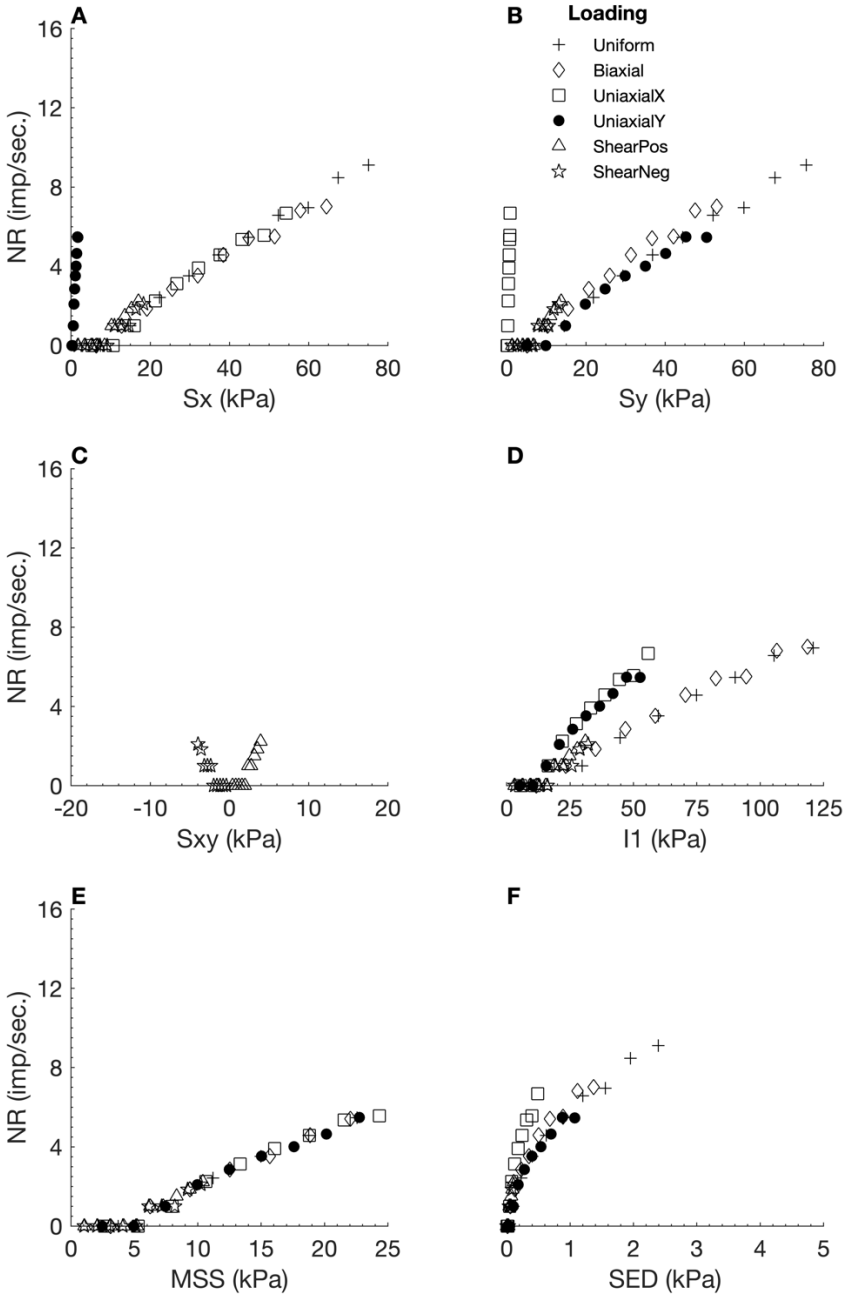

Figure B - 16. Neural responses (NR) output by the orthotropic elastic FEBio model 1 using ShearC as the neural model input, plotted against six different stress variables. Sx: X stress. Sy: Y stress. Sxy: shear stress. I1: 1st invariant stress tensor. MSS: maximum shear stress. SED: strain energy density.

Table B - 18. Linear regression measures for individual loading regime results from the orthotropic elastic model 1, with ShearC as neural model input.

Loading Regime	R^2	RMSE	Slope
Uniform	0.9901	0.3247	0.6436
Biaxial	0.4274	1.2339	4.6912
Uniaxial X	0.0886	1.2490	-0.1689
Uniaxial Y	0.9380	0.4128	1.0852
Shear Positive	0.3035	0.3809	0.0461
Shear Negative	NaN	0.0000	0.0000

B.1.17 X Strain (Ex)

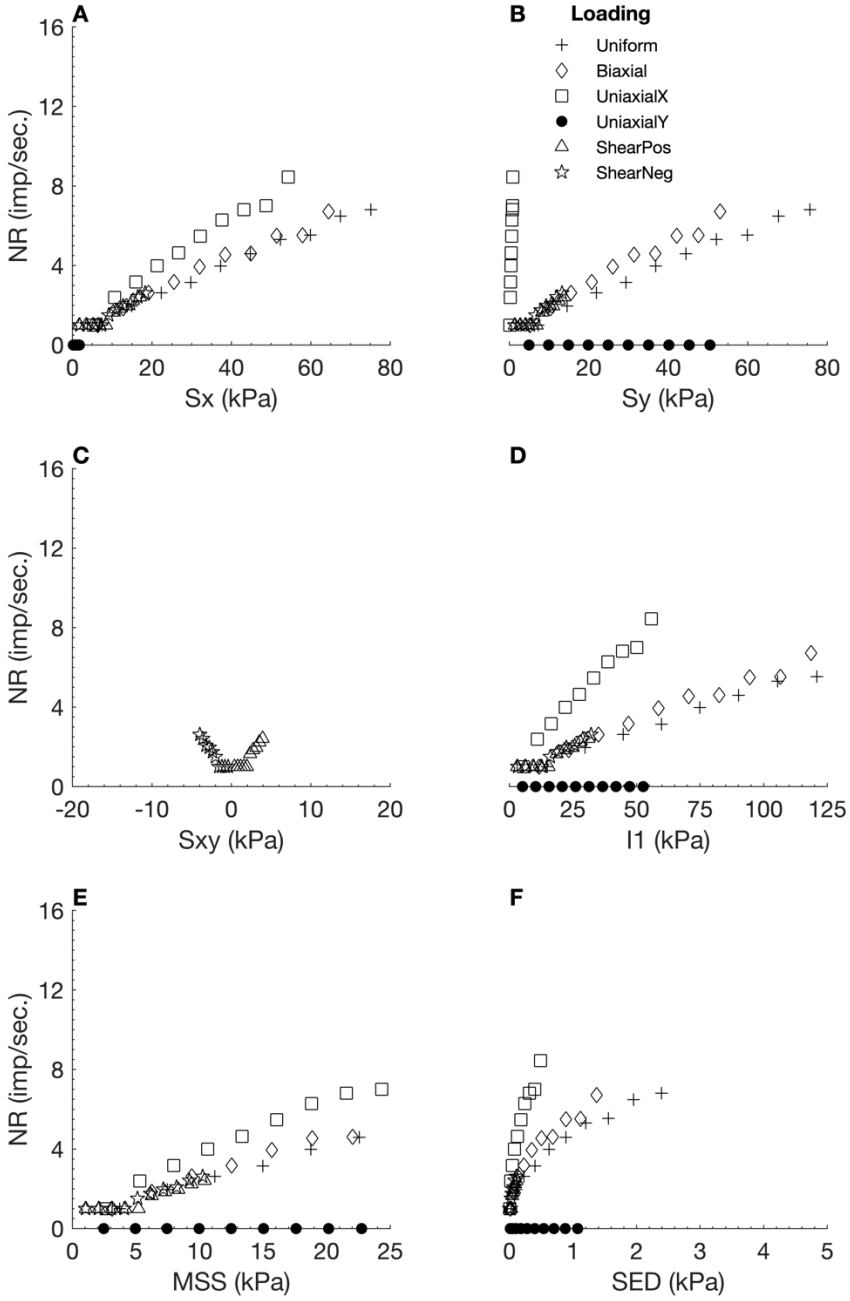

Figure B - 17. Neural responses (NR) output by the orthotropic elastic FEBio model 1 using Ex as the neural model input, plotted against six different stress variables. Sx: X stress. Sy: Y stress. Sxy: shear stress. I1: 1st invariant stress tensor. MSS: maximum shear stress. SED: strain energy density.

Table B - 19. Linear regression measures for individual loading regime results from the orthotropic elastic model 1, with Ex as neural model input.

Loading Regime	R^2	RMSE	Slope
Uniform	0.9883	0.2233	0.4064
Biaxial	0.4081	1.0158	3.7120
Uniaxial X	0.5165	1.0832	-0.4854
Uniaxial Y	NaN	0.0000	0.0000
Shear Positive	0.3035	0.2479	0.0300
Shear Negative	0.2318	0.2272	0.0651

B.1.18 Y Strain (Ey)

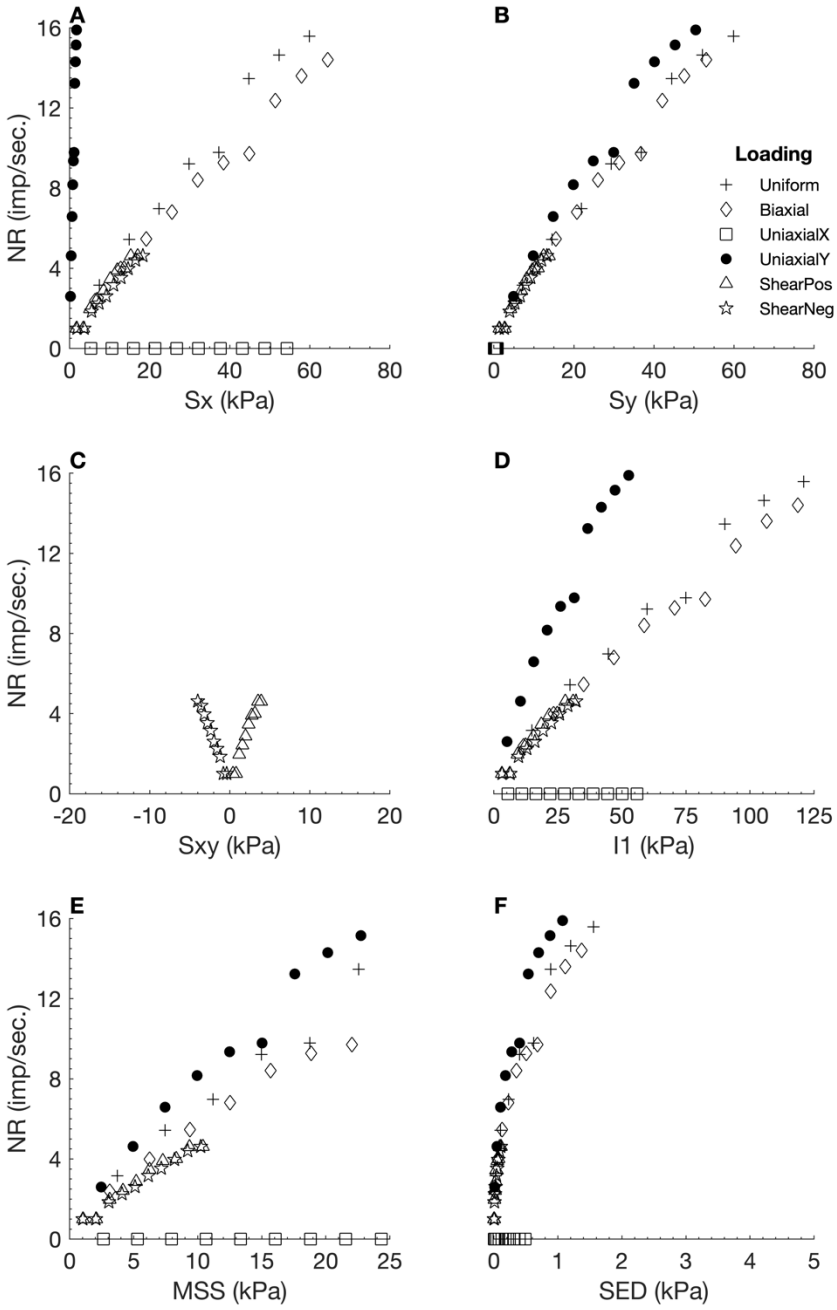

Figure B - 18. Neural responses (NR) output by the orthotropic elastic FEBio model 1 using Ey as the neural model input, plotted against six different stress variables. Sx: X stress. Sy: Y stress. Sxy: shear stress. I1: 1st invariant stress tensor. MSS: maximum shear stress. SED: strain energy density.

Table B - 20. Linear regression measures for individual loading regime results from the orthotropic elastic model 1, with Ey as neural model input.

Loading Regime	R^2	RMSE	Slope
Uniform	0.9893	0.5439	1.0364
Biaxial	0.3872	2.1237	7.4290
Uniaxial X	NaN	0.0000	0.0000
Uniaxial Y	0.8450	1.2402	1.9564
Shear Positive	0.8824	0.3838	0.1928
Shear Negative	0.8050	0.3715	0.3938

B.2 Test 2

Table B - 21. Values selected for material properties during FEBio implementation of orthotropic elastic material test 2.

Orthotropic Material Property	Value Selected
Density	1
Young's Modulus (X)	9.4
Young's Modulus (Y)	1
Young's Modulus (Z)	1
Shear Modulus (XY)	3.62
Shear Modulus (YZ)	0.385
Shear Modulus (XZ)	0.385
Poisson's Ratio (XY)	0.299
Poisson's Ratio (YZ)	0.299
Poisson's Ratio (XZ)	0.299

Table B - 22. Linear regression measures for total plot results (i.e. considering all loading regimes combined), for each input stimulus tested with the orthotropic elastic model 2.

Input Stimuli	R^2	RMSE	Slope
X Stress (Sx)	0.1693	4.4584	0.4446
Y Stress (Sy)	0.2800	4.1261	0.5684
Shear Stress (Sxy)	0.0756	1.6098	0.1017
1st Invariant Stress Tensor (I1)	0.2616	5.8521	0.7695
Maximum Shear Stress (MSS)	0.2667	2.2999	0.3064
SED (Strain Energy Density)	0.1747	1.2614	0.1282
Hydrostatic Pressure (HS)	0.2453	2.9957	0.3772
1st Principal Stress (S1)	0.2776	4.0427	0.5536
2nd Principal Stress (S2)	0.2009	4.1762	0.4625
3rd Principal Stress (S3)	0.1827	7.8902	0.8240
Deviatoric Stress 1 (Dev1)	0.2492	1.7930	0.2282
Deviatoric Stress 2 (Dev2)	0.1841	1.1386	0.1195
Deviatoric Stress 3 (Dev3)	NaN	0.0000	0.0000
Shear A	0.0141	0.7536	0.0199
Shear B	0.1927	2.1446	0.2315
Shear C	0.2667	2.2999	0.3064
X Strain (Ex)	0.1288	0.7420	0.0630
Y Strain (Ey)	0.3496	4.4746	0.7246
Average	**0.2070**	**2.8922**	**0.3461**

B.2.1 X Stress (Sx)

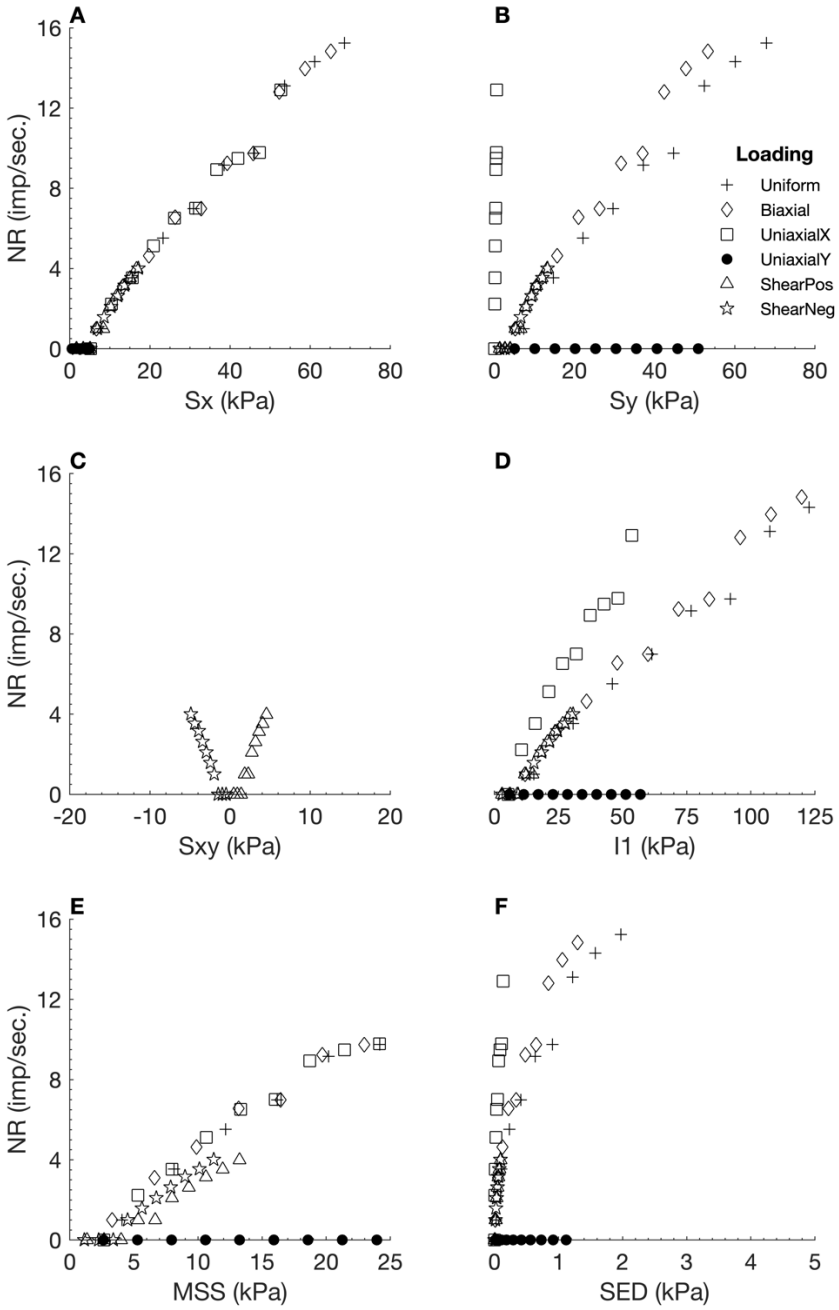

Figure B - 19. Neural responses (NR) output by the orthotropic elastic FEBio model 2 using Sx as the neural model input, plotted against six different stress variables. Sx: X stress. Sy: Y stress. Sxy: shear stress. I1: 1st invariant stress tensor. MSS: maximum shear stress. SED: strain energy density.

Table B - 23. Linear regression measures for individual loading regime results from the orthotropic elastic model 2, with Sx as neural model input.

Loading Regime	R^2	RMSE	Slope
Uniform	0.9843	0.6904	1.0830
Biaxial	0.5073	2.0125	8.9864
Uniaxial X	0.4743	1.9235	-0.7922
Uniaxial Y	NaN	0.0000	0.0000
Shear Positive	0.6748	0.5406	0.1428
Shear Negative	0.4736	0.6155	0.3047

B.2.2 Y Stress (Sy)

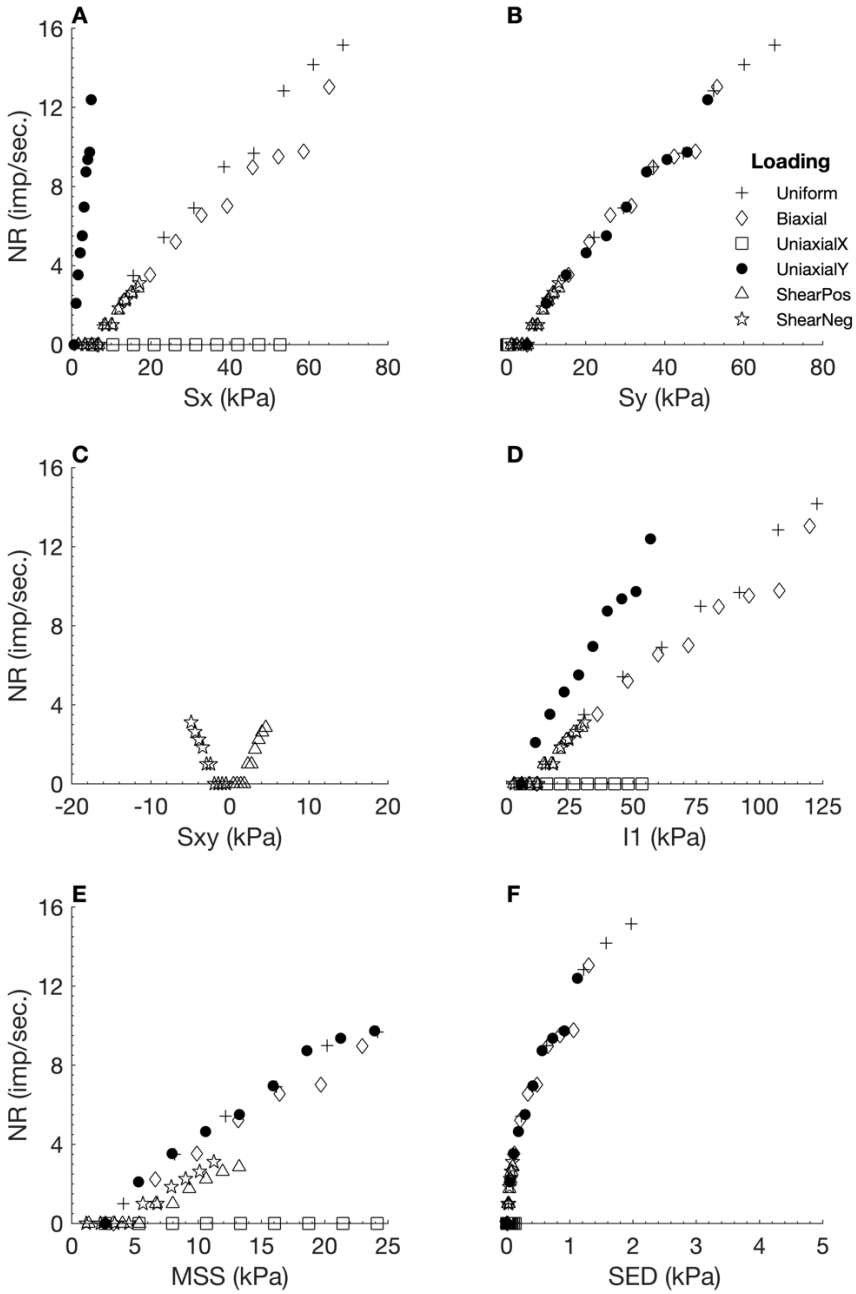

Figure B - 20. Neural responses (NR) output by the orthotropic elastic FEBio model 2 using Sy as the neural model input, plotted against six different stress variables. Sx: X stress. Sy: Y stress. Sxy: shear stress. I1: 1st invariant stress tensor. MSS: maximum shear stress. SED: strain energy density.

Table B - 24. Linear regression measures for individual loading regime results from the orthotropic elastic model 2, with Sy as neural model input.

Loading Regime	R^2	RMSE	Slope
Uniform	0.9855	0.6582	1.0768
Biaxial	0.4005	2.2830	8.2117
Uniaxial X	NaN	0.0000	0.0000
Uniaxial Y	0.8835	0.9508	1.7695
Shear Positive	0.5096	0.4043	0.0756
Shear Negative	0.2318	0.4526	0.1297

B.2.3 Shear Stress (Sxy)

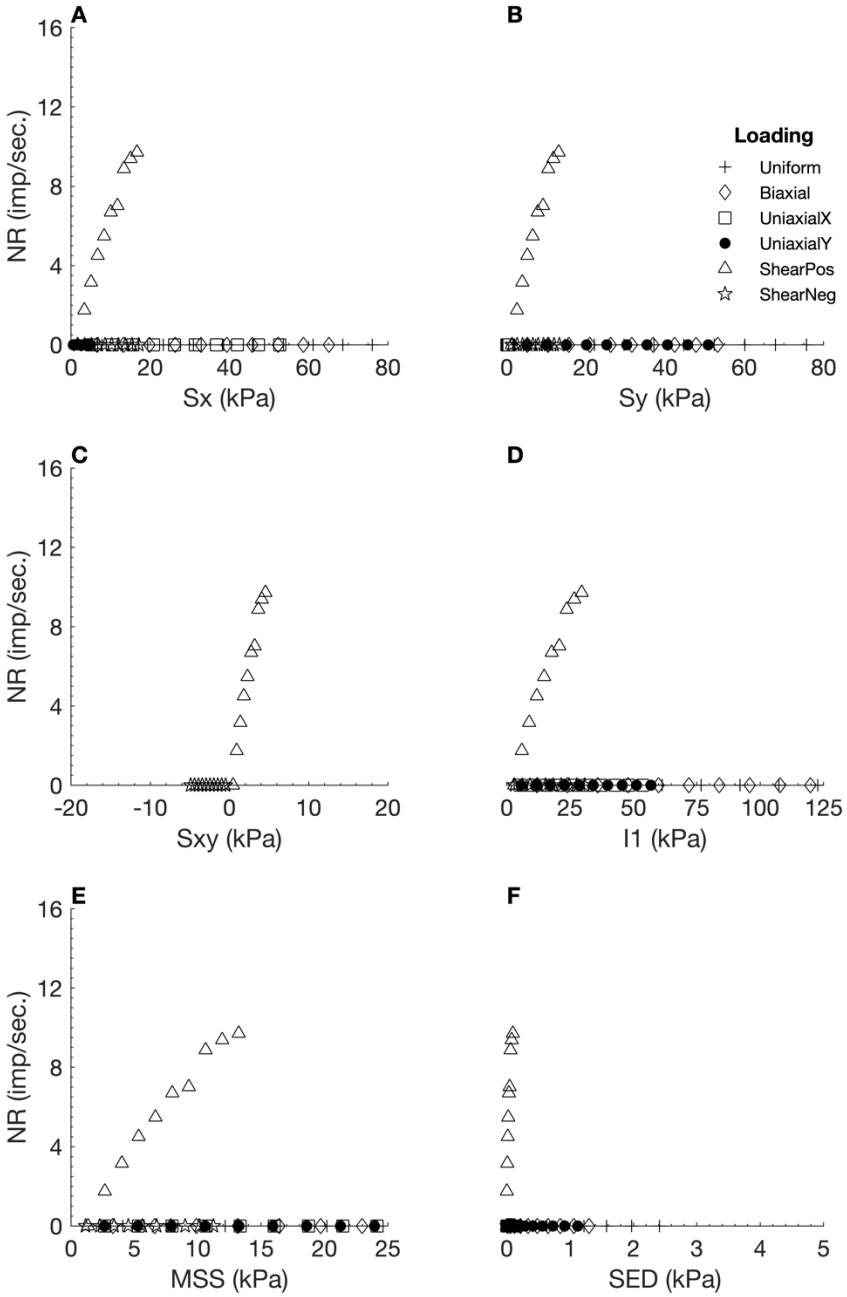

Figure B - 21. Neural responses (NR) output by the orthotropic elastic FEBio model 2 using Sxy as the neural model input, plotted against six different stress variables. Sx: X stress. Sy: Y stress. Sxy: shear stress. I1: 1st invariant stress tensor. MSS: maximum shear stress. SED: strain energy density.

Table B - 25. Linear regression measures for individual loading regime results from the orthotropic elastic model 2, with Sxy as neural model input.

Loading Regime	R^2	RMSE	Slope
Uniform	NaN	0.0000	0.0000
Biaxial	NaN	0.0000	0.0000
Uniaxial X	NaN	0.0000	0.0000
Uniaxial Y	NaN	0.0000	0.0000
Shear Positive	0.9797	0.3935	0.5017
Shear Negative	NaN	0.0000	0.0000

B.2.4 1st Invariant Stress Tensor (I1)

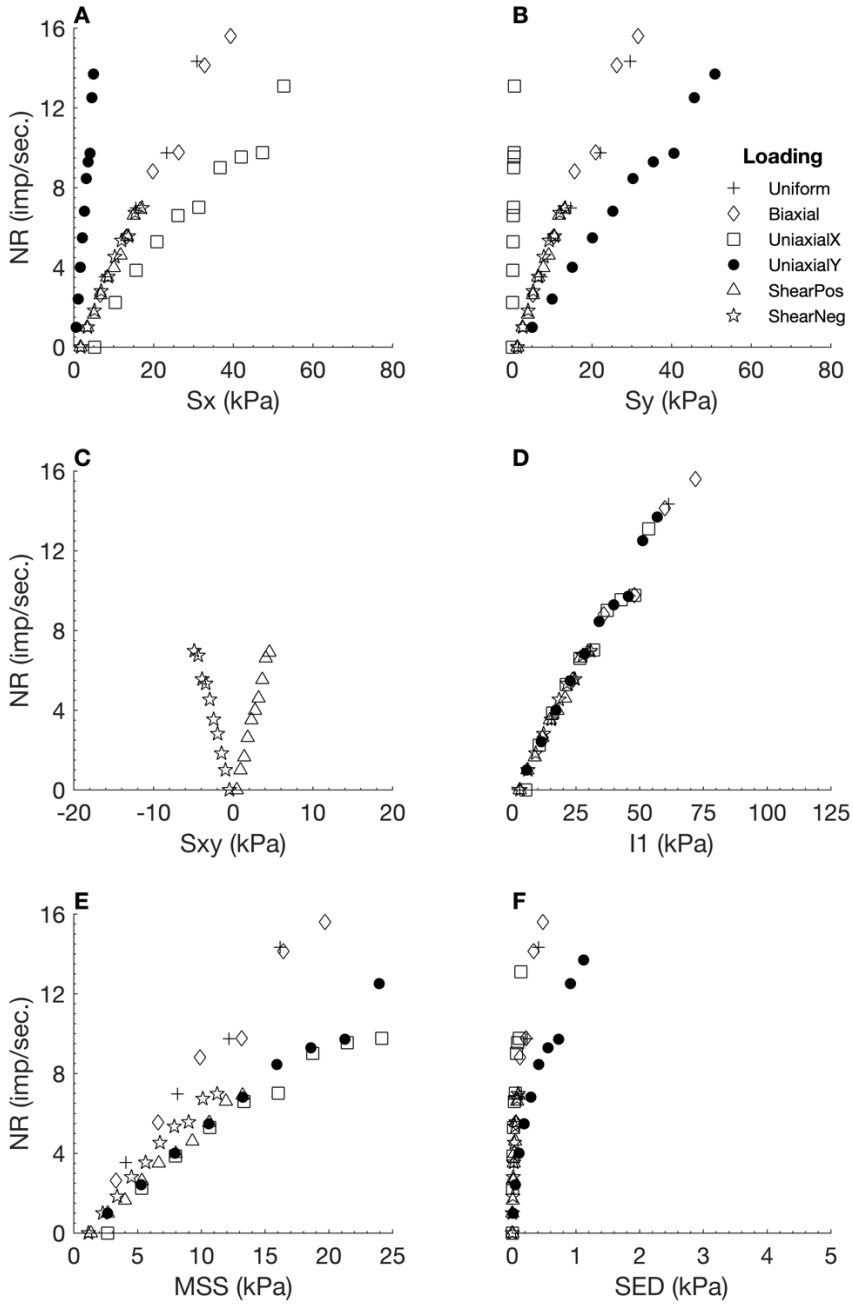

Figure B - 22. Neural responses (NR) output by the orthotropic elastic FEBio model 2 using I1 as the neural model input, plotted against six different stress variables. Sx: X stress. Sy: Y stress. Sxy: shear stress. I1: 1st invariant stress tensor. MSS: maximum shear stress. SED: strain energy density.

Table B - 26. Linear regression measures for individual loading regime results from the orthotropic elastic model 2, with I1 as neural model input.

Loading Regime	R^2	RMSE	Slope
Uniform	0.9631	1.3161	1.3343
Biaxial	0.3471	4.0716	13.0653
Uniaxial X	0.4814	2.0033	-0.8369
Uniaxial Y	0.9420	0.7484	2.0373
Shear Positive	0.9561	0.3578	0.3061
Shear Negative	0.8970	0.5214	0.8030

B.2.5 Maximum Shear Stress (MSS)

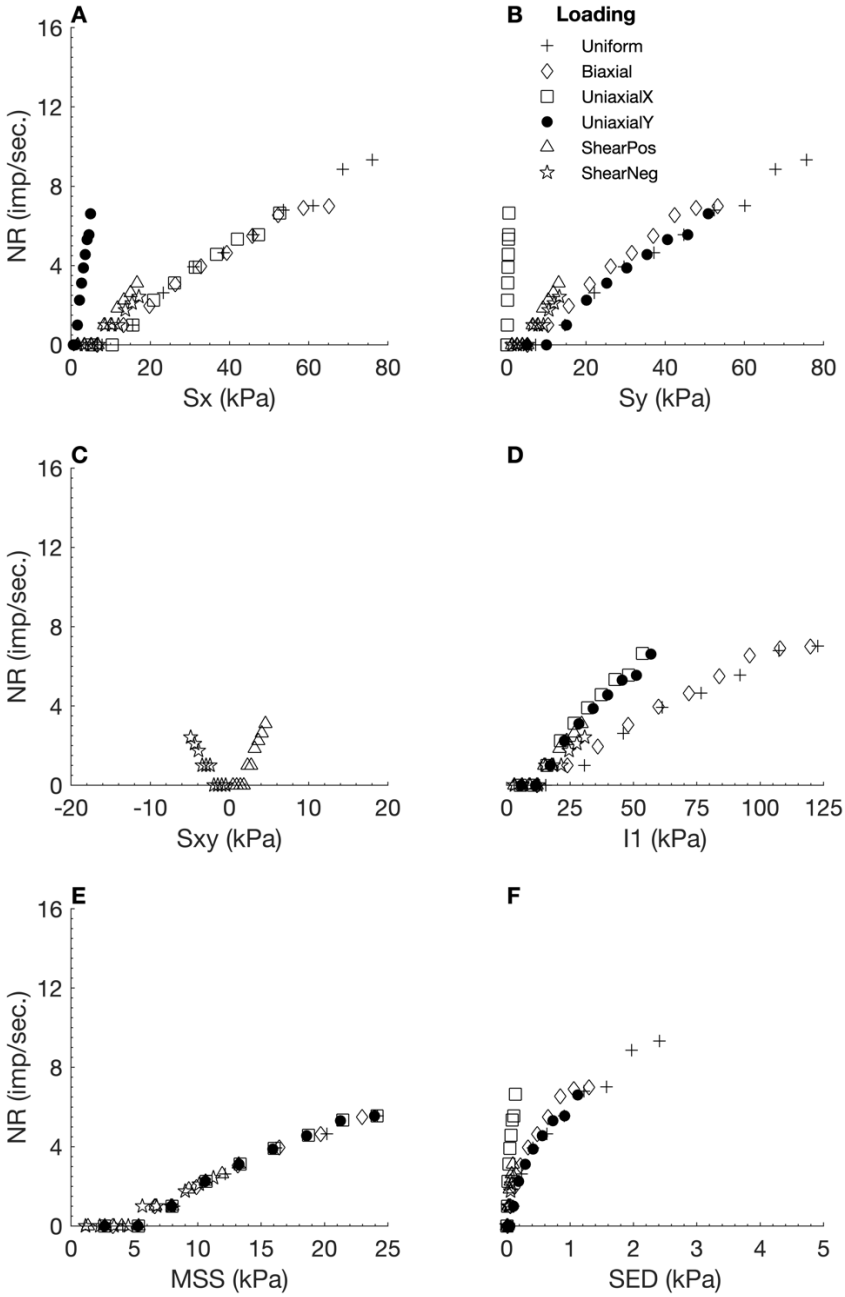

Figure B - 23. Neural responses (NR) output by the orthotropic elastic FEBio model 2 using MSS as the neural model input, plotted against six different stress variables. Sx: X stress. Sy: Y stress. Sxy: shear stress. I1: 1st invariant stress tensor. MSS: maximum shear stress. SED: strain energy density.

Table B - 27. Linear regression measures for individual loading regime results from the orthotropic elastic model 2, with MSS as neural model input.

Loading Regime	R^2	RMSE	Slope
Uniform	0.9859	0.3970	0.6577
Biaxial	0.3983	1.4145	5.0649
Uniaxial X	0.0886	1.2491	-0.1689
Uniaxial Y	0.9464	0.4222	1.1991
Shear Positive	0.5096	0.4043	0.0756
Shear Negative	0.2318	0.4526	0.1297

B.2.6 Strain Energy Density (SED)

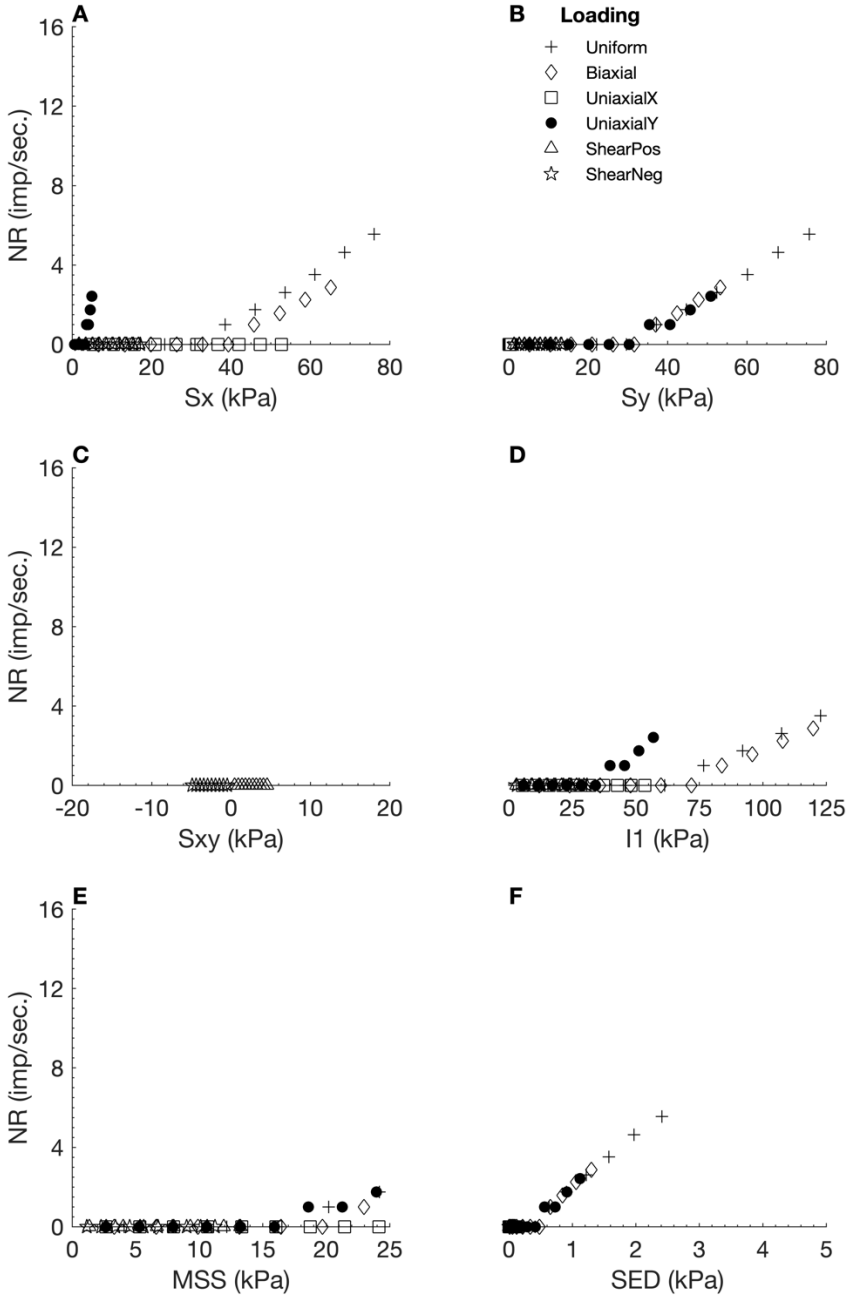

Figure B - 24. Neural responses (NR) output by the orthotropic elastic FEBio model 2 using SED as the neural model input, plotted against six different stress variables. Sx: X stress. Sy: Y stress. Sxy: shear stress. I1: 1st invariant stress tensor. MSS: maximum shear stress. SED: strain energy density.

Table B - 28. Linear regression measures for individual loading regime results from the orthotropic elastic model 2, with SED as neural model input.

Loading Regime	R^2	RMSE	Slope
Uniform	0.8521	0.8521	0.4056
Biaxial	NaN	0.0000	0.0000
Uniaxial X	NaN	0.0000	0.0000
Uniaxial Y	NaN	0.0000	0.0000
Shear Positive	NaN	0.0000	0.0000
Shear Negative	NaN	0.0000	0.0000

B.2.7 Hydrostatic Pressure (HS)

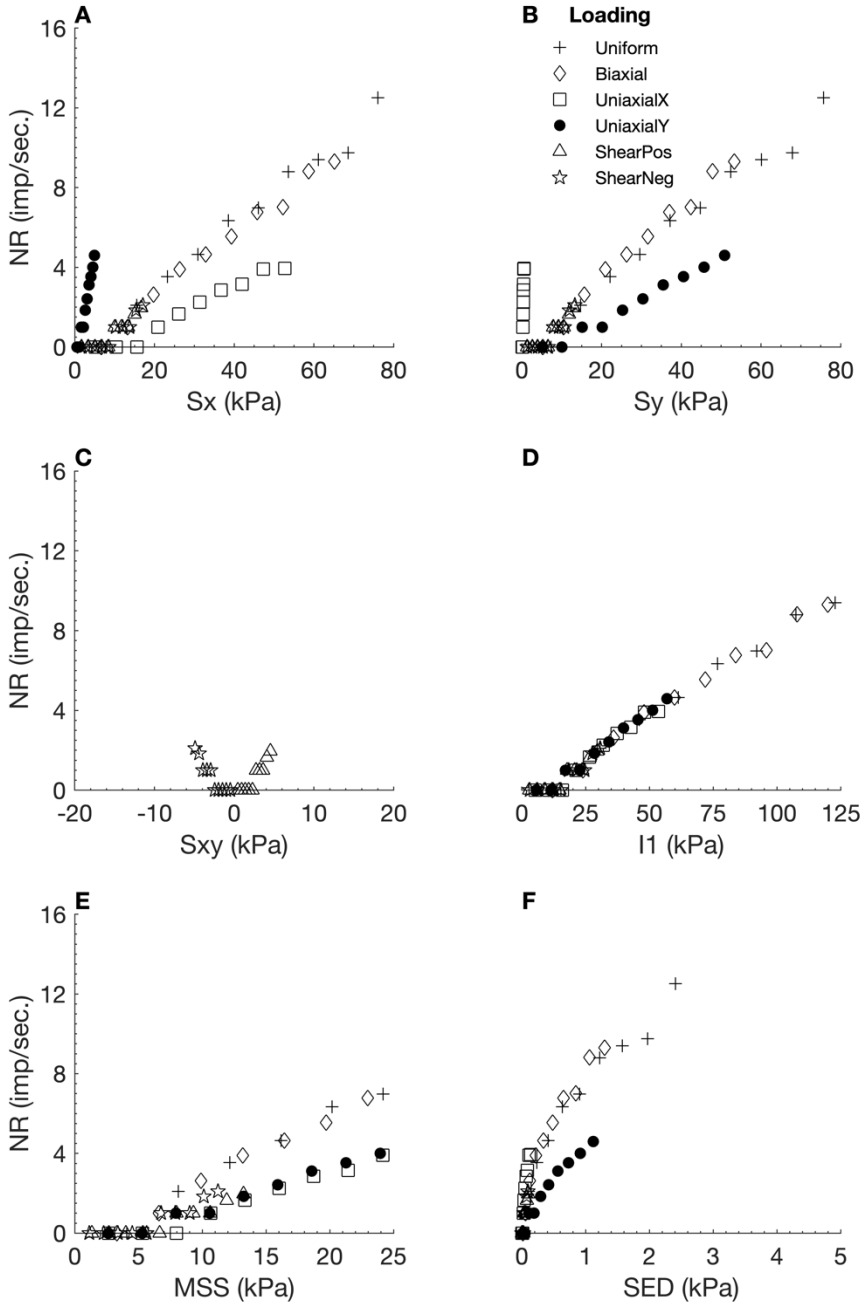

Figure B - 25. Neural responses (NR) output by the orthotropic elastic FEBio model 2 using HS as the neural model input, plotted against six different stress variables. Sx: X stress. Sy: Y stress. Sxy: shear stress. I1: 1st invariant stress tensor. MSS: maximum shear stress. SED: strain energy density.

Table B - 29. Linear regression measures for individual loading regime results from the orthotropic elastic model 2, with HS as neural model input.

Loading Regime	R^2	RMSE	Slope
Uniform	0.9676	0.7380	0.7995
Biaxial	0.5022	1.5803	6.9847
Uniaxial X	0.0076	0.6100	-0.0232
Uniaxial Y	0.8888	0.3626	0.6929
Shear Positive	0.3035	0.3809	0.0461
Shear Negative	NaN	0.0000	0.0000

B.2.8 1st Principle Stress (S1)

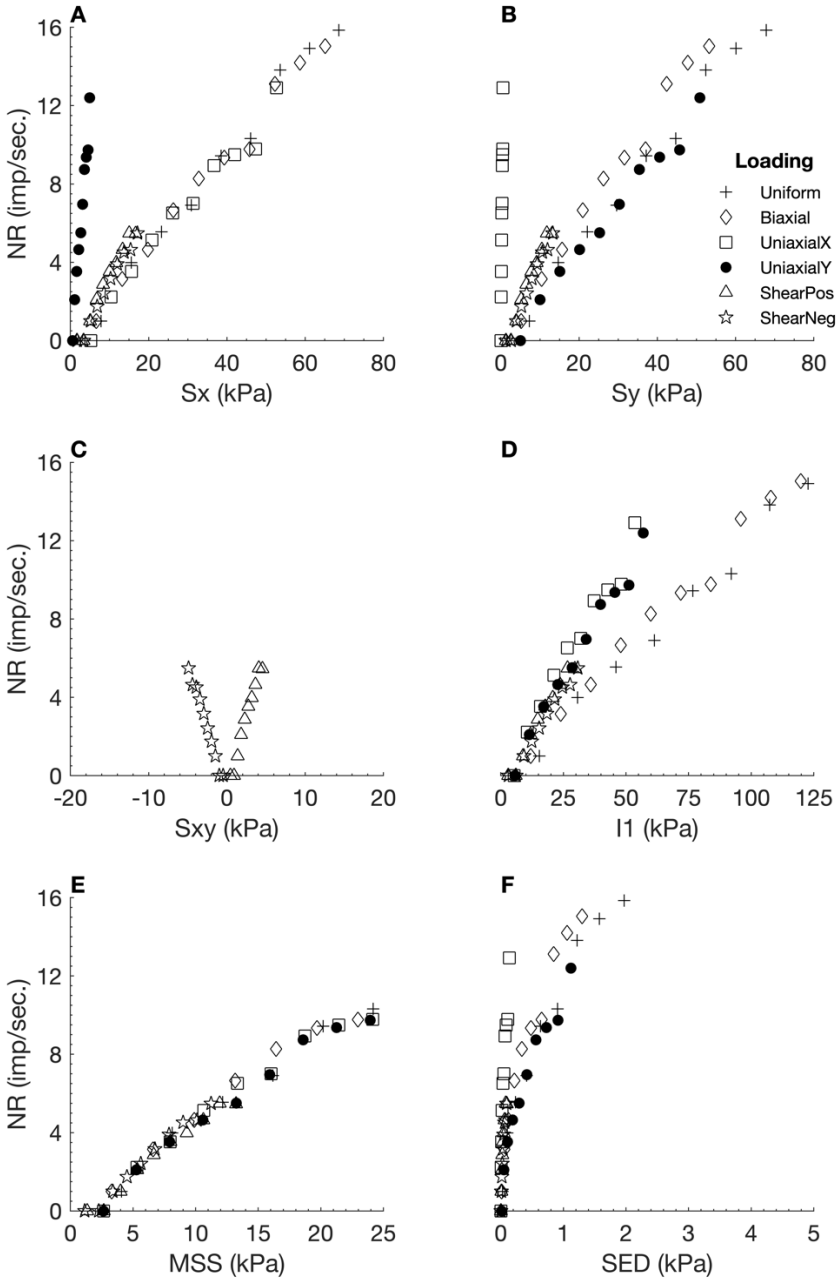

Figure B - 26. Neural responses (NR) output by the orthotropic elastic FEBio model 2 using S1 as the neural model input, plotted against six different stress variables. Sx: X stress. Sy: Y stress. Sxy: shear stress. I1: 1st invariant stress tensor. MSS: maximum shear stress. SED: strain energy density.

Table B - 30. Linear regression measures for individual loading regime results from the orthotropic elastic model 2, with S1 as neural model input.

Loading Regime	R^2	RMSE	Slope
Uniform	0.9819	0.7745	1.1303
Biaxial	0.3872	2.5832	9.0363
Uniaxial X	0.4728	1.9303	-0.7926
Uniaxial Y	0.8835	0.9508	1.7694
Shear Positive	0.8570	0.6297	0.2828
Shear Negative	0.7544	0.6108	0.5586

B.2.9 2nd Principle Stress (S2)

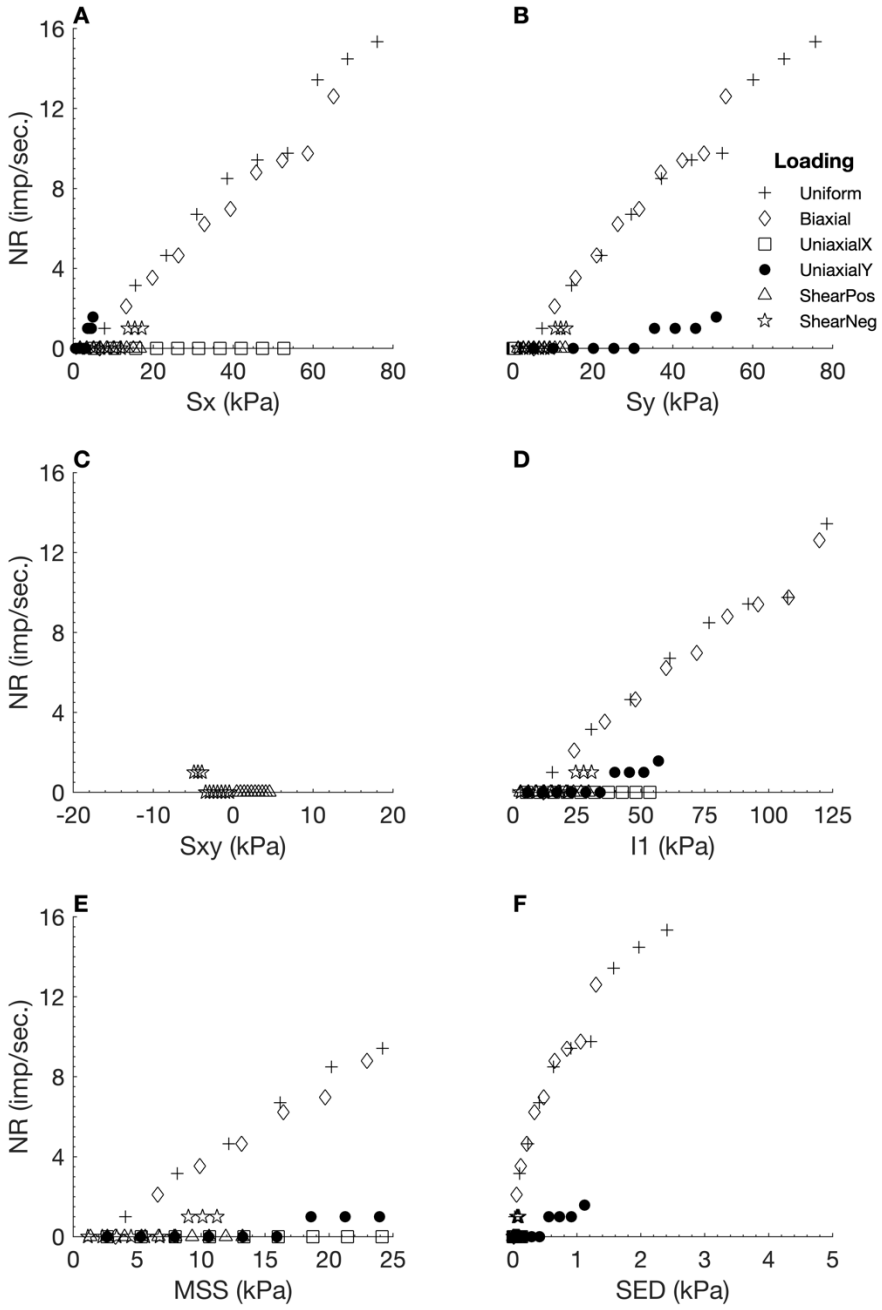

Figure B - 27. Neural responses (NR) output by the orthotropic elastic FEBio model 2 using S2 as the neural model input, plotted against six different stress variables. Sx: X stress. Sy: Y stress. Sxy: shear stress. I1: 1st invariant stress tensor. MSS: maximum shear stress. SED: strain energy density.

Table B - 31. Linear regression measures for individual loading regime results from the orthotropic elastic model 2, with S2 as neural model input.

Loading Regime	R^2	RMSE	Slope
Uniform	0.9723	0.8568	1.0069
Biaxial	0.3999	2.1330	7.6621
Uniaxial X	NaN	0.0000	0.0000
Uniaxial Y	NaN	0.0000	0.0000
Shear Positive	NaN	0.0000	0.0000
Shear Negative	NaN	0.0000	0.0000

B.2.10 3rd Principle Stress (S3)

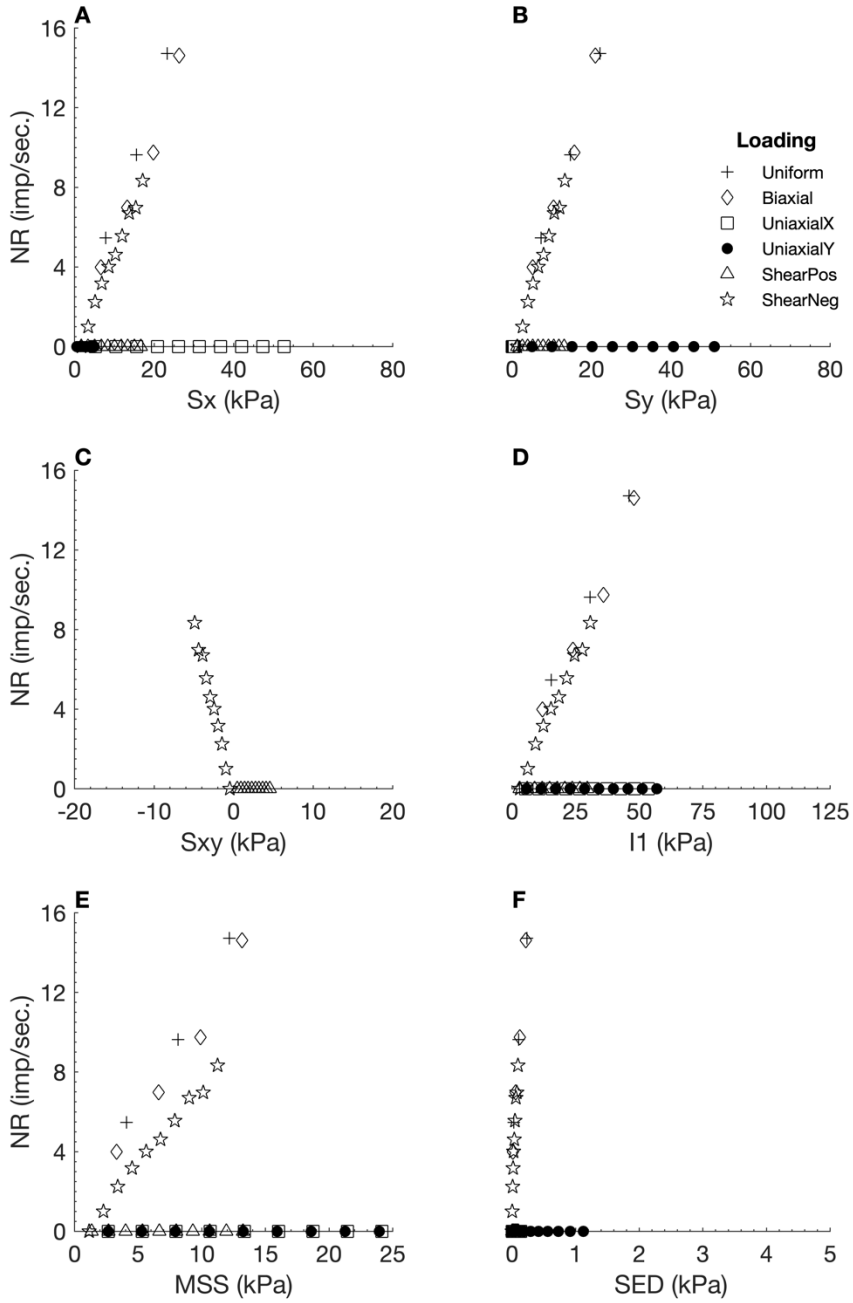

Figure B - 28. Neural responses (NR) output by the orthotropic elastic FEBio model 2 using S3 as the neural model input, plotted against six different stress variables. Sx: X stress. Sy: Y stress. Sxy: shear stress. I1: 1st invariant stress tensor. MSS: maximum shear stress. SED: strain energy density.

Table B - 32. Linear regression measures for individual loading regime results from the orthotropic elastic model 2, with S3 as neural model input.

Loading Regime	R^2	RMSE	Slope
Uniform	0.9497	1.4970	1.2899
Biaxial	0.4235	4.4959	16.9576
Uniaxial X	NaN	0.0000	0.0000
Uniaxial Y	NaN	0.0000	0.0000
Shear Positive	NaN	0.0000	0.0000
Shear Negative	0.9108	0.5572	0.9289

B.2.11 Deviatoric Stress 1 (Dev1)

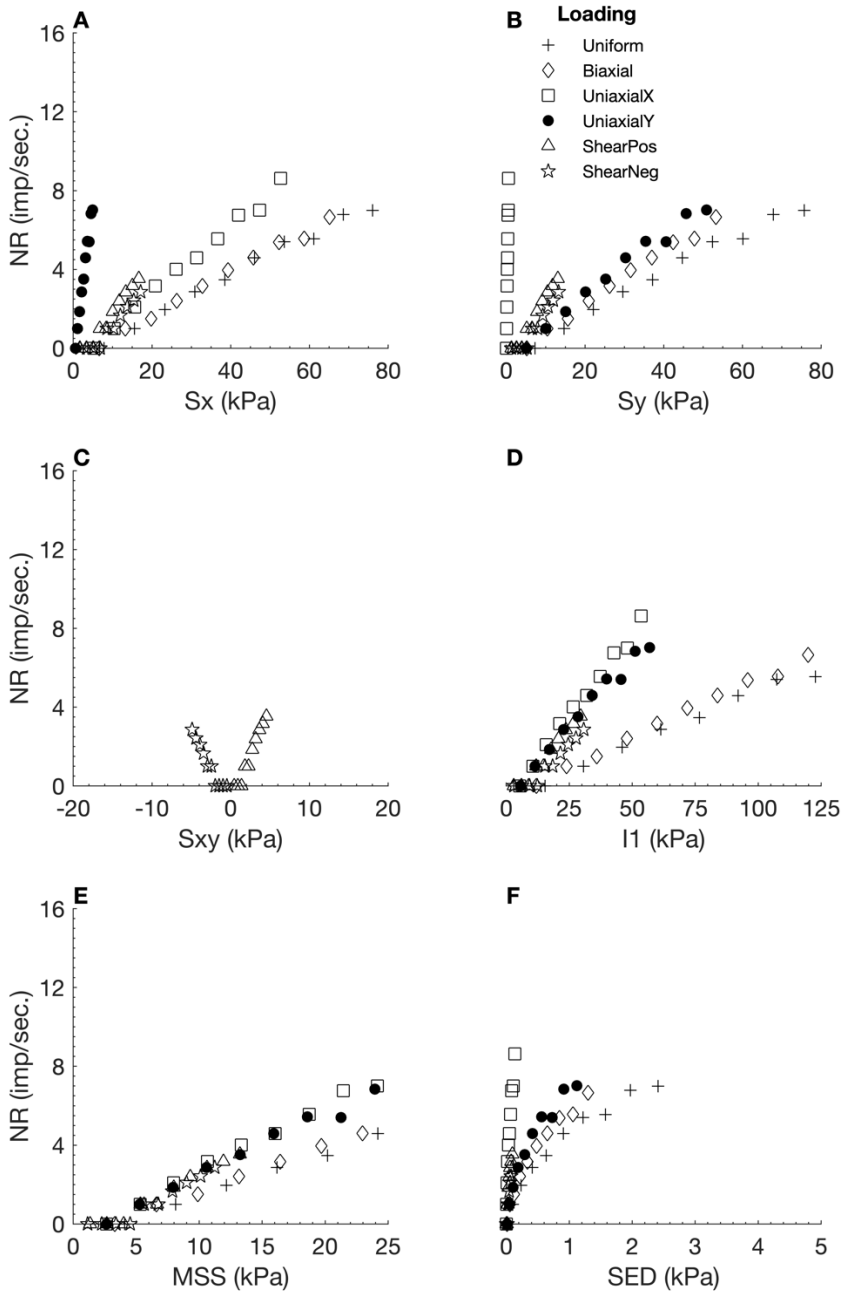

Figure B - 29. Neural responses (NR) output by the orthotropic elastic FEBio model 2 using Dev1 as the neural model input, plotted against six different stress variables. Sx: X stress. Sy: Y stress. Sxy: shear stress. I1: 1st invariant stress tensor. MSS: maximum shear stress. SED: strain energy density.

Table B - 33. Linear regression measures for individual loading regime results from the orthotropic elastic model 2, with Dev1 as neural model input.

Loading Regime	R^2	RMSE	Slope
Uniform	0.9924	0.2219	0.5036
Biaxial	0.3476	1.1445	3.6767
Uniaxial X	0.3584	1.3410	-0.4346
Uniaxial Y	0.9380	0.4695	1.2340
Shear Positive	0.6964	0.4741	0.1317
Shear Negative	0.2318	0.4526	0.1297

B.2.12 Deviatoric Stress 2 (Dev2)

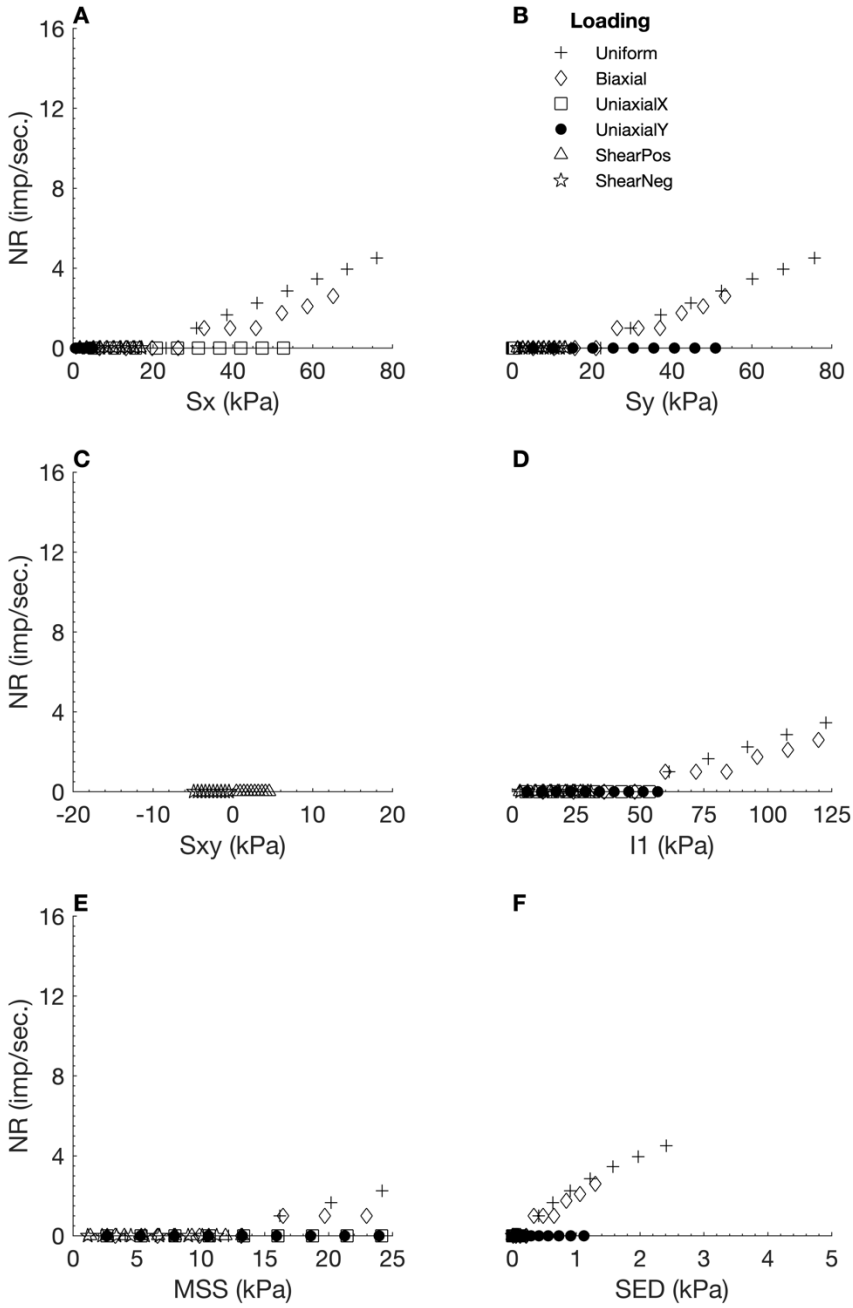

Figure B - 30. Neural responses (NR) output by the orthotropic elastic FEBio model 2 using Dev2 as the neural model input, plotted against six different stress variables. Sx: X stress. Sy: Y stress. Sxy: shear stress. I1: 1st invariant stress tensor. MSS: maximum shear stress. SED: strain energy density.

Table B - 34. Linear regression measures for individual loading regime results from the orthotropic elastic model 2, with Dev2 as neural model input.

Loading Regime	R^2	RMSE	Slope
Uniform	0.9481	0.4117	0.3491
Biaxial	0.0001	0.5164	-0.0233
Uniaxial X	NaN	0.0000	0.0000
Uniaxial Y	NaN	0.0000	0.0000
Shear Positive	NaN	0.0000	0.0000
Shear Negative	NaN	0.0000	0.0000

B.2.13 Deviatoric Stress 3 (Dev3)

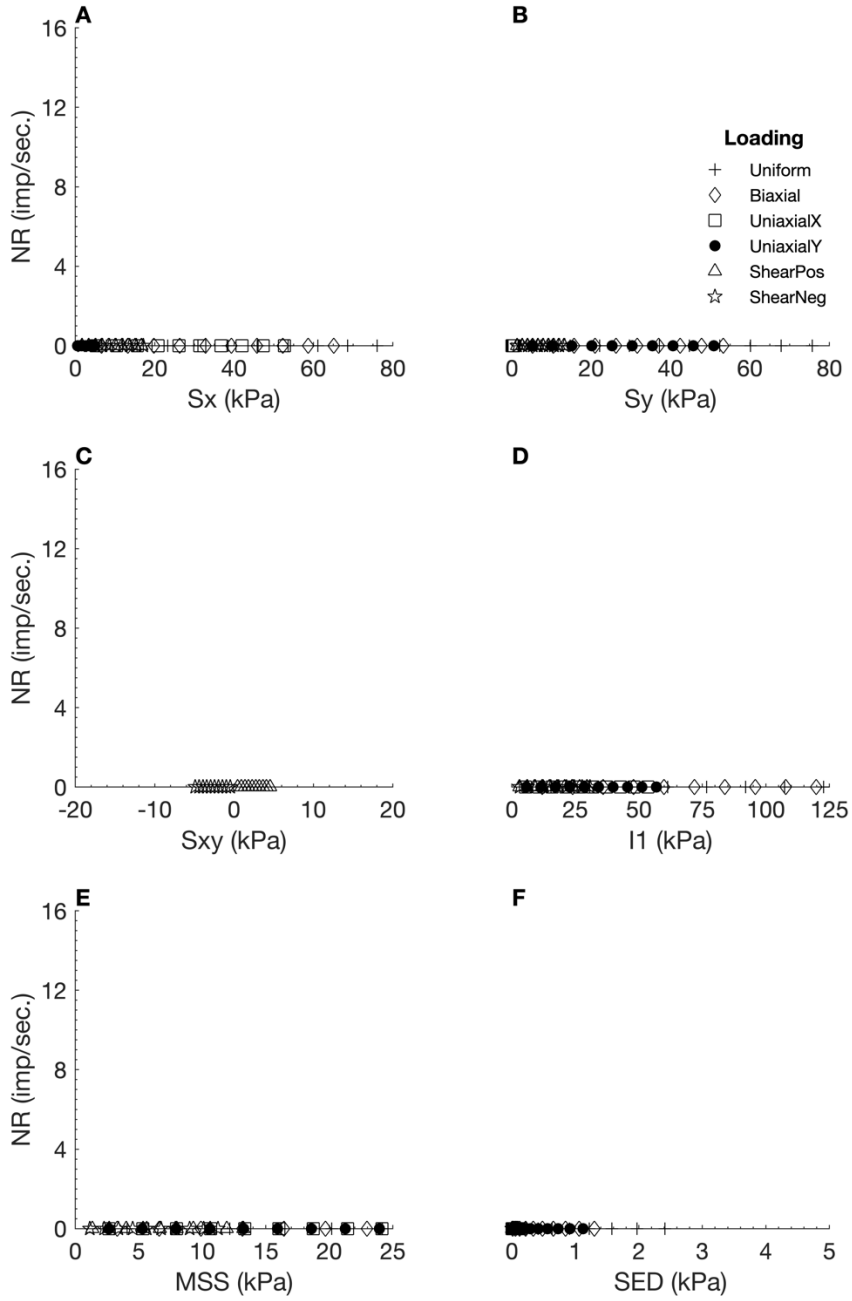

Figure B - 31. Neural responses (NR) output by the orthotropic elastic FEBio model 2 using Dev3 as the neural model input, plotted against six different stress variables. Sx: X stress. Sy: Y stress. Sxy: shear stress. I1: 1st invariant stress tensor. MSS: maximum shear stress. SED: strain energy density.

Table B - 35. Linear regression measures for individual loading regime results from the orthotropic elastic model 2, with Dev3 as neural model input.

Loading Regime	R^2	RMSE	Slope
Uniform	NaN	0.0000	0.0000
Biaxial	NaN	0.0000	0.0000
Uniaxial X	NaN	0.0000	0.0000
Uniaxial Y	NaN	0.0000	0.0000
Shear Positive	NaN	0.0000	0.0000
Shear Negative	NaN	0.0000	0.0000

B.2.14 Shear Stress A

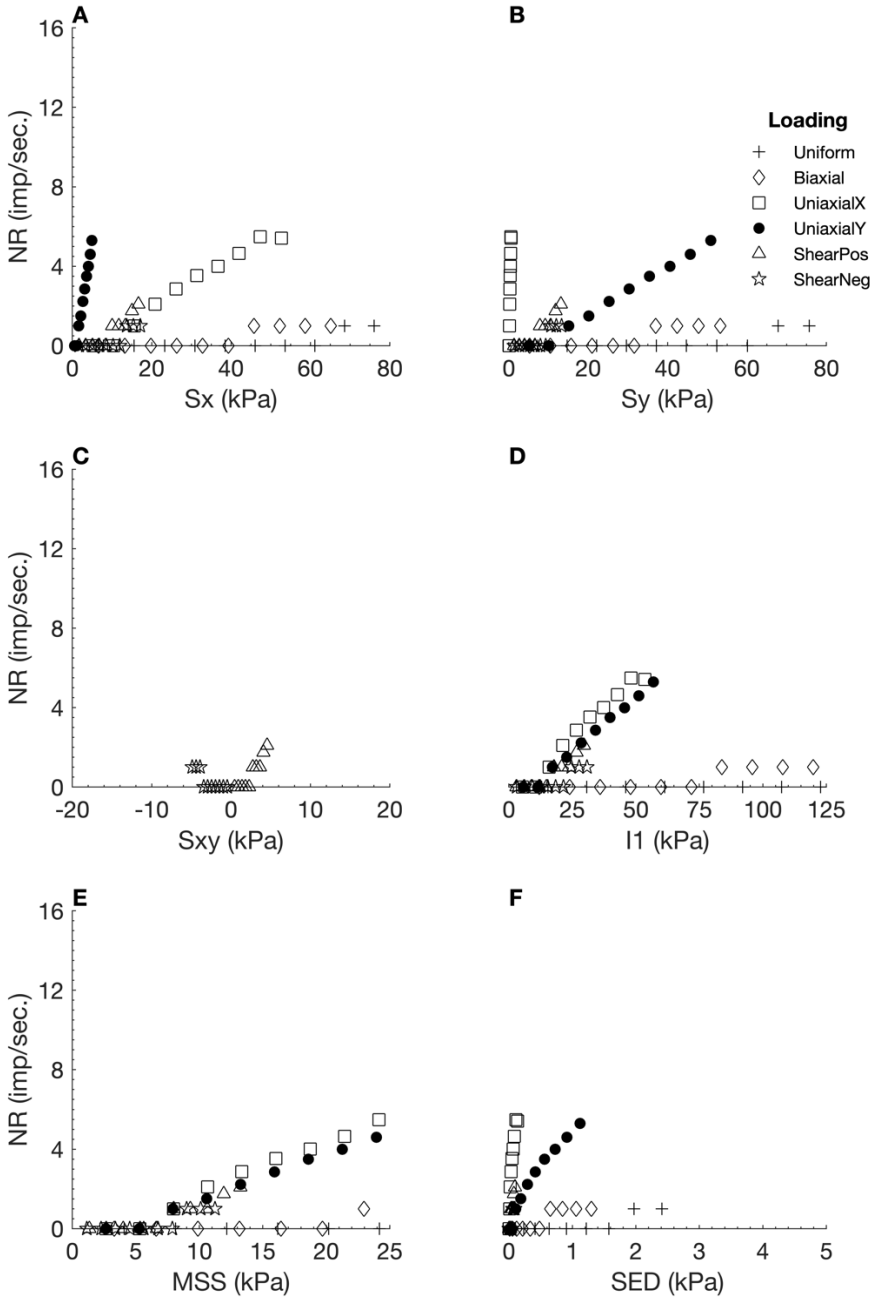

Figure B - 32. Neural responses (NR) output by the orthotropic elastic FEBio model 2 using ShearA as the neural model input, plotted against six different stress variables. Sx: X stress. Sy: Y stress. Sxy: shear stress. I1: 1st invariant stress tensor. MSS: maximum shear stress. SED: strain energy density.

Table B - 36. Linear regression measures for individual loading regime results from the orthotropic elastic model 2, with ShearA as neural model input.

Loading Regime	R^2	RMSE	Slope
Uniform	0.3998	0.3465	0.0561
Biaxial	NaN	0.0000	0.0000
Uniaxial X	0.0970	1.1626	-0.1653
Uniaxial Y	0.9243	0.3585	0.8468
Shear Positive	0.3035	0.3809	0.0461
Shear Negative	NaN	0.0000	0.0000

B.2.15 Shear Stress B

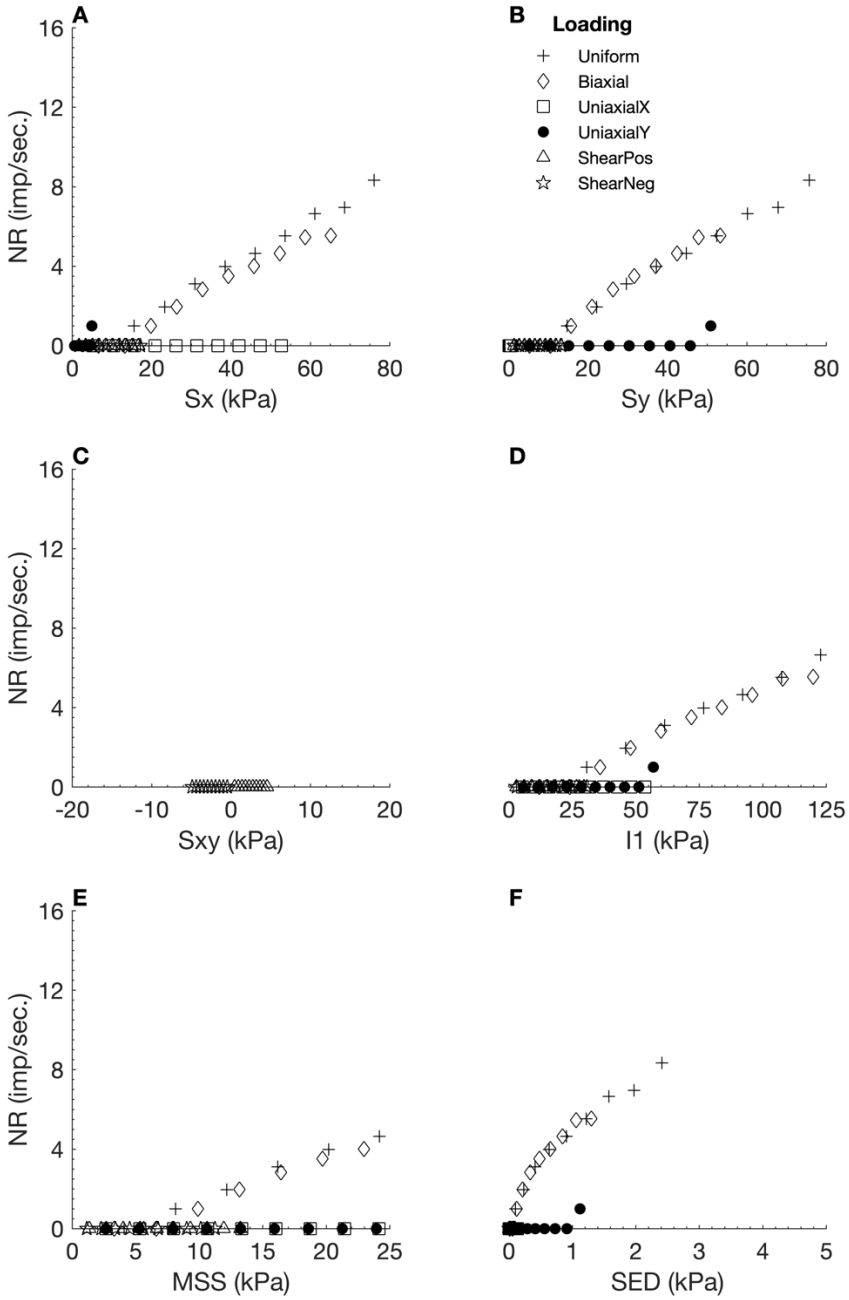

Figure B - 33. Neural responses (NR) output by the orthotropic elastic FEBio model 2 using ShearB as the neural model input, plotted against six different stress variables. Sx: X stress. Sy: Y stress. Sxy: shear stress. I1: 1st invariant stress tensor. MSS: maximum shear stress. SED: strain energy density.

Table B - 37. Linear regression measures for individual loading regime results from the orthotropic elastic model 2, with ShearB as neural model input.

Loading Regime	R^2	RMSE	Slope
Uniform	0.9822	0.3855	0.5683
Biaxial	0.3527	1.1539	3.7485
Uniaxial X	NaN	0.0000	0.0000
Uniaxial Y	NaN	0.0000	0.0000
Shear Positive	NaN	0.0000	0.0000
Shear Negative	NaN	0.0000	0.0000

B.2.16 Shear Stress C

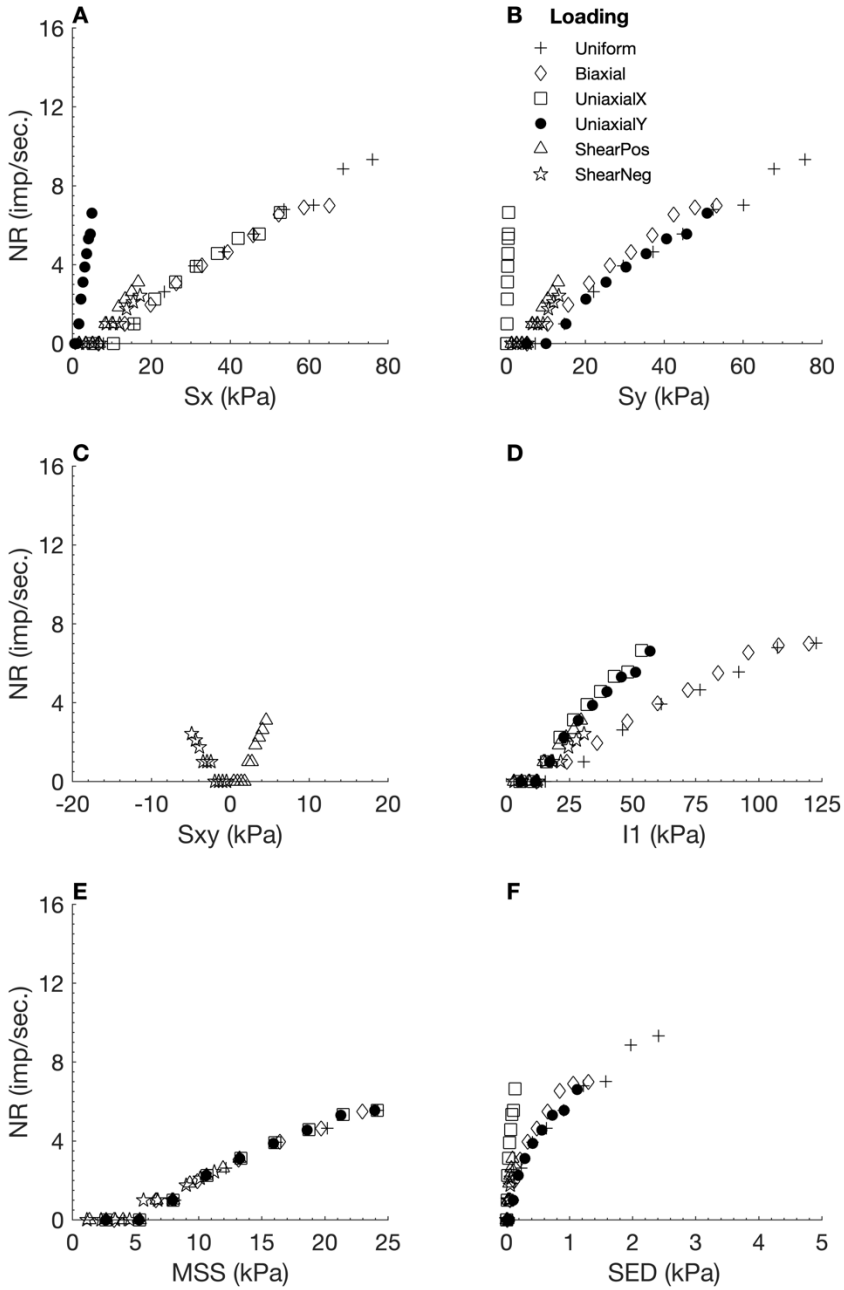

Figure B - 34. Neural responses (NR) output by the orthotropic elastic FEBio model 2 using ShearC as the neural model input, plotted against six different stress variables. Sx: X stress. Sy: Y stress. Sxy: shear stress. I1: 1st invariant stress tensor. MSS: maximum shear stress. SED: strain energy density.

Table B - 38. Linear regression measures for individual loading regime results from the orthotropic elastic model 2, with ShearC as neural model input.

Loading Regime	R^2	RMSE	Slope
Uniform	0.9859	0.3970	0.6577
Biaxial	0.3983	1.4145	5.0649
Uniaxial X	0.0886	1.2491	-0.1689
Uniaxial Y	0.9464	0.4222	1.1991
Shear Positive	0.5096	0.4043	0.0756
Shear Negative	0.2318	0.4526	0.1297

B.2.17 X Strain (Ex)

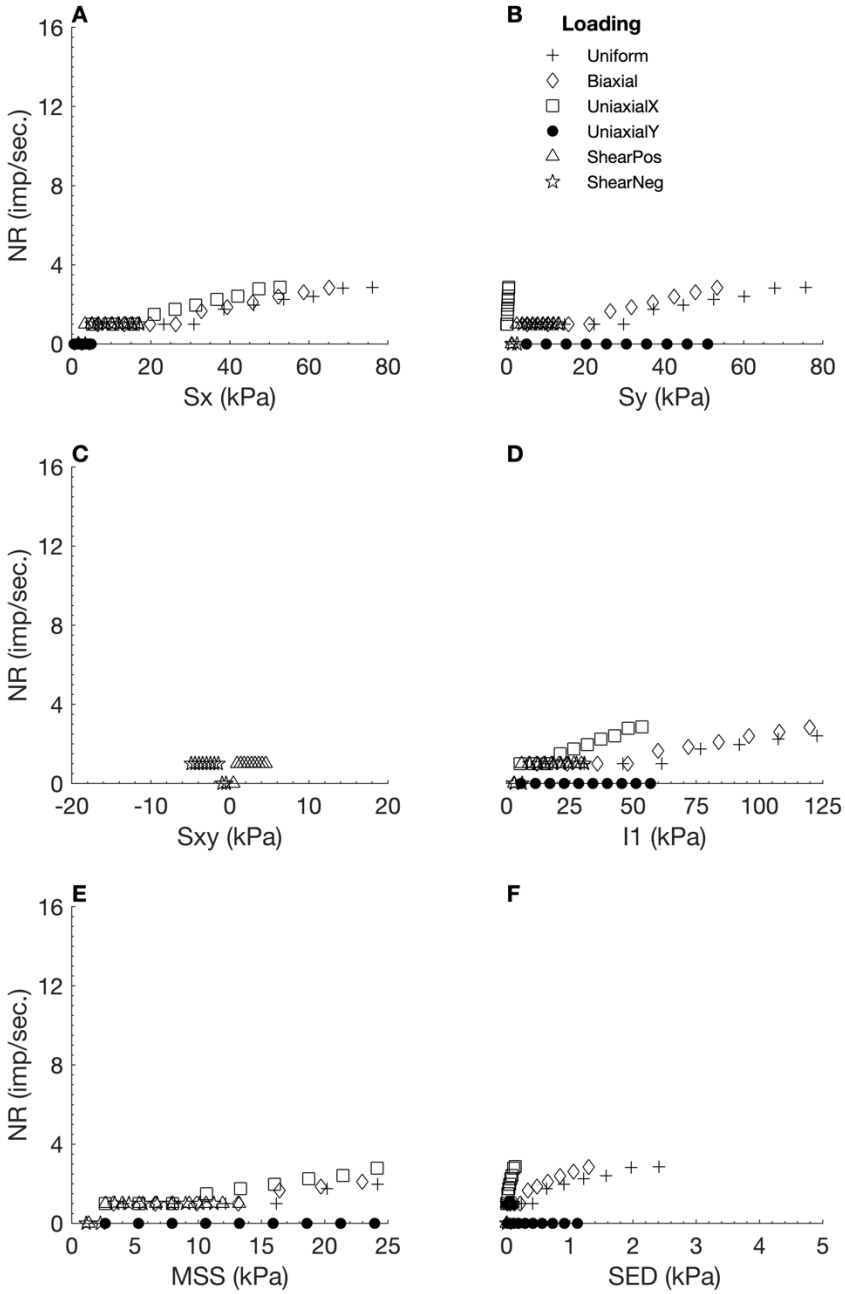

Figure B - 35. Neural responses (NR) output by the orthotropic elastic FEBio model 2 using Ex as the neural model input, plotted against six different stress variables. Sx: X stress. Sy: Y stress. Sxy: shear stress. I1: 1st invariant stress tensor. MSS: maximum shear stress. SED: strain energy density.

Table B - 39. Linear regression measures for individual loading regime results from the orthotropic elastic model 2, with Ex as neural model input.

Loading Regime	R^2	RMSE	Slope
Uniform	0.9071	0.2486	0.1541
Biaxial	0.0001	0.3390	-0.0153
Uniaxial X	0.0076	0.3053	-0.0116
Uniaxial Y	NaN	0.0000	0.0000
Shear Positive	0.6424	0.2730	0.0671
Shear Negative	0.8275	0.2627	0.3002

B.2.18 Y Strain (Ey)

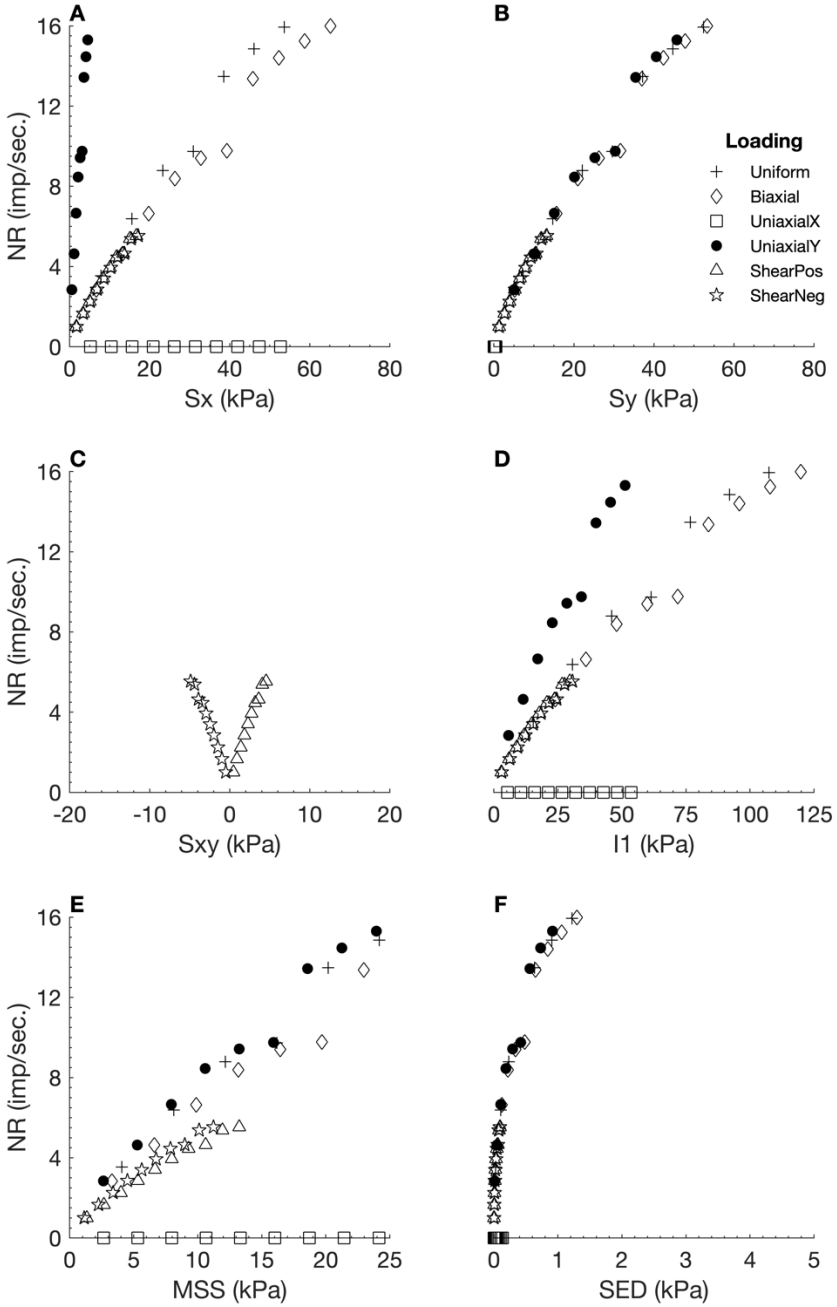

Figure B - 36. Neural responses (NR) output by the orthotropic elastic FEBio model 2 using Ey as the neural model input, plotted against six different stress variables. Sx: X stress. Sy: Y stress. Sxy: shear stress. I1: 1st invariant stress tensor. MSS: maximum shear stress. SED: strain energy density.

Table B - 40. Linear regression measures for individual loading regime results from the orthotropic elastic model 2, with Ey as neural model input.

Loading Regime	R^2	RMSE	Slope
Uniform	0.9764	0.8452	1.0786
Biaxial	0.4896	2.2153	9.5488
Uniaxial X	NaN	0.0000	0.0000
Uniaxial Y	0.8331	1.2685	1.9151
Shear Positive	0.9604	0.2446	0.2211
Shear Negative	0.8961	0.3529	0.5408

B.3 Test 3

Table B - 41. Values selected for material properties during FEBio implementation of orthotropic elastic material test 3.

Orthotropic Material Property	**Value Selected**
Density	1
Young's Modulus (X)	7.4
Young's Modulus (Y)	1
Young's Modulus (Z)	1
Shear Modulus (XY)	2.85
Shear Modulus (YZ)	0.336
Shear Modulus (XZ)	0.385
Poisson's Ratio (XY)	0.299
Poisson's Ratio (YZ)	0.488
Poisson's Ratio (XZ)	0.299

B.3.1 X Stress (Sx)

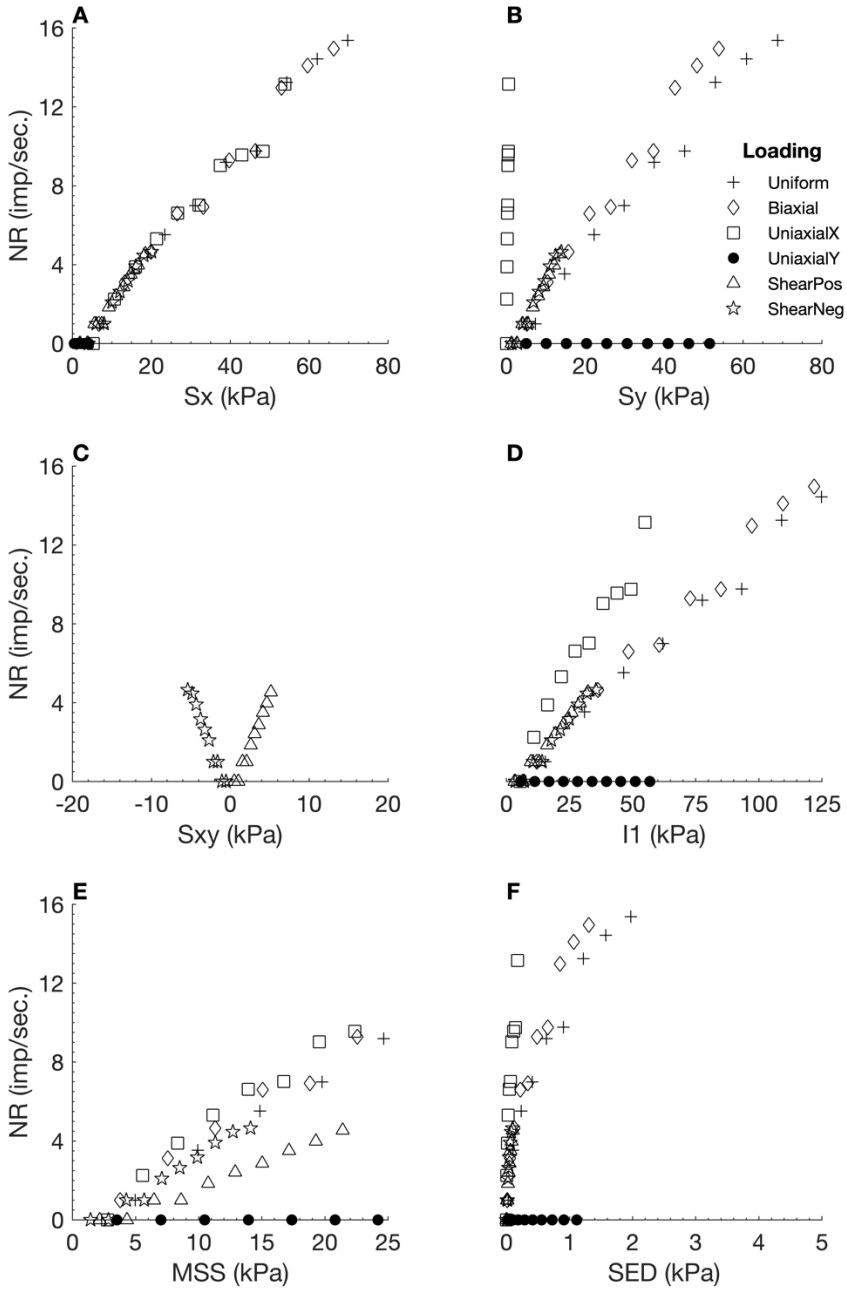

Figure B - 37. Neural responses (NR) output by the orthotropic elastic FEBio model 3 using Sx as the neural model input, plotted against six different stress variables. Sx: X stress. Sy: Y stress. Sxy: shear stress. I1: 1st invariant stress tensor. MSS: maximum shear stress. SED: strain energy density.

Table B - 42. Linear regression measures for individual loading regime results from the orthotropic elastic model 3, with Sx as neural model input.

Loading Regime	R^2	RMSE	Slope
Uniform	0.9836	0.7123	1.0953
Biaxial	0.5149	1.9886	9.0160
Uniaxial X	0.4813	2.0130	-0.8408
Uniaxial Y	NaN	0.0000	0.0000
Shear Positive	0.8407	0.4334	0.1826
Shear Negative	0.7102	0.5413	0.4421

B.3.2 Y Stress (Sy)

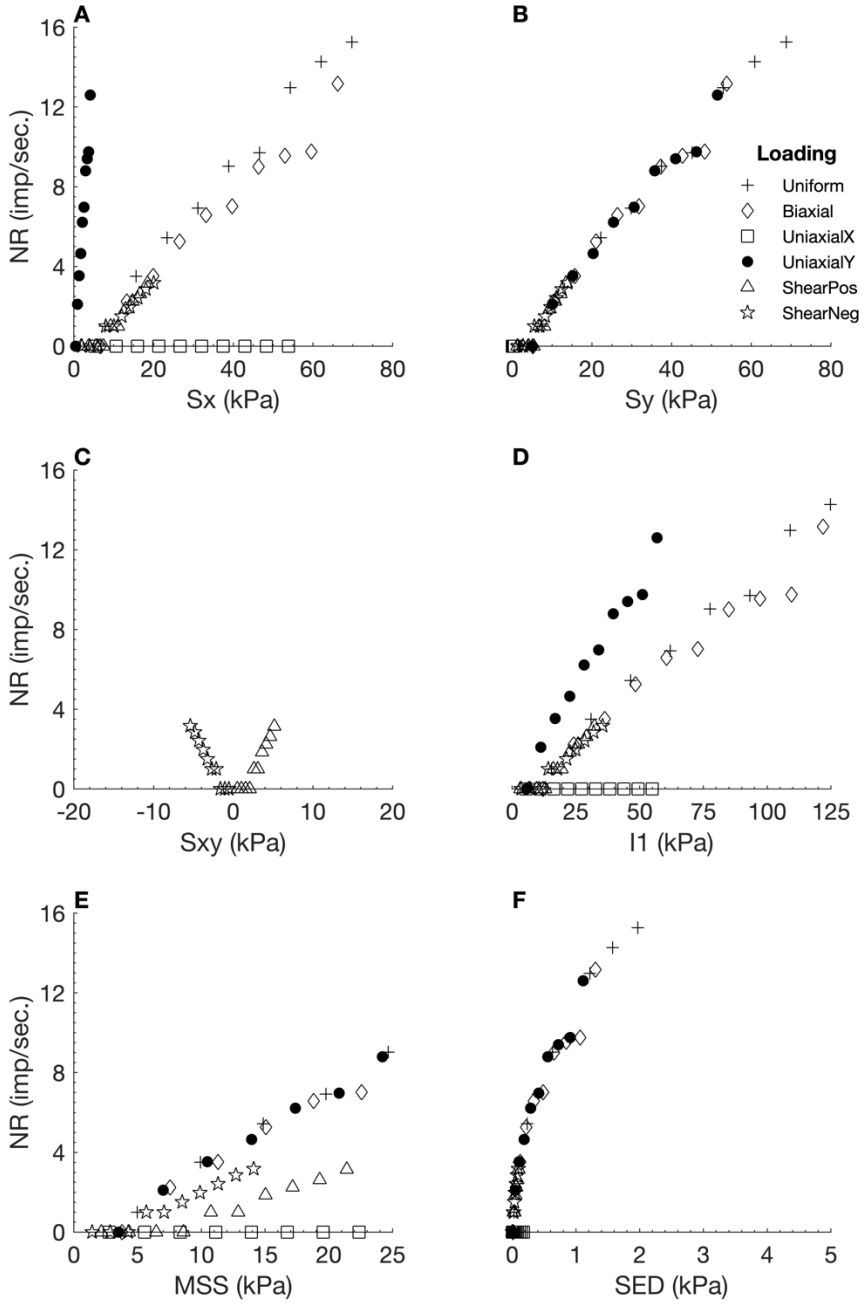

Figure B - 38. Neural responses (NR) output by the orthotropic elastic FEBio model 3 using Sy as the neural model input, plotted against six different stress variables. Sx: X stress. Sy: Y stress. Sxy: shear stress. I1: 1st invariant stress tensor. MSS: maximum shear stress. SED: strain energy density.

Table B - 43. Linear regression measures for individual loading regime results from the orthotropic elastic model 3, with Sy as neural model input.

Loading Regime	R^2	RMSE	Slope
Uniform	0.9850	0.6766	1.0865
Biaxial	0.3991	2.2999	8.2485
Uniaxial X	NaN	0.0000	0.0000
Uniaxial Y	0.8959	0.9403	1.8640
Shear Positive	0.5096	0.4043	0.0756
Shear Negative	0.4848	0.4540	0.2298

B.3.3 Shear Stress (Sxy)

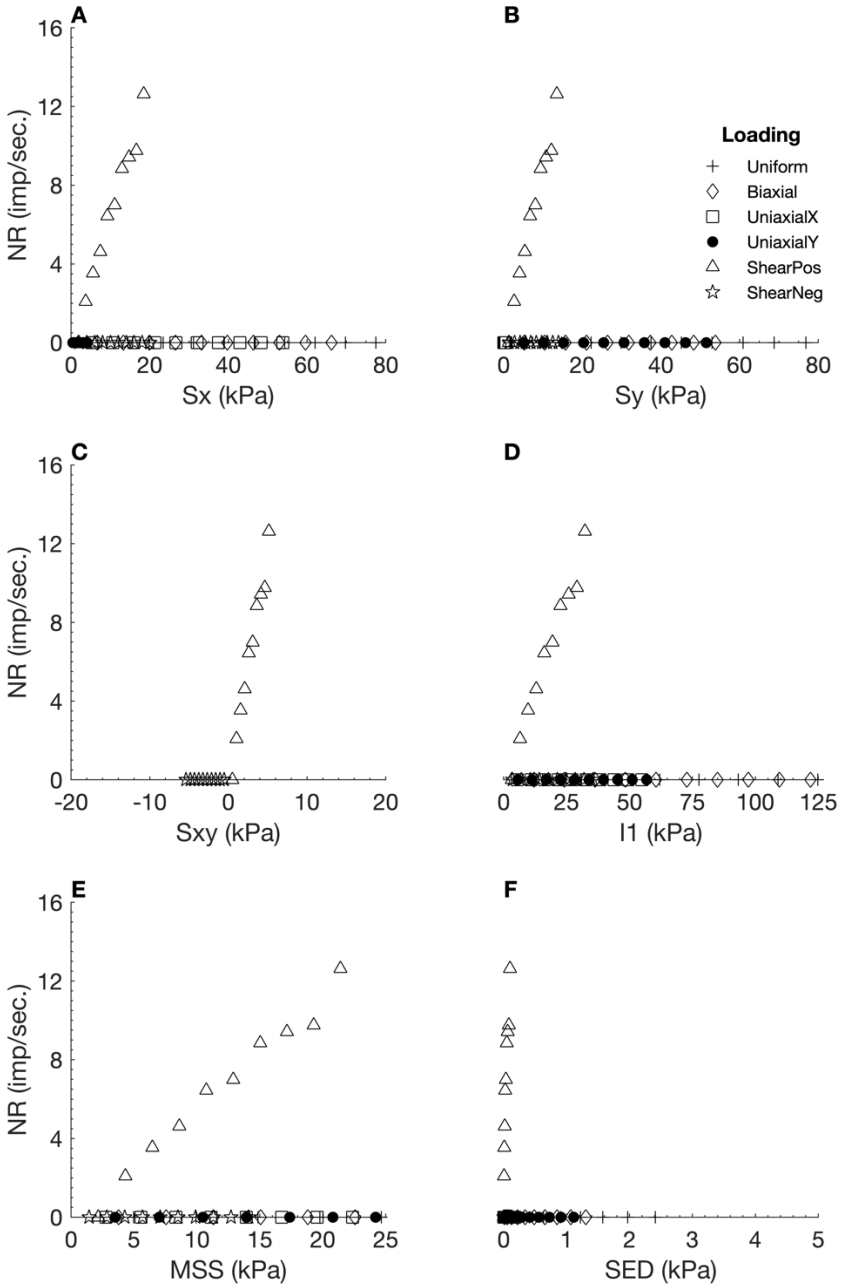

Figure B - 39. Neural responses (NR) output by the orthotropic elastic FEBio model 3 using Sxy as the neural model input, plotted against six different stress variables. Sx: X stress. Sy: Y stress. Sxy: shear stress. I1: 1st invariant stress tensor. MSS: maximum shear stress. SED: strain energy density.

Table B - 44. Linear regression measures for individual loading regime results from the orthotropic elastic model 3, with Sxy as neural model input.

Loading Regime	R^2	RMSE	Slope
Uniform	NaN	0.0000	0.0000
Biaxial	NaN	0.0000	0.0000
Uniaxial X	NaN	0.0000	0.0000
Uniaxial Y	NaN	0.0000	0.0000
Shear Positive	0.9749	0.4693	0.5369
Shear Negative	NaN	0.0000	0.0000

B.3.4 1st Invariant Stress Tensor (I1)

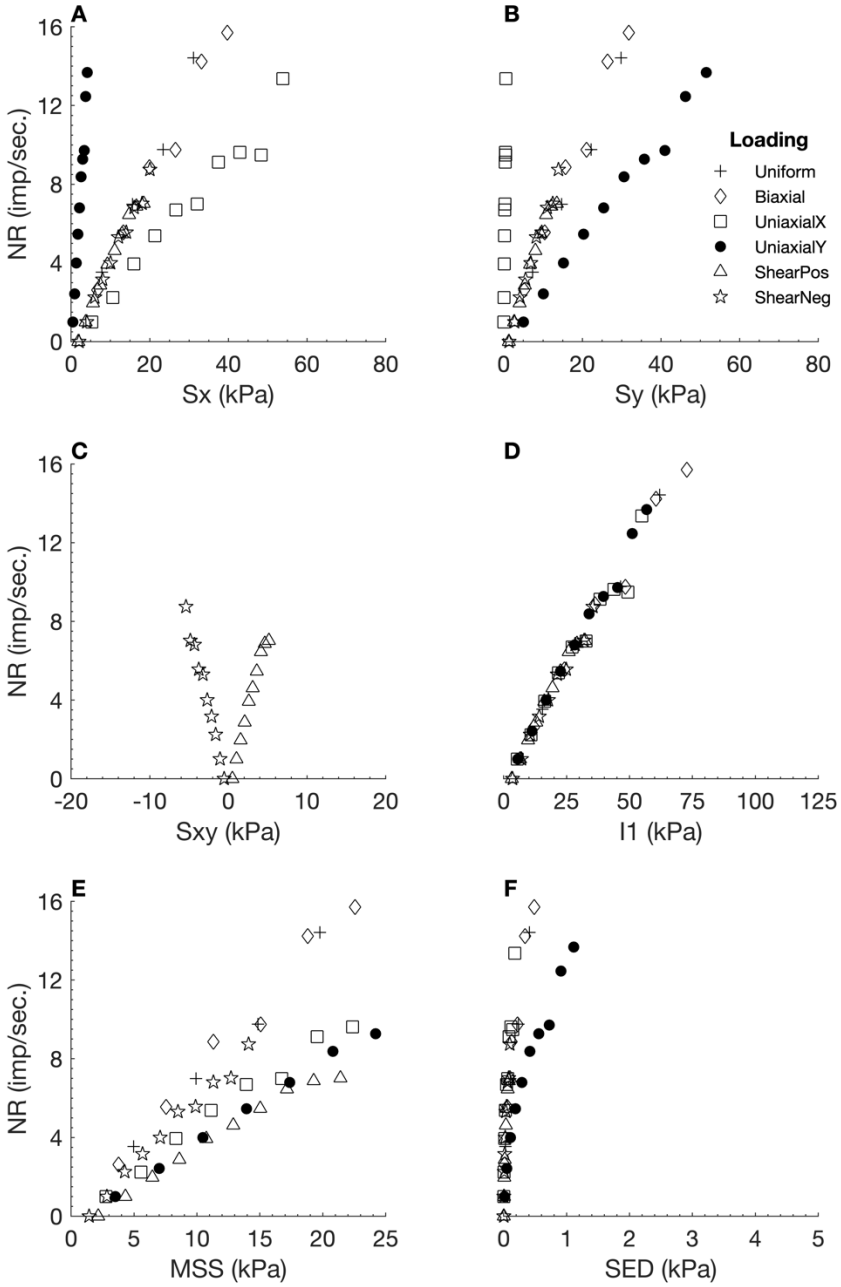

Figure B - 40. Neural responses (NR) output by the orthotropic elastic FEBio model 3 using I1 as the neural model input, plotted against six different stress variables. Sx: X stress. Sy: Y stress. Sxy: shear stress. I1: 1st invariant stress tensor. MSS: maximum shear stress. SED: strain energy density.

Table B - 45. Linear regression measures for individual loading regime results from the orthotropic elastic model 3, with I1 as neural model input.

Loading Regime	R^2	RMSE	Slope
Uniform	0.9639	1.3179	1.3508
Biaxial	0.3432	4.1133	13.0858
Uniaxial X	0.3358	1.9177	-0.5913
Uniaxial Y	0.9408	0.7486	2.0170
Shear Positive	0.9548	0.4173	0.3518
Shear Negative	0.9126	0.5497	0.9267

B.3.5 Maximum Shear Stress (MSS)

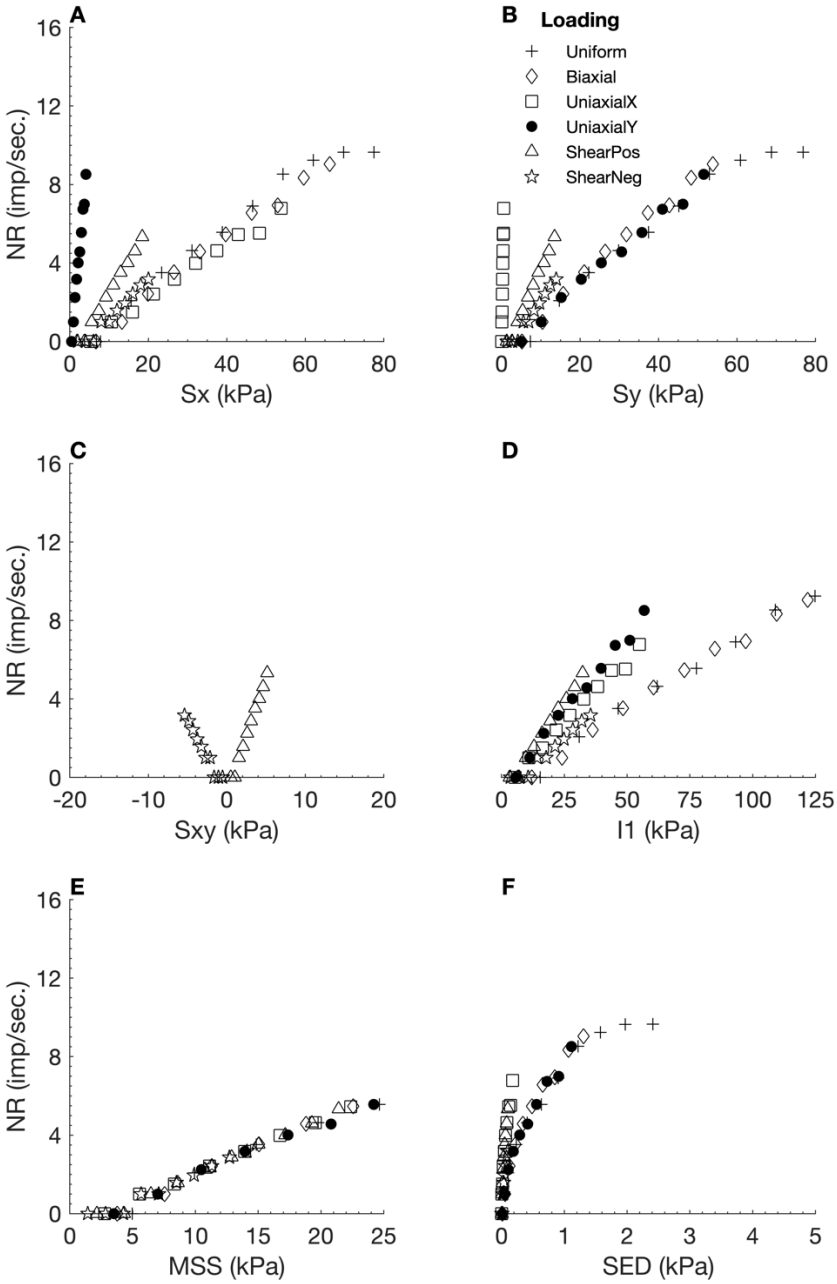

Figure B - 41. Neural responses (NR) output by the orthotropic elastic FEBio model 3 using MSS as the neural model input, plotted against six different stress variables. Sx: X stress. Sy: Y stress. Sxy: shear stress. I1: 1st invariant stress tensor. MSS: maximum shear stress. SED: strain energy density.

Table B - 46. Linear regression measures for individual loading regime results from the orthotropic elastic model 3, with MSS as neural model input.

Loading Regime	R^2	RMSE	Slope
Uniform	0.9839	0.4577	0.7091
Biaxial	0.4418	1.5966	6.2507
Uniaxial X	0.4230	0.9393	-0.3487
Uniaxial Y	0.8924	0.6474	1.2596
Shear Positive	0.8702	0.4738	0.2251
Shear Negative	0.4848	0.4540	0.2298

B.3.6 Strain Energy Density (SED)

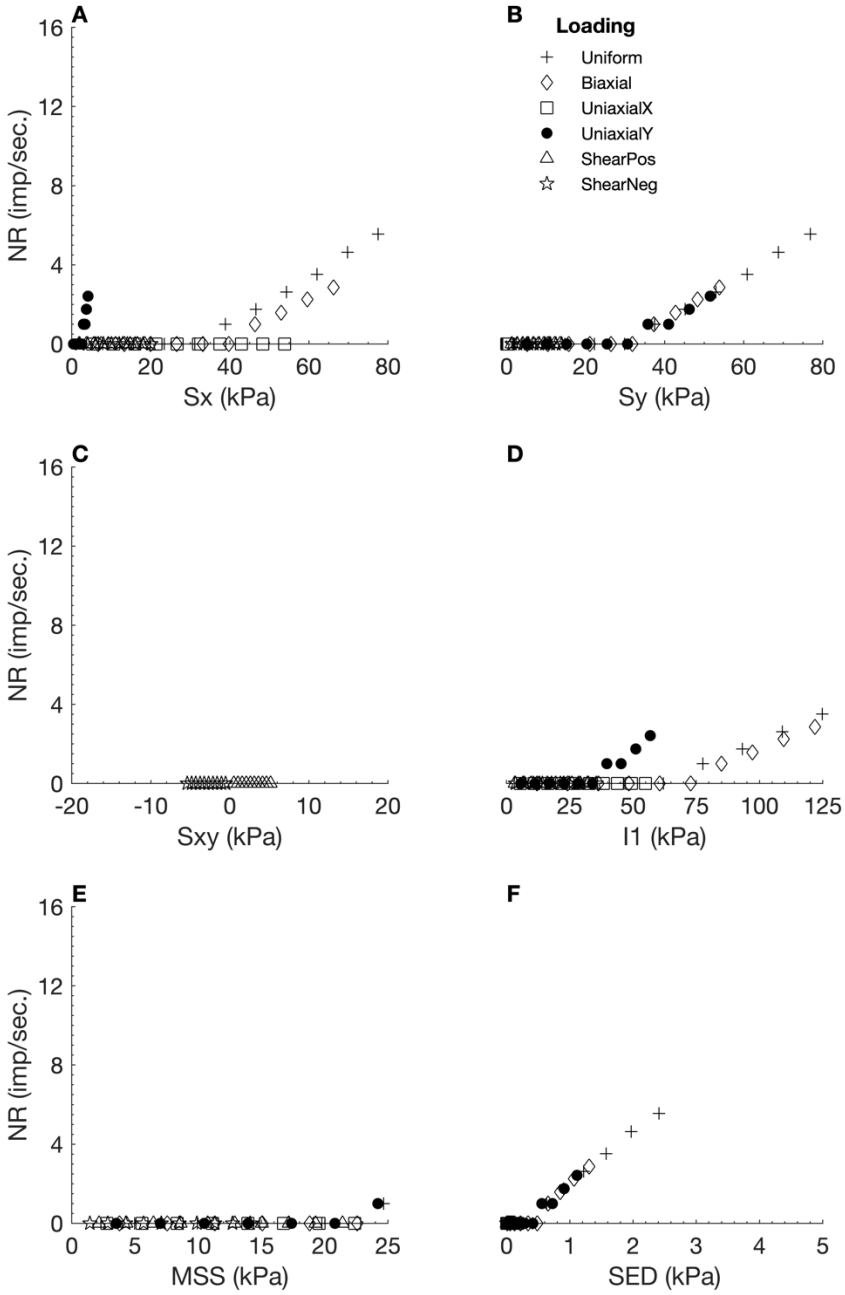

Figure B - 42. Neural responses (NR) output by the orthotropic elastic FEBio model 3 using SED as the neural model input, plotted against six different stress variables. Sx: X stress. Sy: Y stress. Sxy: shear stress. I1: 1st invariant stress tensor. MSS: maximum shear stress. SED: strain energy density.

Table B - 47. Linear regression measures for individual loading regime results from the orthotropic elastic model 3, with SED as neural model input.

Loading Regime	R^2	RMSE	Slope
Uniform	0.8522	0.8518	0.4057
Biaxial	NaN	0.0000	0.0000
Uniaxial X	NaN	0.0000	0.0000
Uniaxial Y	NaN	0.0000	0.0000
Shear Positive	NaN	0.0000	0.0000
Shear Negative	NaN	0.0000	0.0000

B.3.7 Hydrostatic Pressure (HS)

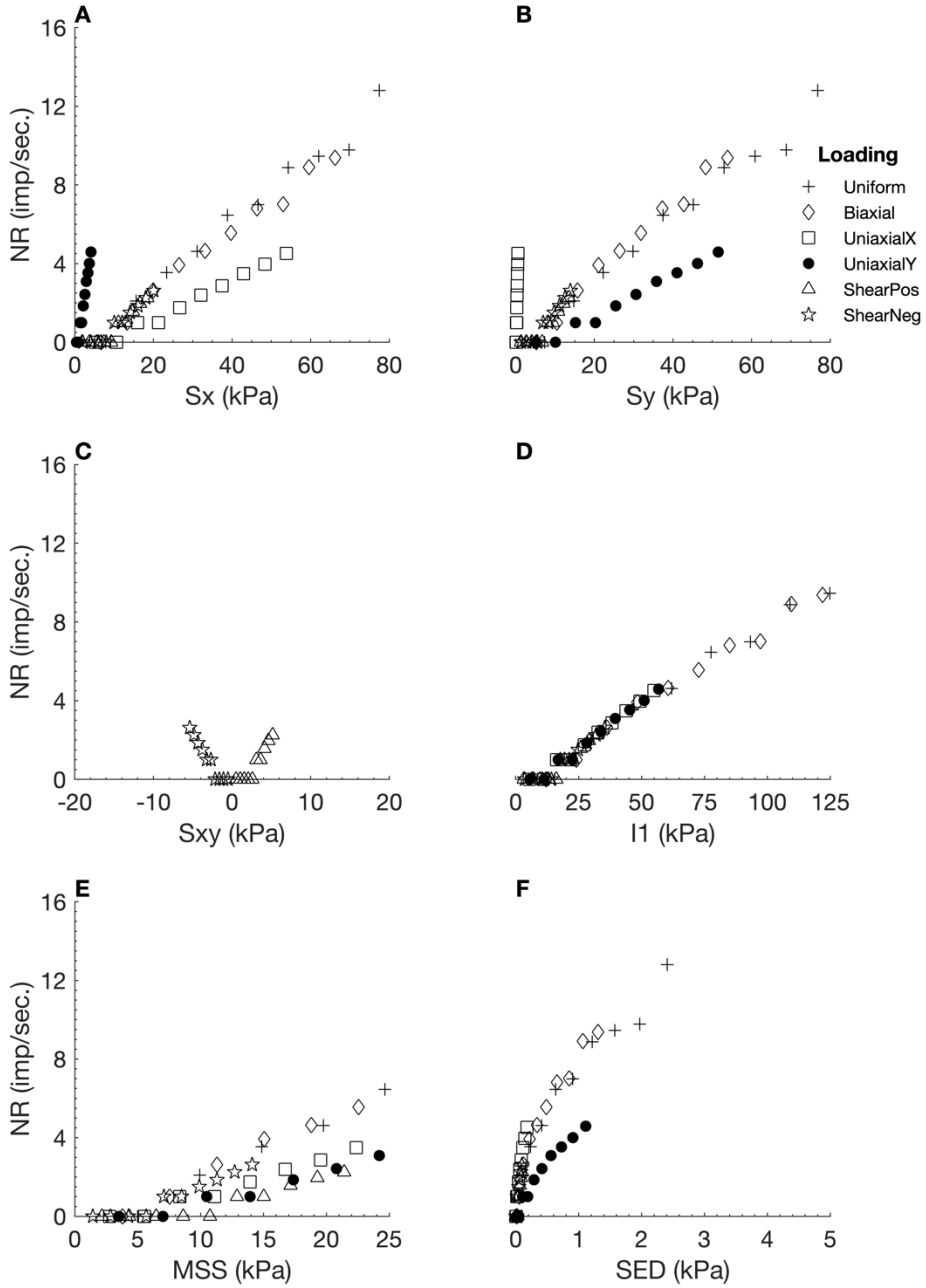

Figure B - 43. Neural responses (NR) output by the orthotropic elastic FEBio model 3 using HS as the neural model input, plotted against six different stress variables. Sx: X stress. Sy: Y stress. Sxy: shear stress. I1: 1st invariant stress tensor. MSS: maximum shear stress. SED: strain energy density.

Table B - 48. Linear regression measures for individual loading regime results from the orthotropic elastic model 3, with HS as neural model input.

Loading Regime	R^2	RMSE	Slope
Uniform	0.9626	0.8058	0.8112
Biaxial	0.5045	1.5824	7.0263
Uniaxial X	0.2082	0.6292	-0.1399
Uniaxial Y	0.8891	0.3628	0.6942
Shear Positive	0.3035	0.3809	0.0461
Shear Negative	0.2318	0.4526	0.1297

B.3.8 1st Principle Stress (S1)

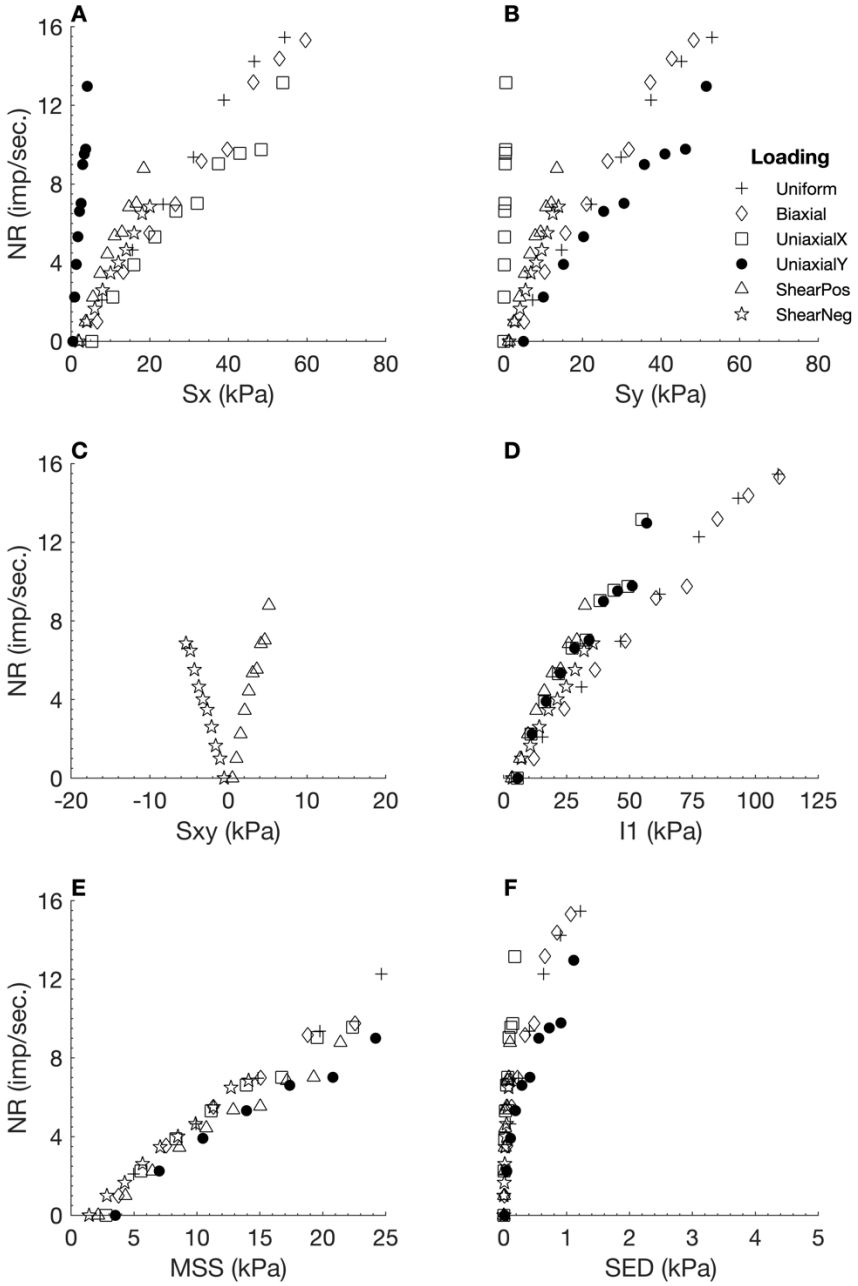

Figure B - 44. Neural responses (NR) output by the orthotropic elastic FEBio model 3 using S1 as the neural model input, plotted against six different stress variables. Sx: X stress. Sy: Y stress. Sxy: shear stress. I1: 1st invariant stress tensor. MSS: maximum shear stress. SED: strain energy density.

Table B - 49. Linear regression measures for individual loading regime results from the orthotropic elastic model 3, with S1 as neural model input.

Loading Regime	R^2	RMSE	Slope
Uniform	0.9833	0.7804	1.1875
Biaxial	0.3954	2.8186	10.0316
Uniaxial X	0.4812	2.0138	-0.8410
Uniaxial Y	0.8497	1.1723	1.8832
Shear Positive	0.9524	0.4999	0.4101
Shear Negative	0.8706	0.5629	0.7617

B.3.9 2nd Principle Stress (S2)

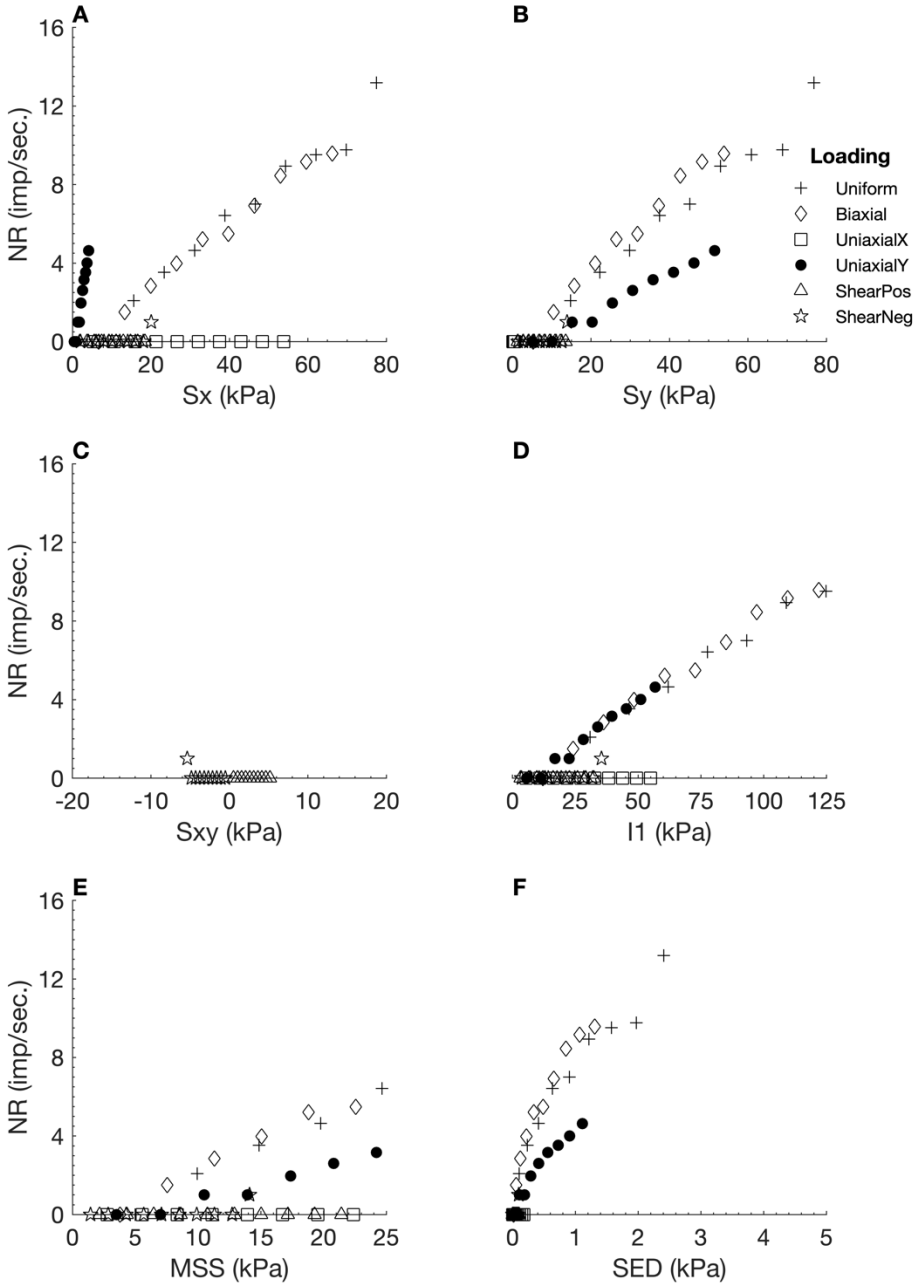

Figure B - 45. Neural responses (NR) output by the orthotropic elastic FEBio model 3 using S2 as the neural model input, plotted against six different stress variables. Sx: X stress. Sy: Y stress. Sxy: shear stress. I1: 1st invariant stress tensor. MSS: maximum shear stress. SED: strain energy density.

Table B - 50. Linear regression measures for individual loading regime results from the orthotropic elastic model 3, with S2 as neural model input.

Loading Regime	R^2	RMSE	Slope
Uniform	0.9561	0.8912	0.8247
Biaxial	0.4186	1.8012	6.7256
Uniaxial X	NaN	0.0000	0.0000
Uniaxial Y	0.8999	0.3699	0.7497
Shear Positive	NaN	0.0000	0.0000
Shear Negative	NaN	0.0000	0.0000

B.3.10 3rd Principle Stress (S3)

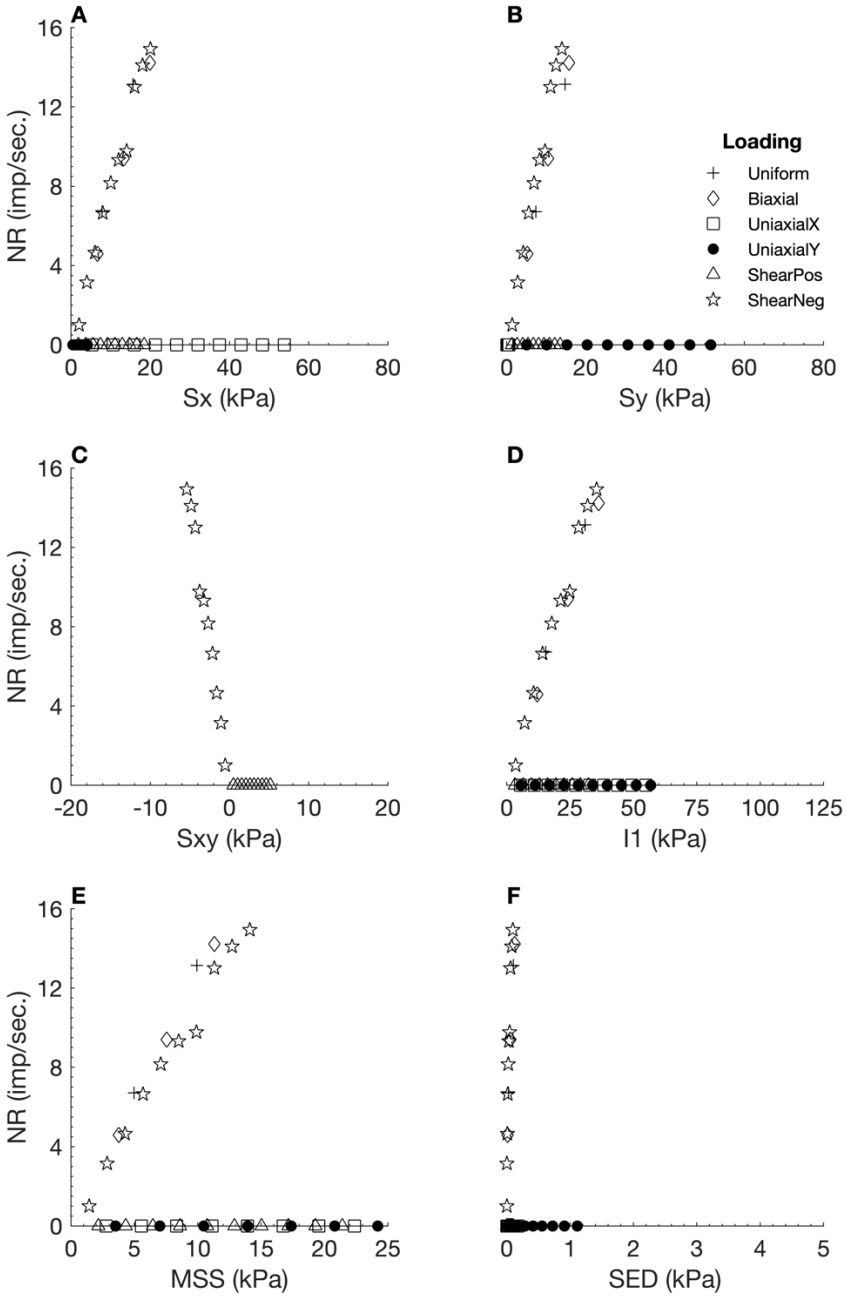

Figure B - 46. Neural responses (NR) output by the orthotropic elastic FEBio model 3 using S3 as the neural model input, plotted against six different stress variables. Sx: X stress. Sy: Y stress. Sxy: shear stress. I1: 1st invariant stress tensor. MSS: maximum shear stress. SED: strain energy density.

Table B - 51. Linear regression measures for individual loading regime results from the orthotropic elastic model 3, with S3 as neural model input.

Loading Regime	R^2	RMSE	Slope
Uniform	0.9544	1.5286	1.3863
Biaxial	0.5590	4.2443	21.0309
Uniaxial X	NaN	0.0000	0.0000
Uniaxial Y	NaN	0.0000	0.0000
Shear Positive	NaN	0.0000	0.0000
Shear Negative	0.8937	1.0625	1.6072

B.3.11 Deviatoric Stress 1 (Dev1)

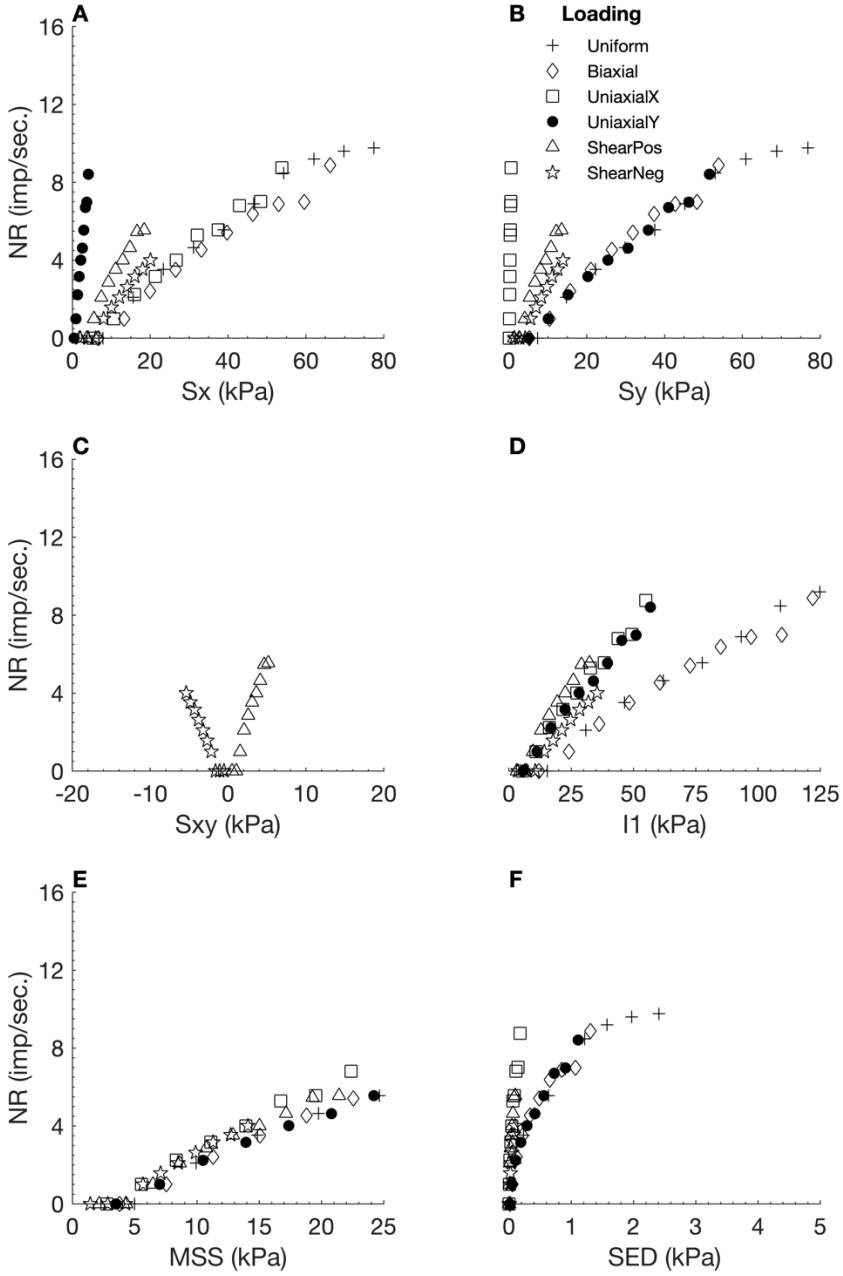

Figure B - 47. Neural responses (NR) output by the orthotropic elastic FEBio model 3 using Dev1 as the neural model input, plotted against six different stress variables. Sx: X stress. Sy: Y stress. Sxy: shear stress. I1: 1st invariant stress tensor. MSS: maximum shear stress. SED: strain energy density.

Table B - 52. Linear regression measures for individual loading regime results from the orthotropic elastic model 3, with Dev1 as neural model input.

Loading Regime	R^2	RMSE	Slope
Uniform	0.9854	0.4347	0.7089
Biaxial	0.4456	1.5771	6.2224
Uniaxial X	0.3760	1.3451	-0.4527
Uniaxial Y	0.8978	0.6358	1.2733
Shear Positive	0.8573	0.6276	0.2822
Shear Negative	0.4739	0.6142	0.3042

B.3.12 Deviatoric Stress 2 (Dev2)

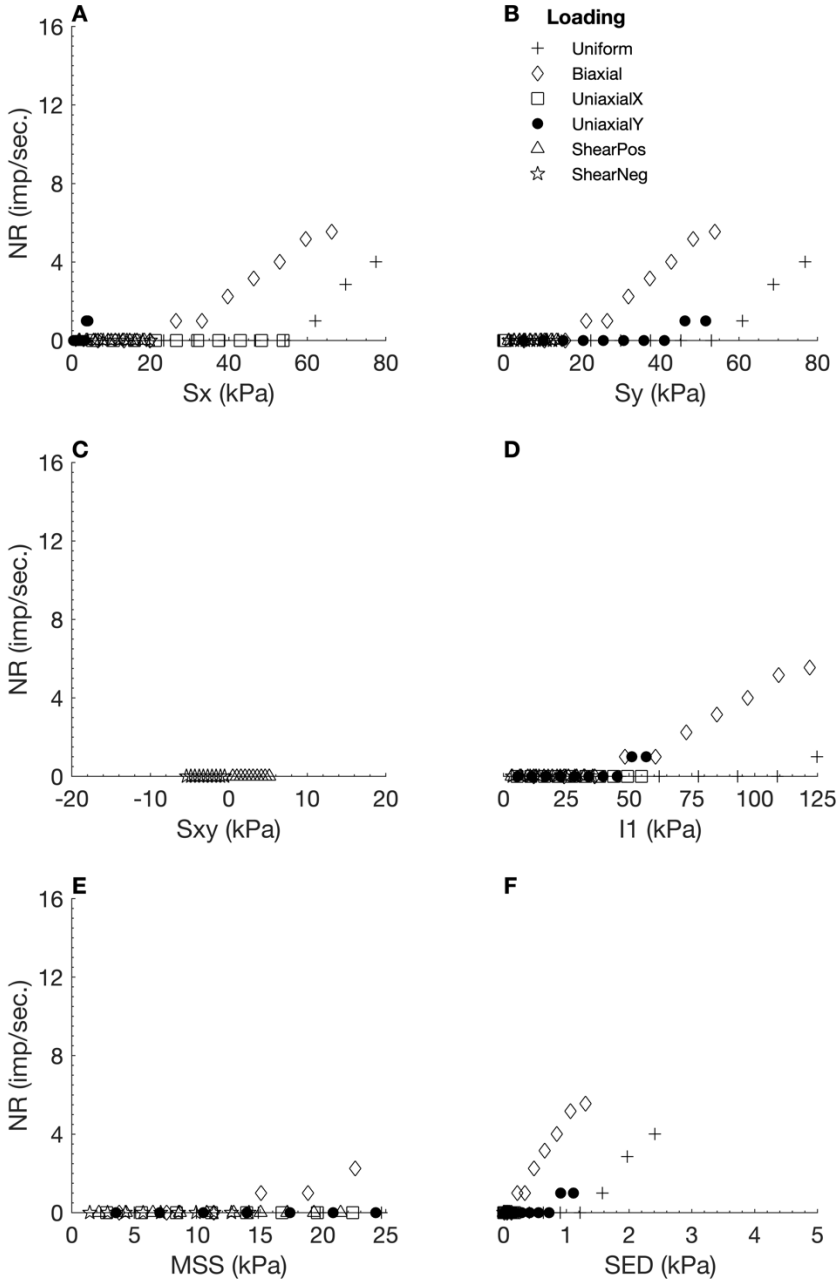

Figure B - 48. Neural responses (NR) output by the orthotropic elastic FEBio model 3 using Dev2 as the neural model input, plotted against six different stress variables. Sx: X stress. Sy: Y stress. Sxy: shear stress. I1: 1st invariant stress tensor. MSS: maximum shear stress. SED: strain energy density.

Table B - 53. Linear regression measures for individual loading regime results from the orthotropic elastic model 3, with Dev2 as neural model input.

Loading Regime	R^2	RMSE	Slope
Uniform	0.4931	1.0978	0.2148
Biaxial	0.2119	0.5615	1.2811
Uniaxial X	NaN	0.0000	0.0000
Uniaxial Y	NaN	0.0000	0.0000
Shear Positive	NaN	0.0000	0.0000
Shear Negative	NaN	0.0000	0.0000

B.3.13 Deviatoric Stress 3 (Dev3)

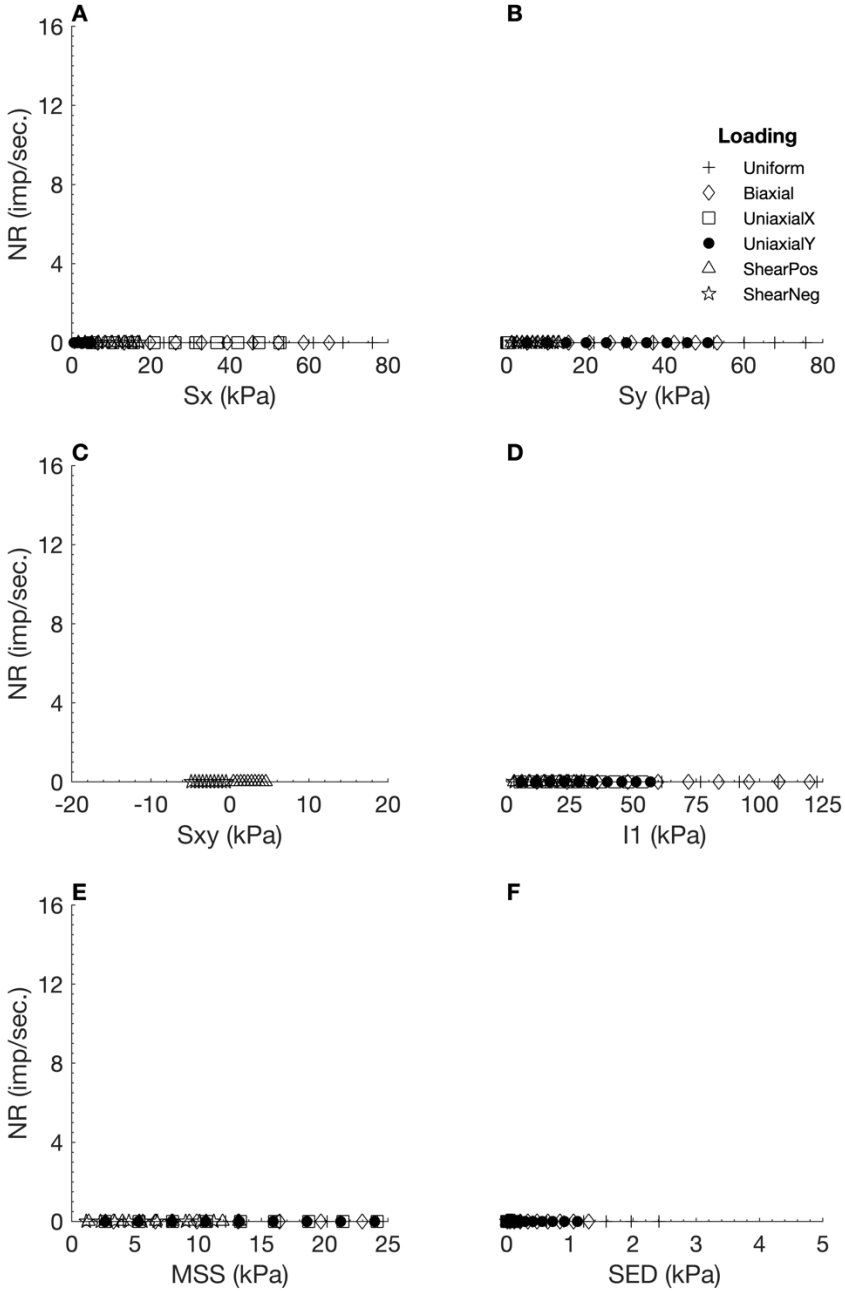

Figure B - 49. Neural responses (NR) output by the orthotropic elastic FEBio model 3 using Dev3 as the neural model input, plotted against six different stress variables. Sx: X stress. Sy: Y stress. Sxy: shear stress. I1: 1st invariant stress tensor. MSS: maximum shear stress. SED: strain energy density.

Table B - 54. Linear regression measures for individual loading regime results from the orthotropic elastic model 3, with Dev3 as neural model input.

Loading Regime	R^2	RMSE	Slope
Uniform	NaN	0.0000	0.0000
Biaxial	NaN	0.0000	0.0000
Uniaxial X	NaN	0.0000	0.0000
Uniaxial Y	NaN	0.0000	0.0000
Shear Positive	NaN	0.0000	0.0000
Shear Negative	NaN	0.0000	0.0000

B.3.14 Shear Stress A

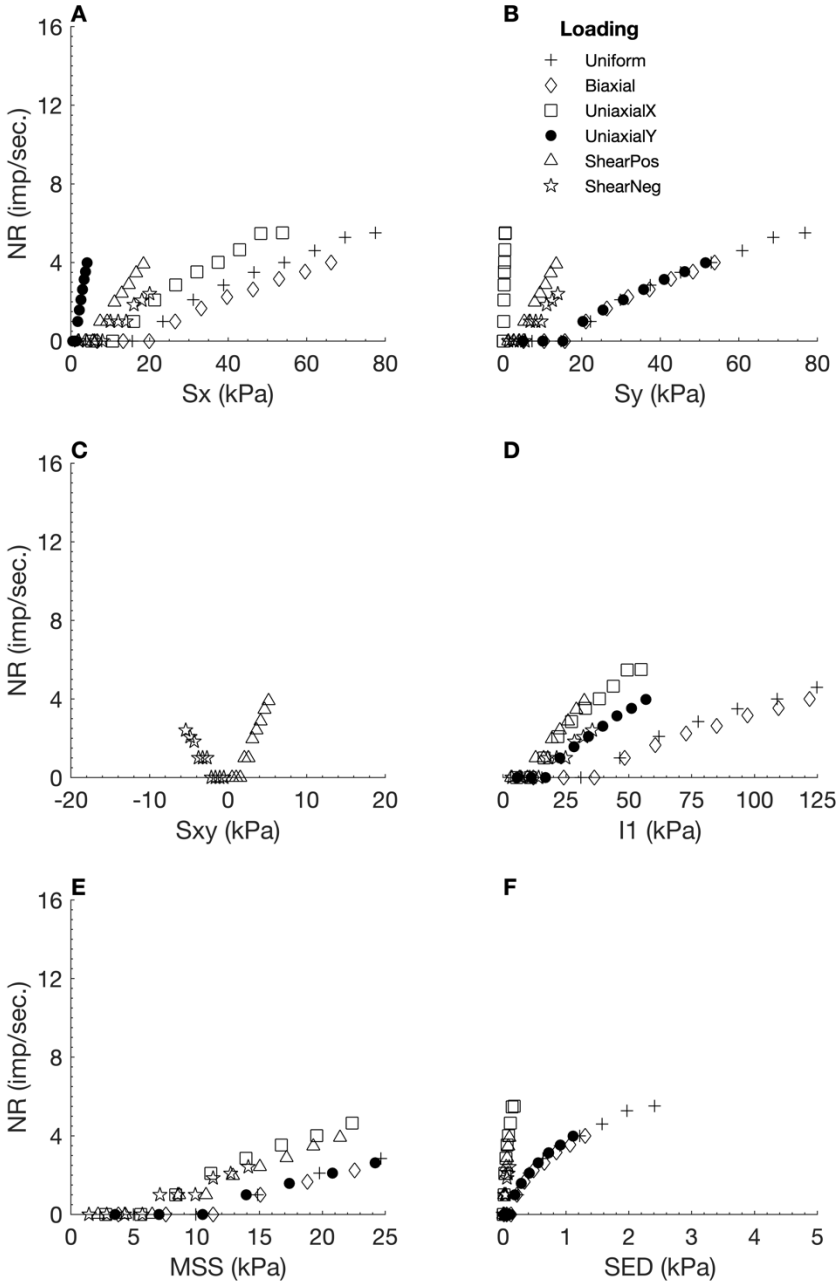

Figure B - 50. Neural responses (NR) output by the orthotropic elastic FEBio model 3 using ShearA as the neural model input, plotted against six different stress variables. Sx: X stress. Sy: Y stress. Sxy: shear stress. I1: 1st invariant stress tensor. MSS: maximum shear stress. SED: strain energy density.

Table B - 55. Linear regression measures for individual loading regime results from the orthotropic elastic model 3, with ShearA as neural model input.

Loading Regime	R^2	RMSE	Slope
Uniform	0.9879	0.2398	0.4296
Biaxial	0.1061	0.8348	1.2657
Uniaxial X	0.0976	1.1576	-0.1651
Uniaxial Y	0.9689	0.1819	0.6858
Shear Positive	0.6864	0.5049	0.1370
Shear Negative	0.2318	0.4526	0.1297

B.3.15 Shear Stress B

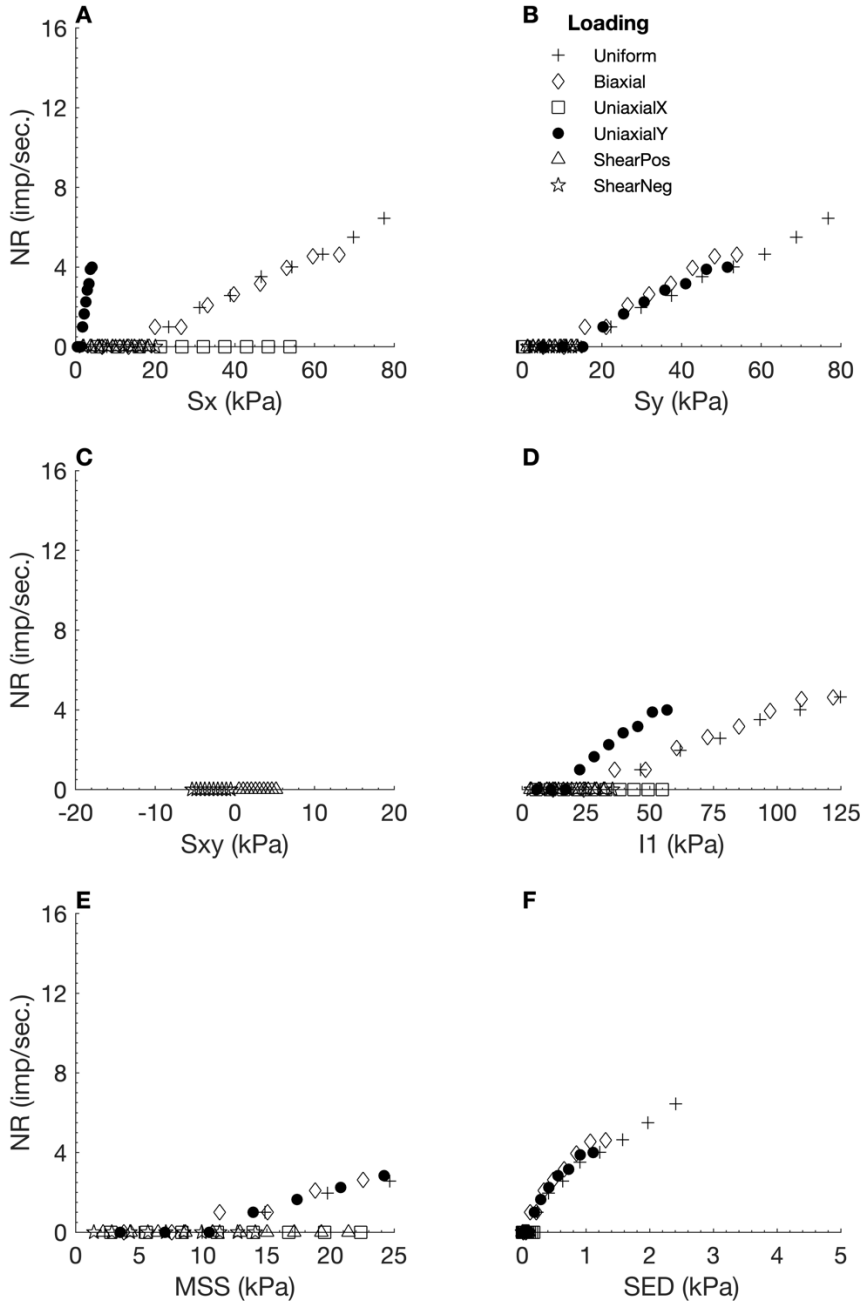

Figure B - 51. Neural responses (NR) output by the orthotropic elastic FEBio model 3 using ShearB as the neural model input, plotted against six different stress variables. Sx: X stress. Sy: Y stress. Sxy: shear stress. I1: 1st invariant stress tensor. MSS: maximum shear stress. SED: strain energy density.

Table B - 56. Linear regression measures for individual loading regime results from the orthotropic elastic model 3, with ShearB as neural model input.

Loading Regime	R^2	RMSE	Slope
Uniform	0.9771	0.3603	0.4671
Biaxial	0.3209	0.8275	2.5032
Uniaxial X	NaN	0.0000	0.0000
Uniaxial Y	0.9716	0.1841	0.7282
Shear Positive	NaN	0.0000	0.0000
Shear Negative	NaN	0.0000	0.0000

B.3.16 Shear Stress C

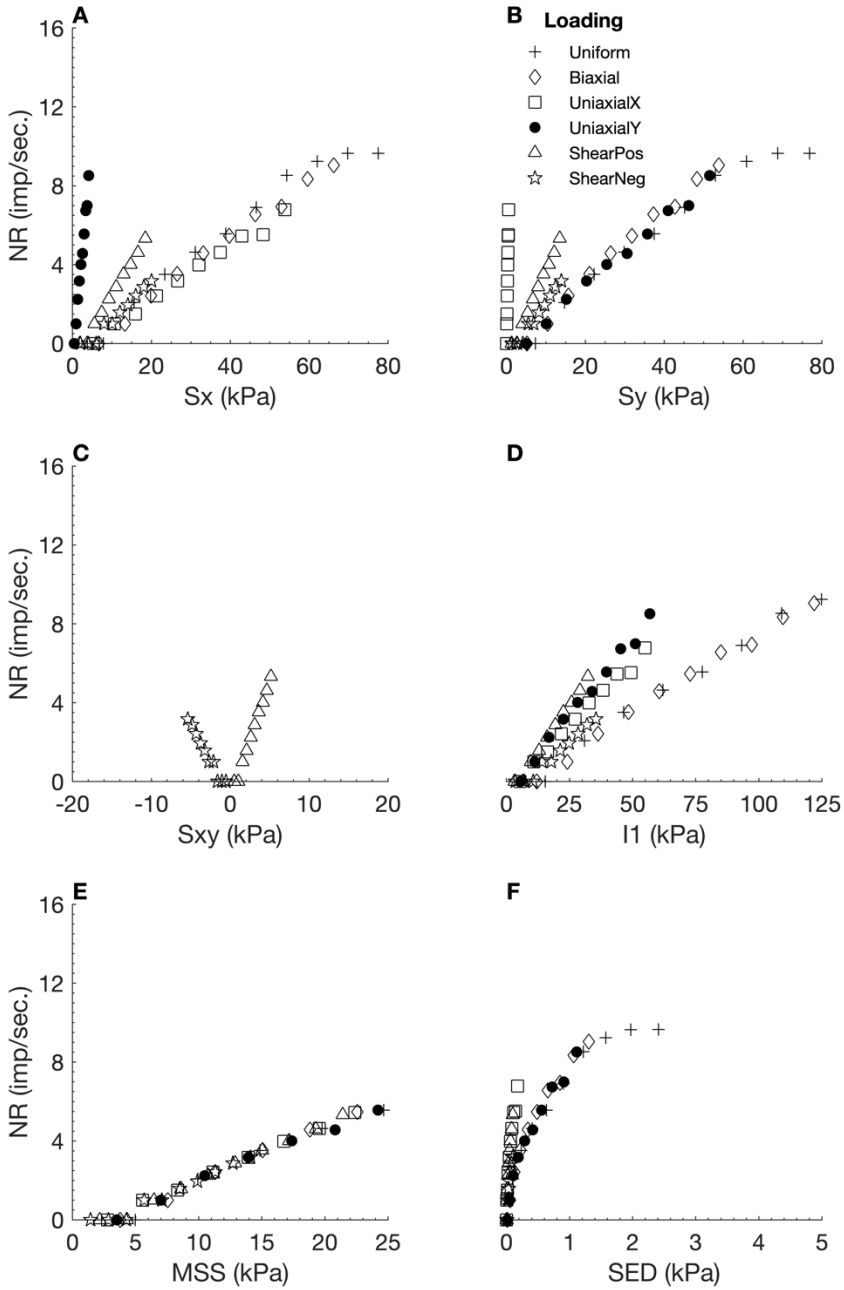

Figure B - 52. Neural responses (NR) output by the orthotropic elastic FEBio model 3 using ShearC as the neural model input, plotted against six different stress variables. Sx: X stress. Sy: Y stress. Sxy: shear stress. I1: 1st invariant stress tensor. MSS: maximum shear stress. SED: strain energy density.

Table B - 57. Linear regression measures for individual loading regime results from the orthotropic elastic model 3, with ShearC as neural model input.

Loading Regime	R^2	RMSE	Slope
Uniform	0.9839	0.4577	0.7091
Biaxial	0.4418	1.5966	6.2507
Uniaxial X	0.4230	0.9393	-0.3487
Uniaxial Y	0.8924	0.6474	1.2596
Shear Positive	0.8702	0.4738	0.2251
Shear Negative	0.4848	0.4540	0.2298

B.3.17 X Strain (Ex)

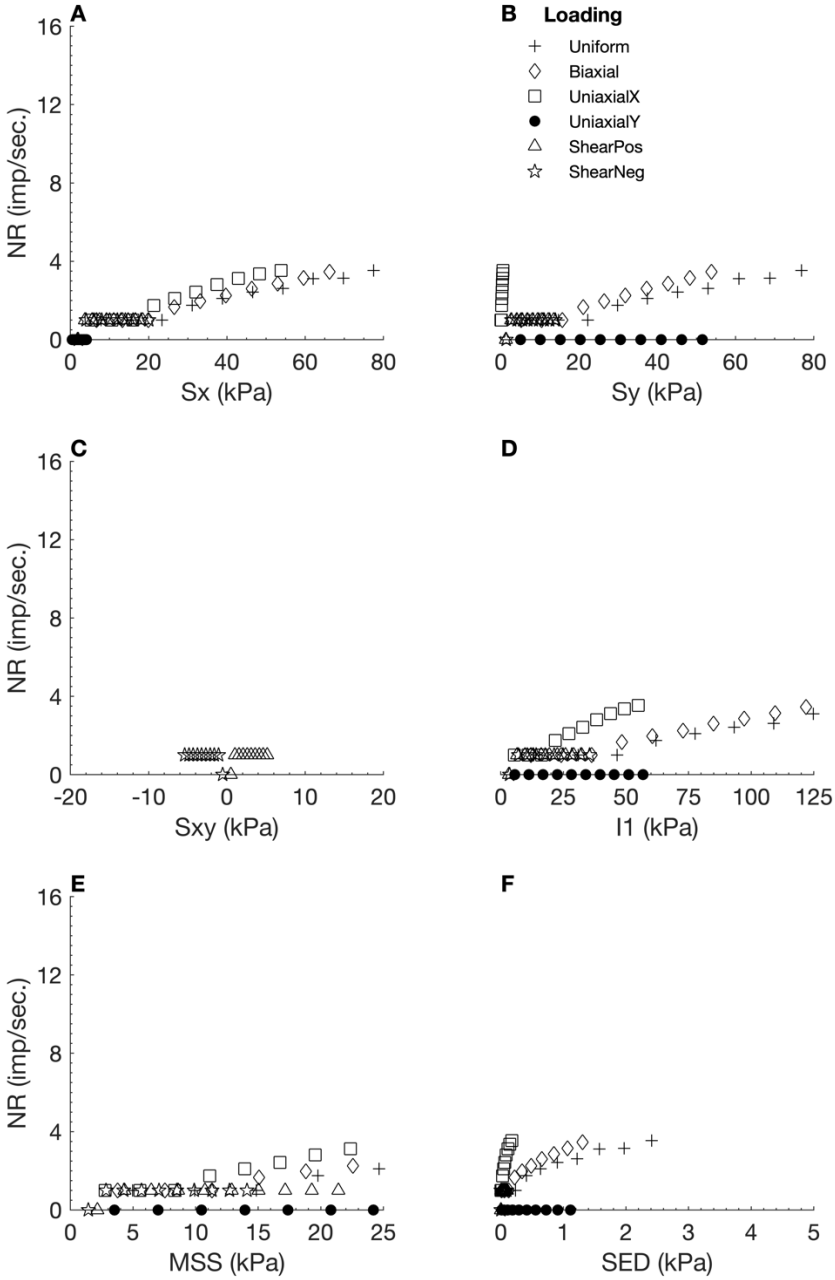

Figure B - 53. Neural responses (NR) output by the orthotropic elastic FEBio model 3 using Ex as the neural model input, plotted against six different stress variables. Sx: X stress. Sy: Y stress. Sxy: shear stress. I1: 1st invariant stress tensor. MSS: maximum shear stress. SED: strain energy density.

Table B - 58. Linear regression measures for individual loading regime results from the orthotropic elastic model 3, with Ex as neural model input.

Loading Regime	R^2	RMSE	Slope
Uniform	0.9500	0.2270	0.1962
Biaxial	0.1291	0.4948	0.8383
Uniaxial X	0.0076	0.4551	-0.0173
Uniaxial Y	NaN	0.0000	0.0000
Shear Positive	0.6424	0.2730	0.0671
Shear Negative	0.7507	0.2579	0.2334

B.3.18 Y Strain (Ey)

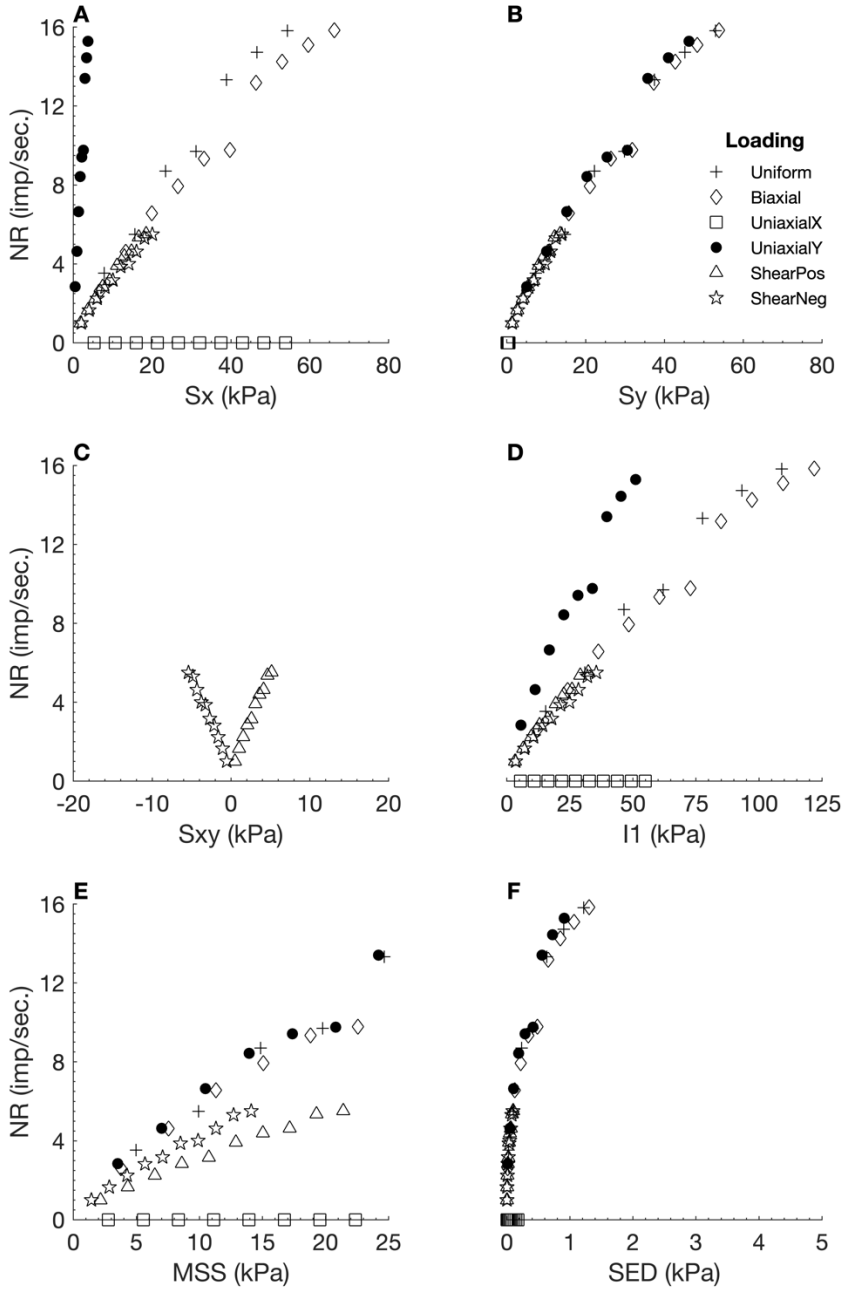

Figure B - 54. Neural responses (NR) output by the orthotropic elastic FEBio model 3 using Ey as the neural model input, plotted against six different stress variables. Sx: X stress. Sy: Y stress. Sxy: shear stress. I1: 1st invariant stress tensor. MSS: maximum shear stress. SED: strain energy density.

B.4 Test 4

Table B - 59. Values selected for material properties during FEBio implementation of orthotropic elastic material test 4.

Orthotropic Material Property	Value Selected
Density	1
Young's Modulus (X)	1
Young's Modulus (Y)	2.6
Young's Modulus (Z)	1
Shear Modulus (XY)	0.345
Shear Modulus (YZ)	0.9
Shear Modulus (XZ)	0.345
Poisson's Ratio (XY)	0.45
Poisson's Ratio (YZ)	0.45
Poisson's Ratio (XZ)	0.45

Table B - 60. Linear regression measures for total plot results (i.e. considering all loading regimes combined), for each input stimulus tested with the orthotropic elastic model 4.

Input Stimuli	R^2	RMSE	Slope
X Stress (Sx)	0.1619	4.4193	0.4290
Y Stress (Sy)	0.2900	3.8589	0.5447
Shear Stress (Sxy)	0.0898	0.7181	0.0498
1st Invariant Stress Tensor (I1)	0.2531	5.7533	0.7398
Maximum Shear Stress (MSS)	0.2457	2.2094	0.2785
Strain Energy Density (SED)	0.1602	0.4938	0.0476
Hydrostatic Pressure (HS)	0.2214	2.7780	0.3272
1st Principal Stress (S1)	0.2480	3.9374	0.4994
2nd Principal Stress (S2)	0.2080	4.1837	0.4735
3rd Principal Stress (S3)	0.2109	6.0172	0.6872
Deviatoric Stress 1 (Dev1)	0.1913	1.7654	0.1896
Deviatoric Stress 2 (Dev2)	0.1619	1.3875	0.1347
Deviatoric Stress 3 (Dev3)	NaN	0.0000	0.0000
Shear A	0.0000	0.8594	-0.0011
Shear B	0.1918	2.1790	0.2345
Shear C	0.2457	2.2094	0.2785
X Strain (Ex)	0.0917	3.8468	0.2700
Y Strain (Ey)	0.0251	1.3824	0.0490
Average	**0.1763**	**2.6666**	**0.2907**

B.4.1 X Stress (Sx)

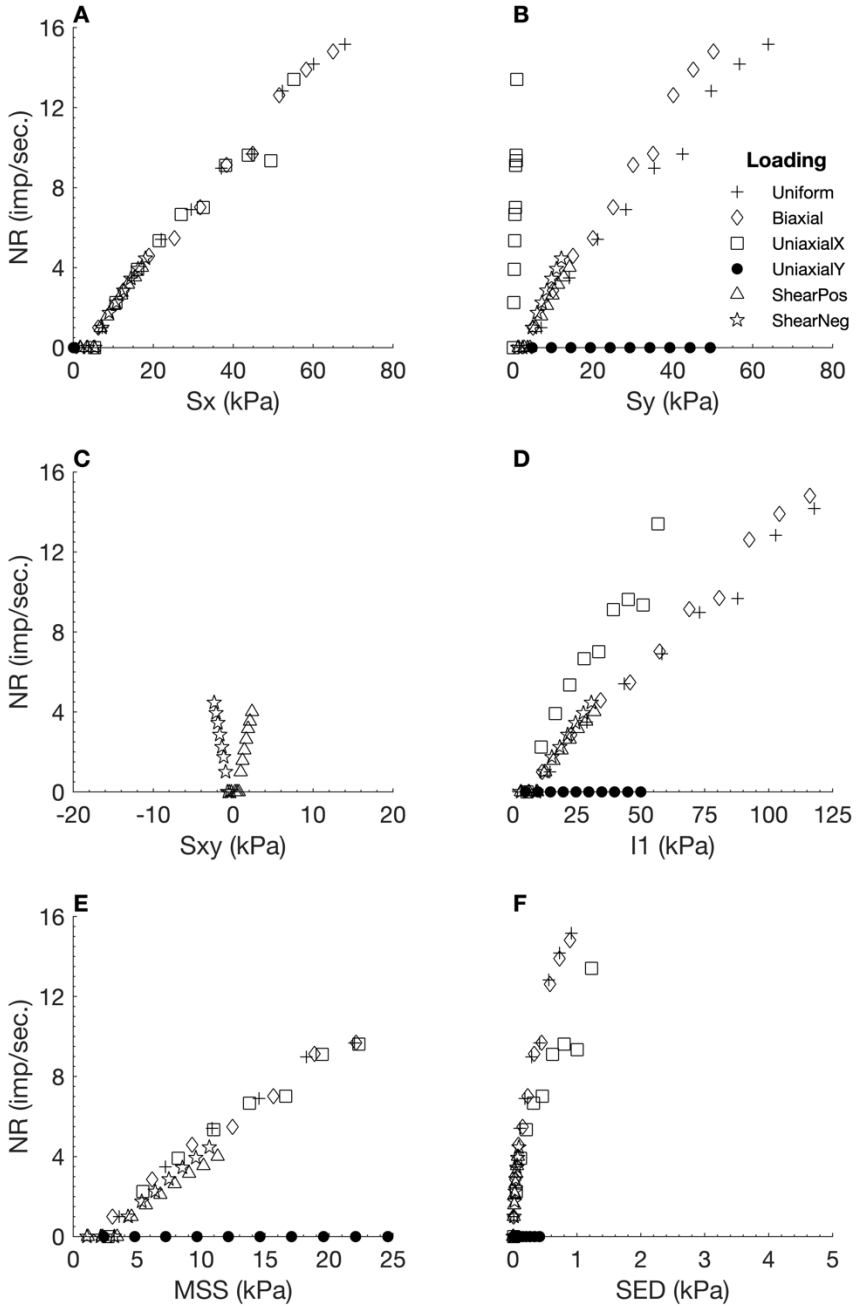

Figure B - 55. Neural responses (NR) output by the orthotropic elastic FEBio model 4 using Sx as the neural model input, plotted against six different stress variables. Sx: X stress. Sy: Y stress. Sxy: shear stress. I1: 1st invariant stress tensor. MSS: maximum shear stress. SED: strain energy density.

Table B - 61. Linear regression measures for individual loading regime results from the orthotropic elastic model 4, with Sx as neural model input.

Loading Regime	R^2	RMSE	Slope
Uniform	0.9856	0.6571	1.0781
Biaxial	0.4348	2.0247	7.8153
Uniaxial X	0.4790	2.0320	-0.8448
Uniaxial Y	NaN	0.0000	0.0000
Shear Positive	0.7165	0.5488	0.1600
Shear Negative	0.4624	0.6753	0.3268

B.4.2 Y Stress (Sy)

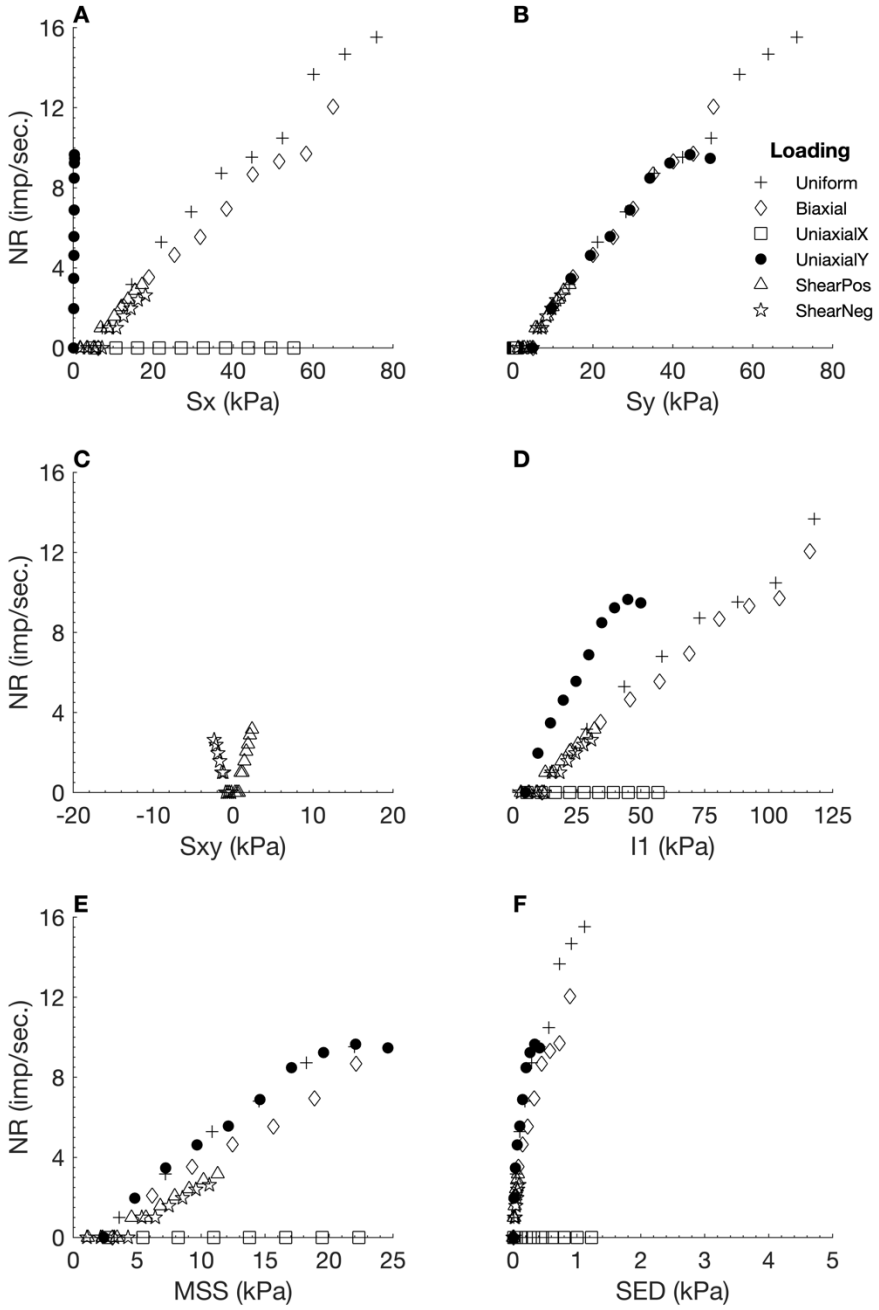

Figure B - 56. Neural responses (NR) output by the orthotropic elastic FEBio model 4 using Sy as the neural model input, plotted against six different stress variables. Sx: X stress. Sy: Y stress. Sxy: shear stress. I1: 1st invariant stress tensor. MSS: maximum shear stress. SED: strain energy density.

Table B - 62. Linear regression measures for individual loading regime results from the orthotropic elastic model 4, with Sy as neural model input.

Loading Regime	R^2	RMSE	Slope
Uniform	0.9811	0.7145	1.0197
Biaxial	0.4765	1.8277	7.6745
Uniaxial X	NaN	0.0000	0.0000
Uniaxial Y	0.8877	0.9362	1.7785
Shear Positive	0.7143	0.4101	0.1189
Shear Negative	0.2318	0.4526	0.1297

B.4.3 Shear Stress (Sxy)

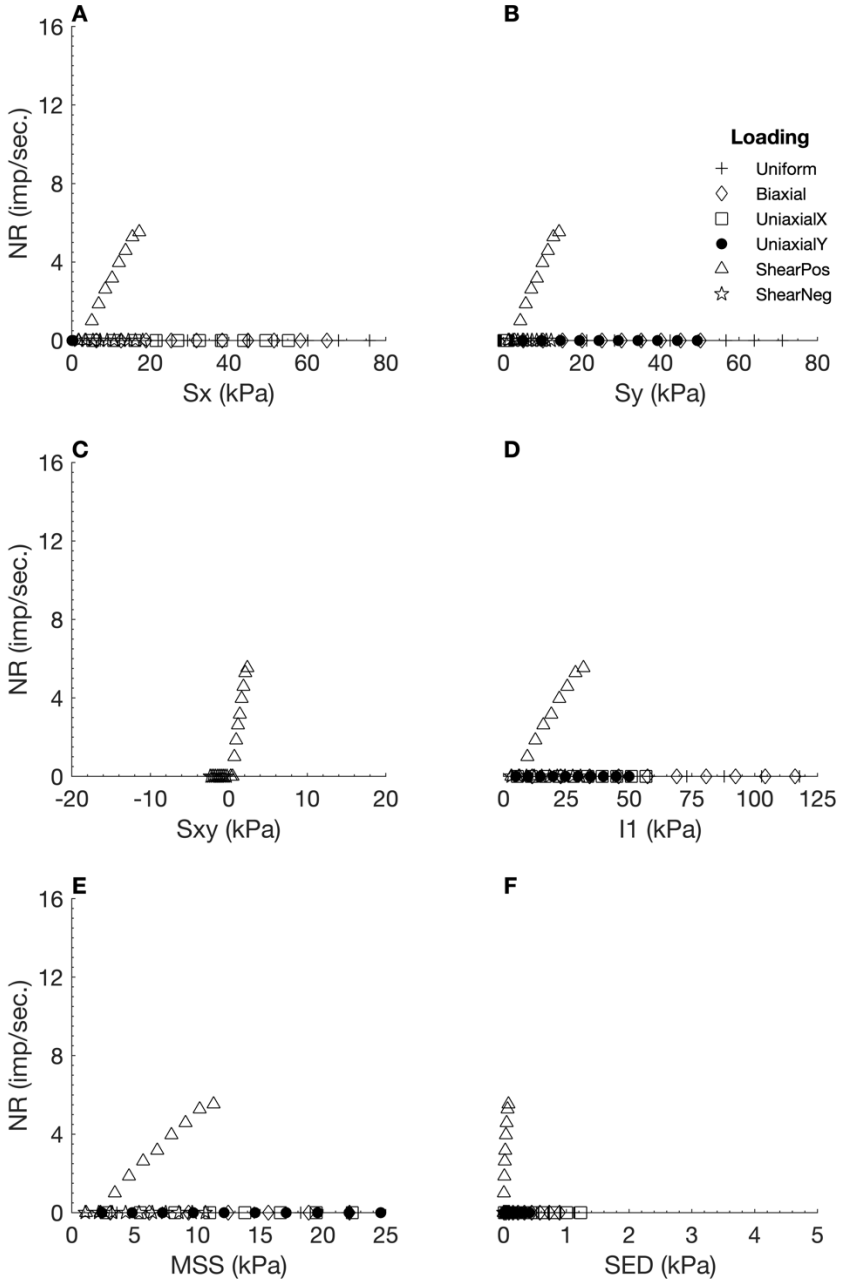

Figure B - 57. Neural responses (NR) output by the orthotropic elastic FEBio model 4 using Sxy as the neural model input, plotted against six different stress variables. Sx: X stress. Sy: Y stress. Sxy: shear stress. I1: 1st invariant stress tensor. MSS: maximum shear stress. SED: strain energy density.

Table B - 63. Linear regression measures for individual loading regime results from the orthotropic elastic model 4, with Sxy as neural model input.

Loading Regime	R^2	RMSE	Slope
Uniform	NaN	0.0000	0.0000
Biaxial	NaN	0.0000	0.0000
Uniaxial X	NaN	0.0000	0.0000
Uniaxial Y	NaN	0.0000	0.0000
Shear Positive	0.8647	0.5485	0.2543
Shear Negative	NaN	0.0000	0.0000

B.4.4 1st Invariant Stress Tensor (I1)

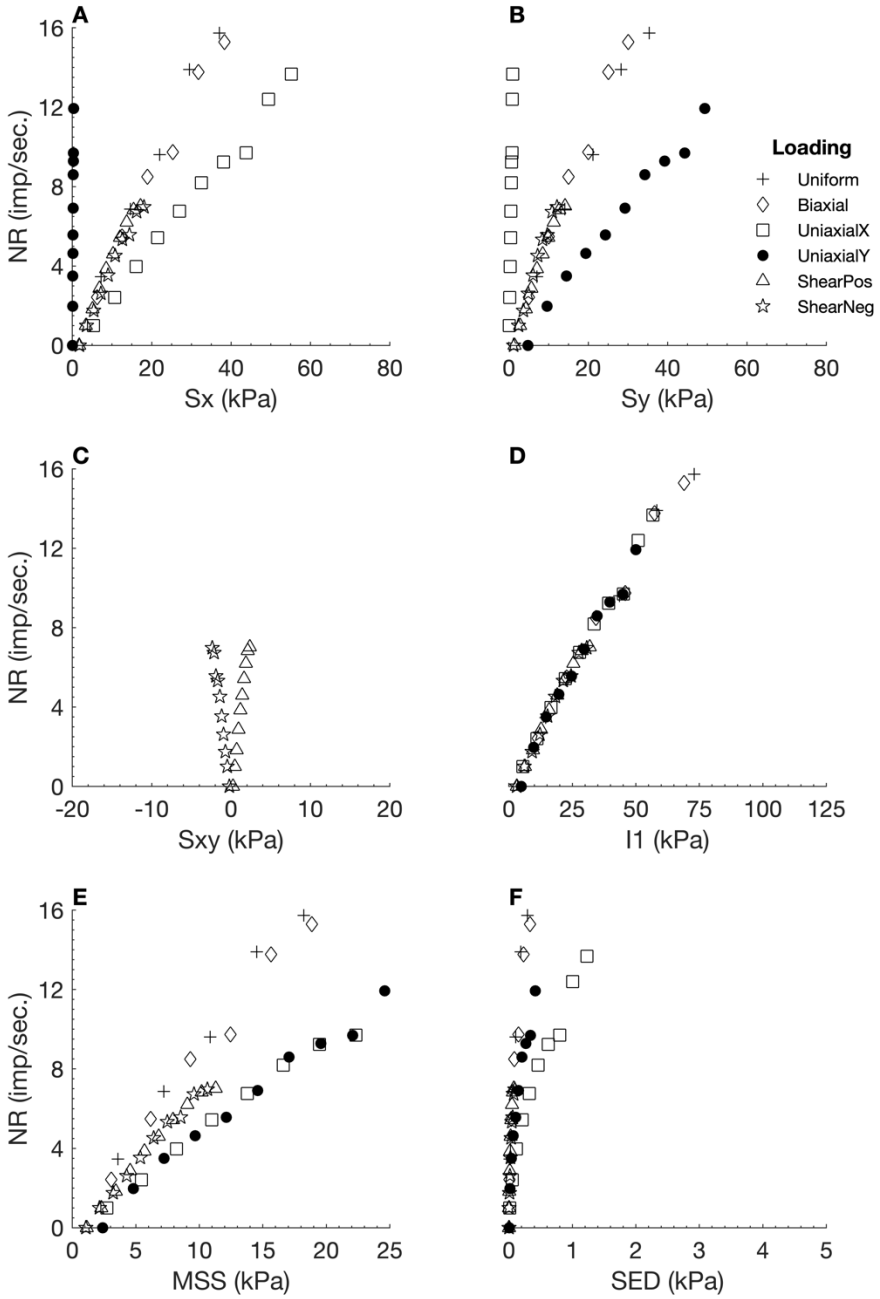

Figure B - 58. Neural responses (NR) output by the orthotropic elastic FEBio model 4 using I1 as the neural model input, plotted against six different stress variables. Sx: X stress. Sy: Y stress. Sxy: shear stress. I1: 1st invariant stress tensor. MSS: maximum shear stress. SED: strain energy density.

Table B - 64. Linear regression measures for individual loading regime results from the orthotropic elastic model 4, with I1 as neural model input.

Loading Regime	R^2	RMSE	Slope
Uniform	0.9660	1.2387	1.3087
Biaxial	0.3518	3.9977	12.9618
Uniaxial X	0.3649	1.8728	-0.6155
Uniaxial Y	0.8863	0.9447	1.7822
Shear Positive	0.9497	0.4374	0.3485
Shear Negative	0.8796	0.5507	0.7767

B.4.5 Maximum Shear Stress (MSS)

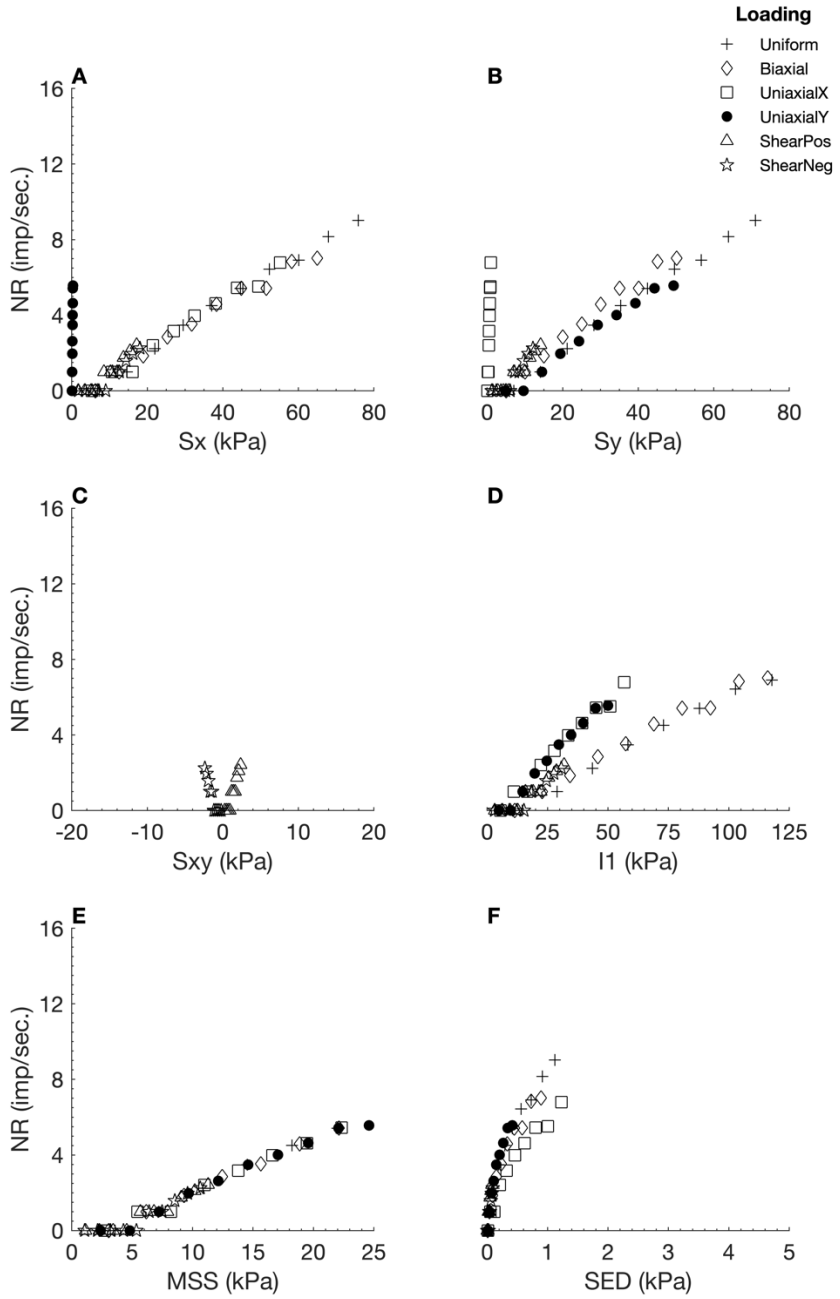

Figure B - 59. Neural responses (NR) output by the orthotropic elastic FEBio model 4 using MSS as the neural model input, plotted against six different stress variables. Sx: X stress. Sy: Y stress. Sxy: shear stress. I1: 1st invariant stress tensor. MSS: maximum shear stress. SED: strain energy density.

Table B - 65. Linear regression measures for individual loading regime results from the orthotropic elastic model 4, with MSS as neural model input.

Loading Regime	R^2	RMSE	Slope
Uniform	0.9898	0.3243	0.6333
Biaxial	0.4250	1.2365	4.6784
Uniaxial X	0.3035	1.0123	-0.2898
Uniaxial Y	0.9393	0.3932	1.0452
Shear Positive	0.5096	0.4043	0.0756
Shear Negative	NaN	0.0000	0.0000

B.4.6 Strain Energy Density (SED)

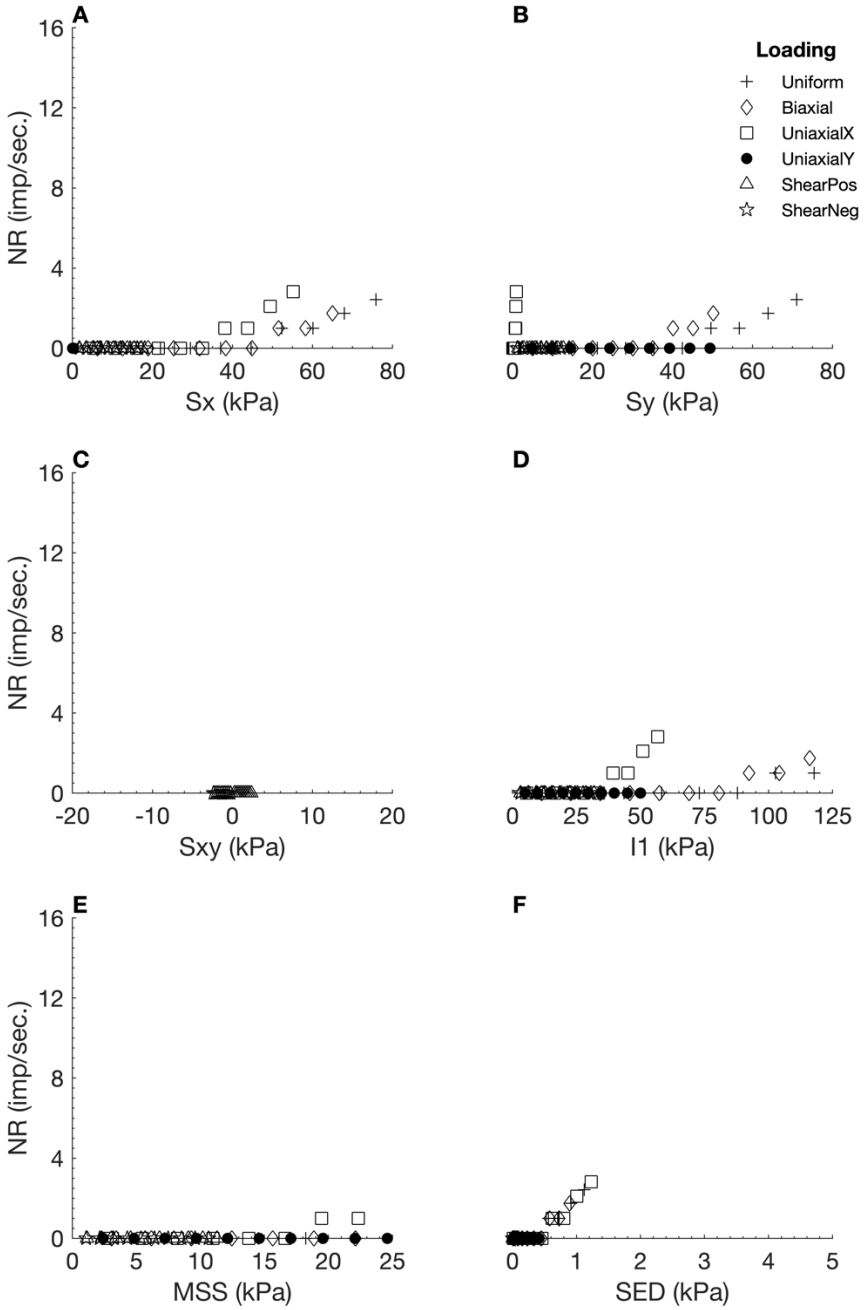

Figure B - 60. Neural responses (NR) output by the orthotropic elastic FEBio model 4 using SED as the neural model input, plotted against six different stress variables. Sx: X stress. Sy: Y stress. Sxy: shear stress. I1: 1st invariant stress tensor. MSS: maximum shear stress. SED: strain energy density.

Table B - 66. Linear regression measures for individual loading regime results from the orthotropic elastic model 4, with SED as neural model input.

Loading Regime	R^2	RMSE	Slope
Uniform	0.6625	0.5481	0.1523
Biaxial	NaN	0.0000	0.0000
Uniaxial X	NaN	0.0000	0.0000
Uniaxial Y	NaN	0.0000	0.0000
Shear Positive	NaN	0.0000	0.0000
Shear Negative	NaN	0.0000	0.0000

B.4.7 Hydrostatic Pressure (HS)

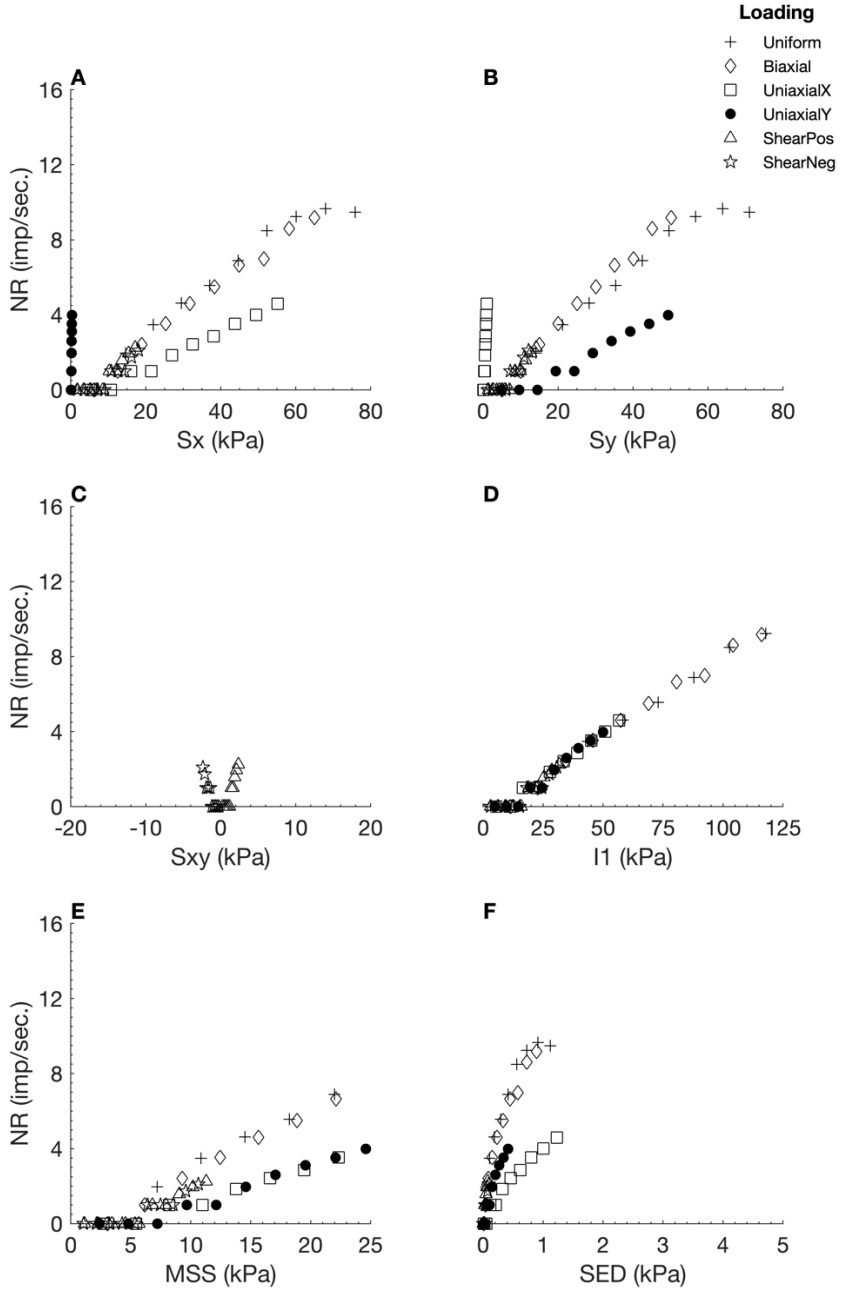

Figure B - 61. Neural responses (NR) output by the orthotropic elastic FEBio model 4 using HS as the neural model input, plotted against six different stress variables. Sx: X stress. Sy: Y stress. Sxy: shear stress. I1: 1st invariant stress tensor. MSS: maximum shear stress. SED: strain energy density.

Table B - 67. Linear regression measures for individual loading regime results from the orthotropic elastic model 4, with HS as neural model input.

Loading Regime	R^2	RMSE	Slope
Uniform	0.9831	0.4681	0.7076
Biaxial	0.4379	1.6100	6.2530
Uniaxial X	0.2082	0.6292	-0.1399
Uniaxial Y	0.9123	0.2659	0.5794
Shear Positive	0.3035	0.3809	0.0461
Shear Negative	NaN	0.0000	0.0000

B.4.8 1st Principle Stress (S1)

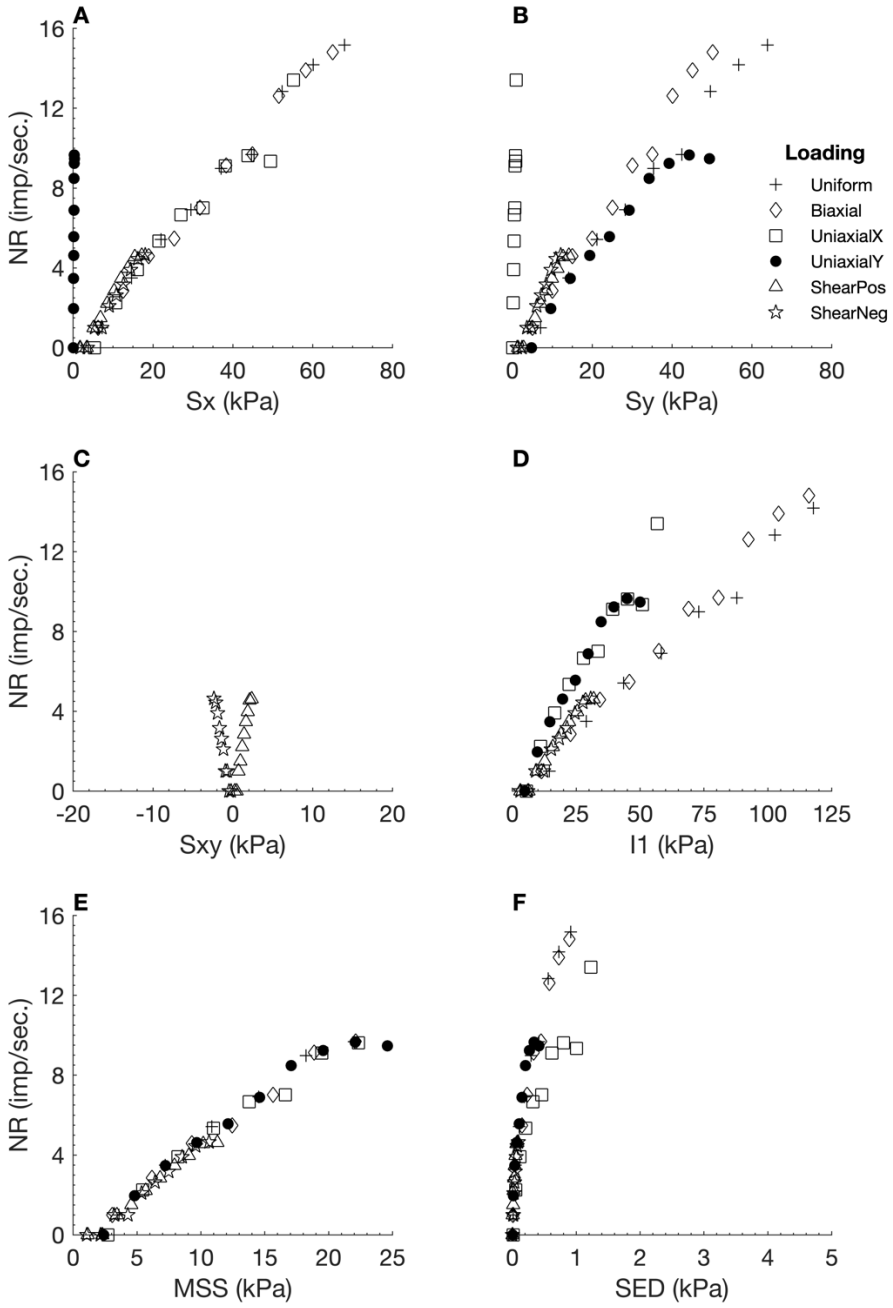

Figure B - 62. Neural responses (NR) output by the orthotropic elastic FEBio model 4 using S1 as the neural model input, plotted against six different stress variables. Sx: X stress. Sy: Y stress. Sxy: shear stress. I1: 1st invariant stress tensor. MSS: maximum shear stress. SED: strain energy density.

Table B - 68. Linear regression measures for individual loading regime results from the orthotropic elastic model 4, with S1 as neural model input.

Loading Regime	R^2	RMSE	Slope
Uniform	0.9855	0.6591	1.0780
Biaxial	0.4347	2.0248	7.8144
Uniaxial X	0.4790	2.0320	-0.8448
Uniaxial Y	0.8877	0.9362	1.7785
Shear Positive	0.8675	0.4728	0.2219
Shear Negative	0.7104	0.5407	0.4419

B.4.9 2nd Principle Stress (S2)

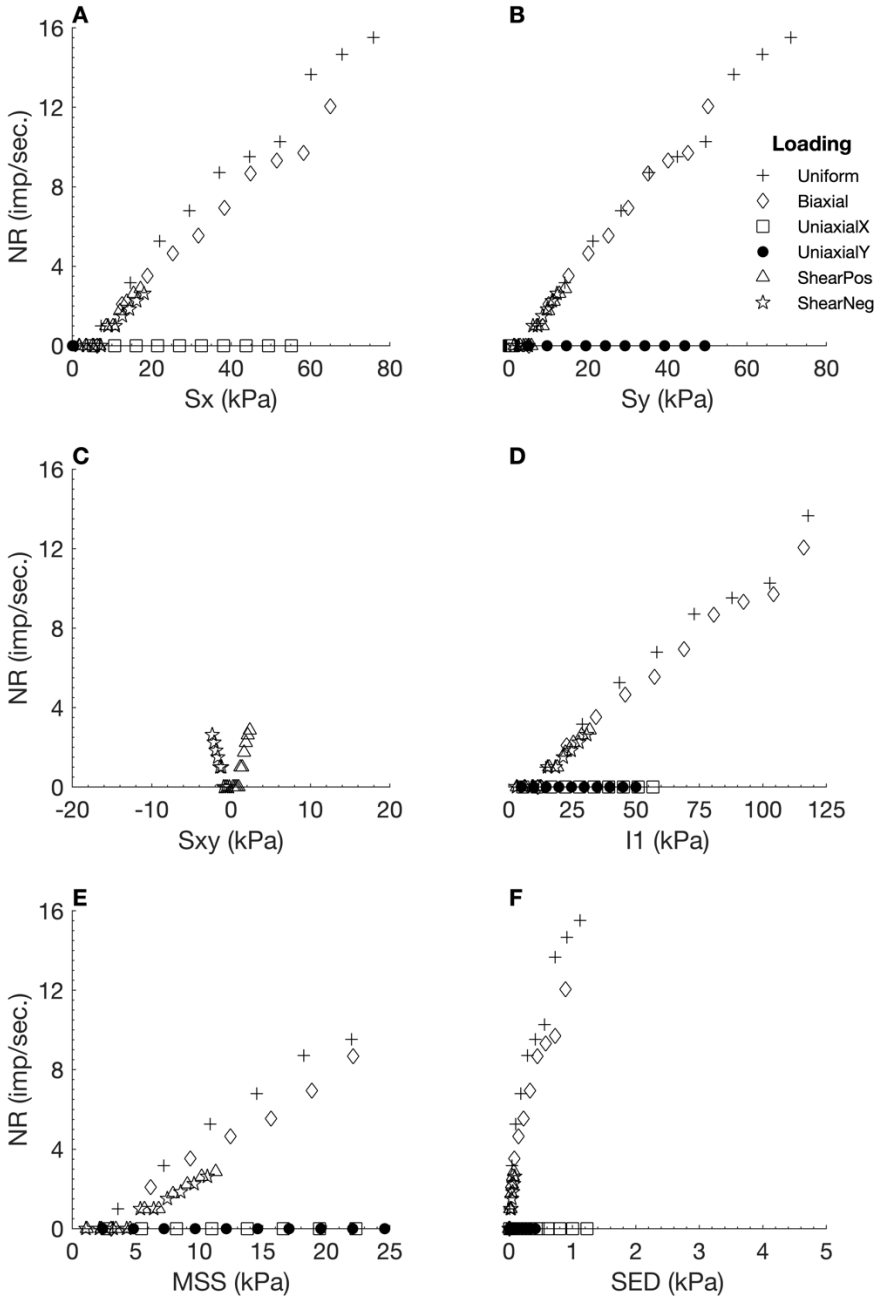

Figure B - 63. Neural responses (NR) output by the orthotropic elastic FEBio model 4 using S2 as the neural model input, plotted against six different stress variables. Sx: X stress. Sy: Y stress. Sxy: shear stress. I1: 1st invariant stress tensor. MSS: maximum shear stress. SED: strain energy density.

Table B - 69. Linear regression measures for individual loading regime results from the orthotropic elastic model 4, with S2 as neural model input.

Loading Regime	R^2	RMSE	Slope
Uniform	0.9785	0.7604	1.0169
Biaxial	0.4765	1.8280	7.6744
Uniaxial X	NaN	0.0000	0.0000
Uniaxial Y	NaN	0.0000	0.0000
Shear Positive	0.5096	0.4043	0.0756
Shear Negative	0.2318	0.4526	0.1297

B.4.10 3rd Principle Stress (S3)

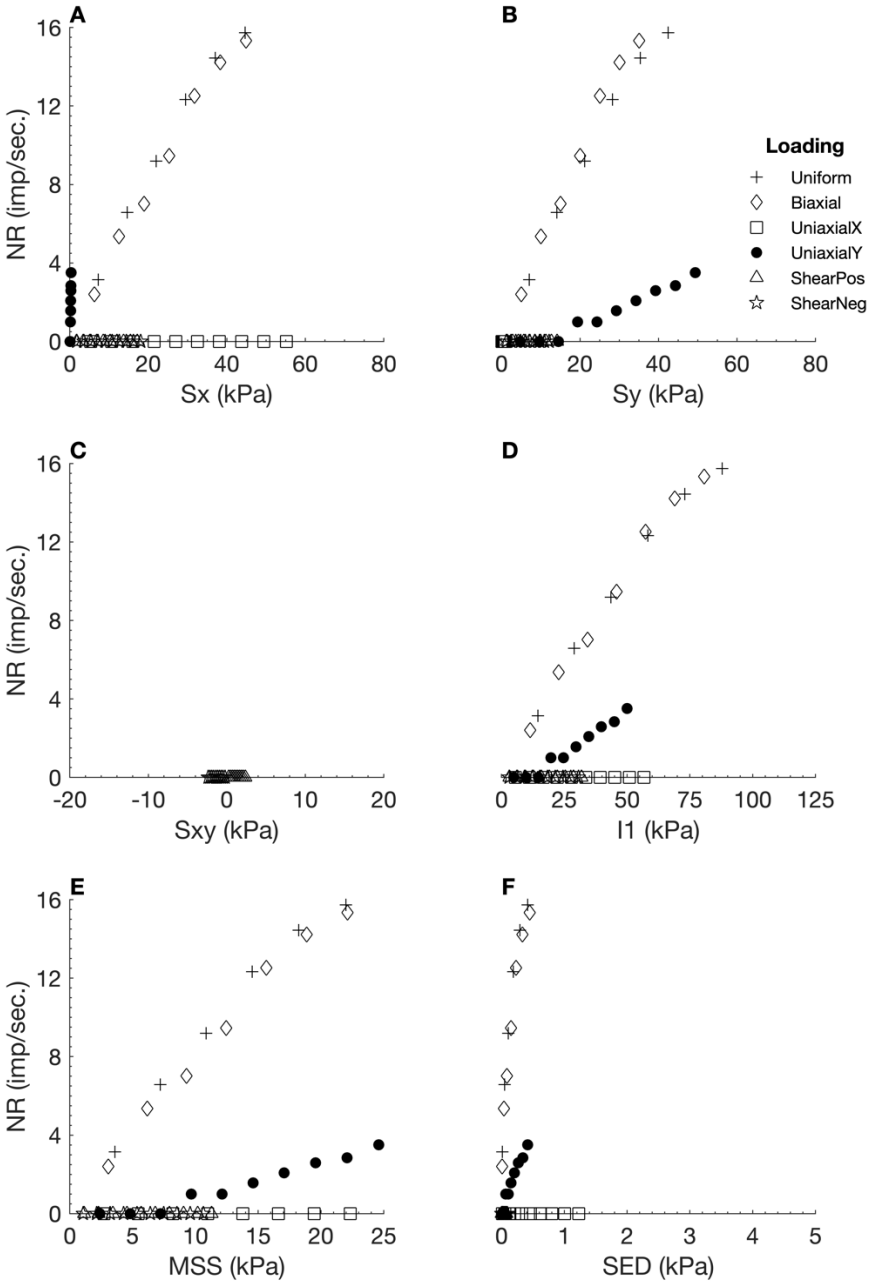

Figure B - 64. Neural responses (NR) output by the orthotropic elastic FEBio model 4 using S3 as the neural model input, plotted against six different stress variables. Sx: X stress. Sy: Y stress. Sxy: shear stress. I1: 1st invariant stress tensor. MSS: maximum shear stress. SED: strain energy density.

Table B - 70. Linear regression measures for individual loading regime results from the orthotropic elastic model 4, with S3 as neural model input.

Loading Regime	R^2	RMSE	Slope
Uniform	0.9584	1.1891	1.1324
Biaxial	0.3125	3.7006	10.9791
Uniaxial X	NaN	0.0000	0.0000
Uniaxial Y	0.9108	0.2279	0.4922
Shear Positive	NaN	0.0000	0.0000
Shear Negative	NaN	0.0000	0.0000

B.4.11 Deviatoric Stress 1 (Dev1)

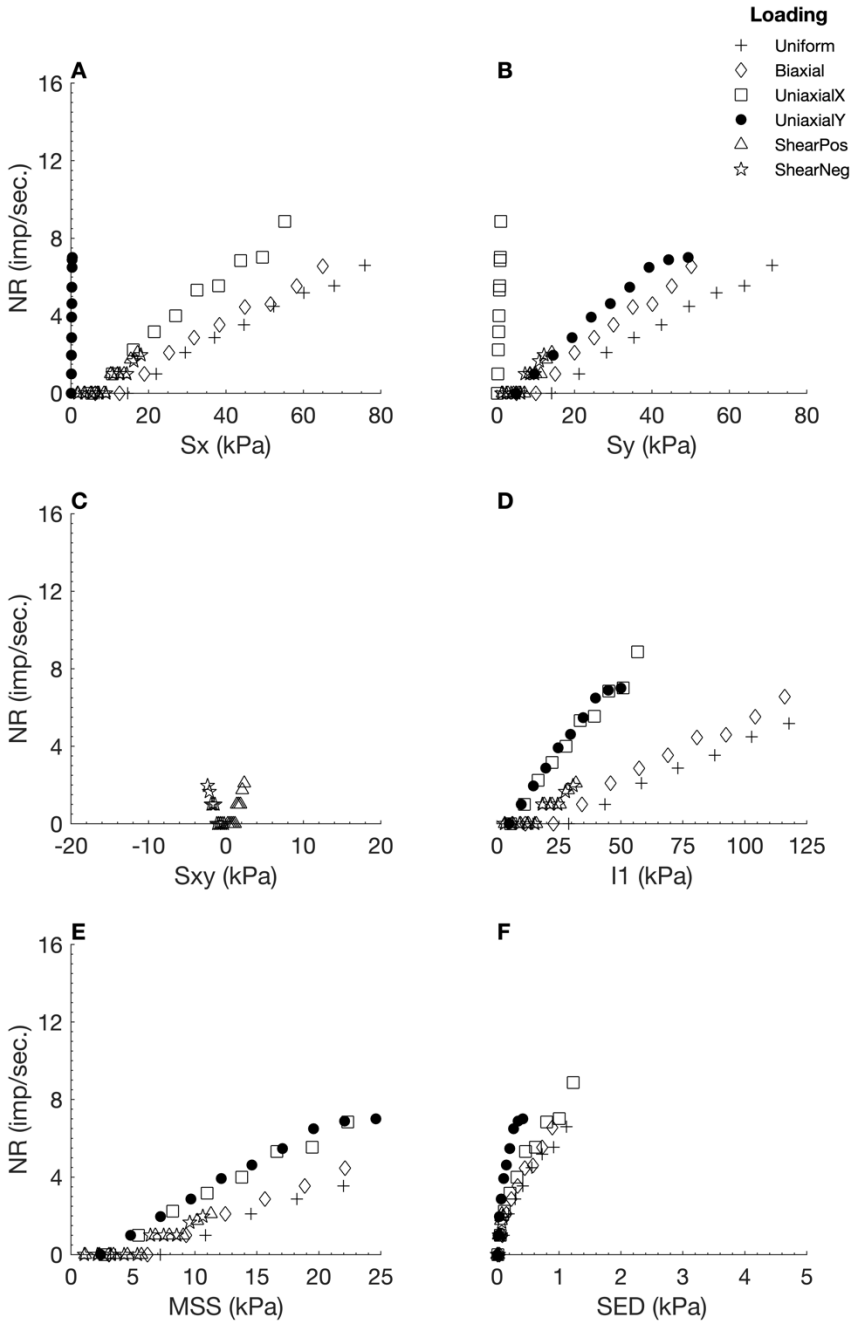

Figure B - 65. Neural responses (NR) output by the orthotropic elastic FEBio model 4 using Dev1 as the neural model input, plotted against six different stress variables. Sx: X stress. Sy: Y stress. Sxy: shear stress. I1: 1st invariant stress tensor. MSS: maximum shear stress. SED: strain energy density.

Table B - 71. Linear regression measures for individual loading regime results from the orthotropic elastic model 4, with Dev1 as neural model input.

Loading Regime	R^2	RMSE	Slope
Uniform	0.9804	0.3478	0.4876
Biaxial	0.3650	1.1736	3.9159
Uniaxial X	0.3763	1.3442	-0.4527
Uniaxial Y	0.9371	0.4919	1.2834
Shear Positive	0.3035	0.3809	0.0461
Shear Negative	NaN	0.0000	0.0000

B.4.12 Deviatoric Stress 2 (Dev2)

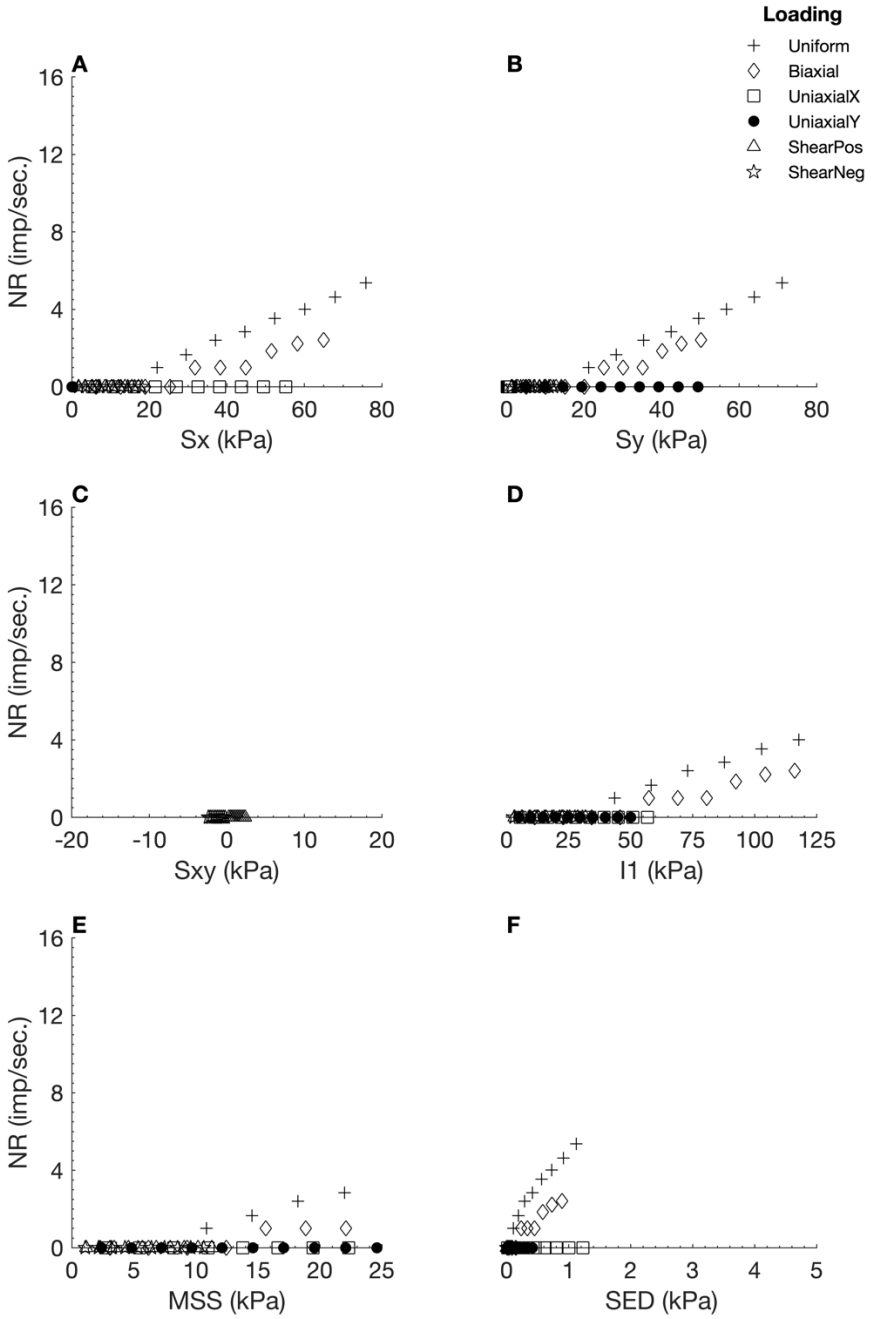

Figure B - 66. Neural responses (NR) output by the orthotropic elastic FEBio model 4 using Dev2 as the neural model input, plotted against six different stress variables. Sx: X stress. Sy: Y stress. Sxy: shear stress. I1: 1st invariant stress tensor. MSS: maximum shear stress. SED: strain energy density.

Table B - 72. Linear regression measures for individual loading regime results from the orthotropic elastic model 4, with Dev2 as neural model input.

Loading Regime	R^2	RMSE	Slope
Uniform	0.9814	0.2717	0.3912
Biaxial	0.0001	0.5164	-0.0233
Uniaxial X	NaN	0.0000	0.0000
Uniaxial Y	NaN	0.0000	0.0000
Shear Positive	NaN	0.0000	0.0000
Shear Negative	NaN	0.0000	0.0000

B.4.13 Deviatoric Stress 3 (Dev3)

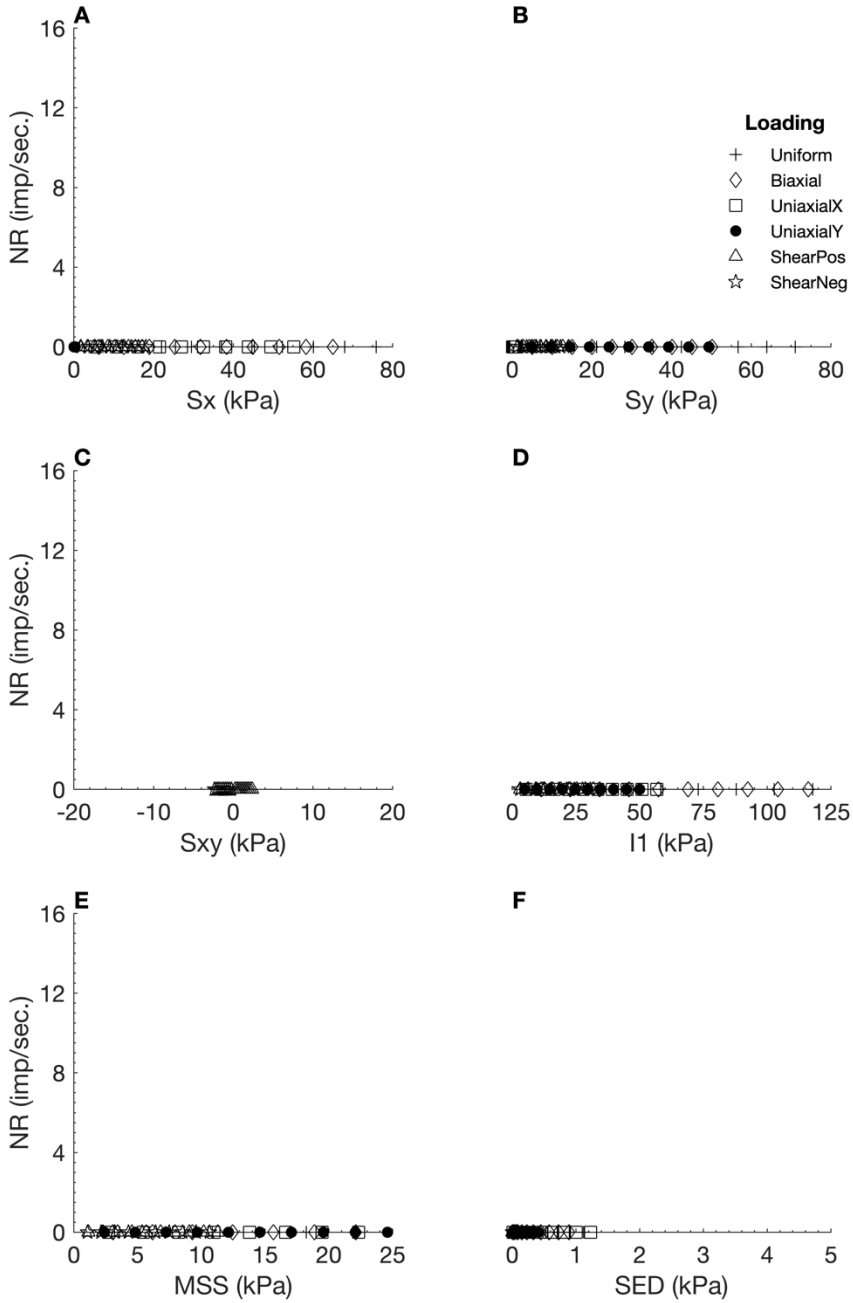

Figure B - 67. Neural responses (NR) output by the orthotropic elastic FEBio model 4 using Dev3 as the neural model input, plotted against six different stress variables. Sx: X stress. Sy: Y stress. Sxy: shear stress. I1: 1st invariant stress tensor. MSS: maximum shear stress. SED: strain energy density.

Table B - 73. Linear regression measures for individual loading regime results from the orthotropic elastic model 4, with Dev3 as neural model input.

Loading Regime	R^2	RMSE	Slope
Uniform	NaN	0.0000	0.0000
Biaxial	NaN	0.0000	0.0000
Uniaxial X	NaN	0.0000	0.0000
Uniaxial Y	NaN	0.0000	0.0000
Shear Positive	NaN	0.0000	0.0000
Shear Negative	NaN	0.0000	0.0000

B.4.14 Shear Stress A

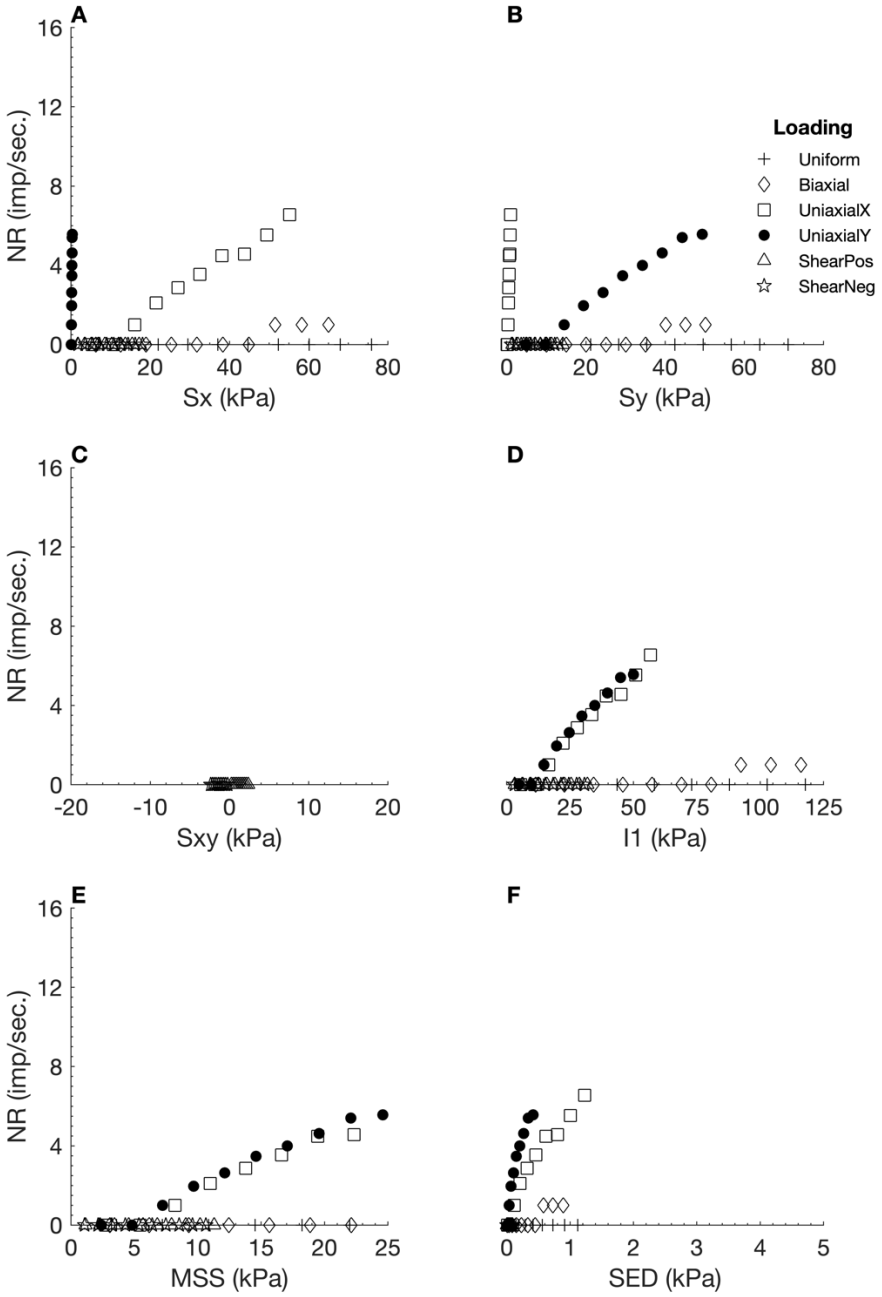

Figure B - 68. Neural responses (NR) output by the orthotropic elastic FEBio model 4 using ShearA as the neural model input, plotted against six different stress variables. Sx: X stress. Sy: Y stress. Sxy: shear stress. I1: 1st invariant stress tensor. MSS: maximum shear stress. SED: strain energy density.

Table B - 74. Linear regression measures for individual loading regime results from the orthotropic elastic model 4, with ShearA as neural model input.

Loading Regime	R^2	RMSE	Slope
Uniform	NaN	0.0000	0.0000
Biaxial	NaN	0.0000	0.0000
Uniaxial X	0.0967	1.1658	-0.1654
Uniaxial Y	0.9391	0.3925	1.0416
Shear Positive	NaN	0.0000	0.0000
Shear Negative	NaN	0.0000	0.0000

B.4.15 Shear Stress B

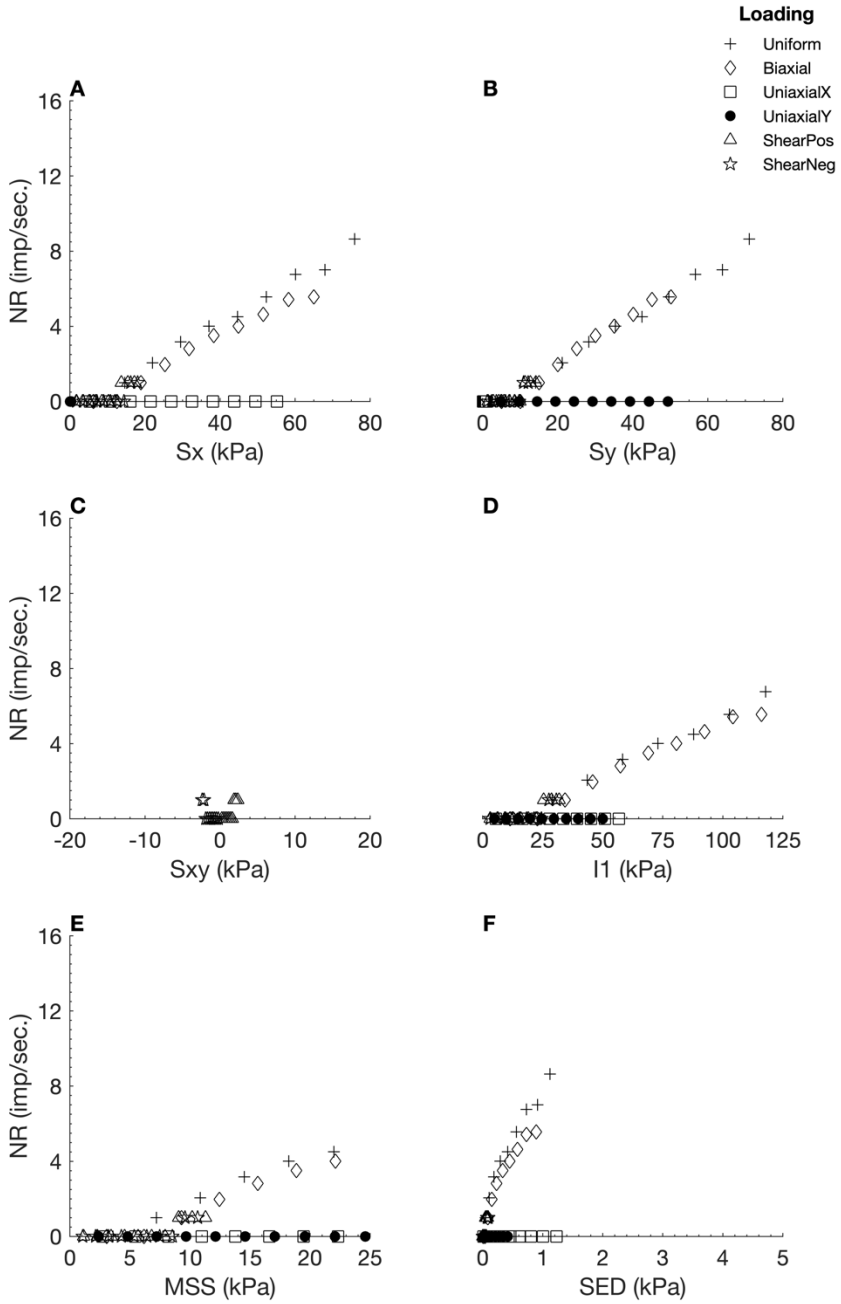

Figure B - 69. Neural responses (NR) output by the orthotropic elastic FEBio model 4 using ShearB as the neural model input, plotted against six different stress variables. Sx: X stress. Sy: Y stress. Sxy: shear stress. I1: 1st invariant stress tensor. MSS: maximum shear stress. SED: strain energy density.

Table B - 75. Linear regression measures for individual loading regime results from the orthotropic elastic model 4, with ShearB as neural model input.

Loading Regime	R^2	RMSE	Slope
Uniform	0.9743	0.4731	0.5780
Biaxial	0.3562	1.1455	3.7499
Uniaxial X	NaN	0.0000	0.0000
Uniaxial Y	NaN	0.0000	0.0000
Shear Positive	NaN	0.0000	0.0000
Shear Negative	NaN	0.0000	0.0000

B.4.16 Shear Stress C

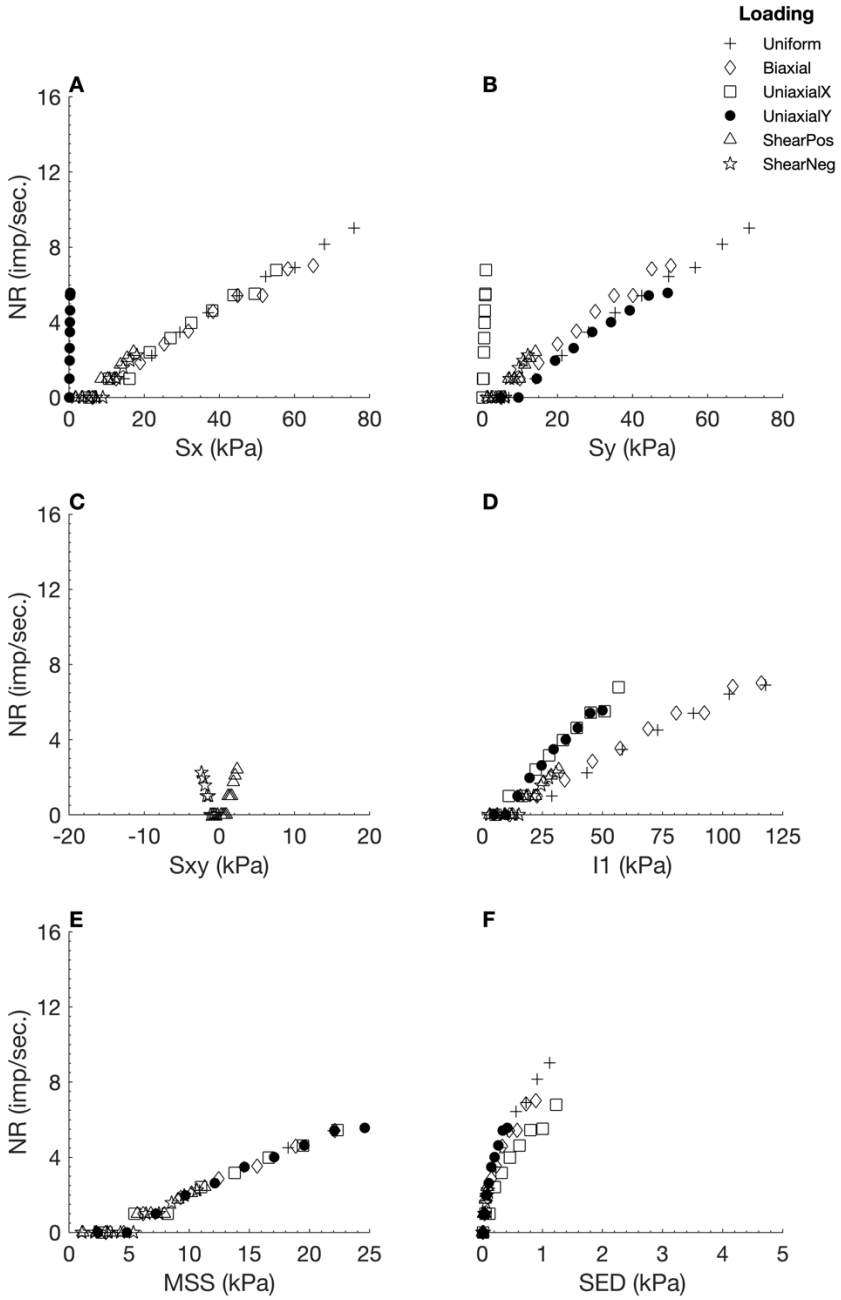

Figure B - 70. Neural responses (NR) output by the orthotropic elastic FEBio model 4 using ShearC as the neural model input, plotted against six different stress variables. Sx: X stress. Sy: Y stress. Sxy: shear stress. I1: 1st invariant stress tensor. MSS: maximum shear stress. SED: strain energy density.

Table B - 76. Linear regression measures for individual loading regime results from the orthotropic elastic model 4, with ShearC as neural model input.

Loading Regime	R^2	RMSE	Slope
Uniform	0.9898	0.3243	0.6333
Biaxial	0.4250	1.2365	4.6784
Uniaxial X	0.3035	1.0123	-0.2898
Uniaxial Y	0.9393	0.3932	1.0452
Shear Positive	0.5096	0.4043	0.0756
Shear Negative	NaN	0.0000	0.0000

B.4.17 X Strain (Ex)

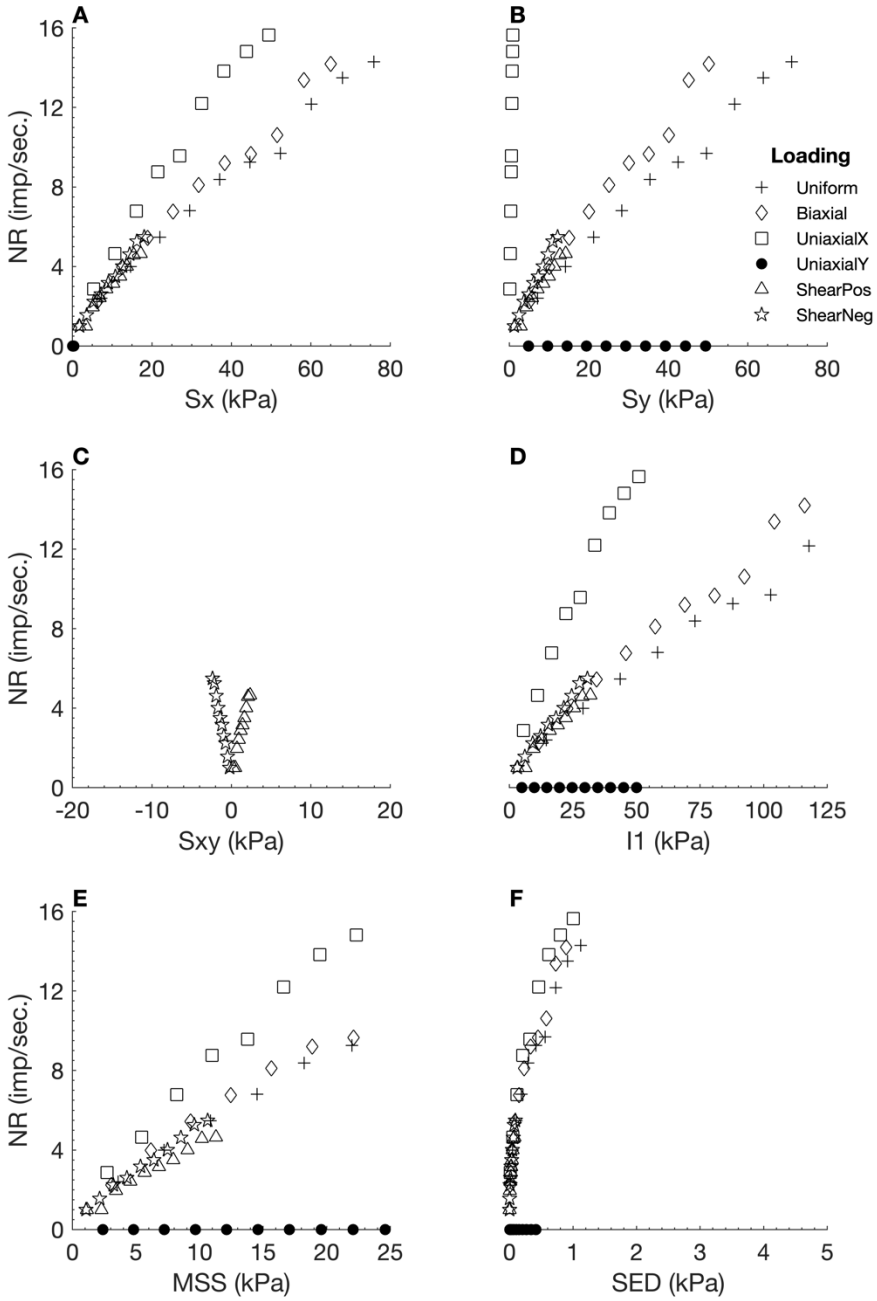

Figure B - 71. Neural responses (NR) output by the orthotropic elastic FEBio model 4 using Ex as the neural model input, plotted against six different stress variables. Sx: X stress. Sy: Y stress. Sxy: shear stress. I1: 1st invariant stress tensor. MSS: maximum shear stress. SED: strain energy density.

Table B - 77. Linear regression measures for individual loading regime results from the orthotropic elastic model 4, with Ex as neural model input.

Loading Regime	R^2	RMSE	Slope
Uniform	0.9777	0.6322	0.8305
Biaxial	0.4178	2.0253	7.5510
Uniaxial X	0.3474	2.5310	-0.8007
Uniaxial Y	NaN	0.0000	0.0000
Shear Positive	0.8904	0.3409	0.1782
Shear Negative	0.9123	0.2919	0.4913

B.4.18 Y Strain (Ey)

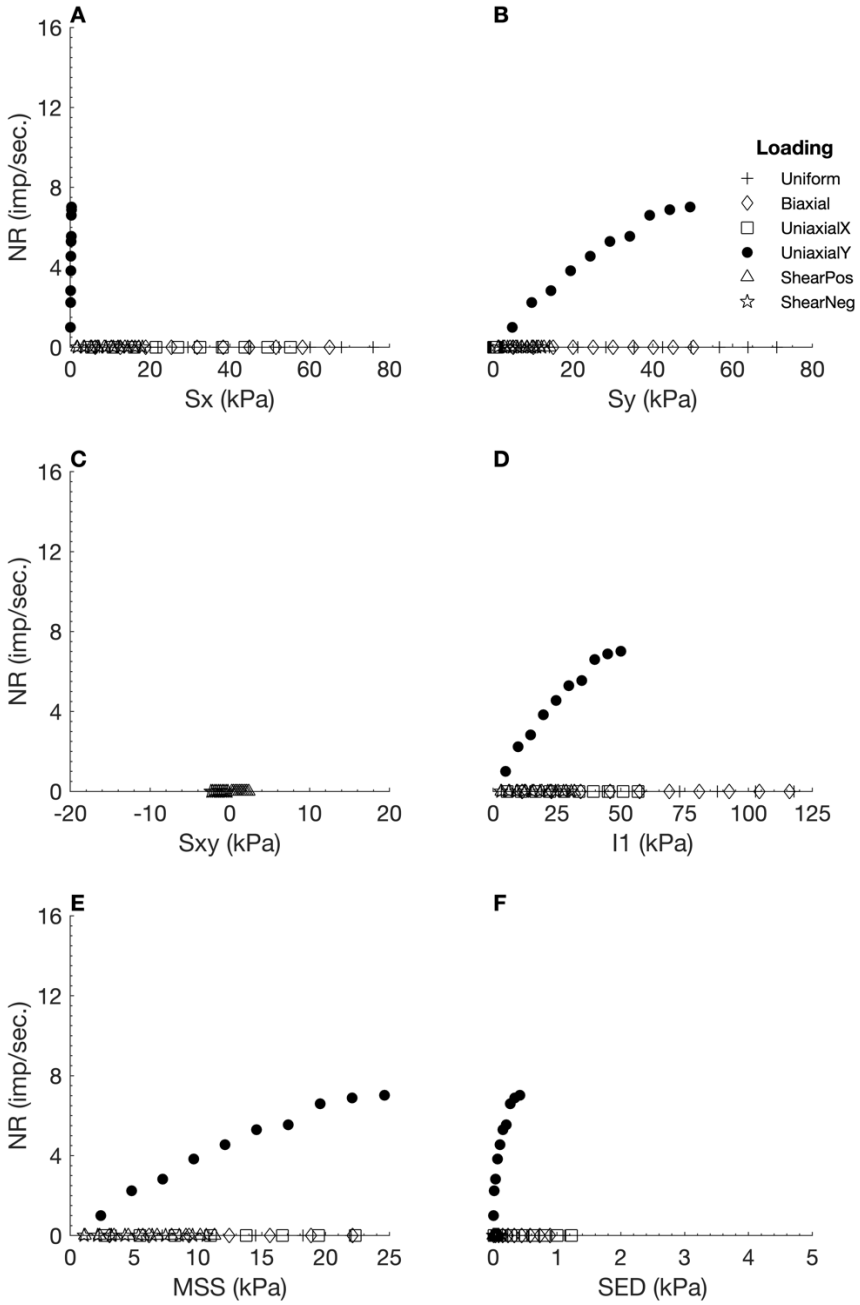

Figure B - 72. Neural responses (NR) output by the orthotropic elastic FEBio model 4 using Ey as the neural model input, plotted against six different stress variables. Sx: X stress. Sy: Y stress. Sxy: shear stress. I1: 1st invariant stress tensor. MSS: maximum shear stress. SED: strain energy density.

Table B - 78. Linear regression measures for individual loading regime results from the orthotropic elastic model 4, with Ey as neural model input.

Loading Regime	R^2	RMSE	Slope
Uniform	NaN	0.0000	0.0000
Biaxial	NaN	0.0000	0.0000
Uniaxial X	NaN	0.0000	0.0000
Uniaxial Y	0.9313	0.4629	1.1517
Shear Positive	NaN	0.0000	0.0000
Shear Negative	NaN	0.0000	0.0000

B.5 Test 5

Table B - 79. Values selected for material properties during FEBio implementation of orthotropic elastic material test 5.

Orthotropic Material Property	Value Selected
Density	1
Young's Modulus (X)	1
Young's Modulus (Y)	9.4
Young's Modulus (Z)	1
Shear Modulus (XY)	0.385
Shear Modulus (YZ)	3.62
Shear Modulus (XZ)	0.385
Poisson's Ratio (XY)	0.299
Poisson's Ratio (YZ)	0.299
Poisson's Ratio (XZ)	0.299

Table B - 80. Linear regression measures for total plot results (i.e. considering all loading regimes combined), for each input stimulus tested with the orthotropic elastic model 5.

Input Stimuli	R^2	RMSE	Slope
X Stress (Sx)	0.1623	4.3806	0.4259
Y Stress (Sy)	0.2904	3.7956	0.5363
Shear Stress (Sxy)	0.0908	0.4323	0.0302
1st Invariant Stress Tensor (I1)	0.2516	5.7047	0.7306
Maximum Shear Stress (MSS)	0.3047	1.9997	0.2924
Strain Energy Density (SED)	0.1606	0.5014	0.0484
Hydrostatic Pressure (HS)	0.2230	2.7709	0.3279
1st Principal Stress (S1)	0.2941	3.6532	0.5208
2nd Principal Stress (S2)	0.2228	3.9674	0.4692
3rd Principal Stress (S3)	0.2200	4.5314	0.5317
Deviatoric Stress 1 (Dev1)	0.2696	1.6095	0.2160
Deviatoric Stress 2 (Dev2)	0.1695	1.1861	0.1184
Deviatoric Stress 3 (Dev3)	NaN	0.0000	0.0000
Shear A	0.0042	0.8626	0.0124
Shear B	0.2415	1.9108	0.2382
Shear C	0.3047	1.9997	0.2924
X Strain (Ex)	0.1116	4.3760	0.3427
Y Strain (Ey)	0.0226	0.5082	0.0171
Average	**0.1967**	**2.4550**	**0.2861**

B.5.1 X Stress (Sx)

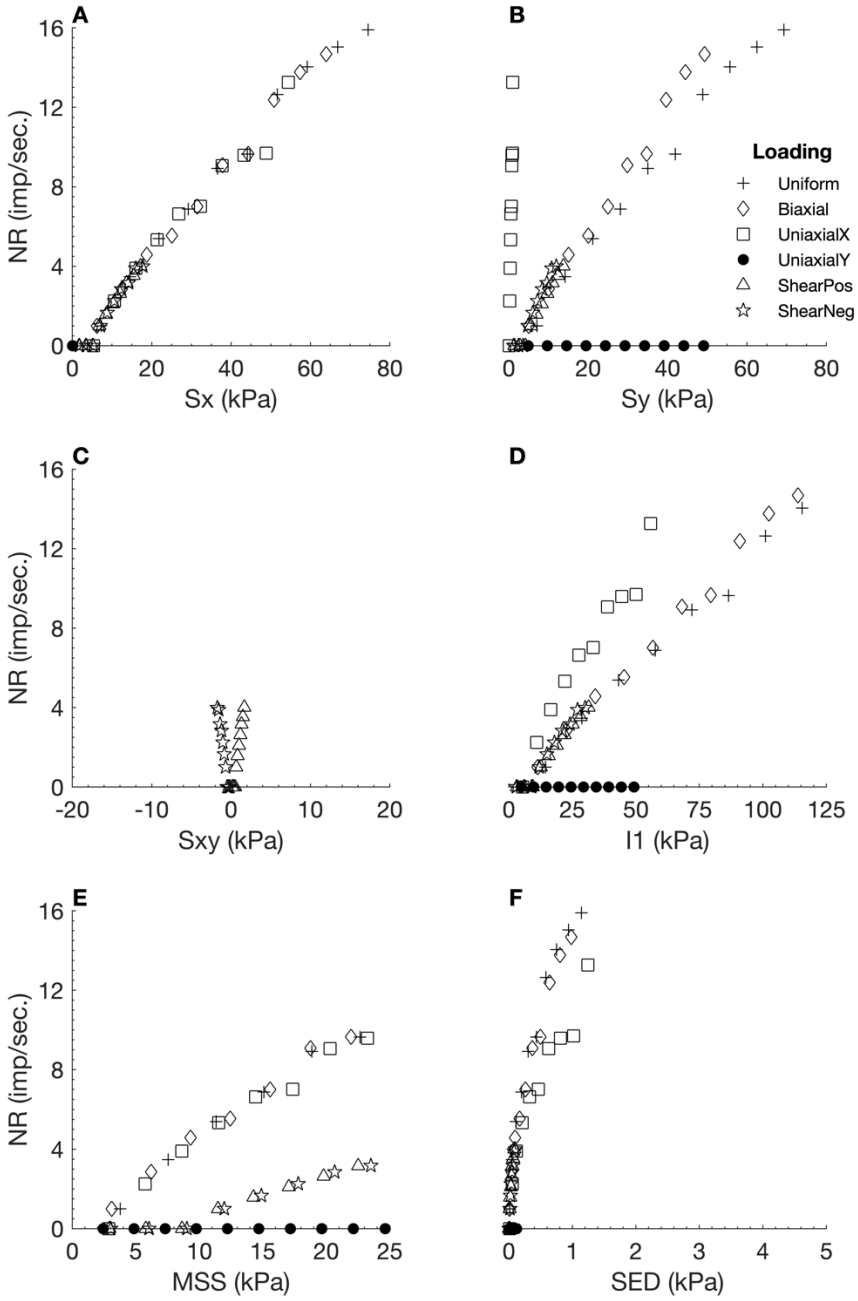

Figure B - 73. Neural responses (NR) output by the orthotropic elastic FEBio model 5 using Sx as the neural model input, plotted against six different stress variables. Sx: X stress. Sy: Y stress. Sxy: shear stress. I1: 1st invariant stress tensor. MSS: maximum shear stress. SED: strain energy density.

Table B - 81. Linear regression measures for individual loading regime results from the orthotropic elastic model 5, with Sx as neural model input.

Loading Regime	R^2	RMSE	Slope
Uniform	0.9863	0.6326	1.0662
Biaxial	0.4402	2.0208	7.8857
Uniaxial X	0.4803	2.0221	-0.8429
Uniaxial Y	NaN	0.0000	0.0000
Shear Positive	0.7165	0.5487	0.1600
Shear Negative	0.4684	0.6437	0.3153

B.5.2 Y Stress (Sy)

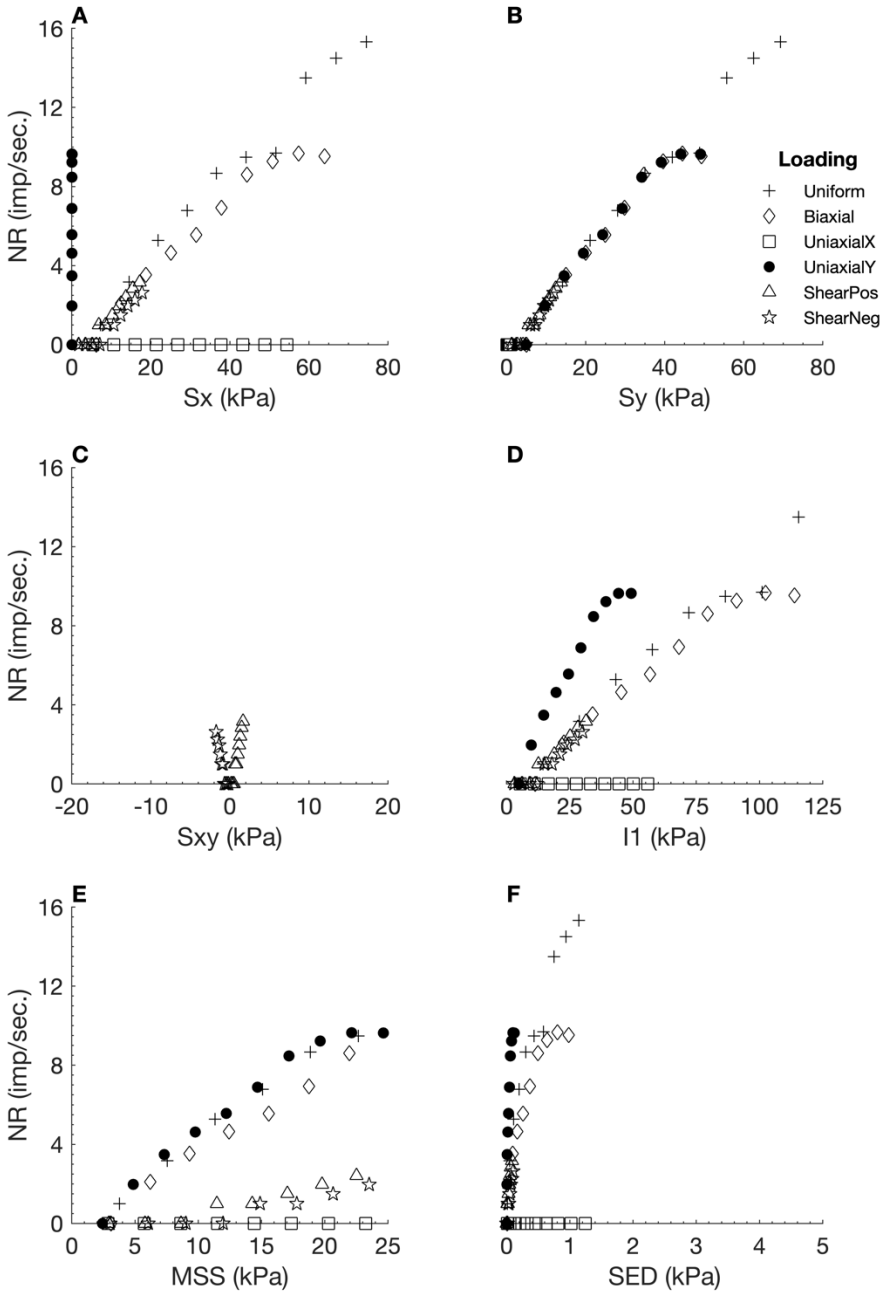

Figure B - 74. Neural responses (NR) output by the orthotropic elastic FEBio model 5 using Sy as the neural model input, plotted against six different stress variables. Sx: X stress. Sy: Y stress. Sxy: shear stress. I1: 1st invariant stress tensor. MSS: maximum shear stress. SED: strain energy density.

Table B - 82. Linear regression measures for individual loading regime results from the orthotropic elastic model 5, with Sy as neural model input.

Loading Regime	R^2	RMSE	Slope
Uniform	0.9713	0.8619	0.9952
Biaxial	0.4750	1.8325	7.6703
Uniaxial X	NaN	0.0000	0.0000
Uniaxial Y	0.8868	0.9399	1.7772
Shear Positive	0.7167	0.3960	0.1155
Shear Negative	0.2318	0.4526	0.1297

B.5.3 Shear Stress (Sxy)

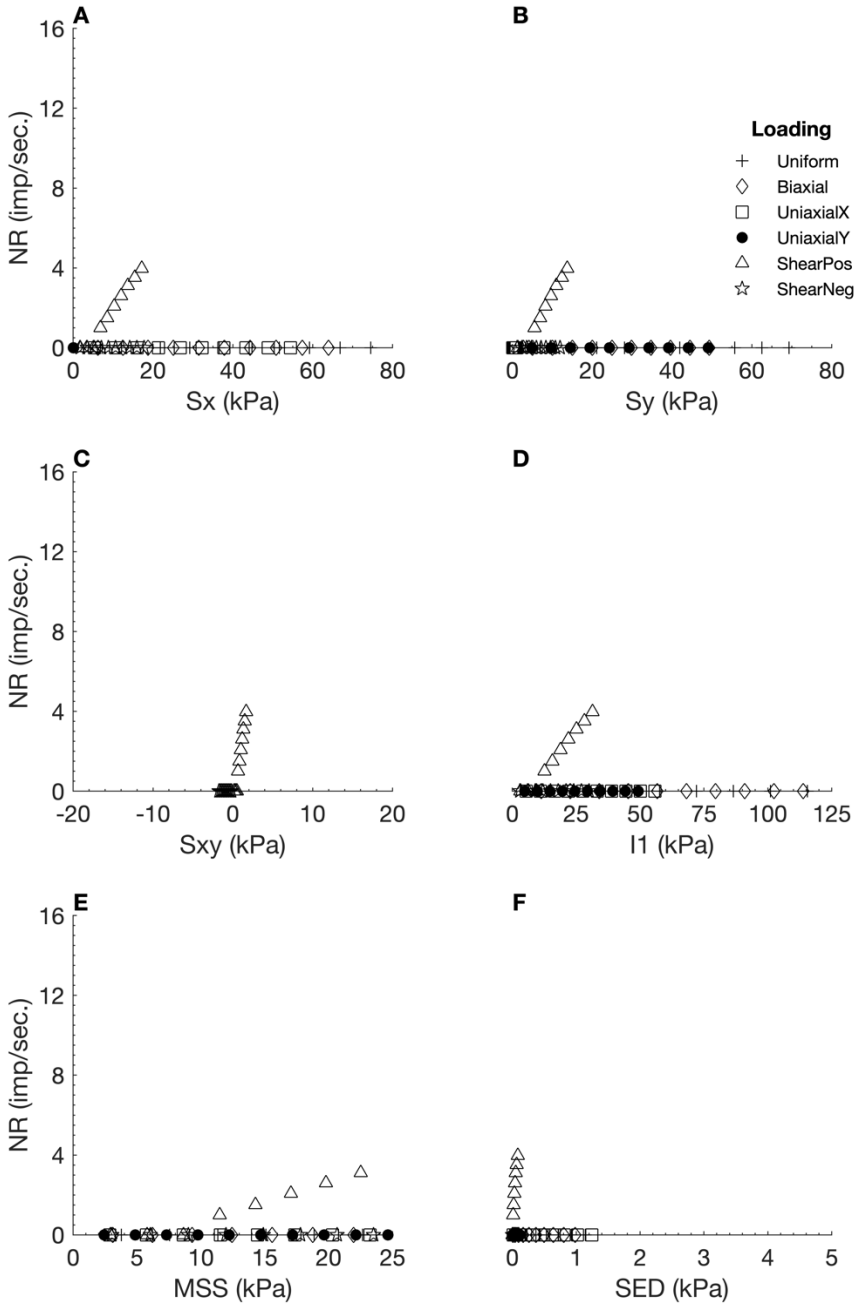

Figure B - 75. Neural responses (NR) output by the orthotropic elastic FEBio model 5 using Sxy as the neural model input, plotted against six different stress variables. Sx: X stress. Sy: Y stress. Sxy: shear stress. I1: 1st invariant stress tensor. MSS: maximum shear stress. SED: strain energy density.

Table B - 83. Linear regression measures for individual loading regime results from the orthotropic elastic model 5, with Sxy as neural model input.

Loading Regime	R^2	RMSE	Slope
Uniform	NaN	0.0000	0.0000
Biaxial	NaN	0.0000	0.0000
Uniaxial X	NaN	0.0000	0.0000
Uniaxial Y	NaN	0.0000	0.0000
Shear Positive	0.7172	0.5368	0.1568
Shear Negative	NaN	0.0000	0.0000

B.5.4 1st Invariant Stress Tensor (I1)

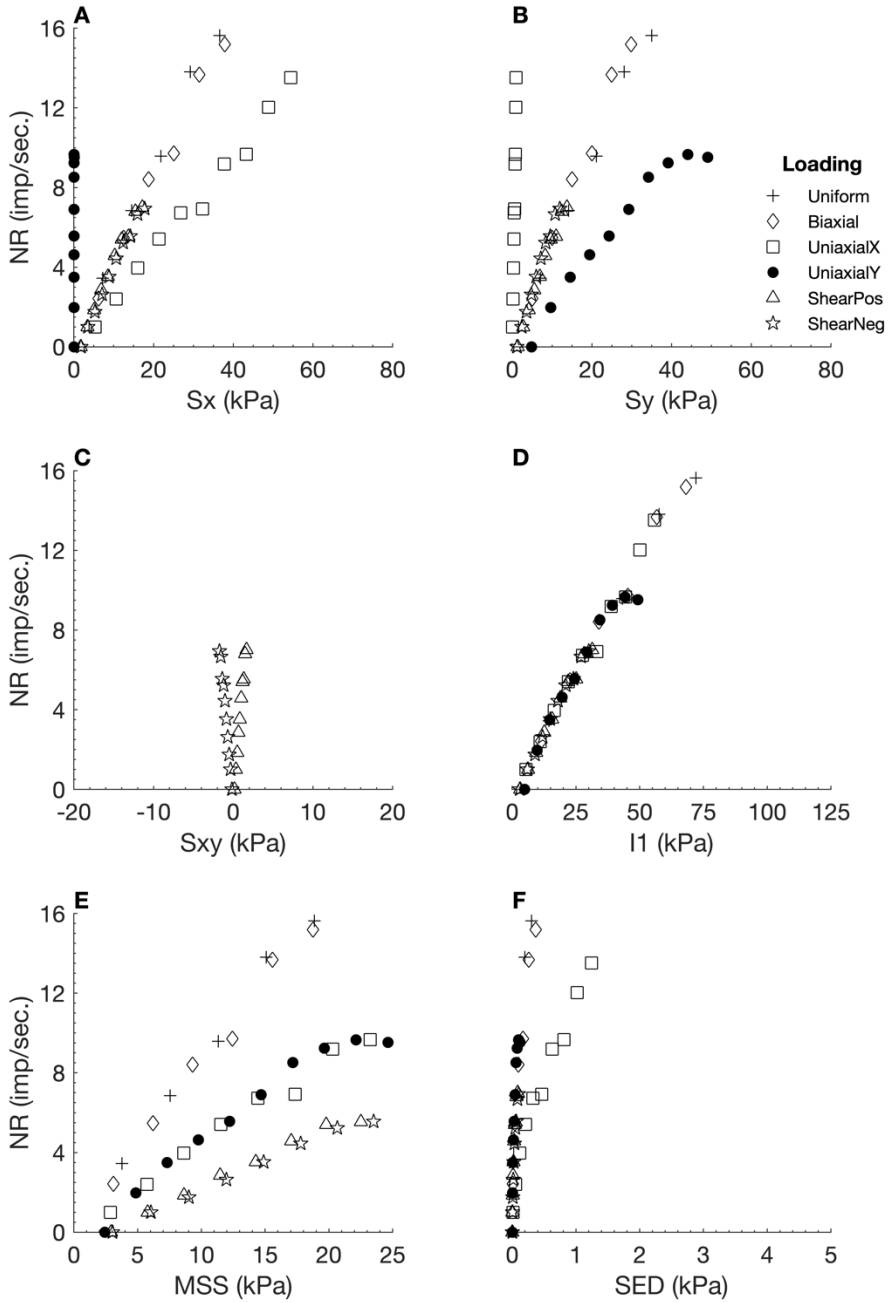

Figure B - 76. Neural responses (NR) output by the orthotropic elastic FEBio model 5 using I1 as the neural model input, plotted against six different stress variables. Sx: X stress. Sy: Y stress. Sxy: shear stress. I1: 1st invariant stress tensor. MSS: maximum shear stress. SED: strain energy density.

Table B - 84. Linear regression measures for individual loading regime results from the orthotropic elastic model 5, with I1 as neural model input.

Loading Regime	R^2	RMSE	Slope
Uniform	0.9648	1.2426	1.2907
Biaxial	0.3519	3.9640	12.8556
Uniaxial X	0.3646	1.8657	-0.6128
Uniaxial Y	0.8863	0.9427	1.7788
Shear Positive	0.9554	0.3979	0.3378
Shear Negative	0.8815	0.5456	0.7766

B.5.5 Maximum Shear Stress (MSS)

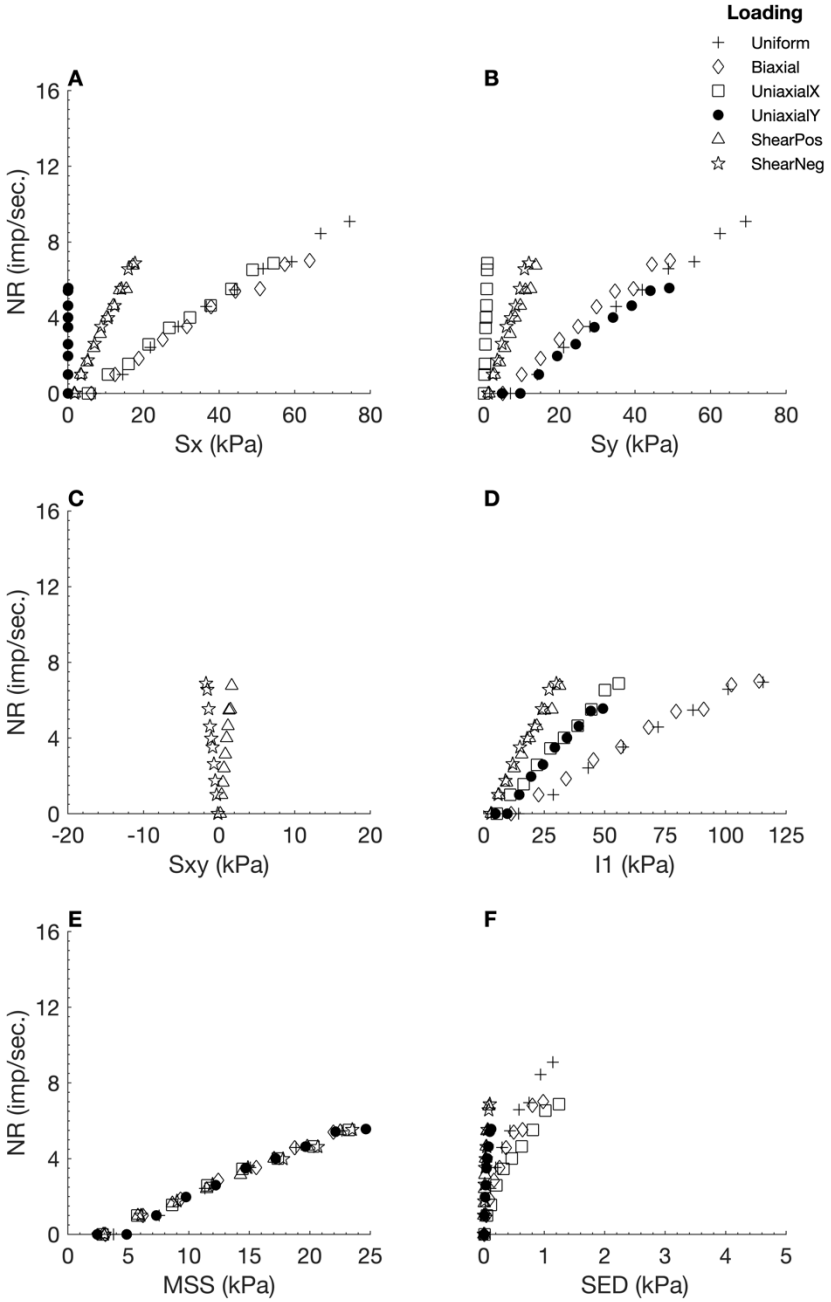

Figure B - 77. Neural responses (NR) output by the orthotropic elastic FEBio model 5 using MSS as the neural model input, plotted against six different stress variables. Sx: X stress. Sy: Y stress. Sxy: shear stress. I1: 1st invariant stress tensor. MSS: maximum shear stress. SED: strain energy density.

Table B - 85. Linear regression measures for individual loading regime results from the orthotropic elastic model 5, with MSS as neural model input.

Loading Regime	R^2	RMSE	Slope
Uniform	0.9903	0.3204	0.6426
Biaxial	0.4244	1.2380	4.6776
Uniaxial X	0.3911	1.0328	-0.3589
Uniaxial Y	0.9388	0.3948	1.0446
Shear Positive	0.9578	0.3344	0.2924
Shear Negative	0.8824	0.5428	0.7759

B.5.6 Strain Energy Density (SED)

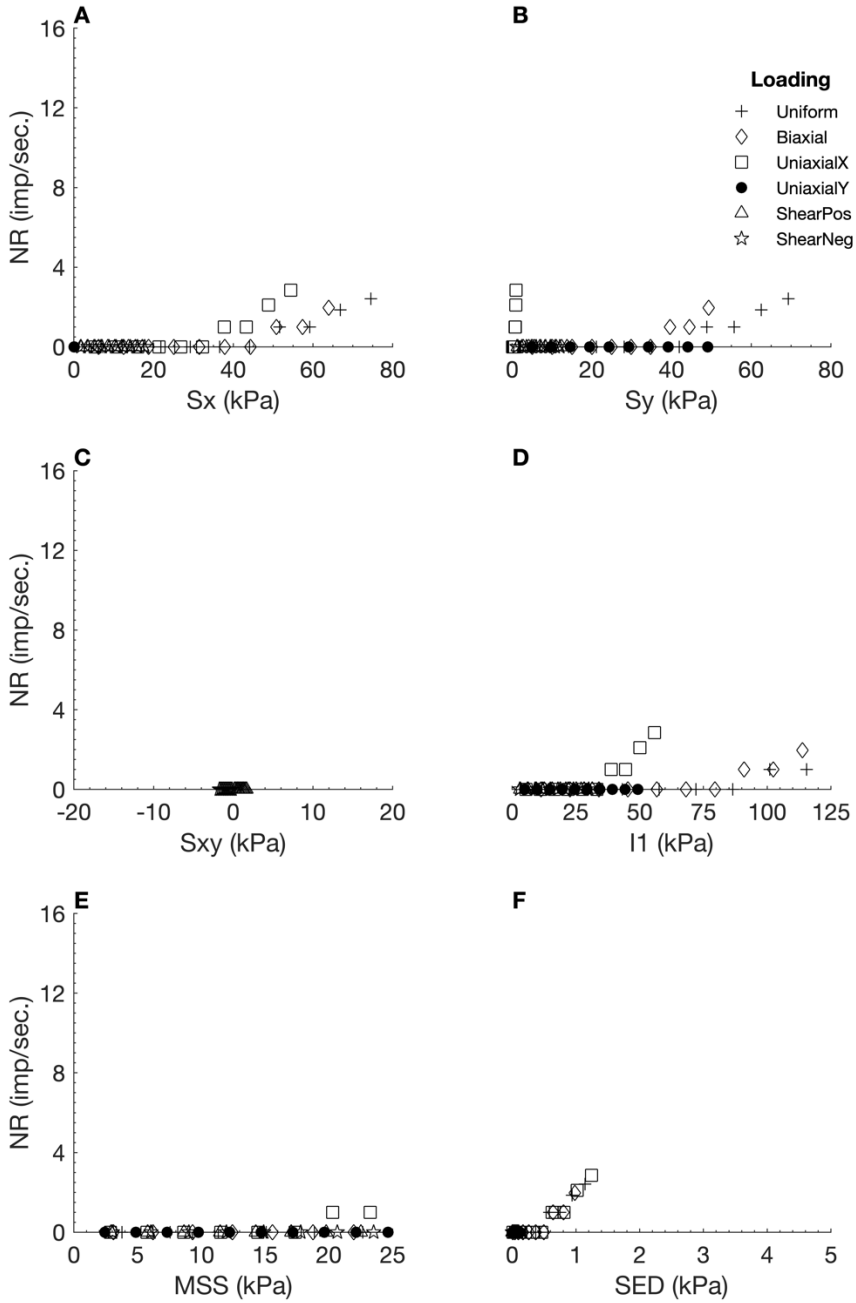

Figure B - 78. Neural responses (NR) output by the orthotropic elastic FEBio model 5 using SED as the neural model input, plotted against six different stress variables. Sx: X stress. Sy: Y stress. Sxy: shear stress. I1: 1st invariant stress tensor. MSS: maximum shear stress. SED: strain energy density.

Table B - 86. Linear regression measures for individual loading regime results from the orthotropic elastic model 5, with SED as neural model input.

Loading Regime	R^2	RMSE	Slope
Uniform	0.6646	0.5549	0.1549
Biaxial	NaN	0.0000	0.0000
Uniaxial X	NaN	0.0000	0.0000
Uniaxial Y	NaN	0.0000	0.0000
Shear Positive	NaN	0.0000	0.0000
Shear Negative	NaN	0.0000	0.0000

B.5.7 Hydrostatic Pressure (HS)

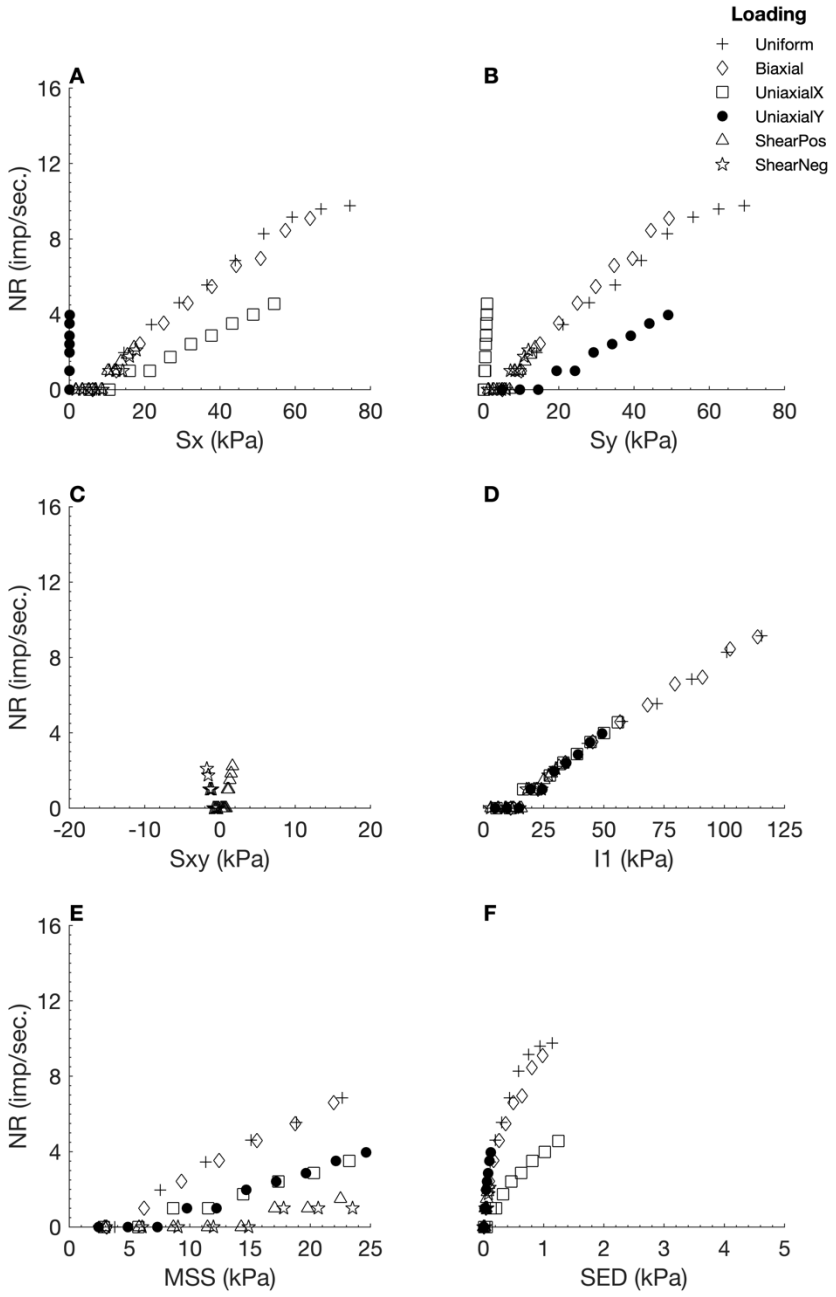

Figure B - 79. Neural responses (NR) output by the orthotropic elastic FEBio model 5 using HS as the neural model input, plotted against six different stress variables. Sx: X stress. Sy: Y stress. Sxy: shear stress. I1: 1st invariant stress tensor. MSS: maximum shear stress. SED: strain energy density.

Table B - 87. Linear regression measures for individual loading regime results from the orthotropic elastic model 5, with HS as neural model input.

Loading Regime	R^2	RMSE	Slope
Uniform	0.9884	0.3873	0.7104
Biaxial	0.4407	1.6011	6.2542
Uniaxial X	0.2082	0.6292	-0.1399
Uniaxial Y	0.9119	0.2677	0.5818
Shear Positive	0.3035	0.3809	0.0461
Shear Negative	NaN	0.0000	0.0000

B.5.8 1st Principle Stress (S1)

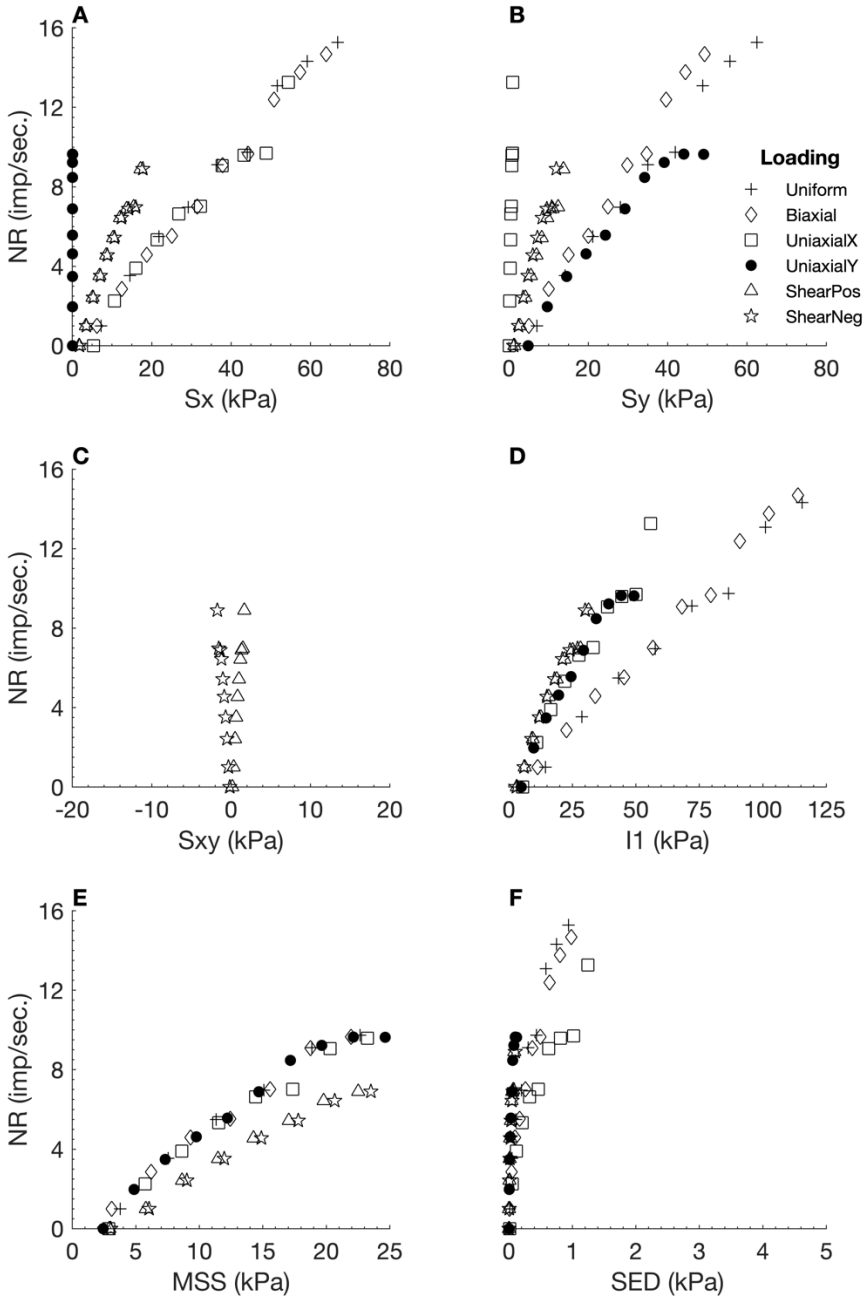

Figure B - 80. Neural responses (NR) output by the orthotropic elastic FEBio model 5 using S1 as the neural model input, plotted against six different stress variables. Sx: X stress. Sy: Y stress. Sxy: shear stress. I1: 1st invariant stress tensor. MSS: maximum shear stress. SED: strain energy density.

Table B - 88. Linear regression measures for individual loading regime results from the orthotropic elastic model 5, with S1 as neural model input.

Loading Regime	R^2	RMSE	Slope
Uniform	0.9844	0.6893	1.0863
Biaxial	0.4397	2.0202	7.8760
Uniaxial X	0.4802	2.0222	-0.8428
Uniaxial Y	0.8868	0.9399	1.7772
Shear Positive	0.9570	0.4836	0.4182
Shear Negative	0.8903	0.7040	1.0467

B.5.9 2nd Principle Stress (S2)

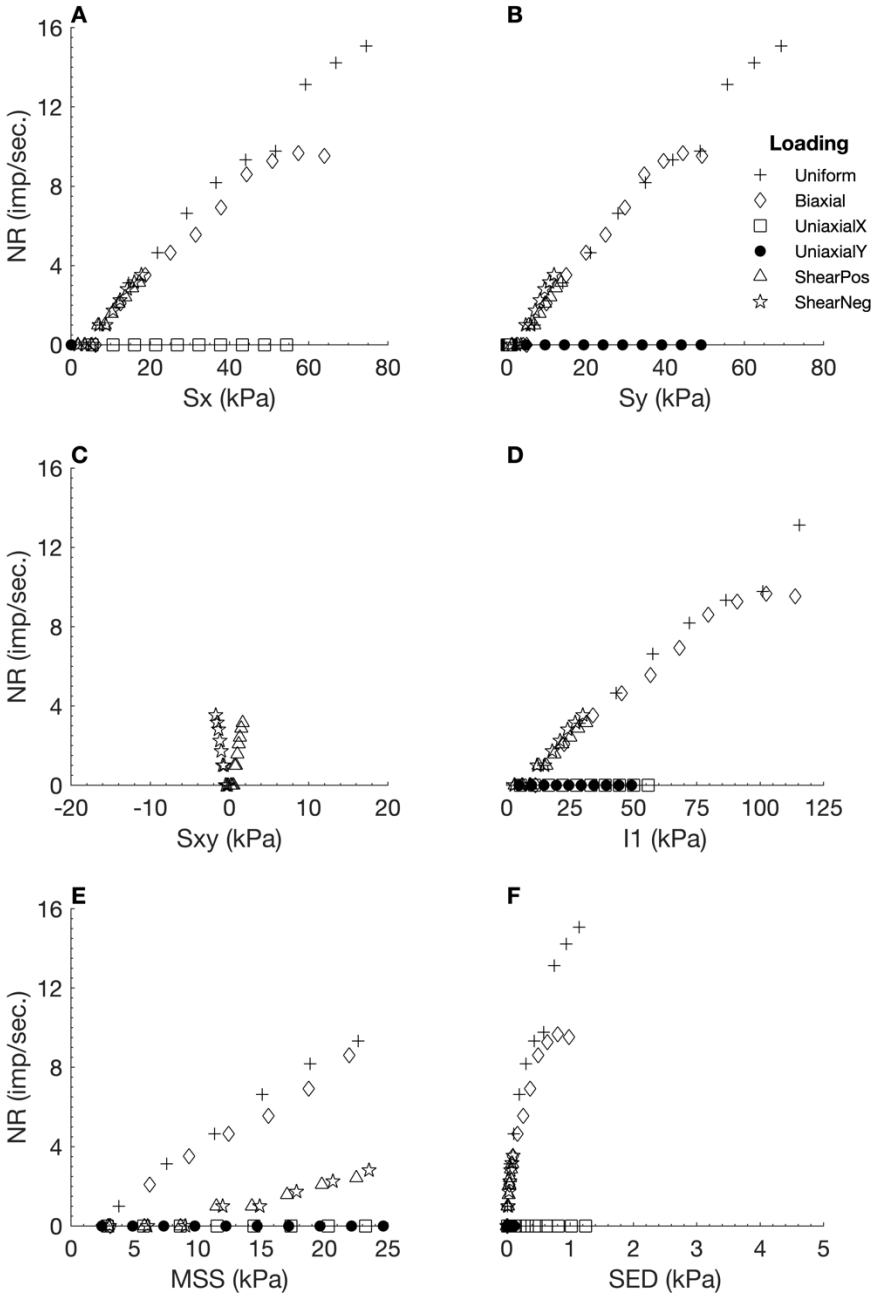

Figure B - 81. Neural responses (NR) output by the orthotropic elastic FEBio model 5 using S2 as the neural model input, plotted against six different stress variables. Sx: X stress. Sy: Y stress. Sxy: shear stress. I1: 1st invariant stress tensor. MSS: maximum shear stress. SED: strain energy density.

Table B - 89. Linear regression measures for individual loading regime results from the orthotropic elastic model 5, with S2 as neural model input.

Loading Regime	R^2	RMSE	Slope
Uniform	0.9769	0.7657	0.9881
Biaxial	0.4750	1.8334	7.6741
Uniaxial X	NaN	0.0000	0.0000
Uniaxial Y	NaN	0.0000	0.0000
Shear Positive	0.7143	0.4102	0.1190
Shear Negative	0.4848	0.4540	0.2298

B.5.10 3rd Principle Stress (S3)

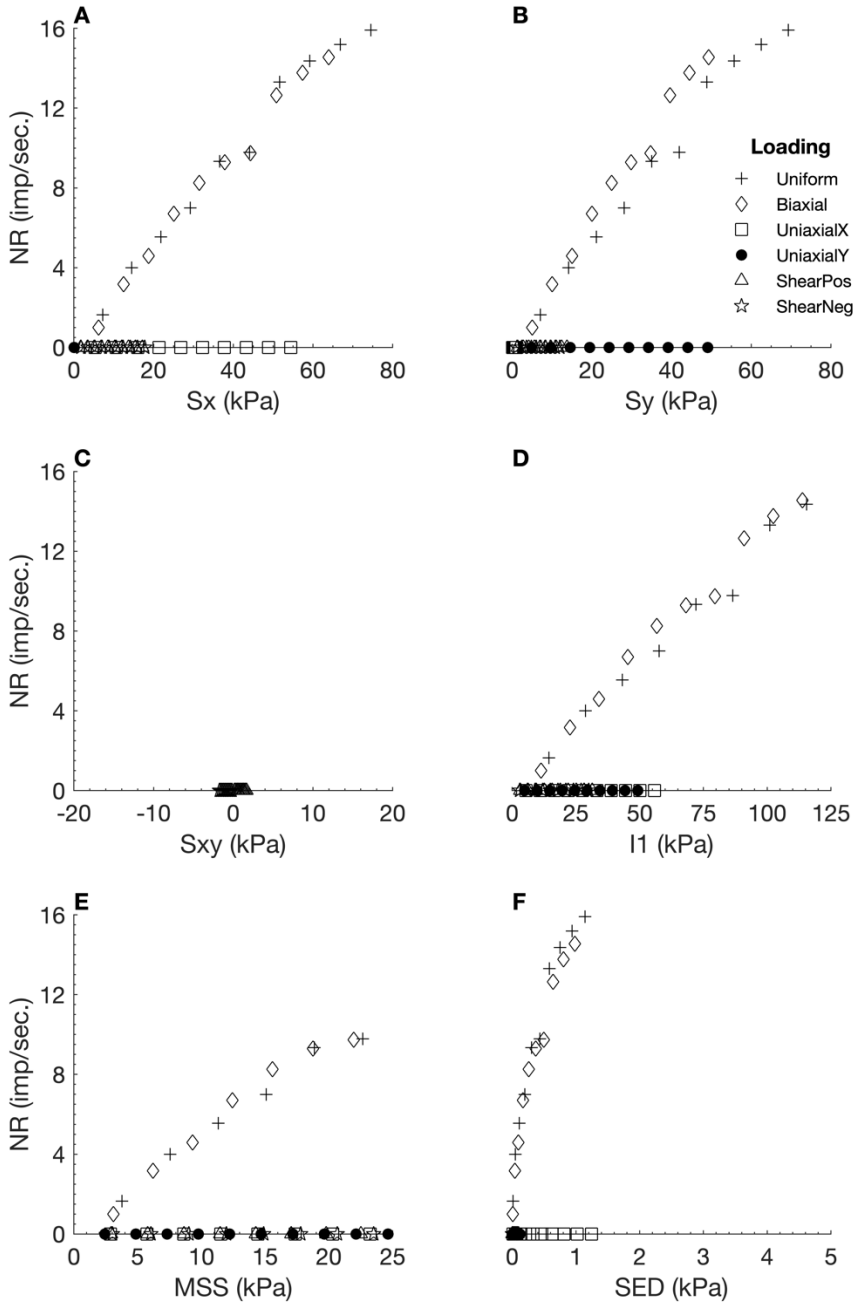

Figure B - 82. Neural responses (NR) output by the orthotropic elastic FEBio model 5 using S3 as the neural model input, plotted against six different stress variables. Sx: X stress. Sy: Y stress. Sxy: shear stress. I1: 1st invariant stress tensor. MSS: maximum shear stress. SED: strain energy density.

Table B - 90. Linear regression measures for individual loading regime results from the orthotropic elastic model 5, with S3 as neural model input.

Loading Regime	R^2	RMSE	Slope
Uniform	0.9800	0.7501	1.0423
Biaxial	0.3832	2.5925	8.9919
Uniaxial X	NaN	0.0000	0.0000
Uniaxial Y	NaN	0.0000	0.0000
Shear Positive	NaN	0.0000	0.0000
Shear Negative	NaN	0.0000	0.0000

B.5.11 Deviatoric Stress 1 (Dev1)

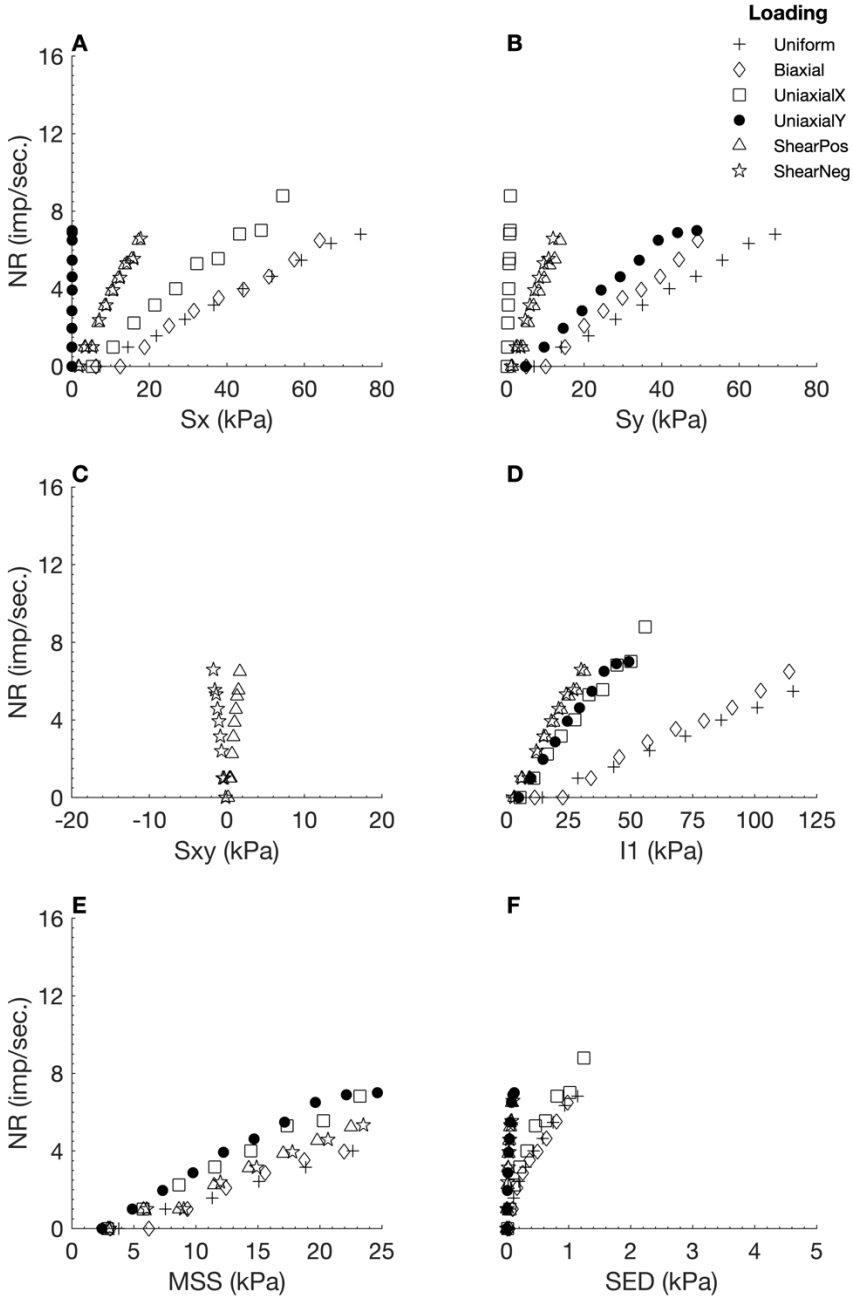

Figure B - 83. Neural responses (NR) output by the orthotropic elastic FEBio model 5 using Dev1 as the neural model input, plotted against six different stress variables. Sx: X stress. Sy: Y stress. Sxy: shear stress. I1: 1st invariant stress tensor. MSS: maximum shear stress. SED: strain energy density.

Table B - 91. Linear regression measures for individual loading regime results from the orthotropic elastic model 5, with Dev1 as neural model input.

Loading Regime	R^2	RMSE	Slope
Uniform	0.9862	0.2875	0.4826
Biaxial	0.3657	1.1708	3.9126
Uniaxial X	0.3759	1.3450	-0.4526
Uniaxial Y	0.9369	0.4939	1.2855
Shear Positive	0.8872	0.5508	0.2834
Shear Negative	0.7462	0.7288	0.6521

B.5.12 Deviatoric Stress 2 (Dev2)

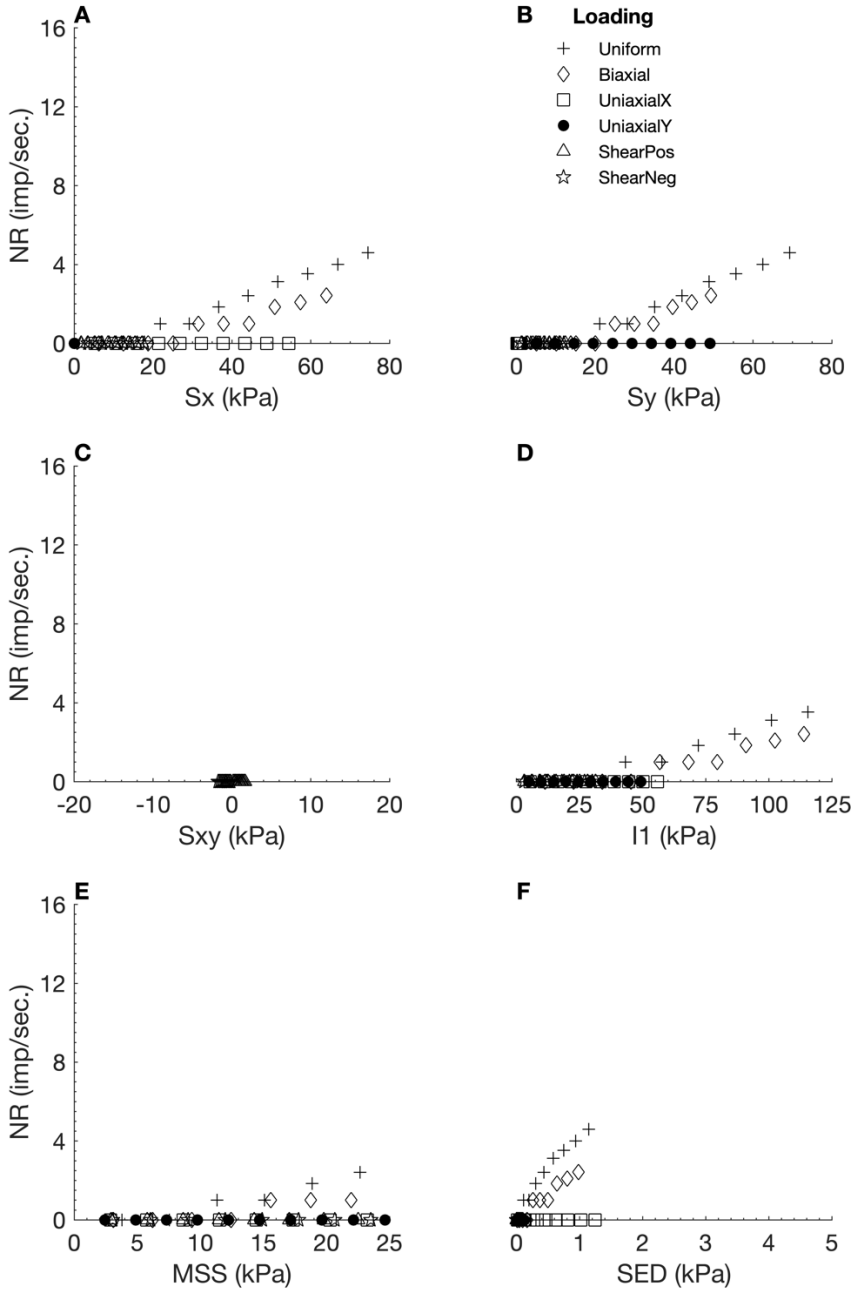

Figure B - 84. Neural responses (NR) output by the orthotropic elastic FEBio model 5 using Dev2 as the neural model input, plotted against six different stress variables. Sx: X stress. Sy: Y stress. Sxy: shear stress. I1: 1st invariant stress tensor. MSS: maximum shear stress. SED: strain energy density.

Table B - 92. Linear regression measures for individual loading regime results from the orthotropic elastic model 5, with Dev2 as neural model input.

Loading Regime	R^2	RMSE	Slope
Uniform	0.9779	0.2596	0.3422
Biaxial	0.0001	0.5164	-0.0233
Uniaxial X	NaN	0.0000	0.0000
Uniaxial Y	NaN	0.0000	0.0000
Shear Positive	NaN	0.0000	0.0000
Shear Negative	NaN	0.0000	0.0000

B.5.13 Deviatoric Stress 3 (Dev3)

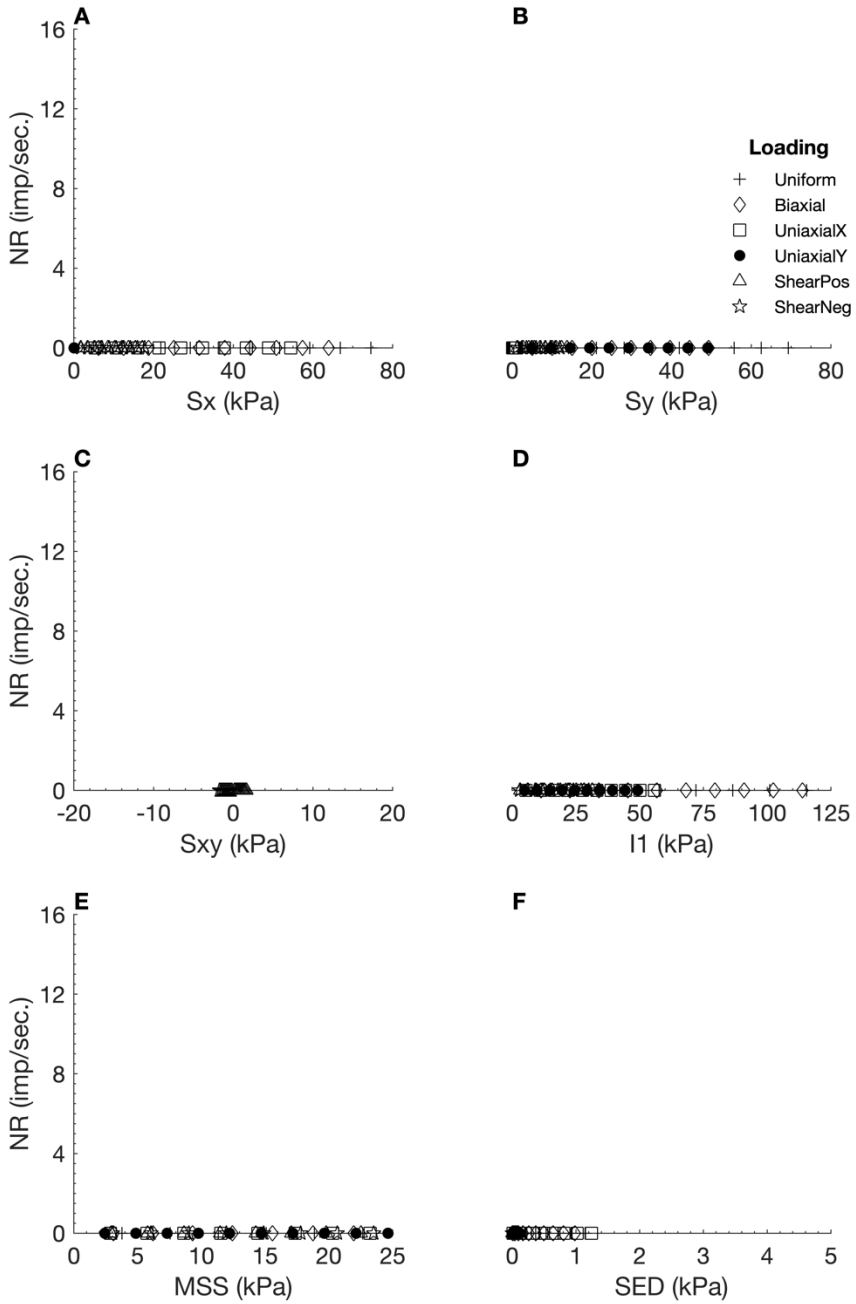

Figure B - 85. Neural responses (NR) output by the orthotropic elastic FEBio model 5 using Dev3 as the neural model input, plotted against six different stress variables. Sx: X stress. Sy: Y stress. Sxy: shear stress. I1: 1st invariant stress tensor. MSS: maximum shear stress. SED: strain energy density.

Table B - 93. Linear regression measures for individual loading regime results from the orthotropic elastic model 5, with Dev3 as neural model input.

Loading Regime	R^2	RMSE	Slope
Uniform	NaN	0.0000	0.0000
Biaxial	NaN	0.0000	0.0000
Uniaxial X	NaN	0.0000	0.0000
Uniaxial Y	NaN	0.0000	0.0000
Shear Positive	NaN	0.0000	0.0000
Shear Negative	NaN	0.0000	0.0000

B.5.14 Shear Stress A

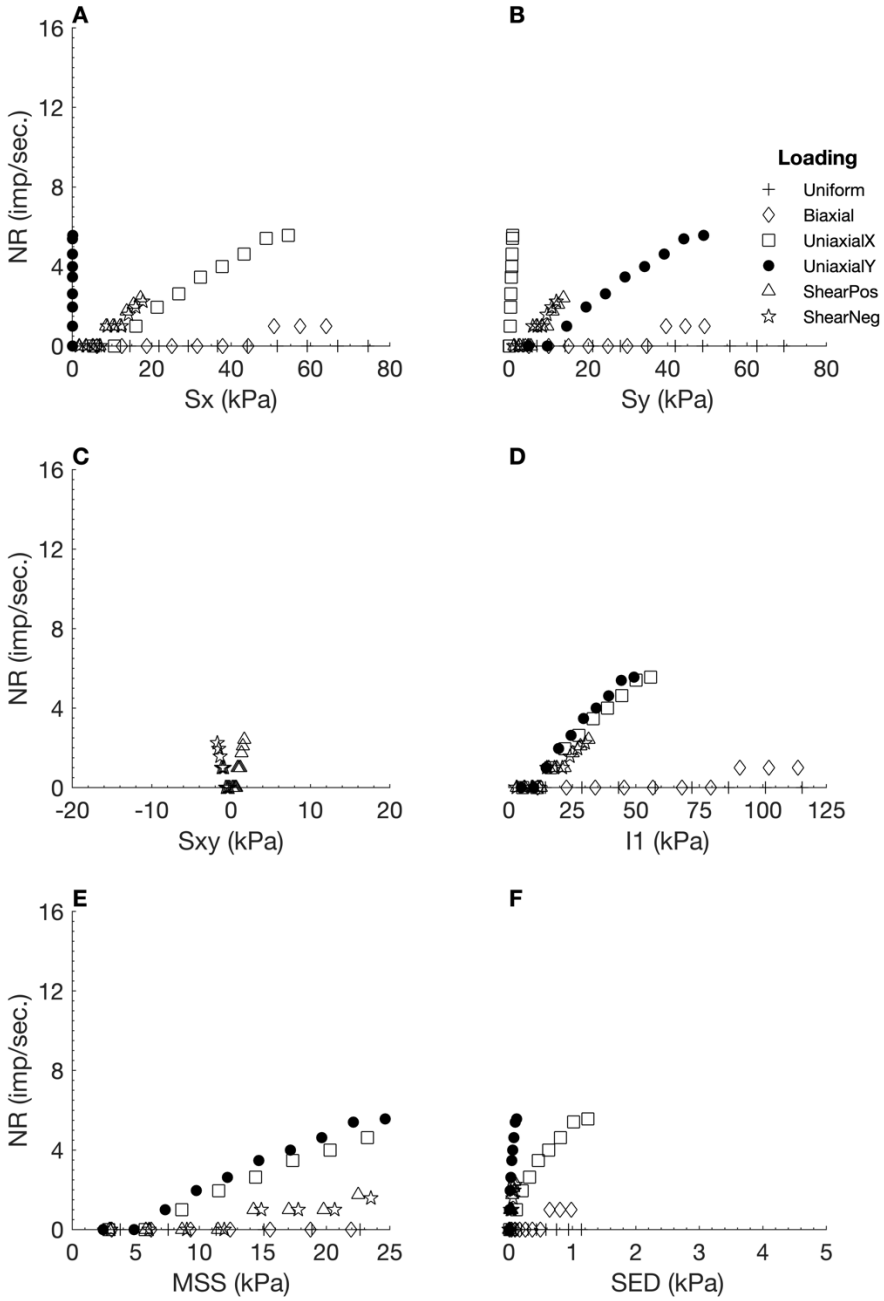

Figure B - 86. Neural responses (NR) output by the orthotropic elastic FEBio model 5 using ShearA as the neural model input, plotted against six different stress variables. Sx: X stress. Sy: Y stress. Sxy: shear stress. I1: 1st invariant stress tensor. MSS: maximum shear stress. SED: strain energy density.

Table B - 94. Linear regression measures for individual loading regime results from the orthotropic elastic model 5, with ShearA as neural model input.

Loading Regime	R^2	RMSE	Slope
Uniform	NaN	0.0000	0.0000
Biaxial	NaN	0.0000	0.0000
Uniaxial X	0.1058	1.0863	-0.1620
Uniaxial Y	0.9390	0.3931	1.0426
Shear Positive	0.5096	0.4043	0.0756
Shear Negative	0.2318	0.4526	0.1297

B.5.15 Shear Stress B

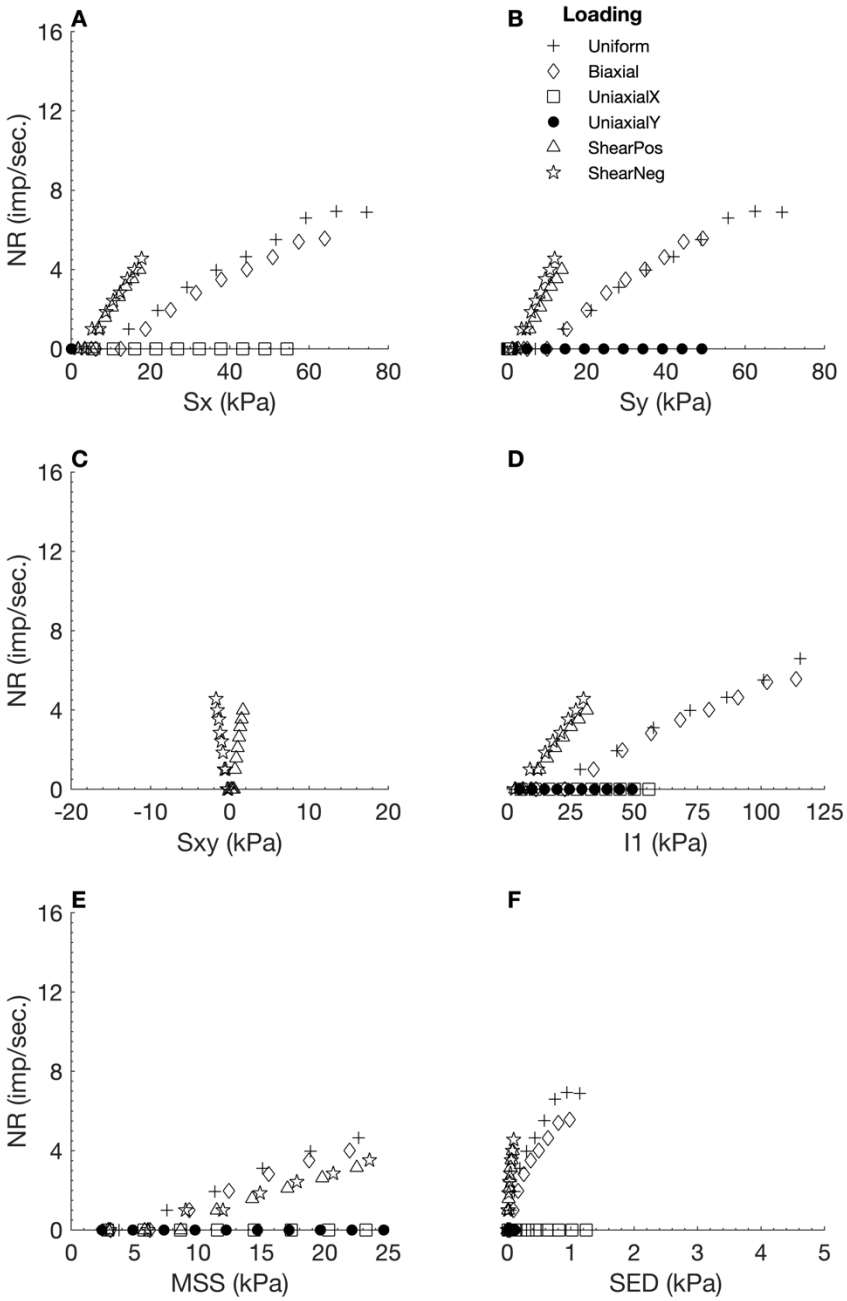

Figure B - 87. Neural responses (NR) output by the orthotropic elastic FEBio model 5 using ShearB as the neural model input, plotted against six different stress variables. Sx: X stress. Sy: Y stress. Sxy: shear stress. I1: 1st invariant stress tensor. MSS: maximum shear stress. SED: strain energy density.

Table B - 95. Linear regression measures for individual loading regime results from the orthotropic elastic model 5, with ShearB as neural model input.

Loading Regime	R^2	RMSE	Slope
Uniform	0.9892	0.2763	0.5239
Biaxial	0.3544	1.1494	3.7477
Uniaxial X	NaN	0.0000	0.0000
Uniaxial Y	NaN	0.0000	0.0000
Shear Positive	0.7165	0.5490	0.1601
Shear Negative	0.7546	0.4490	0.4109

B.5.16 Shear Stress C

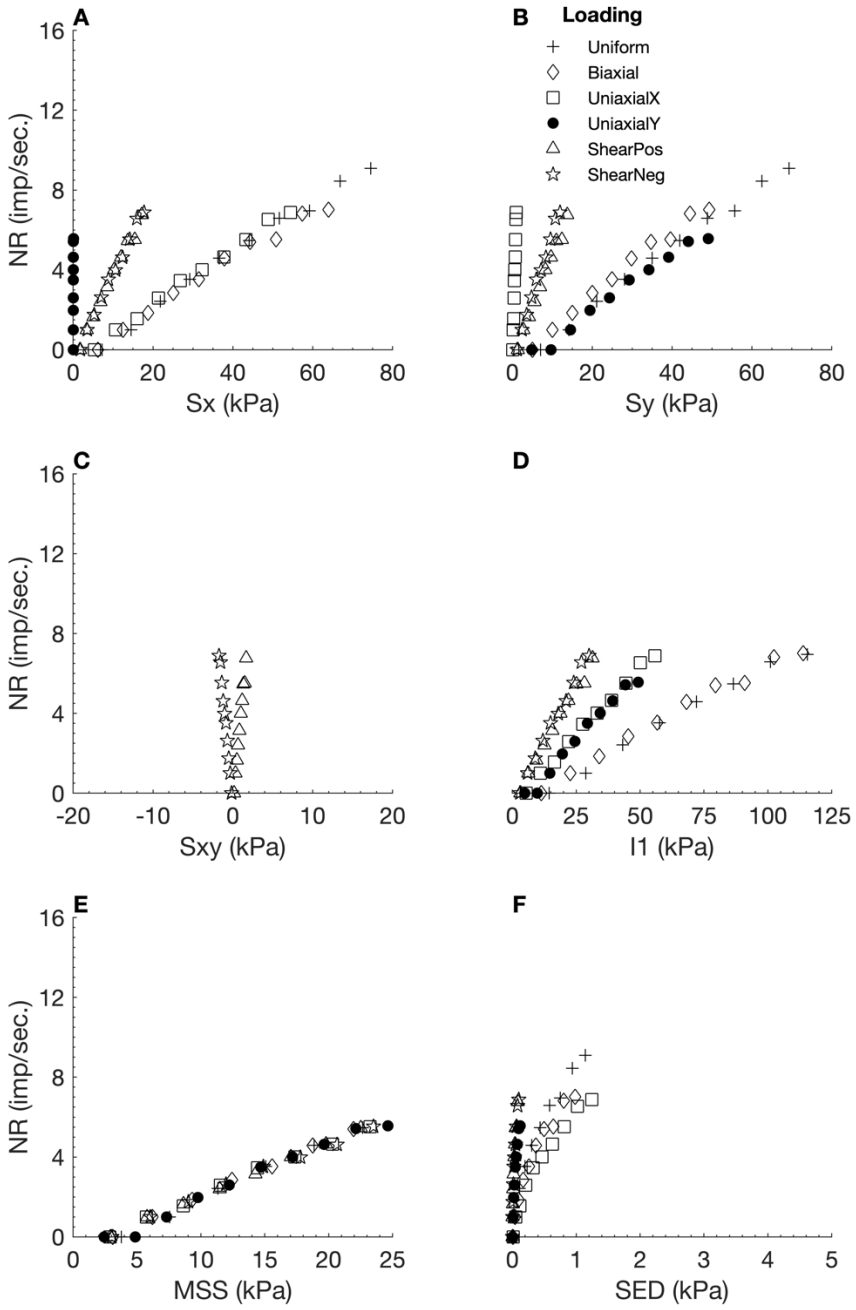

Figure B - 88. Neural responses (NR) output by the orthotropic elastic FEBio model 5 using ShearC as the neural model input, plotted against six different stress variables. Sx: X stress. Sy: Y stress. Sxy: shear stress. I1: 1st invariant stress tensor. MSS: maximum shear stress. SED: strain energy density.

Table B - 96. Linear regression measures for individual loading regime results from the orthotropic elastic model 5, with ShearC as neural model input.

Loading Regime	R^2	RMSE	Slope
Uniform	0.9903	0.3204	0.6426
Biaxial	0.4244	1.2380	4.6776
Uniaxial X	0.3911	1.0328	-0.3589
Uniaxial Y	0.9388	0.3948	1.0446
Shear Positive	0.9578	0.3344	0.2924
Shear Negative	0.8824	0.5428	0.7759

B.5.17 X Strain (Ex)

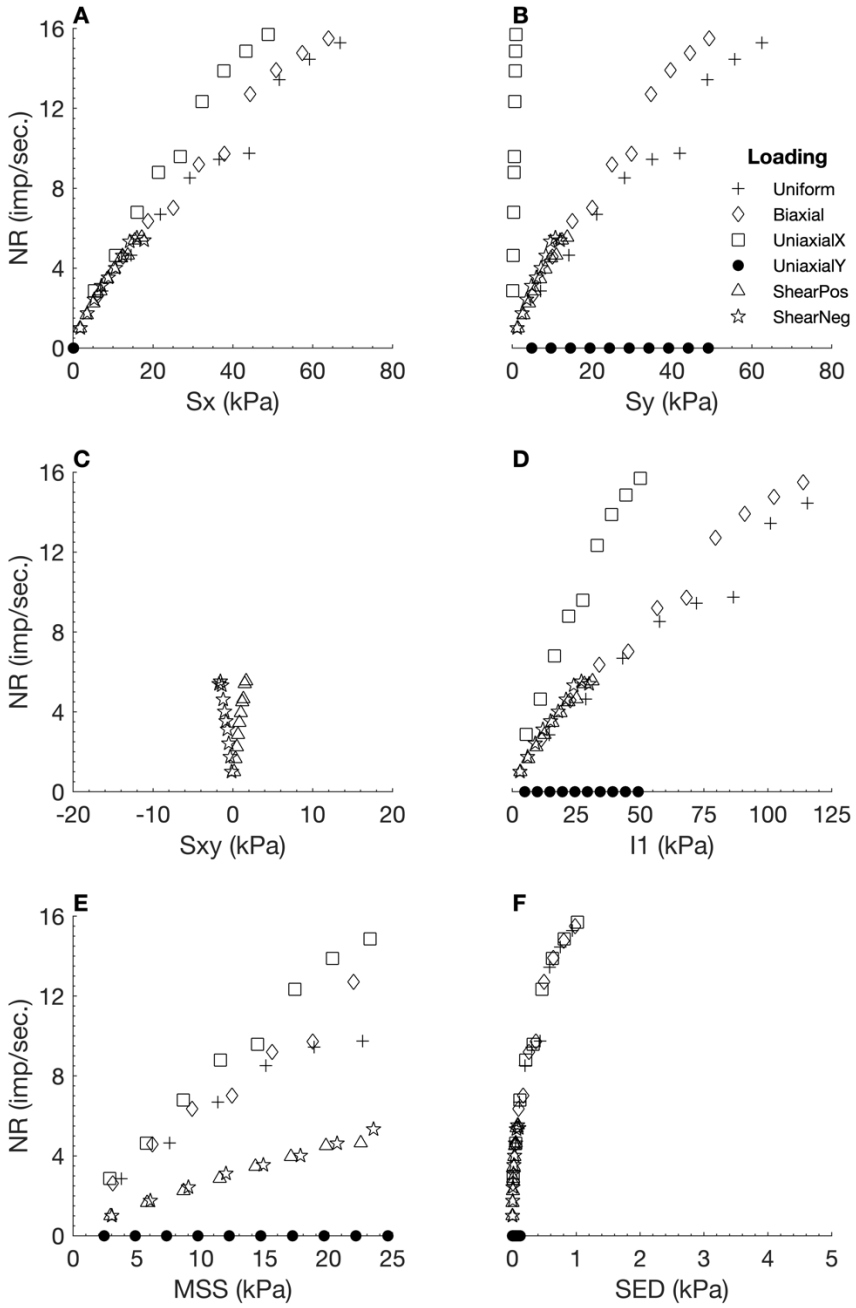

Figure B - 89. Neural responses (NR) output by the orthotropic elastic FEBio model 5 using Ex as the neural model input, plotted against six different stress variables. Sx: X stress. Sy: Y stress. Sxy: shear stress. I1: 1st invariant stress tensor. MSS: maximum shear stress. SED: strain energy density.

Table B - 97. Linear regression measures for individual loading regime results from the orthotropic elastic model 5, with Ex as neural model input.

Loading Regime	R^2	RMSE	Slope
Uniform	0.9750	0.7688	0.9513
Biaxial	0.3756	2.2701	7.7484
Uniaxial X	0.3442	2.5540	-0.8022
Uniaxial Y	NaN	0.0000	0.0000
Shear Positive	0.9584	0.2539	0.2236
Shear Negative	0.9203	0.3334	0.5910

B.5.18 Y Strain (Ey)

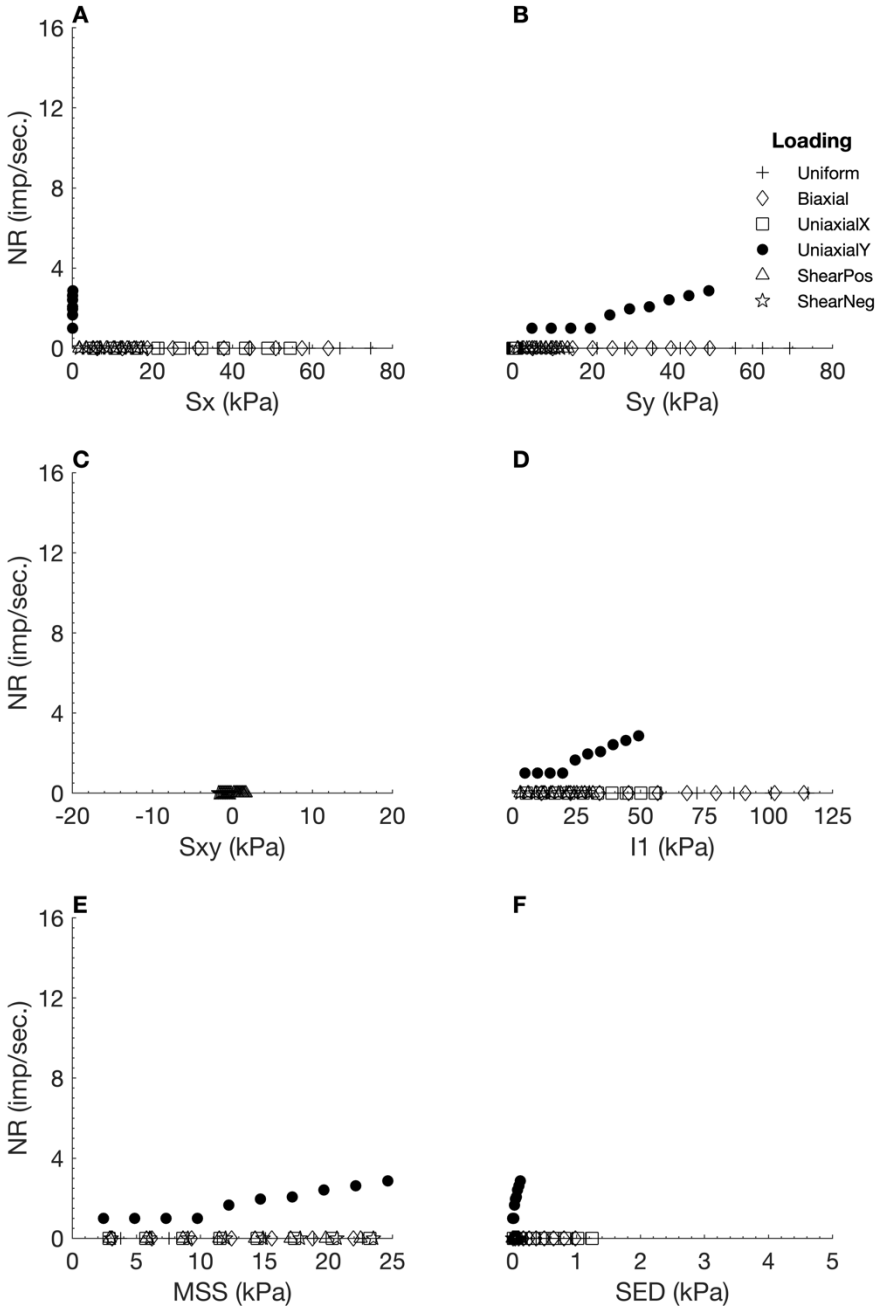

Figure B - 90. Neural responses (NR) output by the orthotropic elastic FEBio model 5 using Ey as the neural model input, plotted against six different stress variables. Sx: X stress. Sy: Y stress. Sxy: shear stress. I1: 1st invariant stress tensor. MSS: maximum shear stress. SED: strain energy density.

Table B - 98. Linear regression measures for individual loading regime results from the orthotropic elastic model 5, with Ey as neural model input.

Loading Regime	R^2	RMSE	Slope
Uniform	NaN	0.0000	0.0000
Biaxial	NaN	0.0000	0.0000
Uniaxial X	NaN	0.0000	0.0000
Uniaxial Y	0.8473	0.1874	0.2983
Shear Positive	NaN	0.0000	0.0000
Shear Negative	NaN	0.0000	0.0000

B.6 Test 6

Table B - 99. Values selected for material properties during FEBio implementation of orthotropic elastic material test 6.

Orthotropic Material Property	Value Selected
Density	1
Young's Modulus (X)	1
Young's Modulus (Y)	7.4
Young's Modulus (Z)	1
Shear Modulus (XY)	0.385
Shear Modulus (YZ)	2.85
Shear Modulus (XZ)	0.336
Poisson's Ratio (XY)	0.299
Poisson's Ratio (YZ)	0.299
Poisson's Ratio (XZ)	0.488

Table B - 100. Linear regression measures for total plot results (i.e. considering all loading regimes combined), for each input stimulus tested with the orthotropic elastic model 6.

Input Stimuli	R^2	RMSE	Slope
X Stress (Sx)	0.1613	4.4218	0.4283
Y Stress (Sy)	0.2770	4.0022	0.5472
Shear Stress (Sxy)	0.0889	0.3818	0.0263
1st Invariant Stress Tensor (I1)	0.2514	5.7834	0.7403
Maximum Shear Stress (MSS)	0.2867	2.2642	0.3170
Strain Energy Density (SED)	0.1586	0.5348	0.0513
Hydrostatic Pressure (HS)	0.2288	2.8364	0.3412
1st Principal Stress (S1)	0.3051	3.9153	0.5731
2nd Principal Stress (S2)	0.2220	3.5283	0.4164
3rd Principal Stress (S3)	0.1988	7.5955	0.8358
Deviatoric Stress 1 (Dev1)	0.3341	1.9817	0.3101
Deviatoric Stress 2 (Dev2)	0.1708	0.4950	0.0496
Deviatoric Stress 3 (Dev3)	NaN	0.0000	0.0000
Shear A	0.2541	0.9368	0.1208
Shear B	0.2617	1.7145	0.2255
Shear C	0.2867	2.2642	0.3170
X Strain (Ex)	0.1112	4.3581	0.3405
Y Strain (Ey)	0.0243	0.6264	0.0218
Average	**0.2130**	**2.6467**	**0.3146**

B.6.1 X Stress (Sx)

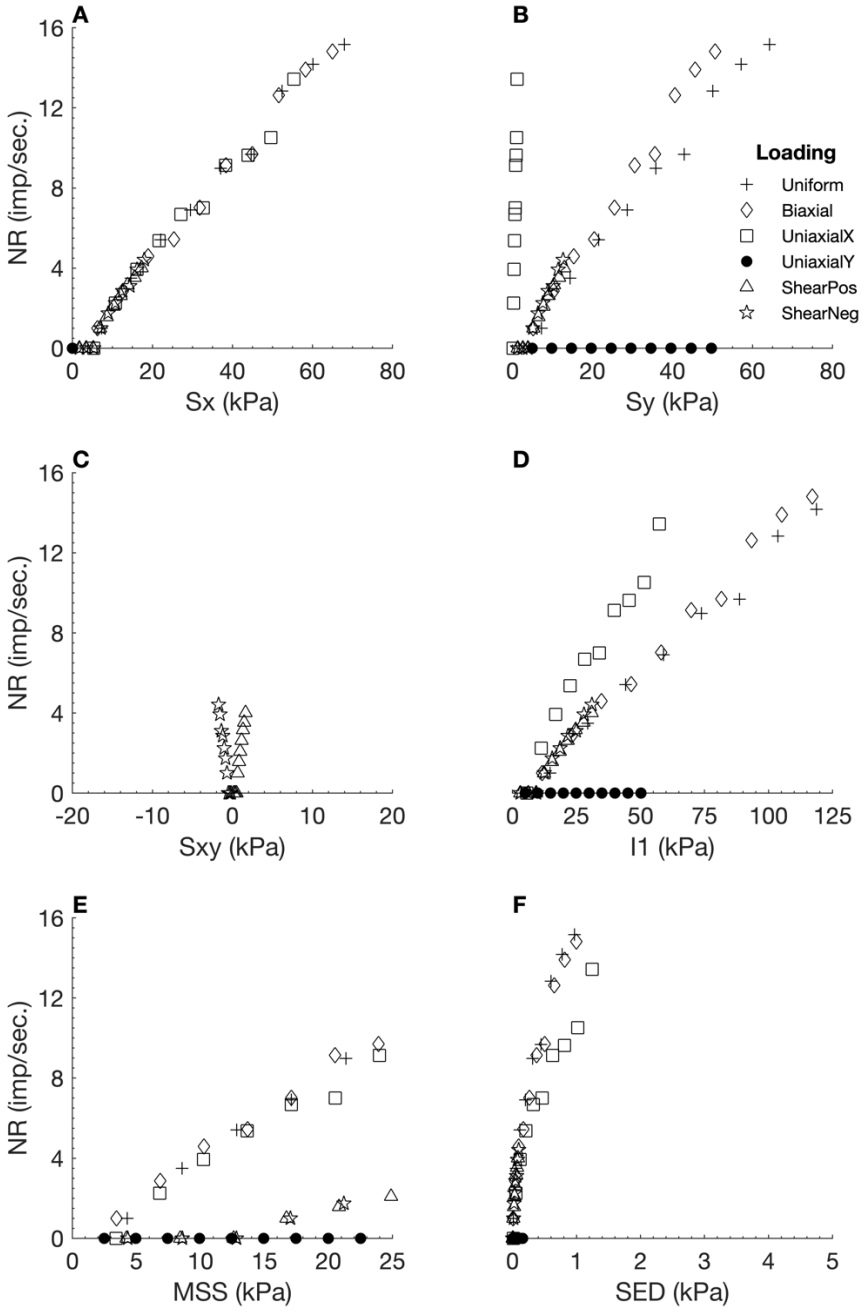

Figure B - 91. Neural responses (NR) output by the orthotropic elastic FEBio model 6 using Sx as the neural model input, plotted against six different stress variables. Sx: X stress. Sy: Y stress. Sxy: shear stress. I1: 1st invariant stress tensor. MSS: maximum shear stress. SED: strain energy density.

Table B - 101. Linear regression measures for individual loading regime results from the orthotropic elastic model 6, with Sx as neural model input.

Loading Regime	R^2	RMSE	Slope
Uniform	0.9856	0.6580	1.0780
Biaxial	0.4316	2.0263	7.7703
Uniaxial X	0.4778	2.0430	-0.8473
Uniaxial Y	NaN	0.0000	0.0000
Shear Positive	0.7170	0.5456	0.1593
Shear Negative	0.4629	0.6724	0.3257

B.6.2 Y Stress (Sy)

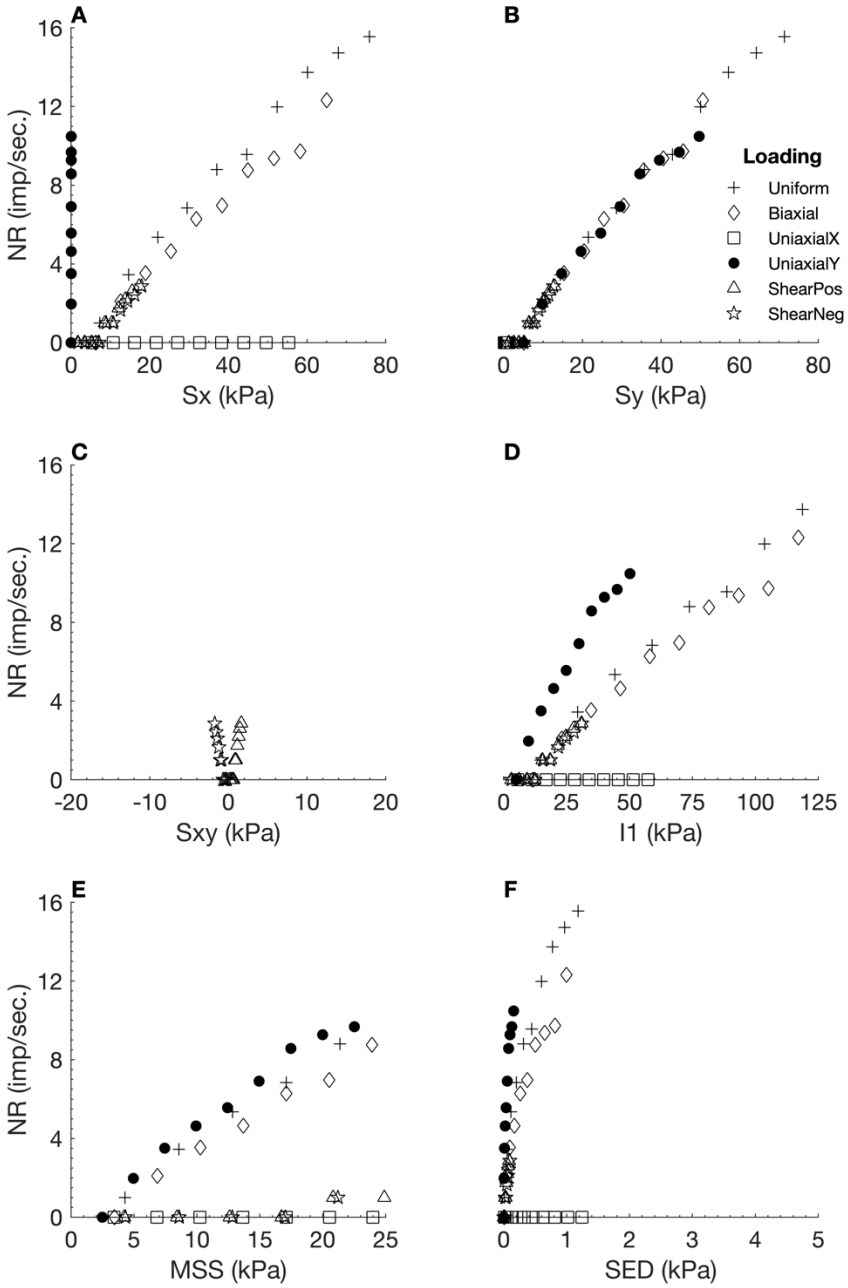

Figure B - 92. Neural responses (NR) output by the orthotropic elastic FEBio model 6 using Sy as the neural model input, plotted against six different stress variables. Sx: X stress. Sy: Y stress. Sxy: shear stress. I1: 1st invariant stress tensor. MSS: maximum shear stress. SED: strain energy density.

Table B - 102. Linear regression measures for individual loading regime results from the orthotropic elastic model 6, with Sy as neural model input.

Loading Regime	R^2	RMSE	Slope
Uniform	0.9878	0.5794	1.0339
Biaxial	0.3937	2.1601	7.6603
Uniaxial X	NaN	0.0000	0.0000
Uniaxial Y	0.8858	0.9465	1.7813
Shear Positive	0.5096	0.4043	0.0756
Shear Negative	0.2318	0.4526	0.1297

B.6.3 Shear Stress (Sxy)

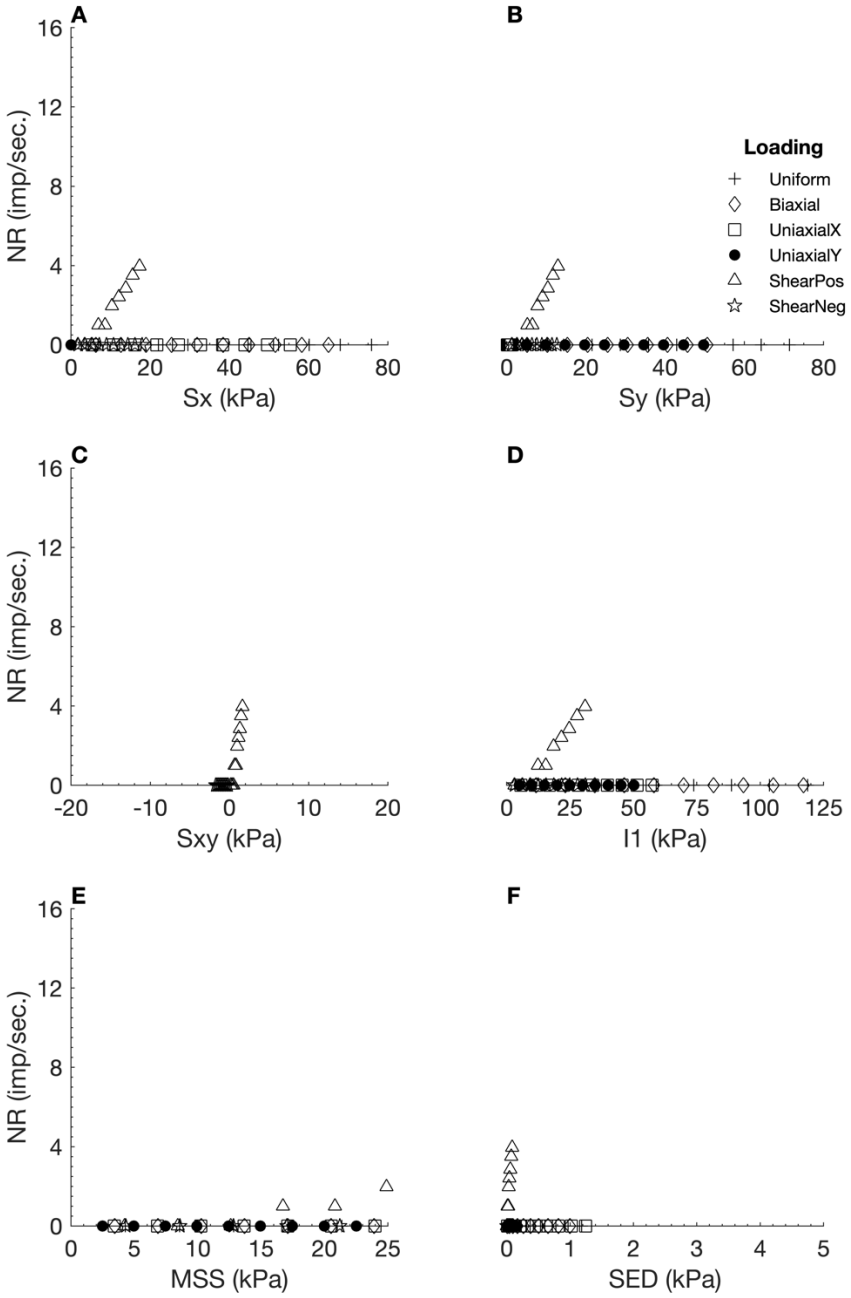

Figure B - 93. Neural responses (NR) output by the orthotropic elastic FEBio model 6 using Sxy as the neural model input, plotted against six different stress variables. Sx: X stress. Sy: Y stress. Sxy: shear stress. I1: 1st invariant stress tensor. MSS: maximum shear stress. SED: strain energy density.

Table B - 103. Linear regression measures for individual loading regime results from the orthotropic elastic model 6, with Sxy as neural model input.

Loading Regime	R^2	RMSE	Slope
Uniform	NaN	0.0000	0.0000
Biaxial	NaN	0.0000	0.0000
Uniaxial X	NaN	0.0000	0.0000
Uniaxial Y	NaN	0.0000	0.0000
Shear Positive	0.6864	0.5048	0.1370
Shear Negative	NaN	0.0000	0.0000

B.6.4 1st Invariant Stress Tensor (I1)

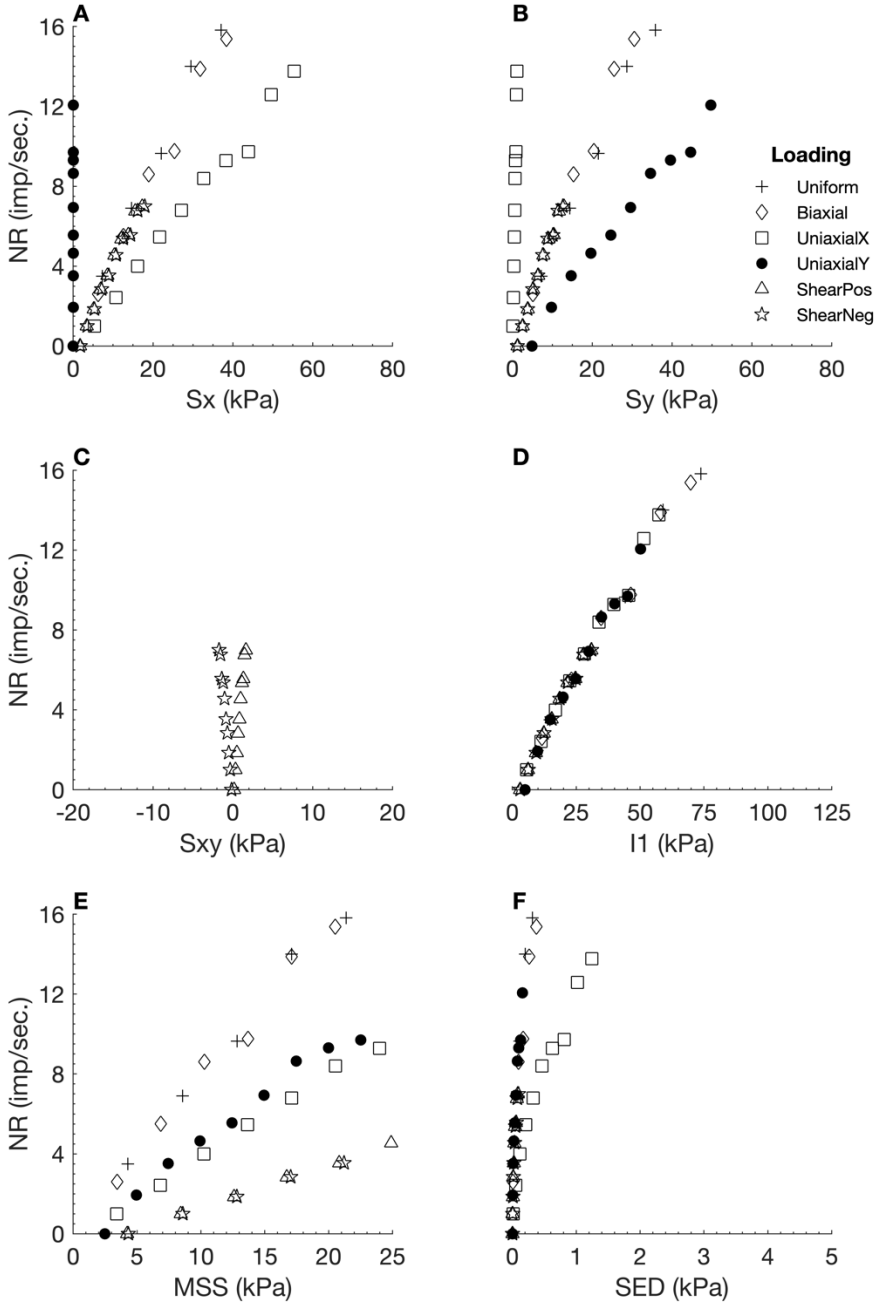

Figure B - 94. Neural responses (NR) output by the orthotropic elastic FEBio model 6 using I1 as the neural model input, plotted against six different stress variables. Sx: X stress. Sy: Y stress. Sxy: shear stress. I1: 1st invariant stress tensor. MSS: maximum shear stress. SED: strain energy density.

Table B - 104. Linear regression measures for individual loading regime results from the orthotropic elastic model 6, with I1 as neural model input.

Loading Regime	R^2	RMSE	Slope
Uniform	0.9651	1.2565	1.3113
Biaxial	0.3503	3.9860	12.8807
Uniaxial X	0.3652	1.8838	-0.6195
Uniaxial Y	0.8851	0.9527	1.7870
Shear Positive	0.9558	0.3941	0.3361
Shear Negative	0.8992	0.5180	0.8071

B.6.5 Maximum Shear Stress (MSS)

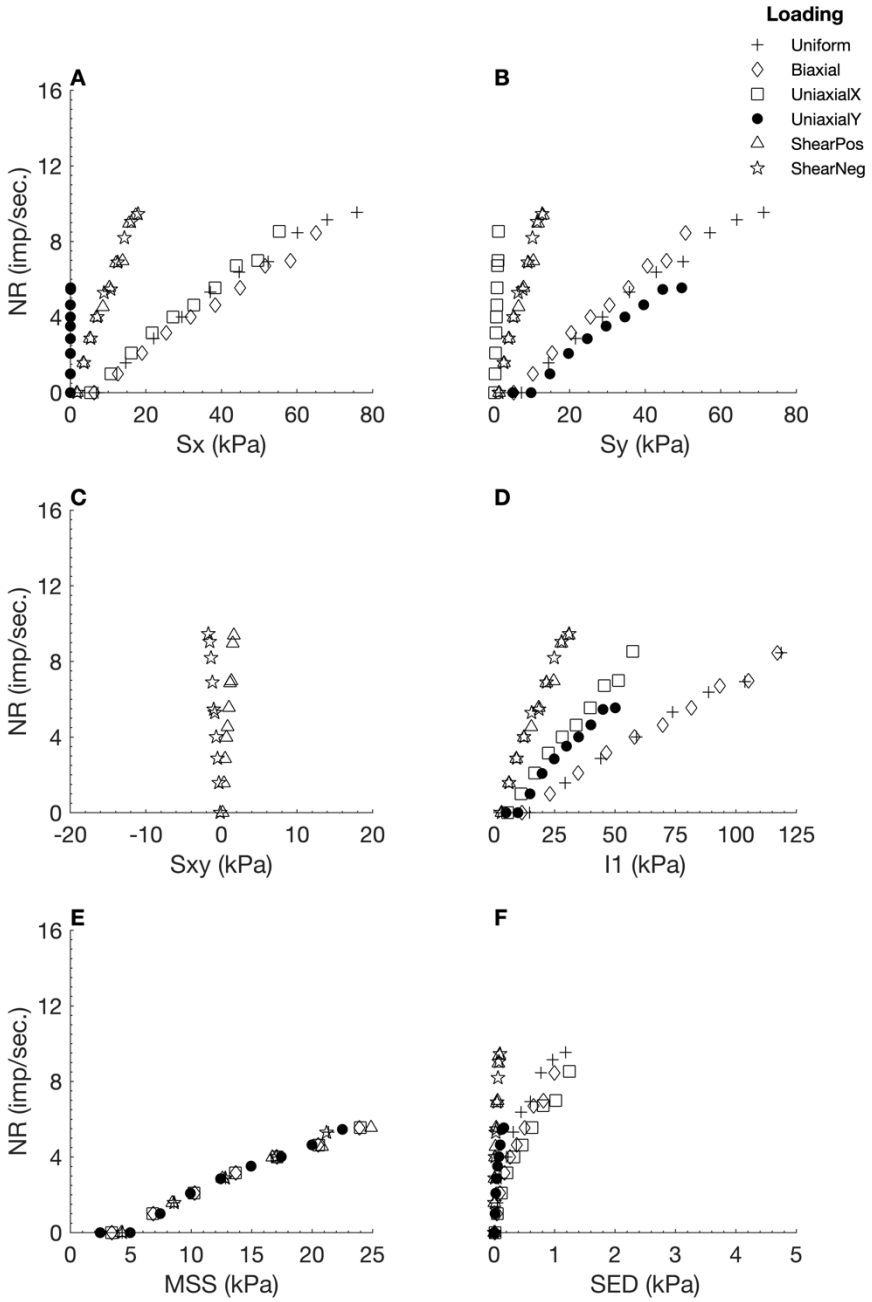

Figure B - 95. Neural responses (NR) output by the orthotropic elastic FEBio model 6 using MSS as the neural model input, plotted against six different stress variables. Sx: X stress. Sy: Y stress. Sxy: shear stress. I1: 1st invariant stress tensor. MSS: maximum shear stress. SED: strain energy density.

Table B - 105. Linear regression measures for individual loading regime results from the orthotropic elastic model 6, with MSS as neural model input.

Loading Regime	R^2	RMSE	Slope
Uniform	0.9922	0.3057	0.6844
Biaxial	0.4320	1.4013	5.3775
Uniaxial X	0.3607	1.3375	-0.4356
Uniaxial Y	0.9381	0.4119	1.0833
Shear Positive	0.9897	0.2324	0.4171
Shear Negative	0.9096	0.7155	1.1841

B.6.6 Strain Energy Density (SED)

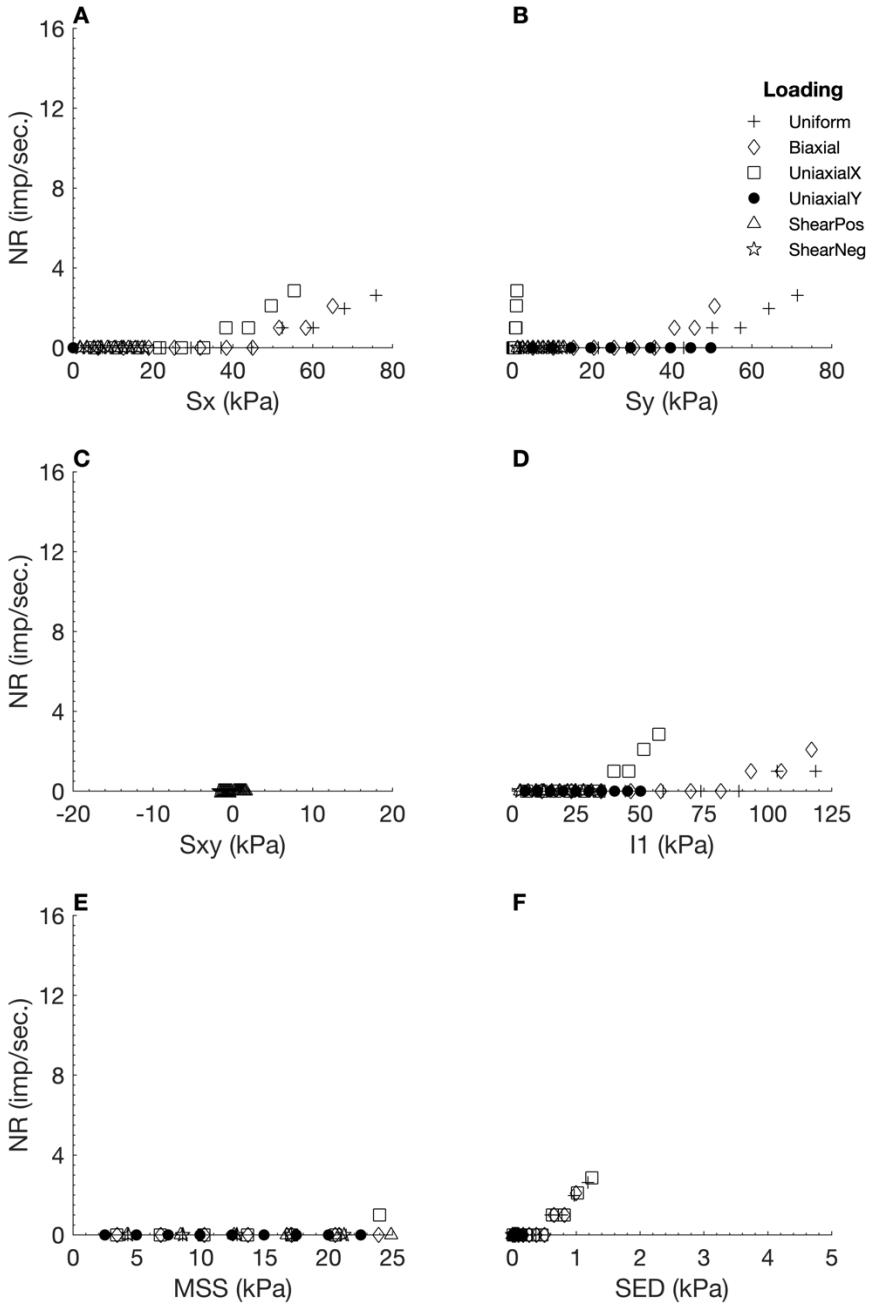

Figure B - 96. Neural responses (NR) output by the orthotropic elastic FEBio model 6 using SED as the neural model input, plotted against six different stress variables. Sx: X stress. Sy: Y stress. Sxy: shear stress. I1: 1st invariant stress tensor. MSS: maximum shear stress. SED: strain energy density.

Table B - 106. Linear regression measures for individual loading regime results from the orthotropic elastic model 6, with SED as neural model input.

Loading Regime	R^2	RMSE	Slope
Uniform	0.6506	0.6063	0.1641
Biaxial	NaN	0.0000	0.0000
Uniaxial X	NaN	0.0000	0.0000
Uniaxial Y	NaN	0.0000	0.0000
Shear Positive	NaN	0.0000	0.0000
Shear Negative	NaN	0.0000	0.0000

B.6.7 Hydrostatic Pressure (HS)

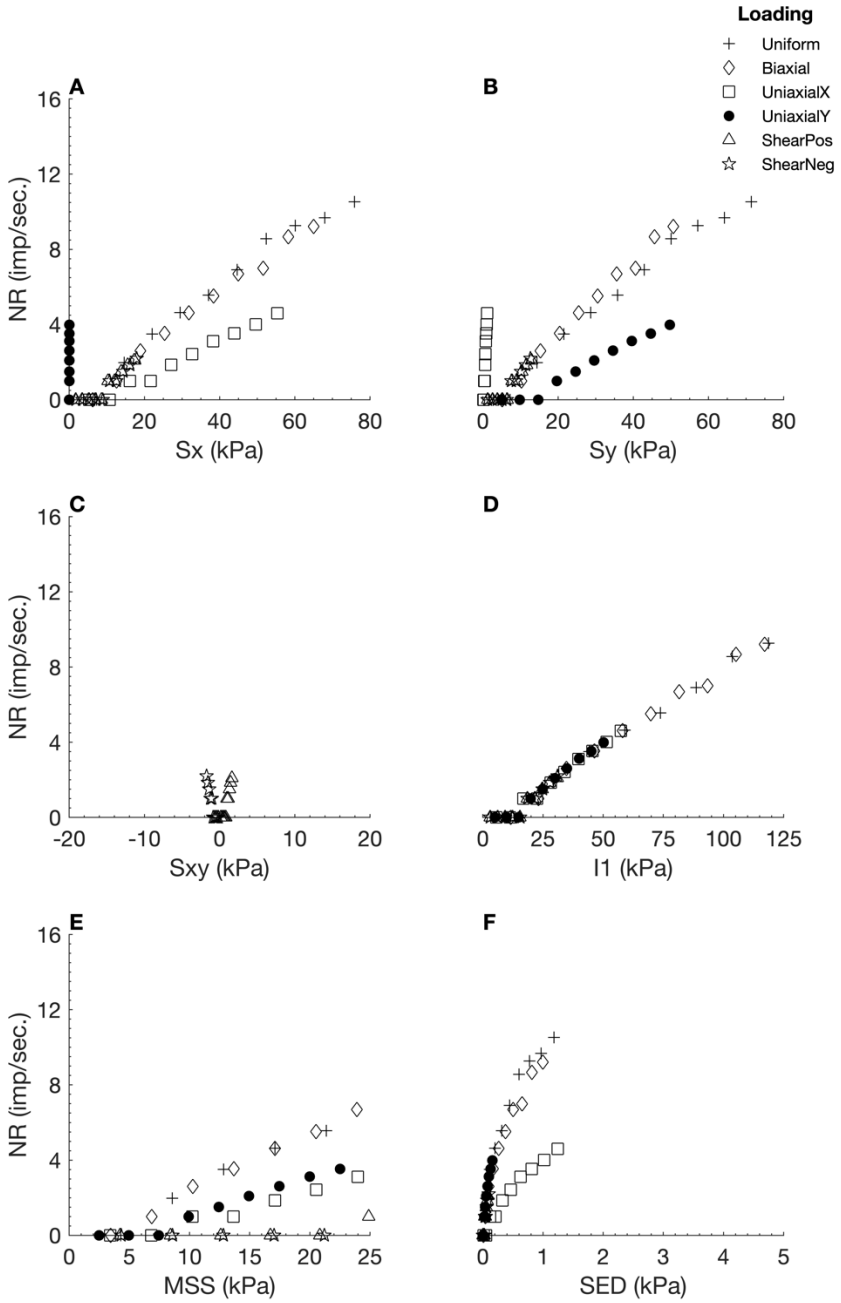

Figure B - 97. Neural responses (NR) output by the orthotropic elastic FEBio model 6 using HS as the neural model input, plotted against six different stress variables. Sx: X stress. Sy: Y stress. Sxy: shear stress. I1: 1st invariant stress tensor. MSS: maximum shear stress. SED: strain energy density.

Table B - 107. Linear regression measures for individual loading regime results from the orthotropic elastic model 6, with HS as neural model input.

Loading Regime	R^2	RMSE	Slope
Uniform	0.9901	0.3729	0.7404
Biaxial	0.4661	1.5770	6.4847
Uniaxial X	0.2082	0.6292	-0.1399
Uniaxial Y	0.9676	0.1824	0.6733
Shear Positive	0.3035	0.3809	0.0461
Shear Negative	NaN	0.0000	0.0000

B.6.8 1st Principle Stress (S1)

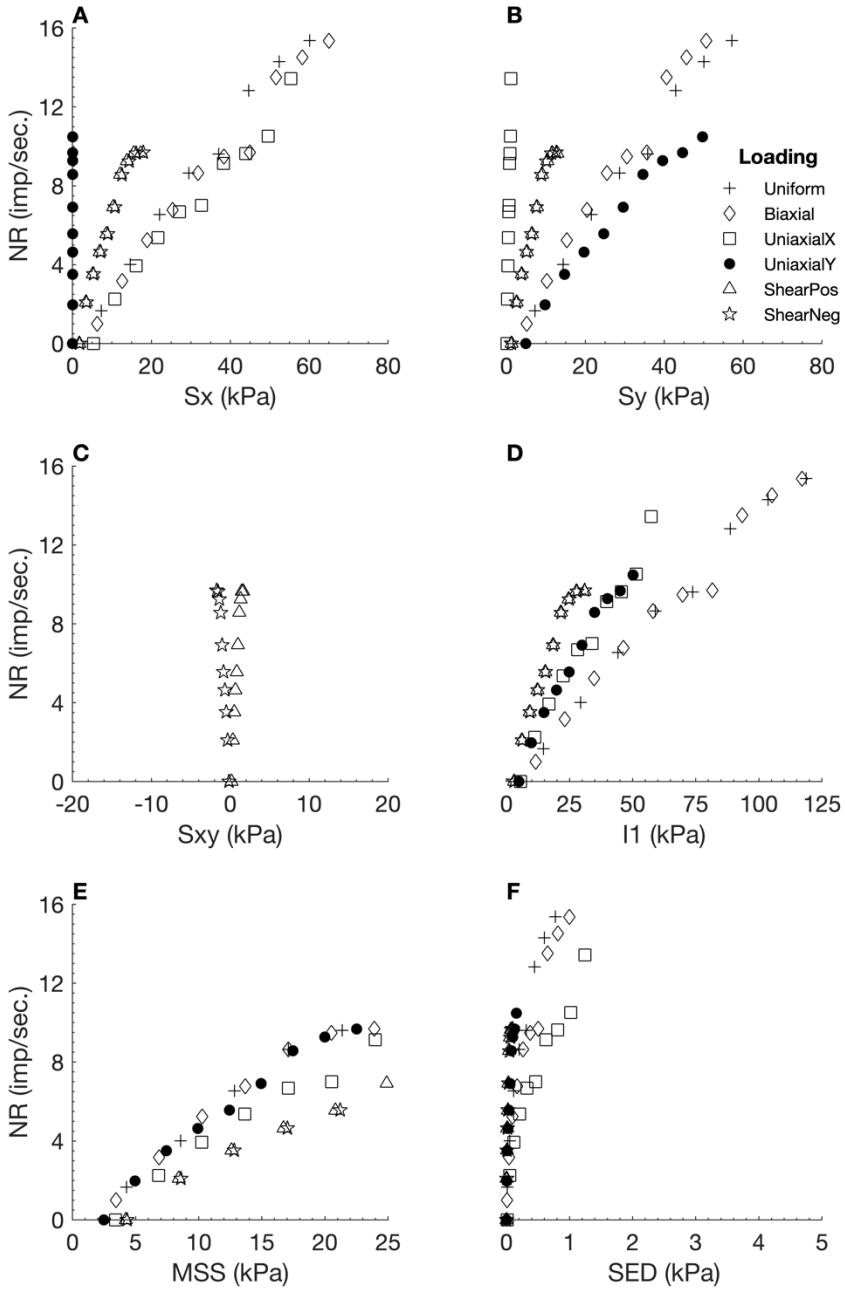

Figure B - 98. Neural responses (NR) output by the orthotropic elastic FEBio model 6 using S1 as the neural model input, plotted against six different stress variables. Sx: X stress. Sy: Y stress. Sxy: shear stress. I1: 1st invariant stress tensor. MSS: maximum shear stress. SED: strain energy density.

Table B - 108. Linear regression measures for individual loading regime results from the orthotropic elastic model 6, with S1 as neural model input.

Loading Regime	R^2	RMSE	Slope
Uniform	0.9942	0.4367	1.1307
Biaxial	0.4227	2.6274	9.8933
Uniaxial X	0.4778	2.0430	-0.8473
Uniaxial Y	0.8858	0.9465	1.7813
Shear Positive	0.9899	0.2799	0.5079
Shear Negative	0.9607	0.5019	1.2942

B.6.9 2nd Principle Stress (S2)

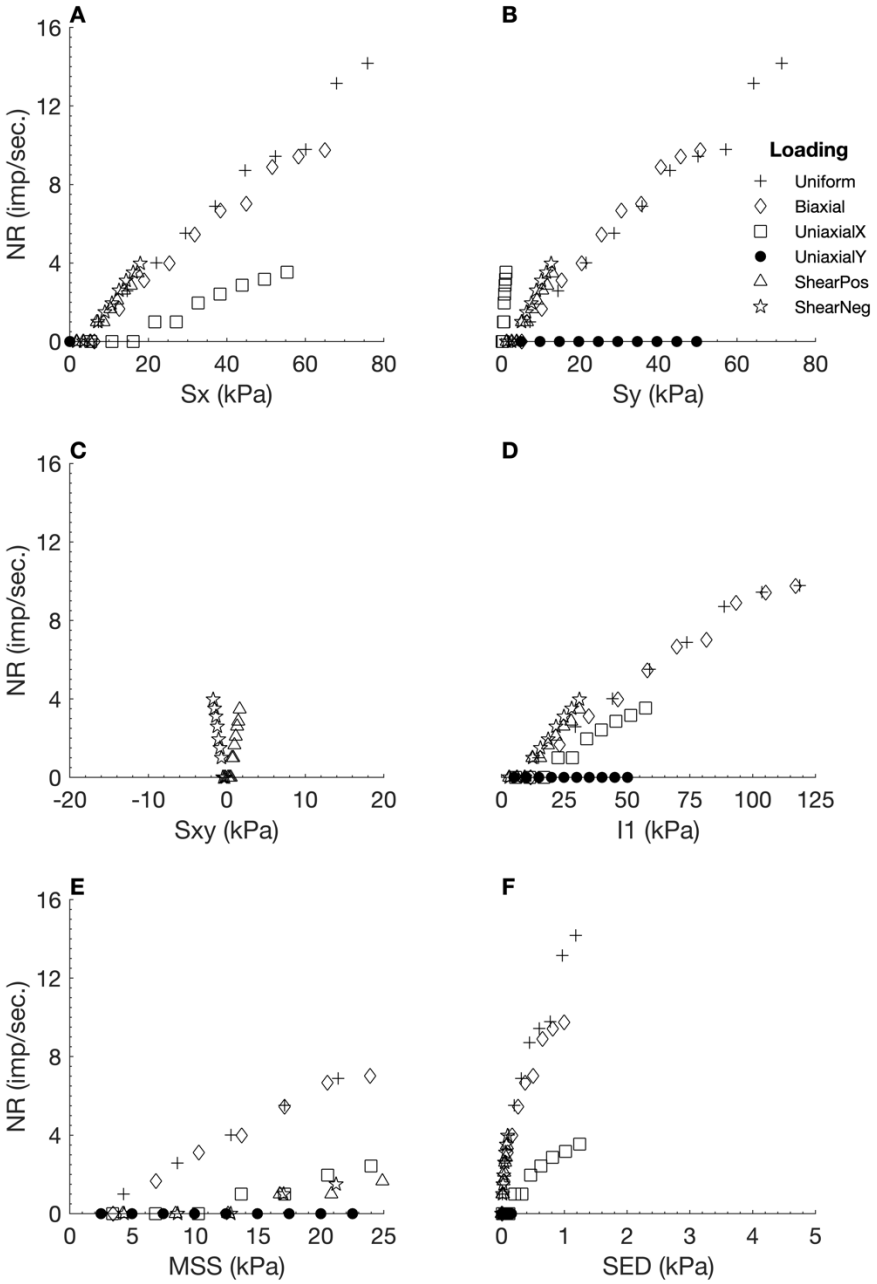

Figure B - 99. Neural responses (NR) output by the orthotropic elastic FEBio model 6 using S2 as the neural model input, plotted against six different stress variables. Sx: X stress. Sy: Y stress. Sxy: shear stress. I1: 1st invariant stress tensor. MSS: maximum shear stress. SED: strain energy density.

Table B - 109. Linear regression measures for individual loading regime results from the orthotropic elastic model 6, with S2 as neural model input.

Loading Regime	R^2	RMSE	Slope
Uniform	0.9675	0.8311	0.8992
Biaxial	0.4114	1.8607	6.8462
Uniaxial X	0.0076	0.6100	-0.0232
Uniaxial Y	NaN	0.0000	0.0000
Shear Positive	0.7103	0.4272	0.1227
Shear Negative	0.4782	0.5901	0.2948

B.6.10 3rd Principle Stress (S3)

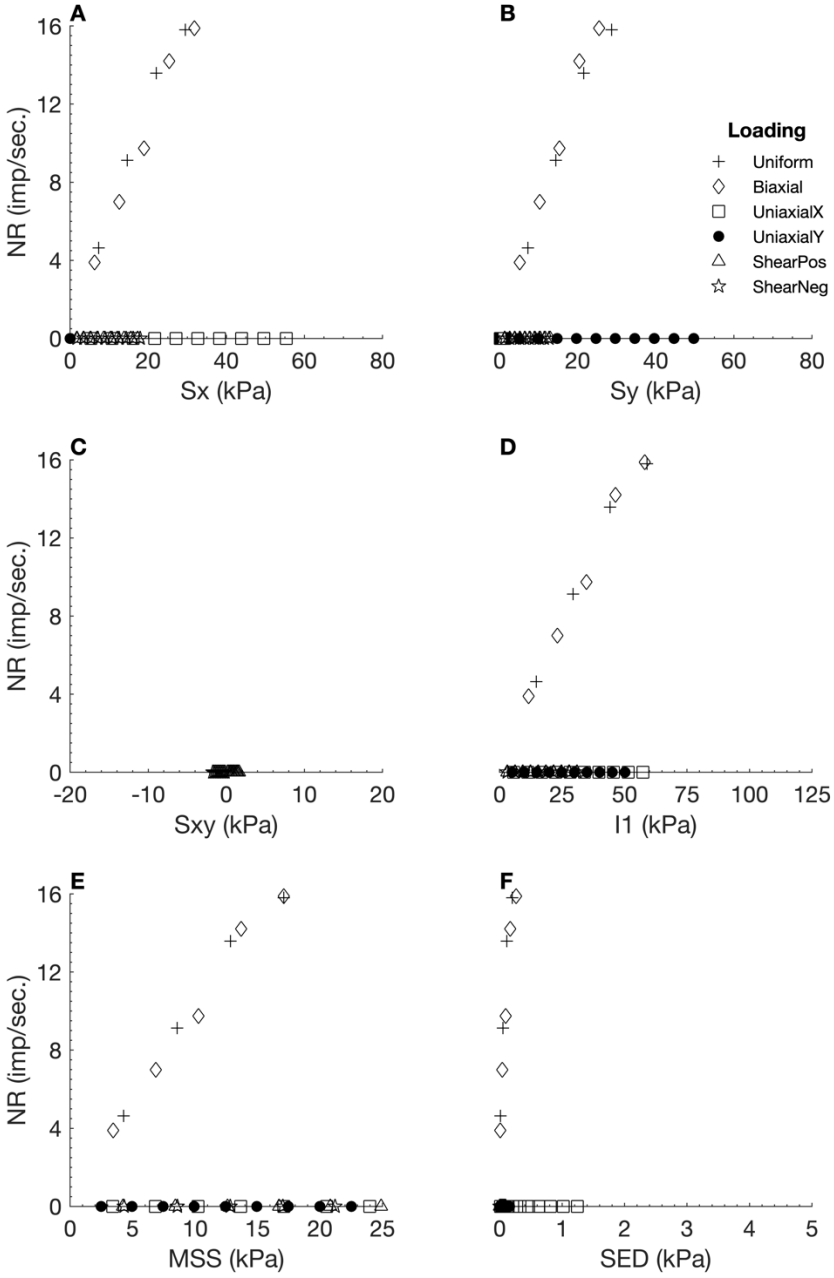

Figure B - 100. Neural responses (NR) output by the orthotropic elastic FEBio model 6 using S3 as the neural model input, plotted against six different stress variables. Sx: X stress. Sy: Y stress. Sxy: shear stress. I1: 1st invariant stress tensor. MSS: maximum shear stress. SED: strain energy density.

Table B - 110. Linear regression measures for individual loading regime results from the orthotropic elastic model 6, with S3 as neural model input.

Loading Regime	R^2	RMSE	Slope
Uniform	0.9512	1.4445	1.2651
Biaxial	0.4294	4.3307	16.5319
Uniaxial X	NaN	0.0000	0.0000
Uniaxial Y	NaN	0.0000	0.0000
Shear Positive	NaN	0.0000	0.0000
Shear Negative	NaN	0.0000	0.0000

B.6.11 Deviatoric Stress 1 (Dev1)

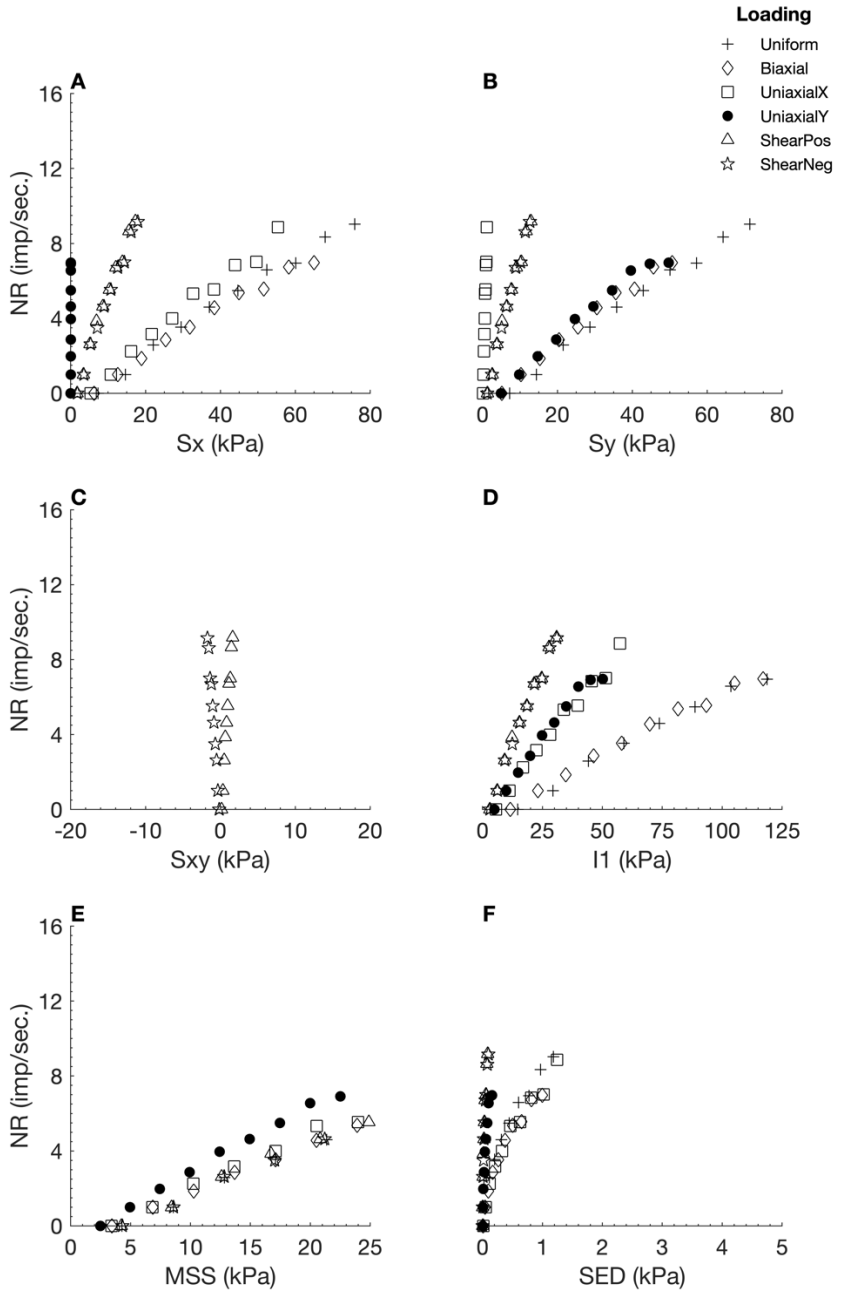

Figure B - 101. Neural responses (NR) output by the orthotropic elastic FEBio model 6 using Dev1 as the neural model input, plotted against six different stress variables. Sx: X stress. Sy: Y stress. Sxy: shear stress. I1: 1st invariant stress tensor. MSS: maximum shear stress. SED: strain energy density.

Table B - 111. Linear regression measures for individual loading regime results from the orthotropic elastic model 6, with Dev1 as neural model input.

Loading Regime	R^2	RMSE	Slope
Uniform	0.9914	0.2989	0.6352
Biaxial	0.4258	1.2376	4.6899
Uniaxial X	0.3767	1.3436	-0.4529
Uniaxial Y	0.9375	0.4928	1.2898
Shear Positive	0.9626	0.4637	0.4313
Shear Negative	0.9027	0.6727	1.0693

B.6.12 Deviatoric Stress 2 (Dev2)

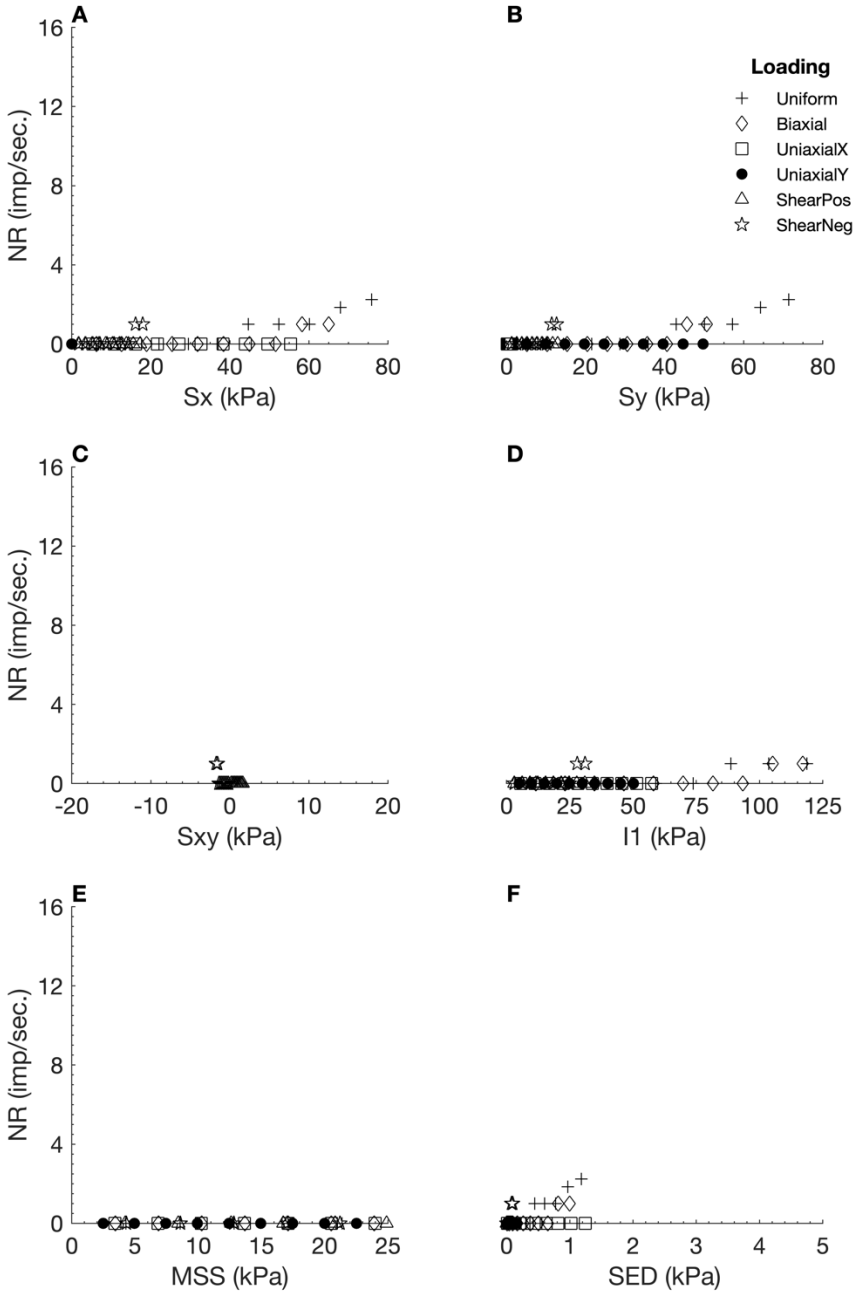

Figure B - 102. Neural responses (NR) output by the orthotropic elastic FEBio model 6 using Dev2 as the neural model input, plotted against six different stress variables. Sx: X stress. Sy: Y stress. Sxy: shear stress. I1: 1st invariant stress tensor. MSS: maximum shear stress. SED: strain energy density.

Table B - 112. Linear regression measures for individual loading regime results from the orthotropic elastic model 6, with Dev2 as neural model input.

Loading Regime	R^2	RMSE	Slope
Uniform	0.7863	0.4140	0.1575
Biaxial	NaN	0.0000	0.0000
Uniaxial X	NaN	0.0000	0.0000
Uniaxial Y	NaN	0.0000	0.0000
Shear Positive	NaN	0.0000	0.0000
Shear Negative	NaN	0.0000	0.0000

B.6.13 Deviatoric Stress 3 (Dev3)

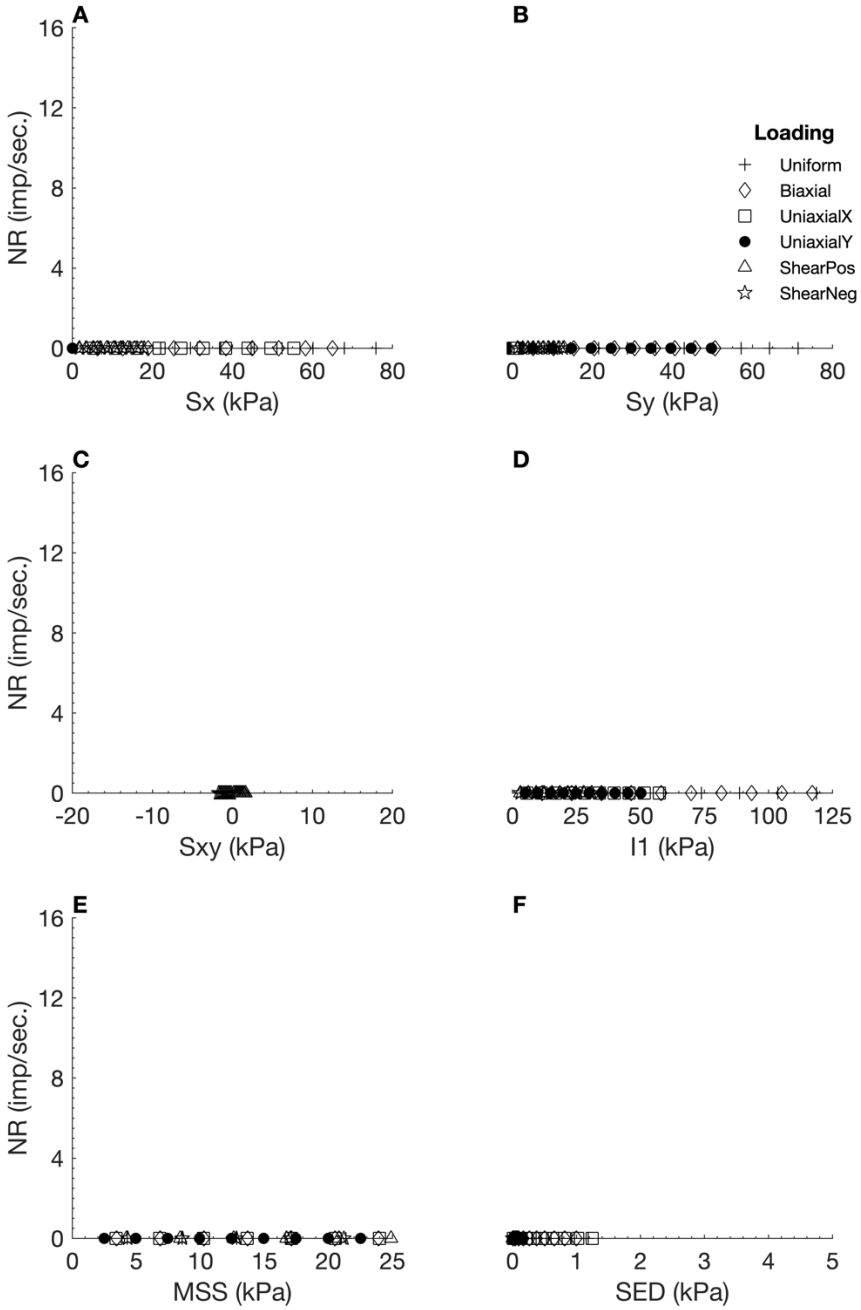

Figure B - 103. Neural responses (NR) output by the orthotropic elastic FEBio model 6 using Dev3 as the neural model input, plotted against six different stress variables. Sx: X stress. Sy: Y stress. Sxy: shear stress. I1: 1st invariant stress tensor. MSS: maximum shear stress. SED: strain energy density.

Table B - 113. Linear regression measures for individual loading regime results from the orthotropic elastic model 6, with Dev3 as neural model input.

Loading Regime	R^2	RMSE	Slope
Uniform	NaN	0.0000	0.0000
Biaxial	NaN	0.0000	0.0000
Uniaxial X	NaN	0.0000	0.0000
Uniaxial Y	NaN	0.0000	0.0000
Shear Positive	NaN	0.0000	0.0000
Shear Negative	NaN	0.0000	0.0000

B.6.14 Shear Stress A

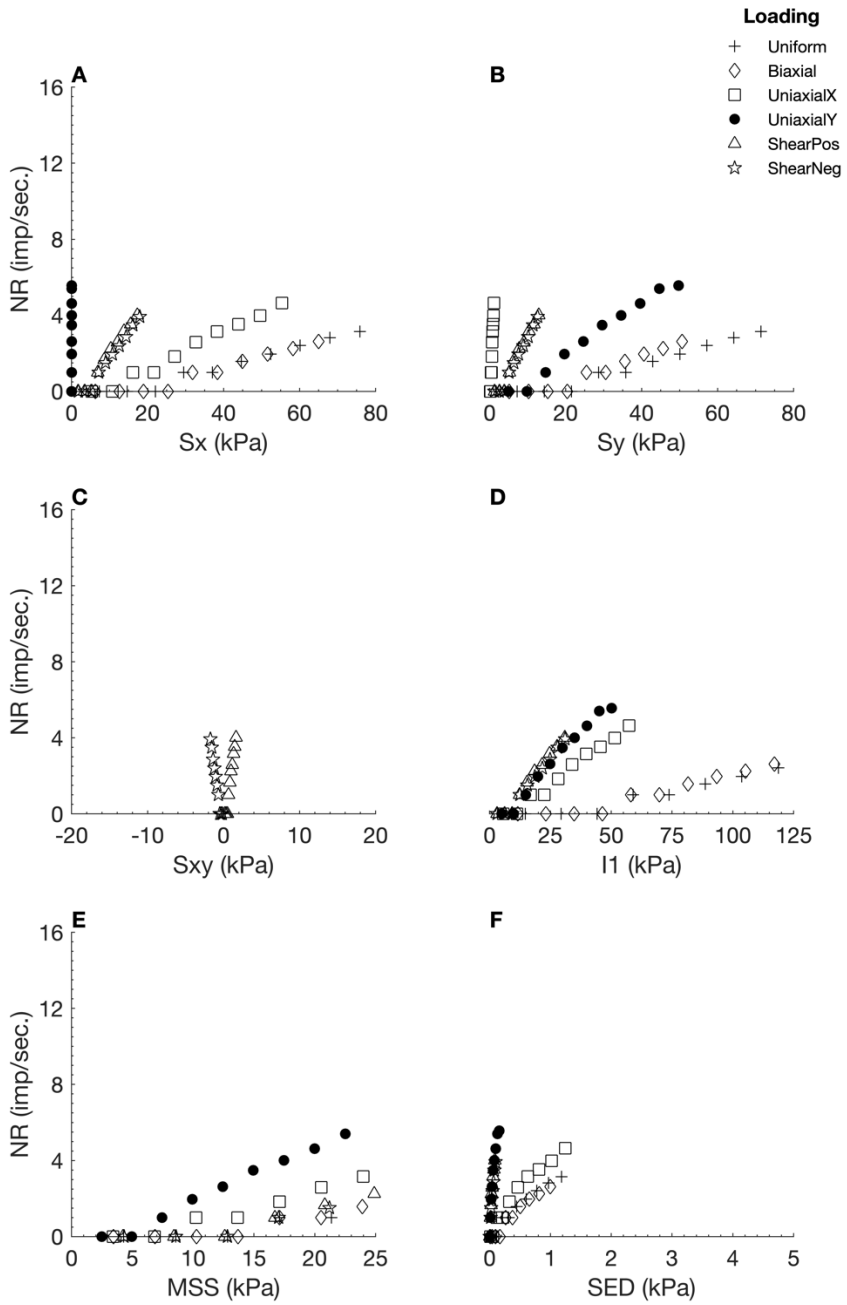

Figure B - 104. Neural responses (NR) output by the orthotropic elastic FEBio model 6 using ShearA as the neural model input, plotted against six different stress variables. Sx: X stress. Sy: Y stress. Sxy: shear stress. I1: 1st invariant stress tensor. MSS: maximum shear stress. SED: strain energy density.

Table B - 114. Linear regression measures for individual loading regime results from the orthotropic elastic model 6, with ShearA as neural model input.

Loading Regime	R^2	RMSE	Slope
Uniform	0.9440	0.2976	0.2424
Biaxial	0.0001	0.5164	-0.0233
Uniaxial X	0.2082	0.6292	-0.1399
Uniaxial Y	0.9391	0.3932	1.0438
Shear Positive	0.7112	0.5880	0.1692
Shear Negative	0.4781	0.5908	0.2950

B.6.15 Shear Stress B

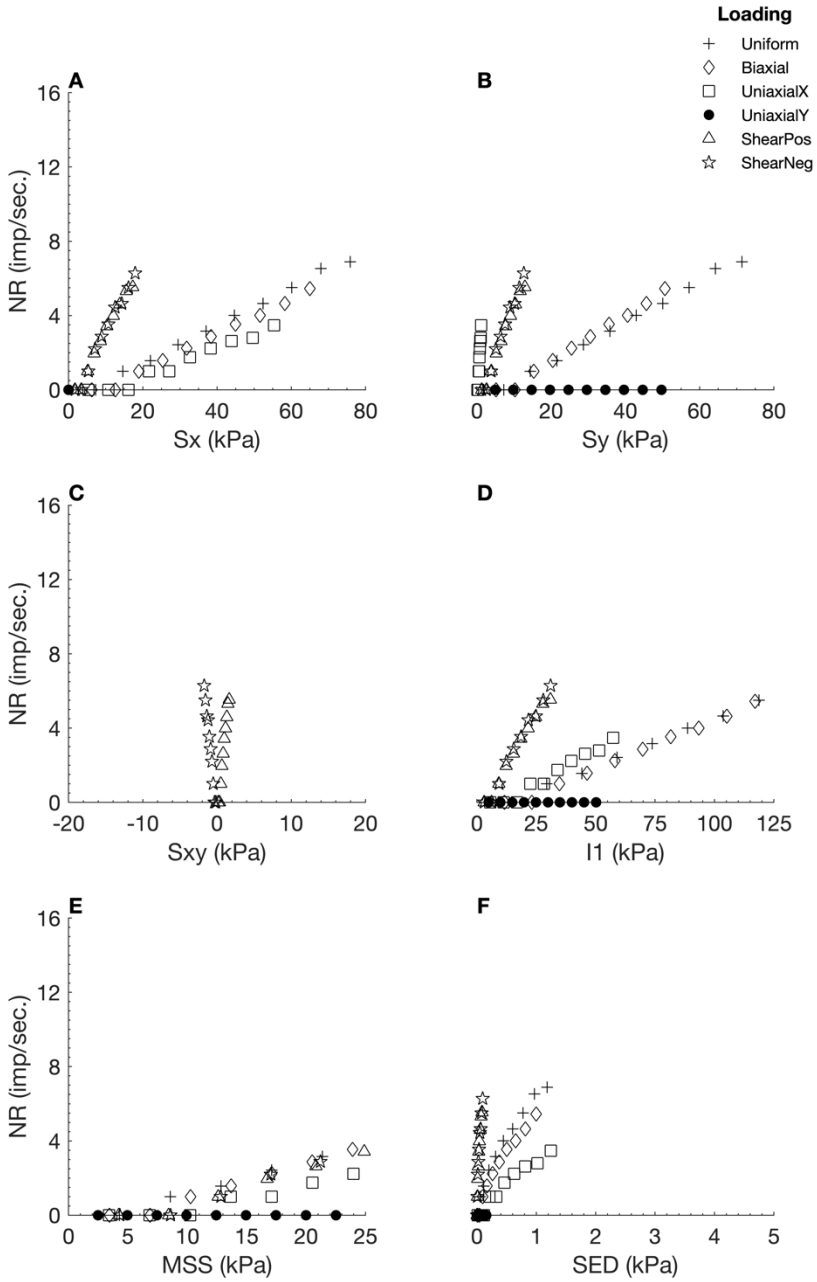

Figure B - 105. Neural responses (NR) output by the orthotropic elastic FEBio model 6 using ShearB as the neural model input, plotted against six different stress variables. Sx: X stress. Sy: Y stress. Sxy: shear stress. I1: 1st invariant stress tensor. MSS: maximum shear stress. SED: strain energy density.

Table B - 115. Linear regression measures for individual loading regime results from the orthotropic elastic model 6, with ShearB as neural model input.

Loading Regime	R^2	RMSE	Slope
Uniform	0.9840	0.3151	0.4904
Biaxial	0.4220	0.8639	3.2484
Uniaxial X	0.0076	0.6100	-0.0232
Uniaxial Y	NaN	0.0000	0.0000
Shear Positive	0.8600	0.5907	0.2685
Shear Negative	0.7214	0.7895	0.6630

B.6.16 Shear Stress C

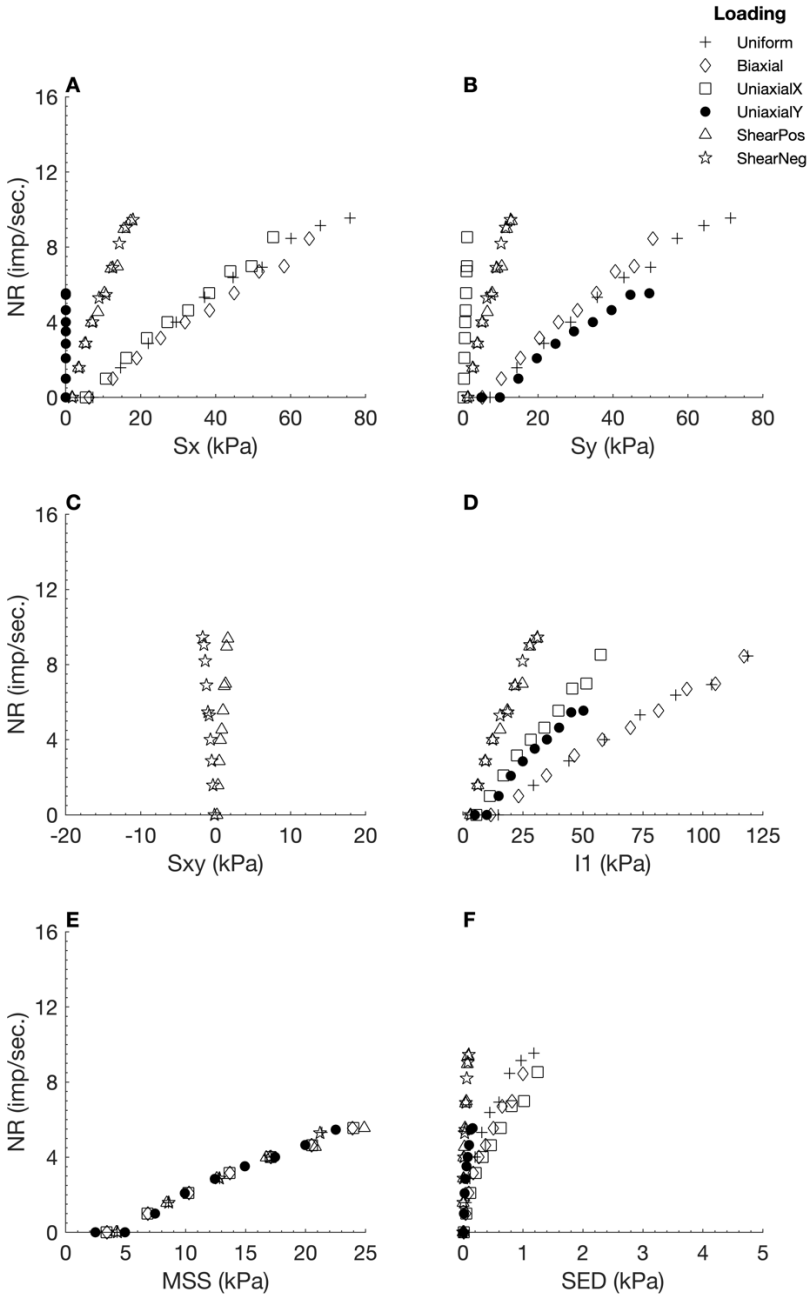

Figure B - 106. Neural responses (NR) output by the orthotropic elastic FEBio model 6 using ShearC as the neural model input, plotted against six different stress variables. Sx: X stress. Sy: Y stress. Sxy: shear stress. I1: 1st invariant stress tensor. MSS: maximum shear stress. SED: strain energy density.

Table B - 116. Linear regression measures for individual loading regime results from the orthotropic elastic model 6, with ShearC as neural model input.

Loading Regime	R^2	RMSE	Slope
Uniform	0.9922	0.3057	0.6844
Biaxial	0.4320	1.4013	5.3775
Uniaxial X	0.3607	1.3375	-0.4356
Uniaxial Y	0.9381	0.4119	1.0833
Shear Positive	0.9897	0.2324	0.4171
Shear Negative	0.9096	0.7155	1.1841

B.6.17 X Strain (Ex)

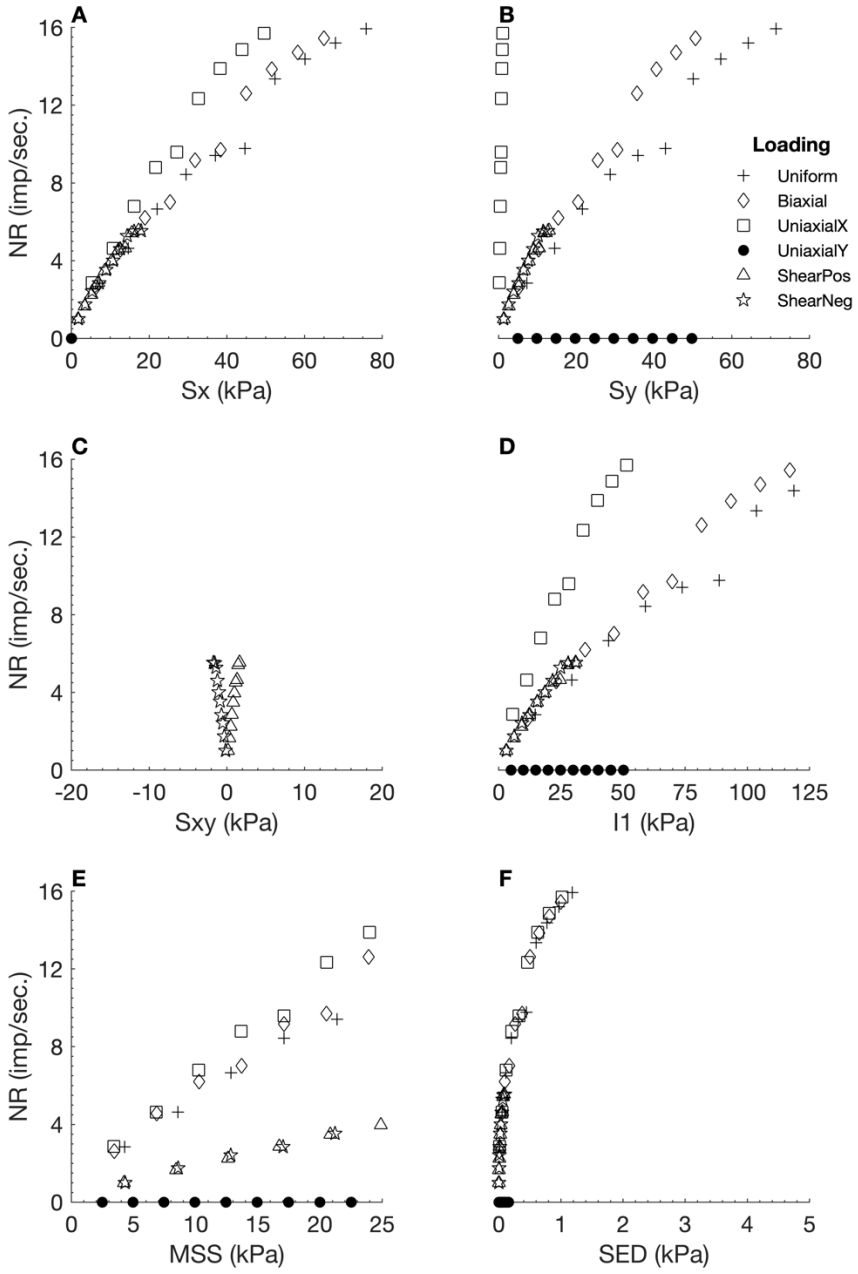

Figure B - 107. Neural responses (NR) output by the orthotropic elastic FEBio model 6 using Ex as the neural model input, plotted against six different stress variables. Sx: X stress. Sy: Y stress. Sxy: shear stress. I1: 1st invariant stress tensor. MSS: maximum shear stress. SED: strain energy density.

Table B - 117. Linear regression measures for individual loading regime results from the orthotropic elastic model 6, with Ex as neural model input.

Loading Regime	R^2	RMSE	Slope
Uniform	0.9767	0.7371	0.9465
Biaxial	0.3623	2.2823	7.5714
Uniaxial X	0.3440	2.5546	-0.8022
Uniaxial Y	NaN	0.0000	0.0000
Shear Positive	0.9571	0.2596	0.2248
Shear Negative	0.9139	0.3309	0.5625

B.6.18 Y Strain (Ey)

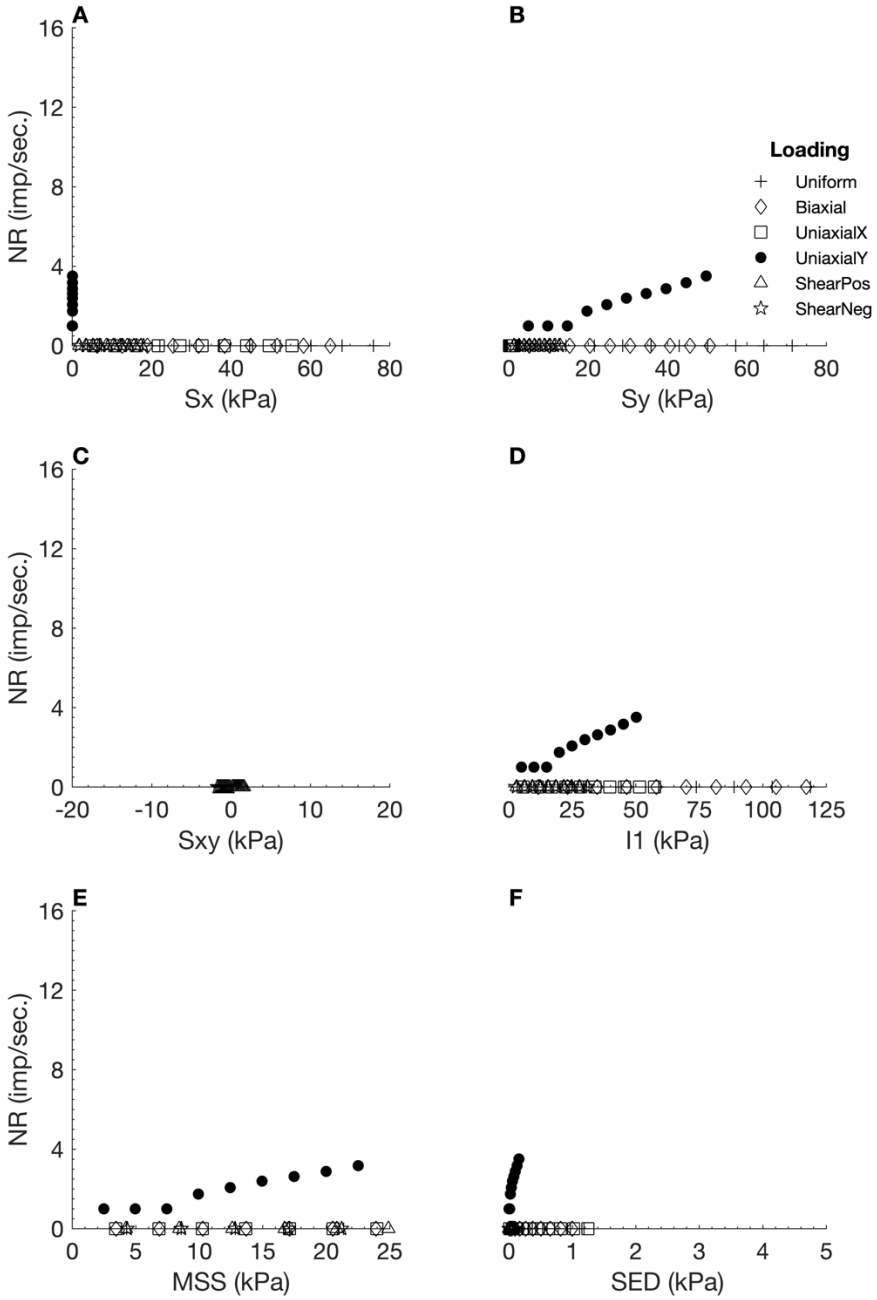

Figure B - 108. Neural responses (NR) output by the orthotropic elastic FEBio model 6 using Ey as the neural model input, plotted against six different stress variables. Sx: X stress. Sy: Y stress. Sxy: shear stress. I1: 1st invariant stress tensor. MSS: maximum shear stress. SED: strain energy density.

Table B - 118. Linear regression measures for individual loading regime results from the orthotropic elastic model 6, with Ey as neural model input.

Loading Regime	R^2	RMSE	Slope
Uniform	NaN	0.0000	0.0000
Biaxial	NaN	0.0000	0.0000
Uniaxial X	NaN	0.0000	0.0000
Uniaxial Y	0.9594	0.1394	0.4579
Shear Positive	NaN	0.0000	0.0000
Shear Negative	NaN	0.0000	0.0000

Appendix C: Coupled Transversely Isotropic Mooney Rivlin Material Results

C.1 Test 1

C.1.1 X Stress (Sx)

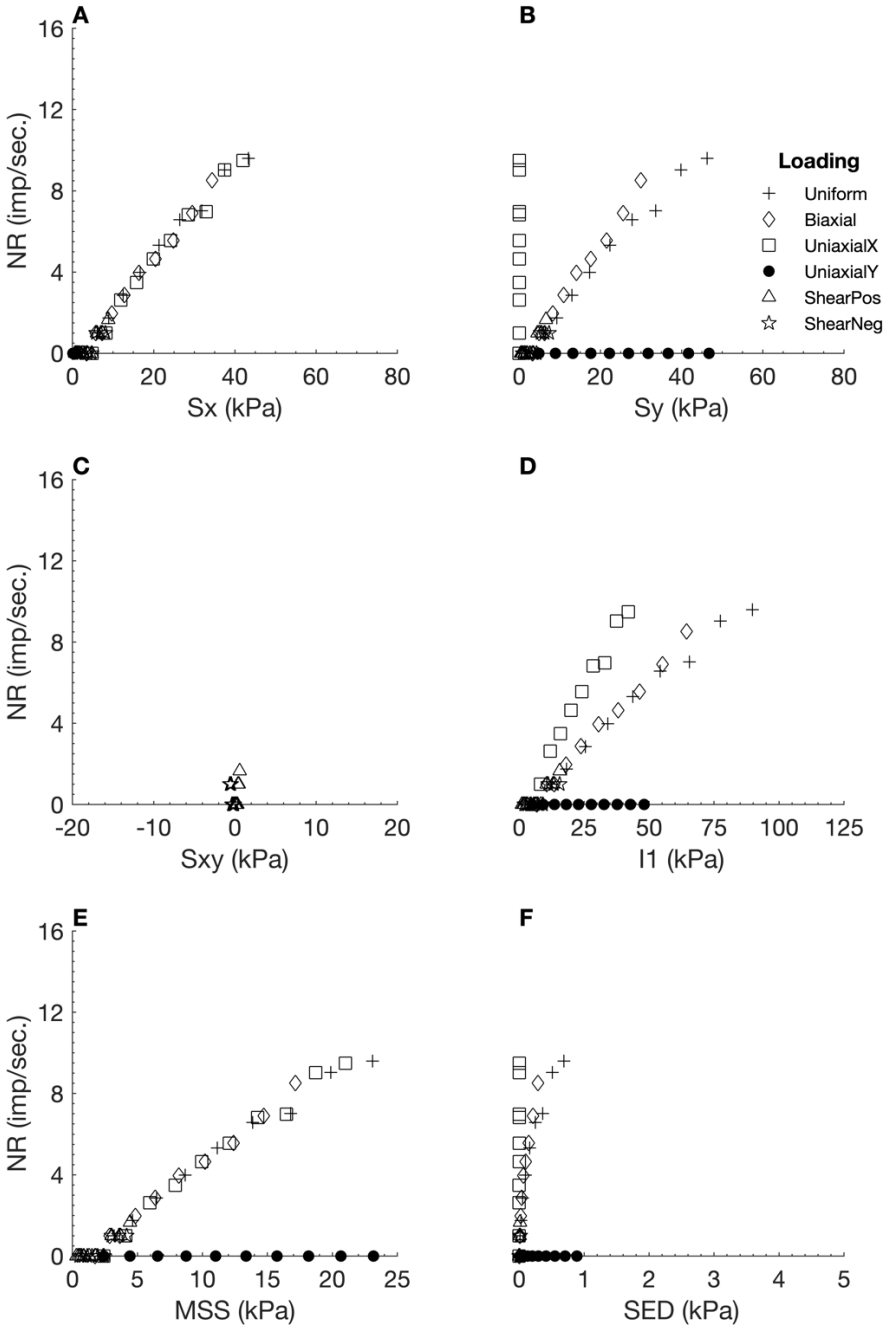

Figure C - 1. Neural responses (NR) output by the Mooney Rivlin FEBio model 1 using Sx as the neural model input, plotted against six different stress variables. Sx: X stress. Sy: Y stress. Sxy: shear stress. I1: 1st invariant stress tensor. MSS: maximum shear stress. SED: strain energy density.

Table C - 1. Linear regression measures for individual loading regime results from the Mooney Rivlin model 1, with Sx as neural model input.

Loading Regime	**R^2**	**RMSE**	**Slope**
Uniform	0.9751	0.5592	0.6940
Biaxial	0.1997	1.1273	2.4783
Uniaxial X	0.3658	1.5328	-0.5048
Uniaxial Y	NaN	0.0000	0.0000
Shear Positive	NaN	0.0000	0.0000
Shear Negative	NaN	0.0000	0.0000

C.1.2 Y Stress (Sy)

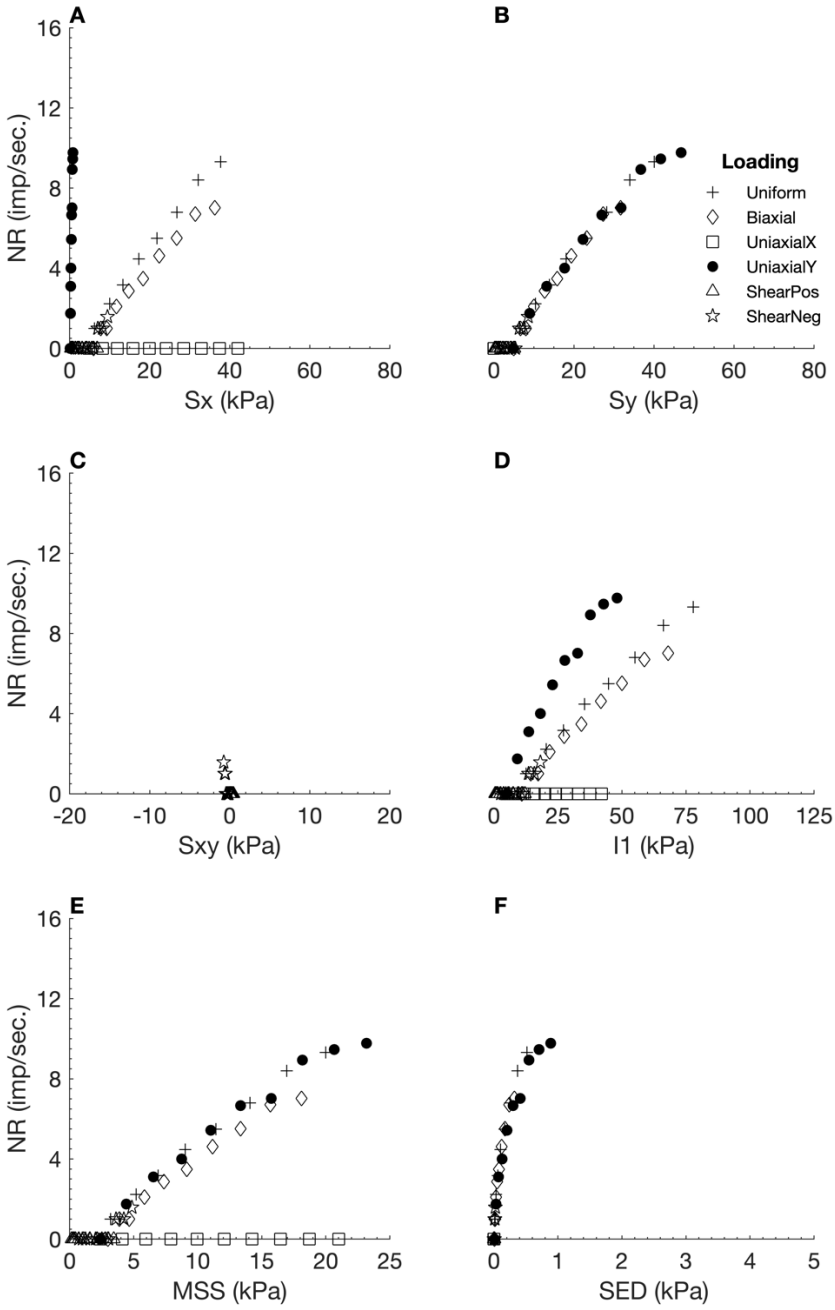

Figure C - 2. Neural responses (NR) output by the Mooney Rivlin FEBio model 1 using Sy as the neural model input, plotted against six different stress variables. Sx: X stress. Sy: Y stress. Sxy: shear stress. I1: 1st invariant stress tensor. MSS: maximum shear stress. SED: strain energy density.

Table C - 2. Linear regression measures for individual loading regime results from the Mooney Rivlin model 1, with Sy as neural model input.

Loading Regime	R^2	RMSE	Slope
Uniform	0.9437	0.8196	0.6654
Biaxial	0.2200	1.1308	2.6429
Uniaxial X	NaN	0.0000	0.0000
Uniaxial Y	0.9217	0.7596	1.7609
Shear Positive	NaN	0.0000	0.0000
Shear Negative	NaN	0.0000	0.0000

C.1.3 Shear Stress (Sxy)

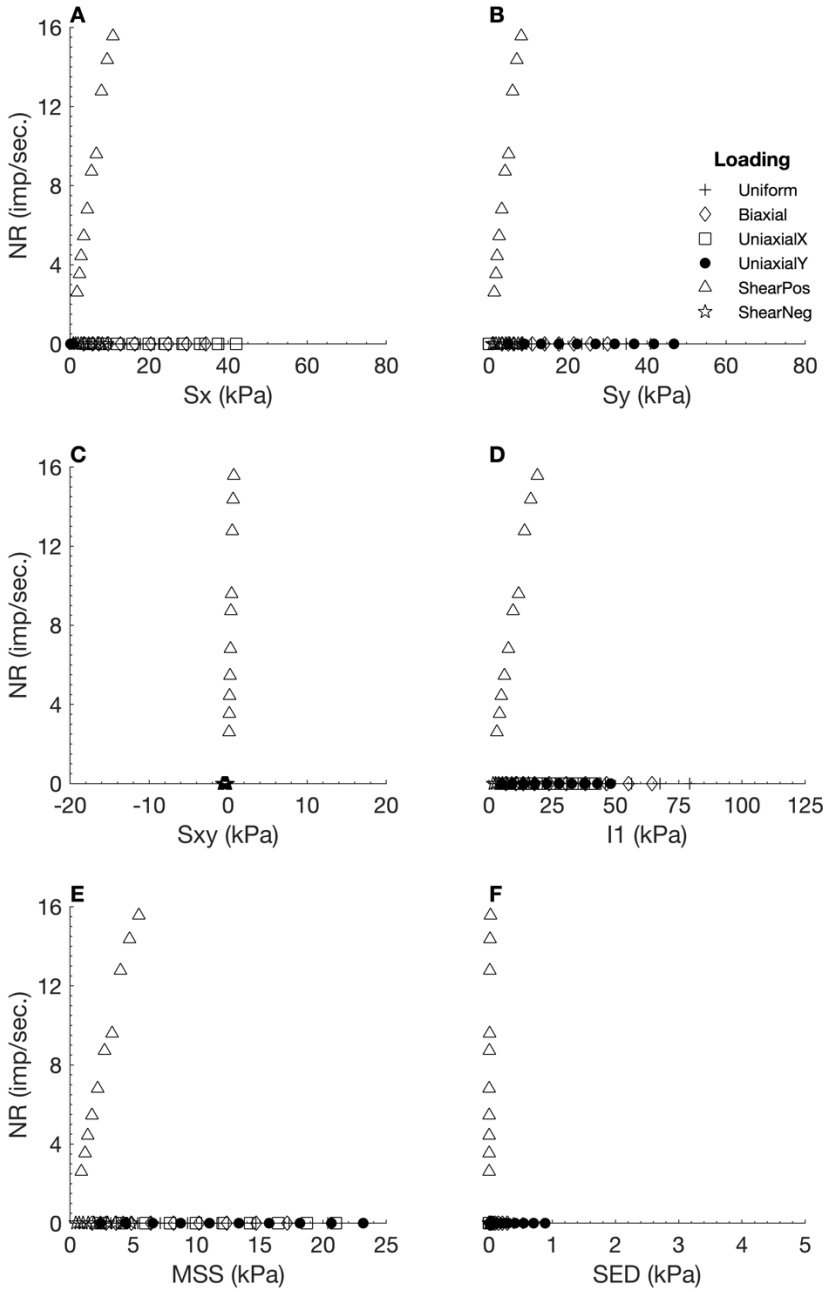

Figure C - 3. Neural responses (NR) output by the Mooney Rivlin FEBio model 1 using Sxy as the neural model input, plotted against six different stress variables. Sx: X stress. Sy: Y stress. Sxy: shear stress. I1: 1st invariant stress tensor. MSS: maximum shear stress. SED: strain energy density.

Table C - 3. Linear regression measures for individual loading regime results from the Mooney Rivlin model 1, with Sxy as neural model input.

Loading Regime	R^2	RMSE	Slope
Uniform	NaN	0.0000	0.0000
Biaxial	NaN	0.0000	0.0000
Uniaxial X	NaN	0.0000	0.0000
Uniaxial Y	NaN	0.0000	0.0000
Shear Positive	0.8755	0.8839	0.4300
Shear Negative	NaN	0.0000	0.0000

C.1.4 1st Invariant Stress Tensor (I1)

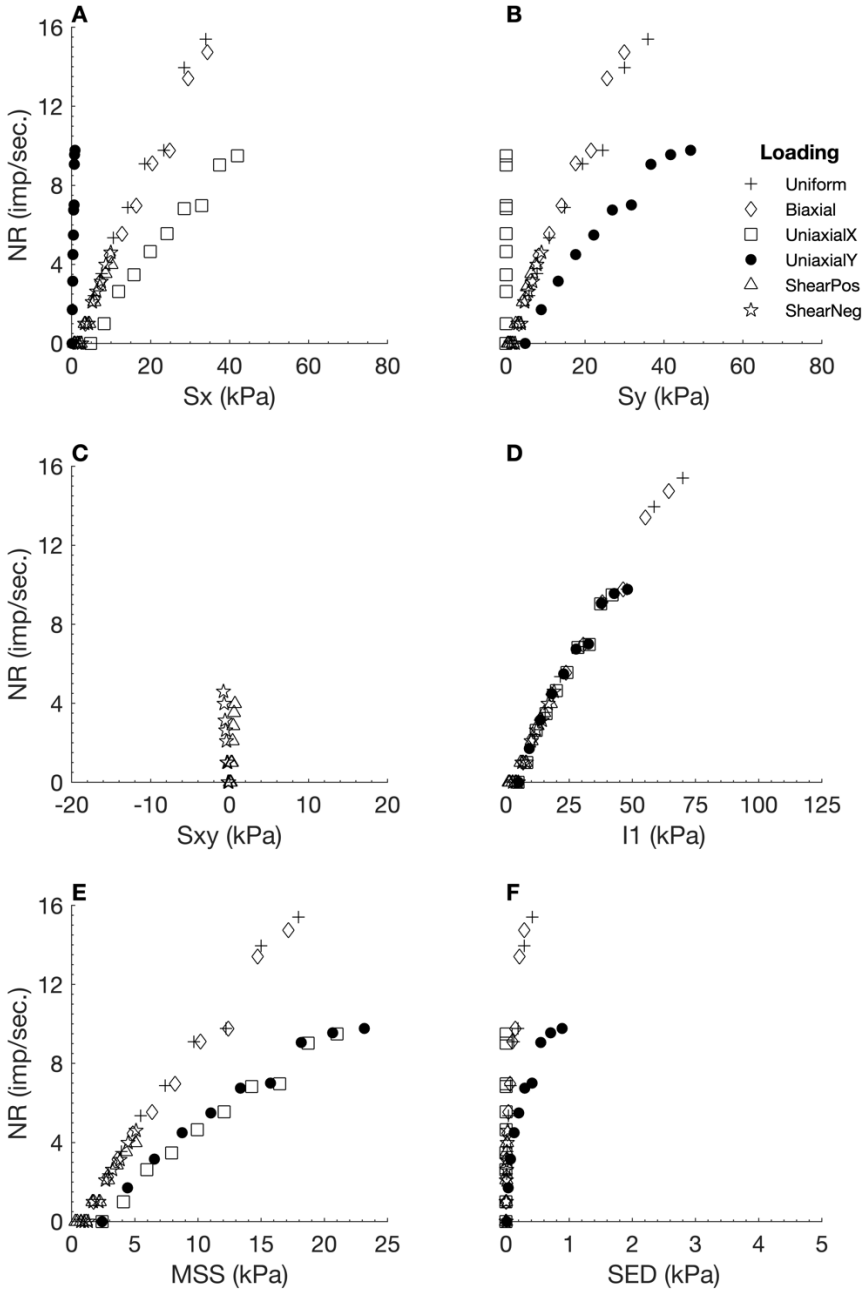

Figure C - 4. Neural responses (NR) output by the Mooney Rivlin FEBio model 1 using I1 as the neural model input, plotted against six different stress variables. Sx: X stress. Sy: Y stress. Sxy: shear stress. I1: 1st invariant stress tensor. MSS: maximum shear stress. SED: strain energy density.

Table C - 4. Linear regression measures for individual loading regime results from the Mooney Rivlin model 1, with I1 as neural model input.

Loading Regime	R^2	RMSE	Slope
Uniform	0.9704	1.0212	1.1606
Biaxial	0.3662	1.6432	5.4966
Uniaxial X	0.3674	1.5270	-0.5045
Uniaxial Y	0.9087	0.8416	1.7939
Shear Positive	0.5096	0.4043	0.0756
Shear Negative	0.4848	0.4540	0.2298

C.1.5 Maximum Shear Stress (MSS)

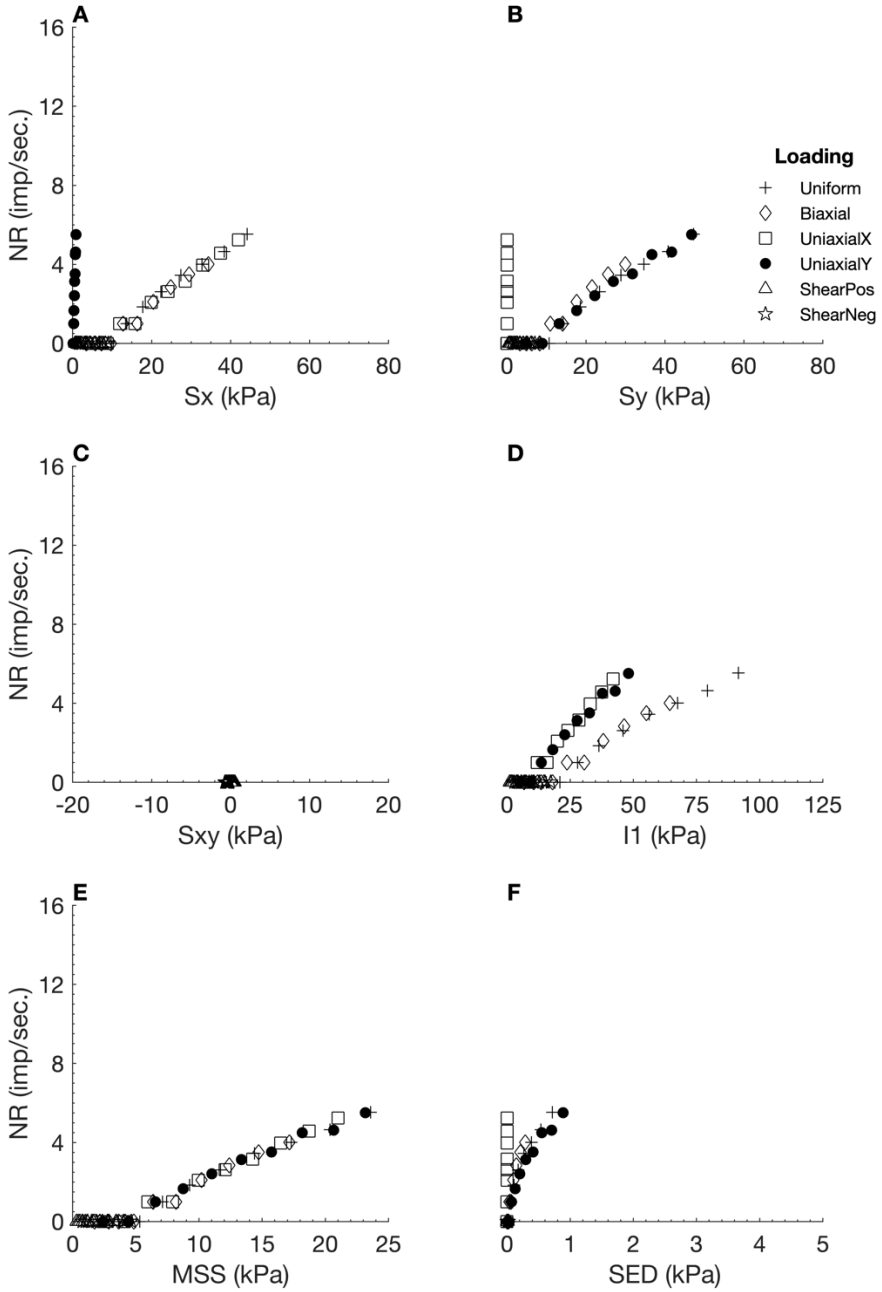

Figure C - 5. Neural responses (NR) output by the Mooney Rivlin FEBio model 1 using MSS as the neural model input, plotted against six different stress variables. Sx: X stress. Sy: Y stress. Sxy: shear stress. I1: 1st invariant stress tensor. MSS: maximum shear stress. SED: strain energy density.

Table C - 5. Linear regression measures for individual loading regime results from the Mooney Rivlin model 1, with MSS as neural model input.

Loading Regime	R^2	RMSE	Slope
Uniform	0.9396	0.5361	0.4195
Biaxial	0.0001	0.5164	-0.0233
Uniaxial X	0.2082	0.6292	-0.1399
Uniaxial Y	0.9352	0.3637	0.9336
Shear Positive	NaN	0.0000	0.0000
Shear Negative	NaN	0.0000	0.0000

C.1.6 Strain Energy Density (SED)

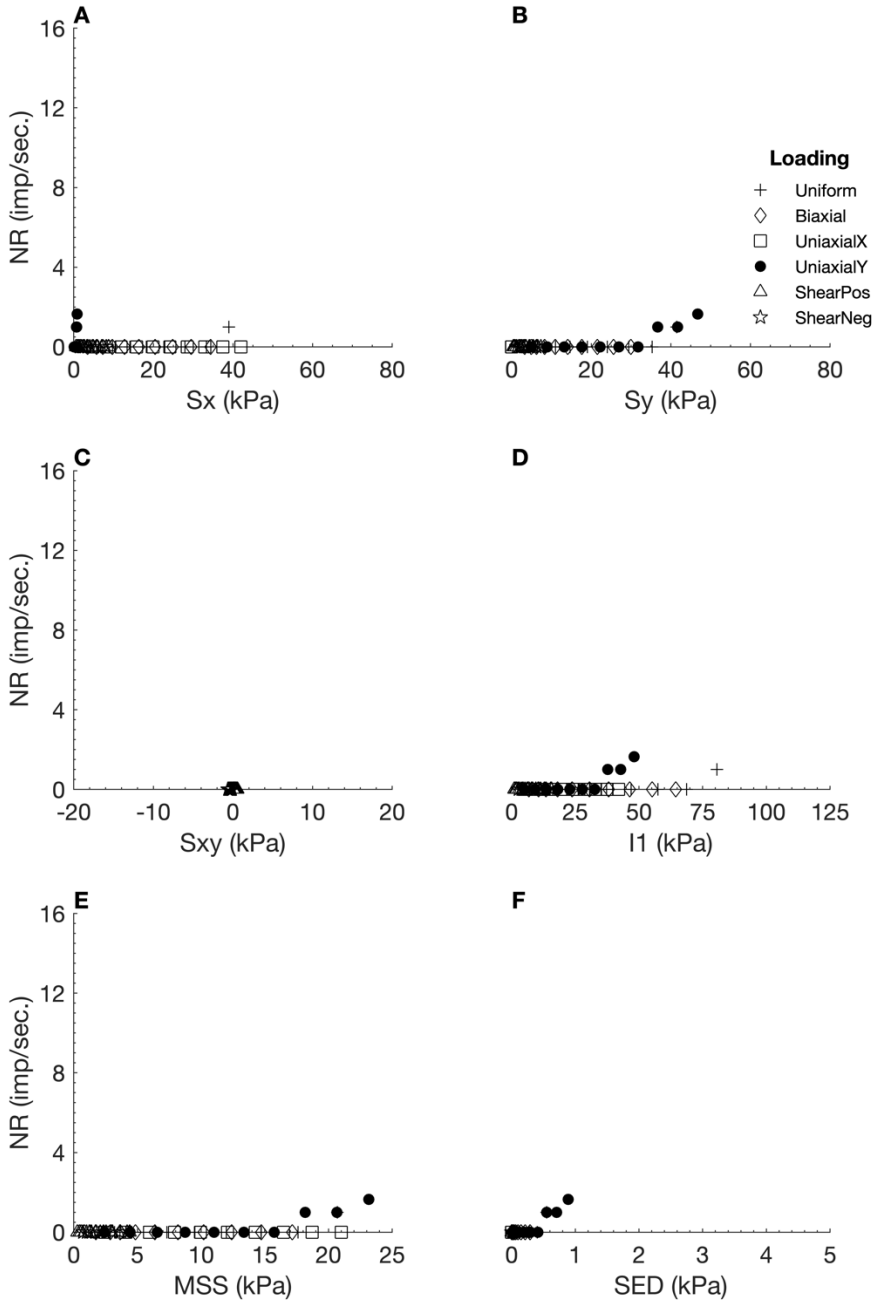

Figure C - 6. Neural responses (NR) output by the Mooney Rivlin FEBio model 1 using SED as the neural model input, plotted against six different stress variables. Sx: X stress. Sy: Y stress. Sxy: shear stress. I1: 1st invariant stress tensor. MSS: maximum shear stress. SED: strain energy density.

Table C - 6. Linear regression measures for individual loading regime results from the Mooney Rivlin model 1, with SED as neural model input.

Loading Regime	R^2	RMSE	Slope
Uniform	0.1966	0.3006	0.0295
Biaxial	NaN	0.0000	0.0000
Uniaxial X	NaN	0.0000	0.0000
Uniaxial Y	NaN	0.0000	0.0000
Shear Positive	NaN	0.0000	0.0000
Shear Negative	NaN	0.0000	0.0000

C.1.7 Hydrostatic Pressure (HS)

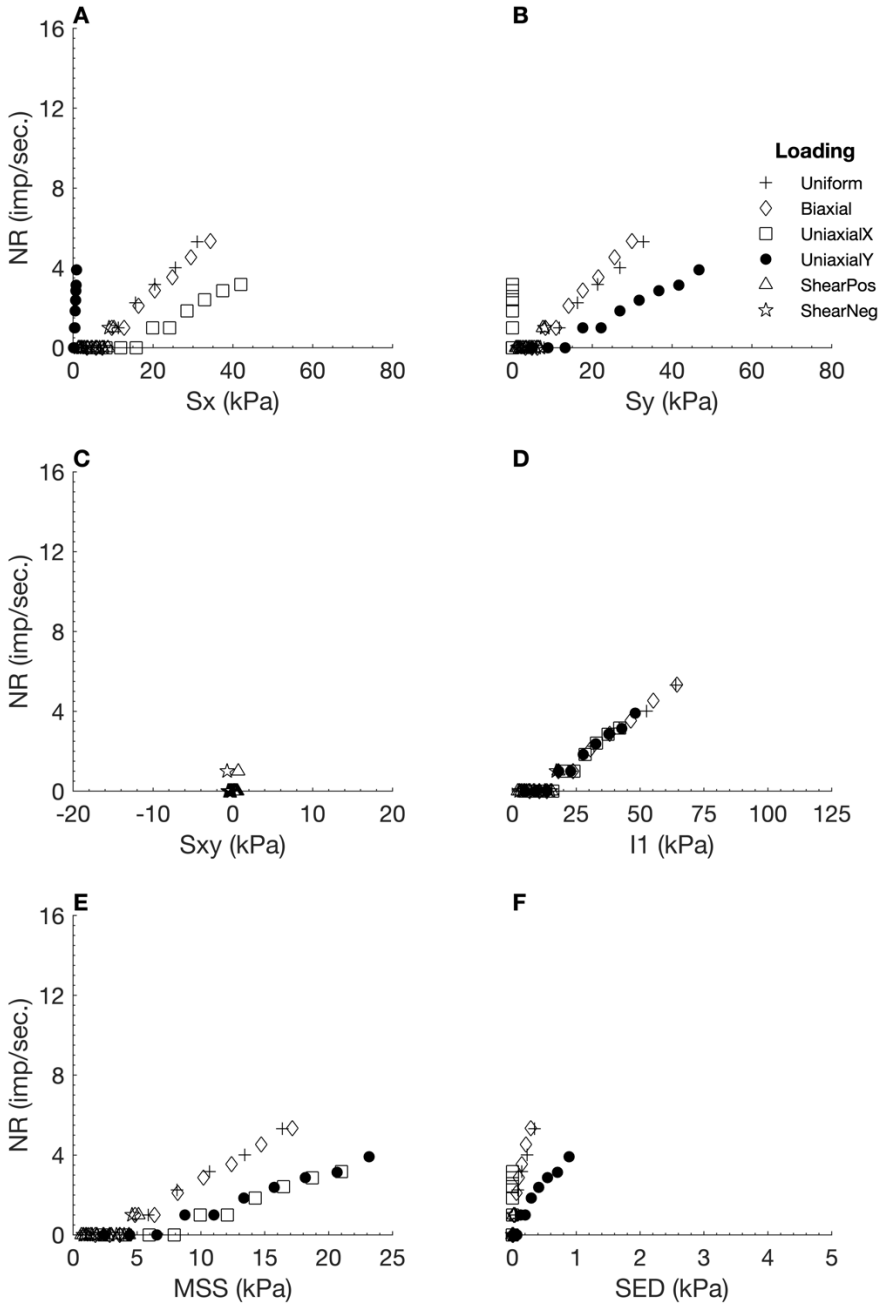

Figure C - 7. Neural responses (NR) output by the Mooney Rivlin FEBio model 1 using HS as the neural model input, plotted against six different stress variables. Sx: X stress. Sy: Y stress. Sxy: shear stress. I1: 1st invariant stress tensor. MSS: maximum shear stress. SED: strain energy density.

Table C - 7. Linear regression measures for individual loading regime results from the Mooney Rivlin model 1, with HS as neural model input.

Loading Regime	R^2	RMSE	Slope
Uniform	0.7707	1.0110	0.3676
Biaxial	0.2119	0.5615	1.2811
Uniaxial X	NaN	0.0000	0.0000
Uniaxial Y	0.9155	0.2492	0.5544
Shear Positive	NaN	0.0000	0.0000
Shear Negative	NaN	0.0000	0.0000

C.1.8 1st Principle Stress (S1)

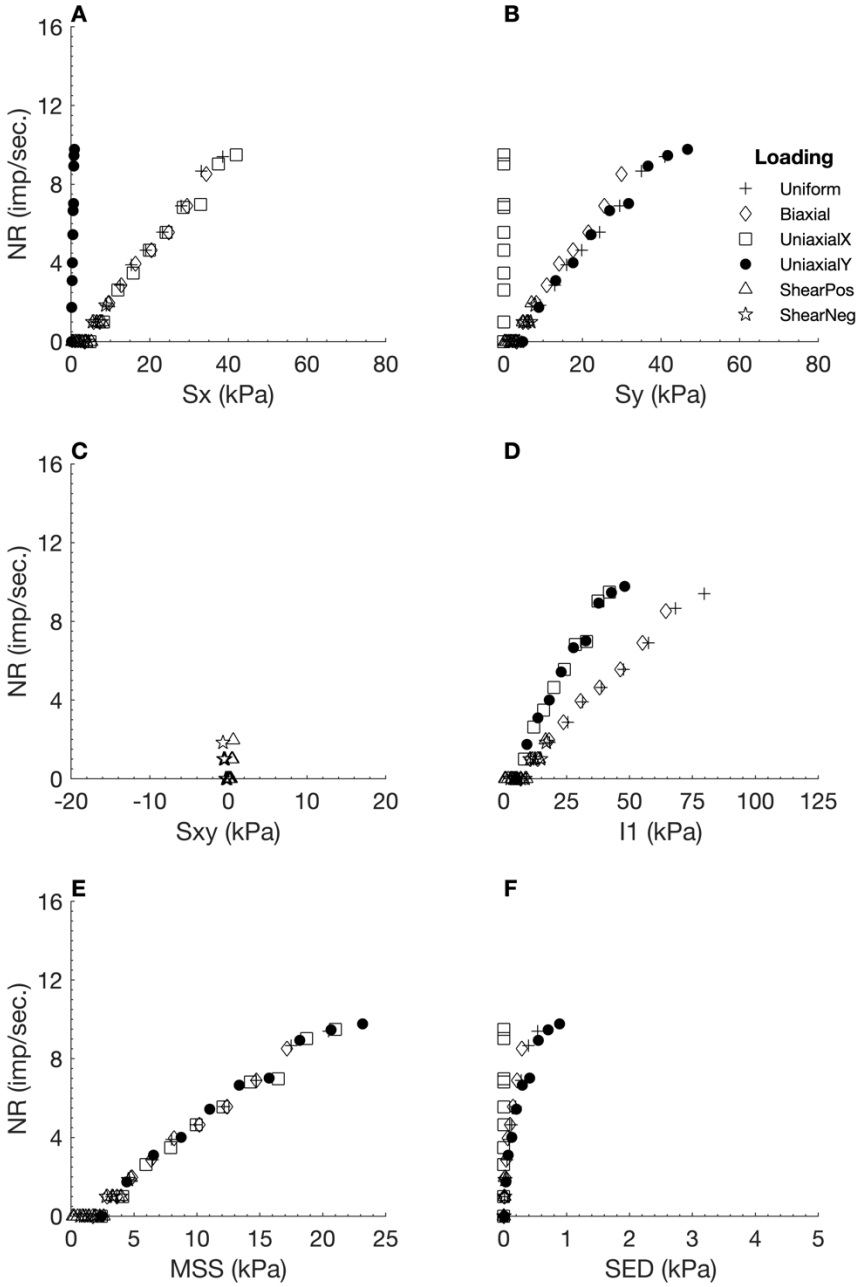

Figure C - 8. Neural responses (NR) output by the Mooney Rivlin FEBio model 1 using S1 as the neural model input, plotted against six different stress variables. Sx: X stress. Sy: Y stress. Sxy: shear stress. I1: 1st invariant stress tensor. MSS: maximum shear stress. SED: strain energy density.

Table C - 8. Linear regression measures for individual loading regime results from the Mooney Rivlin model 1, with S1 as neural model input.

Loading Regime	R^2	RMSE	Slope
Uniform	0.9614	0.6623	0.6554
Biaxial	0.1997	1.1273	2.4783
Uniaxial X	0.3658	1.5328	-0.5048
Uniaxial Y	0.9217	0.7598	1.7609
Shear Positive	NaN	0.0000	0.0000
Shear Negative	NaN	0.0000	0.0000

C.1.9 2nd Principle Stress (S2)

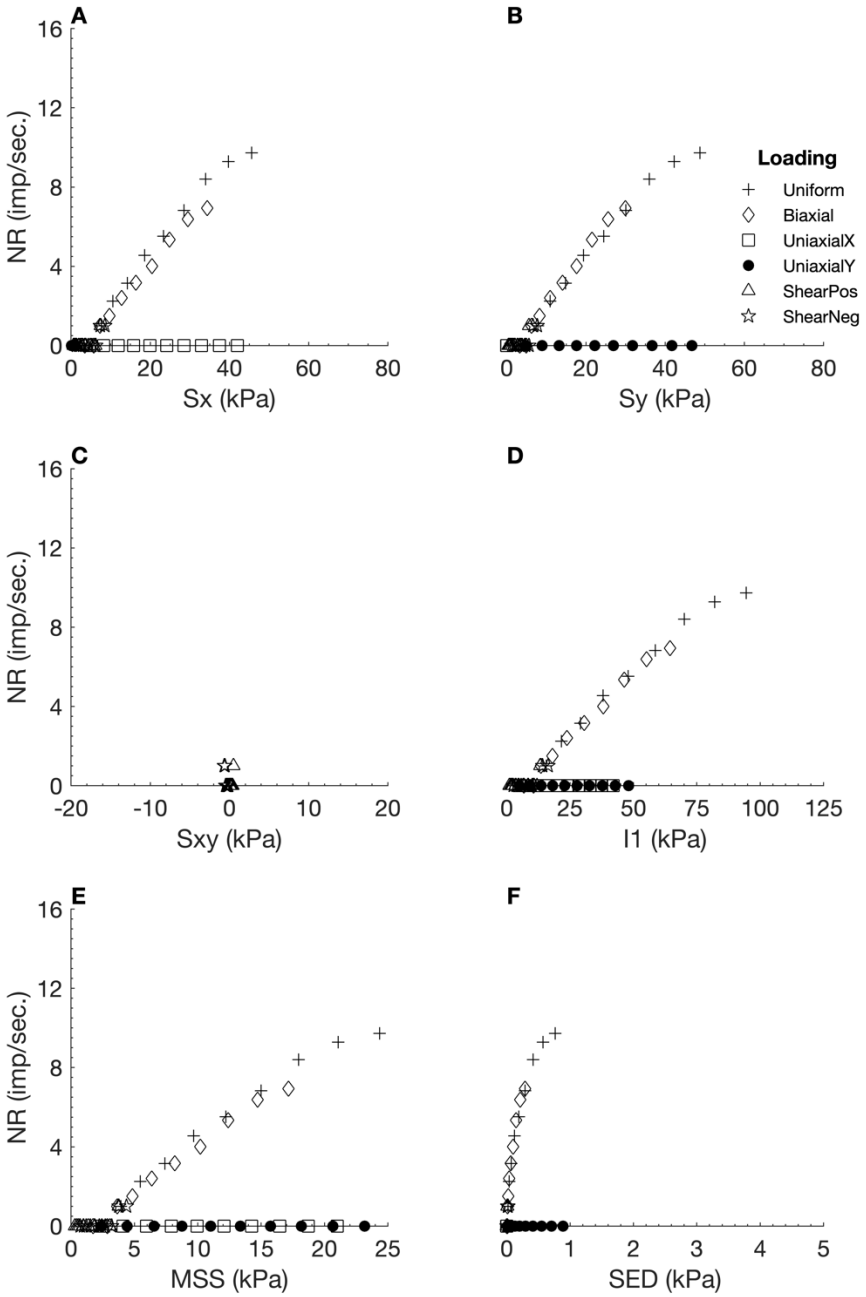

Figure C - 9. Neural responses (NR) output by the Mooney Rivlin FEBio model 1 using S2 as the neural model input, plotted against six different stress variables. Sx: X stress. Sy: Y stress. Sxy: shear stress. I1: 1st invariant stress tensor. MSS: maximum shear stress. SED: strain energy density.

Table C - 9. Linear regression measures for individual loading regime results from the Mooney Rivlin model 1, with S2 as neural model input.

Loading Regime	R^2	RMSE	Slope
Uniform	0.9876	0.4089	0.7244
Biaxial	0.3637	0.9474	3.1522
Uniaxial X	NaN	0.0000	0.0000
Uniaxial Y	NaN	0.0000	0.0000
Shear Positive	NaN	0.0000	0.0000
Shear Negative	NaN	0.0000	0.0000

C.1.10 3rd Principle Stress (S3)

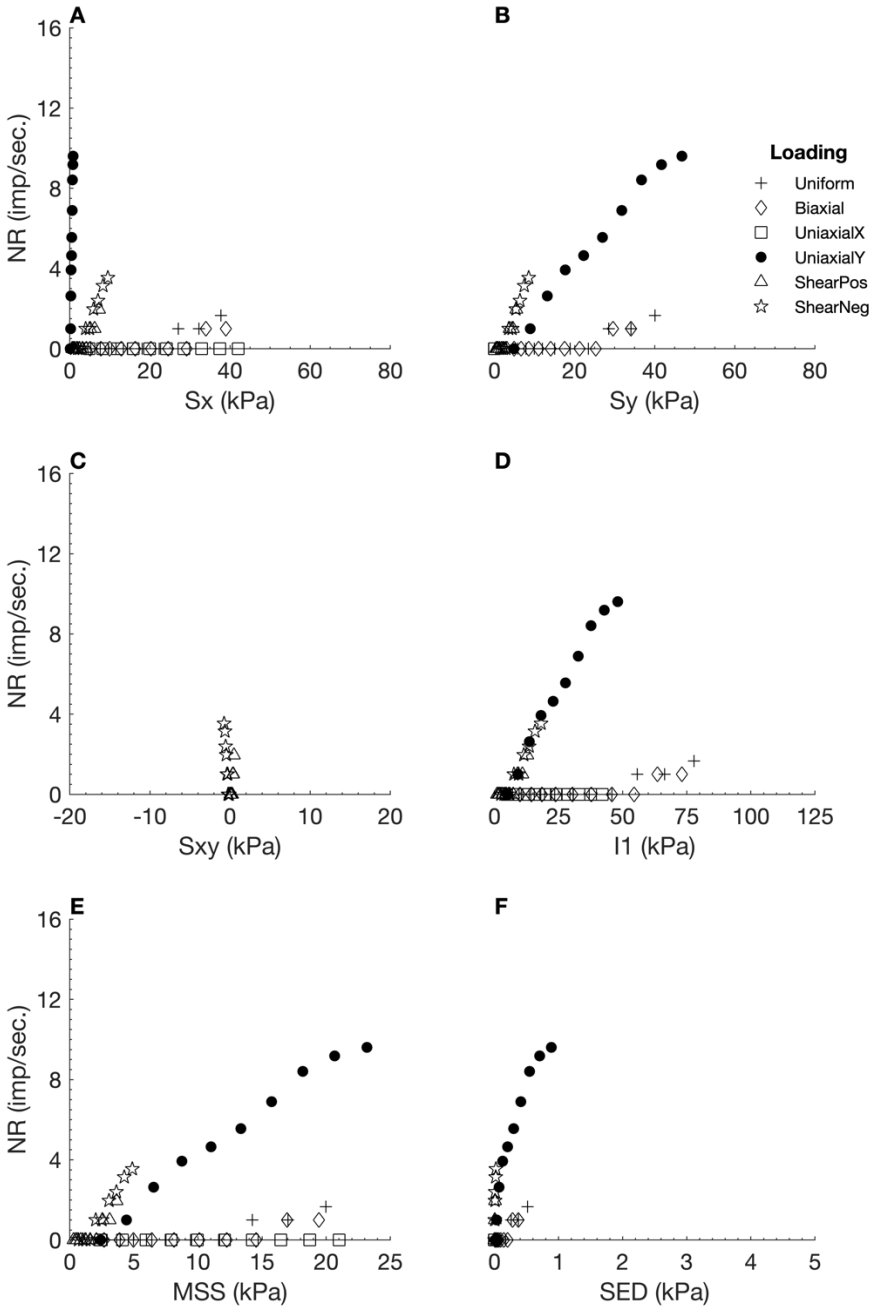

Figure C - 10. Neural responses (NR) output by the Mooney Rivlin FEBio model 1 using S3 as the neural model input, plotted against six different stress variables. Sx: X stress. Sy: Y stress. Sxy: shear stress. I1: 1st invariant stress tensor. MSS: maximum shear stress. SED: strain energy density.

Table C - 10. Linear regression measures for individual loading regime results from the Mooney Rivlin model 1, with S3 as neural model input.

Loading Regime	R^2	RMSE	Slope
Uniform	0.5511	0.4378	0.0962
Biaxial	NaN	0.0000	0.0000
Uniaxial X	NaN	0.0000	0.0000
Uniaxial Y	0.8875	0.8088	1.5347
Shear Positive	NaN	0.0000	0.0000
Shear Negative	0.2318	0.4526	0.1297

C.1.11 Deviatoric Stress 1 (Dev1)

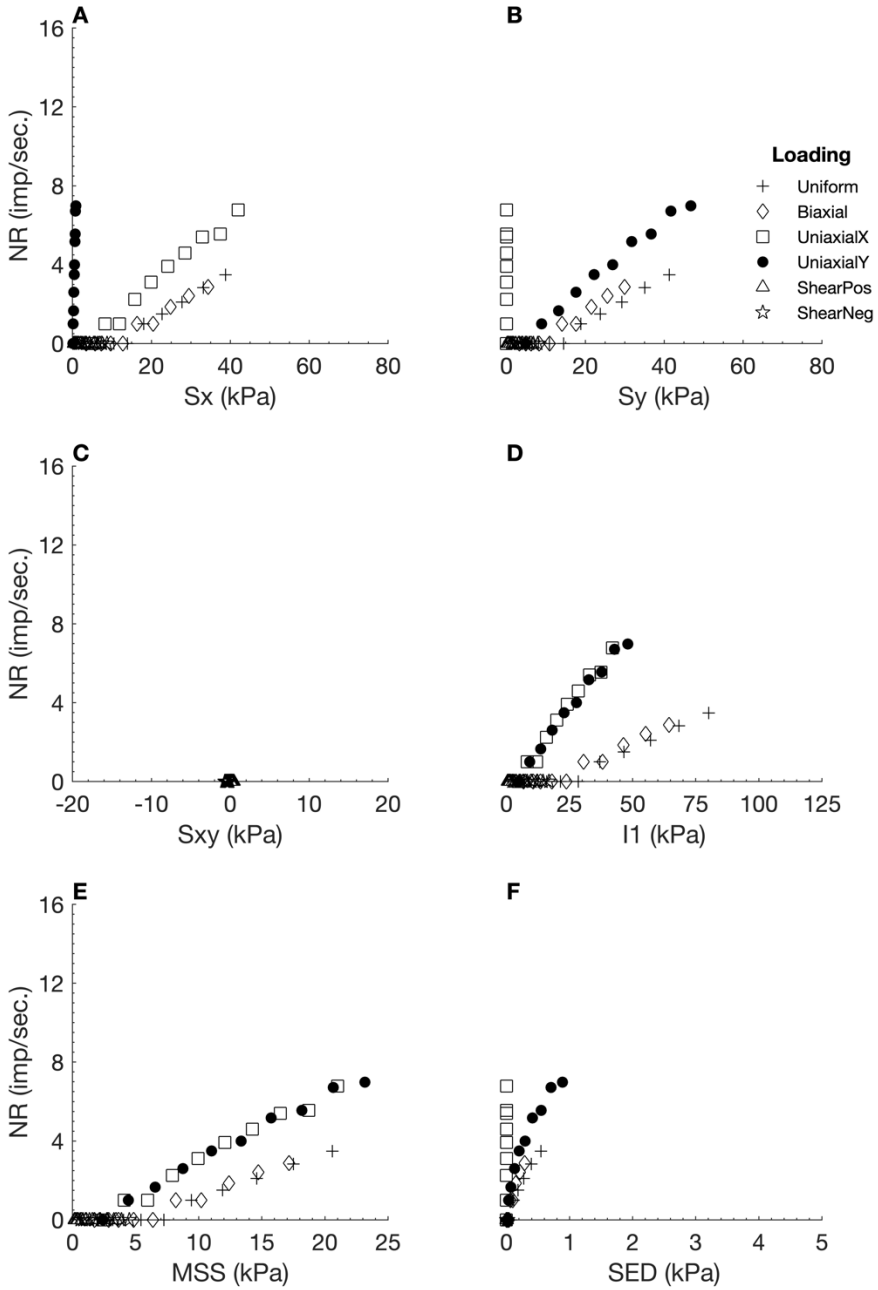

Figure C - 11. Neural responses (NR) output by the Mooney Rivlin FEBio model 1 using Dev1 as the neural model input, plotted against six different stress variables. Sx: X stress. Sy: Y stress. Sxy: shear stress. I1: 1st invariant stress tensor. MSS: maximum shear stress. SED: strain energy density.

Table C - 11. Linear regression measures for individual loading regime results from the Mooney Rivlin model 1, with Dev1 as neural model input.

Loading Regime	R^2	RMSE	Slope
Uniform	0.7987	0.6325	0.2499
Biaxial	NaN	0.0000	0.0000
Uniaxial X	0.3429	0.9130	-0.2860
Uniaxial Y	0.9385	0.4223	1.1150
Shear Positive	NaN	0.0000	0.0000
Shear Negative	NaN	0.0000	0.0000

C.1.12 Deviatoric Stress 2 (Dev2)

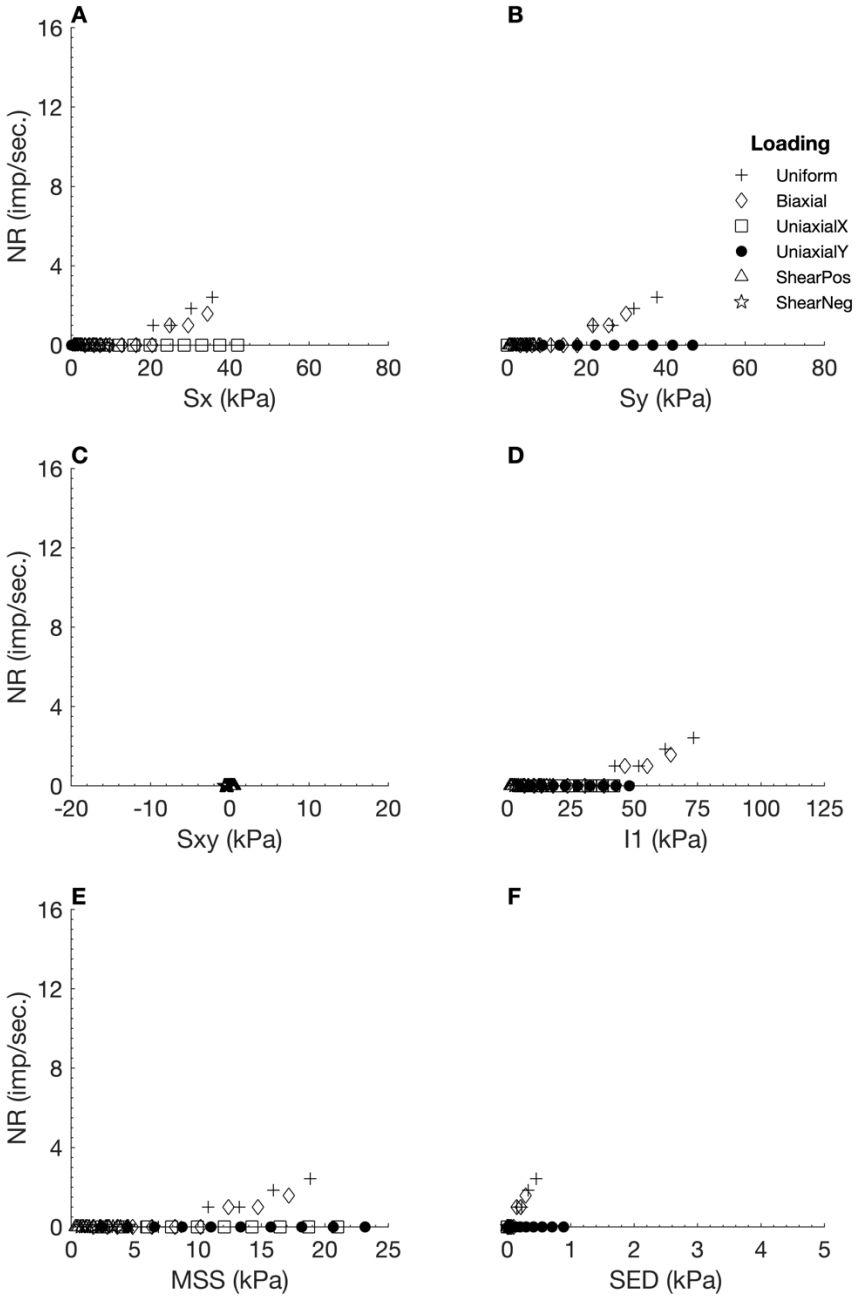

Figure C - 12. Neural responses (NR) output by the Mooney Rivlin FEBio model 1 using Dev2 as the neural model input, plotted against six different stress variables. Sx: X stress. Sy: Y stress. Sxy: shear stress. I1: 1st invariant stress tensor. MSS: maximum shear stress. SED: strain energy density.

Table C - 12. Linear regression measures for individual loading regime results from the Mooney Rivlin model 1, with Dev2 as neural model input.

Loading Regime	R^2	RMSE	Slope
Uniform	0.6642	0.5551	0.1548
Biaxial	NaN	0.0000	0.0000
Uniaxial X	NaN	0.0000	0.0000
Uniaxial Y	NaN	0.0000	0.0000
Shear Positive	NaN	0.0000	0.0000
Shear Negative	NaN	0.0000	0.0000

C.1.13 Deviatoric Stress 3 (Dev3)

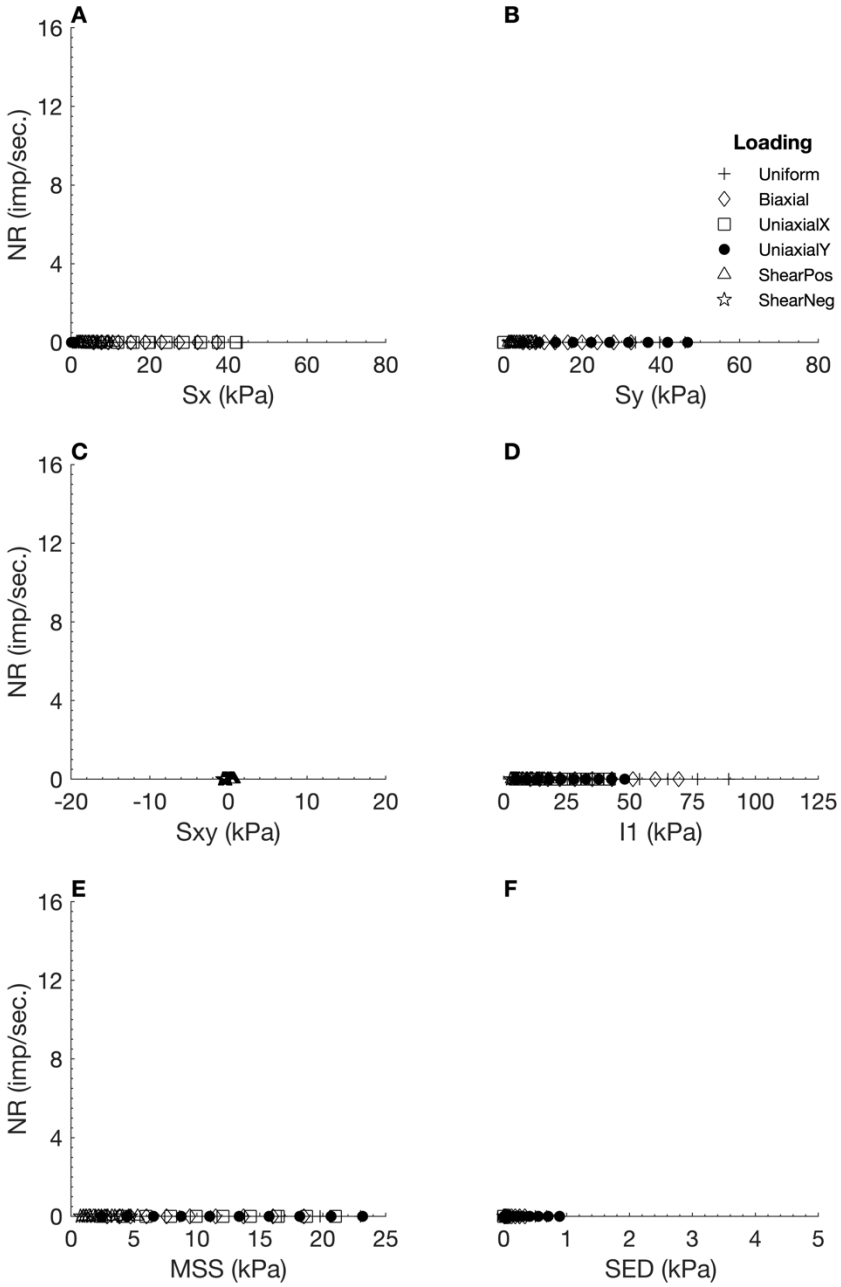

Figure C - 13. Neural responses (NR) output by the Mooney Rivlin FEBio model 1 using Dev3 as the neural model input, plotted against six different stress variables. Sx: X stress. Sy: Y stress. Sxy: shear stress. I1: 1st invariant stress tensor. MSS: maximum shear stress. SED: strain energy density.

Table C - 13. Linear regression measures for individual loading regime results from the Mooney Rivlin model 1, with Dev3 as neural model input.

Loading Regime	R^2	RMSE	Slope
Uniform	NaN	0.0000	0.0000
Biaxial	NaN	0.0000	0.0000
Uniaxial X	NaN	0.0000	0.0000
Uniaxial Y	NaN	0.0000	0.0000
Shear Positive	NaN	0.0000	0.0000
Shear Negative	NaN	0.0000	0.0000

C.1.14 Shear Stress A

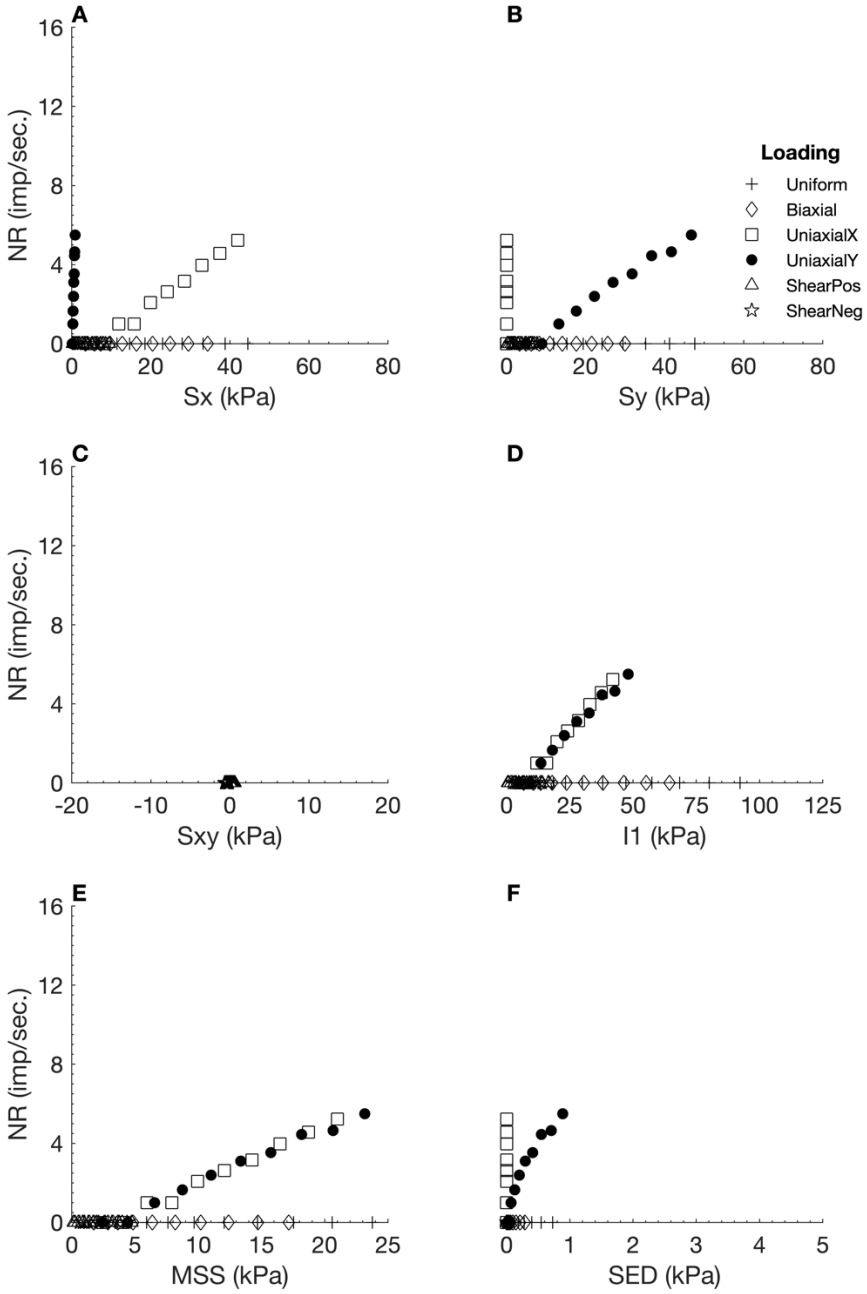

Figure C - 14. Neural responses (NR) output by the Mooney Rivlin FEBio model 1 using ShearA as the neural model input, plotted against six different stress variables. Sx: X stress. Sy: Y stress. Sxy: shear stress. I1: 1st invariant stress tensor. MSS: maximum shear stress. SED: strain energy density.

Table C - 14. Linear regression measures for individual loading regime results from the Mooney Rivlin model 1, with ShearA as neural model input.

Loading Regime	R^2	RMSE	Slope
Uniform	NaN	0.0000	0.0000
Biaxial	NaN	0.0000	0.0000
Uniaxial X	0.2082	0.6292	-0.1399
Uniaxial Y	0.9340	0.3640	0.9251
Shear Positive	NaN	0.0000	0.0000
Shear Negative	NaN	0.0000	0.0000

C.1.15 Shear Stress B

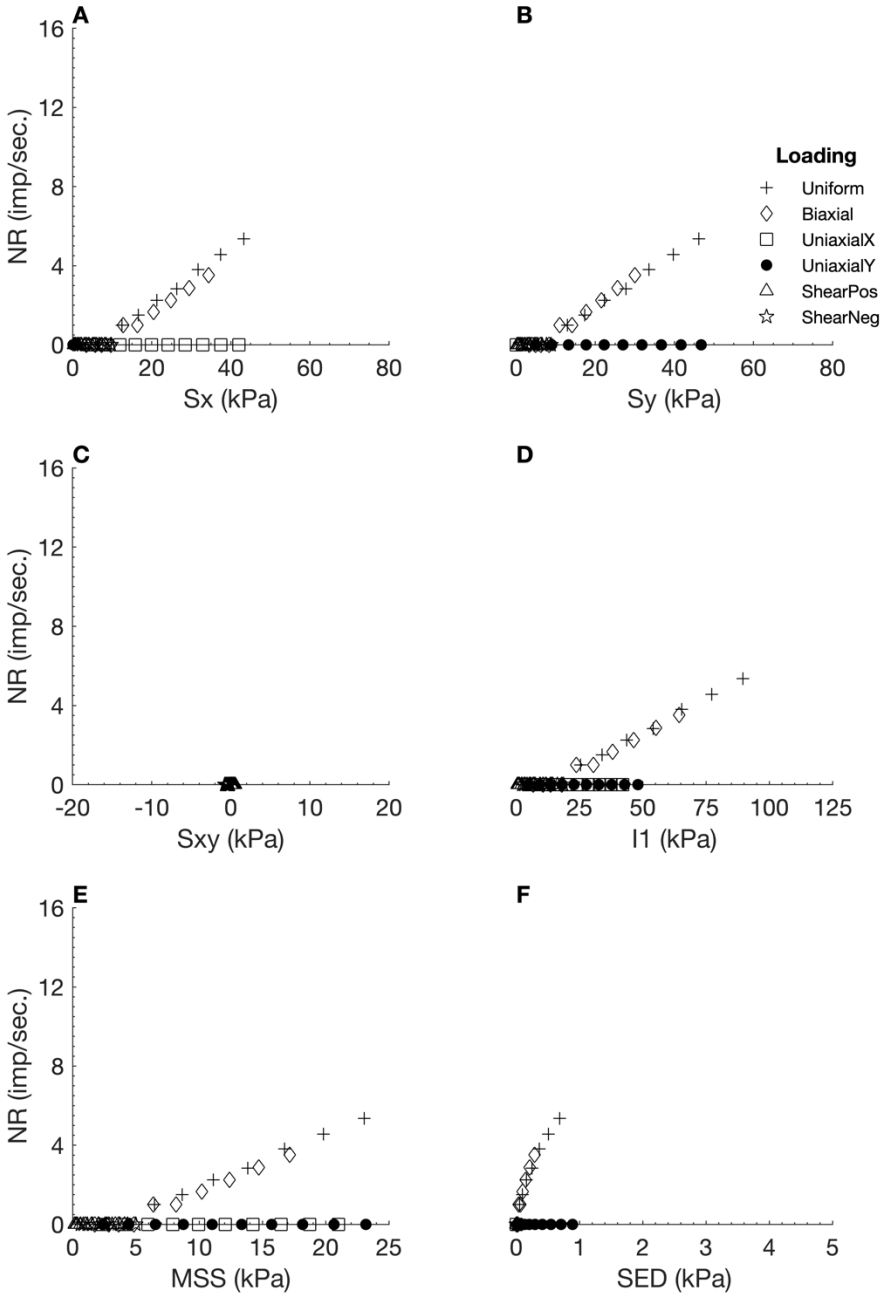

Figure C - 15. Neural responses (NR) output by the Mooney Rivlin FEBio model 1 using ShearB as the neural model input, plotted against six different stress variables. Sx: X stress. Sy: Y stress. Sxy: shear stress. I1: 1st invariant stress tensor. MSS: maximum shear stress. SED: strain energy density.

Table C - 15. Linear regression measures for individual loading regime results from the Mooney Rivlin model 1, with ShearB as neural model input.

Loading Regime	R^2	RMSE	Slope
Uniform	0.9212	0.5871	0.3981
Biaxial	0.0001	0.5164	-0.0233
Uniaxial X	NaN	0.0000	0.0000
Uniaxial Y	NaN	0.0000	0.0000
Shear Positive	NaN	0.0000	0.0000
Shear Negative	NaN	0.0000	0.0000

C.1.16 Shear Stress C

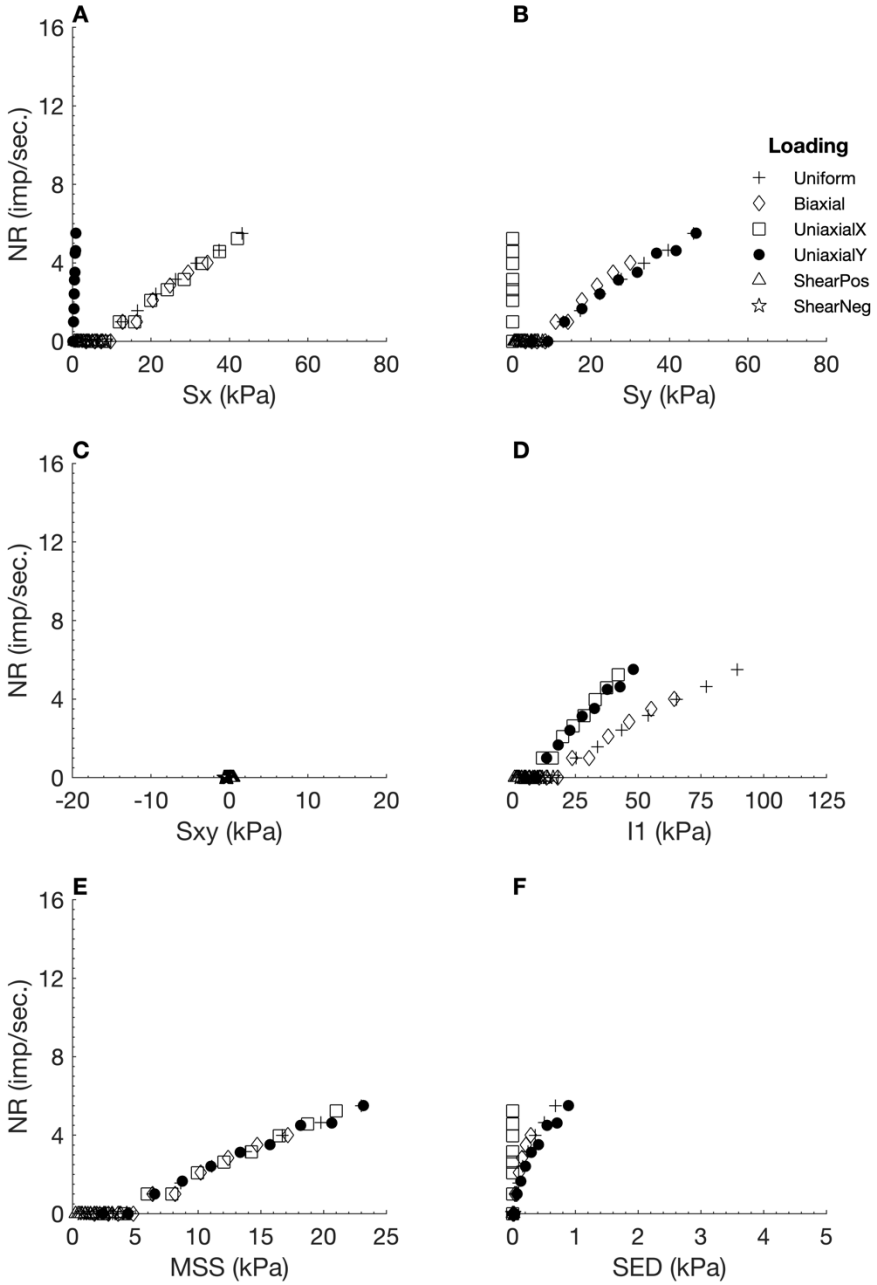

Figure C - 16. Neural responses (NR) output by the Mooney Rivlin FEBio model 1 using ShearC as the neural model input, plotted against six different stress variables. Sx: X stress. Sy: Y stress. Sxy: shear stress. I1: 1st invariant stress tensor. MSS: maximum shear stress. SED: strain energy density.

Table C - 16. Linear regression measures for individual loading regime results from the Mooney Rivlin model 1, with ShearC as neural model input.

Loading Regime	R^2	RMSE	Slope
Uniform	0.9300	0.5719	0.4135
Biaxial	0.0001	0.5164	-0.0233
Uniaxial X	0.2082	0.6292	-0.1399
Uniaxial Y	0.9352	0.3637	0.9336
Shear Positive	NaN	0.0000	0.0000
Shear Negative	NaN	0.0000	0.0000

C.1.17 X Strain (Ex)

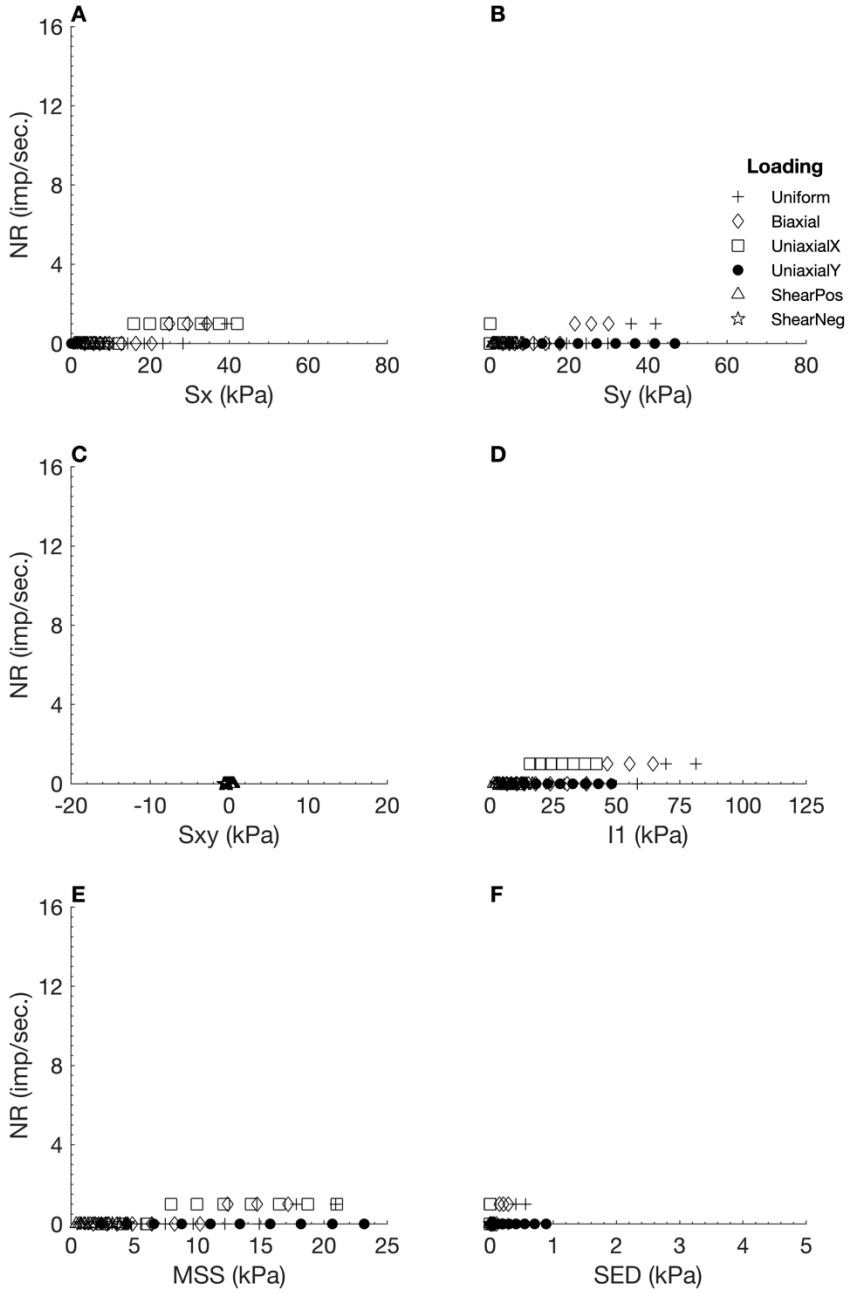

Figure C - 17. Neural responses (NR) output by the Mooney Rivlin FEBio model 1 using Ex as the neural model input, plotted against six different stress variables. Sx: X stress. Sy: Y stress. Sxy: shear stress. I1: 1st invariant stress tensor. MSS: maximum shear stress. SED: strain energy density.

Table C - 17. Linear regression measures for individual loading regime results from the Mooney Rivlin model 1, with Ex as neural model input.

Loading Regime	R^2	RMSE	Slope
Uniform	0.3998	0.3465	0.0561
Biaxial	NaN	0.0000	0.0000
Uniaxial X	0.0076	0.6100	-0.0232
Uniaxial Y	NaN	0.0000	0.0000
Shear Positive	NaN	0.0000	0.0000
Shear Negative	NaN	0.0000	0.0000

C.1.18 Y Strain (Ey)

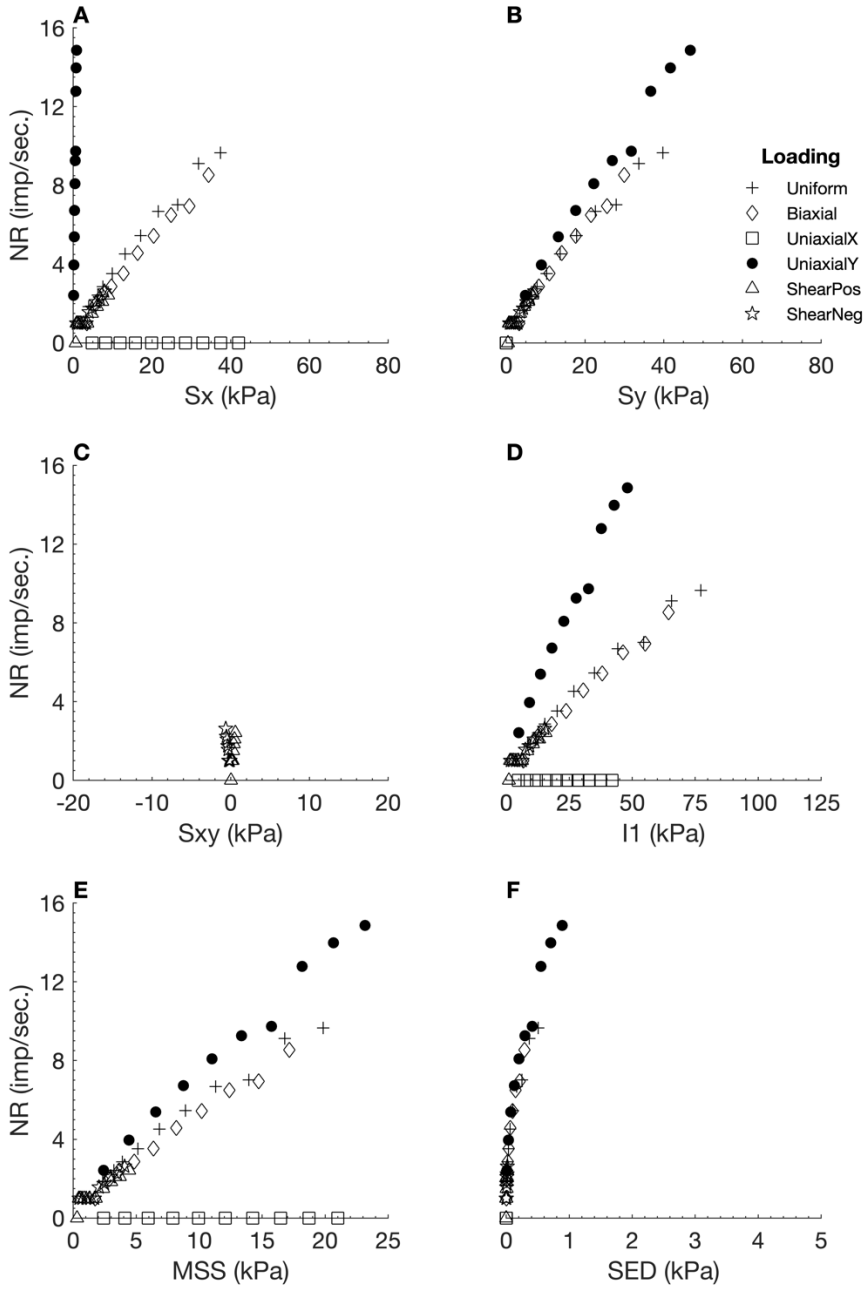

Figure C - 18. Neural responses (NR) output by the Mooney Rivlin FEBio model 1 using Ey as the neural model input, plotted against six different stress variables. Sx: X stress. Sy: Y stress. Sxy: shear stress. I1: 1st invariant stress tensor. MSS: maximum shear stress. SED: strain energy density.

C.2 Test 2

Table C - 18. Values selected for material properties during FEBio implementation of coupled transversely isotropic Mooney Rivlin model 2.

Mooney Rivlin Material Property	**Value Selected**
Density	1
Mooney Rivlin Parameter 1 (C1)	0.195
Mooney Rivlin Parameter 2 (C2)	0
Exponential Multiplier (C3)	0.0139
Fibre Scale Factor (C4)	116.22
Fibre Modulus - Linear Region (C5)	535.039
Bulk-like Modulus (K)	73.2
Max. Fibre Straightening Stretch (Lambda)	1
Fibre Direction	Y

Table C - 19. Linear regression measures for total plot results (i.e. considering all loading regimes combined), for each input stimulus tested with the Mooney Rivlin model 2.

Input Stimuli	**R^2**	**RMSE**	**Slope**
X Stress (Sx)	0.0732	2.6860	0.1668
Y Stress (Sy)	0.2310	2.6438	0.3200
Shear Stress (Sxy)	0.0532	0.1645	0.0086
1st Invariant Stress Tensor (I1)	0.1536	4.9325	0.4642
Maximum Shear Stress (MSS)	0.1470	1.1072	0.1015
Strain Energy Density (SED)	0.1117	0.2221	0.0174
Hydrostatic Pressure (HS)	0.1357	1.8422	0.1613
1st Principal Stress (S1)	0.1152	2.5948	0.2068
2nd Principal Stress (S2)	0.1783	2.4794	0.2551
3rd Principal Stress (S3)	0.0337	2.0138	-0.0830
Deviatoric Stress 1 (Dev1)	0.0724	1.2797	0.0790
Deviatoric Stress 2 (Dev2)	0.1743	0.6250	0.0634
Deviatoric Stress 3 (Dev3)	NaN	0.0000	0.0000
Shear A	0.0018	0.6937	-0.0065
Shear B	0.1655	1.2660	0.1246
Shear C	0.1376	1.5192	0.1341
X Strain (Ex)	0.0411	3.2378	0.1482
Y Strain (Ey)	0.1592	0.3516	0.0338
Average	**0.1167**	**1.6477**	**0.1220**

C.2.1 X Stress (Sx)

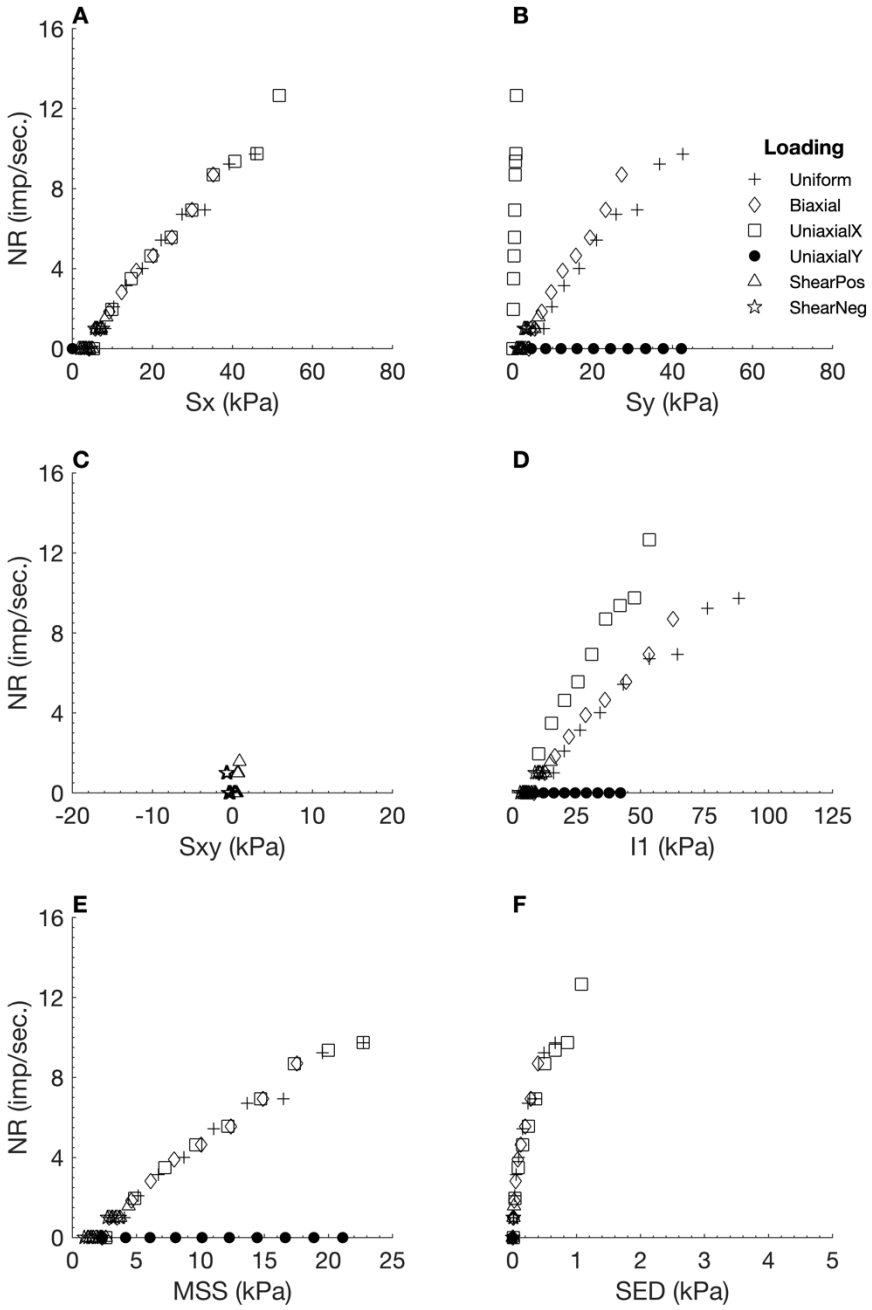

Figure C - 19. Neural responses (NR) output by the Mooney Rivlin FEBio model 2 using Sx as the neural model input, plotted against six different stress variables. Sx: X stress. Sy: Y stress. Sxy: shear stress. I1: 1st invariant stress tensor. MSS: maximum shear stress. SED: strain energy density.

Table C - 20. Linear regression measures for individual loading regime results from the Mooney Rivlin model 2, with Sx as neural model input.

Loading Regime	R^2	RMSE	Slope
Uniform	0.9598	0.6796	0.6589
Biaxial	0.1864	1.1014	2.3201
Uniaxial X	0.4892	1.7565	-0.7453
Uniaxial Y	NaN	0.0000	0.0000
Shear Positive	NaN	0.0000	0.0000
Shear Negative	NaN	0.0000	0.0000

C.2.2 Y Stress (Sy)

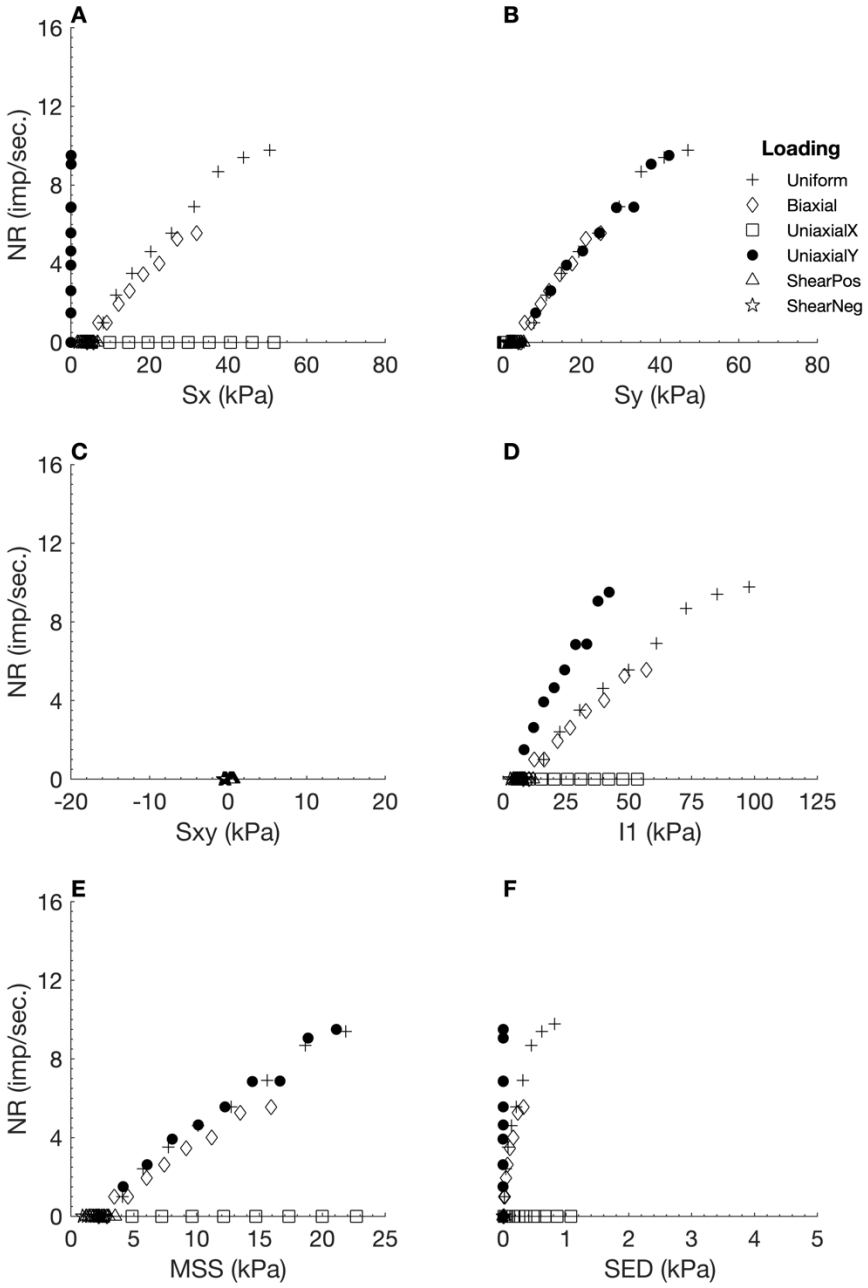

Figure C - 20. Neural responses (NR) output by the Mooney Rivlin FEBio model 2 using Sy as the neural model input, plotted against six different stress variables. Sx: X stress. Sy: Y stress. Sxy: shear stress. I1: 1st invariant stress tensor. MSS: maximum shear stress. SED: strain energy density.

Table C - 21. Linear regression measures for individual loading regime results from the Mooney Rivlin model 2, with Sy as neural model input.

Loading Regime	R^2	RMSE	Slope
Uniform	0.9882	0.4011	0.7294
Biaxial	0.3635	0.7538	2.5066
Uniaxial X	NaN	0.0000	0.0000
Uniaxial Y	0.8992	0.7363	1.4863
Shear Positive	NaN	0.0000	0.0000
Shear Negative	NaN	0.0000	0.0000

C.2.3 Shear Stress (Sxy)

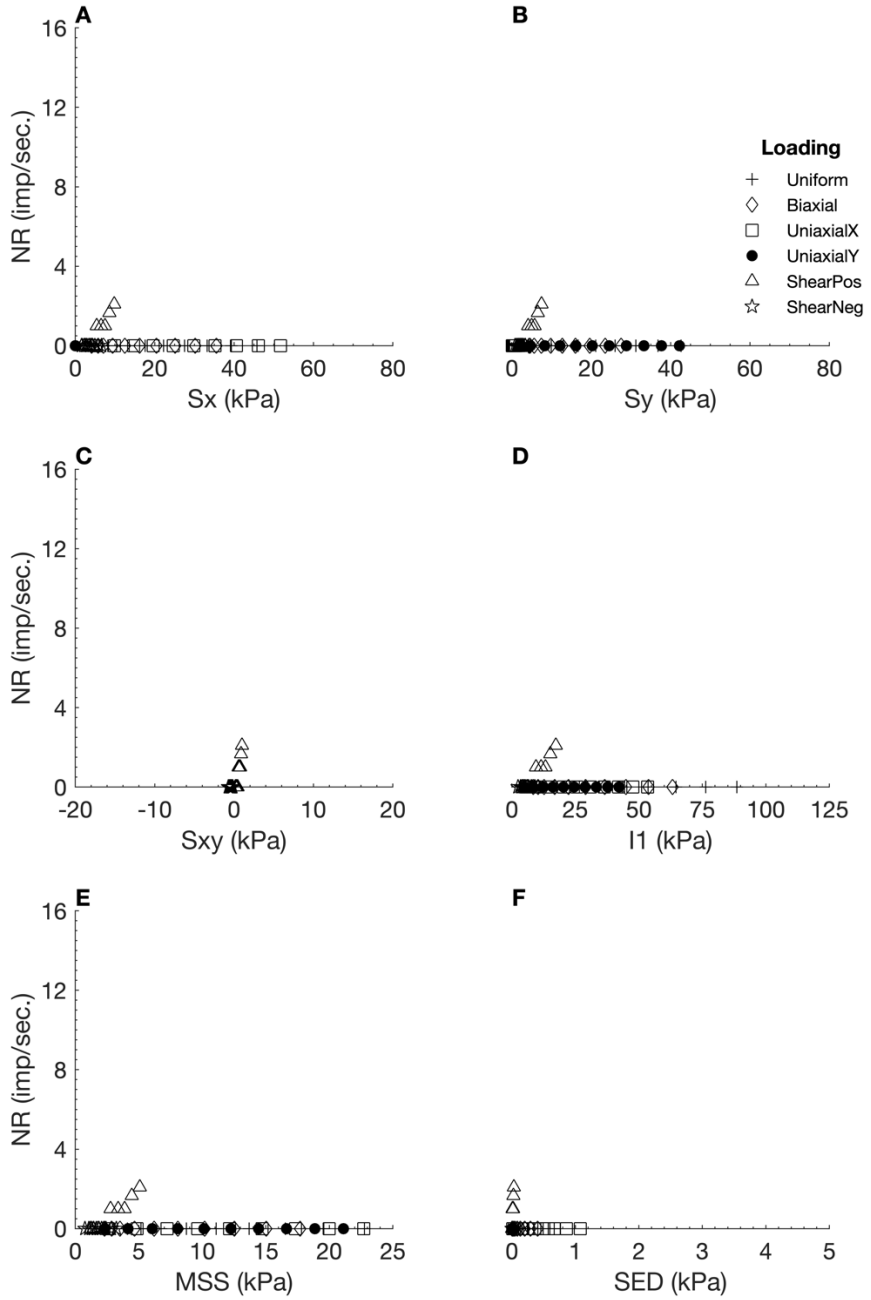

Figure C - 21. Neural responses (NR) output by the Mooney Rivlin FEBio model 2 using Sxy as the neural model input, plotted against six different stress variables. Sx: X stress. Sy: Y stress. Sxy: shear stress. I1: 1st invariant stress tensor. MSS: maximum shear stress. SED: strain energy density.

Table C - 22. Linear regression measures for individual loading regime results from the Mooney Rivlin model 2, with Sxy as neural model input.

Loading Regime	R^2	RMSE	Slope
Uniform	NaN	0.0000	0.0000
Biaxial	NaN	0.0000	0.0000
Uniaxial X	NaN	0.0000	0.0000
Uniaxial Y	NaN	0.0000	0.0000
Shear Positive	0.3035	0.3809	0.0461
Shear Negative	NaN	0.0000	0.0000

C.2.4 1st Invariant Stress Tensor (I1)

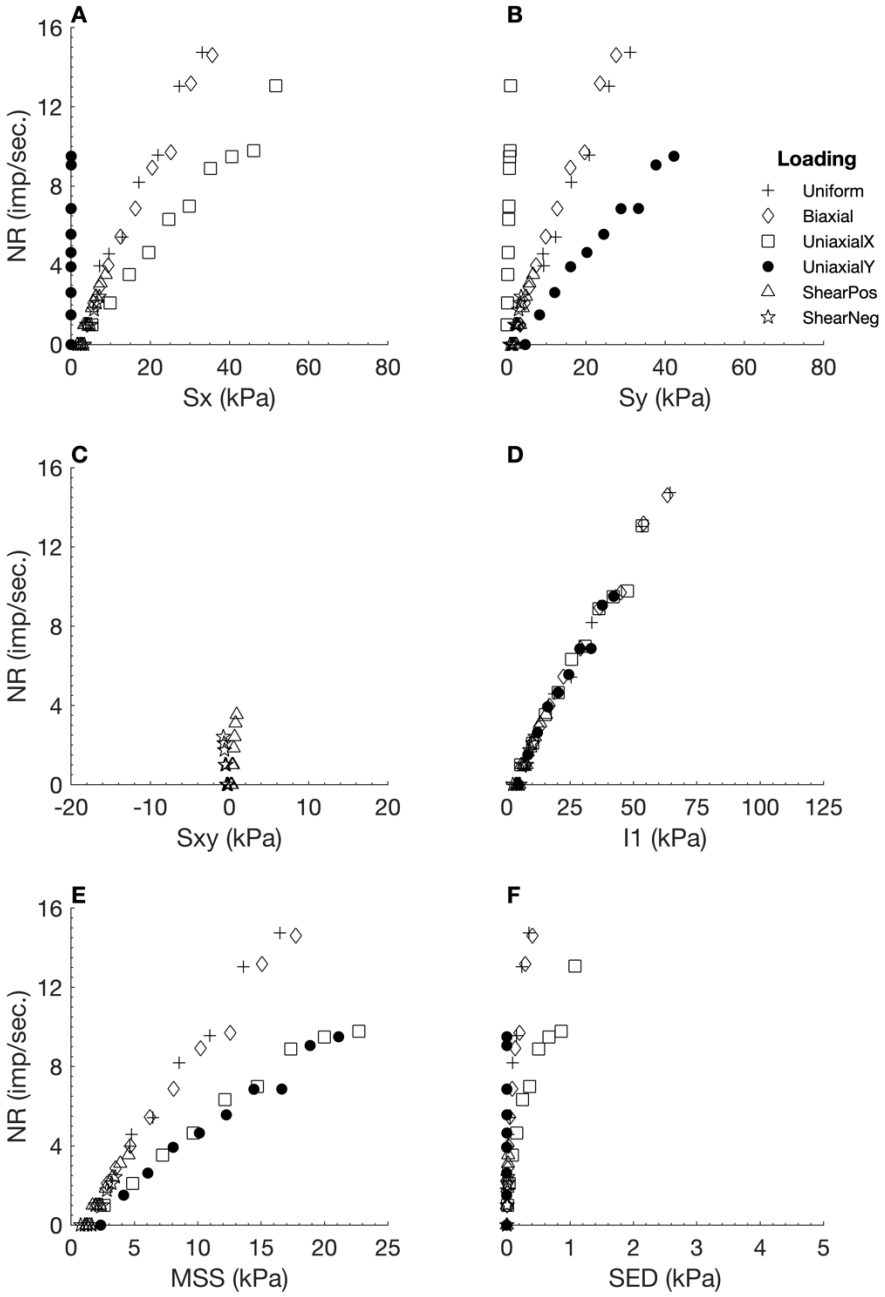

Figure C - 22. Neural responses (NR) output by the Mooney Rivlin FEBio model 2 using I1 as the neural model input, plotted against six different stress variables. Sx: X stress. Sy: Y stress. Sxy: shear stress. I1: 1st invariant stress tensor. MSS: maximum shear stress. SED: strain energy density.

Table C - 23. Linear regression measures for individual loading regime results from the Mooney Rivlin model 2, with I1 as neural model input.

Loading Regime	R^2	RMSE	Slope
Uniform	0.9767	0.8890	1.1409
Biaxial	0.2947	1.6651	4.7367
Uniaxial X	0.3590	1.5692	-0.5092
Uniaxial Y	0.8992	0.7364	1.4863
Shear Positive	0.6756	0.3488	0.0923
Shear Negative	0.2318	0.4526	0.1297

C.2.5 Maximum Shear Stress (MSS)

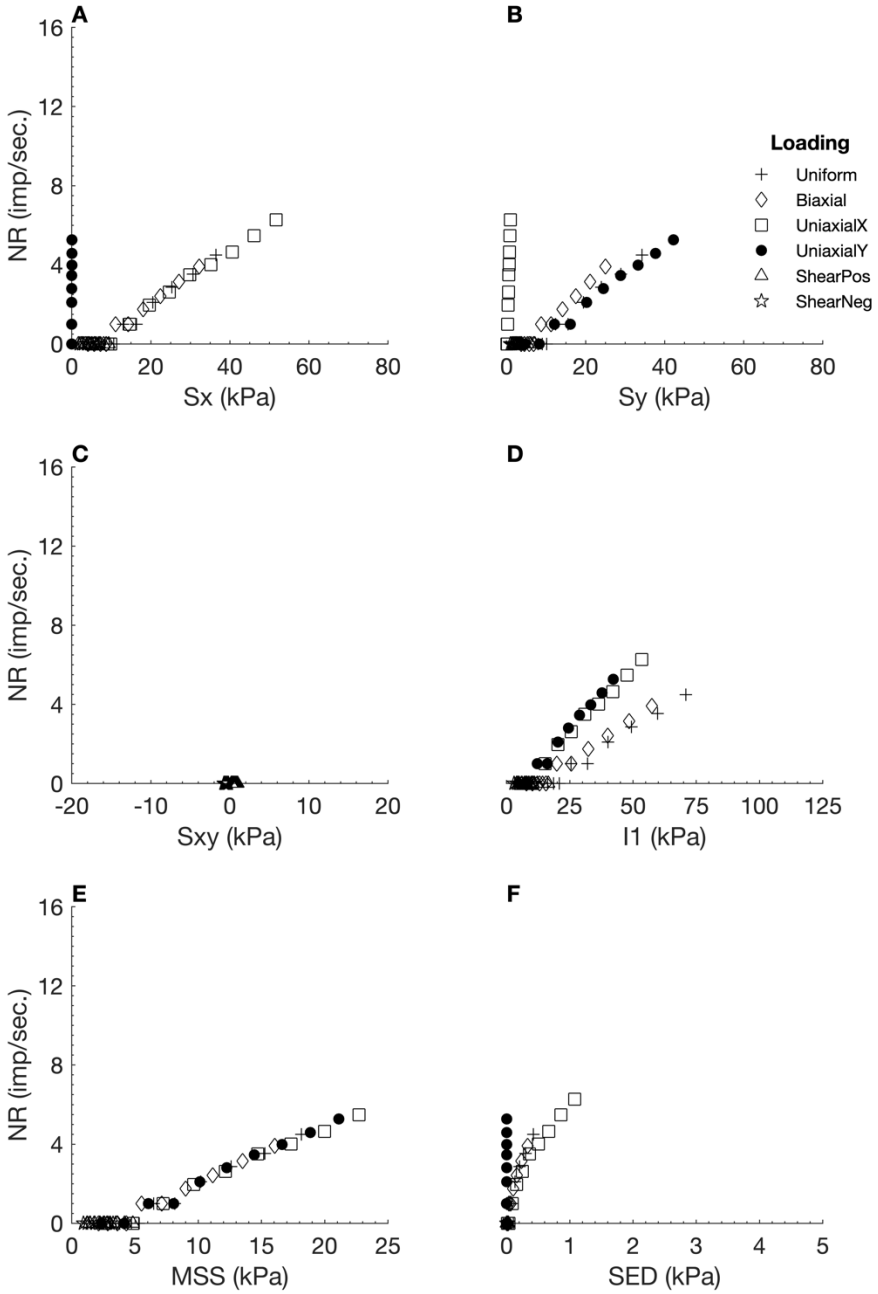

Figure C - 23. Neural responses (NR) output by the Mooney Rivlin FEBio model 2 using MSS as the neural model input, plotted against six different stress variables. Sx: X stress. Sy: Y stress. Sxy: shear stress. I1: 1st invariant stress tensor. MSS: maximum shear stress. SED: strain energy density.

Table C - 24. Linear regression measures for individual loading regime results from the Mooney Rivlin model 2, with MSS as neural model input.

Loading Regime	R^2	RMSE	Slope
Uniform	0.8307	0.7248	0.3185
Biaxial	0.0001	0.5164	-0.0233
Uniaxial X	0.1051	1.0921	-0.1623
Uniaxial Y	0.9082	0.3811	0.8099
Shear Positive	NaN	0.0000	0.0000
Shear Negative	NaN	0.0000	0.0000

C.2.6 Strain Energy Density (SED)

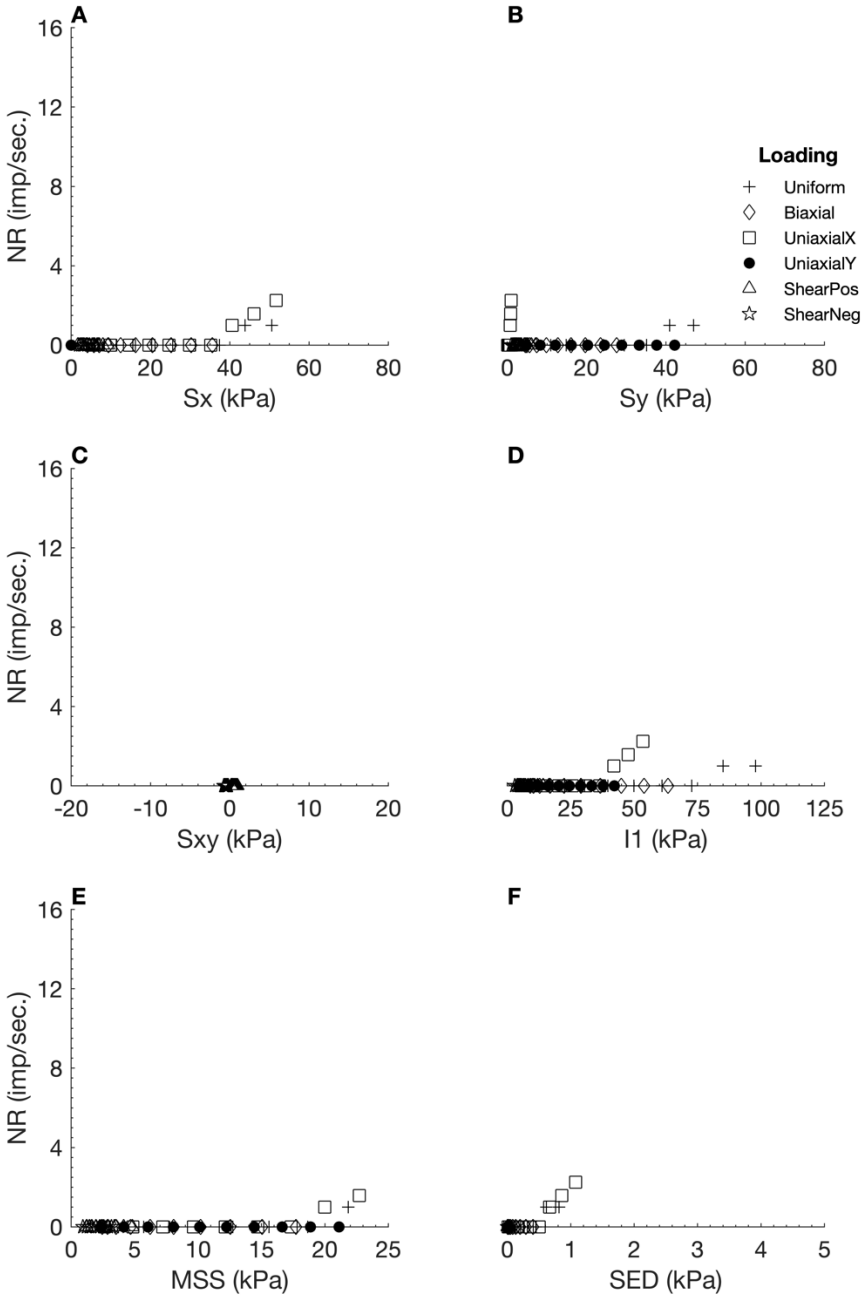

Figure C - 24. Neural responses (NR) output by the Mooney Rivlin FEBio model 2 using SED as the neural model input, plotted against six different stress variables. Sx: X stress. Sy: Y stress. Sxy: shear stress. I1: 1st invariant stress tensor. MSS: maximum shear stress. SED: strain energy density.

Table C - 25. Linear regression measures for individual loading regime results from the Mooney Rivlin model 2, with SED as neural model input.

Loading Regime	R^2	RMSE	Slope
Uniform	0.3998	0.3465	0.0561
Biaxial	NaN	0.0000	0.0000
Uniaxial X	NaN	0.0000	0.0000
Uniaxial Y	NaN	0.0000	0.0000
Shear Positive	NaN	0.0000	0.0000
Shear Negative	NaN	0.0000	0.0000

C.2.7 Hydrostatic Pressure (HS)

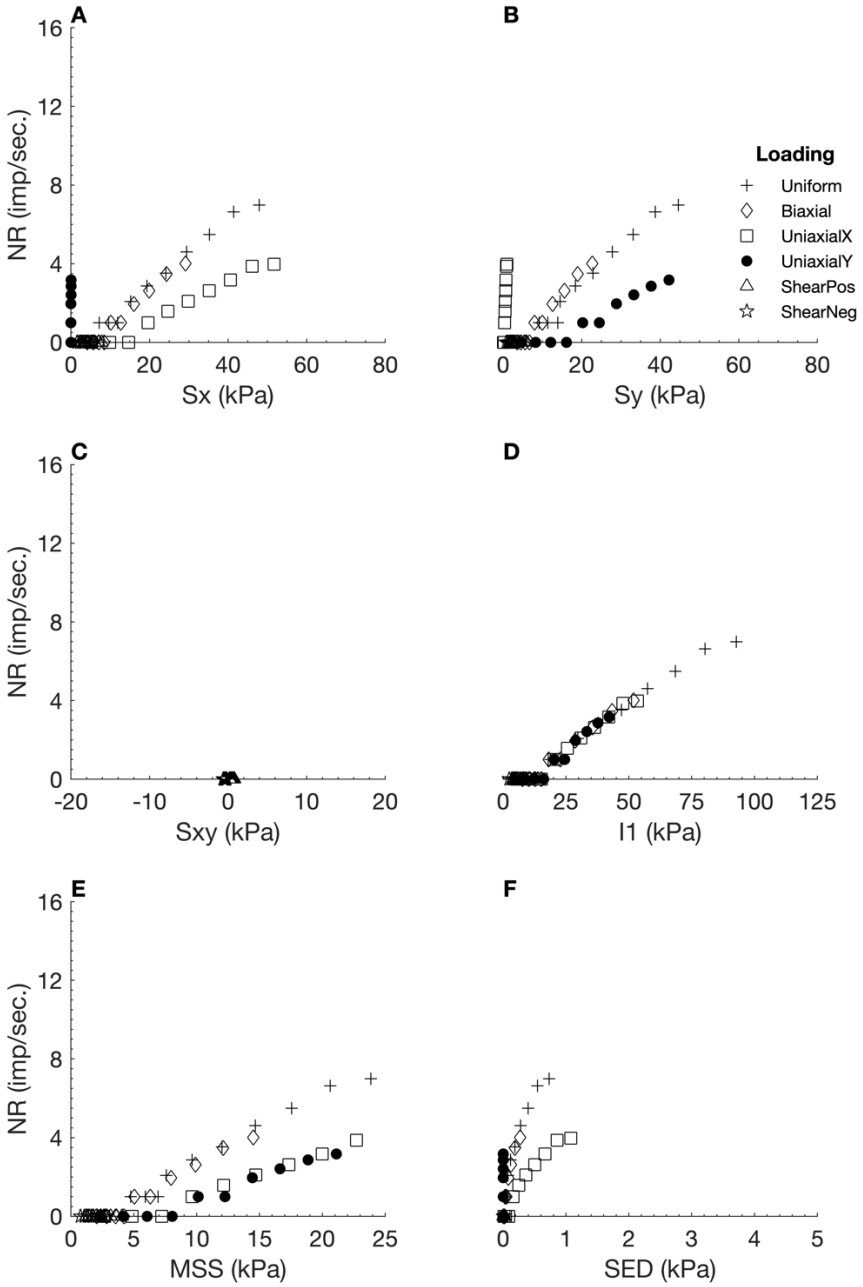

Figure C - 25. Neural responses (NR) output by the Mooney Rivlin FEBio model 2 using HS as the neural model input, plotted against six different stress variables. Sx: X stress. Sy: Y stress. Sxy: shear stress. I1: 1st invariant stress tensor. MSS: maximum shear stress. SED: strain energy density.

Table C - 26. Linear regression measures for individual loading regime results from the Mooney Rivlin model 2, with HS as neural model input.

Loading Regime	R^2	RMSE	Slope
Uniform	0.9272	0.6634	0.4695
Biaxial	0.0001	0.5164	-0.0233
Uniaxial X	0.0076	0.6100	-0.0232
Uniaxial Y	0.8107	0.2512	0.3513
Shear Positive	NaN	0.0000	0.0000
Shear Negative	NaN	0.0000	0.0000

C.2.8 1st Principle Stress (S1)

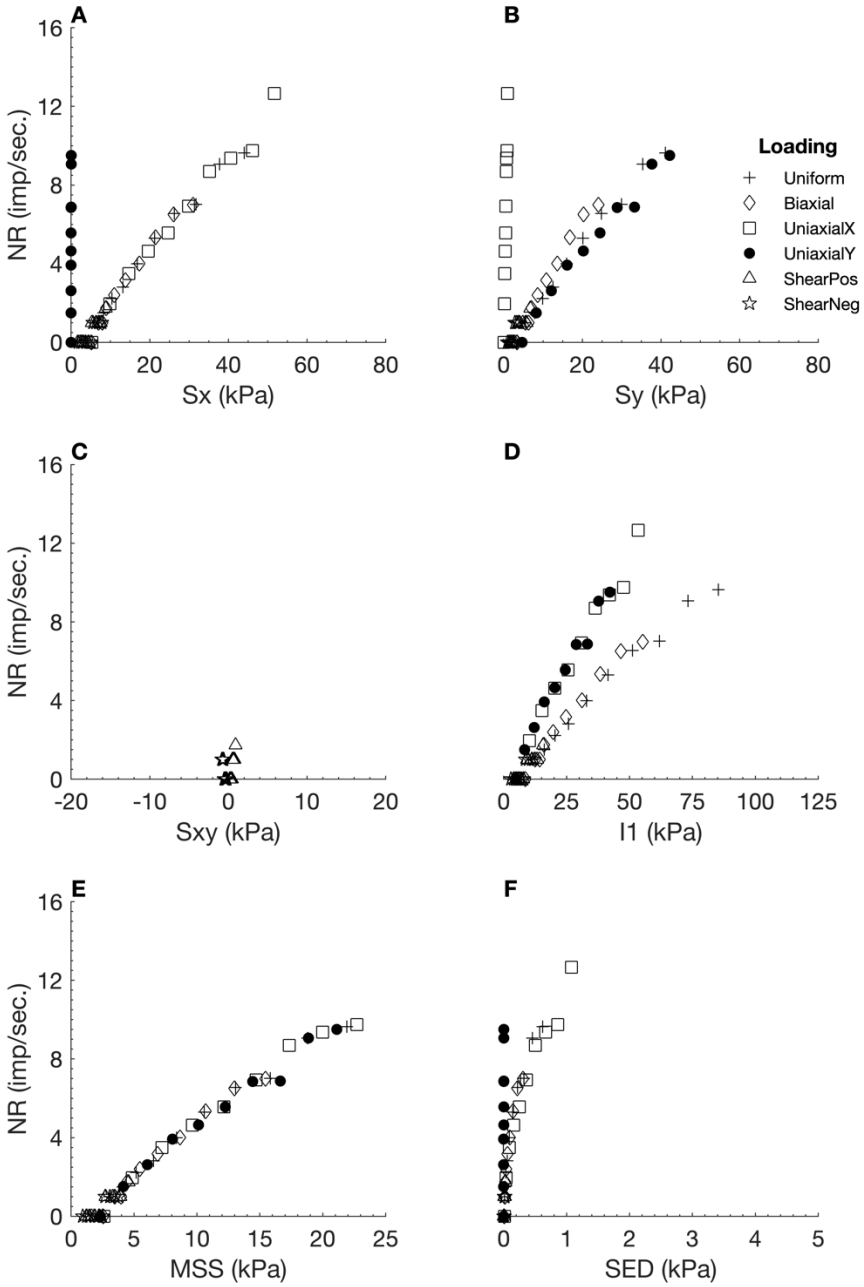

Figure C - 26. Neural responses (NR) output by the Mooney Rivlin FEBio model 2 using S1 as the neural model input, plotted against six different stress variables. Sx: X stress. Sy: Y stress. Sxy: shear stress. I1: 1st invariant stress tensor. MSS: maximum shear stress. SED: strain energy density.

Table C - 27. Linear regression measures for individual loading regime results from the Mooney Rivlin model 2, with S1 as neural model input.

Loading Regime	R^2	RMSE	Slope
Uniform	0.9547	0.6989	0.6363
Biaxial	0.2293	0.9151	2.1969
Uniaxial X	0.4892	1.7565	-0.7453
Uniaxial Y	0.8992	0.7363	1.4863
Shear Positive	NaN	0.0000	0.0000
Shear Negative	NaN	0.0000	0.0000

C.2.9 2nd Principle Stress (S2)

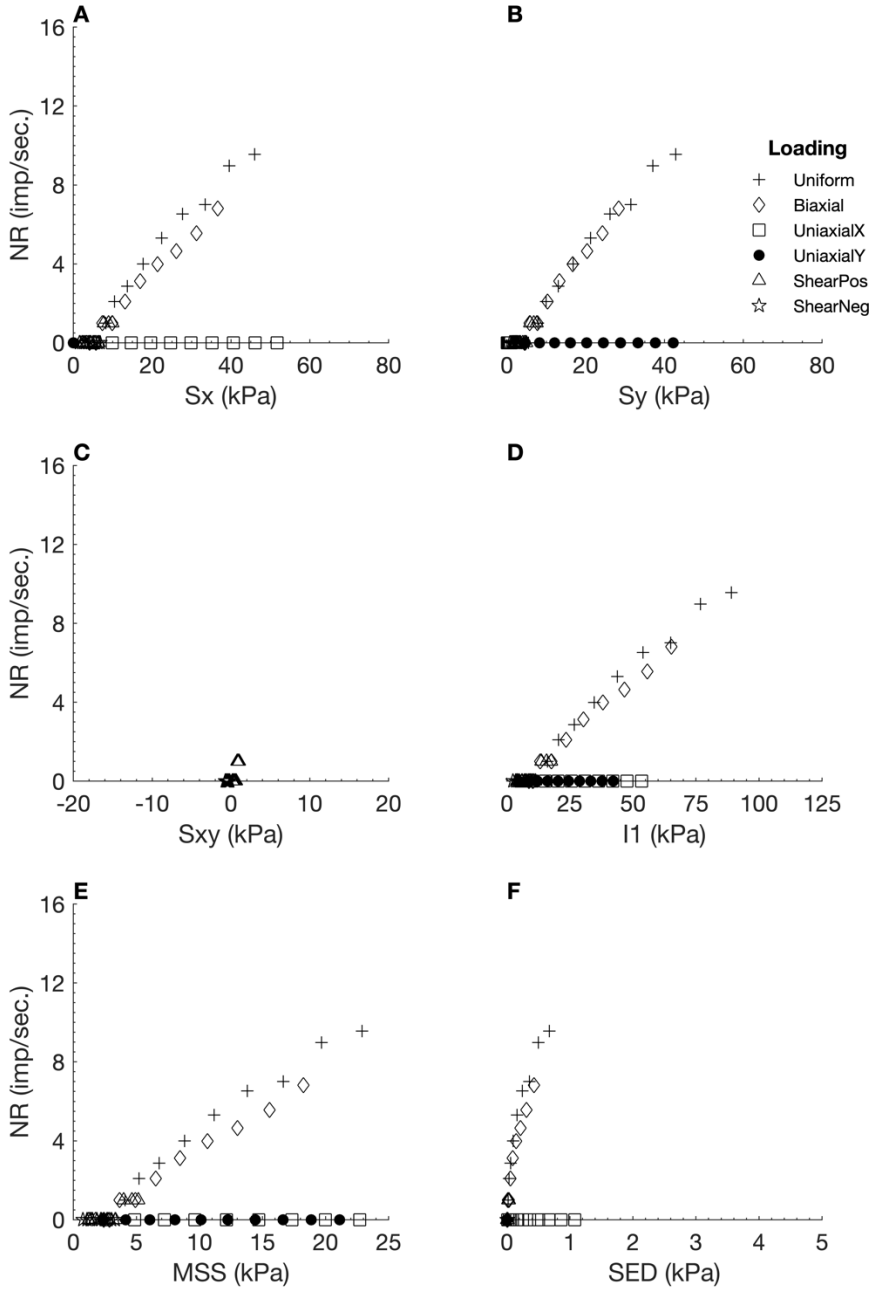

Figure C - 27. . Neural responses (NR) output by the Mooney Rivlin FEBio model 2 using S2 as the neural model input, plotted against six different stress variables. Sx: X stress. Sy: Y stress. Sxy: shear stress. I1: 1st invariant stress tensor. MSS: maximum shear stress. SED: strain energy density.

Table C - 28. Linear regression measures for individual loading regime results from the Mooney Rivlin model 2, with S2 as neural model input.

Loading Regime	R^2	RMSE	Slope
Uniform	0.9786	0.5108	0.6845
Biaxial	0.3209	0.8275	2.5032
Uniaxial X	NaN	0.0000	0.0000
Uniaxial Y	NaN	0.0000	0.0000
Shear Positive	NaN	0.0000	0.0000
Shear Negative	NaN	0.0000	0.0000

C.2.10 3rd Principle Stress (S3)

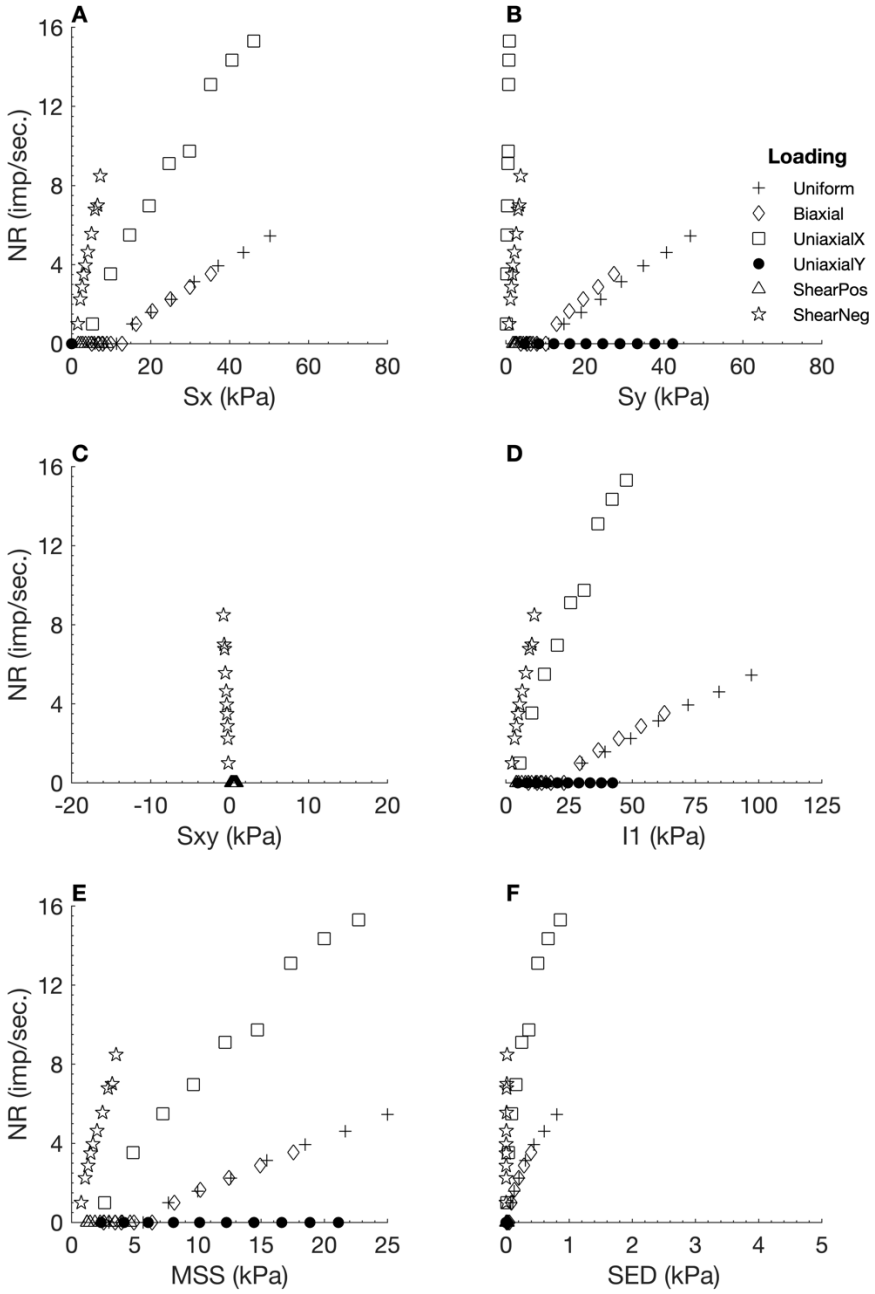

Figure C - 28. Neural responses (NR) output by the Mooney Rivlin FEBio model 2 using S3 as the neural model input, plotted against six different stress variables. Sx: X stress. Sy: Y stress. Sxy: shear stress. I1: 1st invariant stress tensor. MSS: maximum shear stress. SED: strain energy density.

Table C - 29. Linear regression measures for individual loading regime results from the Mooney Rivlin model 2, with S3 as neural model input.

Loading Regime	R^2	RMSE	Slope
Uniform	0.9258	0.5830	0.4085
Biaxial	NaN	0.0000	0.0000
Uniaxial X	0.4902	2.2589	-0.9604
Uniaxial Y	NaN	0.0000	0.0000
Shear Positive	NaN	0.0000	0.0000
Shear Negative	0.9594	0.2691	0.6826

C.2.11 Deviatoric Stress 1 (Dev1)

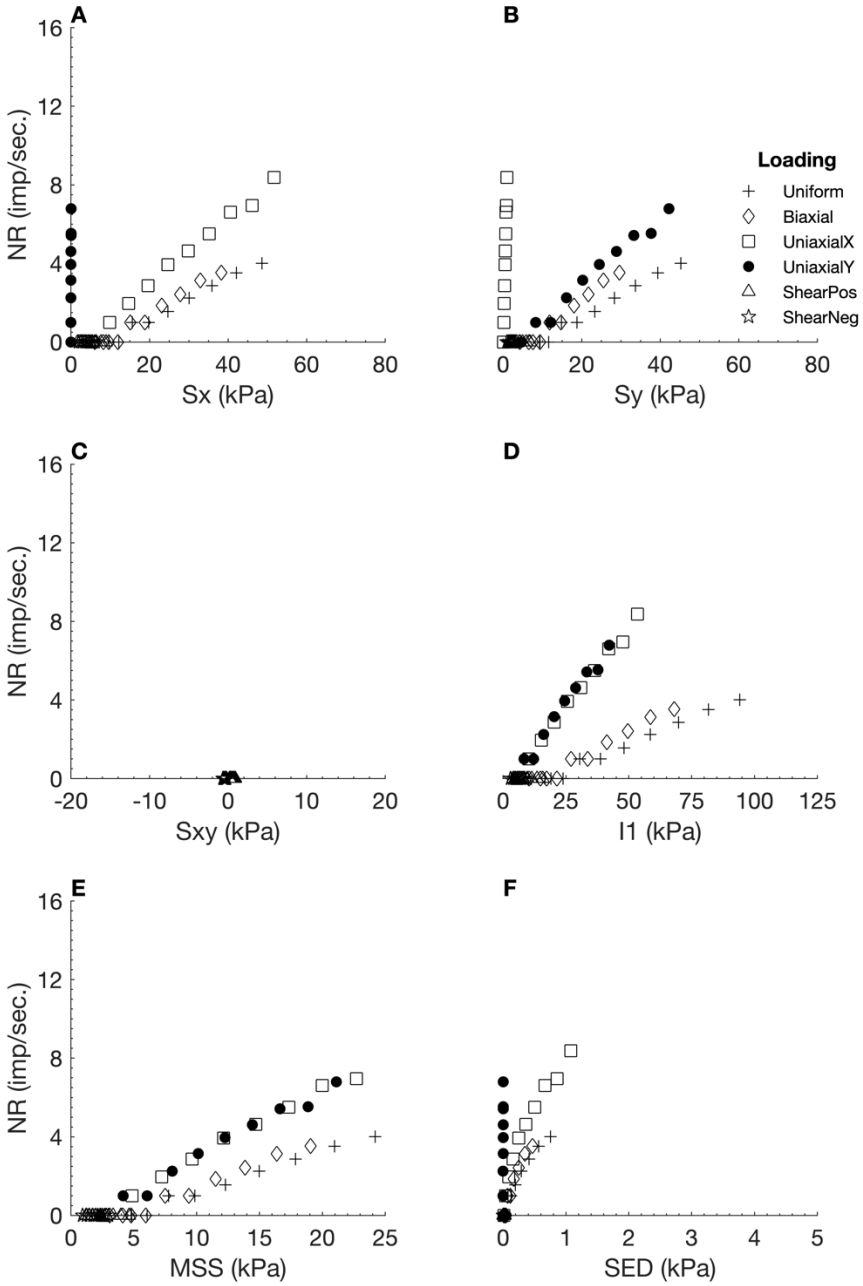

Figure C - 29. Neural responses (NR) output by the Mooney Rivlin FEBio model 2 using Dev1 as the neural model input, plotted against six different stress variables. Sx: X stress. Sy: Y stress. Sxy: shear stress. I1: 1st invariant stress tensor. MSS: maximum shear stress. SED: strain energy density.

Table C - 30. Linear regression measures for individual loading regime results from the Mooney Rivlin model 2, with Dev1 as neural model input.

Loading Regime	R^2	RMSE	Slope
Uniform	0.9153	0.4591	0.2993
Biaxial	0.0001	0.5164	-0.0233
Uniaxial X	0.3947	1.1789	-0.4127
Uniaxial Y	0.9884	0.1801	1.1209
Shear Positive	NaN	0.0000	0.0000
Shear Negative	NaN	0.0000	0.0000

C.2.12 Deviatoric Stress 2 (Dev2)

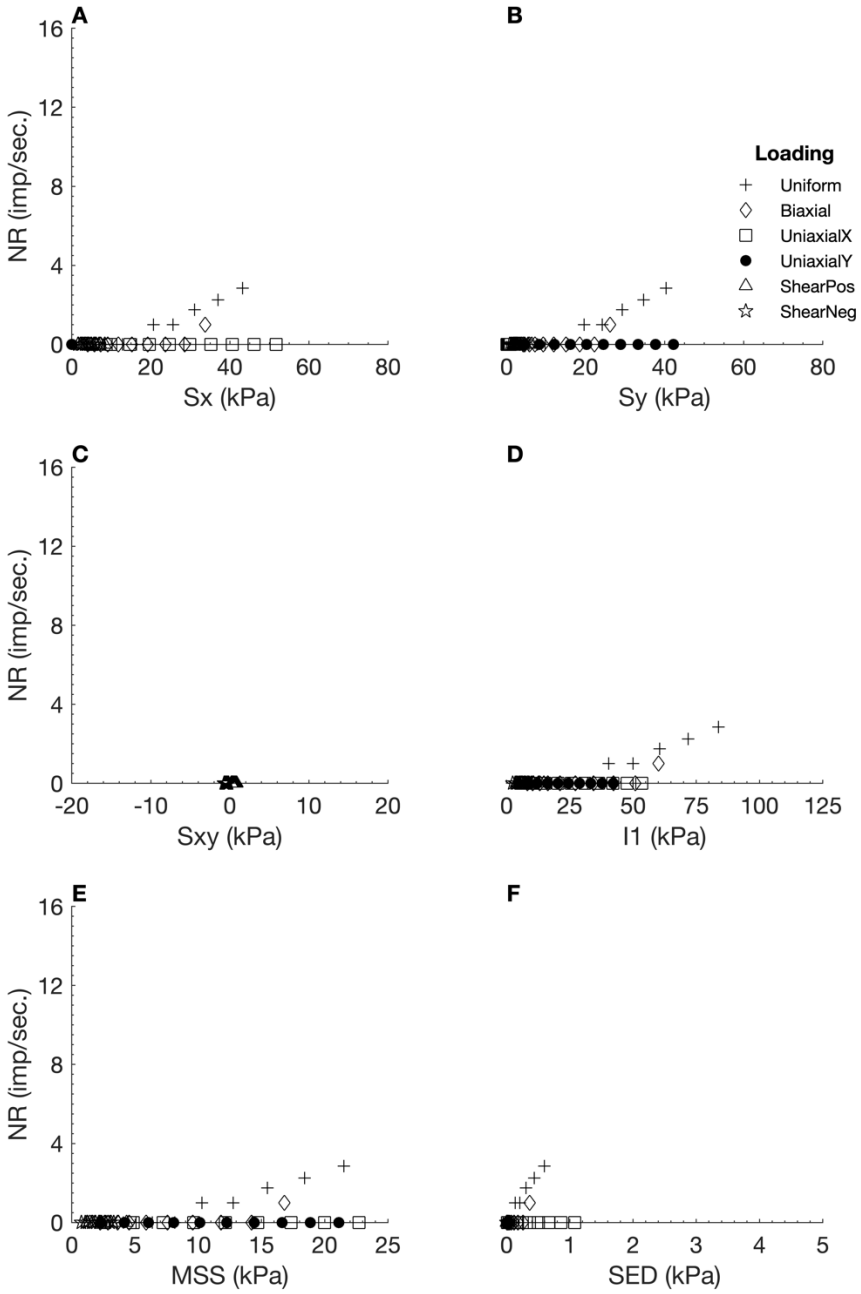

Figure C - 30. Neural responses (NR) output by the Mooney Rivlin FEBio model 2 using Dev2 as the neural model input, plotted against six different stress variables. Sx: X stress. Sy: Y stress. Sxy: shear stress. I1: 1st invariant stress tensor. MSS: maximum shear stress. SED: strain energy density.

Table C - 31. Linear regression measures for individual loading regime results from the Mooney Rivlin model 2, with Dev2 as neural model input.

Loading Regime	R^2	RMSE	Slope
Uniform	0.7936	0.5185	0.2017
Biaxial	NaN	0.0000	0.0000
Uniaxial X	NaN	0.0000	0.0000
Uniaxial Y	NaN	0.0000	0.0000
Shear Positive	NaN	0.0000	0.0000
Shear Negative	NaN	0.0000	0.0000

C.2.13 Deviatoric Stress 3 (Dev3)

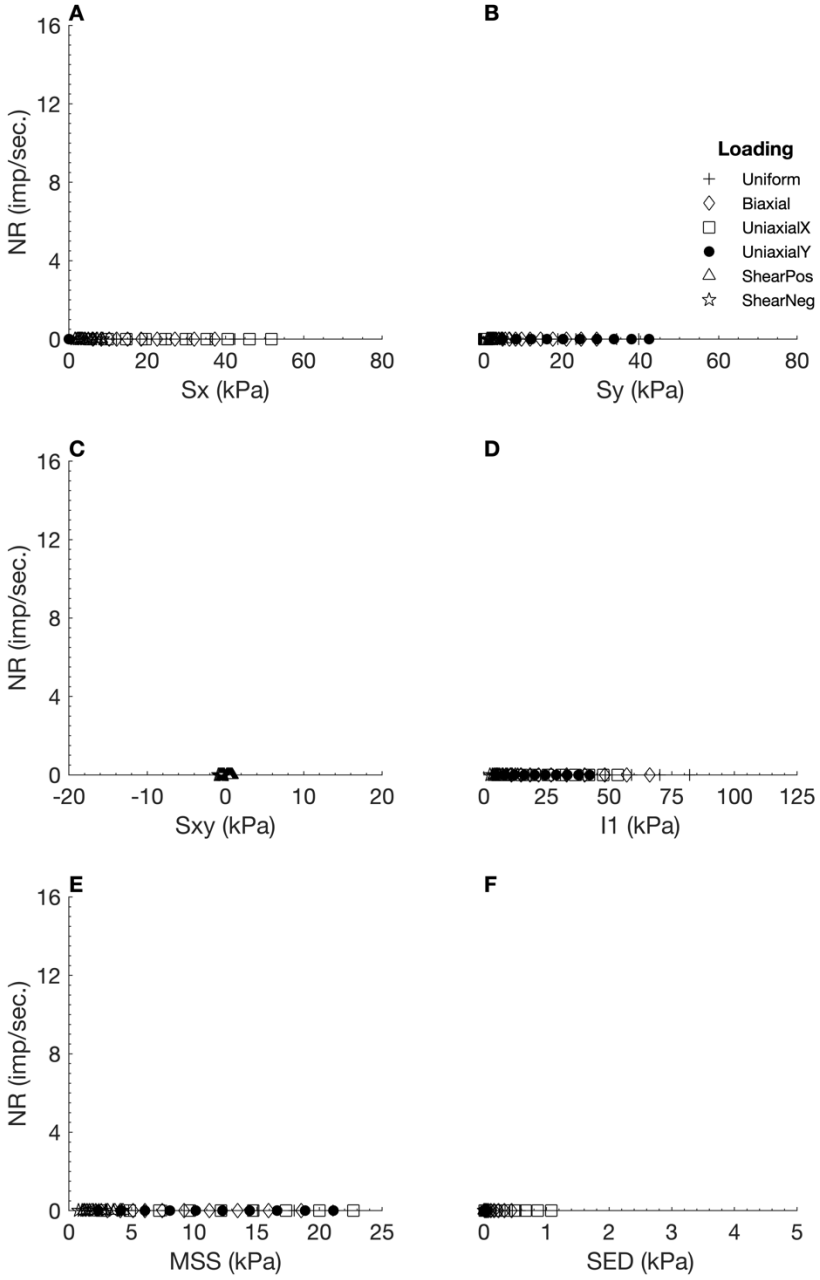

Figure C - 31. Neural responses (NR) output by the Mooney Rivlin FEBio model 2 using Dev3 as the neural model input, plotted against six different stress variables. Sx: X stress. Sy: Y stress. Sxy: shear stress. I1: 1st invariant stress tensor. MSS: maximum shear stress. SED: strain energy density.

Table C - 32. Linear regression measures for individual loading regime results from the Mooney Rivlin model 2, with Dev3 as neural model input.

Loading Regime	R^2	RMSE	Slope
Uniform	NaN	0.0000	0.0000
Biaxial	NaN	0.0000	0.0000
Uniaxial X	NaN	0.0000	0.0000
Uniaxial Y	NaN	0.0000	0.0000
Shear Positive	NaN	0.0000	0.0000
Shear Negative	NaN	0.0000	0.0000

C.2.14 Shear Stress A

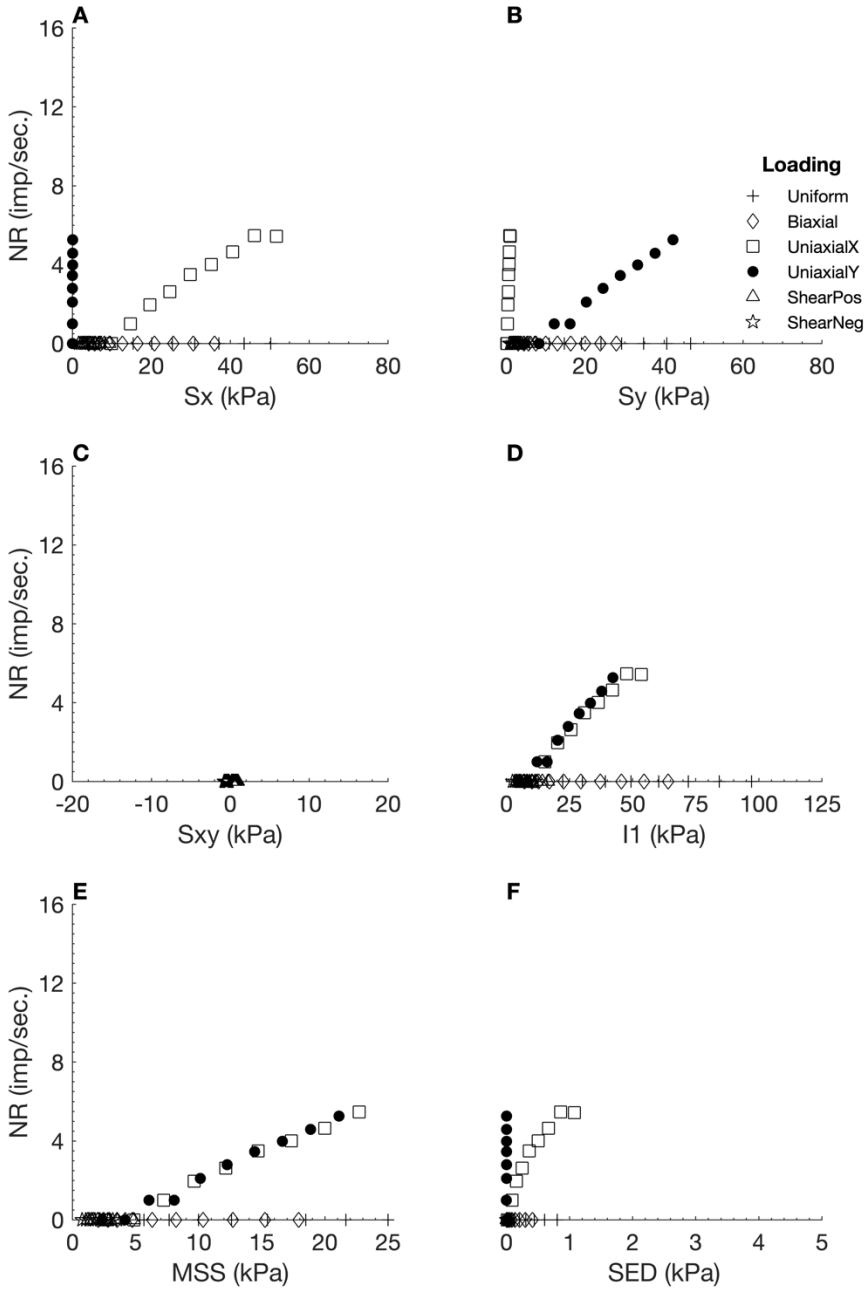

Figure C - 32. Neural responses (NR) output by the Mooney Rivlin FEBio model 2 using ShearA as the neural model input, plotted against six different stress variables. Sx: X stress. Sy: Y stress. Sxy: shear stress. I1: 1st invariant stress tensor. MSS: maximum shear stress. SED: strain energy density.

Table C - 33. Linear regression measures for individual loading regime results from the Mooney Rivlin model 2, with ShearA as neural model input.

Loading Regime	R^2	RMSE	Slope
Uniform	NaN	0.0000	0.0000
Biaxial	NaN	0.0000	0.0000
Uniaxial X	0.1053	1.0903	-0.1622
Uniaxial Y	0.9081	0.3808	0.8088
Shear Positive	NaN	0.0000	0.0000
Shear Negative	NaN	0.0000	0.0000

C.2.15 Shear Stress B

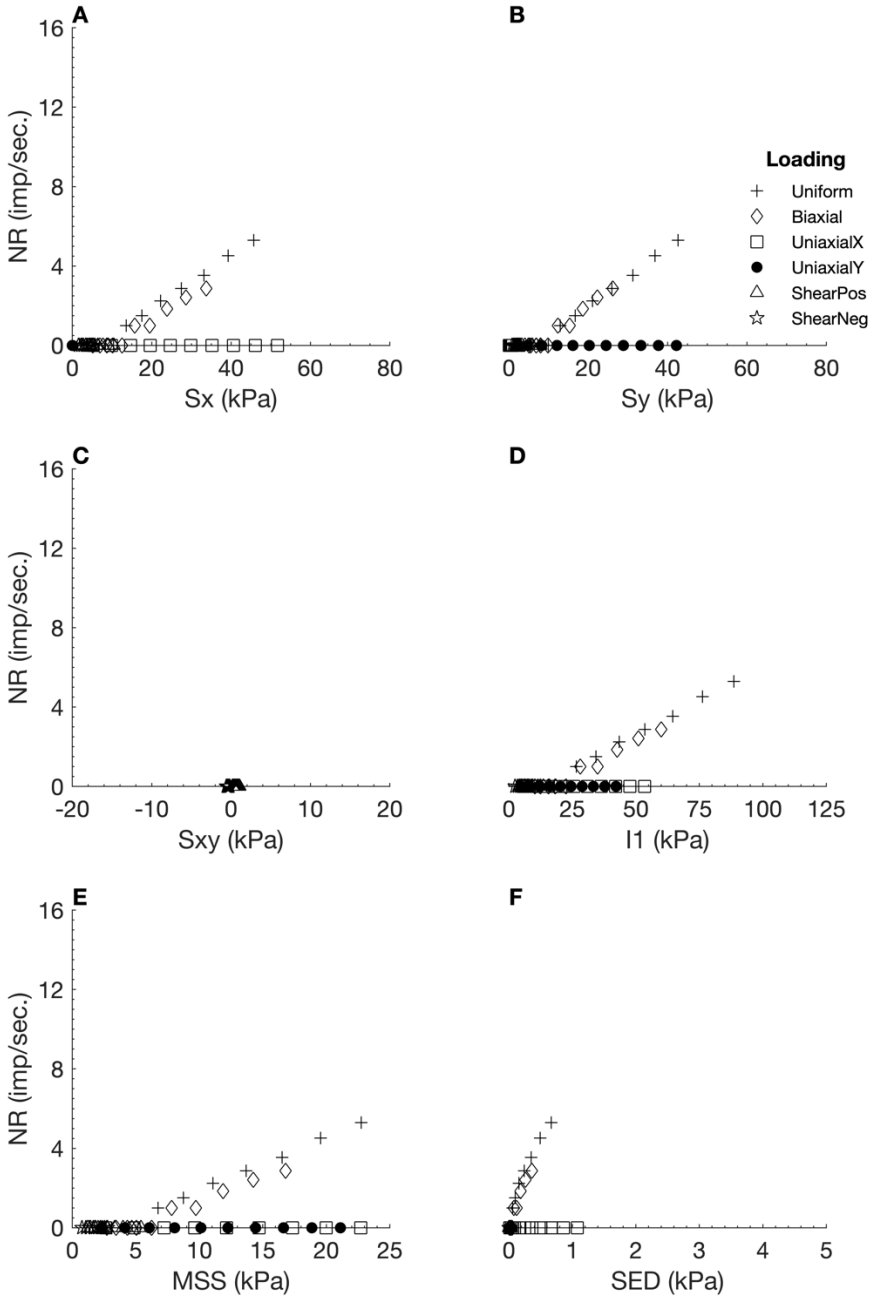

Figure C - 33. Neural responses (NR) output by the Mooney Rivlin FEBio model 2 using ShearB as the neural model input, plotted against six different stress variables. Sx: X stress. Sy: Y stress. Sxy: shear stress. I1: 1st invariant stress tensor. MSS: maximum shear stress. SED: strain energy density.

Table C - 34. Linear regression measures for individual loading regime results from the Mooney Rivlin model 2, with ShearB as neural model input.

Loading Regime	R^2	RMSE	Slope
Uniform	0.9210	0.5756	0.3898
Biaxial	NaN	0.0000	0.0000
Uniaxial X	NaN	0.0000	0.0000
Uniaxial Y	NaN	0.0000	0.0000
Shear Positive	NaN	0.0000	0.0000
Shear Negative	NaN	0.0000	0.0000

C.2.16 Shear Stress C

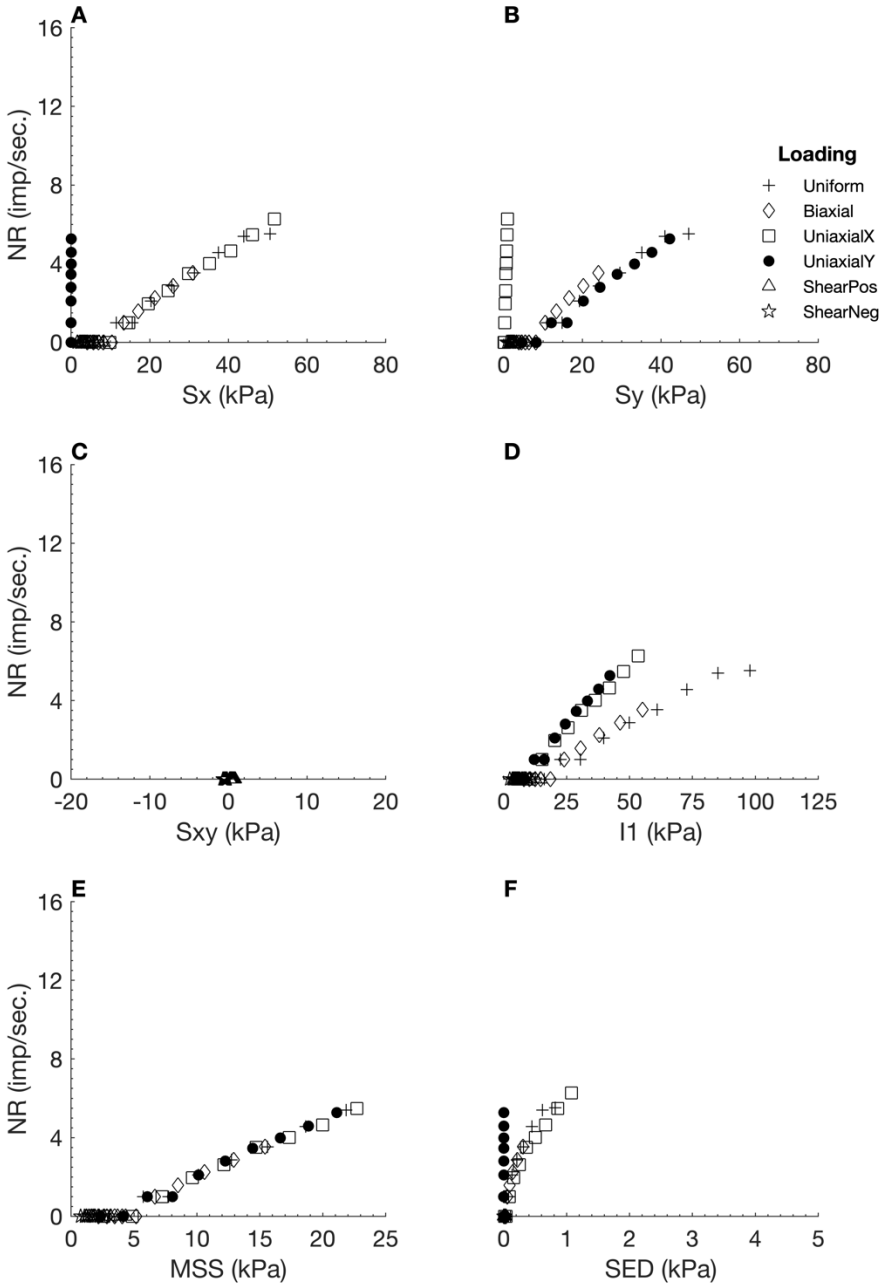

Figure C - 34. Neural responses (NR) output by the Mooney Rivlin FEBio model 2 using ShearC as the neural model input, plotted against six different stress variables. Sx: X stress. Sy: Y stress. Sxy: shear stress. I1: 1st invariant stress tensor. MSS: maximum shear stress. SED: strain energy density.

Table C - 35. Linear regression measures for individual loading regime results from the Mooney Rivlin model 2, with ShearC as neural model input.

Loading Regime	R^2	RMSE	Slope
Uniform	0.9648	0.4199	0.4358
Biaxial	NaN	0.0000	0.0000
Uniaxial X	0.1051	1.0921	-0.1623
Uniaxial Y	0.9082	0.3811	0.8099
Shear Positive	NaN	0.0000	0.0000
Shear Negative	NaN	0.0000	0.0000

C.2.17 X Strain (Ex)

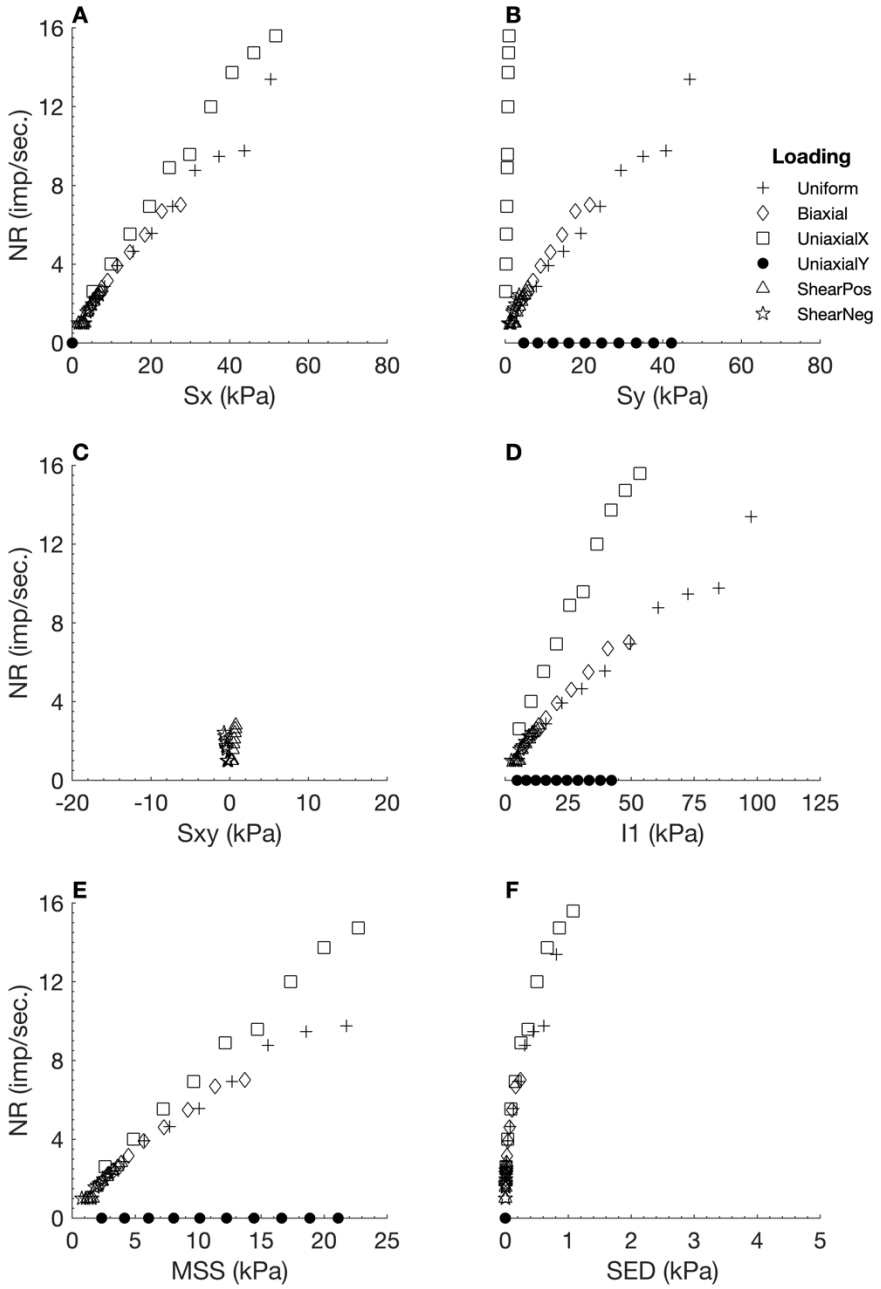

Figure C - 35. Neural responses (NR) output by the Mooney Rivlin FEBio model 2 using Ex as the neural model input, plotted against six different stress variables. Sx: X stress. Sy: Y stress. Sxy: shear stress. I1: 1st invariant stress tensor. MSS: maximum shear stress. SED: strain energy density.

Table C - 36. Linear regression measures for individual loading regime results from the Mooney Rivlin model 2, with Ex as neural model input.

Loading Regime	R^2	RMSE	Slope
Uniform	0.9208	1.0607	0.7176
Biaxial	0.2366	0.5191	1.2719
Uniaxial X	0.3705	1.8174	-0.6045
Uniaxial Y	NaN	0.0000	0.0000
Shear Positive	0.5234	0.2908	0.0559
Shear Negative	0.2318	0.2579	0.0739

C.2.18 Y Strain (Ey)

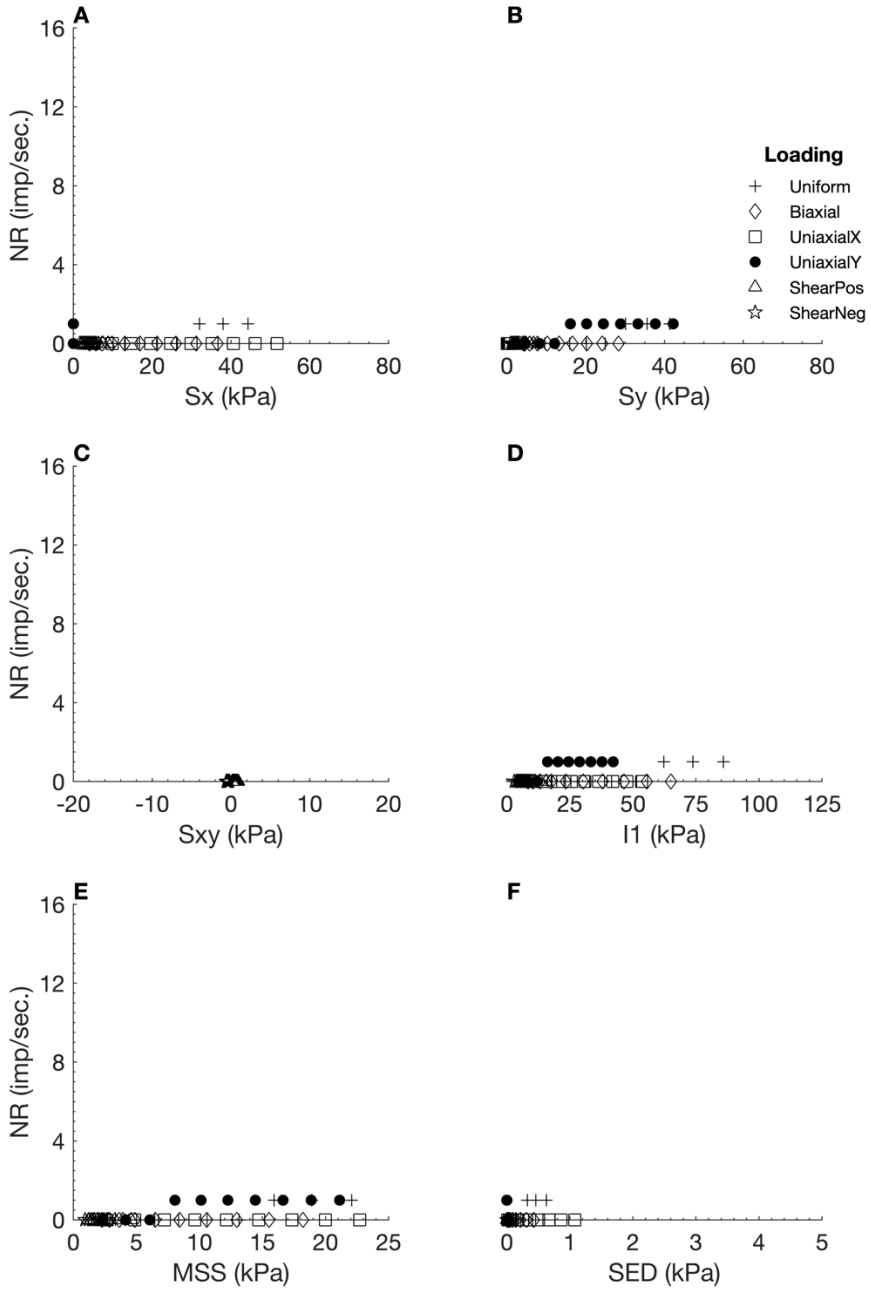

Figure C - 36. Neural responses (NR) output by the Mooney Rivlin FEBio model 2 using Ey as the neural model input, plotted against six different stress variables. Sx: X stress. Sy: Y stress. Sxy: shear stress. I1: 1st invariant stress tensor. MSS: maximum shear stress. SED: strain energy density.

Table C - 37. Linear regression measures for individual loading regime results from the Mooney Rivlin model 2, with Ey as neural model input.

Loading Regime	R^2	RMSE	Slope
Uniform	0.5703	0.3358	0.0767
Biaxial	NaN	0.0000	0.0000
Uniaxial X	NaN	0.0000	0.0000
Uniaxial Y	0.7874	0.2824	0.3672
Shear Positive	NaN	0.0000	0.0000
Shear Negative	NaN	0.0000	0.0000

Appendix D: Matlab Code

The relevant Matlab scripts that were developed and/or adapted for this project are included in this appendix.

D.1 HH_ruffini.m

```
function [V, I_ST] = HH_ruffini( stresses, dt)
%        [V, I_ST] = HH_ruffini( stresses, dt, varargs)
%
% Function for calculating the cell membranne potential V (mV) of a ruffini
% neuron given a time series of stresses (kPa) and a time step dt (ms) (ie
% the sampling period).
% Based on the work of Xu et al 1996 on nociception of skin
% Code adapted from http://andysbrainblog.blogspot.com/2013/10/introduction-
to-computational-modeling.html
% Adapted for ruffini neurons 2019, Daina Ross, Kenneth Pope

%% write some code to parse the inputs
assert( isvector( stresses), 'stresses must be a vector of stresses');
assert( isscalar( dt), 'dt must be a scalar');
assert( dt > 0, 'dt must be positive');

% extract useful information
Ns = numel( stresses);

%% Constants and definitions
% Hogdkin Huxley constants
Cnst_Cm = 1;         % uF/cm^2; Membrane Capcitance;  Cm=0.01
Cnst_ENa = 55;       % mv; Na reversal potential;  ENa=55
Cnst_EK = -72;       % mv; K reversal potential; EK=-72
Cnst_El = 10;        % mv; Leakage reversal potential; El=10;
Cnst_gbarNa = 120;   % mS/cm^2; Na conductance gbar; Na=1.2
Cnst_gbarK = 36;     % mS/cm^2; K conductance gbar
Cnst_gbarl = 0.3;    % mS/cm^2; Leakage conductance gbarl
Cnst_gbarA = 47.7;

% original code from Gwen made these comments
% Cnst_ENa controls amplitude of voltage
% Cnst_El controls firing frequency

% Shapiro and Lenherr 1972 vary epsilon between 1 and 10
epsilon = 1;         % default value is 1, not sure why
```

```
% fudge factor introduced by Xu to stop firing below threshold value. This
% influences the threshold of firing.
% If Cnst_ENa=50, I_shift = -1
% If Cnst_ENa=55, I_shift = -4
% If Cnst_ENa=100, I_shift = -15
I_shift = -4;

% experimental conditions
V0 = -40;       % initial membrane voltage

% These are defined but never used, delete them?
% REF_I = 0.00;   % external applied current
% GL = 0.3;

% These determine the mapping from stress to current I_ST
Ch1 = 0.382;
Ch2 = 0.064;
Ch3 = 0.355;
FF = 1; % Fudge factor to scale stress input to the I_ST value necessary for
an output response
MN = 25;  % Our magic number to scale how far above threshold we are to
sensible current

% Not sure what these are
VA = -50;       % default value is -50
A_fac = 7;
B_fac = 7;
m_fac = 0.263;
h_fac = 0.263;
n_fac = 2.63;
k = 0.15;       % This influences the rate of firing, range 0.03 to 0.15 is
reasonable

%% calculate the outputs
% make space for the state variables and the output
A = zeros( 1, Ns);
B = zeros( 1, Ns);
n = zeros( 1, Ns);
m = zeros( 1, Ns);
h = zeros( 1, Ns);
I_ST = zeros( 1, Ns);
alpha_n = zeros( 1, Ns);
```

```
beta_n = zeros( 1, Ns);
alpha_m = zeros( 1, Ns);
beta_m = zeros( 1, Ns);
alpha_h = zeros( 1, Ns);
beta_h = zeros( 1, Ns);
alpha_A = zeros( 1, Ns);
beta_A = zeros( 1, Ns);
alpha_B = zeros( 1, Ns);
beta_B = zeros( 1, Ns);
V = [ V0 zeros( 1, Ns - 1)];

% loop over time
for ti = 1:( Ns - 1)

    % Calculate the HH model - lots of magic numbers etc :-(
    % Equations 12, 13, 20, 21, 23, 24
    alpha_n( ti) = (1/n_fac) * (epsilon*( -.01 * ( (50+V(ti)) / (exp(-
(V(ti)+50)/10)-1) )));
    beta_n( ti) = (1/n_fac) * ( epsilon*(.125*exp((-(V(ti)+60)/80))));
    alpha_m( ti) = (1/m_fac) * (-0.1*( (V(ti)+35) / (exp(-(V(ti)+35)/10)-1)
));
    beta_m( ti) = (1/m_fac) * (4*exp(-(V(ti)+60)/18));
    alpha_h( ti) = (1/h_fac) * (0.07*exp(-(V(ti)+60)/20));
    beta_h( ti) = (1/h_fac) * (1/(exp(-(V(ti)+30)/10)+1));
    % more equations
    A_inf =
((0.0761*exp((V(ti)+94.22)/31.84))/(1+exp((V(ti)+1.17)/28.93)))^(1/3);
    Ta_A = A_fac*(0.3632+(1.158/(1+exp((V(ti)+55.96)/20.12))));
    alpha_A( ti) = A_inf/Ta_A;
    beta_A( ti) = (1-A_inf)/Ta_A;
    B_inf = (1/(1+exp((V(ti)+53.3)/14.54)))^4;
    Ta_B = B_fac*(1.24+(2.678/(1+exp((V(ti)+50)/16.027))));
    alpha_B( ti) = B_inf/Ta_B;
    beta_B( ti) = (1-B_inf)/Ta_B;

    % Handle initial conditions for A, B, n, m and h separately
    if ti == 1
        A(1) = alpha_A( 1) / ( alpha_A( 1) + beta_A( 1));
        B(1) = alpha_B( 1) / ( alpha_B( 1) + beta_B( 1));
        n(1) = alpha_n( 1) / ( alpha_n( 1) + beta_n( 1)); % equation 9
        m(1) = alpha_m( 1) / ( alpha_m( 1) + beta_m( 1)); % equation 18
        h(1) = alpha_h( 1) / ( alpha_h( 1) + beta_h( 1)); % equation 18
    end
```

```
    % calculate I_ST (total stimulation-induced current, comprised of
    % current from heat, mechanical and chemical gated ion-channels)
    % Based off of the temperature-sensitive nociceptors
    IST_min = 0.737;      % I_ST min value that produces firing
    IST_max = 30.2631;    % I_ST max value that produces firing
    mech_min = 5;         % min stress threshold reported by Khalsa (5)
    mech_max = 125;       % max stress threshold reported by Khalsa (125)
%     mech_min = 0;       % min strain threshold reported by Khalsa (0)
%     mech_max = 0.08;    % max strain threshold reported by Khalsa (0.8)

    I_ST( ti) = ((((stresses( ti) - mech_min) * ( IST_max - IST_min)) / (
mech_max - mech_min)) + IST_min) + I_shift;
%     I_ST( ti) = stresses( ti) * FF + I_shift;
%     I_ST( ti) = ( Ch1 * exp((( stresses( ti) - 5) / 5) / Ch2) + Ch3) +
I_shift;

    %  calculate the currents
    I_Na = ( m( ti)^3) * Cnst_gbarNa * h(ti) * ( V(ti) - Cnst_ENa); %
equations 3 and 14
    I_K = ( n( ti)^4) * Cnst_gbarK * ( V( ti) - Cnst_EK); % equations 4 and 6
    I_L = Cnst_gbarl * ( V( ti) - Cnst_El); % equation 5
    I_k2 = Cnst_gbarA * ( A( ti)^3) * B( ti) * ( V(ti) - VA); % not sure
about VA
    I_ion = I_ST( ti) - I_K - I_Na - I_L - I_k2;

    % calculate initial conditions for next time sample
    % using the derivatives from the Euler first order approximation
    V( ti+1) = V( ti) + dt * I_ion/Cnst_Cm;
    n( ti+1) = n( ti) + dt * (( alpha_n( ti) * (1-n( ti)) - beta_n( ti) * n(
ti))*k); % equation 7
    m( ti+1) = m( ti) + dt * (( alpha_m( ti) * (1-m( ti)) - beta_m( ti) * m(
ti))*k); % equation 15
    h( ti+1) = h( ti) + dt * (( alpha_h( ti) * (1-h( ti)) - beta_h( ti) * h(
ti))*k); % equation 16
    A( ti+1) = A( ti) + dt * ( alpha_A( ti) * (1-A( ti)) - beta_A( ti) * A(
ti)); % for Ik2
    B( ti+1) = B( ti) + dt * ( alpha_B( ti) * (1-B( ti)) - beta_B( ti) * B(
ti)); % for Ik2

end
```

D.2 Pipeline.m

```
% pipeline for running feobio and analysing the results automatically
% Developed to replicate Khalsa et al. (1996) experiment
% Written 2019 by Kenneth Pope, adapted 2019 by Daina Ross

%% definitions

% what experiments do we want to run
loading_forces = linspace( 0, 1, 10);
experiments( 1).type = 'Uniform'; % etc etc
experiments( 2).type = 'Biaxial';
experiments( 3).type = 'Uniaxial X';
experiments( 4).type = 'Uniaxial Y';
experiments( 5).type = '+Shear';
experiments( 6).type = '-Shear';

% definitions
folder = '/Users/dainaross/Desktop/Uni/Masters/Practical/Testing';
febio_files = { 'khalsa_uniform_matlab', 'khalsa_biaxial_matlab', ...
    'khalsa_uniaxial_x_matlab', 'khalsa_uniaxial_y_matlab', ...
    'khalsa_pos_shear_matlab', 'khalsa_neg_shear_matlab'};

subplots = { '321', 'sx'; '322', 'sy'; '323', 'sxy'; ...
    '324', 'I1'; '325', 'MSS'; '326', 'sed'};

% display definitions
display_variables = { 'Sx', 'Sy', 'Sxy', 'I1', 'MSS', 'SED'};
experiment_markers = { 'k+', 'kd', 'ks', 'k.', 'k^', 'kp'};

% the test material is 16 x 11 x 2, with distance 0.5 between nodes
[ nodes, elements] = make_febio_box( [ 16 11 2], [ 0.5 0.5 0.5]);

% HH model time step in ms
dt = 0.05;
% The input to the HH model is some weighted combination of the following:
% sx, sy , sz, sxy, sxz, syz, SED, MSS, HS, I1, Dev1, Dev2, Dev3, s1, s2, s3
% HH_model_input should be a set of pairs of variable name and weight
HH_model_input = { 'sx', 1.0; 'sy', 0.0; 'sxy', 0.0; ...
    'I1', 0.0; 'MSS', 0.0; 'sed', 0.0; 'HS', 0.0; 's1', 0.0; ...
    's2', 0.0; 's3', 0.0; 'Dev1', 0.0; 'Dev2', 0.0; 'Dev3', 0.0; ...
    'shearA', 0.0; 'shearB', 0.0; 'shearC', 0.0; 'Ex', 0.0; 'Ey', 0.0};

% derived
Ndisplay_variables = numel( display_variables);
Nexperiments = numel( experiments);
Nloads = numel( loading_forces);
Ninputs = size( HH_model_input, 1);
firing_freqs = zeros( Nexperiments, Nloads);
save_input = zeros( Nexperiments, Nloads);


%% loop over each experiment

% for each experiment
for ei = 1:Nexperiments

    % prepare the febio .feb file

    % what experiment will we run?
    experiment = [];
    switch experiments( ei).type
```

```
        case 'Uniform'
            % define the type of experiment
            experiment.boundary( 1).face = 'left';
            experiment.boundary( 1).axis = 'x';
            experiment.boundary( 2).face = 'front';
            experiment.boundary( 2).axis = 'y';
            experiment.boundary( 3).face = 'origin';
            experiment.boundary( 3).axis = 'z';
            experiment.load( 1).face = 'right';
            experiment.load( 1).type = 'load';
            experiment.load( 1).axis = 'x';
            experiment.load( 1).scale = 0.00818;
            experiment.load( 1).relative = 0;
            experiment.load( 2).face = 'back';
            experiment.load( 2).type = 'load';
            experiment.load( 2).axis = 'y';
            experiment.load( 2).scale = 0.00844;
            experiment.load( 2).relative = 0;
            experiment.displacement = [];

            % constraints
            [ boundaries, nodesets] = make_febio_constraints( nodes,
experiment, ...
                'front', 'y', 'left', 'x' , 'origin', 'z');

            % write out to file
            write_dot_feb( fullfile( folder, [ febio_files{ ei} '.feb']), ...
                'displacement', experiment.displacement, ...
                'load', experiment.load, 'nodes', nodes, 'elements',
elements, ...
                'nodesets', nodesets, 'boundaries', boundaries)

         case 'Biaxial'
            % define the type of experiment
            experiment.boundary( 1).face = 'left';
            experiment.boundary( 1).axis = 'x';
            experiment.boundary( 2).face = 'front';
            experiment.boundary( 2).axis = 'y';
            experiment.boundary( 3).face = 'origin';
            experiment.boundary( 3).axis = 'z';
            experiment.load( 1).face = 'right';
            experiment.load( 1).type = 'load';
            experiment.load( 1).axis = 'x';
            experiment.load( 1).scale = 0.00705;
            experiment.load( 1).relative = 0;
            experiment.load( 2).face = 'back';
            experiment.load( 2).type = 'load';
            experiment.load( 2).axis = 'y';
            experiment.load( 2).scale = 0.00598;
            experiment.load( 2).relative = 0;
            experiment.displacement = [];

            % constraints
            [ boundaries, nodesets] = make_febio_constraints( nodes,
experiment, ...
                'front', 'y', 'left', 'x' , 'origin', 'z');

            % write out to file
            write_dot_feb( fullfile( folder, [ febio_files{ ei} '.feb']), ...
                'displacement', experiment.displacement, ...
                'load', experiment.load, 'nodes', nodes, 'elements',
elements, ...
                'nodesets', nodesets, 'boundaries', boundaries)
```

```
        case 'Uniaxial X'
            % define the type of experiment
            experiment.boundary( 1).face = 'left';
            experiment.boundary( 1).axis = 'x';
            experiment.boundary( 2).face = 'front';
            experiment.boundary( 2).axis = 'y';
            experiment.boundary( 3).face = 'origin';
            experiment.boundary( 3).axis = 'z';
            experiment.load.face = 'right';
            experiment.load.type = 'load';
            experiment.load.axis = 'x';
            experiment.load.scale = 0.00602;
            experiment.load.relative = 0;
            experiment.displacement = [];

            % constraints
            [ boundaries, nodesets] = make_febio_constraints( nodes,
experiment, ...
                'front', 'y', 'left', 'x' , 'origin', 'z');

            % write out to file
            write_dot_feb( fullfile( folder, [ febio_files{ ei} '.feb']), ...
                'displacement', experiment.displacement, ...
                'load', experiment.load, 'nodes', nodes, 'elements',
elements, ...
                'nodesets', nodesets, 'boundaries', boundaries)

        case 'Uniaxial Y'
            % define the type of experiment
            experiment.boundary( 1).face = 'left';
            experiment.boundary( 1).axis = 'x';
            experiment.boundary( 2).face = 'front';
            experiment.boundary( 2).axis = 'y';
            experiment.boundary( 3).face = 'origin';
            experiment.boundary( 3).axis = 'z';
            experiment.load.face = 'back';
            experiment.load.type = 'load';
            experiment.load.axis = 'y';
            experiment.load.scale = 0.00586;
            experiment.load.relative = 0;
            experiment.displacement = [];

            % constraints
            [ boundaries, nodesets] = make_febio_constraints( nodes,
experiment, ...
                'front', 'y', 'left', 'x' , 'origin', 'z');

            % write out to file
            write_dot_feb( fullfile( folder, [ febio_files{ ei} '.feb']), ...
                'displacement', experiment.displacement, ...
                'load', experiment.load, 'nodes', nodes, 'elements',
elements, ...
                'nodesets', nodesets, 'boundaries', boundaries)


        case '+Shear'
            % define the type of experiment
            experiment.boundary( 1).face = 'left';
            experiment.boundary( 1).axis = 'x';
            experiment.boundary( 2).face = 'front';
            experiment.boundary( 2).axis = 'y';
            experiment.boundary( 3).face = 'origin';
            experiment.boundary( 3).axis = 'z';
            experiment.load( 1).face = 'right_vertical1/3';
```

```
            experiment.load( 1).type = 'load';
            experiment.load( 1).axis = 'x';
            experiment.load( 1).scale = 0.000985;
            experiment.load( 1).relative = 0;
            experiment.load( 2).face = 'right_vertical2/3';
            experiment.load( 2).type = 'load';
            experiment.load( 2).axis = 'x';
            experiment.load( 2).scale = 0.00197;
            experiment.load( 2).relative = 0;
            experiment.load( 3).face = 'right_vertical3/3';
            experiment.load( 3).type = 'load';
            experiment.load( 3).axis = 'x';
            experiment.load( 3).scale = 0.00295;
            experiment.load( 3).relative = 0;
            experiment.load( 4).face = 'back_vertical1/3';
            experiment.load( 4).type = 'load';
            experiment.load( 4).axis = 'y';
            experiment.load( 4).scale = 0.000684;
            experiment.load( 4).relative = 0;
            experiment.load( 5).face = 'back_vertical2/3';
            experiment.load( 5).type = 'load';
            experiment.load( 5).axis = 'y';
            experiment.load( 5).scale = 0.00137;
            experiment.load( 5).relative = 0;
            experiment.load( 6).face = 'back_vertical3/3';
            experiment.load( 6).type = 'load';
            experiment.load( 6).axis = 'y';
            experiment.load( 6).scale = 0.00205;
            experiment.load( 6).relative = 0;
            experiment.displacement = [];

            % constraints
            [ boundaries, nodesets] = make_febio_constraints( nodes,
experiment, ...
                'front', 'y', 'left', 'x' , 'origin', 'z');

            % write out to file
            write_dot_feb( fullfile( folder, [ febio_files{ ei} '.feb']), ...
                'displacement', experiment.displacement, ...
                'load', experiment.load, 'nodes', nodes, 'elements',
elements, ...
                'nodesets', nodesets, 'boundaries', boundaries)

        case '-Shear'
            % define the type of experiment
            experiment.boundary( 1).face = 'left';
            experiment.boundary( 1).axis = 'x';
            experiment.boundary( 2).face = 'front';
            experiment.boundary( 2).axis = 'y';
            experiment.boundary( 3).face = 'origin';
            experiment.boundary( 3).axis = 'z';
            experiment.load( 1).face = 'right_vertical1/3';
            experiment.load( 1).type = 'load';
            experiment.load( 1).axis = 'x';
            experiment.load( 1).scale =  0.00295;
            experiment.load( 1).relative = 0;
            experiment.load( 2).face = 'right_vertical2/3';
            experiment.load( 2).type = 'load';
            experiment.load( 2).axis = 'x';
            experiment.load( 2).scale = 0.00197;
            experiment.load( 2).relative = 0;
            experiment.load( 3).face = 'right_vertical3/3';
            experiment.load( 3).type = 'load';
            experiment.load( 3).axis = 'x';
            experiment.load( 3).scale = 0.000985;
```

```
            experiment.load( 3).relative = 0;
            experiment.load( 4).face = 'back_vertical1/3';
            experiment.load( 4).type = 'load';
            experiment.load( 4).axis = 'y';
            experiment.load( 4).scale = 0.00199;
            experiment.load( 4).relative = 0;
            experiment.load( 5).face = 'back_vertical2/3';
            experiment.load( 5).type = 'load';
            experiment.load( 5).axis = 'y';
            experiment.load( 5).scale = 0.00133;
            experiment.load( 5).relative = 0;
            experiment.load( 6).face = 'back_vertical3/3';
            experiment.load( 6).type = 'load';
            experiment.load( 6).axis = 'y';
            experiment.load( 6).scale = 0.000664;
            experiment.load( 6).relative = 0;
            experiment.displacement = [];

            % constraints
            [ boundaries, nodesets] = make_febio_constraints( nodes,
experiment, ...
                'front', 'y', 'left', 'x' , 'origin', 'z');

            % write out to file
            write_dot_feb( fullfile( folder, [ febio_files{ ei} '.feb']), ...
                'displacement', experiment.displacement, ...
                'load', experiment.load, 'nodes', nodes, 'elements',
elements, ...
                'nodesets', nodesets, 'boundaries', boundaries)

        otherwise
            warning( 'Unknown experiment %s', experiments( ei).type);
            continue
    end

    % run febio
    run_febio( 'fpath', folder, 'configfile', [ febio_files{ ei} '.feb']);


    %% read in the results from febio

    % load the febio output
    febio_output{ ei} = readfebio( fullfile( folder, [ febio_files{ ei}
'_stress.txt']));

    % calculate some things if required
%     if ~isfield( febio_output{ ei}, 's1')
%         febio_output{ ei}.s1 = febio_output{ ei}.sx - febio_output{ ei}.sy;
%     end
%     if ~isfield( febio_output{ ei}, 's2')
%         febio_output{ ei}.s2 = febio_output{ ei}.sx - febio_output{ ei}.sz;
%     end
%     if ~isfield( febio_output{ ei}, 's3')
%         febio_output{ ei}.s3 = febio_output{ ei}.sy - febio_output{ ei}.sz;
%     end
%     if ~isfield( febio_output{ ei}, 'SED')
%         febio_output{ ei}.SED = febio_output{ ei}.sx - febio_output{
ei}.sy;
%     end

    % Check if SED is provided by FEBIO output
    assert( isfield( febio_output{ ei}, 'sed'), 'SED not calculated in
febio');
```

```
    % derived
    febio_output{ ei}.shearA = abs( febio_output{ ei}.s1 - febio_output{
ei}.s2) / 2;
    febio_output{ ei}.shearB = abs( febio_output{ ei}.s2 - febio_output{
ei}.s3) / 2;
    febio_output{ ei}.shearC = abs( febio_output{ ei}.s1 - febio_output{
ei}.s3) / 2;

    % calculate extra display variables for the
    % 1st invariant of stress tensor, strain energy density, max shear
stress,
    % hydrostatic stress, deviatoric stress 1, 2 and 3
    febio_output{ ei}.I1 = febio_output{ ei}.s1 + febio_output{ ei}.s2 +
febio_output{ ei}.s3;
    febio_output{ ei}.MSS = max( cat( 3, febio_output{ ei}.shearA,
febio_output{ ei}.shearB, febio_output{ ei}.shearC), [], 3);
    febio_output{ ei}.HS = febio_output{ ei}.I1 / 3;
    febio_output{ ei}.Dev1 = febio_output{ ei}.s1 - febio_output{ ei}.HS;
    febio_output{ ei}.Dev2 = febio_output{ ei}.s2 - febio_output{ ei}.HS;
    febio_output{ ei}.Dev3 = febio_output{ ei}.s3 - febio_output{ ei}.HS;

    % and for convenience
    febio_output{ ei}.Nelements = size( febio_output{ ei}.sx, 1);


    %% do our analysis

    % HH model experiment length
    HH_total_time = 2000; %1000
    HH_calculation_time = 1000; %500
    freq_MPP = 10;

    % derived
    element = ceil( febio_output{ ei}.Nelements / 2);


    for lfi = 1:Nloads
        input = 0;

        % loop over the inputs to the HH model, multiply by 1000 to convert
        % from Mpa to Kpa
        for ii = 1:Ninputs
            input = input + ...
                HH_model_input{ ii, 2} * ...
                febio_output{ ei}.( HH_model_input{ ii, 1})( element,
lfi)*1000;

        end

        [ V, I_ST] = HH_ruffini( input * ones( 1, HH_total_time / dt), dt);

        % estimate the firing frequency
        [ ~, peak_locations] = findpeaks( V( ( end - HH_calculation_time /
dt):end), ...
            'MinPeakProminence', freq_MPP);
        if isempty( peak_locations)
            ff = 0;
        elseif isscalar( peak_locations)
            ff = 1 / ( HH_calculation_time / 1000);
        else
            ff = 1 / ( mean( diff( peak_locations)) * dt / 1000);
        end
```

```
        firing_freqs( ei, lfi) = ff;

    end
end
%% display the results
Khalsa_figure6

%% Reproduce Khalsa Fig 6 digitized results
% ReproduceKhalsa_Fig6

%% Show linear regression of results
results
```

D.3 Khalsa_figure6.m

```
% script to recreate Figure 6 from the Khalsa paper

    % reproduce Figure 6 in the Khalsa paper
    % febio model should give us stresses/strains at increasing applied
    % loads, we use the central node and loop over the applied loads,
    % taking the output for that load and replicating it in time for the HH
    % model to settle and allow us to estimate the firing frequency. They
    % run the experiment for 4 seconds and estimate from the last 0.5
    % seconds. We need to identify the settling time, and then estimate
    % carefully from the last few action potential.

    % Created by Kenneth Pope 2019, adapted by Daina Ross 2020

%% pull together all the results and make the figure

% definitions
Force_axes_to_match_Khalsa = true;
subplots = { '321', 'sx'; '322', 'sy'; '323', 'sxy'; ...
    '324', 'I1'; '325', 'MSS'; '326', 'sed'};
loading_regimes = { 'Uniform', 'k+', 6; 'Biaxial', 'kd', 6; ...
    'UniaxialX', 'ks', 8; 'UniaxialY', 'k.', 20; ...
    'ShearPos', 'k^', 6; 'ShearNeg', 'kp', 8};

% derived
Nloading_regimes = size( loading_regimes, 1);
Nloading_forces = numel( loading_forces);
Nsubplots = size( subplots, 1);


%% display the results

% figure( 1), clf, hold off;
% subplot( 3, 3, 1), plot( febio_output.sx( element, :)), title( 'sx')
% subplot( 3, 3, 2), plot( febio_output.sy( element, :)), title( 'sy')
% subplot( 3, 3, 3), plot( febio_output.sxy( element, :)), title( 'sxy')
% subplot( 3, 3, 4), plot( febio_output.I1( element, :)), title( 'I1')
% subplot( 3, 3, 5), plot( febio_output.MSS( element, :)), title( 'MSS')
% subplot( 3, 3, 6), plot( febio_output.SED( element, :)), title( 'SED')
% subplot( 3, 3, 7), plot( shearA( element, :)), title( 'shearA')
% subplot( 3, 3, 8), plot( shearB( element, :)), title( 'shearB')
% subplot( 3, 3, 9), plot( shearC( element, :)), title( 'shearC')

% set up figure
figure( 1), hold off, clf;
save_input = 0;
% loop over subplots
for spi = 1:Nsubplots
    % prepare subplot
    subplot( subplots{ spi, 1});
    if spi == 2
        hld = zeros( 1, Nloading_regimes);
        for lri = 1:Nloading_regimes
            hld( lri) = plot( -rand * 25 - 12, -rand, loading_regimes{ lri,
2}, 'MarkerSize', loading_regimes{ lri, 3});
            hold on
        end
        hl = legend( loading_regimes( :, 1), 'AutoUpdate', 'off', ...
            'Box', 'off', 'Location', 'SouthEast');
        title(hl,'Loading');
        delete( hld);
    end
```

```
    % loop over loading regimes and load forces
    for lri = 1:Nloading_regimes
        if ( ( spi == 3) && ( lri ~= 5) && ( lri ~= 6))
            continue
        else
            for lfi = 1:Nloading_forces
                plot( febio_output{ lri}.(subplots{ spi, 2})( element,
lfi)*1000, firing_freqs( lri, lfi), ...
                    loading_regimes{ lri, 2}, 'MarkerSize', loading_regimes{
lri, 3});
                hold on

                %save input stresses and firing freqs for later
                febio_results{ lri}.( subplots{ spi, 2})( lfi,1) =
febio_output{ lri}.(subplots{ spi, 2})( element, lfi)*1000;
                febio_results{ lri}.( subplots{ spi, 2})( lfi,2) =
firing_freqs( lri, lfi);
            end

        end

    end

    % label the graph
    xlabel( [ display_variables{ spi} ' (kPa)']);
    ylabel( 'NR (imp/sec.)');
    % adjust each subplot axes limits to match khalsa figure to allow for
    % direct comparisons
    if Force_axes_to_match_Khalsa == true
        switch ( spi)
            %subplot A - sx
            case 1
                set( gca, 'XLim', [ 0 80], 'XTick', 0:20:80, 'YLim', [ 0 16],
'YTick', 0:4:16);
                set( gca, 'XAxisLocation', 'origin', 'YAxisLocation',
'origin');
                set( gca, 'XMinorTick', 'on', 'YMinorTick', 'on');
            %subplot B - sy
            case 2
                set( gca, 'XLim', [ 0 80], 'XTick', 0:20:80, 'YLim', [ 0 16],
'YTick', 0:4:16);
                set( gca, 'XAxisLocation', 'origin', 'YAxisLocation',
'origin');
                set( gca, 'XMinorTick', 'on', 'YMinorTick', 'on');
                set( get( gca, 'YAxis'), 'Visible', 'off');
            %subplot C - sxy
            case 3
                set( gca, 'XLim', [ -20 20], 'XTick', -20:10:20, 'YLim', [ 0
16], 'YTick', 0:4:16);
                set( gca, 'XAxisLocation', 'origin');
                set( gca, 'XMinorTick', 'on', 'YMinorTick', 'on');
            %subplot D - I1
            case 4
                set( gca, 'XLim', [ 0 125], 'XTick', 0:25:125, 'YLim', [ 0
16], 'YTick', 0:4:16);
                set( gca, 'XAxisLocation', 'origin', 'YAxisLocation',
'origin');
                set( gca, 'XMinorTick', 'on', 'YMinorTick', 'on');
                set( get( gca, 'YAxis'), 'Visible', 'off');
            %subplot E - MSS
            case 5
```

```
                set( gca, 'XLim', [ 0 25], 'XTick', 0:5:25, 'YLim', [ 0 16],
'YTick', 0:4:16);
                set( gca, 'XAxisLocation', 'origin', 'YAxisLocation',
'origin');
                set( gca, 'XMinorTick', 'on', 'YMinorTick', 'on');
            %subplot F - SED
            case 6
                set( gca, 'XLim', [ 0 5], 'XTick', 0:1:5, 'YLim', [ 0 16],
'YTick', 0:4:16);
                set( gca, 'XAxisLocation', 'origin', 'YAxisLocation',
'origin');
                set( gca, 'XMinorTick', 'on', 'YMinorTick', 'on');
                set( get( gca, 'YAxis'), 'Visible', 'off');
            %if none of the other cases match
            otherwise
                set( gca, 'YLim', [ 0 16], 'YTick', 0:4:16, 'YMinorTick',
'on');
        end
    end

    % a few more adjustments so figure looks more like Khalsa Fig 6
    xlim = get( gca, 'XLim');
    ylim = get( gca, 'YLim');
    text( xlim(1), ylim(2), char( 'A' + spi - 1), ...
        'FontSize', 12, 'FontWeight', 'bold', ...
        'HorizontalAlignment', 'left', 'VerticalAlignment', 'bottom');
    axis square;
    set( gca, 'Box', 'off');

end

% adjust figure size to be big but like Khalsa
mp = get( 0, 'MonitorPositions');
pos = get( gcf, 'Position');
set( gcf, 'Color', [ 1 1 1])
best_height = mp( 1, 4) - 120;
set( gcf, 'Position', floor( [ 25, 40, best_height / 1.54, best_height]));
```

D.4 ReproduceKhalsa_Fig6.m

```
% script to recreate Figure 6 from the Khalsa paper
    % reproduce Figure 6 in the Khalsa paper
    % using that data from the figures in the Khalsa paper
    % obtained via Grabit

% Adapted from Khalsa_figure6.m (Kenneth Pope 2019)
% Adapted by Daina Ross 2020

% definitions
folder =
'/Users/dainaross/Desktop/Uni/Masters/Practical/Matlab_Code/Khalsa_Fig6_grabi
t/';
subplots = { '321', 'sx'; '322', 'sy'; '323', 'sxy'; ...
    '324', 'I1'; '325', 'MSS'; '326', 'sed'};
loading_regimes = { 'Uniform', 'k+', 6; 'Biaxial', 'kd', 6; ...
    'UniaxialX', 'ks', 8; 'UniaxialY', 'k.', 20; ...
    'ShearPos', 'k^', 6; 'ShearNeg', 'kp', 8};
display_names = { 'Sx'; 'Sy'; 'Sxy'; ...
    'I1'; 'MSS'; 'SED'};

loading_forces = linspace( 0, 1, 10); %number of points on plot
Force_axes_to_match_Khalsa = true;

% derived
Nloading_regimes = size( loading_regimes, 1);
Nloading_forces = numel( loading_forces);
Nsubplots = size( subplots, 1);

%% display the results
% set up figure
figure( 2), hold off, clf;

%set up subplots to plot the khalsa data
Khalsa_output = cell( 1, Nloading_regimes);
%Fill with NaN instead of zeros
% Khalsa_output(:,:) = {NaN};
for spi = 1:Nsubplots
    %prepare subplot
    subplot( subplots{ spi, 1});
    if spi == 2
        hld = zeros( 1, Nloading_regimes);
        for lri = 1:Nloading_regimes
            hld( lri) = plot( -rand * 25 - 12, -rand, loading_regimes{ lri,
2}, 'MarkerSize', loading_regimes{ lri, 3});
            hold on
        end
        hl = legend( loading_regimes( :, 1), 'AutoUpdate', 'off', ...
            'Box', 'off', 'Location', 'SouthEast');
        title(hl,'Loading');
        delete( hld);
    end

    for lri = 1:Nloading_regimes
        if (isfile(fullfile( folder, [ loading_regimes{ lri, 1} '/' subplots{
spi, 2} '.mat'])))
            load(fullfile( folder, [ loading_regimes{ lri, 1} '/' subplots{
spi, 2} '.mat']));
        else
            continue
        end

        switch( spi)
```

```
            case 1
                [~, idx] = sort([sx(:,1)], 'ascend');
                 Khalsa_output{ lri}.( subplots{ spi, 2}) = ...
                    sx(idx,:);
                plot( sx(:,1), sx(:,2), loading_regimes{ lri, 2},
'MarkerSize', loading_regimes{ lri, 3});

            case 2
                [~, idx] = sort([sy(:,1)], 'ascend');
                 Khalsa_output{ lri}.( subplots{ spi, 2}) = ...
                    sy(idx,:);
                plot( sy(:,1), sy(:,2), loading_regimes{ lri, 2},
'MarkerSize', loading_regimes{ lri, 3});

            case 3
                [~, idx] = sort([sxy(:,1)], 'ascend');
                 Khalsa_output{ lri}.( subplots{ spi, 2}) = ...
                    sxy(idx,:);
                plot( sxy(:,1), sxy(:,2), loading_regimes{ lri, 2},
'MarkerSize', loading_regimes{ lri, 3});

            case 4
                [~, idx] = sort([I1(:,1)], 'ascend');
                 Khalsa_output{ lri}.( subplots{ spi, 2}) = ...
                    I1(idx,:);
                plot( I1(:,1), I1(:,2), loading_regimes{ lri, 2},
'MarkerSize', loading_regimes{ lri, 3});

            case 5
                [~, idx] = sort([MSS(:,1)], 'ascend');
                 Khalsa_output{ lri}.( subplots{ spi, 2}) = ...
                    MSS(idx,:);
                plot( MSS(:,1), MSS(:,2), loading_regimes{ lri, 2},
'MarkerSize', loading_regimes{ lri, 3});

            case 6
                [~, idx] = sort([SED(:,1)], 'ascend');
                 Khalsa_output{ lri}.( subplots{ spi, 2}) = ...
                    SED(idx,:);
                plot( SED(:,1), SED(:,2), loading_regimes{ lri, 2},
'MarkerSize', loading_regimes{ lri, 3});

        end
        hold on

    end

    % adjust each subplot axes limits to match khalsa figure to allow for
    % direct comparisons

    if Force_axes_to_match_Khalsa == true
        switch ( spi)
            %subplot A - sx
            case 1
                set( gca, 'XLim', [ -1 80], 'XTick', 0:20:80, 'YLim', [ 0
17], 'YTick', 0:4:16);
                set( gca, 'XAxisLocation', 'origin', 'YAxisLocation',
'origin');
                set( gca, 'XMinorTick', 'on', 'YMinorTick', 'on');

            %subplot B - sy
            case 2
```

```
                set( gca, 'XLim', [ 0 80], 'XTick', 0:20:80, 'YLim', [ 0 16],
'YTick', 0:4:16);
                set( gca, 'XAxisLocation', 'origin', 'YAxisLocation',
'origin');
                set( gca, 'XMinorTick', 'on', 'YMinorTick', 'on');
                set( get( gca, 'YAxis'), 'Visible', 'off');
            %subplot C - sxy
            case 3
                set( gca, 'XLim', [ -20 20], 'XTick', -20:10:20, 'YLim', [ 0
16], 'YTick', 0:4:16);
                set( gca, 'XAxisLocation', 'origin');
                set( gca, 'XMinorTick', 'on', 'YMinorTick', 'on');
            %subplot D - I1
            case 4
                set( gca, 'XLim', [ 0 125], 'XTick', 0:25:125, 'YLim', [ 0
16], 'YTick', 0:4:16);
                set( gca, 'XAxisLocation', 'origin', 'YAxisLocation',
'origin');
                set( gca, 'XMinorTick', 'on', 'YMinorTick', 'on');
                set( get( gca, 'YAxis'), 'Visible', 'off');
            %subplot E - MSS
            case 5
                set( gca, 'XLim', [ 0 27], 'XTick', 0:5:25, 'YLim', [ -0.25
16], 'YTick', 0:4:16);
                set( gca, 'XAxisLocation', 'origin', 'YAxisLocation',
'origin');
                set( gca, 'XMinorTick', 'on', 'YMinorTick', 'on');
            %subplot F - SED
            case 6
                set( gca, 'XLim', [ -0.25 5.5], 'XTick', 0:1:5, 'YLim', [ -
0.25 16], 'YTick', 0:4:16);
                set( gca, 'XAxisLocation', 'origin', 'YAxisLocation',
'origin');
                set( gca, 'XMinorTick', 'on', 'YMinorTick', 'on');
                set( get( gca, 'YAxis'), 'Visible', 'off');
                xticks(gca,0:1:5);
                xticklabels(gca,{'0','1','2','3','4', '5'})
                yticks(gca,0:4:16);
                yticklabels(gca,{'0','4','8','12','16'})
            %if none of the other cases match
            otherwise
                set( gca, 'YLim', [ 0 16], 'YTick', 0:4:16, 'YMinorTick',
'on');
        end
    end


    % a few more adjustments so figure looks more like Khalsa Fig 6
    xlim = get( gca, 'XLim');
    ylim = get( gca, 'YLim');
    text( xlim(1), ylim(2), char( 'A' + spi - 1), ...
        'FontSize', 16, 'FontWeight', 'bold', ...
        'HorizontalAlignment', 'left', 'VerticalAlignment', 'bottom');
    axis square;
    set( gca, 'Box', 'off');

    % label the graph
    if spi == 5 || spi == 6
        xlabel( [ display_names{ spi} ' (kPa)'], 'HorizontalAlignment',
'center','VerticalAlignment', 'middle', 'Position', [xlim(2)/2 -3]);
    else
        xlabel( [ display_names{ spi} ' (kPa)']);
    end
    if spi == 1
```

```
        ylabel( 'NR (imp/sec.)', 'HorizontalAlignment',
'center','VerticalAlignment', 'middle', 'Rotation', 90, 'Position', [-17,
ylim(2)/2]);
    else
        ylabel( 'NR (imp/sec.)');
    end

    %change font size of axes labels and tick labels
    x_title = get(gca,'XLabel');
    y_title = get(gca,'YLabel');
    x_ticks = get(gca,'XAxis');
    y_ticks = get(gca,'YAxis');
    set(x_ticks,'FontSize', 12);
    set(y_ticks,'FontSize', 12);
    set(x_title, 'FontSize', 14);
    set(y_title, 'FontSize', 14);

end

% adjust figure size
mp = get( 0, 'MonitorPositions');
pos = get( gcf, 'Position');
set( gcf, 'Color', [ 1 1 1])
best_height = mp( 1, 4) - 120;
set( gcf, 'Position', floor( [ 25, 40, best_height / 1.54, best_height]));
set(gcf, 'PaperUnits', 'centimeters', 'PaperPosition', [1, 1, 15, 15])
```

D.5 Regression_results.m

```
% Script to plot the linear regressions of the results of FEBio experiment
% versus the Khalsa et al. (1996) experiment results

% Adapted from Khalsa_figure6.m (Kenneth Pope 2019)
% Adapted by Daina Ross 2020

%% derived
Khalsa_ff = zeros( Nexperiments, Nloads);
khalsa_lfi = {10; 5; 4; 6; 6; 5};

% Average the Khalsa output for each loading regime (i.e. for lri = #, avg of
all
% firing rates for that lri from the subplots)
% i.e. sorting the Khalsa data into the correct format

for lri = 1:Nloading_regimes
    % get the name of each subplot
    subplots_khalsa = (fieldnames(Khalsa_output{ lri}));

    for lfi = 1:Nloads
        if lfi > khalsa_lfi{ lri }
            %fill with NaN if less than 10 firing rates for that loading
regime
            Khalsa_ff( lri, lfi) = NaN;
        else
        % For each subplot applicable for the loading regime find the
        % average firing rate
            for rpi = 1:numel(fieldnames(Khalsa_output{ lri}))
                    Khalsa_ff( lri, lfi) = Khalsa_ff( lri, lfi) +
Khalsa_output{ lri}.( subplots_khalsa{ rpi, 1})( lfi, 2);
            end
            Khalsa_ff( lri, lfi) = Khalsa_ff( lri, lfi) / rpi;
        end
    end
end

%% Plot figure
% plot comparison figure
figure( 3), hold off, clf;

hld = zeros( 1, Nloading_regimes);
for lri = 1:Nloading_regimes
    hld( lri) = plot( -rand * 25 - 12, -rand, loading_regimes{ lri, 2},
'MarkerSize', loading_regimes{ lri, 3});
    hold on
end
hl = legend( loading_regimes( :, 1), 'AutoUpdate', 'off', ...
    'Box', 'off', 'Location', 'SouthEast');
title(hl,'Loading');
delete( hld);

    % loop over loading regimes and load forces
for lri = 1:Nloading_regimes
    for lfi = 1:Nloading_forces
        if isnan(Khalsa_ff( lri, lfi))
            continue
        else
%             plot( Khalsa_ff( lri, lfi), firing_freqs( lri, lfi), ...
            plot( Khalsa_ff( lri, lfi), Khalsa_ff( lri, lfi), ...
              loading_regimes{ lri, 2}, 'MarkerSize', loading_regimes{ lri,
3});
            hold on
```

```
        end
    end
end

% Combine data for comparing all loading regime points together
all_Khalsa = horzcat(Khalsa_ff( 1, 1:khalsa_lfi{1}), Khalsa_ff( 2,
1:khalsa_lfi{2}), Khalsa_ff( 3, 1:khalsa_lfi{3}), Khalsa_ff( 4,
1:khalsa_lfi{4}), Khalsa_ff( 5, 1:khalsa_lfi{5}), Khalsa_ff( 6,
1:khalsa_lfi{6}));
all_Febio = horzcat(firing_freqs( 1, 1:khalsa_lfi{1}), firing_freqs( 2,
1:khalsa_lfi{2}), firing_freqs( 3, 1:khalsa_lfi{3}), firing_freqs( 4,
1:khalsa_lfi{4}), firing_freqs( 5, 1:khalsa_lfi{5}), firing_freqs( 6,
1:khalsa_lfi{6}));

% label the graph
xlabel( ' Khalsa NR (imp/sec.)');
ylabel( 'FeBio NR (imp/sec.)');
set( gca, 'YLim', [ 0 18], 'YTick', 0:2:18, 'YMinorTick', 'on');
set( gca, 'XLim', [ 0 18], 'XTick', 0:2:18, 'XMinorTick', 'on');

% a few more adjustments so figure looks more presentable
xlim = get( gca, 'XLim');
ylim = get( gca, 'YLim');
axis square;
set( gca, 'Box', 'off');
mp = get( 0, 'MonitorPositions');
pos = get( gcf, 'Position');
set( gcf, 'Color', [ 1 1 1])
best_height = mp( 1, 4) - 120;
set( gcf, 'Position', floor( [ 25, 40, best_height / 1.54, best_height]));

%% Calculate linear regression
% For each individual set of loading regime points and for the whole plot
uniform = fitlm( Khalsa_ff( 1, 1:khalsa_lfi{1}), firing_freqs( 1,
1:khalsa_lfi{1}));
biaxial = fitlm( Khalsa_ff( 2, 1:khalsa_lfi{2}), firing_freqs( 2,
1:khalsa_lfi{2}));
uniaxialX = fitlm( Khalsa_ff( 3, 1:khalsa_lfi{3}), firing_freqs( 3,
1:khalsa_lfi{3}));
uniaxialY = fitlm( Khalsa_ff( 4, 1:khalsa_lfi{4}), firing_freqs( 4,
1:khalsa_lfi{4}));
PosShear = fitlm( Khalsa_ff( 5, 1:khalsa_lfi{5}), firing_freqs( 5,
1:khalsa_lfi{5}));
NegShear = fitlm( Khalsa_ff( 6, 1:khalsa_lfi{6}), firing_freqs( 6,
1:khalsa_lfi{6}));
total_regression = fitlm( all_Khalsa( :, :), all_Febio( :, :));

%Store in an array for use later
lin_regression(1,1) = uniform.Rsquared.Ordinary;
lin_regression (1,2) = uniform.RMSE;
lin_regression (1,3) = uniform.Coefficients.Estimate(2,1);
lin_regression (2,1) = biaxial.Rsquared.Ordinary;
lin_regression (2,2) = biaxial.RMSE;
lin_regression (2,3) = biaxial.Coefficients.Estimate(2,1);
lin_regression (3,1) = uniaxialX.Rsquared.Ordinary;
lin_regression (3,2) = uniaxialX.RMSE;
lin_regression (3,3) = uniaxialX.Coefficients.Estimate(2,1);
lin_regression (4,1) = uniaxialY.Rsquared.Ordinary;
lin_regression (4,2) = uniaxialY.RMSE;
lin_regression (4,3) = uniaxialY.Coefficients.Estimate(2,1);
lin_regression (5,1) = PosShear.Rsquared.Ordinary;
lin_regression (5,2) = PosShear.RMSE;
lin_regression (5,3) = PosShear.Coefficients.Estimate(2,1);
```

```
lin_regression (6,1) = NegShear.Rsquared.Ordinary;
lin_regression (6,2) = NegShear.RMSE;
lin_regression (6,3) = NegShear.Coefficients.Estimate(2,1);
lin_regression (7,1) = total_regression.Rsquared.Ordinary;
lin_regression (7,2) = total_regression.RMSE;
lin_regression (7,3) = total_regression.Coefficients.Estimate(2,1);
```

D.6 FEBio Automation

D.6.1 Make_febio_box.m

```
function [ nodes, elements] = make_febio_box( Nelements, separations, name)

% Written 2019 by Kenneth Pope

% parse inputs
assert( all( size( Nelements) == [ 1 3]), ...
    'Nelements must be 1 row vector of length 3 (it specifies the number of
elements in the x, y and z axes)');
assert( all( isint( Nelements) & ( Nelements > 0)), ...
    'Nelements must contain positive integers (it specifies the number of
elements in the x, y and z axes)');
assert( all( size( separations) == [ 1 3]), ...
    'separations must be 1 row vector of length 3 (it specifies the
separation between nodes in the x, y and z axes)');
assert( all( separations > 0), ...
    'separations must contain positive numbers (it specifies the separation
between nodes in the x, y and z axes)');
if ~exist( 'name', 'var') || isempty( name)
    name = 'Object01';
end

% Work out the first and last node (x,y,z) coordinates
% We are assuming that the box is centred on zero in the x and y axes,
% whereas in the z axis we start at zero and increase in value
node1n = [ ( 1 - Nelements( 1:2)) / 2 .* separations( 1:2), 0];
nodeNn = [ -node1n( 1:2), ( Nelements( 3) - 1) * separations( 3)];

% put together the nodes structure
nodes.name = name;
nodes.locations = [ kron( ( node1n( 1):separations( 1):nodeNn( 1))', ...
    ones( prod( Nelements( 2:3)), 1)), ...
    kron( kron( ones( Nelements( 1), 1), ...
    ( node1n( 2):separations( 2):nodeNn( 2))'), ...
    ones( Nelements( 3), 1)), ...
    kron( ones( prod( Nelements( 1:2)), 1), ...
    ( node1n( 3):separations( 3):nodeNn( 3))')];

% which nodes go into making an element?
base = [ 0, Nelements( 2), Nelements( 2) + 1, 1] * Nelements( 3);
nodeinds = [ base, base + 1] + 1;
nodeinds = kron( ones( Nelements( 3) - 1, 1), nodeinds) + ...
    kron( ( 0:( Nelements( 3) - 2))', ones( size( nodeinds)));
nodeinds = kron( ones( Nelements( 2) - 1, 1), nodeinds) + ...
    kron( ( 0:( Nelements( 2) - 2))', ones( size( nodeinds))) * Nelements(
3);
nodeinds = kron( ones( Nelements( 1) - 1, 1), nodeinds) + ...
    kron( ( 0:( Nelements( 1) - 2))', ones( size( nodeinds))) * prod(
Nelements( 2:3));

% put together the elements structure
elements.name = 'Part1';
elements.material = '1';
elements.nodes = nodeinds;
```

D.6.2 Make_febio_constraints.m

```
function [ boundaries, nodesets] = make_febio_constraints( varargin)

% Written 2019 by Kenneth Pope

% parse inputs
p = inputParser;
p.KeepUnmatched = true;
addRequired( p, 'nodes', @isstruct);
addRequired( p, 'experiment', @isstruct);
parse( p, varargin{ :});

% extract useful things
nls = p.Results.nodes.locations;
boundary_faces = { p.Results.experiment.boundary.face};
load_faces = { p.Results.experiment.load.face};
if isfield( p.Results.experiment.displacement, 'face')
    displacement_faces = { p.Results.experiment.displacement.face};
else
    displacement_faces = [];
end
constraint_faces = fieldnames( p.Unmatched)';
unique_faces = unique( cat( 2, boundary_faces, load_faces, ...
    displacement_faces, constraint_faces));

% make the sets
for bi = numel( constraint_faces):-1:1
    boundaries( bi).nodeset = constraint_faces{ bi};
    boundaries( bi).axes = p.Unmatched.( constraint_faces{ bi});
end

% make the nodesets
for nsi = numel( unique_faces):-1:1
    % which face of the box are we after?
    switch unique_faces{ nsi}
        case 'right_vertical1/3'
            threshold = max( nls( :, 2)) / 3 + min( nls( :, 2)) * 2 / 3;
            nodeids = find( ( nls( :, 1) == max( nls( :, 1))) & ...
                ( nls( :, 2) <= threshold));
        case 'right_vertical2/3'
            low_threshold = max( nls( :, 2)) / 3 + min( nls( :, 2)) * 2 / 3;
            high_threshold = max( nls( :, 2)) * 2 / 3 + min( nls( :, 2)) / 3;
            nodeids = find( ( nls( :, 1) == max( nls( :, 1))) & ...
                ( nls( :, 2) <= high_threshold) & ( nls( :, 2) >=
low_threshold));
        case 'right_vertical3/3'
            threshold = max( nls( :, 2)) * 2 / 3 + min( nls( :, 2)) / 3;
            nodeids = find( ( nls( :, 1) == max( nls( :, 1))) & ...
                ( nls( :, 2) >= threshold));
        case 'back_vertical1/3'
            threshold = max( nls( :, 1)) / 3 + min( nls( :, 1)) * 2 / 3;
            nodeids = find( ( nls( :, 2) == max( nls( :, 2))) & ...
                ( nls( :, 1) <= threshold));
        case 'back_vertical2/3'
            low_threshold = max( nls( :, 1)) / 3 + min( nls( :, 1)) * 2 / 3;
            high_threshold = max( nls( :, 1)) * 2 / 3 + min( nls( :, 1)) / 3;
            nodeids = find( ( nls( :, 2) == max( nls( :, 2))) & ...
                ( nls( :, 1) <= high_threshold) & ( nls( :, 1) >=
low_threshold));
        case 'back_vertical3/3'
            threshold = max( nls( :, 1)) * 2 / 3 + min( nls( :, 1)) / 3;
            nodeids = find( ( nls( :, 2) == max( nls( :, 2))) & ...
                ( nls( :, 1) >= threshold));
        case 'right'
```

```
            nodeids = find( nls( :, 1) == max( nls( :, 1)));
        case 'left'
            nodeids = find( nls( :, 1) == min( nls( :, 1)));
        case 'back'
            nodeids = find( nls( :, 2) == max( nls( :, 2)));
        case 'front'
            nodeids = find( nls( :, 2) == min( nls( :, 2)));
        case 'top'
            nodeids = find( nls( :, 3) == max( nls( :, 3)));
        case 'bottom'
            nodeids = find( nls( :, 3) == min( nls( :, 3)));
        case 'origin'
            nodeids = intersect( intersect( ...
                find( nls( :, 1) == min( nls( :, 1))), ...
                find( nls( :, 2) == min( nls( :, 2)))), ...
                find( nls( :, 3) == min( nls( :, 3))));
        otherwise
    end
    nodesets( nsi).name = unique_faces{ nsi};
    nodesets( nsi).ids = nodeids;
end
```

D.6.3 Write_dot_feb.m

```
function write_dot_feb( fout, varargin)
%        write_dot_feb( fout, varargin)
%
% Function for creating .feb file from FEBio model
% Written 2019 by Kenneth Pope, adapted 2019 by Daina Ross

% useful materials
%isotropic elastic
isotropic_elastic.id = 1;
isotropic_elastic.name = 'Material1';
isotropic_elastic.type = 'isotropic elastic';
isotropic_elastic.density = 1;
isotropic_elastic.E = 1;
isotropic_elastic.v = 0.49;

% orthotropic elastic
orthotropic_elastic.id = 1;
orthotropic_elastic.name = 'Material1';
orthotropic_elastic.type = 'orthotropic elastic';
orthotropic_elastic.density = 1;
orthotropic_elastic.E1 = 1;
orthotropic_elastic.E2 = 7.4;
orthotropic_elastic.E3 = 1;
orthotropic_elastic.G12 = 0.385;
orthotropic_elastic.G23 = 2.85;
orthotropic_elastic.G31 = 0.336;
orthotropic_elastic.v12 = 0.299;
orthotropic_elastic.v23 = 0.299;
orthotropic_elastic.v31 = 0.488;

%Mooney Rivlin
mooney_rivlin.id = 1;
mooney_rivlin.name = 'Material1';
mooney_rivlin.type = 'coupled trans-iso Mooney-Rivlin';
mooney_rivlin.density = 1;
mooney_rivlin.c1 = 0.195;
mooney_rivlin.c2 = 0;
mooney_rivlin.c3 = 0.0139;
mooney_rivlin.c4 = 116.22;
mooney_rivlin.c5 = 535.039;
mooney_rivlin.k = 73.2;
mooney_rivlin.lambda = 1;
mooney_rivlin.fiber_type = '0,1,0';

% default simple box
[ nodes0, elements0] = make_febio_box( [ 3 3 3], [ 1 1 1]);

% standard experiment
experiment0.boundary( 1).face = 'left';
experiment0.boundary( 1).axis = 'x';
experiment0.boundary( 2).face = 'front';
experiment0.boundary( 2).axis = 'y';
experiment0.boundary( 3).face = 'origin';
experiment0.boundary( 3).axis = 'z';
experiment0.load.face = 'right';
experiment0.load.type = 'load';
experiment0.load.axis = 'x';
experiment0.load.scale = 1;
experiment0.load.relative = 0;
experiment0.displacement = [];

% parse inputs to control what we put in the .feb file
```

```
p = inputParser;
addParameter( p, 'spec_version', 2.5, @isscalar);
addParameter( p, 'module_type', 'solid', @isstring);
addParameter( p, 'globals', { 'T', 0; 'R', 0; 'Fc', 0}, @iscell);
addParameter( p, 'materials', isotropic_elastic, @isstruct);
% addParameter( p, 'materials', orthotropic_elastic, @isstruct);
% addParameter( p, 'materials', mooney_rivlin, @isstruct);
addParameter( p, 'nodes', nodes0, @isstruct);
addParameter( p, 'elements', elements0, @isstruct);
addParameter( p, 'nodesets', [], @isstruct);
addParameter( p, 'boundaries', experiment0.boundary, @isstruct);
addParameter( p, 'load_curve', 'linear', @ischar);
addParameter( p, 'output', { 'displacement', 'stress'}, @iscell);
addParameter( p, 'time_steps', 10, @isscalar);
addParameter( p, 'step_size', 0.1, @isscalar);
addParameter( p, 'load', experiment0.load, @isstruct);
addParameter( p, 'displacement', experiment0.displacement, @( x) isempty( x)
|| isstruct( x));
addParameter( p, 'logfile_outputs', { 'stress', 'strain'}, @iscell);
parse( p, varargin{ :});
pr = p.Results;

% open file to write
[ folder, filename, extension] = fileparts( fout);
fid = fopen( fout, 'w');

% header information
fprintf( fid, '<?xml version="1.0" encoding="ISO-8859-1"?>\n');
fprintf( fid, '<febio_spec version="%0.1f">\n', pr.spec_version);
fprintf( fid, '\t<Module type="%s"/>\n', pr.module_type);

% global variables
fprintf( fid, '\t<Globals>\n');
fprintf( fid, '\t\t<Constants>\n');
for i = 1:size( pr.globals, 1)
    fprintf( fid, '\t\t\t<%s>%d</%s>\n', pr.globals{ i, [ 1 2 1]}); %, ...
    %         pr.globals{ i, 2}, pr.globals{ i, 1});
end
fprintf( fid, '\t\t</Constants>\n');
fprintf( fid, '\t</Globals>\n');

% material
fprintf( fid, '\t<Material>\n');
for i = 1:numel( pr.materials)
    fprintf( fid, '\t\t<material id="%d" name="%s" type="%s">\n', ...
        pr.materials( i).id, pr.materials( i).name, pr.materials( i).type);
    fprintf( fid, '\t\t\t<density>%d</density>\n', pr.materials( i).density);

% uncomment section for required material type
% Orthotropic material
%     fprintf( fid, '\t\t\t<E1>%d</E1>\n', pr.materials( i).E1);
%     fprintf( fid, '\t\t\t<E2>%d</E2>\n', pr.materials( i).E2);
%     fprintf( fid, '\t\t\t<E3>%d</E3>\n', pr.materials( i).E3);
%     fprintf( fid, '\t\t\t<G12>%d</G12>\n', pr.materials( i).G12);
%     fprintf( fid, '\t\t\t<G23>%d</G23>\n', pr.materials( i).G23);
%     fprintf( fid, '\t\t\t<G31>%d</G31>\n', pr.materials( i).G31);
%     fprintf( fid, '\t\t\t<v12>%d</v12>\n', pr.materials( i).v12);
%     fprintf( fid, '\t\t\t<v23>%d</v23>\n', pr.materials( i).v23);
%     fprintf( fid, '\t\t\t<v31>%d</v31>\n', pr.materials( i).v31);

% Isotropic material
    fprintf( fid, '\t\t\t<E>%d</E>\n', pr.materials( i).E);
    fprintf( fid, '\t\t\t<v>%d</v>\n', pr.materials( i).v);
```

```
% Mooney-Rivlin material
%     fprintf( fid, '\t\t\t<c1>%d</c1>\n', pr.materials( i).c1);
%     fprintf( fid, '\t\t\t<c2>%d</c2>\n', pr.materials( i).c2);
%     fprintf( fid, '\t\t\t<c3>%d</c3>\n', pr.materials( i).c3);
%     fprintf( fid, '\t\t\t<c4>%d</c4>\n', pr.materials( i).c4);
%     fprintf( fid, '\t\t\t<c5>%d</c5>\n', pr.materials( i).c5);
%     fprintf( fid, '\t\t\t<k>%d</k>\n', pr.materials( i).k);
%     fprintf( fid, '\t\t\t<lambda>%d</lambda>\n', pr.materials( i).lambda);
%     fprintf( fid, '\t\t\t<fiber type="vector">%s</fiber>\n', pr.materials(
i).fiber_type);

    fprintf( fid, '\t\t</material>\n');
end
fprintf( fid, '\t</Material>\n');

% start geometry
fprintf( fid, '\t<Geometry>\n');

% nodes
for ni = 1:numel( pr.nodes)
    fprintf( fid, '\t\t<Nodes name="%s">\n', pr.nodes( ni).name);
    for li = 1:size( pr.nodes( ni).locations, 1)
        fprintf( fid, '\t\t\t<node id="%d"> % 0.7e, % 0.7e, % 0.7e</node>\n',
...
            li, pr.nodes( ni).locations( li, :));
    end
    fprintf( fid, '\t\t</Nodes>\n');
end

% elements
for ei = 1:numel( pr.elements)
    fprintf( fid, '\t\t<Elements type="hex8" mat="%s" name="%s">\n', ...
        pr.elements( ei).material, pr.elements( ei).name);
    for ni = 1:size( pr.elements( ei).nodes, 1)
        fprintf( fid, '\t\t\t<elem id="%d"> %5d, %5d, %5d, %5d, %5d, %5d,
%5d, %5d</elem>\n', ...
            ni, pr.elements( ei).nodes( ni, :));
    end
    fprintf( fid, '\t\t</Elements>\n');
end

% nodesets
for nsi = 1:numel( pr.nodesets)
    fprintf( fid, '\t\t<NodeSet name="%s">\n', pr.nodesets( nsi).name);
    for nii = 1:numel( pr.nodesets( nsi).ids)
        fprintf( fid, '\t\t\t<node id="%d"/>\n', pr.nodesets( nsi).ids(
nii));
    end
    fprintf( fid, '\t\t</NodeSet>\n');
end

% finished geometry
fprintf( fid, '\t</Geometry>\n');

% boundary conditions
fprintf( fid, '\t<Boundary>\n');
for bi = 1:numel( pr.boundaries)
    fprintf( fid, '\t\t<fix bc="%s" node_set="%s"/>\n', ...
        pr.boundaries( bi).axes, pr.boundaries( bi).nodeset);
end
fprintf( fid, '\t</Boundary>\n');

% load curve data
switch pr.load_curve
```

```
    case 'linear'
        points = [ 0 0; 1 1];
    case 'constant'
        points = [ 0 1; 1 1];
    otherwise
        error( 'unknown load curve');
end
fprintf( fid, '\t<LoadData>\n');
fprintf( fid, '\t\t<loadcurve id="1" type="smooth">\n');
for pi = 1:size( points, 1)
    fprintf( fid, '\t\t\t<point>%d,%d</point>\n', points( pi, :));
end
fprintf( fid, '\t\t</loadcurve>\n');
fprintf( fid, '\t\t<loadcurve id="2" type="smooth">\n');
for pi = 1:size( points, 1)
    fprintf( fid, '\t\t\t<point>%d,%d</point>\n', points( pi, :));
end
fprintf( fid, '\t\t</loadcurve>\n');
fprintf( fid, '\t</LoadData>\n');

% output
fprintf( fid, '\t<Output>\n');
fprintf( fid, '\t\t<plotfile type="febio">\n');
for oi = 1:numel( pr.output)
    fprintf( fid, '\t\t\t<var type="%s"/>\n', pr.output{ oi});
end
fprintf( fid, '\t\t</plotfile>\n');
for li = 1:numel( pr.logfile_outputs)
    fprintf( fid, '\t\t<logfile>\n');
    switch pr.logfile_outputs{ li}
        case 'stress'
            fprintf( fid, '\t\t\t<element_data
data="sx;sy;sz;sxy;sxz;syz;s1;s2;s3;sed;Ex;Ey" delim=", " file="%s"/>\n', ...
                [ filename '_' pr.logfile_outputs{ li} '.txt']);
        case 'strain'
            fprintf( fid, '\t\t\t<element_data
data="Ex;Ey;Ez;Exy;Exz;Eyz;E1;E2;E3" delim=", " file = "%s"/>\n', ...
                [ filename '_' pr.logfile_outputs{ li} '.txt']);
        otherwise
            error( 'Unknown logfile');
    end
    fprintf( fid, '\t\t</logfile>\n');
end
fprintf( fid, '\t</Output>\n');

% steps in the control algorithm
fprintf( fid, '\t<Step name="Step1">\n');
fprintf( fid, '\t\t<Control>\n');
fprintf( fid, '\t\t\t<time_steps>%d</time_steps>\n', pr.time_steps);
fprintf( fid, '\t\t\t<step_size>%d</step_size>\n', pr.step_size);
fprintf( fid, '\t\t\t<max_refs>15</max_refs>\n');
fprintf( fid, '\t\t\t<max_ups>10</max_ups>\n');
fprintf( fid, '\t\t\t<diverge_reform>1</diverge_reform>\n');
fprintf( fid, '\t\t\t<reform_each_time_step>1</reform_each_time_step>\n');
fprintf( fid, '\t\t\t<dtol>0.001</dtol>\n');
fprintf( fid, '\t\t\t<etol>0.01</etol>\n');
fprintf( fid, '\t\t\t<rtol>0</rtol>\n');
fprintf( fid, '\t\t\t<lstol>0.9</lstol>\n');
fprintf( fid, '\t\t\t<min_residual>1e-20</min_residual>\n');
fprintf( fid, '\t\t\t<qnmethod>0</qnmethod>\n');
fprintf( fid, '\t\t\t<time_stepper>\n');
fprintf( fid, '\t\t\t\t<dtmin>0.01</dtmin>\n');
fprintf( fid, '\t\t\t\t<dtmax>0.1</dtmax>\n');
fprintf( fid, '\t\t\t\t<max_retries>5</max_retries>\n');
fprintf( fid, '\t\t\t\t<opt_iter>10</opt_iter>\n');
```

```
fprintf( fid, '\t\t\t</time_stepper>\n');
fprintf( fid, '\t\t\t<analysis type="static"/>\n');
fprintf( fid, '\t\t</Control>\n');
% applied displacements?
if ~isempty( pr.displacement)
    fprintf( fid, '\t\t<Boundary>\n');
    for bi = 1:numel( pr.displacement)
        fprintf( fid, '\t\t\t<prescribe bc="%s" node_set="%s">\n', ...
            pr.displacement( bi).axis, pr.displacement( bi).face);
        fprintf( fid, '\t\t\t\t<scale lc="1">%d</scale>\n', ...
            pr.displacement( bi).scale);
        fprintf( fid, '\t\t\t\t<relative>%d</relative>\n', ...
            pr.displacement( bi).relative);
        fprintf( fid, '\t\t\t</prescribe>\n');
    end
    fprintf( fid, '\t\t</Boundary>\n');
end
% applied forces
if ~isempty( pr.load)
    fprintf( fid, '\t\t<Loads>\n');
    for li = 1:numel( pr.load)
        if ~isempty( pr.load( li).face)
            fprintf( fid, '\t\t\t<nodal_load bc="%s" node_set="%s">\n', ...
                pr.load( li).axis, pr.load( li).face);
        elseif ~isempty( pr.load( li).node)
            fprintf( fid, '\t\t\t<nodal_load bc="%s" node_set="%s">\n', ...
                pr.load( li).axis, pr.load( li).node);
        else
            error( 'unknown load location');
        end
        fprintf( fid, '\t\t\t\t<scale lc="1">%d</scale>\n', ...
            pr.load( li).scale);
%         fprintf( fid, '\t\t\t\t<relative>%d</relative>\n', ...
%             pr.load( li).relative);
        fprintf( fid, '\t\t\t</nodal_load>\n');
    end
    fprintf( fid, '\t\t</Loads>\n');
end
fprintf( fid, '\t</Step>\n');

% \Boundary \prescribe for fixed displacements as a load
% \Loads \nodal_load for fixed force as a load

% finalise and tidy up
fprintf( fid, '</febio_spec>\n');
fclose( fid);
```

D.6.4 Run_febio.m

```
function status = run_febio( varargin)
% code for running febio
% parameter pairs allowed:
% fpath : path for input and output files
% configfile : filename for configuration file
% febiopath : path and filename for executable

% Written 2019 by Kenneth Pope

% parse inputs
p = inputParser;
addParameter( p, 'fpath',
'/Users/dainaross/Desktop/Uni/Masters/Practical/Matlab_Code/', ...
    @ischar);
addParameter( p, 'febiopath', '/Applications/FEBio2.9.1/bin/febio2', ...
    @ischar);
addParameter( p, 'configfile', 'temp.feb', @ischar);
parse( p, varargin{ :});
pr = p.Results;

% Execute system command to run febio .feb file
status = system(  [ pr.febiopath ' -i ' fullfile( pr.fpath, pr.configfile)]);

% % check the system command was successful
% assert( status == 0, ...
%     ' System command was not executed successfully');
```

D.6.5 Readfebio.m

```
function data = readfebio( fname)
%        output = readfebio( fname)
% Read in stress or strain values from febio output file
% This is version 3, might be worth generalising this to identify what sort
% of output file we are looking at (headers / no headers etc) and calling
% the appropriate read function

% parse inputs
assert( exist( fname, 'file') == 2, 'Input file does not exist');

% open file
fid = fopen( fname, 'r');

% for each time step
step = 0;
while ~feof( fid)

    % might be worth generalising this to allow any headers etc

    % read in the *Step line
    l = fgetl( fid);
    assert( strcmp( l( 1:5), '*Step'), ...
        'First line of step %d isn''t "*Step"', step + 1);
    [ ~, stepstr] = strtok( l, '=');
    step = sscanf( stepstr( 3:end), '%d');

    % read in the *Time line
    l = fgetl( fid);
    assert( strcmp( l( 1:5), '*Time'), ...
        'Second line of step %d isn''t "*Time"', step);
    [ ~, timestr] = strtok( l, '=');
    data.time( step) = sscanf( timestr( 3:end), '%f');

    % read in the *Data line
    l = fgetl( fid);
    assert( strcmp( l( 1:5), '*Data'), ...
        'Third line of step %d isn''t "*Data"', step);
    [ ~, datastr] = strtok( l, '=');
    outputs = strsplit( datastr( 3:end), ';');
    Noutputs = numel( outputs);
    data.outputs = outputs;

    % parse the data
    while ~feof( fid)
        l = fgetl( fid);
        if strcmp( l( 1:5), '*Step')
            fseek( fid, -( 1 + numel( l)), 'cof');
            break
        end
        data_line = sscanf( l, '%f,');
        assert( numel( data_line) == Noutputs + 1, ...
            'Wrong number of data for node %d', data_line( 1));
        for oi = 1:Noutputs
            data.( outputs{ oi})( data_line( 1), step) = data_line( oi + 1);
        end
    end

end

% add some more useful information
[ data.Nnodes, data.Nsteps] = size( data.outputs{ 1});
```